TESIS DE LA UNIVERSIDAD DE ZARAGOZA
2023
71

María San Anselmo Jarauta

Novel dendritic multifunctional nanocarriers and their application in biomedicine

Director/es
Serrano Ostáriz, José Luis
Hernández Ainsa, Silvia

ISSN 2254-7606

Prensas de la Universidad
Universidad Zaragoza

ISSN 2254-7606

Universidad Zaragoza
1542

Tesis Doctoral

NOVEL DENDRITIC MULTIFUNCTIONAL NANOCARRIERS AND THEIR APPLICATION IN BIOMEDICINE

Autor

María San Anselmo Jarauta

Director/es

Serrano Ostáriz, José Luis
Hernández Ainsa, Silvia

UNIVERSIDAD DE ZARAGOZA
Escuela de Doctorado

2021

Departamento de Química Orgánica
Universidad Zaragoza
1542

INMA
INSTITUTO DE NANOCIENCIA Y MATERIALES DE ARAGÓN

TESIS DOCTORAL

Novel dendritic multifunctional nanocarriers and their application in biomedicine

María San Anselmo Jarauta

Memoria presentada en la Universidad de Zaragoza para optar al Grado de Doctor

Dpto. de Química Orgánica

Universidad de Zaragoza-INMA

Zaragoza, Julio de 2021

El **Prof. José Luis Serrano Ostáriz**, Catedrático del Departamento de Química Orgánica de la Facultad de Ciencias de la Universidad de Zaragoza y miembro del Instituto de Nanociencia y Materiales de Aragón y

la **Dra. Silvia Hernández Ainsa**, Investigadora de la Fundación Agencia Aragonesa para la Investigación y el Desarrollo, y miembro del Instituto de Nanociencia y Materiales de Aragón

HACEN CONSTAR:

Que la memoria titulada: "**NOVEL DENDRITIC MULTIFUNCTIONAL NANOCARRIERS AND THEIR APPLICATION IN BIOMEDICINE"** ha sido realizada bajo nuestra dirección por **María San Anselmo Jarauta** en el Departamento de Química Orgánica de esta Universidad y reúne las condiciones requeridas para su presentación como tesis doctoral.

Zaragoza a 1 de Julio de 2021

Fdo. Prof. José Luis Serrano Ostáriz Fdo. Dra. Silvia Hernández Ainsa

List of acronyms

AAV	Adeno-associated virus
ACN	Acetonitrile
ACT	Artemisinin-based combination therapies
AFM	Atomic force microscopy
ANOVA	one-way analysis of variance
ATR	Attenuated total reflection
BCG	Bacillus Calmette–Guérin
BF	Bright field
bis-GMPA	2,2'-*bis*(glyciloxymethyl)propionic acid
bis-MPA	2,2'-*bis*(hydroxymethyl)propionic acid
BnBr	Benzyl bromide
bs	Broad signal (in ^{1}H NMR and FTIR characterisation)
BSA	Bovine serum albumin
CAC	Critical aggregation concentration
CC_{50}	50% cytostatic concentration
CDI	1,1'-carbonyldiimidazole
CFU	Colony-forming unit
CPT	Camptothecin
CQ	Chloroquine
CuAAC	Copper(I) catalysed Azide-Alkyne 1,3-dipolar Cycloaddition
δ	Bending (in FTIR) or chemical shift (in NMR)
Đ	Dispersity
DAPI	4′,6-Diamidine-2′-phenylindole dihydrochloride
DCC	N,N′-dicyclohexylcarbodiimide
DCM	Dichloromethane
DCU	N,N'-dicyclohexylurea
dH_2O	Distilled H_2O
D_H	Hydrodynamic diameter
DHP	Dendronized hyperbranched polymer
DLC	Drug loading content
DLS	Dynamic light scattering
DMAP	4-dimethylaminopyridine
DMEM	Dulbecco's Modified Eagle's Medium

DMF	Dimethylformamide
DMSO	Dimethyl sulfoxide
DNA	Deoxyribonucleic acid
DPTS	4-(dimethylamino)pyridinium 4-toluenesulfonate
EC_{40}	40% effective concentration
EDA	Ethylenediamine
EDC	N-Ethyl-N′-(3-dimethylaminopropyl)carbodiimide
EDTA	Ethylenedinitrilotetraacetic acid
ESI^+	Positive electrospray ionisation
Et_2O	Diethyl ether
EtOH	Ethanol
FBS	Fetal bovine serum
FDA	Food and Drug Administration
FIC	Fractional inhibitory concentration
FSC	Forward scatter channel
FTIR	Fourier transform infrared spectroscopy
G0, G1, G2…	Number of generations of dendrons or dendrimers
GFP	Green fluorescent protein
GIA	Growth inhibition assay
Glyboc(OH)	N-(*tert*-butoxycarbonyl)glycine
HCV	Hepatitis C virus
HDLDBCs	Hybrid dendritic-linear-dendritic block copolymers
HeLa	Henrietta Lacks (cell line)
Hep	Heparin
HIV	Human immunodeficiency virus
HOBt	1-hydroxybenzotriazole hydrate
HP	Hyperbranched polymer
HPLC	High-performance liquid chromatography
Huh	Human hepatoma (cell line)
HUVEC	Human umbilical vein endothelial cells
IA	Iopanoic acid
IC_{50}	50% inhibitory concentration
INH	Isoniazid

ITC	Isothermal titration calorimetry
K_a	Association constant
Lc	Lipophilic content
logP	Logarithm of the partition coefficient
LS	Light scattering
LV	Lentivirus or lateral view
MALDI-TOF	Matrix assisted laser desorption/ionization - Time of flight
MB	Methylene blue
MDR-TB	Multidrug resistant tuberculosis
MeOH	Methanol
MIC	Minimum inhibitory concentration
miRNA	Micro RNA
mMSCs	Mesenchymal stem cells from mouse
mRNA	Messenger RNA
MS	Mass spectrometry
Mtb	*Mycobacterium tuberculosis*
Mtb-THP1	Macrophages derived from monocytes THP1 and infected by *Mtb*
MW	Mass average molecular weight
Mw	Molecular weight
MWCO	Molecular weight cut off
N/P ratio	Ratio between N^+ terminal groups and P^- groups of different molecules
NPs	Nanoparticles
p	Packing parameter
P.	*Plasmodium*
PAMAM	Poly(amidoamine)
PBS	Phosphate-buffered saline
pDNA	Plasmid DNA
PEG	Poly(ethylene glycol)
PEI	Poly(ethylene imine)
PG	Polyglycerol
PLL	Poly-(*L*)-lysine
PMMA	Poly(methyl methacrylate)
PPI	Poly(propylene imine)

PQ	Primaquine
pRBCs	*Plasmodium*-infected red blood cells
QN	Quinacrine
RBCs	Red blood cells
Rh or RhB	Rhodamine B
RIF	Rifampicin
RNA	Ribonucleic acid
RPMI	Roswell Park Memorial Institute (culture medium)
RR-TB	Rifampicin resistant tuberculosis
RT	Room temperature (in synthetic procedures) or retention time (in HPLC)
SD	Standard deviation
SEC	Size exclusion chromatography
SFM	Serum free medium
siRNA	Small interfering RNA
SSC	Side scatter channel
st	Stretching (in FTIR)
$t_{1/2}$	Half-life
TAE	TRIS-acetate-EDTA
TB	Tuberculosis
t-Boc	*Tert*-butoxycarbonyl
TBTA	Tris(benzyltriazolylmethyl)amine
TEM	Transmission electron microscopy
TFA	Trifluoroacetic acid
THF	Tetrahydrofuran
TMS	Tetramethylsilane
TRIAC	3,3',5-triiodothyroacetic acid or tiratricol
TRIS	Tris(hydroxymethyl)aminomethane
TsOH	p-Toluenesulfonic acid
UV-Vis	Ultraviolet-visible
WHO	World Health Organisation
XDR-TB	Extensively drug resistant tuberculosis

Index

Introduction

Science is a discipline that has historically evolved together with the necessities of the society. For that reason, there is a close relationship between **science and society**, and without forgetting that science is developed by human beings, there is an unavoidable sense of responsibility in the context of scientific research and innovation[1].

The particular area of **nanoscience** emerged as an interdisciplinary field to provide solutions to the challenges of a changing society. Specifically, it is composed of three main areas: chemistry, physics and biology (Figure 1).

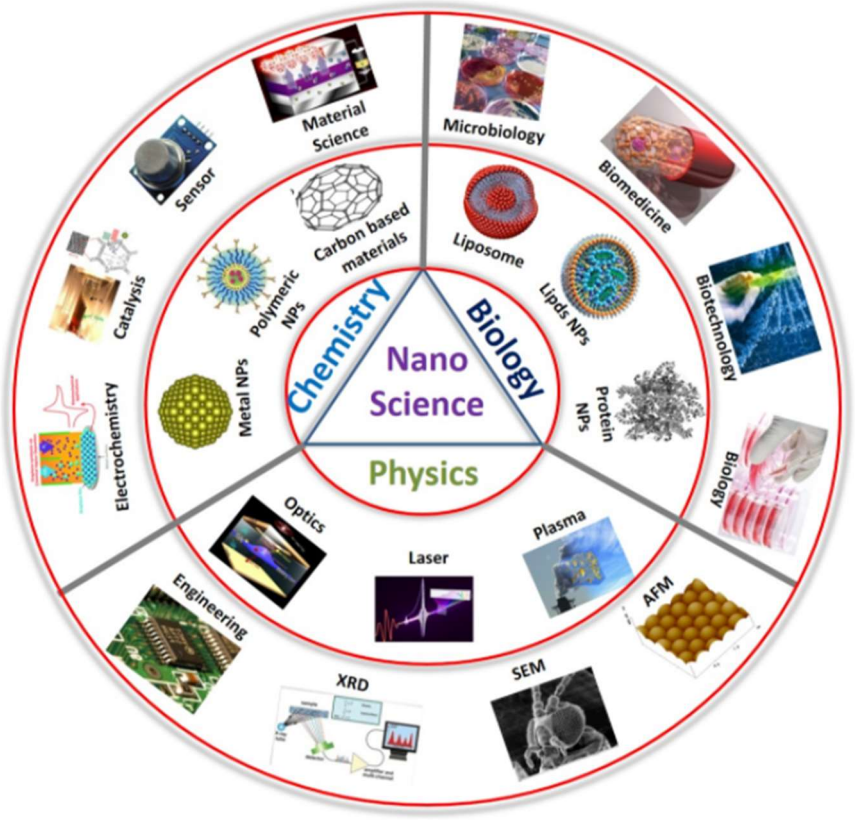

Figure 1. Graphical representation of the interdisciplinarity intrinsic to nanoscience, obtained from Bayda et al[2].

On the other hand, the ability to work at the nanometer scale given by **nanotechnology** was introduced in 1959 by Richard P. Feynman[3]. The different behaviour observed in the materials when modifying the scale (Figure 2) and the unique properties of the nanomaterials, make them highly interesting for a wide range of applications[4].

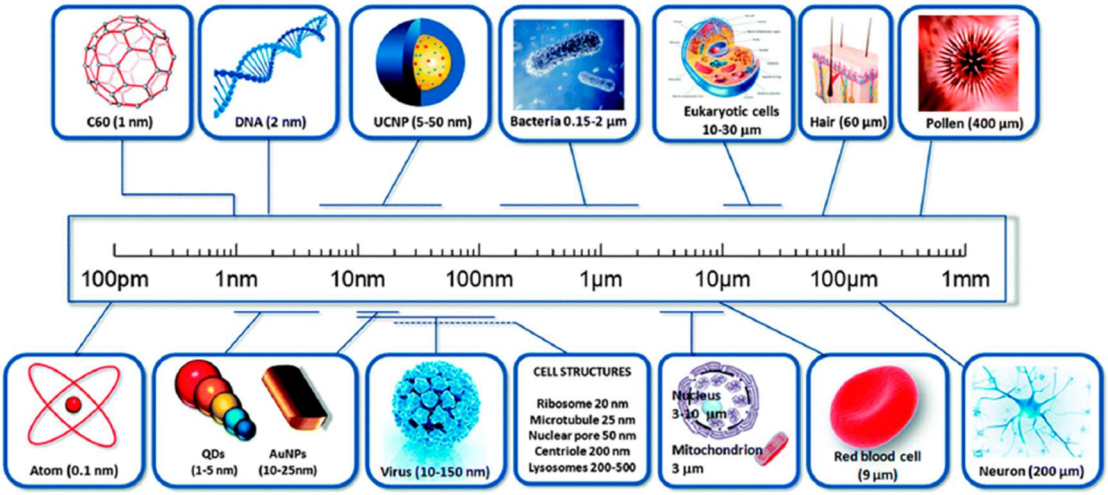

Figure 2. Size scale from picometres (pm) to millimetres (mm), with different examples of structures found at these sizes, obtained from Bayda et al[2].

The range of possible **applications of nanotechnology** include the fields of energy, water treatment, food, the environment, health or cultural heritage conservation[5,6]. Focusing on the health wellness, the introduction of nanotechnology in biomedical research has allowed incredible progress in the diagnosis and treatment of diseases, with the encouraging possibility to develop a personalized management of the health[7]. However, there are still some issues related to reproducibility, specificity, economical or legal aspects that need to be overcome[8].

The main contributions of nanotechnology in the **biomedical field** together with their challenges are summarised by Kaushik in a quite successful way[8]. On the one hand, the nanoscale allows a versatile modification of some characteristics such as surface functionalisation, stimuli-responsive or physical properties, although reaching the desired targeted application is quite challenging. The early-stage diagnosis through miniaturised biosensors integrated in smartphones is a promising area under research that involves bioinformatics with multiple clinical applications[9]. Additionally, bio-mimic materials constitute a powerful tool in regenerative medicine, while compatibility, scaling up and legal issues still need to be addressed[10]. The targeted drug delivery area has been successfully explored in the last century, although the long-term side effects are a matter of concern. For this reason, efforts are being made towards least-component based

nanocarriers, biocompatible and stimuli-responsive[11,12]. Combinational therapy assisted by nanotechnology or gene therapy constitute other powerful approaches in the field but all these cutting-edge progresses in research require the support of the corresponding organisations and an adequate level of social awareness to succeed.

In the exceptional global situation provoked by the **COVID-19 pandemic**, the search for rapid and effective formulations for the prevention and treatment of the SARS-CoV-2 infection has turned to nanotechnology for solutions[13,14]. Different strategies are being studied such as nanoformulations to deliver therapeutic agents, nanomaterials to deactivate the virus in the external environment or nanotechnological approaches for the quick detection of the virus. Above all, it is remarkable the development of new vaccines based on mRNA delivered in a liposomal formulation, which entails a huge achievement in the biomedical field of nanotechnology.

Within this **doctoral thesis**, different areas of biomedical research have been covered using **new dendritic platforms** as nanocarriers. Specifically, **drug delivery** has been applied to the treatment of various diseases, i.e., hepatitis C, tuberculosis and malaria. On the other hand, the **gene transfection** approach has been studied as a general tool to introduce genetic material inside cells with multiple future biomedical applications. Regarding the dendritic materials, a compilation of the structures employed in previous works developed in our group has been done, taking the best of each one to finally design potential nanocarriers based on polyester or poly(esteramide) structures.

In order to establish a coherent structure, this thesis has been divided into eight different chapters as follows. Firstly, in chapter 1, an updated revision of the main topics of interest is made (state of the art) and the objectives of the thesis are set. Then, chapter 2 gathers the synthesis and characterisation of the dendritic materials, as well as the study of their behaviour in water. Later, chapters 3 to 6 are dedicated to the study of these dendritic materials in different biomedical applications. Namely, chapter 3 is about the hepatitis C studies, chapter 4 about tuberculosis, chapter 5 about malaria and chapter 6 about gene transfection. In each of these chapters a specific introduction and the corresponding working

plan to fulfil the set objectives are included. Then, the experimental procedures are detailed in chapter 7 and finally, the summary and general conclusions of the thesis are exposed in chapter 8.

(1) Owen, R.; Macnaghten, P.; Stilgoe, J. Responsible Research and Innovation: From Science in Society to Science for Society, with Society. *Science and Public Policy* **2012**, *39* (6), 751–760. https://doi.org/10.1093/scipol/scs093.

(2) Bayda, S.; Adeel, M.; Tuccinardi, T.; Cordani, M.; Rizzolio, F. The History of Nanoscience and Nanotechnology: From Chemical–Physical Applications to Nanomedicine. *Molecules* **2020**, *25* (1), 112. https://doi.org/10.3390/molecules25010112.

(3) Feynman, R. P. There's Plenty of Room at the Bottom. *Engineering and Science* **1960**, *23* (5), 22–36.

(4) Gatoo, M. A.; Naseem, S.; Arfat, M. Y.; Mahmood Dar, A.; Qasim, K.; Zubair, S. Physicochemical Properties of Nanomaterials: Implication in Associated Toxic Manifestations. *BioMed Research International* **2014**, *2014*, e498420. https://doi.org/10.1155/2014/498420.

(5) Parak, W. J.; Nel, A. E.; Weiss, P. S. Grand Challenges for Nanoscience and Nanotechnology. *ACS Nano* **2015**, *9* (7), 6637–6640. https://doi.org/10.1021/acsnano.5b04386.

(6) Franco-Castillo, I.; Hierro, L.; Fuente, J. M. de la; Seral-Ascaso, A.; Mitchell, S. G. Perspectives for Antimicrobial Nanomaterials in Cultural Heritage Conservation. *Chem* **2021**, *7* (3), 629–669. https://doi.org/10.1016/j.chempr.2021.01.006.

(7) *Advances in Personalized Nanotherapeutics*; Kaushik, A. K., Jayant, R. D., Nair, M., Eds.; Springer International Publishing, 2017. https://doi.org/10.1007/978-3-319-63633-7.

(8) Kaushik, A. Biomedical Nanotechnology Related Grand Challenges and Perspectives. *Front. Nanotechnol.* **2019**, *1*. https://doi.org/10.3389/fnano.2019.00001.

(9) Kaushik, A.; Mujawar, M. A. Point of Care Sensing Devices: Better Care for Everyone. *Sensors (Basel)* **2018**, *18* (12). https://doi.org/10.3390/s18124303.

(10) Sharma, K.; Mujawar, M. A.; Kaushik, A. State-of-Art Functional Biomaterials for Tissue Engineering. *Front. Mater.* **2019**, *6*. https://doi.org/10.3389/fmats.2019.00172.

(11) Vashist, A.; Kaushik, A.; Vashist, A.; Bala, J.; Nikkhah-Moshaie, R.; Sagar, V.; Nair, M. Nanogels as Potential Drug Nanocarriers for CNS Drug Delivery. *Drug Discov Today* **2018**, *23* (7), 1436–1443. https://doi.org/10.1016/j.drudis.2018.05.018.

(12) Rodriguez, M.; Lapierre, J.; Ojha, C. R.; Kaushik, A.; Batrakova, E.; Kashanchi, F.; Dever, S. M.; Nair, M.; El-Hage, N. Intranasal Drug Delivery of Small Interfering RNA Targeting Beclin1 Encapsulated with Polyethylenimine (PEI) in Mouse Brain to Achieve HIV Attenuation. *Scientific Reports* **2017**, *7* (1), 1862.

https://doi.org/10.1038/s41598-017-01819-9.
(13) Yang, D. Application of Nanotechnology in the COVID-19 Pandemic. *IJN* **2021**, *Volume 16*, 623–649. https://doi.org/10.2147/IJN.S296383.
(14) Machhi, J.; Shahjin, F.; Das, S.; Patel, M.; Abdelmoaty, M. M.; Cohen, J. D.; Singh, P. A.; Baldi, A.; Bajwa, N.; Kumar, R.; Vora, L. K.; Patel, T. A.; Oleynikov, M. D.; Soni, D.; Yeapuri, P.; Mukadam, I.; Chakraborty, R.; Saksena, C. G.; Herskovitz, J.; Hasan, M.; Oupicky, D.; Das, S.; Donnelly, R. F.; Hettie, K. S.; Chang, L.; Gendelman, H. E.; Kevadiya, B. D. Nanocarrier Vaccines for SARS-CoV-2. *Advanced Drug Delivery Reviews* **2021**, *171*, 215–239. https://doi.org/10.1016/j.addr.2021.01.002.

Chapter 1:

State of the art and Objectives

1.1. State of the art

The main concepts and works related to the nanotechnological approaches of **drug delivery** and **gene transfection** are discussed in the following sections. The specific issues concerning each studied disease or application will be included in the corresponding chapter.

1.1.1. Nanotechnology applied to drug delivery

Drug delivery systems could be defined as the methods to deliver drugs to the desired targets employing a nanocarrier[1]. The first publication that introduces the drug delivery methodology dates from 1964, when Folkman *et al*. explored silicone capsules as carriers to incorporate a therapeutic agent[2], although some other authors points at the research developed at the Smith, Kline & French Laboratories in 1952 as the first formulations for a sustained drug delivery[3,4].

The **objectives** of the drug delivery approach are usually focused on improving the aqueous solubility and chemical stability of active agents, increasing the pharmacological activity of drugs and reducing the side effects[1]. A great battery of **nanocarriers** have been explored with these purposes till date including micelles, liposomes, lipid-based or polymer-based formulations, dendrimers, nanocapsules, nanospheres, inorganic particles, etc; and the number of approved nanoformulations is continuously increasing[5–11].

The properties of these systems in terms of **biocompatibility** and **biodegradability** arise as crucial to reach the desired pharmacological effect. In addition, some other issues need to be addressed within this field. To cite some, the **entrapment** of the drug can be achieved by different methods (physical entrapment, covalent conjugation, etc.), the **targeting** (active or passive) of the drug delivery systems and their **circulation time** can be modulated, and a proper **cellular uptake** is usually required. Notably, the **controlled drug release** has attracted great attention within this field and a wide variety of strategies have been explored in this sense to create nanocarriers sensitive to different stimuli, like temperature, light, pH, redox changes, enzymatic activity, etc[1,12]. Another interesting possibility offered by the drug delivery systems is the combination of

more than one drug in a nanocarrier in order to reach a **combinational therapy** enhanced by the properties of the nanocarrier[13–15]. This constitutes a recently developed tool with a huge potential to co-deliver two agents at optimal dosages in a specific tissue[16].

1.1.2. Nanotechnology applied to gene transfection

The insertion of exogenous genetic material inside cells constitutes a promising alternative to drug or surgery-based treatment for several diseases. This **gene therapy** approach allows multiple therapeutic strategies like the replacement of defective genes, the inactivation of mutated genes or the insertion of new genes with protective purposes[17]. The **stability** of the foreign genetic molecule and its **delivery** to the target location remains the main issue for the application of this technology. Since the emergence of the first viral vectors in the 1980´s for the effective **gene delivery**, new methodologies have been developed such as physical methods (electroporation, ultrasound, gene gun…) or the non-viral synthetic vectors. The latter, although with some transfection efficiency limitations, arise as a promising alternative to overcome the **immune responses** and safety issues derived from the viral vectors[18,19].

An important aspect to consider in the design of gene delivery vectors is the balance between a good genetic material **complexation,** generally established by the N/P ratio (the ratio of positive charges of cationic amines in the vector with respect to negative charges of the phosphate groups of genetic material), and a proper **release** upon cellular internalisation to finally reach the nucleus or the corresponding cellular compartment and achieve good transfection efficiency[20] (Figure 1.1).

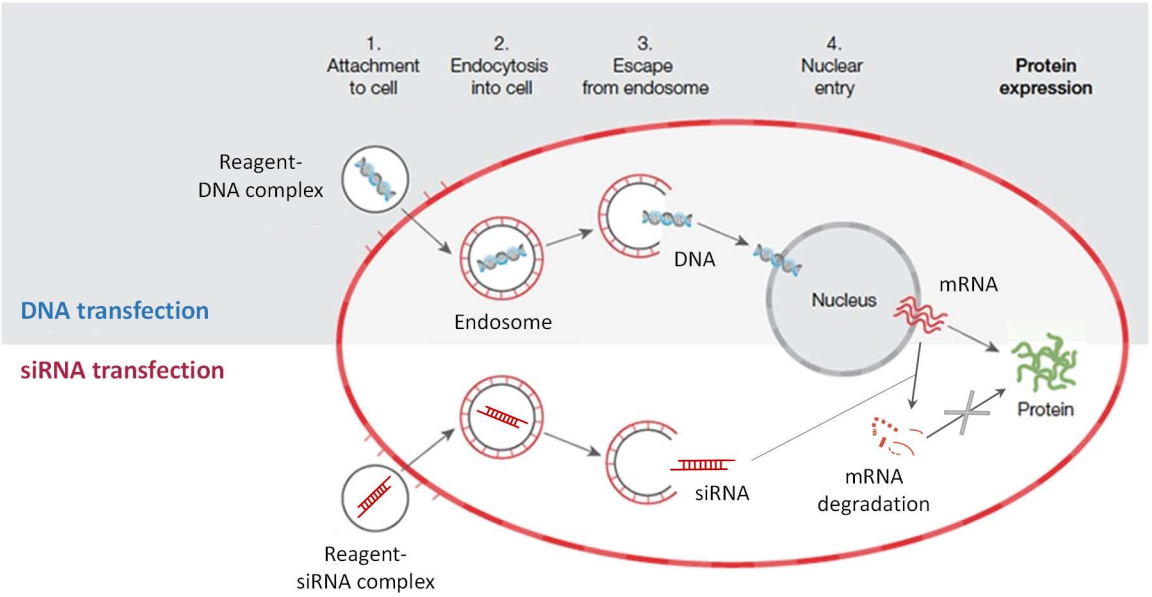

Figure 1.1. Schematic representation of DNA (above) and siRNA (below) transfection processes. Adapted from ThermoFisher[21].

Among the **non-viral vectors**, some formulations have shown good transfection abilities, mainly cationic lipids and polymers (including dendrimers), although toxicity is usually their principal drawback[22,23]. In this regard, some **commercial** formulations can be found like Lipofectin®, Lipofectamine® 2000 and 3000, ExpiFectamine™, FuGENE® or Optifect™ as lipidic formulations; jetPEI®, TurboFect™ or ExpressFect™ as polymeric formulations; Polyfect® or Superfect® as dendrimeric formulations and Arrest-In™ as a lipo-polymeric formulation[24].

1.1.3. Dendritic materials for biomedical applications

Dendritic materials show unique properties that make them good candidates for multiple applications[25]. Within the biomedical field, dendrimers have been used as nanocarriers for **drug**[26–30] and **gene delivery**[31–33], for tissue engineering[34], as antibacterial[35] or antiviral[36] agents, as contrast agents, as adjuvants, as antioxidants and so on, being the first two the most widely explored applications (Figure 1.2)[37].

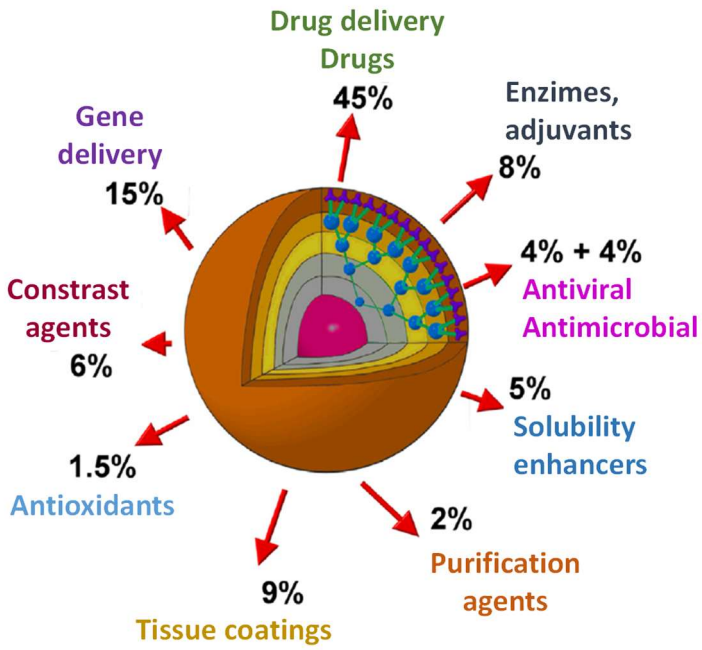

Figure 1.2. Distribution of patents of dendrimers in biomedicine, in percentage, obtained from Pedziwiatr-Werbicka et al[37].

In the following sections, the main characteristics of the dendrimers and the concepts related to their application in the biomedical field are gathered. In addition, a detailed collection of the dendritic materials employed for drug and gene delivery is presented in section 1.1.4.

1.1.3.1. Dendrimers: definition and properties

Dendrimers are a particular type of synthetic polymers with a treelike structure inspired in patterns observed in nature at different scales (Figure 1.3). The etymology of the word comes from the Greek word “dendri-” (tree-branch-like) and the suffix “-meros” (part of)[38,39]. The origin of dendrimers date back to 1978 with the “cascade molecules” described by Vögtle[40]. However, many authors attribute their origin to Tomalia´s group, who described in 1985 the “starburst dendrimers”, introducing for the first time the term dendrimer[41]. Simultaneously, Newkome described a new class of cascade structures called “arborols” because of their arboreal design[42].

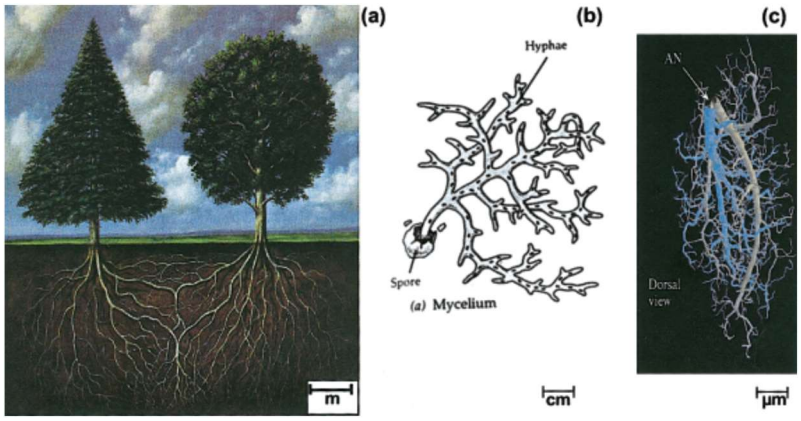

Figure 1.3. Different examples of the dendrimeric structure found in nature at different scales: a) trees, b) fungus and c) neurons. Obtained from Tomalia et al[43].

Their **structure** consists of a central core composed by an atom or group of atoms, from which the branches or arms of dendrons grow exponentially establishing the generation of the dendrimer as the number of layers of repetitive units. Finally, a large number of terminal groups remains exposed to the peripheral surface of the molecule[44] (Figure 1.4).

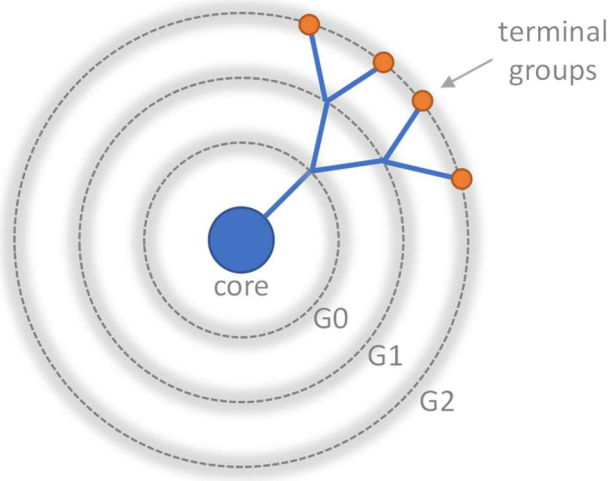

Figure 1.4. Schematic structure of a dendrimer: core, growing generations (G0, G1, G2, etc.) and terminal groups on the periphery.

This special architecture allows the **hosting** of different molecules within the cavities of the dendritic structure and provides a great **versatile functionalisation** of the peripheral groups[44]. On the other hand, the change in the traditional polymerisation strategies allow to obtain these **monodisperse**

synthetic macromolecules with a higher level of control than in the synthesis of the usual polydisperse polymers[43]. Moreover, the high **biocompatibility** and **biodegradability**, dependent on their chemical structure but usually exhibited by these macromolecules, have prompted their application in the biomedical field. Other remarkable characteristic is their ability to **self-assembly** by establishing intermolecular forces, which will be treated deeper in section 1.1.3.3. There are several types of dendrimers attending to their structure, as discussed in the next section.

1.1.3.2. Hybrids between dendrimers and polymers

An interesting type of materials are the hybrids between dendrimers and polymers, which combine the advantageous properties of both[45]. **Hyperbranched polymers** (HPs) are highly branched three-dimensional globular macromolecules with multiple terminal groups randomly distributed[46–48]. They are in the midway between linear polymers and dendrimers, and a good comparative of the properties of the three structures is established in Figure 1.5. Compared to linear polymers, they present lower intrinsic viscosity, good solubility, and higher degree of branching. With respect to dendrimers, HPs are easier synthesised in a one-step polymerisation reaction, but in return, their structure is more irregular and their dispersity cannot be controlled as precisely as in dendrimers, thus obtaining a broader molecular weight distribution[49,50].

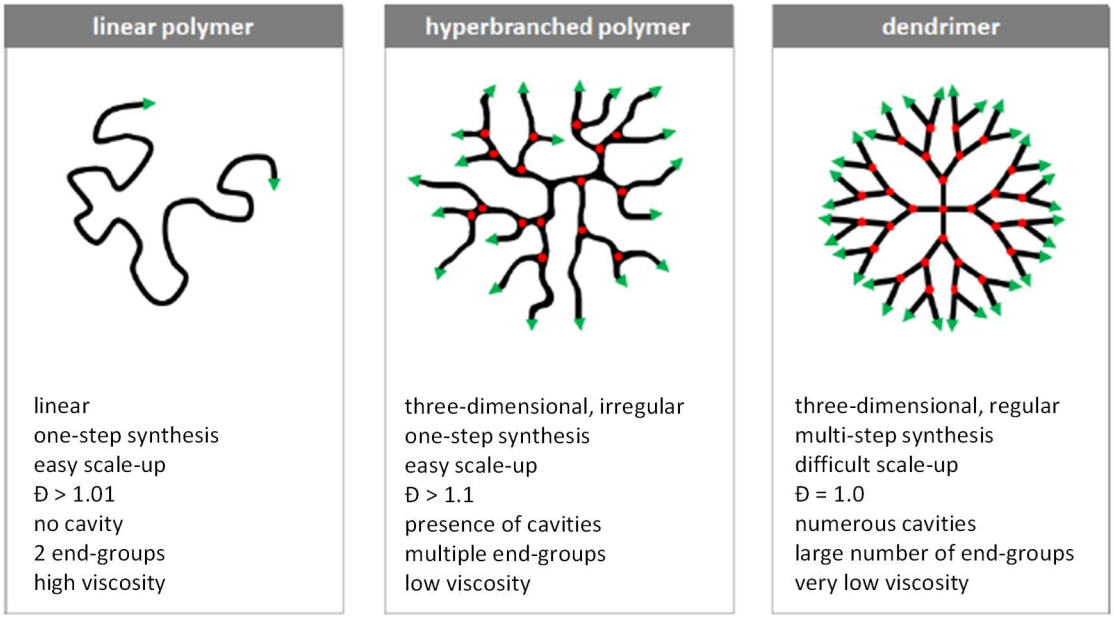

Figure 1.5. Comparative of some properties of linear polymers, hyperbranched polymers and dendrimers. Đ: dispersity. Obtained from Kavand et al[49].

To reduce this undesired polydispersity of HPs, a successful strategy consists in the attachment of dendrons to the surface of HPs, obtaining the **dendronized hyperbranched polymers (DHPs)** also named pseudo-dendrimers[51,52] (Figure 1.6). Frey *et al*. described in 1998 for the first time the post-modification of a polycarbosilane HP with dendrons of the 1st generation in order to enhance the branching degree of the former polymer[53]. Later, in 2012, Lederer *et al*. described the attachment of higher generation dendrons to HPs[51]. With this modification, a decrease on the polydispersity of the HPs was achieved and in addition, similar properties to those of high-generation dendrimers were reached with a reduced synthetic effort[54,55].

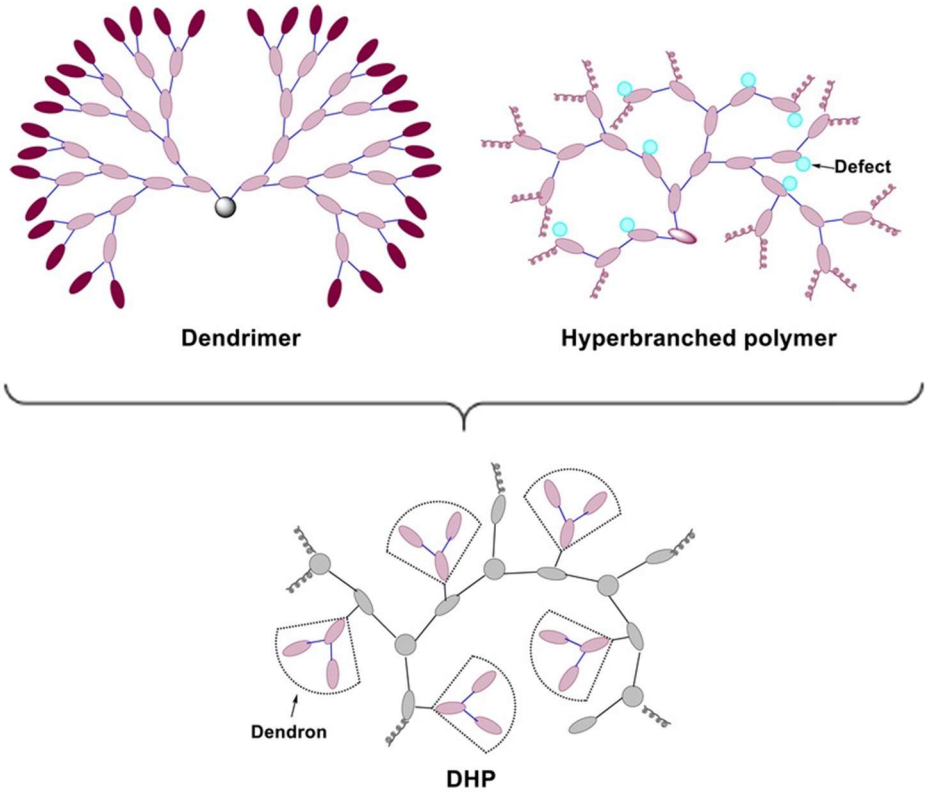

Figure 1.6. DHP structure as a combination of hyperbranched polymers and dendrimers. Adapted from Tang et al[54].

1.1.3.3. Self-assembly in water of amphiphilic dendrimers

The **self-assembly** or self-organisation of a compound is an essential step to obtain supramolecular **aggregates**[56–60]. The characteristics of these aggregates will lead their final applications, so much effort has been made towards a rational design of the compounds and the subsequent formation of aggregates[61].

The **amphiphilic** character of the molecules favours its self-assembly in aqueous media, yielding aggregates in which the lipophilic parts remain in the inner part of the aggregate to escape from the water, and the hydrophilic parts are exposed to the surface of the aggregate. This balance between the lipophilic/hydrophilic parts of the amphiphilic molecule contributes to the arrangement in aggregates with **different morphologies**[62–64]. Considering thermodynamics, interaction free energies and geometrical aspects, the "packing parameter" (p) serves to predict the structure of the aggregates resulting from the self-assembly of amphiphilic molecules through the following equation: $p = \frac{v}{a \cdot l}$; where v is the volume of the

lipophilic part, a is the polar head surface and l is the length of the lipophilic region of the amphiphile[65,66]. Briefly, the more stable structures for the self-assembly of amphiphiles with p<1 are spherical micelles, while 1/3<p<1/2 indicates the formation of cylindrical micelles. When the value of p ranges from 1/2 to 1, the most energetically favourable conformation consists of bilayers, either flexible bilayers leading to vesicles (1/2<p<1) or flat bilayers (p≈1) (Figure 1.7). For p values higher than 1, the assemblies arrange into inverted micelles with the hydrophobic region exposed to the outer part[66,67].

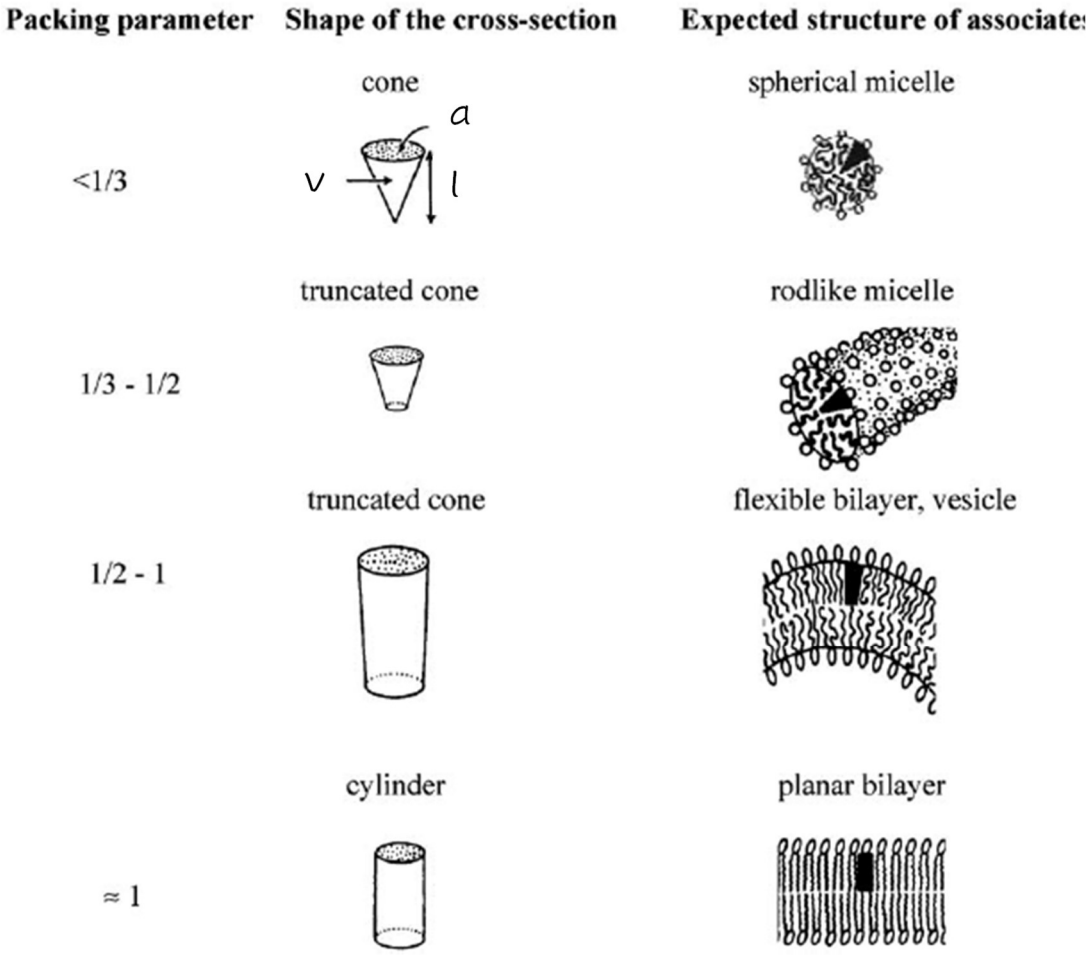

Figure 1.7. Prediction of the structures of the self-assemblies of amphiphilic molecules according to the packing parameter. Obtained from Šegota et al.[66].

The self-assemblies have been found to be also reliant on the preparation technique employed[68]. Different techniques for the **preparation of aggregates** have been developed including the film rehydration method, the solvent injection,

the oil-in-water emulsion or the microfluidic approaches[69]. In this thesis, the **oil-in-water emulsion** has been widely employed for the preparation of aggregates from amphiphilic dendrimers non soluble in water. Briefly, the preformed dendrimers were dissolved into an organic volatile solvent immiscible with water, dichloromethane (DCM), and then, an equal volume of water was added. After vigorous stirring, the whole organic solvent was evaporated and a dispersion of the aggregates in water was obtained. The loading of drugs into the dendrimers can be easily achieved by following the same solvent evaporation methodology with the addition of the drug of interest into the initial mixture (Figure 1.8).

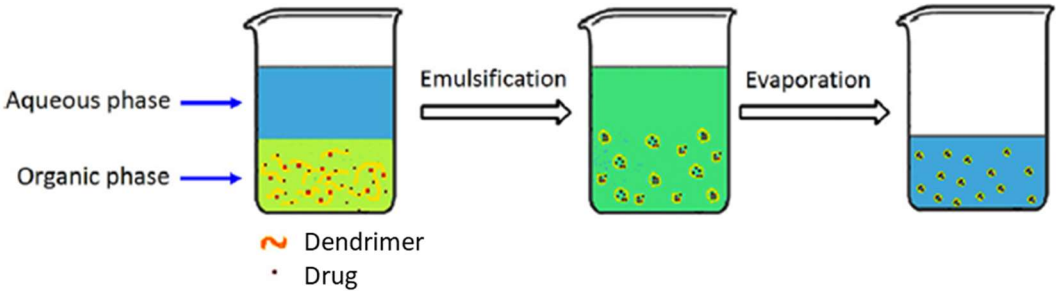

Figure 1.8. Preparation of drug-loaded aggregates by the oil-in-water method. Adapted from George et al.[61].

Another factor to consider in the formation of aggregates is the **Critical Aggregation Concentration** (CAC). It depends on the amphiphile nature, the solvent, the temperature, the pressure and the ionic force, and defines the concentration limit above which aggregates can be formed. That is, below this concentration, interactions between molecules do not regularly occur and the aggregates are not spontaneously formed[70,71]. It is known that low CAC values are beneficial to avoid dilution effects in the blood circulation[72], however, when administered as drug nanocarriers, aggregates usually undergo dilution processes under their CAC. In this sense, it has been described for some polymeric formulations that the stability of the polymeric aggregates was prolonged up to 7 days after they dilution, which is important for drug delivery applications[72–74].

Additionally, the assembly/dissociation of the aggregates can be triggered by some **stimuli**, either intracellular or external, a great advantage for controlled drug release purposes. Some examples of this strategy include aggregates sensitive to light irradiation, to pH or temperature changes and to different enzymatic activities. Regarding the cleavable chemical groups involved, tertiary amines, acetals, ketals, disulfide bonds and peptide bonds can be cited among the most widely used as stimuli-sensitive motifs[63,75].

1.1.4. Examples of dendritic materials employed for drug or gene delivery

In this section, a detailed collection of dendritic materials employed for drug and gene delivery is presented attending to the chemical composition of the nanocarriers. Dendrimers are grouped into nitrogen-based, oxygen-based, or other composing elements in the principal groups of their structure.

1.1.4.1. Nitrogen-based dendritic materials

a. Poly(amidoamine) (PAMAM) dendrimers. They were the structures synthesised by Tomalia in 1985[41] that introduced for the first time the term dendrimer, and have been widely studied since then. Their structure consists of the repetition of amides and tertiary amines growing in an arborescent way and ending up with primary amine groups at the periphery (Figure 1.9). The synthesis of these dendrimers till 11th generation has been described as the highest generation energetically stable[76]. The dendrimer core is composed of different linear chains containing primary amines, being the most common the ethylenediamine (EDA) core present in Figure 1.9, which allows the attachment of four dendritic branches[77].

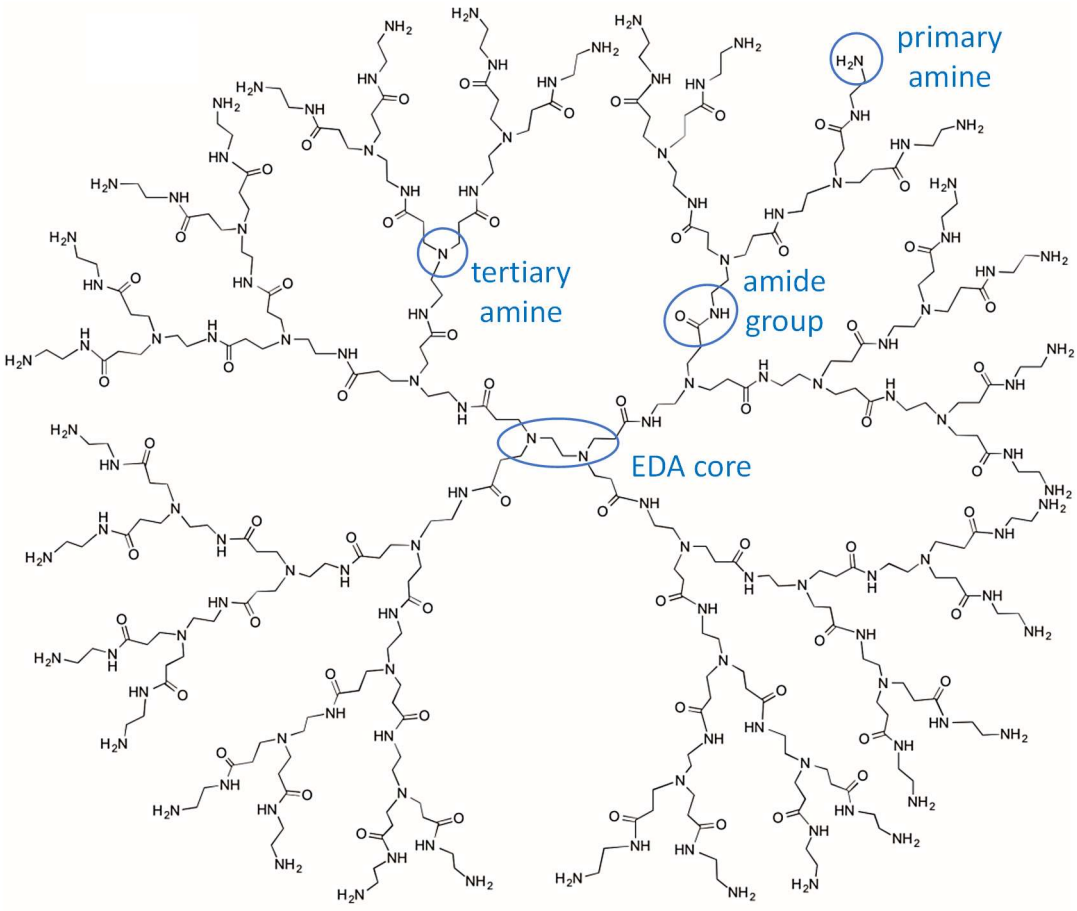

Figure 1.9. Chemical structure of poly(amidoamine) (PAMAM) dendrimer of 3rd generation with an EDA core. Adapted from Najlah et al.[78].

The PAMAM dendrimers, together with the poly(propylene imine) or PPI, are the most widely used dendrimers in the biomedical field[25,79]. Among the biomedical applications of interest, PAMAM dendrimers have been used as drug delivery systems for the treatment of several diseases like cancer[80], Parkinson´s disease[81], Alzheimer's´ and other prion related diseases[82], HIV-1[83] or tuberculosis[84,85] among others. The polycationic PAMAM dendrimers have also attracted interest as gene delivery vectors, either free[86] or modified with Au (AuPAMAM)[87] or other molecules. The genetic material transferred within PAMAM dendrimers include plasmid DNA (pDNA), antisense oligonucleotides, ribozymes, small interfering RNA (siRNA) or messenger RNA (mRNA)[88,89], establishing stable dendriplexes mainly through electrostatic interactions and also through some hydrogen bonds dependent on the pH[90]. In addition, these PAMAM dendrimers have also been explored as co-delivery systems in combination

therapy to deliver two drugs[91] or a drug and a genetic material[92,93] and prevent the emergence of resistances.

They are commercially available and the main concerns of this type of dendrimers are issues related to their toxicity and safety. This cytotoxic effect has been observed to be dependent on the charge, being the positively charged dendrimers the most cytotoxic, while the increase in generation and concentration also leads to an increased cytotoxicity[94]. In this regard, the functionalisation of PAMAM dendrimers on the surface with poly(ethylene glycol) (PEG) has been assayed to enhance the biocompatibility of these dendrimers[95].

This surface post-modification strategy has been widely used in several works to improve the viability, the pharmacokinetics of the PAMAM dendrimers employed as drug nanocarriers, the immunogenic response or their targeting. For example, diethylene glycol, lauroyl[78], pyrrolidone[96] or aptamers[97] have been attached to their surface. However, a good balance in the design must be considered, since the reduction in the cationic peripheral groups also leads to decreased cellular uptake and transfection efficiencies[89].

b. Poly(imine) dendrimers. They constitute another family of nitrogen-based dendrimers that comprises the **poly(ethylene imine) (PEI)** dendrimers and the **poly(propylene imine) (PPI)** dendrimers (Figure 1.10). PPI dendrimers were firstly synthesised by Vögtle´s group in 1978 under the name of “cascade molecules”[40], and the derivatives PEI dendrimers were described later in 2008 by Imae *et al*.[98], although linear PEI polymers were previously described. Both are characterised by a high number of tertiary amino groups in the inner structure and primary amino groups located at the periphery. The structural differences between both types of dendrimers reside in the central core and the length of the alkyl chains joining the amino groups, as indicated by their names, being chains of two carbon atoms (ethylene) for PEI (Figure 1.10a) or three (propylene) in the case of PPI (Figure 1.10b). With respect to PAMAM dendrimers, these poly(imine) dendrimers are smaller, since half number of amino peripheral groups are reached in PEI and PPI when comparing the same generation of dendrimers with PAMAM[99–101].

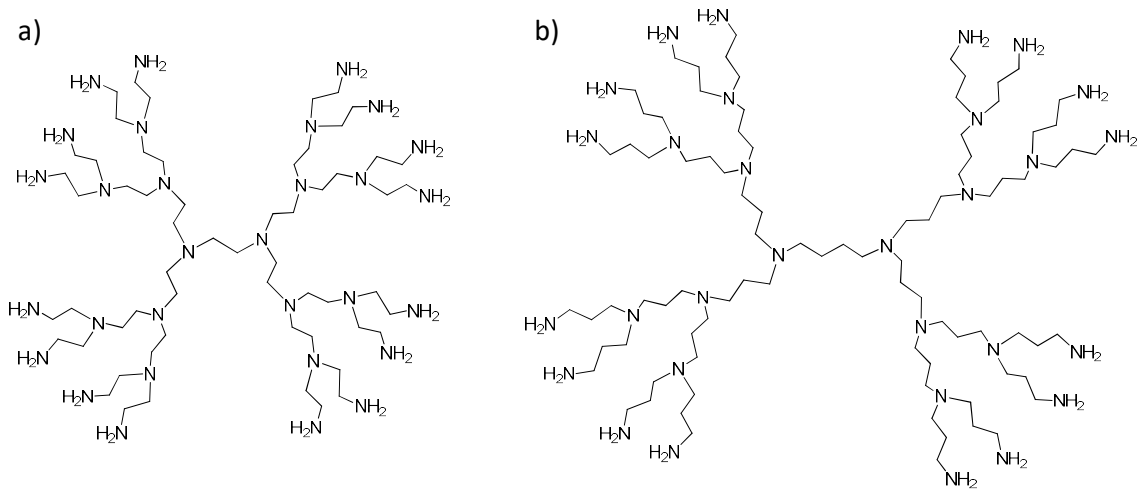

Figure 1.10. a) Poly(ethylene imine) (PEI) and b) poly(propylene imine) (PPI) structures, both of the 3rd generation.

They are commercially available and it is remarkable the interest of these dendrimers as gene delivery vectors, being PEI more studied than PPI for siRNA transfection[102]. On the other hand, PPI dendrimers of different generations have been explored as drug delivery carriers for cancer[103–105], diabetes[106] or tuberculosis[107], and PEI dendrimers have also found their application as drug delivery systems[108,109]. In an interesting recent study, a hybrid Janus dendrimer combining a lipophilic PPI dendron with a hydrophilic PAMAM dendron has been designed an employed to solubilise two lipophilic drugs[110].

As for PAMAM dendrimers, to reduce cytotoxicity and enhance the activity efficiency, surface modifications with sugar maltose[105,111,112], PEG[32], heterocyclic amines[113] or tyrosine[114] have been explored within these poly(imine) dendrimers.

On the other hand, the **triazine-based dendrimers** have been synthesised by Simanek *et al.*[115,116]. They are not commercially available, but their applications have also reached the biomedical field[117]. They have been studied as drug delivery nanocarriers in anticancer therapy[118–120], and in gene delivery as vectors to transfect DNA[121,122] and RNA[123].

c. Polyamide dendrimers. Among them, **poly-(*L*)-lysine (PLL) dendrimers** are peptide-based dendrimers built by amidation from *L*-lysine aminoacid, an analogue of linear oligopeptides, but with a hyperbranched structure[124] (Figure 1.11). They were firstly synthesised and patented by Denkewalter *et al*. in 1979[125–127] and are commercially available.

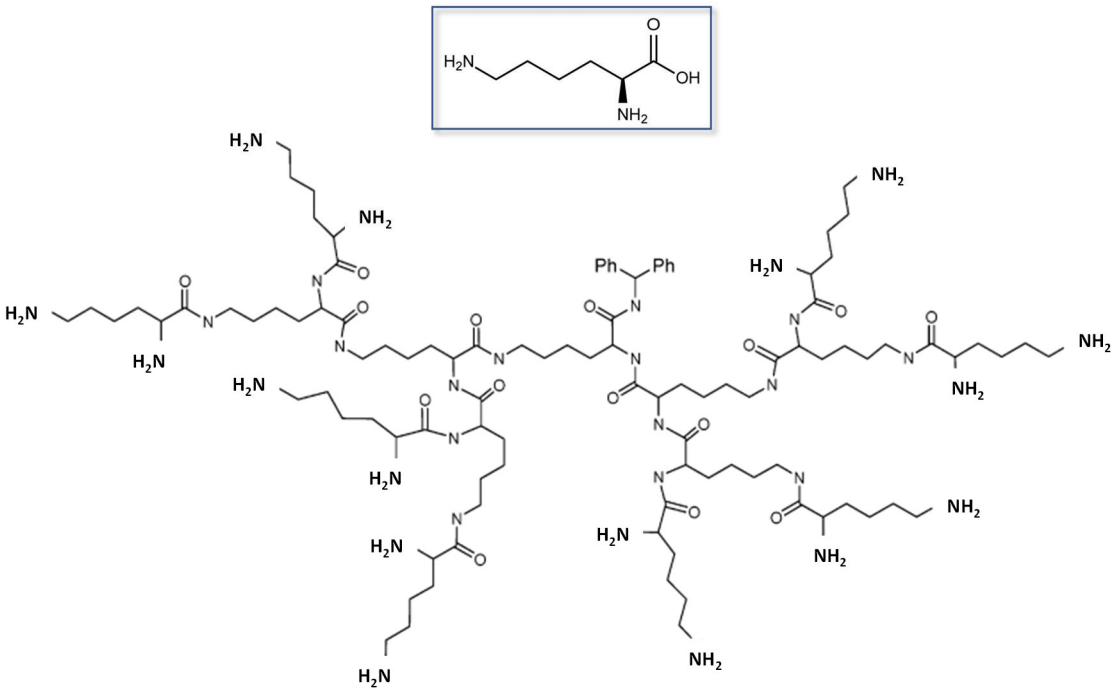

Figure 1.11. Structure of a poly-(L)-lysine (PLL) dendrimer of 3rd generation, and structure of the composing L-lysine aminoacid (in the box). Adapted from Boyd et al.[128].

Their applications in biomedicine include drug delivery in the cancer field[129] and more importantly, their use for gene delivery purposes as efficient vectors of DNA[130] and siRNA[131–133]. The main advantage of these dendrimers over other dendritic nanocarriers is their high biocompatibility exhibited due to the easy degradation carried out by proteases[33,134,135].

Other type of polyamide dendrimers is the **gallic acid triethylene glycol (GATG)** dendritic family, firstly described by Roy *et al*.[136]. This kind of dendrimers has also been used for drug and gene delivery[137,138].

Polycarbamate dendrimers have also been reported and used in the design of anticancer prodrugs, taking advantage of the easy degradation of the carbamate groups when exposed to acidic conditions or to enzymatic activity[139].

1.1.4.2. Oxygen-based dendritic materials

a. Polyester dendrimers. Commercial **2,2'-*bis*(hydroxymethyl) propionic acid (*bis*-MPA) dendrimers** were firstly described by Ihre *et al*. in 1996[140] and are the most common polyester dendrimers. The basic structure of *bis*-MPA dendrimers is composed of ester groups with hydroxyl groups at the periphery (Figure 1.12). However, lots of modifications have been described, the synthetic approaches have been improved and a large number of dendritic polymers have been developed based on *bis*-MPA (Figure 1.13)[141–145]. For instance, heterofunctional dendrimers like Janus dendrimers, hyperbranched polymers (HPs) and dendronized hyperbranched polymers (DHPs), or hybrid dendritic-linear-dendritic block copolymers (HDLDBCs) have been developed based on *bis*-MPA.

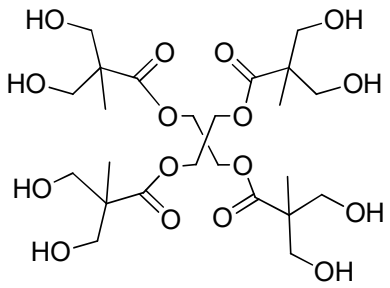

Figure 1.12. Structure of a 2,2'-bis(hydroxymethyl) propionic acid (bis-MPA) dendrimer.

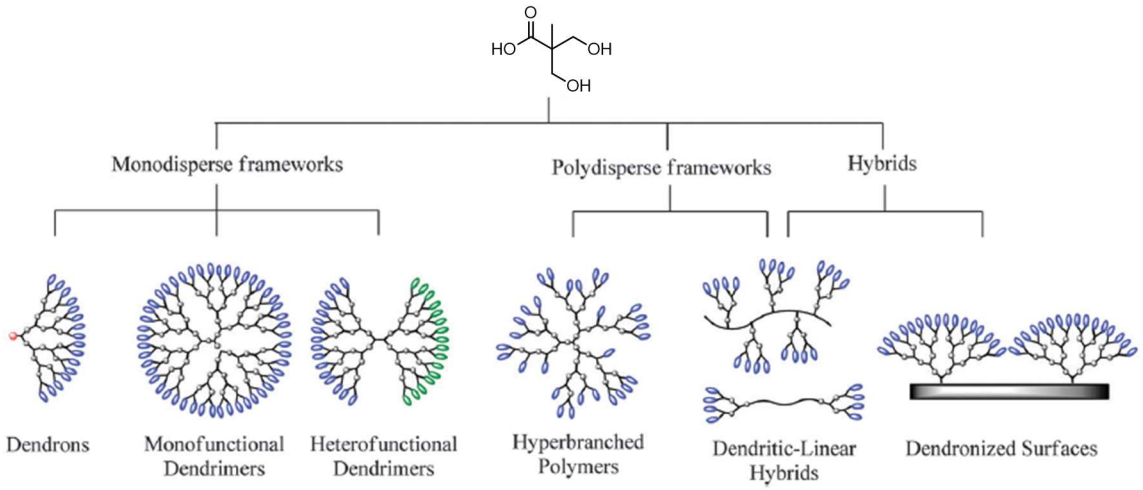

Figure 1.13. bis-MPA monomer and schematic representation of the different types of dendritic polymers based on it, obtained from Carlmark et al[141].

These dendritic materials exhibit amphiphilic behaviour, with a moderated lipophilic inner core and a hydrophilic periphery, which gives them the ability to self-assembly in water. Moreover, they have shown good biocompatibility and biodegradability properties, which postulate them as powerful materials for biomedical applications[146,147].

Among this field, *bis*-MPA based dendritic structures have been employed in several drug delivery studies with lipophilic and hydrophilic drugs. Namely, just to cite some recent examples, unimolecular HP micelles based on *bis*-MPA have encapsulated a natural anticancer substance[148], PEGylated *bis*-MPA dendrimers have been explored as aerosol devices for efficient drug deliver on the lungs[149], globular DHP structures have been explored as antimalarial carriers[26], linear O-alkylated polyesters have encapsulated doxorubicin in high yields[150], or Janus dendrimers have been employed as anti-hepatitis C nanocarriers[151,152].

The use of *bis*-MPA dendritic structures as gene delivery carriers include several polycationic DHPs for the transfection of pDNA[153], amino-functional globular dendrimers to deliver siRNA[154], or linear and hyperbranched polyester cores bearing low Mw PEI and PEG for micro RNA (miRNA) transfection[155].

Other polyester dendrimers developed include **poly(glycerol-succinic acid) (PGLSA) dendrimers**, employed as drug nanocarriers for cancer therapy[156,157].

b. Poly(ester amide) dendrimers. This is a recent family of dendritic materials based on **2,2'-*bis*(glyciloxymethyl)propionic acid (*bis*-GMPA)**. This skeleton combining ester and amide groups has been recently developed within our group by Lancelot *et al.*[158]. In Figure 1.14, the structure of the *bis*-GMPA monomer protected with *t*-Boc moieties can be observed (left), as well as an example of an amino-terminated dendron of the 2nd generation based on *bis*-GMPA (right). This synthesis involves iterative amidation reactions and allows the design of multiple dendritic platforms, as described for *bis*-MPA dendrimers (see Figure 1.13).

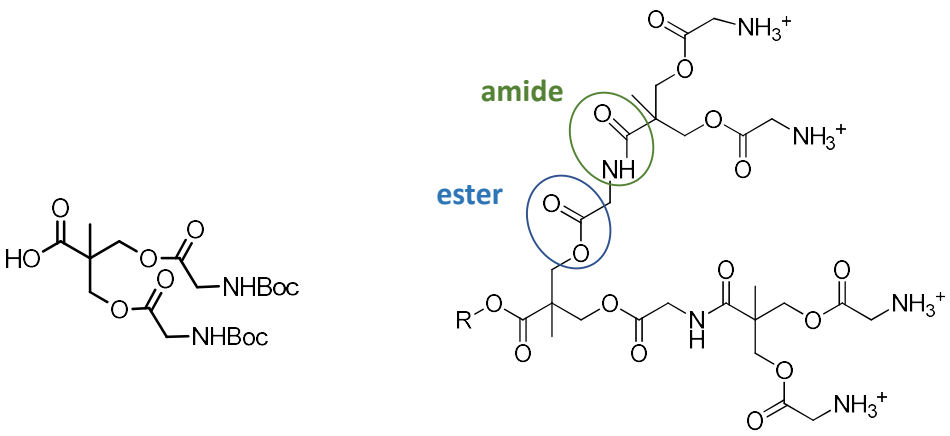

Figure 1.14. Structure of t-Boc protected 2,2'-bis(glyciloxymethyl)propionic acid (bis-GMPA) monomer (left) and an example of bis-GMPA dendron of 2nd generation (right). R: generic substituent.

With respect to the *bis*-MPA architecture, these biocompatible *bis*-GMPA structures include the possibility to establish hydrogen bonds though the amide groups. Then, they are proposed to enhance the interactions with the cargo (drugs or genetic material) and thus, improve their effective loading and maybe, the further delivery. Till date, different structures have been employed for drug delivery, like HDLDBCs based on Pluronic F-127 bearing *bis*-GMPA dendrons for the treatment of malaria[26], hybrid *bis*-MPA/*bis*-GMPA amphiphilic Janus dendrimers for hepatitis C[152] and tripodal poly(ester amide) dendrimers with a tripropargylamine core surrounded by *bis*-GMPA dendrons for the study of the

cited hepatic disease[158]. The latter dendritic structures have also been studied as gene delivery vehicles due to their high density of peripheral cationic groups[158].

c. Polyether dendrimers. Although some other polyether dendrimers date from earlier dates[159,160], the most common ones employed in biomedicine[161] among this subtype of O-based dendritic material, the commercial **polyglycerol (PG) dendrimers** (Figure 1.15), were synthesised by Fréchet *et al*. in 1998, following a convergent pathway[162].

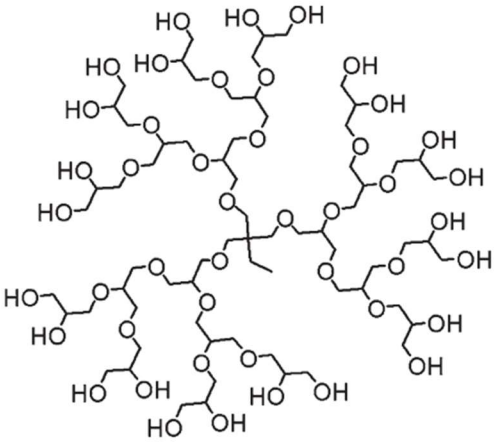

Figure 1.15. Structure of polyglycerol (PG) dendrimer of 3rd generation, obtained from Calderón et al[161].

Either symmetrical dendrimers, hyperbranched polymers or block copolymers, all based on PG, have been used in drug delivery to carry anticancer drugs[163–166], thermoresponsive nanogels based on PG were used as protein transdermal delivery systems[167] or recently, hyperbranched PG dendrimers have been explored as nanodrugs themselves to inhibit protein aggregation[168]. Interestingly, some hybrid nanocarriers between mesoporous silica and PG have been developed for the co-delivery of two drugs in cancer stem cells[169]. Additionally, some constructs containing PG were used as gene vectors for pDNA[170–172], or siRNA[173,174], demonstrating the latter a higher level of safety than other commercial transfectants in *in vivo* models. Finally, a co-delivery system for drug and gene delivery has been created by combining a β-cyclodextrin with an hyperbranched PG by supramolecular interactions[175].

1.1.4.3. Other dendritic materials

Apart from the dendritic materials included in the above sections, there exist other types of dendrimers, less abundant in the biomedical field that are listed below.

a. The family of **silicon-containing dendrimers** include the **carbosilane** (C-Si) and the **carbosiloxane** (Si-O)[176] (Figure 1.16a). The application of these dendrimers in the biomedical field[177] include different examples as drug delivery systems[178,179] and for gene delivery[180], for instance to transfect siRNA[181] even in the brain, crossing the blood brain barrier[182].

b. The family of **phosphorous-containing dendrimers** include a variety of dendrimers that generally consist of a core of thiophosphate or cyclotriphosphazene bearing branches of aromatic thiophosphohydrazones[33,183–185] (Figure 1.16b). Apart for some biomedical applications in which the phosphorous dendrimers were used as therapeutic agents themselves (against inflammation, neurodegenerative diseases or other infections)[184,186], these dendrimers have been explored for drug delivery towards ocular hypertension[187] or cancer[188]. In the gene delivery field, some examples of the transfection of siRNA[188–190] or pDNA[191] can be found.

An interesting study for siRNA delivery compared three dendritic nanocarriers, PAMAM, phosphorous and carbosilane, pointing out at phosphorous containing dendrimers as the most effective, but also the most cytotoxic ones[192].

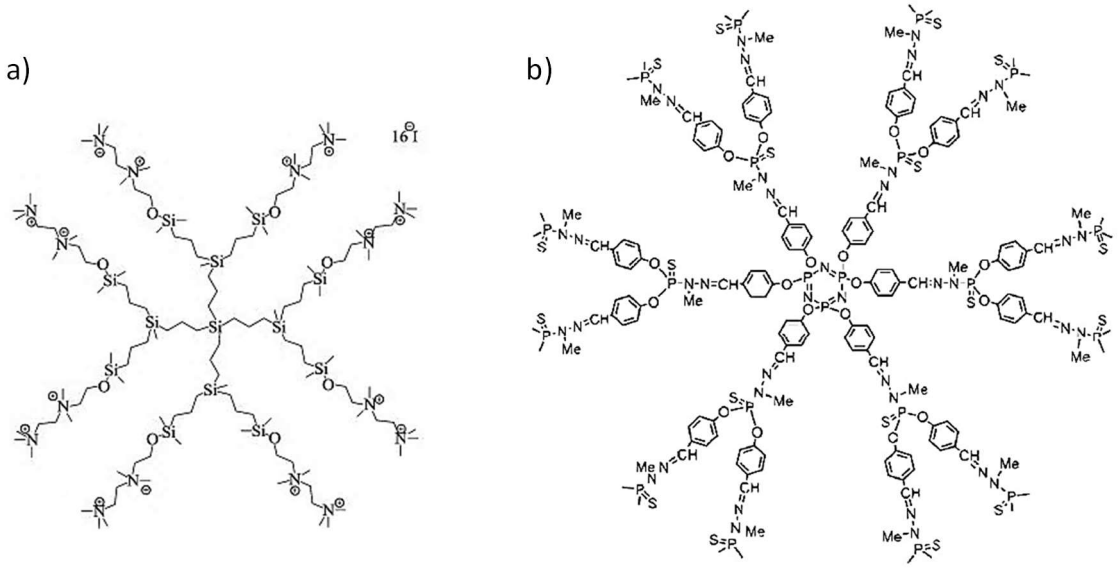

Figure 1.16. Examples of a) silicon-containing and b) phosphorous-containing dendrimers. Obtained from Perisé-Barrios et al[181] and Dzmitruk et al[33], respectively.

1.2. Objectives

The objectives of this doctoral thesis can be summarised and divided into five main blocks concerning the preparation of the dendritic materials and their subsequent employment for the different biomedical applications, i.e., drug delivery or gene transfection. It must be indicated that the **drug delivery** approach has been directly applied to the treatment of specific diseases (hepatitis C, tuberculosis or malaria), while **gene transfection** has been addressed as a general biotechnological tool without any specific biomedical application in mind.

I. **Synthesis and characterisation** of new amphiphilic dendritic structures based on *bis*-MPA and *bis*-GMPA and study of their aggregates formed in water. Specifically, two different types of dendritic derivatives have been designed:
   a. Amphiphilic Janus dendrimers
   b. Globular polycationic dendronized hyperbranched polymers (DHPs)

   This objective is addressed in chapter 2.

II. Study of the ability of the **Janus dendrimers** to deliver antiviral compounds for the treatment of **Hepatitis C** infection.
   This work has been developed in collaboration with Dr. Olga Abián Franco of the Biocomputation and Physics of Complex Systems (BIFI).

   This objective is addressed in chapter 3.

III. Study of the ability of the **Janus dendrimers** to deliver antibiotic compounds for the treatment of **Tuberculosis** infection.

   This work has been developed in collaboration with Dr. José Antonio Ainsa Claver of the Microbiology Department, University of Zaragoza.

   This objective is addressed in chapter 4.

IV. Study of the ability of the globular **DHPs** to enhance the properties of a polysaccharide for the treatment of **Malaria** infection.

This work has been developed in collaboration with Dr. Xavier Fernàndez-Busquets of the Barcelona Institute for Global Health (ISGlobal) and the Institute for Bioengineering of Catalonia (IBEC).

This objective is addressed in chapter 5.

V. Study of the ability of the globular **DHPs** as non-viral vectors for **gene transfection**, namely, to transfect pDNA and siRNA.

This objective is addressed in chapter 6.

1.3. References

(1) Li, C.; Wang, J.; Wang, Y.; Gao, H.; Wei, G.; Huang, Y.; Yu, H.; Gan, Y.; Wang, Y.; Mei, L.; Chen, H.; Hu, H.; Zhang, Z.; Jin, Y. Recent Progress in Drug Delivery. *Acta Pharmaceutica Sinica B* **2019**, *9* (6), 1145–1162. https://doi.org/10.1016/j.apsb.2019.08.003.

(2) Folkman, J.; Long, D. M. The Use of Silicone Rubber as a Carrier for Prolonged Drug Therapy. *J Surg Res* **1964**, *4*, 139–142. https://doi.org/10.1016/s0022-4804(64)80040-8.

(3) Helfand, W. H.; Cowen, D. L. Evolution of Pharmaceutical Oral Dosage Forms. *Pharmacy in History* **1983**, *25* (1), 3, 5, 7–18.

(4) Park, K. Controlled Drug Delivery Systems: Past Forward and Future Back. *Journal of Controlled Release* **2014**, *190*, 3–8. https://doi.org/10.1016/j.jconrel.2014.03.054.

(5) Machhi, J.; Shahjin, F.; Das, S.; Patel, M.; Abdelmoaty, M. M.; Cohen, J. D.; Singh, P. A.; Baldi, A.; Bajwa, N.; Kumar, R.; Vora, L. K.; Patel, T. A.; Oleynikov, M. D.; Soni, D.; Yeapuri, P.; Mukadam, I.; Chakraborty, R.; Saksena, C. G.; Herskovitz, J.; Hasan, M.; Oupicky, D.; Das, S.; Donnelly, R. F.; Hettie, K. S.; Chang, L.; Gendelman, H. E.; Kevadiya, B. D. Nanocarrier Vaccines for SARS-CoV-2. *Advanced Drug Delivery Reviews* **2021**, *171*, 215–239. https://doi.org/10.1016/j.addr.2021.01.002.

(6) Weissig, V.; Pettinger, T. K.; Murdock, N. Nanopharmaceuticals (Part 1): Products on the Market. *Int J Nanomedicine* **2014**, *9*, 4357–4373. https://doi.org/10.2147/IJN.S46900.

(7) Torchilin, V. P. Nanocarriers. *Pharm Res* **2007**, *24* (12), 2333–2334. https://doi.org/10.1007/s11095-007-9463-5.

(8) Khiev, D.; Mohamed, Z. A.; Vichare, R.; Paulson, R.; Bhatia, S.; Mohapatra, S.; Lobo, G. P.; Valapala, M.; Kerur, N.; Passaglia, C. L.; Mohapatra, S. S.; Biswal, M. R. Emerging Nano-Formulations and Nanomedicines Applications for Ocular Drug Delivery. *Nanomaterials (Basel)* **2021**, *11* (1). https://doi.org/10.3390/nano11010173.

(9) Nazlı, E.; Safiye, A.; Erem, B. Nanocapsules for Drug Delivery: An Updated Review of the Last Decade. *Recent Patents on Drug Delivery & Formulation* **2018**, *12* (4), 252–266. https://doi.org/10.2174/1872211313666190123153711.

(10) Babu, A.; Templeton, A. K.; Munshi, A.; Ramesh, R. Nanodrug Delivery Systems: A Promising Technology for Detection, Diagnosis, and Treatment of Cancer. *AAPS PharmSciTech* **2014**, *15* (3), 709–721. https://doi.org/10.1208/s12249-014-0089-8.

(11) Chariou, P. L.; Ortega-Rivera, O. A.; Steinmetz, N. F. Nanocarriers for the Delivery of Medical, Veterinary, and Agricultural Active Ingredients. *ACS Nano* **2020**, *14* (3), 2678–2701. https://doi.org/10.1021/acsnano.0c00173.

(12) Kamaly, N.; Yameen, B.; Wu, J.; Farokhzad, O. C. Degradable Controlled-Release Polymers and Polymeric Nanoparticles: Mechanisms of Controlling Drug Release. *Chem. Rev.* **2016**, *116* (4), 2602–2663. https://doi.org/10.1021/acs.chemrev.5b00346.

(13) Kaushik, A. Biomedical Nanotechnology Related Grand Challenges and Perspectives. *Front. Nanotechnol.* **2019**, *1*. https://doi.org/10.3389/fnano.2019.00001.
(14) Parhi, P.; Mohanty, C.; Sahoo, S. K. Nanotechnology-Based Combinational Drug Delivery: An Emerging Approach for Cancer Therapy. *Drug Discovery Today* **2012**, *17* (17–18), 1044–1052. https://doi.org/10.1016/j.drudis.2012.05.010.
(15) Tekade, R. K.; Dutta, T.; Gajbhiye, V.; Jain, N. K. Exploring Dendrimer towards Dual Drug Delivery: PH Responsive Simultaneous Drug-Release Kinetics. *Journal of Microencapsulation* **2009**, *26* (4), 287–296. https://doi.org/10.1080/02652040802312572.
(16) Sun, J.; Chen, Y.; Xu, J.; Song, X.; Wan, Z.; Du, Y.; Ma, W.; Li, X.; Zhang, L.; Li, S. High Loading of Hydrophobic and Hydrophilic Agents via Small Immunostimulatory Carrier for Enhanced Tumor Penetration and Combinational Therapy. *Theranostics* **2020**, *10* (3), 1136–1150. https://doi.org/10.7150/thno.38287.
(17) Sung, Y.; Kim, S. Recent Advances in the Development of Gene Delivery Systems. *Biomater Res* **2019**, *23* (1), 8. https://doi.org/10.1186/s40824-019-0156-z.
(18) Shirley, J. L.; de Jong, Y. P.; Terhorst, C.; Herzog, R. W. Immune Responses to Viral Gene Therapy Vectors. *Molecular Therapy* **2020**, *28* (3), 709–722. https://doi.org/10.1016/j.ymthe.2020.01.001.
(19) Nyamay'Antu, A.; Dumont, M.; Kedinger, V.; Erbacher, P. Non-Viral Vector Mediated Gene Delivery: The Outsider to Watch Out For in Gene Therapy. *Cell Gene Therapy Insights* **2019**, *5* (S1), 51–57. https://doi.org/10.18609/cgti.2019.007.
(20) Yellepeddi, V. K. Vectors for Non-Viral Gene Delivery - Clinical and Biomedical Applications. *Austin Therapeutics* **2015**, *2* (1), 8.
(21) Neurobiology Transfection Guide - ES //www.thermofisher.com/es/es/home/life-science/cell-culture/cell-culture-learning-center/cell-culture-resource-library/cell-culture-transfection-application-notes/neurobiology-transfection-guide.html (accessed Apr 12, 2021).
(22) Santos, J. de A.; Liarte, D. B.; Ribeiro, A. B.; Rizzo, M. dos S.; Costa, M. P. da; Osajima, J. A.; Silva-Filho, E. C. Biopolymeric Materials Used as Nonviral Vectors: A Review. *Polysaccharides* **2021**, *2* (1), 100–109. https://doi.org/10.3390/polysaccharides2010007.
(23) Ma, K.; Mi, C.-L.; Cao, X.-X.; Wang, T.-Y. Progress of Cationic Gene Delivery Reagents for Non-Viral Vector. *Appl Microbiol Biotechnol* **2021**, *105* (2), 525–538. https://doi.org/10.1007/s00253-020-11028-6.
(24) Yamano, S.; Dai, J.; Moursi, A. M. Comparison of Transfection Efficiency of Nonviral Gene Transfer Reagents. *Mol Biotechnol* **2010**, *46* (3), 287–300. https://doi.org/10.1007/s12033-010-9302-5.
(25) Campora, S.; Ghersi, G. Smart Nanoparticles in Biomedicine: An Overview of Recent Developments and Applications. **2021**. https://doi.org/10.20944/preprints202102.0619.v1.

(26) Martí Coma-Cros, E.; Lancelot, A.; San Anselmo, M.; Neves Borgheti-Cardoso, L.; Valle-Delgado, J. J.; Serrano, J. L.; Fernàndez-Busquets, X.; Sierra, T. Micelle Carriers Based on Dendritic Macromolecules Containing Bis-MPA and Glycine for Antimalarial Drug Delivery. *Biomater. Sci.* **2019**, *7* (4), 1661–1674. https://doi.org/10.1039/C8BM01600C.

(27) Lu, Y.; Han, S.; Zheng, H.; Ma, R.; Ping, Y.; Zou, J.; Tang, H.; Zhang, Y.; Xu, X.; Li, F. A Novel RGDyC/PEG Co-Modified PAMAM Dendrimer-Loaded Arsenic Trioxide of Glioma Targeting Delivery System. *IJN* **2018**, *13*, 5937–5952. https://doi.org/10.2147/IJN.S175418.

(28) Fana, M.; Gallien, J.; Srinageshwar, B.; Dunbar, G. L.; Rossignol, J. PAMAM Dendrimer Nanomolecules Utilized as Drug Delivery Systems for Potential Treatment of Glioblastoma: A Systematic Review. *Int J Nanomedicine* **2020**, *15*, 2789–2808. https://doi.org/10.2147/IJN.S243155.

(29) Mhlwatika, Z.; Aderibigbe, B. A. Application of Dendrimers for the Treatment of Infectious Diseases. *Molecules* **2018**, *23* (9), 2205. https://doi.org/10.3390/molecules23092205.

(30) Mittal, P.; Saharan, A.; Verma, R.; Altalbawy, F. M. A.; Alfaidi, M. A.; Batiha, G. E.-S.; Akter, W.; Gautam, R. K.; Uddin, M. S.; Rahman, M. S. Dendrimers: A New Race of Pharmaceutical Nanocarriers https://www.hindawi.com/journals/bmri/2021/8844030/ (accessed Feb 28, 2021). https://doi.org/10.1155/2021/8844030.

(31) Palmerston Mendes, L.; Pan, J.; Torchilin, V. P. Dendrimers as Nanocarriers for Nucleic Acid and Drug Delivery in Cancer Therapy. *Molecules* **2017**, *22* (9). https://doi.org/10.3390/molecules22091401.

(32) Somani, S.; Laskar, P.; Altwaijry, N.; Kewcharoenvong, P.; Irving, C.; Robb, G.; Pickard, B. S.; Dufès, C. PEGylation of Polypropylenimine Dendrimers: Effects on Cytotoxicity, DNA Condensation, Gene Delivery and Expression in Cancer Cells. *Scientific Reports* **2018**, *8* (1), 9410. https://doi.org/10.1038/s41598-018-27400-6.

(33) Dzmitruk, V.; Apartsin, E.; Ihnatsyeu-Kachan, A.; Abashkin, V.; Shcharbin, D.; Bryszewska, M. Dendrimers Show Promise for SiRNA and MicroRNA Therapeutics. *Pharmaceutics* **2018**, *10* (3), 126. https://doi.org/10.3390/pharmaceutics10030126.

(34) Gorain, B.; Tekade, M.; Kesharwani, P.; Iyer, A. K.; Kalia, K.; Tekade, R. K. The Use of Nanoscaffolds and Dendrimers in Tissue Engineering. *Drug Discovery Today* **2017**, *22* (4), 652–664. https://doi.org/10.1016/j.drudis.2016.12.007.

(35) Kannan, R.; Prabakaran, P.; Basu, R.; Pindi, C.; Senapati, S.; Muthuvijayan, V.; Prasad, E. Mechanistic Study on the Antibacterial Activity of Self-Assembled Poly(Aryl Ether)-Based Amphiphilic Dendrimers. *ACS Appl. Bio Mater.* **2019**, *2* (8), 3212–3224. https://doi.org/10.1021/acsabm.9b00140.

(36) Asaftei, S.; De Clercq, E. "Viologen" Dendrimers as Antiviral Agents: The Effect of Charge Number and Distance †. *J. Med. Chem.* **2010**, *53* (9), 3480–3488. https://doi.org/10.1021/jm100093p.

(37) Pedziwiatr-Werbicka, E.; Milowska, K.; Dzmitruk, V.; Ionov, M.; Shcharbin, D.; Bryszewska, M. Dendrimers and Hyperbranched Structures for Biomedical Applications. *European Polymer Journal* **2019**, *119*, 61–73. https://doi.org/10.1016/j.eurpolymj.2019.07.013.
(38) Dvornic, P. R.; Tomalia, D. A. Recent Advances in Dendritic Polymers. **1996**, 15.
(39) Tomalia, D. A. The Dendritic State. *Materials Today* **2005**, *8* (3), 34–46. https://doi.org/10.1016/S1369-7021(05)00746-7.
(40) Buhleier, E.; Wehner, W.; Voegtle, F. ′Cascade′- and ′nonskid-Chain-Like′ Syntheses of Molecular Cavity Topologies. **1978**. https://doi.org/10.1002/CHIN.197825228.
(41) Tomalia, D. A.; Baker, H.; Dewald, J.; Hall, M.; Kallos, G.; Martin, S.; Roeck, J.; Ryder, J.; Smith, P. A New Class of Polymers: Starburst-Dendritic Macromolecules. *Polym J* **1985**, *17* (1), 117–132. https://doi.org/10.1295/polymj.17.117.
(42) Newkome, G. R.; Yao, Z.; Baker, G. R.; Gupta, V. K. Micelles. Part 1. Cascade Molecules: A New Approach to Micelles. A [27]-Arborol. *J. Org. Chem.* **1985**, *50* (11), 2003–2004. https://doi.org/10.1021/jo00211a052.
(43) Tomalia, D. A.; Fréchet, J. M. J. Discovery of Dendrimers and Dendritic Polymers: A Brief Historical Perspective*. *Journal of Polymer Science Part A: Polymer Chemistry* **2002**, *40* (16), 2719–2728. https://doi.org/10.1002/pola.10301.
(44) Abbasi, E.; Aval, S. F.; Akbarzadeh, A.; Milani, M.; Nasrabadi, H. T.; Joo, S. W.; Hanifehpour, Y.; Nejati-Koshki, K.; Pashaei-Asl, R. Dendrimers: Synthesis, Applications, and Properties. *Nanoscale Res Lett* **2014**, *9* (1), 247. https://doi.org/10.1186/1556-276X-9-247.
(45) Zhang, X.; Dai, Y.; Dai, G. Advances in Amphiphilic Hyperbranched Copolymers with an Aliphatic Hyperbranched 2,2-Bis(Methylol)Propionic Acid-Based Polyester Core. *Polym. Chem.* **2020**, 10.1039.C9PY01608B. https://doi.org/10.1039/C9PY01608B.
(46) Jikei, M.; Kakimoto, M. Hyperbranched Polymers: A Promising New Class of Materials. *Progress in Polymer Science* **2001**, *26* (8), 1233–1285. https://doi.org/10.1016/S0079-6700(01)00018-1.
(47) Voit, B. Hyperbranched Polymers—All Problems Solved after 15 Years of Research? *Journal of Polymer Science Part A: Polymer Chemistry* **2005**, *43* (13), 2679–2699. https://doi.org/10.1002/pola.20821.
(48) Bhat, S. I.; Ahmadi, Y.; Ahmad, S. Recent Advances in Structural Modifications of Hyperbranched Polymers and Their Applications. *Ind. Eng. Chem. Res.* **2018**, *57* (32), 10754–10785. https://doi.org/10.1021/acs.iecr.8b01969.
(49) Kavand, A.; Anton, N.; Vandamme, T.; Serra, C. A.; Chan-Seng, D. Synthesis and Functionalization of Hyperbranched Polymers for Targeted Drug Delivery. *Journal of Controlled Release* **2020**, *321*, 285–311. https://doi.org/10.1016/j.jconrel.2020.02.019.
(50) Caminade, A.-M.; Yan, D.; K. Smith, D. Dendrimers and Hyperbranched Polymers. *Chemical Society Reviews* **2015**, *44* (12), 3870–3873. https://doi.org/10.1039/C5CS90049B.

(51) Lederer, A.; Hartmann, T.; Komber, H. Sphere-Like Fourth Generation Pseudo-Dendrimers with a Hyperbranched Core. *Macromolecular Rapid Communications* **2012**, *33* (17), 1440–1444. https://doi.org/10.1002/marc.201200223.
(52) Wu, W.; Huang, L.; Fu, Y.; Ye, C.; Qin, J.; Li, Z. Design, Synthesis and Nonlinear Optical Properties of “Dendronized Hyperbranched Polymers.” *Chin. Sci. Bull.* **2013**, *58* (22), 2753–2761. https://doi.org/10.1007/s11434-013-5938-4.
(53) Lach, C.; Frey, H. Enhancing the Degree of Branching of Hyperbranched Polymers by Postsynthetic Modification. **1998**, 3.
(54) Tang, R.; Li, Z. Second-Order Nonlinear Optical Dendrimers and Dendronized Hyperbranched Polymers. *The Chemical Record* **2017**, *17* (1), 71–89. https://doi.org/10.1002/tcr.201600065.
(55) Lederer, A.; Burchard, W.; Hartmann, T.; Haataja, J. S.; Houbenov, N.; Janke, A.; Friedel, P.; Schweins, R.; Lindner, P. Dendronized Hyperbranched Macromolecules: Soft Matter with a Novel Type of Segmental Distribution. *Angew. Chem. Int. Ed. Engl.* **2015**, *54* (43), 12578–12583. https://doi.org/10.1002/anie.201504059.
(56) Ariga, K.; Nishikawa, M.; Mori, T.; Takeya, J.; Shrestha, L. K.; Hill, J. P. Self-Assembly as a Key Player for Materials Nanoarchitectonics. *Science and Technology of Advanced Materials* **2019**, *20* (1), 51–95. https://doi.org/10.1080/14686996.2018.1553108.
(57) Stupp, S. I.; LeBonheur, V.; Walker, K.; Li, L. S.; Huggins, K. E.; Keser, M.; Amstutz, A. Supramolecular Materials: Self-Organized Nanostructures. *Science* **1997**, *276* (5311), 384–389. https://doi.org/10.1126/science.276.5311.384.
(58) Amabilino, D. B.; Smith, D. K.; Steed, J. W. Supramolecular Materials. *Chem. Soc. Rev.* **2017**, *46* (9), 2404–2420. https://doi.org/10.1039/C7CS00163K.
(59) Calandra, P.; Caschera, D.; Turco Liveri, V.; Lombardo, D. How Self-Assembly of Amphiphilic Molecules Can Generate Complexity in the Nanoscale. *Colloids and Surfaces A: Physicochemical and Engineering Aspects* **2015**, *484*, 164–183. https://doi.org/10.1016/j.colsurfa.2015.07.058.
(60) Zhu, Y.; Liu, L.; Du, J. Probing into Homopolymer Self-Assembly: How Does Hydrogen Bonding Influence Morphology? *Macromolecules* **2013**, *46* (1), 194–203. https://doi.org/10.1021/ma302176a.
(61) George, A.; Shah, P. A.; Shrivastav, P. S. Natural Biodegradable Polymers Based Nano-Formulations for Drug Delivery: A Review. *International Journal of Pharmaceutics* **2019**, *561*, 244–264. https://doi.org/10.1016/j.ijpharm.2019.03.011.
(62) Israelachvil, B. Y. J.; Ninham, B. Theory of Self-Assembly of Hydrocarbon Amphiphiles into Micelles and Bilayers. **1976**, 44.
(63) Zhang, J.; Li, X.; Li, X. Stimuli-Triggered Structural Engineering of Synthetic and Biological Polymeric Assemblies. *Progress in Polymer Science* **2012**, *37* (8), 1130–1176. https://doi.org/10.1016/j.progpolymsci.2011.11.005.

(64) Zhang, Q.; Lin, J.; Wang, L.; Xu, Z. Theoretical Modeling and Simulations of Self-Assembly of Copolymers in Solution. *Progress in Polymer Science* **2017**, *75*, 1–30. https://doi.org/10.1016/j.progpolymsci.2017.04.003.

(65) Israelachvili, J. N.; Mitchell, D. J.; Ninham, B. W. Theory of Self-Assembly of Hydrocarbon Amphiphiles into Micelles and Bilayers. *J. Chem. Soc., Faraday Trans. 2* **1976**, *72*, 1525. https://doi.org/10.1039/f29767201525.

(66) Šegota, S.; Težak, D. Spontaneous Formation of Vesicles. *Advances in Colloid and Interface Science* **2006**, *121* (1–3), 51–75. https://doi.org/10.1016/j.cis.2006.01.002.

(67) Hernández-Ainsa, S. Nuevos materiales funcionales basados en dendrímeros cristales líquidos iónicos, 2011.

(68) Dionzou, M.; Morère, A.; Roux, C.; Lonetti, B.; Marty, J.-D.; Mingotaud, C.; Joseph, P.; Goudounèche, D.; Payré, B.; Léonetti, M.; Mingotaud, A.-F. Comparison of Methods for the Fabrication and the Characterization of Polymer Self-Assemblies: What Are the Important Parameters? *Soft Matter* **2016**, *12* (7), 2166–2176. https://doi.org/10.1039/C5SM01863C.

(69) Taabache, S.; Bertin, A. Vesicles from Amphiphilic Dumbbells and Janus Dendrimers: Bioinspired Self-Assembled Structures for Biomedical Applications. *Polymers* **2017**, *9* (12), 280. https://doi.org/10.3390/polym9070280.

(70) Wu, Z.; Zhao, C.; Huang, Y.; Ye, F.; Zhao, G. Molecular Mechanism Underlying the Effects of Temperature and PH on the Size and Surface Charge of Octenylsuccinated Oat β-Glucan Aggregates. *Carbohydrate Polymers* **2020**, *237*, 116115. https://doi.org/10.1016/j.carbpol.2020.116115.

(71) Cho, E. J.; Holback, H.; Liu, K. C.; Abouelmagd, S. A.; Park, J.; Yeo, Y. Nanoparticle Characterization: State of the Art, Challenges, and Emerging Technologies. *Mol Pharm* **2013**, *10* (6), 2093–2110. https://doi.org/10.1021/mp300697h.

(72) Gheybi, H.; Adeli, M. Supramolecular Anticancer Drug Delivery Systems Based on Linear–Dendritic Copolymers. *Polym. Chem.* **2015**, *6* (14), 2580–2615. https://doi.org/10.1039/C4PY01437E.

(73) Opanasopit, P.; Yokoyama, M.; Watanabe, M.; Kawano, K.; Maitani, Y.; Okano, T. Block Copolymer Design for Camptothecin Incorporation into Polymeric Micelles for Passive Tumor Targeting. *Pharm Res* **2004**, *21* (11), 2001–2008. https://doi.org/10.1023/B:PHAM.0000048190.53439.eb.

(74) Lancelot, A. New Dendritic Derivatives for Applications in Nanomedicine: Drug Delivery and Gene Transfection, Universidad de Zaragoza, 2017.

(75) An, X.; Zhu, A.; Luo, H.; Ke, H.; Chen, H.; Zhao, Y. Rational Design of Multi-Stimuli-Responsive Nanoparticles for Precise Cancer Therapy. *ACS Nano* **2016**, *10* (6), 5947–5958. https://doi.org/10.1021/acsnano.6b01296.

(76) Prabal K. Maiti, †; Tahir Çağın; Guofeng Wang, and; William A. Goddard, I. Structure of PAMAM Dendrimers: Generations 1 through 11 https://pubs.acs.org/doi/pdf/10.1021/ma035629b (accessed Apr 13, 2021).

https://doi.org/10.1021/ma035629b.
(77) Araújo, R. V. de; Santos, S. da S.; Igne Ferreira, E.; Giarolla, J. New Advances in General Biomedical Applications of PAMAM Dendrimers. *Molecules* **2018**, *23* (11), 2849. https://doi.org/10.3390/molecules23112849.
(78) Najlah, M.; Freeman, S.; Khoder, M.; Attwood, D.; D'Emanuele, A. In Vitro Evaluation of Third Generation PAMAM Dendrimer Conjugates. *Molecules* **2017**, *22* (10), 1661. https://doi.org/10.3390/molecules22101661.
(79) Tarach, P.; Janaszewska, A. Recent Advances in Preclinical Research Using PAMAM Dendrimers for Cancer Gene Therapy. *IJMS* **2021**, *22* (6), 2912. https://doi.org/10.3390/ijms22062912.
(80) Zhu, J.; Xiong, Z.; Shen, M.; Shi, X. Encapsulation of Doxorubicin within Multifunctional Gadolinium-Loaded Dendrimer Nanocomplexes for Targeted Theranostics of Cancer Cells. *RSC Adv.* **2015**, *5* (38), 30286–30296. https://doi.org/10.1039/C5RA01215E.
(81) Sun, H.-J.; Wang, Y.; Hao, T.; Wang, C.-Y.; Wang, Q.-Y.; Jiang, X.-X. Efficient GSH Delivery Using PAMAM-GSH into MPP-Induced PC12 Cellular Model for Parkinson's Disease. *Regen Biomater* **2016**, *3* (5), 299–307. https://doi.org/10.1093/rb/rbw032.
(82) Klajnert, B.; Cangiotti, M.; Calici, S.; Majoral, J. P.; Caminade, A. M.; Cladera, J.; Bryszewska, M.; Ottaviani, M. F. EPR Study of the Interactions between Dendrimers and Peptides Involved in Alzheimer's and Prion Diseases. *Macromolecular Bioscience* **2007**, *7* (8), 1065–1074. https://doi.org/10.1002/mabi.200700049.
(83) Pyreddy, S.; Kumar, P. D.; Kumar, P. V. Polyethylene Glycolated PAMAM Dendrimers-Efavirenz Conjugates. *International Journal of Pharmaceutical Investigation* **2014**, *4* (1), 4. https://doi.org/10.4103/2230-973X.127735.
(84) Pandurangan, D.; Theivendren, P.; Kilim, D. B.; Kunjiappan, S.; Palanirajan, V. K. Formulation of Rifampicin Loaded PEGylated 5.0G EDA-PAMAM Dendrimers as Effective Long-Duration Release Drug Carriers https://www.eurekaselect.com/152972/article (accessed Mar 7, 2021).
(85) Bellini, R. G.; Guimarães, A. P.; Pacheco, M. A. C.; Dias, D. M.; Furtado, V. R.; de Alencastro, R. B.; Horta, B. A. C. Association of the Anti-Tuberculosis Drug Rifampicin with a PAMAM Dendrimer. *Journal of Molecular Graphics and Modelling* **2015**, *60*, 34–42. https://doi.org/10.1016/j.jmgm.2015.05.012.
(86) Kretzmann, J. A.; Ho, D.; Evans, C. W.; Plani-Lam, J. H. C.; Garcia-Bloj, B.; Mohamed, A. E.; O'Mara, M. L.; Ford, E.; Tan, D. E. K.; Lister, R.; Blancafort, P.; Norret, M.; Iyer, K. S. Synthetically Controlling Dendrimer Flexibility Improves Delivery of Large Plasmid DNA. *Chem. Sci.* **2017**, *8* (4), 2923–2930. https://doi.org/10.1039/C7SC00097A.
(87) Figueroa, E.; Bugga, P.; Asthana, V.; Chen, A. L.; Stephen Yan, J.; Evans, E. R.; Drezek, R. A. A Mechanistic Investigation Exploring the Differential

Transfection Efficiencies between the Easy-to-Transfect SK-BR3 and Difficult-to-Transfect CT26 Cell Lines. *J Nanobiotechnology* **2017**, *15* (1), 36. https://doi.org/10.1186/s12951-017-0271-8.

(88) Dehshahri, A.; Sadeghpour, H. Surface Decorations of Poly(Amidoamine) Dendrimer by Various Pendant Moieties for Improved Delivery of Nucleic Acid Materials. *Colloids and Surfaces B: Biointerfaces* **2015**, *132*, 85–102. https://doi.org/10.1016/j.colsurfb.2015.05.006.

(89) Abedi-Gaballu, F.; Dehghan, G.; Ghaffari, M.; Yekta, R.; Abbaspour-Ravasjani, S.; Baradaran, B.; Dolatabadi, J. E. N.; Hamblin, M. R. PAMAM Dendrimers as Efficient Drug and Gene Delivery Nanosystems for Cancer Therapy. *Appl Mater Today* **2018**, *12*, 177–190. https://doi.org/10.1016/j.apmt.2018.05.002.

(90) Karatasos, K.; Posocco, P.; Laurini, E.; Pricl, S. Poly(Amidoamine)-Based Dendrimer/SiRNA Complexation Studied by Computer Simulations: Effects of PH and Generation on Dendrimer Structure and SiRNA Binding. *Macromolecular Bioscience* **2012**, *12* (2), 225–240. https://doi.org/10.1002/mabi.201100276.

(91) Chen, X.; Liu, Z. Dual Responsive Mesoporous Silica Nanoparticles for Targeted Co-Delivery of Hydrophobic and Hydrophilic Anticancer Drugs to Tumor Cells. *J. Mater. Chem. B* **2016**, *4* (25), 4382–4388. https://doi.org/10.1039/C6TB00694A.

(92) Han, M.; Lv, Q.; Tang, X.-J.; Hu, Y.-L.; Xu, D.-H.; Li, F.-Z.; Liang, W.-Q.; Gao, J.-Q. Overcoming Drug Resistance of MCF-7/ADR Cells by Altering Intracellular Distribution of Doxorubicin via MVP Knockdown with a Novel SiRNA Polyamidoamine-Hyaluronic Acid Complex. *Journal of Controlled Release* **2012**, *163* (2), 136–144. https://doi.org/10.1016/j.jconrel.2012.08.020.

(93) Han, L.; Huang, R.; Li, J.; Liu, S.; Huang, S.; Jiang, C. Plasmid PORF-HTRAIL and Doxorubicin Co-Delivery Targeting to Tumor Using Peptide-Conjugated Polyamidoamine Dendrimer. *Biomaterials* **2011**, *32* (4), 1242–1252. https://doi.org/10.1016/j.biomaterials.2010.09.070.

(94) Martinez, C. S.; Igartúa, D. E.; Calienni, M. N.; Feas, D. A.; Siri, M.; Montanari, J.; Chiaramoni, N. S.; Alonso, S. del V.; Prieto, M. J. Relation between Biophysical Properties of Nanostructures and Their Toxicity on Zebrafish. *Biophys Rev* **2017**, *9* (5), 775–791. https://doi.org/10.1007/s12551-017-0294-2.

(95) Wang, W.; Xiong, W.; Zhu, Y.; Xu, H.; Yang, X. Protective Effect of PEGylation against Poly(Amidoamine) Dendrimer-Induced Hemolysis of Human Red Blood Cells. *Journal of Biomedical Materials Research Part B: Applied Biomaterials* **2010**, *93B* (1), 59–64. https://doi.org/10.1002/jbm.b.31558.

(96) Janaszewska, A.; Gorzkiewicz, M.; Ficker, M.; Petersen, J. F.; Paolucci, V.; Christensen, J. B.; Klajnert-Maculewicz, B. Pyrrolidone Modification Prevents PAMAM Dendrimers from Activation of Pro-Inflammatory Signaling Pathways in Human Monocytes. *Mol. Pharmaceutics* **2018**, *15* (1), 12–20. https://doi.org/10.1021/acs.molpharmaceut.7b00515.

(97) Catuogno, S.; Esposito, C. L.; de Franciscis, V. Aptamer-Mediated Targeted Delivery of Therapeutics: An Update. *Pharmaceuticals (Basel)* **2016**, *9* (4). https://doi.org/10.3390/ph9040069.
(98) Yemul, O.; Imae, T. Synthesis and Characterization of Poly(Ethyleneimine) Dendrimers. *Colloid Polym Sci* **2008**, *286* (6), 747–752. https://doi.org/10.1007/s00396-007-1830-6.
(99) Kaur, D.; Jain, K.; Mehra, N. K.; Kesharwani, P.; Jain, N. K. A Review on Comparative Study of PPI and PAMAM Dendrimers. *J Nanopart Res* **2016**, *18* (6), 146. https://doi.org/10.1007/s11051-016-3423-0.
(100) Shao, N.; Su, Y.; Hu, J.; Zhang, J.; Zhang, H.; Cheng, Y. Comparison of Generation 3 Polyamidoamine Dendrimer and Generation 4 Polypropylenimine Dendrimer on Drug Loading, Complex Structure, Release Behavior, and Cytotoxicity. *Int J Nanomedicine* **2011**, *6*, 3361–3372. https://doi.org/10.2147/IJN.S27028.
(101) Choi, Y. J.; Kang, S. J.; Kim, Y. J.; Lim, Y.; Chung, H. W. Comparative Studies on the Genotoxicity and Cytotoxicity of Polymeric Gene Carriers Polyethylenimine (PEI) and Polyamidoamine (PAMAM) Dendrimer in Jurkat T-Cells. *Drug and Chemical Toxicology* **2010**, *33* (4), 357–366. https://doi.org/10.3109/01480540903493507.
(102) Ewe, A.; Höbel, S.; Heine, C.; Merz, L.; Kallendrusch, S.; Bechmann, I.; Merz, F.; Franke, H.; Aigner, A. Optimized Polyethylenimine (PEI)-Based Nanoparticles for SiRNA Delivery, Analyzed in Vitro and in an Ex Vivo Tumor Tissue Slice Culture Model. *Drug Deliv. and Transl. Res.* **2017**, *7* (2), 206–216. https://doi.org/10.1007/s13346-016-0306-y.
(103) Kaur, A.; Jain, K.; Mehra, N. K.; Jain, N. K. Development and Characterization of Surface Engineered PPI Dendrimers for Targeted Drug Delivery. *Artificial Cells, Nanomedicine, and Biotechnology* **2017**, *45* (3), 414–425. https://doi.org/10.3109/21691401.2016.1160912.
(104) Soltani, F.; Ramezani, M.; Farzad, S. A.; Mokhtarzadeh, A.; Hashemi, M. Comparison Study of the Effect of Alkyl-Modified and Unmodified PAMAM and PPI Dendrimers on Solubility and Antitumor Activity of Crocetin. *Artificial Cells, Nanomedicine, and Biotechnology* **2017**, *45* (7), 1356–1362. https://doi.org/10.1080/21691401.2016.1236805.
(105) Szulc, A.; Pulaski, L.; Appelhans, D.; Voit, B.; Klajnert-Maculewicz, B. Sugar-Modified Poly(Propylene Imine) Dendrimers as Drug Delivery Agents for Cytarabine to Overcome Drug Resistance. *International Journal of Pharmaceutics* **2016**, *513* (1), 572–583. https://doi.org/10.1016/j.ijpharm.2016.09.063.
(106) Parashar, A. K.; Patel, P.; Gupta, A. K.; Jain, N. K.; Kurmi, B. D. Synthesis, Characterization and in Vivo Evaluation of PEGylated PPI Dendrimer for Safe and Prolonged Delivery of Insulin. *Drug Delivery Letters* **2019**, *9* (3), 248–263. https://doi.org/10.2174/2210303109666190401231920.

(107) Vijayaraj Kumar, P.; Agashe, H.; Dutta, T.; Jain, N. PEGylated Dendritic Architecture for Development of a Prolonged Drug Delivery System for an Antitubercular Drug. *CDD* **2007**, *4* (1), 11–19. https://doi.org/10.2174/156720107779314794.

(108) Shi, J.; Zhang, H.; Wang, L.; Li, L.; Wang, H.; Wang, Z.; Li, Z.; Chen, C.; Hou, L.; Zhang, C.; Zhang, Z. PEI-Derivatized Fullerene Drug Delivery Using Folate as a Homing Device Targeting to Tumor. *Biomaterials* **2013**, *34* (1), 251–261. https://doi.org/10.1016/j.biomaterials.2012.09.039.

(109) Pham, D. T.; Saelim, N.; Tiyaboonchai, W. Crosslinked Fibroin Nanoparticles Using EDC or PEI for Drug Delivery: Physicochemical Properties, Crystallinity and Structure. *J Mater Sci* **2018**, *53* (20), 14087–14103. https://doi.org/10.1007/s10853-018-2635-3.

(110) Najafi, F.; Salami-Kalajahi, M.; Roghani-Mamaqani, H. Synthesis of Amphiphilic Janus Dendrimer and Its Application in Improvement of Hydrophobic Drugs Solubility in Aqueous Media. *European Polymer Journal* **2020**, *134*, 109804. https://doi.org/10.1016/j.eurpolymj.2020.109804.

(111) Klajnert, B.; Appelhans, D.; Komber, H.; Morgner, N.; Schwarz, S.; Richter, S.; Brutschy, B.; Ionov, M.; Tonkikh, A. K.; Bryszewska, M.; Voit, B. The Influence of Densely Organized Maltose Shells on the Biological Properties of Poly(Propylene Imine) Dendrimers: New Effects Dependent on Hydrogen Bonding. *Chemistry – A European Journal* **2008**, *14* (23), 7030–7041. https://doi.org/10.1002/chem.200800342.

(112) Tietze, S.; Schau, I.; Michen, S.; Ennen, F.; Janke, A.; Schackert, G.; Aigner, A.; Appelhans, D.; Temme, A. A Poly(Propyleneimine) Dendrimer-Based Polyplex-System for Single-Chain Antibody-Mediated Targeted Delivery and Cellular Uptake of SiRNA. *Small* **2017**, *13* (27), 1700072. https://doi.org/10.1002/smll.201700072.

(113) Hashemi, M.; Tabatabai, S. M.; Parhiz, H.; Milanizadeh, S.; Amel Farzad, S.; Abnous, K.; Ramezani, M. Gene Delivery Efficiency and Cytotoxicity of Heterocyclic Amine-Modified PAMAM and PPI Dendrimers. *Materials Science and Engineering: C* **2016**, *61*, 791–800. https://doi.org/10.1016/j.msec.2016.01.023.

(114) Noske, S.; Karimov, M.; Aigner, A.; Ewe, A. Tyrosine-Modification of Polypropylenimine (PPI) and Polyethylenimine (PEI) Strongly Improves Efficacy of SiRNA-Mediated Gene Knockdown. *Nanomaterials* **2020**, *10* (9), 1809. https://doi.org/10.3390/nano10091809.

(115) Lim, J.; Simanek, E. E. Triazine Dendrimers as Drug Delivery Systems: From Synthesis to Therapy. *Advanced Drug Delivery Reviews* **2012**, *64* (9), 826–835. https://doi.org/10.1016/j.addr.2012.03.008.

(116) Simanek, E. E.; Abdou, H.; Lalwani, S.; Lim, J.; Mintzer, M.; Venditto, V. J.; Vittur, B. The 8 Year Thicket of Triazine Dendrimers: Strategies, Targets and Applications. *Proceedings of the Royal Society A: Mathematical, Physical and Engineering Sciences* **2010**, *466* (2117), 1445–1468.

https://doi.org/10.1098/rspa.2009.0108.
(117) Enciso, A. E.; Neun, B.; Rodriguez, J.; Ranjan, A. P.; Dobrovolskaia, M. A.; Simanek, E. E. Nanoparticle Effects on Human Platelets in Vitro: A Comparison between PAMAM and Triazine Dendrimers. *Molecules* **2016**, *21* (4), 428.
https://doi.org/10.3390/molecules21040428.
(118) Lim, J.; Lo, S.-T.; Hill, S.; Pavan, G. M.; Sun, X.; Simanek, E. E. Antitumor Activity and Molecular Dynamics Simulations of Paclitaxel-Laden Triazine Dendrimers. *Mol. Pharmaceutics* **2012**, *9* (3), 404–412.
https://doi.org/10.1021/mp2005017.
(119) Lim, J.; Guan, B.; Nham, K.; Hao, G.; Sun, X.; Simanek, E. E. Tumor Uptake of Triazine Dendrimers Decorated with Four, Sixteen, and Sixty-Four PSMA-Targeted Ligands: Passive versus Active Tumor Targeting. *Biomolecules* **2019**, *9* (9), 421.
https://doi.org/10.3390/biom9090421.
(120) Landarani-Isfahani, A.; Moghadam, M.; Mohammadi, S.; Royvaran, M.; Moshtael-Arani, N.; Rezaei, S.; Tangestaninejad, S.; Mirkhani, V.; Mohammadpoor-Baltork, I. Elegant PH-Responsive Nanovehicle for Drug Delivery Based on Triazine Dendrimer Modified Magnetic Nanoparticles. *Langmuir* **2017**, *33* (34), 8503–8515.
https://doi.org/10.1021/acs.langmuir.7b00742.
(121) Merkel, O. M.; Mintzer, M. A.; Sitterberg, J.; Bakowsky, U.; Simanek, E. E.; Kissel, T. Triazine Dendrimers as Nonviral Gene Delivery Systems: Effects of Molecular Structure on Biological Activity. *Bioconjugate Chem.* **2009**, *20* (9), 1799–1806.
https://doi.org/10.1021/bc900243r.
(122) Pennetta, C.; Bono, N.; Ponti, F.; Bellucci, M. C.; Viani, F.; Candiani, G.; Volonterio, A. Multifunctional Neomycin-Triazine-Based Cationic Lipids for Gene Delivery with Antibacterial Properties. *Bioconjugate Chem.* **2021**, acs.bioconjchem.0c00616.
https://doi.org/10.1021/acs.bioconjchem.0c00616.
(123) Merkel, O. M.; Mintzer, M. A.; Librizzi, D.; Samsonova, O.; Dicke, T.; Sproat, B.; Garn, H.; Barth, P. J.; Simanek, E. E.; Kissel, T. Triazine Dendrimers as Nonviral Vectors for in Vitro and in Vivo RNAi: The Effects of Peripheral Groups and Core Structure on Biological Activity. *Mol. Pharmaceutics* **2010**, *7* (4), 969–983.
https://doi.org/10.1021/mp100101s.
(124) Crespo, L.; Sanclimens, G.; Pons, M.; Giralt, E.; Royo, M.; Albericio, F. Peptide and Amide Bond-Containing Dendrimers. *Chem. Rev.* **2005**, *105* (5), 1663–1682.
https://doi.org/10.1021/cr030449l.
(125) Denkewalter, R. G.; Kolc, J.; Lukasavage, W. J. Macromolecular Highly Branched Homogeneous Compound Based on Lysine Units. US4289872A, September 15, **1981**.
(126) Denkewalter, R. G.; Kolc, J. F.; Lukasavage, W. J. Macromolecular Highly Branched Homogeneous Compound. US4410688A, October 18, **1983**.
(127) Denkewalter, R. G.; Kolc, J.; Lukasavage, W. J. Preparation of Lysine Based Macromolecular Highly Branched Homogeneous Compound. US4360646A, November 23, **1982**.

(128) Boyd, B. J.; Kaminskas, L. M.; Karellas, P.; Krippner, G.; Lessene, R.; Porter, C. J. H. Cationic Poly- L -Lysine Dendrimers: Pharmacokinetics, Biodistribution, and Evidence for Metabolism and Bioresorption after Intravenous Administration to Rats. *Mol. Pharmaceutics* **2006**, *3* (5), 614–627. https://doi.org/10.1021/mp060032e.

(129) Mehta, D.; Leong, N.; McLeod, V. M.; Kelly, B. D.; Pathak, R.; Owen, D. J.; Porter, C. J. H.; Kaminskas, L. M. Reducing Dendrimer Generation and PEG Chain Length Increases Drug Release and Promotes Anticancer Activity of PEGylated Polylysine Dendrimers Conjugated with Doxorubicin via a Cathepsin-Cleavable Peptide Linker. *Mol. Pharmaceutics* **2018**, *15* (10), 4568–4576. https://doi.org/10.1021/acs.molpharmaceut.8b00581.

(130) Kadlecova, Z.; Rajendra, Y.; Matasci, M.; Baldi, L.; Hacker, D. L.; Wurm, F. M.; Klok, H.-A. DNA Delivery with Hyperbranched Polylysine: A Comparative Study with Linear and Dendritic Polylysine. *Journal of Controlled Release* **2013**, *169* (3), 276–288. https://doi.org/10.1016/j.jconrel.2013.01.019.

(131) Watanabe, K.; Harada-Shiba, M.; Suzuki, A.; Gokuden, R.; Kurihara, R.; Sugao, Y.; Mori, T.; Katayama, Y.; Niidome, T. In Vivo SiRNA Delivery with Dendritic Poly(L-Lysine) for the Treatment of Hypercholesterolemia. *Mol. BioSyst.* **2009**, *5* (11), 1306–1310. https://doi.org/10.1039/B900880B.

(132) Inoue, Y.; Kurihara, R.; Tsuchida, A.; Hasegawa, M.; Nagashima, T.; Mori, T.; Niidome, T.; Katayama, Y.; Okitsu, O. Efficient Delivery of SiRNA Using Dendritic Poly(L-Lysine) for Loss-of-Function Analysis. *J Control Release* **2008**, *126* (1), 59–66. https://doi.org/10.1016/j.jconrel.2007.10.022.

(133) Gorzkiewicz, M.; Kopeć, O.; Janaszewska, A.; Konopka, M.; Pędziwiatr-Werbicka, E.; Tarasenko, I. I.; Bezrodnyi, V. V.; Neelov, I. M.; Klajnert-Maculewicz, B. Poly(Lysine) Dendrimers Form Complexes with SiRNA and Provide Its Efficient Uptake by Myeloid Cells: Model Studies for Therapeutic Nucleic Acid Delivery. *International Journal of Molecular Sciences* **2020**, *21* (9), 3138. https://doi.org/10.3390/ijms21093138.

(134) Okuda, T.; Sugiyama, A.; Niidome, T.; Aoyagi, H. Characters of Dendritic Poly(l-Lysine) Analogues with the Terminal Lysines Replaced with Arginines and Histidines as Gene Carriers in Vitro. *Biomaterials* **2004**, *25* (3), 537–544. https://doi.org/10.1016/S0142-9612(03)00542-8.

(135) Yamagata, M.; Kawano, T.; Shiba, K.; Mori, T.; Katayama, Y.; Niidome, T. Structural Advantage of Dendritic Poly(l-Lysine) for Gene Delivery into Cells. *Bioorganic & Medicinal Chemistry* **2007**, *15* (1), 526–532. https://doi.org/10.1016/j.bmc.2006.09.033.

(136) Roy, R.; Park, W. K. C.; Wu, Q.; Wang, S.-N. Synthesis of Hyper-Branched Dendritic Lactosides. *Tetrahedron Letters* **1995**, *36* (25), 4377–4380. https://doi.org/10.1016/0040-4039(95)00817-V.

(137) de la Fuente, M.; Raviña, M.; Sousa-Herves, A.; Correa, J.; Riguera, R.; Fernandez-Megia, E.; Sánchez, A.; Alonso, M. J. Exploring the Efficiency

of Gallic Acid-Based Dendrimers and Their Block Copolymers with PEG as Gene Carriers. *Nanomedicine* **2012**, *7* (11), 1667–1681. https://doi.org/10.2217/nnm.12.51.
(138) Sousa-Herves, A.; Novoa-Carballal, R.; Riguera, R.; Fernandez-Megia, E. GATG Dendrimers and PEGylated Block Copolymers: From Synthesis to Bioapplications. *AAPS J* **2014**, *16* (5), 948–961. https://doi.org/10.1208/s12248-014-9642-3.
(139) Grinda, M.; Clarhaut, J.; Renoux, B.; Tranoy-Opalinski, I.; Papot, S. A Self-Immolative Dendritic Glucuronide Prodrug of Doxorubicin. *MedChemComm* **2012**, *3* (1), 68–70. https://doi.org/10.1039/C1MD00193K.
(140) Ihre, H.; Hult, A.; Söderlind, E. Synthesis, Characterization, and ^{1}H NMR Self-Diffusion Studies of Dendritic Aliphatic Polyesters Based on 2,2-Bis(Hydroxymethyl)Propionic Acid and 1,1,1-Tris(Hydroxyphenyl)Ethane. *J. Am. Chem. Soc.* **1996**, *118* (27), 6388–6395. https://doi.org/10.1021/ja954171t.
(141) Carlmark, A.; Malmström, E.; Malkoch, M. Dendritic Architectures Based on Bis-MPA: Functional Polymeric Scaffolds for Application-Driven Research. *Chemical Society Reviews* **2013**, *42* (13), 5858–5879. https://doi.org/10.1039/C3CS60101C.
(142) García-Gallego, S.; Stenström, P.; Mesa-Antunez, P.; Zhang, Y.; Malkoch, M. Synthesis of Heterofunctional Polyester Dendrimers with Internal and External Functionalities as Versatile Multipurpose Platforms. **2020**, 7. https://doi.org/10.1021/acs.biomac.0c01068.
(143) Marks, M. A.; Kalaitzidou, K.; Gutekunst, W. R. Synthesis and Characterization of Cationic Dendrimer-PDMS Hybrids. *Macromolecular Rapid Communications* **2020**, *n/a* (n/a), 2000652. https://doi.org/10.1002/marc.202000652.
(144) Giesen, J. A.; Grayson, S. M. Selective Monobenzylation of 2,2-Bis(Hydroxymethyl)Propionic Acid (Bis-MPA) to Yield an AB Linear Monomer and Analogous Linear Oligomers. *Tetrahedron Letters* **2020**, *61* (25), 152016. https://doi.org/10.1016/j.tetlet.2020.152016.
(145) Kareem, O. O.; Daymon, S. P.; Keller, C. B.; Chen, B.; Nazarenko, S.; Grayson, S. M. Synthesis and Characterization of Linear, Homopolyester, Benzoyl-Protected Bis-MPA. **2020**, 11. https://doi.org/10.1021/acs.macromol.0c01045.
(146) Feliu, N.; Walter, M. V.; Montañez, M. I.; Kunzmann, A.; Hult, A.; Nyström, A.; Malkoch, M.; Fadeel, B. Stability and Biocompatibility of a Library of Polyester Dendrimers in Comparison to Polyamidoamine Dendrimers. *Biomaterials* **2012**, *33* (7), 1970–1981. https://doi.org/10.1016/j.biomaterials.2011.11.054.
(147) Malkoch, M.; García-Gallego, S. CHAPTER 2:Bis-MPA Dendrimers and Other Dendritic Polyesters. In *Dendrimer Chemistry*; 2020; pp 21–57. https://doi.org/10.1039/9781788012904-00021.
(148) Jaskula-Sztul, R.; Xu, W.; Chen, G.; Harrison, A.; Dammalapati, A.; Nair, R.; Cheng, Y.; Gong, S.; Chen, H. Thailandepsin A-Loaded and Octreotide-Functionalized Unimolecular Micelles for Targeted Neuroendocrine Cancer Therapy. *Biomaterials* **2016**, *91*, 1–10. https://doi.org/10.1016/j.biomaterials.2016.03.010.

(149) Heyder, R. S.; Zhong, Q.; Bazito, R. C.; da Rocha, S. R. P. Cellular Internalization and Transport of Biodegradable Polyester Dendrimers on a Model of the Pulmonary Epithelium and Their Formulation in Pressurized Metered-Dose Inhalers. *International Journal of Pharmaceutics* **2017**, *520* (1), 181–194. https://doi.org/10.1016/j.ijpharm.2017.01.057.

(150) Santra, S.; Shaw, Z.; Narayanam, R.; Jain, V.; Banerjee, T. Selective O-Alkylation of 2,2′-Bis(Hydroxymethyl)Propionic Acid to Synthesize Biodegradable Polymers for Drug Delivery Applications. *ACS Appl. Polym. Mater.* **2020**, *2* (8), 3465–3473. https://doi.org/10.1021/acsapm.0c00509.

(151) Lancelot, A.; Clavería-Gimeno, R.; Velázquez-Campoy, A.; Abian, O.; Serrano, J. L.; Sierra, T. Nanostructures Based on Ammonium-Terminated Amphiphilic Janus Dendrimers as Camptothecin Carriers with Antiviral Activity. *European Polymer Journal* **2017**, *90*, 136–149. https://doi.org/10.1016/j.eurpolymj.2017.03.012.

(152) San Anselmo, M.; Lancelot, A.; Egido, J. E.; Clavería-Gimeno, R.; Casanova, Á.; Serrano, J. L.; Hernández-Ainsa, S.; Abian, O.; Sierra, T. Janus Dendrimers to Assess the Anti-HCV Activity of Molecules in Cell-Assays. *Pharmaceutics* **2020**, *12* (11), 1062. https://doi.org/10.3390/pharmaceutics12111062.

(153) Lancelot, A.; González-Pastor, R.; Concellón, A.; Sierra, T.; Martín-Duque, P.; Serrano, J. L. DNA Transfection to Mesenchymal Stem Cells Using a Novel Type of Pseudodendrimer Based on 2,2-Bis(Hydroxymethyl)Propionic Acid. *Bioconjugate Chem.* **2017**, *28* (4), 1135–1150. https://doi.org/10.1021/acs.bioconjchem.7b00037.

(154) Stenström, P.; Manzanares, D.; Zhang, Y.; Ceña, V.; Malkoch, M. Evaluation of Amino-Functional Polyester Dendrimers Based on Bis-MPA as Nonviral Vectors for SiRNA Delivery. *Molecules* **2018**, *23* (8), 2028. https://doi.org/10.3390/molecules23082028.

(155) Zhang, X.; Li, Y.; Chen, Y. E.; Chen, J.; Ma, P. X. Cell-Free 3D Scaffold with Two-Stage Delivery of MiRNA-26a to Regenerate Critical-Sized Bone Defects. *Nature Communications* **2016**, *7* (1), 10376. https://doi.org/10.1038/ncomms10376.

(156) Morgan, M. T.; Carnahan, M. A.; Immoos, C. E.; Ribeiro, A. A.; Finkelstein, S.; Lee, S. J.; Grinstaff, M. W. Dendritic Molecular Capsules for Hydrophobic Compounds. *J. Am. Chem. Soc.* **2003**, *125* (50), 15485–15489. https://doi.org/10.1021/ja0347383.

(157) Morgan, M. T.; Nakanishi, Y.; Kroll, D. J.; Griset, A. P.; Carnahan, M. A.; Wathier, M.; Oberlies, N. H.; Manikumar, G.; Wani, M. C.; Grinstaff, M. W. Dendrimer-Encapsulated Camptothecins: Increased Solubility, Cellular Uptake, and Cellular Retention Affords Enhanced Anticancer Activity In Vitro. *Cancer Res* **2006**, *66* (24), 11913–11921. https://doi.org/10.1158/0008-5472.CAN-06-2066.

(158) Lancelot, A.; González-Pastor, R.; Clavería-Gimeno, R.; Romero, P.; Abian, O.; Martín-Duque, P.; Serrano, J. L.; Sierra, T. Cationic Poly(Ester Amide) Dendrimers: Alluring Materials for Biomedical Applications. *J. Mater. Chem. B* **2018**, *6* (23), 3956–3968.

https://doi.org/10.1039/C8TB00639C.
(159) Padias, A. B.; Hall, H. K.; Tomalia, D. A.; McConnell, J. R. Starburst Polyether Dendrimers. *J. Org. Chem.* **1987**, *52* (24), 5305–5312. https://doi.org/10.1021/jo00233a002.
(160) Mourey, T. H.; Turner, S. R.; Rubinstein, M.; Frechet, J. M. J.; Hawker, C. J.; Wooley, K. L. Unique Behavior of Dendritic Macromolecules: Intrinsic Viscosity of Polyether Dendrimers. **1992**, *25* (9), 6.
(161) Calderón, M.; Quadir, M. A.; Sharma, S. K.; Haag, R. Dendritic Polyglycerols for Biomedical Applications. *Adv. Mater.* **2010**, *22* (2), 190–218. https://doi.org/10.1002/adma.200902144.
(162) Jayaraman, M.; Fréchet, J. M. J. A Convergent Route to Novel Aliphatic Polyether Dendrimers. *J. Am. Chem. Soc.* **1998**, *120* (49), 12996–12997. https://doi.org/10.1021/ja983229b.
(163) Hu, M.; Chen, M.; Li, G.; Pang, Y.; Wang, D.; Wu, J.; Qiu, F.; Zhu, X.; Sun, J. Biodegradable Hyperbranched Polyglycerol with Ester Linkages for Drug Delivery. *Biomacromolecules* **2012**, *13* (11), 3552–3561. https://doi.org/10.1021/bm300966d.
(164) Deng, Y.; Saucier-Sawyer, J. K.; Hoimes, C. J.; Zhang, J.; Seo, Y.-E.; Andrejecsk, J. W.; Saltzman, W. M. The Effect of Hyperbranched Polyglycerol Coatings on Drug Delivery Using Degradable Polymer Nanoparticles. *Biomaterials* **2014**, *35* (24), 6595–6602. https://doi.org/10.1016/j.biomaterials.2014.04.038.
(165) Rades, N.; Achazi, K.; Qiu, M.; Deng, C.; Haag, R.; Zhong, Z.; Licha, K. Reductively Cleavable Polymer-Drug Conjugates Based on Dendritic Polyglycerol Sulfate and Monomethyl Auristatin E as Anticancer Drugs. *Journal of Controlled Release* **2019**, *300*, 13–21. https://doi.org/10.1016/j.jconrel.2019.01.035.
(166) Bej, R.; Achazi, K.; Haag, R.; Ghosh, S. Polymersome Formation by Amphiphilic Polyglycerol-b-Polydisulfide-b-Polyglycerol and Glutathione-Triggered Intracellular Drug Delivery. **2020**, 11. https://doi.org/10.1021/acs.biomac.0c00775.
(167) Witting, M.; Molina, M.; Obst, K.; Plank, R.; Eckl, K. M.; Hennies, H. C.; Calderón, M.; Frieß, W.; Hedtrich, S. Thermosensitive Dendritic Polyglycerol-Based Nanogels for Cutaneous Delivery of Biomacromolecules. *Nanomedicine: Nanotechnology, Biology and Medicine* **2015**, *11* (5), 1179–1187. https://doi.org/10.1016/j.nano.2015.02.017.
(168) Mandal, S.; Panja, P.; Debnath, K.; Jana, N. R.; Jana, N. R. Small-Molecule-Functionalized Hyperbranched Polyglycerol Dendrimers for Inhibiting Protein Aggregation. **2020**, 9. https://doi.org/10.1021/acs.biomac.0c00713.
(169) Pan, Y.; Zhou, S.; Li, Y.; Parshad, B.; Li, W.; Haag, R. Novel Dendritic Polyglycerol-Conjugated, Mesoporous Silica-Based Targeting Nanocarriers for Co-Delivery of Doxorubicin and Tariquidar to Overcome Multidrug Resistance in Breast Cancer Stem Cells. *Journal of Controlled Release* **2021**, *330*, 1106–1117. https://doi.org/10.1016/j.jconrel.2020.11.015.
(170) Zhao, L.; Nakae, Y.; Qin, H.; Ito, T.; Kimura, T.; Kojima, H.; Chan, L.; Komatsu, N. Polyglycerol-Functionalized Nanodiamond as a Platform for

Gene Delivery: Derivatization, Characterization, and Hybridization with DNA. *Beilstein J. Org. Chem.* **2014**, *10*, 707–713. https://doi.org/10.3762/bjoc.10.64.

(171) Zhang, L.; Hu, C.-H.; Cheng, S.-X.; Zhuo, R.-X. PEI Grafted Hyperbranched Polymers with Polyglycerol as a Core for Gene Delivery. *Colloids and Surfaces B: Biointerfaces* **2010**, *76* (2), 427–433. https://doi.org/10.1016/j.colsurfb.2009.12.001.

(172) Li, X.; Zhao, L.; Liang, Q.; Ye, J.; Komatsu, N.; Zhang, Q.; Gao, W.; Xu, M.; Chen, X. Cationic Polyarginine Conjugated Mesoporous Bioactive Glass Nanoparticles with Polyglycerol Coating for Efficient DNA Delivery. *Journal of Biomedical Nanotechnology* **2017**, *13* (3), 280–289. https://doi.org/10.1166/jbn.2017.2350.

(173) Staedtler, A. M.; Hellmund, M.; Mehrabadi, F. S.; Thota, B. N. S.; Zollner, T. M.; Koch, M.; Haag, R.; Schmidt, N. Optimized Effective Charge Density and Size of Polyglycerol Amines Leads to Strong Knockdown Efficacy in Vivo. *J. Mater. Chem. B* **2015**, *3* (46), 8993–9000. https://doi.org/10.1039/C5TB01466B.

(174) Tschiche, A.; M. Staedtler, A.; Malhotra, S.; Bauer, H.; Böttcher, C.; Sharbati, S.; Calderón, M.; Koch, M.; M. Zollner, T.; Barnard, A.; K. Smith, D.; Einspanier, R.; Schmidt, N.; Haag, R. Polyglycerol-Based Amphiphilic Dendrons as Potential SiRNA Carriers for in Vivo Applications. *Journal of Materials Chemistry B* **2014**, *2* (15), 2153–2167. https://doi.org/10.1039/C3TB21364A.

(175) Zhou, X.; Xu, L.; Xu, J.; Wu, J.; Kirk, T. B.; Ma, D.; Xue, W. Construction of a High-Efficiency Drug and Gene Co-Delivery System for Cancer Therapy from a PH-Sensitive Supramolecular Inclusion between Oligoethylenimine- *Graft* -β-Cyclodextrin and Hyperbranched Polyglycerol Derivative. *ACS Appl. Mater. Interfaces* **2018**, *10* (42), 35812–35829. https://doi.org/10.1021/acsami.8b14517.

(176) Kim, C.; Hong, J. H. Carbosilane and Carbosiloxane Dendrimers. *Molecules* **2009**, *14* (9), 3719–3730. https://doi.org/10.3390/molecules14093719.

(177) Rabiee, N.; Ahmadvand, S.; Ahmadi, S.; Fatahi, Y.; Dinarvand, R.; Bagherzadeh, M.; Rabiee, M.; Tahriri, M.; Tayebi, L.; Hamblin, M. R. Carbosilane Dendrimers: Drug and Gene Delivery Applications. *Journal of Drug Delivery Science and Technology* **2020**, *59*, 101879. https://doi.org/10.1016/j.jddst.2020.101879.

(178) Aizawa, H.; Otomo, K.; Honsho, N.; Shimazaki, T.; Villeneuve, M.; Matsuoka, K.; Hatano, K.; Terunuma, D. A Carbosilane Dendrimer and a Silacyclopentadiene Analog Carrying Peripheral Lactoses as Drug-Delivery Systems. *Bioorganic & Medicinal Chemistry Letters* **2012**, *22* (10), 3564–3566. https://doi.org/10.1016/j.bmcl.2012.03.034.

(179) Perisé-Barrios, A. J.; Fuentes-Paniagua, E.; San, J.; Alonso, E.; Reguera, R. M.; Gom, R. Improved Efficiency of Ibuprofen by Cationic Carbosilane Dendritic Conjugates. *Mol. Pharmaceutics* **2016**, 12. https://doi.org/10.1021/acs.molpharmaceut.6b00420.

(180) Gómez, R.; Mata, F. J. de la; Jiménez-Fuentes, J. L.; Ortega, P.; Klajnert, B.; Pedziwiatr-Werbicka, E.; Shcharbin, D.; Bryszewska, M.; Maly, M.; Maly, J.; Serramía, M. J.; Lorente, R.; Muñoz-Fernández, M. A. Cationic

Carbosilane Dendrimers as Non-viral Vectors of Nucleic Acids (Oligonucleotide or SiRNA) for Gene Therapy Purposes. In *Dendrimers in Biomedical Applications*; 2013; pp 40–55. https://doi.org/10.1039/9781849737296-00040.

(181) Perisé-Barrios, A. J.; Jiménez, J. L.; Domínguez-Soto, A.; de la Mata, F. J.; Corbí, A. L.; Gomez, R.; Muñoz-Fernandez, M. Á. Carbosilane Dendrimers as Gene Delivery Agents for the Treatment of HIV Infection. *Journal of Controlled Release* **2014**, *184*, 51–57. https://doi.org/10.1016/j.jconrel.2014.03.048.

(182) Serramía, M. J.; Álvarez, S.; Fuentes-Paniagua, E.; Clemente, M. I.; Sánchez-Nieves, J.; Gómez, R.; de la Mata, J.; Muñoz-Fernández, M. Á. In Vivo Delivery of SiRNA to the Brain by Carbosilane Dendrimer. *Journal of Controlled Release* **2015**, *200*, 60–70. https://doi.org/10.1016/j.jconrel.2014.12.042.

(183) Caminade, A.-M.; Majoral, J.-P. Which Dendrimer to Attain the Desired Properties? Focus on Phosphorhydrazone Dendrimers. *Molecules* **2018**, *23* (3), 622. https://doi.org/10.3390/molecules23030622.

(184) Caminade, A.-M.; Majoral, J.-P. Positively Charged Phosphorus Dendrimers. An Overview of Their Properties. *New J. Chem.* **2013**, 16. https://doi.org/10.1039/c3nj00583f.

(185) Shcharbin, D.; Bryszewska, M.; Mignani, S.; Shi, X.; Majoral, J.-P. Phosphorus Dendrimers as Powerful Nanoplatforms for Drug Delivery, as Fluorescent Probes and for Liposome Interaction Studies: A Concise Overview. *European Journal of Medicinal Chemistry* **2020**, *208*, 112788. https://doi.org/10.1016/j.ejmech.2020.112788.

(186) Mignani, S.; Shi, X.; Ceña, V.; Shcharbin, D.; Bryszewska, M.; Majoral, J.-P. In Vivo Therapeutic Applications of Phosphorus Dendrimers: State of the Art. *Drug Discovery Today* **2021**, *26* (3), 677–689. https://doi.org/10.1016/j.drudis.2020.11.034.

(187) Spataro, G.; Malecaze, F.; Turrin, C.-O.; Soler, V.; Duhayon, C.; Elena, P.-P.; Majoral, J.-P.; Caminade, A.-M. Designing Dendrimers for Ocular Drug Delivery. *European Journal of Medicinal Chemistry* **2010**, *45* (1), 326–334. https://doi.org/10.1016/j.ejmech.2009.10.017.

(188) Shcharbin, D.; Dzmitruk, V.; Shakhbazau, A.; Goncharova, N.; Seviaryn, I.; Kosmacheva, S.; Potapnev, M.; Pedziwiatr-Werbicka, E.; Bryszewska, M.; Talabaev, M.; Chernov, A.; Kulchitsky, V.; Caminade, A.-M.; Majoral, J.-P. Fourth Generation Phosphorus-Containing Dendrimers: Prospective Drug and Gene Delivery Carrier. *Pharmaceutics* **2011**, *3* (3), 458–473. https://doi.org/10.3390/pharmaceutics3030458.

(189) Briz, V.; Serramia, M. J.; Madrid, R.; Hameau, A.; Caminade, A.-M.; Majoral, J. P.; Munoz-Fernandez, M. A. Validation of a Generation 4 Phosphorus-Containing Polycationic Dendrimer for Gene Delivery Against HIV-1. *Current Medicinal Chemistry* **2012**, *19* (29), 5044–5051. https://doi.org/10.2174/092986731120902504 4.

(190) Jain, A.; Mahira, S.; Majoral, J.-P.; Bryszewska, M.; Khan, W.; Ionov, M. Dendrimer Mediated Targeting of SiRNA against Polo-like Kinase for the Treatment of Triple Negative Breast Cancer. *Journal of Biomedical Materials Research Part A* **2019**, *107* (9), 1933–1944. https://doi.org/10.1002/jbm.a.36701.

(191) Maksimenko, A. V.; Mandrouguine, V.; Gottikh, M. B.; Bertrand, J.-R.; Majoral, J.-P.; Malvy, C. Optimisation of Dendrimer-Mediated Gene Transfer by Anionic Oligomers. *J Gene Med* **2003**, *5* (1), 61–71. https://doi.org/10.1002/jgm.319.

(192) Dzmitruk, V.; Szulc, A.; Shcharbin, D.; Janaszewska, A.; Shcharbina, N.; Lazniewska, J.; Novopashina, D.; Buyanova, M.; Ionov, M.; Klajnert-Maculewicz, B.; Gómez-Ramirez, R.; Mignani, S.; Majoral, J.-P.; Muñoz-Fernández, M. A.; Bryszewska, M. Anticancer SiRNA Cocktails as a Novel Tool to Treat Cancer Cells. Part (B). Efficiency of Pharmacological Action. *International Journal of Pharmaceutics* **2015**, *485* (1), 288–294. https://doi.org/10.1016/j.ijpharm.2015.03.034.

Chapter 2:

Synthesis and characterisation of the dendritic materials

This chapter includes a general description of the procedures used for the synthesis of the molecules and their characterisation. The detailed description of the synthetic protocols and complete characterisations data for each molecule are gathered in chapter 7.

2.1. *bis*-MPA and *bis*-GMPA dendrons

Following the dendritic line of research of our group, the synthetic part of the present doctoral thesis expands the existing collection of dendritic structures based on 2,2'-*bis*(hydroxymethyl)propionic acid (*bis*-MPA) and 2,2'-*bis*(glyciloxymethyl)propionic acid (*bis*-GMPA) to be applied in different biomedical fields.

Firstly, the synthesis and characterisation of the constituent dendrons of *bis*-MPA and *bis*-GMPA is described and then, their covalent assembly to form the final dendritic structures is shown. This coupling was achieved in all cases by the copper(I) azide-alkyne cycloaddition (CuAAC) reaction, thus involving an azide or an alkyne group in each block to be attached.

The modifications studied among the dendrons include:

- The generation: from 1st to 3rd, to vary their size and the number of peripheral groups
- The focal point: azide or alkyne group, to allow their coupling with the corresponding partner by "click chemistry"
- The terminal moieties: hydrophilic amines or lipophilic stearic acid chains, to modulate their polarity

Notably, the amino-terminated dendrons involved in the CuAAC coupling are protected with *t*-Boc ending groups to favour the reaction conversion and final dendritic structures are obtained after the removal of these protecting groups in the last step.

2.1.1. *bis*-MPA dendrons

The *bis*-MPA dendrons designed and synthesised in this thesis can be classified into two groups attending to their peripheral functionalisation: the amino-terminated dendrons (hydrophilic) and those bearing stearic acid chains (lipophilic).

2.1.1.1. Hydrophilic *bis*-MPA dendrons

bis-MPA dendrons of the 2nd and 3rd generation bearing an azide in the focal point were synthesised following a divergent synthetic route previously used in our group[1] (Scheme 2.1). It should be noted that these dendrons were protected with cleavable *t*-Boc moieties in the periphery that were removed after the CuAAC reaction to form the corresponding dendritic derivative ending in amino groups.

Commercial *bis*-MPA was the starting point from which a succession of esterification and deprotection reactions took place. In a first step, the hydroxyl groups of the commercial reagent were temporarily protected with a ketal group by reaction with 2,2'-dimethoxypropane in dry acetone with *p*-toluenesulfonic acid as catalyst.

Once having this protected *bis*-MPA acetal, an aliphatic chain ending in an azide group was attached to the carboxylic acid in order to provide the molecule with a focal group suitable for later azide-alkyne cycloadditions. This chain containing six carbon atoms was previously obtained from 6-chlorohexan-1-ol in the presence of sodium azide, replacing the chlorine atom with the azide group by bi-molecular nucleophilic substitution (S_N2) to yield 6-azidohexan-1-ol. The attachment of the 6-azidohexan-1-ol to the *bis*-MPA acetal was carried out under anhydrous conditions with N,N'-dicyclohexylcarbodiimide (DCC) as coupling agent and 4-(dimethylamino)pyridinium 4-toluenesulfonate (DPTS) salt as catalyst to yield N_3-[MPA,G1]-(acetal)$_1$. This type of esterification reaction called Steglich's esterification was repeated several times along the synthesis of the dendrons and will be hereinafter referred to as **general procedure I**.

Then, the ketal group was hydrolysed under mild acidic conditions with Dowex® proton exchange resin to yield the dendron with free hydroxyl groups N_3-[MPA,G1]-$(OH)_2$. This highly specific deprotection of ketal groups would be also recurrent within the synthetic route and constitutes the **general procedure II**.

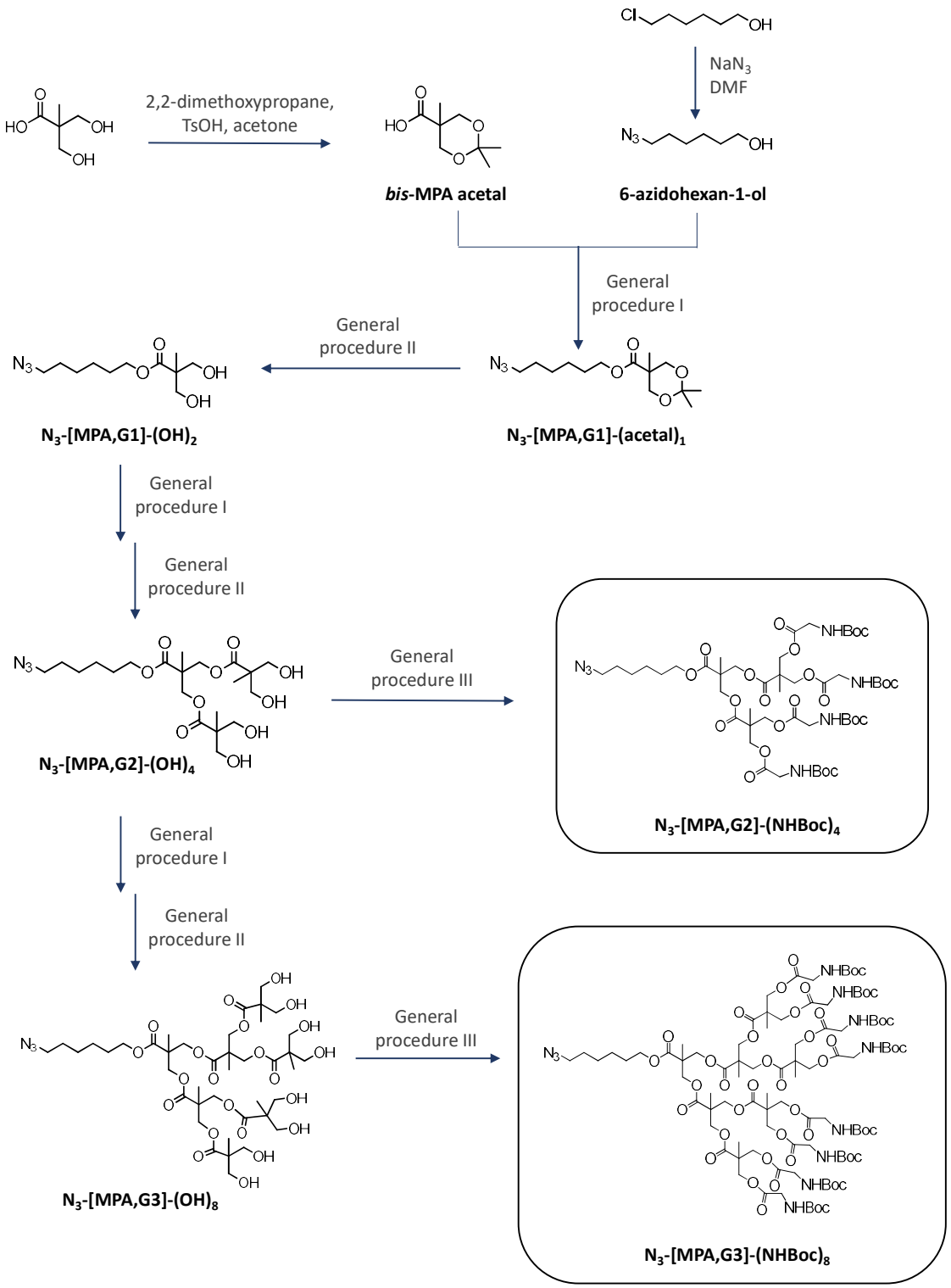

Scheme 2.1. Hydrophilic bis-MPA dendrons synthetic route.

From N_3-[MPA,G1]-$(OH)_2$, the repetition of the esterification and deprotection reactions described above allowed to reach the 2nd and 3rd generation of the dendron bearing hydroxyl groups at the periphery, N_3-[MPA,G2]-$(OH)_4$ and N_3-[MPA,G3]-$(OH)_8$. As a final step, N-(*tert*-butoxycarbonyl)glycine (Glyboc(OH)) was involved in the esterification reaction (**general procedure III**) with the dendrons to render the *t*-Boc amino protected *bis*-MPA dendrons of 2nd and 3rd generation, N_3-[MPA,G2]-$(NHBoc)_4$ and N_3-[MPA,G3]-$(NHBoc)_8$, with 4 and 8 protecting groups in the periphery, respectively.

All the intermediate products as well as the final dendrons were characterised by ^1H and ^{13}C nuclear magnetic resonance (NMR), mass spectrometry (MS) and Fourier transform infrared spectroscopy (FTIR). Additionally, size exclusion chromatography (SEC) of the final *t*-Boc protected dendrons was conducted. See chapter 7 for the complete characterisation of each molecule.

The triplet signal at 3.27 ppm in the ^1H NMR spectra corresponding to the protons of the methylene adjacent to the azide group was observed from N_3-[MPA,G1]-$(acetal)_1$ as a result of the attachment of the 6-azidohexan-1-ol to the dendron and served as an internal reference for the correct quantification of the rest of the protons in the molecule. The presence of the azide group could be also assessed by ^{13}C NMR as denoted the peak observed at 51 ppm corresponding to the C atom adjacent to the azide and by FTIR analyses with a stretching band around 2100 cm^{-1}.

The correct coupling of the *t*-Boc moieties to the dendron was revealed by the appearance of a prominent peak at 1.43 ppm in the ^1H NMR spectrum due to their methyl protons as well as a peak at 3.88 ppm corresponding to the protons of the methylene groups adjacent to the NHBoc. In addition, a broad signal at 5.29 ppm indicated the existence of amide groups. Another indicative signals that corroborate the *t*-Boc protection of the dendron were the new peaks appeared in ^{13}C NMR spectra (170.0, 155.8, 79.8, 42.2 and 28.3 ppm) and the FTIR stretching bands at 3400 cm^{-1} (N-H) and 1720 cm^{-1} (NC=O).

MS analyses confirmed the accurate synthesis of the dendrons as the expected molecular weight was observed. Besides, the narrow distribution given by SEC corroborated their expected monodispersity as discrete molecules.

2.1.1.2. Lipophilic *bis*-MPA dendrons

The lipophilic *bis*-MPA dendrons bearing aliphatic stearic acid chains were grown up till the 2nd generation following again a divergent approach previously used in our group[2] (Scheme 2.2). In this case, the focal point of the dendrons is an alkyne group and protection of the peripheral groups is not necessary.

Initially, the *bis*-MPA protected with the acetal group was functionalised with the propargyl group by Steglich's esterification to yield the 1st generation of acetal protected dendron with the propargyl group at the focal point, ≡-[MPA,G1]-$(acetal)_1$. Then, the protecting acetal group was hydrolysed with Dowex® proton exchange resin (**general procedure II**), obtaining the dendron bearing two hydroxyl groups (≡-[MPA,G1]-$(OH)_2$). The 2nd generation dendron with hydroxyl groups, (≡-[MPA,G2]-$(OH)_4$) was obtained after consecutive esterification and deprotection reactions (**general procedures II** and **III**). Finally, the aliphatic chains were introduced in the periphery of the dendrons of both generations by esterification between the hydroxyl groups of the dendrons and the carboxylic acid of the stearic acid (**general procedure IV**). Thus, the lipophilic dendrons ≡-[MPA,G1]-$(C17)_2$ and ≡-[MPA,G2]-$(C17)_4$ include an alkyne group at the focal point and 2 or 4 aliphatic chains, respectively.

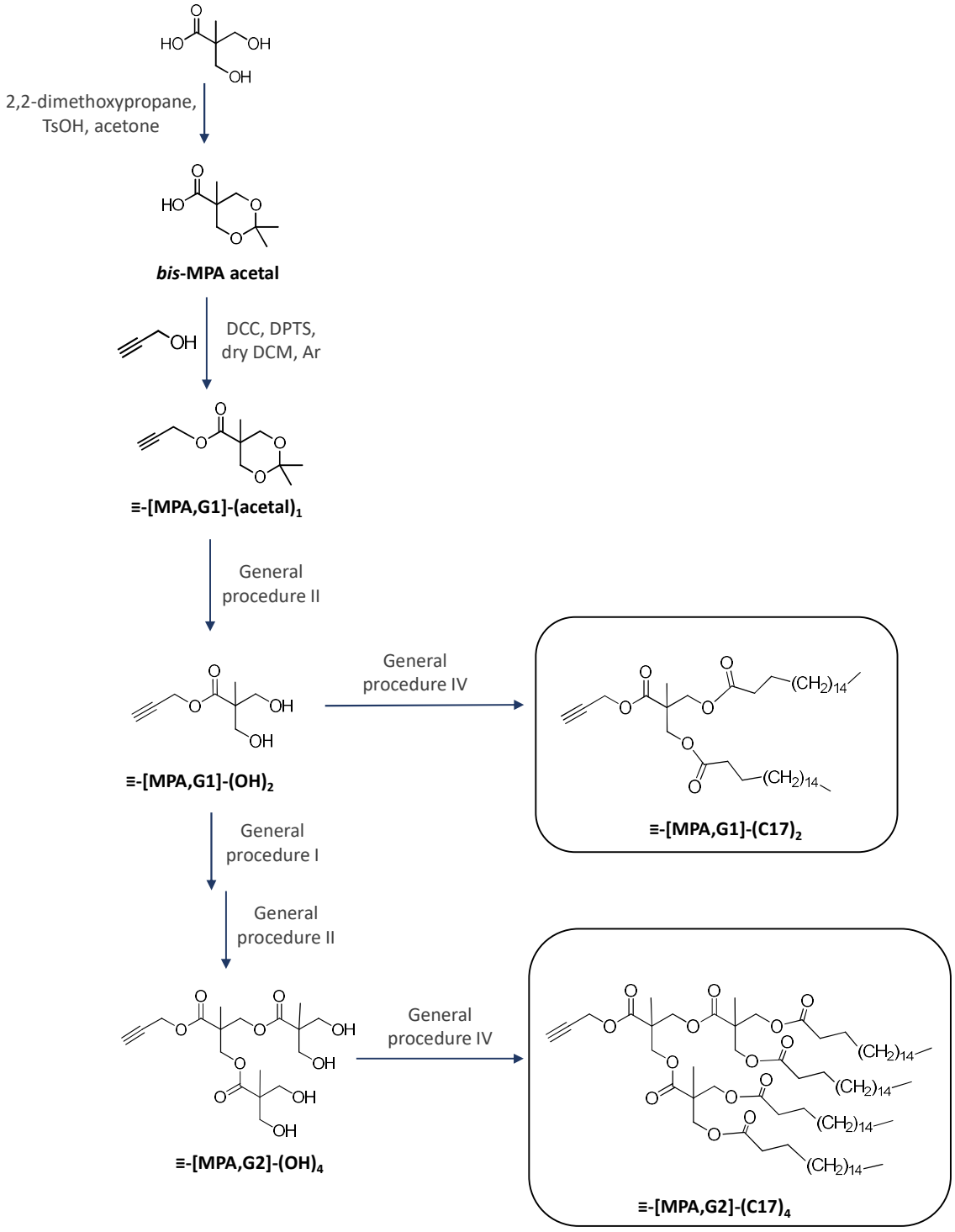

Scheme 2.2. Lipophilic bis-MPA dendrons synthetic route.

All the intermediate products as well as the final dendrons were characterised by ^{1}H and ^{13}C NMR, MS and FTIR. Additionally, SEC of the final *t*-Boc protected dendrons was conducted. See chapter 7 for the complete characterisation of each molecule.

The insertion of the propargyl moiety provoked the appearance of a triplet at 2.50 ppm and a doublet at 4.72 ppm in the ^{1}H NMR spectra. The signals of the C atoms corresponding to this propargyl group were found in ^{13}C NMR spectra at 75.4 and 52.8 ppm.

On the other hand, the presence of the aliphatic chains was confirmed through the appearance of some signals in the ^{1}H NMR spectra due to the protons of the methylene groups, specifically in the region from 2.29 to 1.25 ppm, and the terminal methyl group protons at 0.88 ppm. Regarding the ^{13}C NMR spectrum, the different peaks observed in the region between 34.0 and 17.8, and at 14.1 ppm confirmed the correct functionalisation of the dendrons, as well as the signal at 173.1 ppm corresponding to the ester carbonyl group.

MS analyses confirmed the accurate synthesis of the dendrons as the expected molecular weight was observed. Besides, the narrow distribution given by SEC corroborated their expected monodispersity as discrete molecules.

2.1.2. *bis*-GMPA dendrons

The *bis*-GMPA dendrons designed and synthesised in this thesis can attend the same classification pattern considering the terminal groups: the amino-terminated dendrons (hydrophilic) and those bearing stearic acid chains (lipophilic).

2.1.2.1. Hydrophilic *bis*-GMPA dendrons

The introduction of inner glycine moieties to the *bis*-MPA dendrons to create the *bis*-GMPA derivatives was originally developed in a previous doctoral thesis within our group[3] and has been exploited in subsequent works[4,5]. Here, *t*-Boc terminated *bis*-GMPA dendrons till 3rd generation were synthesised following the

divergent pathway described in Scheme 2.4. The focal point of all of them contained an azide group as in the case of the *bis*-MPA hydrophilic dendrons.

Firstly, the commercial *bis*-MPA was employed as starting point to synthesise the *bis*-GMPA monomer protected with *t*-Boc moieties (Scheme 2.3). This monomer was later used to grow the *bis*-GMPA dendron generation at the same time that amide groups are introduced. Briefly, the carboxylic group of the *bis*-MPA was protected with a benzyl group by reaction with benzyl bromide in basic medium and then, the peripheral hydroxyl groups were allowed to react with *t*-Boc protected glycine. Finally, the benzyl group previously introduced was removed by catalytic hydrogenation and the mentioned synthetic piece of *bis*-GMPA was obtained.

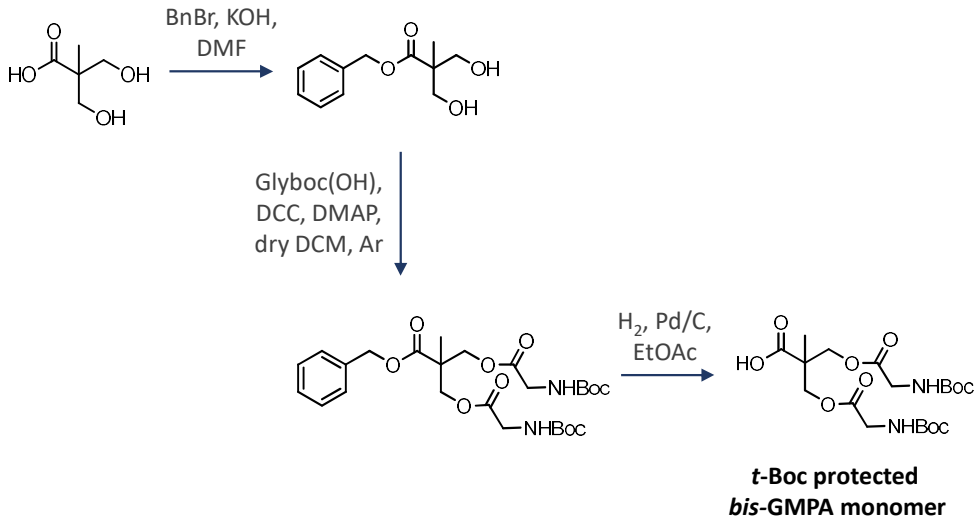

Scheme 2.3. Scheme for the synthesis of the t-Boc protected bis-GMPA monomer.

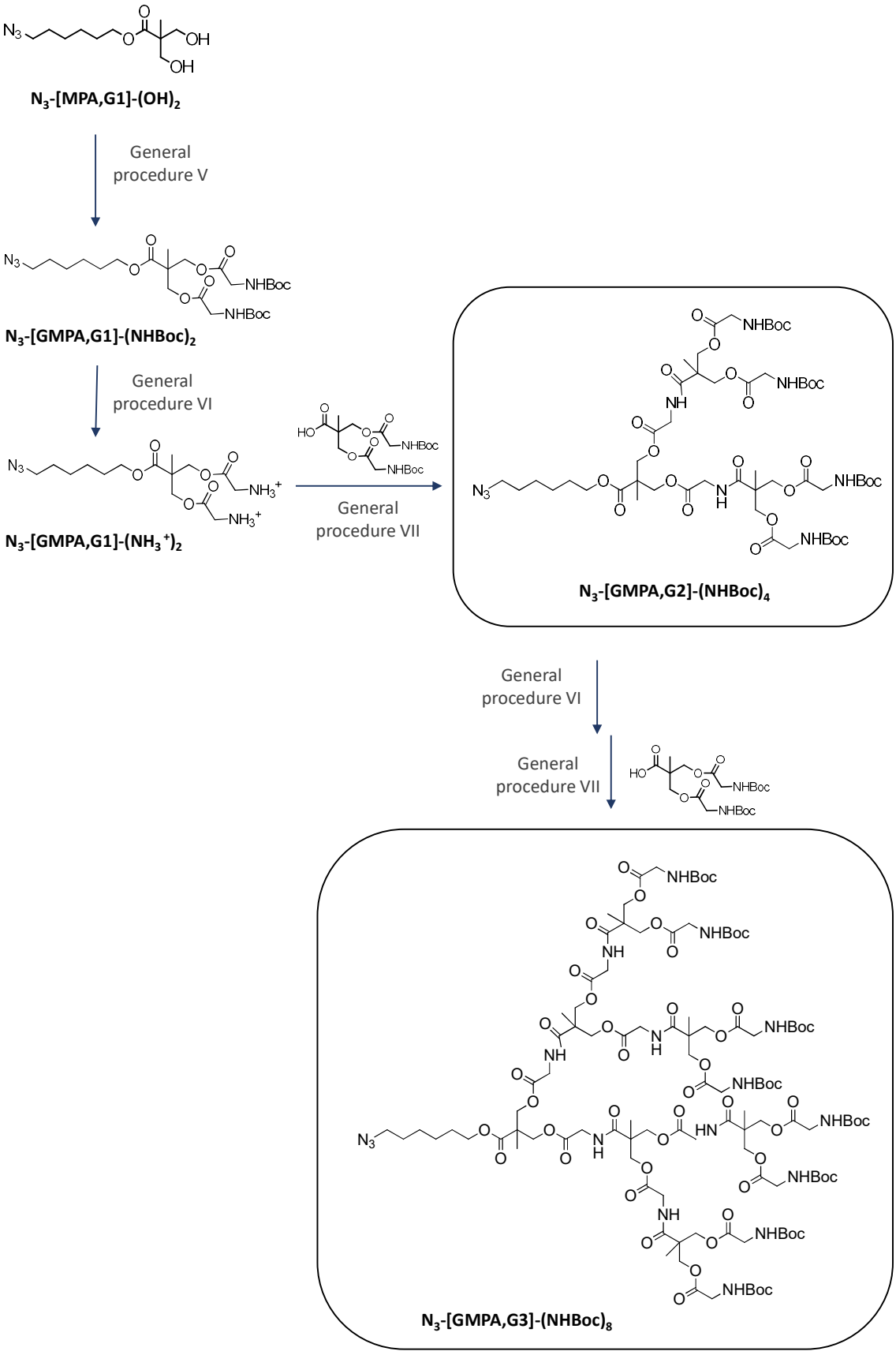

Scheme 2.4. Hydrophilic bis-GMPA dendrons synthetic route.

The *bis*-MPA dendron of 1st generation with hydroxyl groups, N_3-[MPA,G1]-$(OH)_2$, served as base structure to achieve the synthesis of the *bis*-GMPA hydrophilic dendrons with azide groups at the focal point. Namely, N_3-[MPA,G1]-$(OH)_2$ reacted with *t*-Boc protected glycine under Steglich's conditions to yield the 1st generation *bis*-GMPA dendron protected with *t*-Boc moieties, N_3-[MPA,G1]-$(NHBoc)_2$ (**general procedure V**). Then, these protecting groups were removed under acidic conditions (a mixture of trifluoroacetic acid (TFA) and chloroform ($CHCl_3$), **general procedure VI**)[6] to obtain the 1st *bis*-GMPA amino-terminated dendron, N_3-[GMPA,G1]-$(NH_3^+)_2$. A different deprotection method based on hydrochloric acid 3M into ethyl acetate was originally described for the synthesis of these dendrons. However, the observation of some undesirable acidic hydrolysis events guided us to focus into a softer procedure for the *t*-Boc removal.

The dendron growth was carried out by amide coupling of the *bis*-GMPA monomer under similar conditions as those employed in the Steglich's esterification and adapted from Fernández-Megía *et al.*[7] (**general procedure VII**). DCC and HOBt acted as coupling agents while DMAP accomplished two functions, the neutralisation of the ammonium salts of the dendron and the activation of the monomer to the amide coupling[3,4]. A mixture of dry solvents (dichloromethane and dimethylformamide) was employed in order to completely dissolve all the reagents involved in the amidation and the 2nd generation *t*-Boc protected *bis*-GMPA dendron was obtained (N_3-[GMPA,G2]-$(NHBoc)_4$).

To reach the 3rd generation, its deprotection was carried out again under acidic conditions ($CHCl_3$/TFA) to yield N_3-[GMPA,G2]-$(NH_3^+)_4$ and the amide coupling with *t*-Boc protected *bis*-GMPA monomer was performed as described above to yield the N_3-[GMPA,G3]-$(NHBoc)_8$.

All the intermediate products as well as the final dendrons were characterised by ^1H and ^{13}C NMR, MS and FTIR. Additionally, SEC of the final *t*-Boc protected dendrons was conducted. See chapter 7 for the complete characterisation of each molecule.

The presence of the protons of the methylene in the glycine moieties (between the ester groups and the amides or amines) was assessed by the appearance of

a singlet around 3.90 ppm in the ^{1}H NMR spectra. Besides, the protons of the oxymethylene of the ester groups yielded a signal in the region 4.50-4.30 ppm. It is remarkable that these signals can be differentiated when the proton-containing groups are in the peripheral part of the molecule or in the internal one. Specifically, the signal of the protons of the methylene groups in the glycine moieties shifts to higher fields when they are located in the periphery, whereas the protons of the oxymethylene groups shift downfield in the same situation.

The ^{13}C NMR spectra revealed new peaks around 42.0 ppm corresponding to the methylene in the glycine groups and new signals in the carboxylic region were observed as well.

Some differentiating signals of the *bis*-GMPA dendrons could also be observed by FTIR analysis. The presence of a wide band between 3400 and 2600 cm^{-1} corresponding to the stretching vibration of the $N\text{-}H^{+}$ bonds as well as a band around 1500 cm^{-1} corresponding to their bending vibration, confirmed the existence of the ammonium groups in the dendron. Additionally, next to the intense ester band (around 1730 cm^{-1}) a novel band at 1665 cm^{-1} corresponding to the stretching of the carbonyl in the amide groups and another one at around 1520 cm^{-1} due to the bending of N-H were observed.

MS analyses confirmed the accurate synthesis of the dendrons as the expected molecular weight was observed, although in some cases fragmented portions were observed after the ionisation process. Besides, the narrow and symmetrical distribution given by SEC corroborated the expected monodispersity of the dendrons as discrete molecules.

2.1.2.2. Lipophilic *bis*-GMPA dendrons

The synthesis of the *bis*-GMPA dendrons of the 1st and 2nd generation bearing 2 and 4 aliphatic stearic acid chains, respectively, and the alkyne group at the focal point, ≡-[GMPA,G1](C17)$_2$ and ≡-[GMPA,G2](C17)$_4$, has been described for the first time within this doctoral thesis. Besides, the involvement of these dendrons in the synthesis of Janus dendrimers applied in the hepatitis C research (see chapter 3) has been recently published[5].

The synthetic route described in Scheme 2.5 starts with the ≡-[MPA,G1](OH)$_2$ intermediate, whose synthesis was previously described in the pathway followed for the synthesis of the *bis*-MPA lipophilic dendrons (see Scheme 2.2). From that point, the insertion of the *t*-Boc protected glycine moieties under Steglich's esterification conditions leads to the 1st generation *t*-Boc protected *bis*-GMPA dendrons bearing the alkyne group at the focal point, ≡-[GMPA,G1](NHBoc)$_2$. The subsequent deprotection of the amino groups yielded a dendron, ≡-[GMPA,G1](NH$_3^+$)$_2$, with two synthetic possibilities: the growth in the dendron generation by insertion of the *t*-Boc protected *bis*-GMPA monomer or its functionalisation with stearic acid to obtain the 1st generation of the lipophilic *bis*-GMPA dendron with two aliphatic chains, ≡-[GMPA,G1](C17)$_2$ (**general procedure VIII**). In the case of the amidation coupling between the ammonium groups of the dendron and the carboxylic acid of the monomer, the 2nd generation of the *t*-Boc protected *bis*-GMPA dendron, ≡-[GMPA,G2](NHBoc)$_4$, was obtained. In order to reach the 2nd generation lipophilic dendron bearing four aliphatic chains, ≡-[GMPA,G2](C17)$_4$, acidic removal of *t*-Boc groups and functionalisation by amidation with stearic acid chains were consecutively developed under the reaction conditions as described above.

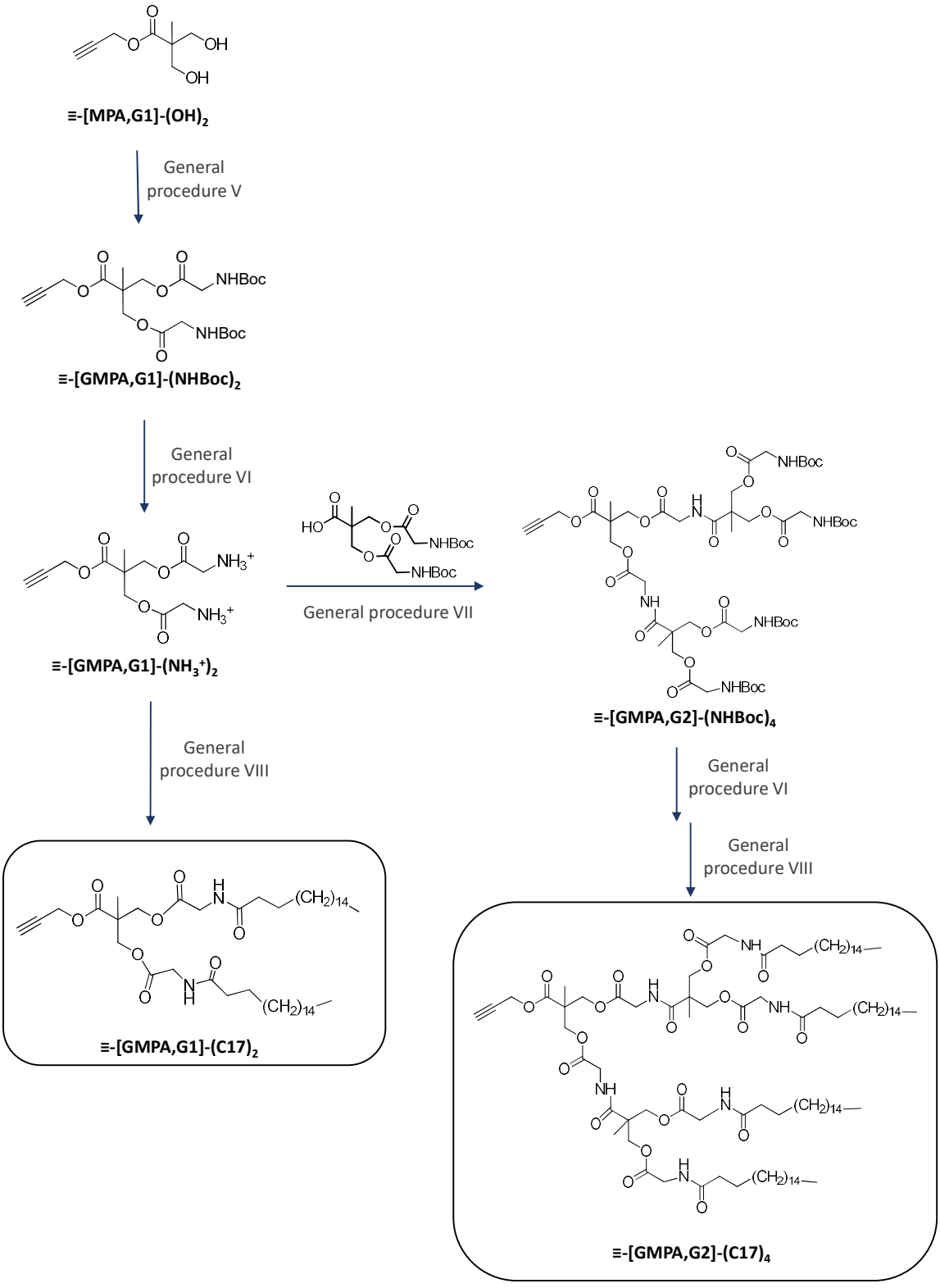

Scheme 2.5. Lipophilic bis-GMPA dendrons synthetic route.

All the intermediate products as well as the final dendrons were characterised by ^{1}H and ^{13}C NMR, MS and FTIR. Additionally, SEC of the final *t*-Boc protected dendrons was conducted. See chapter 7 for the complete characterisation of each molecule. The characterisation of the higher generation dendron, ≡-[GMPA,G2](C17)$_4$, is shown in Figure 2.1 and Figure 2.2 as an explanatory example.

The insertion of the amide groups could be observed through the presence of the protons of the methylene groups corresponding to the glycine moieties around 4.00 ppm in ^{1}H NMR (H-9 and H-15) (Figure 2.1a) and at 41.5 ppm in ^{13}C NMR spectra (C-9 and C-15) (Figure 2.1b). In addition, a broad signal was observed at 6.52 ppm in ^{1}H NMR corresponding to the -NH groups and new peaks appeared in the carbonylic region of the ^{13}C NMR spectrum. The stearic acid chains yielded some characteristic signals in the ^{1}H NMR spectrum as the triplet at 2.24 ppm due to the protons of the methylene groups adjacent to the carbonyl of the peripheral amido groups (H-17), the signal at 1.62 ppm corresponding to their adjacent methylene groups (H-18), the increase on the 1.25 ppm singlet due to the series of protons in the aliphatic chain (H-19) and finally, the triplet at 0.88 ppm corresponding to the peripheral methyl groups of the stearic acid chains (H-20). These groups were also found in the ^{13}C NMR spectrum at 32.1-22.8 ppm (C-17, 18, 19) and at 14.2 ppm (C-20). Finally, as for the lipophilic *bis*-MPA dendrons, a triplet at 2.53 ppm (H-1) and a doublet at 4.74 ppm (H-3) were found in the ^{1}H NMR spectrum corresponding to the protons of the alkyne group and the adjacent methylene group, respectively. Their corresponding carbon atoms were observed in the ^{13}C NMR spectrum at 75.7 and 52.9 ppm (C-1 and C-3).

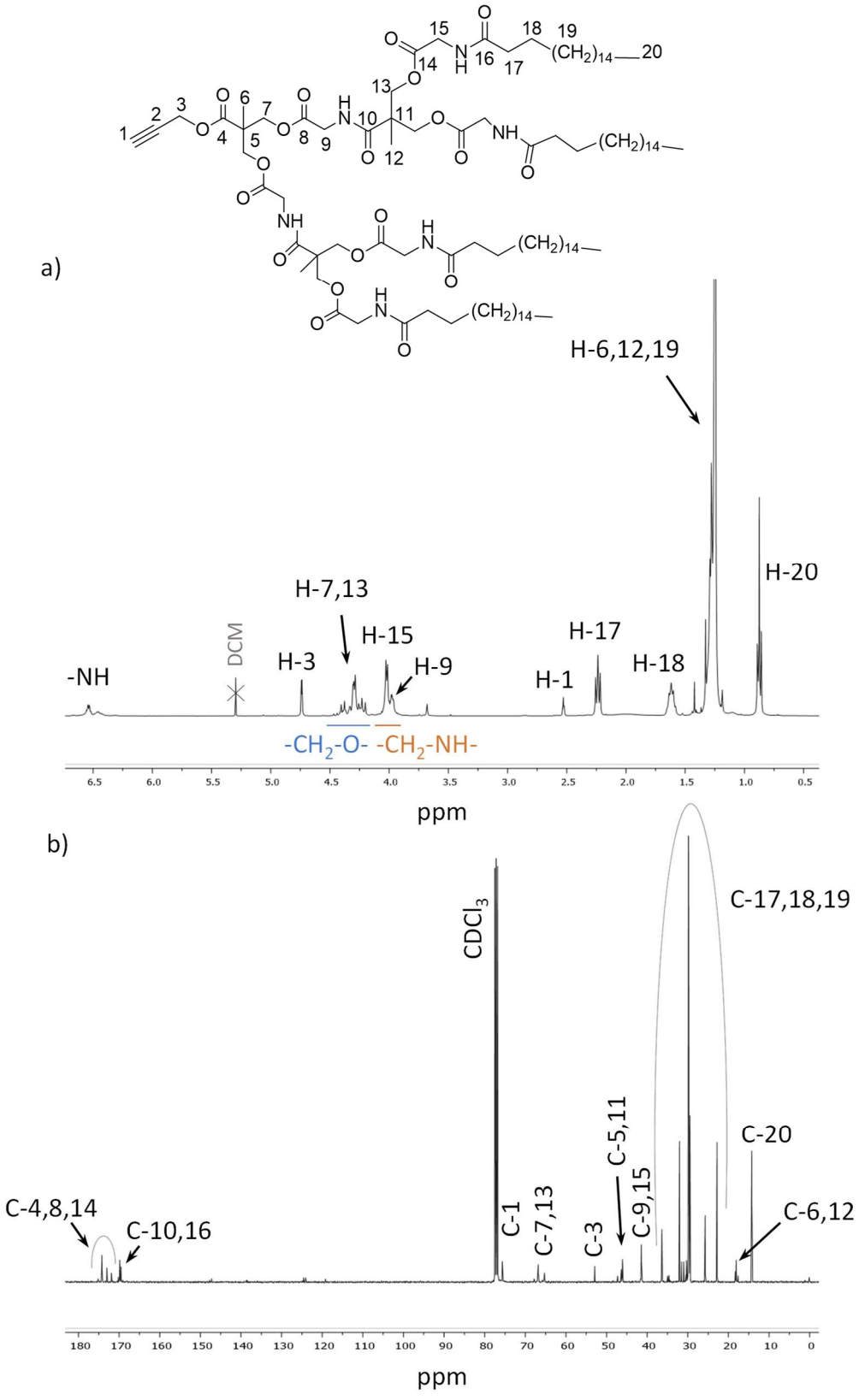

Figure 2.1. NMR spectroscopic characterisation of ≡-[GMPA,G2](C17)$_4$: a) ^{1}H NMR spectrum (CDCl$_3$, 400 MHz) and b) ^{13}C NMR spectrum (CDCl$_3$, 100 MHz).

The FTIR spectroscopy (Figure 2.2a) confirmed the presence of the amide groups of the dendron by showing a broad band at 3301 cm^{-1} corresponding to the stretching vibration of the N-H bond and another band at 1537 cm^{-1} due to its bending. Besides, the band of the carbonyl of the amide group stretching was observed at 1645 cm^{-1}, close to the signal of the carbonyl of the ester group. Finally, two bands were observed around 2900 cm^{-1} corresponding to the C-H stretching.

MS analyses confirmed the accurate synthesis of the dendrons as the expected molecular weight was observed (Figure 2.2b). Besides, the narrow and symmetrical distribution given by SEC corroborated their expected monodispersity as discrete molecules.

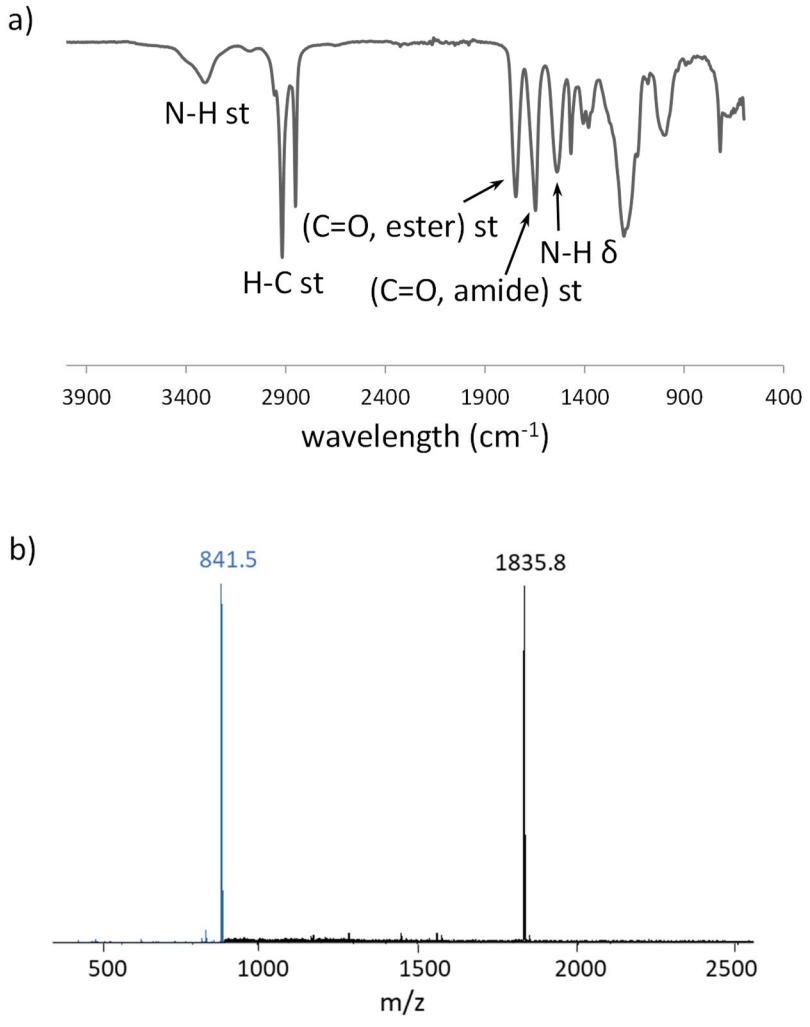

Figure 2.2. Chemical characterisation of bis-GMPA lipophilic dendrons: a) FTIR spectrum in transmission mode of ≡-[GMPA,G2](C17)$_4$ and b) MS spectra overlap of ≡-[GMPA,G1](C17)$_2$ (blue) and ≡-[GMPA,G2](C17)$_4$ (black).

2.2. Amphiphilic Janus dendrimers

The synthesised amphiphilic Janus dendrimers contain ammonium terminated hydrophilic dendrons and stearic acid terminated lipophilic dendrons. In these compounds, the *bis*-MPA/*bis*-GMPA architecture is alternated between both sides and the size of the lipophilic domain varies between two and four chains of stearic acid, whereas the hydrophilic block holds eight ammonium groups at the surface in all cases. Thus, the series of Janus dendrimers designed is comprised by the four following constructs (Figure 2.3):

- **$(NH_3^+)_8$[GMPA]-[MPA](C17)$_2$** that consists of a hydrophilic *bis*-GMPA dendron of 3rd generation and a lipophilic *bis*-MPA dendron of 1st generation,
- **$(NH_3^+)_8$[GMPA]-[MPA](C17)$_4$** that consists of a hydrophilic *bis*-GMPA dendron of 3rd generation and a lipophilic *bis*-MPA dendron of 2nd generation,
- **$(NH_3^+)_8$[MPA]-[GMPA](C17)$_2$** that consists of a hydrophilic *bis*-MPA dendron of 3rd generation and a lipophilic *bis*-GMPA dendron of 1st generation,
- **$(NH_3^+)_8$[MPA]-[GMPA](C17)$_4$** that consists of a hydrophilic *bis*-MPA dendron of 3rd generation and a lipophilic *bis*-GMPA dendron of 2nd generation.

The presence of such chemically different blocks affects the mass average molecular weight (MW) as well as the lipophilic content (Lc) of the amphiphilic compounds obtained. The Lc has been here defined as the percentage in weight of the n-alkylic content in the entire dendrimer. It implies a variation in the calculation of this parameter with respect to previous works in our group where the two dendrons had the same internal composition (*bis*-MPA/*bis*-MPA) and the whole MW of the dendron was considered to calculate the Lc of the dendrimer[8,9]. However, here the internal architecture of the composing dendrons is alternated between *bis*-MPA and *bis*-GMPA. The presence of the inner amides of the *bis*-GMPA in the lipophilic side of the molecule contributes to enlarge the MW of this dendron but they can not be classified as lipophilic groups. Then, their inclusion in the Lc calculation would disturb in some way the real lipophilic contribution of

that dendrons and for that reason, it was finally decided to consider only the MW of the aliphatic chains in the Lc calculation.

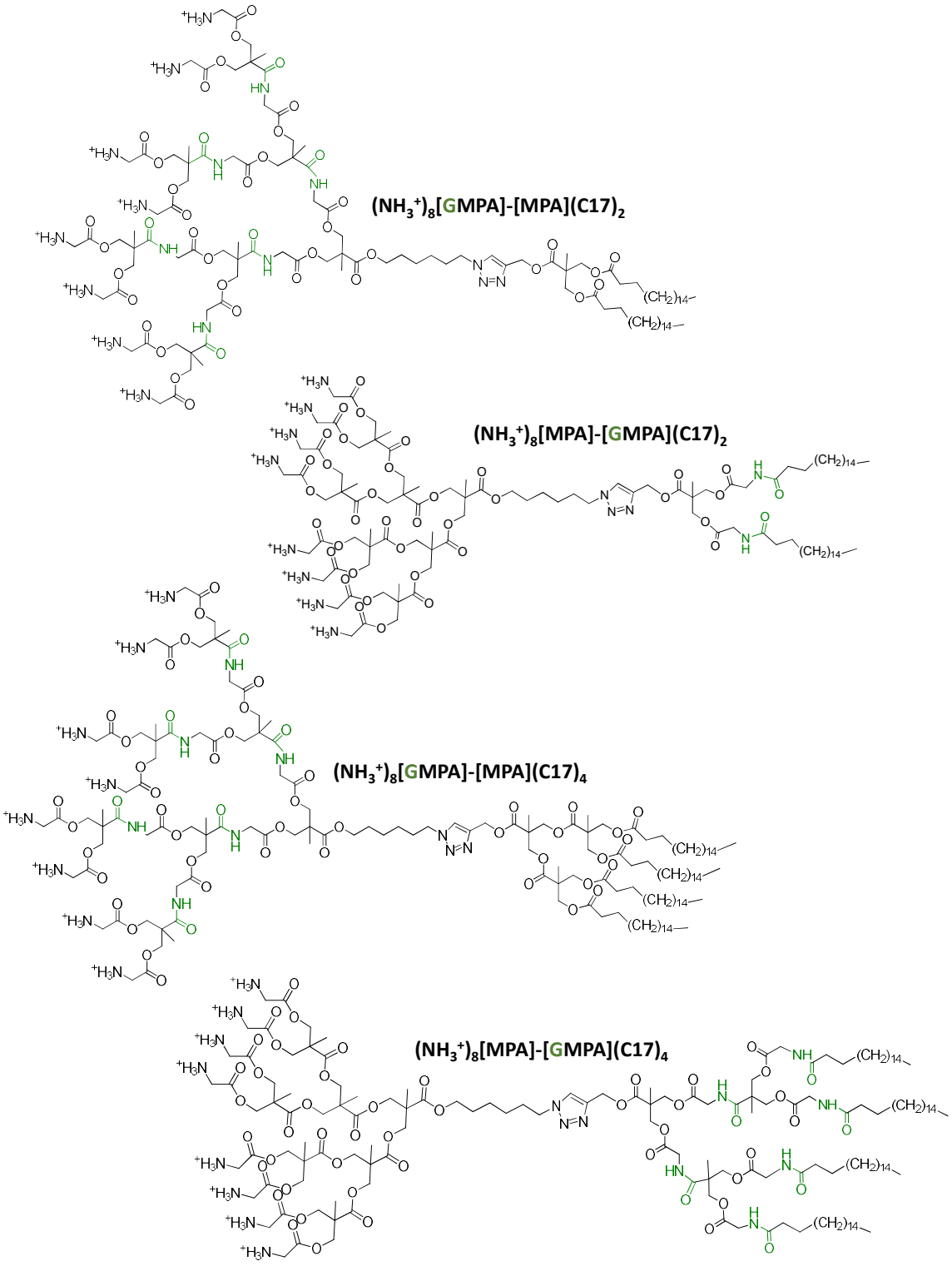

Figure 2.3. Chemical structures of the amphiphilic Janus dendrimers. Glycine moieties of bis-GMPA are denoted in green.

As it can be deduced from Table 2.1, the Janus dendrimers containing the 2nd generation lipophilic dendrons (≡-[MPA]-$(C17)_4$ and ≡-[GMPA]-$(C17)_4$) present a higher Lc (29.6) than those containing the 1st generation ones, due to the contribution of the higher number of stearic acid chains to the whole molecular weight of the dendrimer. The difference between the Lc of the dendrimers with two stearic acid chains, 19.4 and 21.4 for $(NH_3^+)_8$[GMPA]-[MPA]$(C17)_2$ and $(NH_3^+)_8$[MPA]-[GMPA]$(C17)_2$, respectively, can be explained because of the higher number of total amide groups in the case of the $(NH_3^+)_8$[GMPA]-[MPA]$(C17)_2$, which enlarges the dendrimer MW and then, the same number of alkylic chains do not have the same contribution in the entire molecule.

Table 2.1. Molecular weight (MW) and lipophilic content (Lc) of the amphiphilic Janus dendrimers.

	MW (g/mol)		
	Janus dendrimer	Alkylic chains	**Lc (%)**
$(NH_3^+)_8$[GMPA]-[MPA]$(C17)_2$	2468	479	19.4
$(NH_3^+)_8$[GMPA]-[MPA]$(C17)_4$	3233	958	29.6
$(NH_3^+)_8$[MPA]-[GMPA]$(C17)_2$	2240	479	21.4
$(NH_3^+)_8$[MPA]-[GMPA]$(C17)_4$	3233	958	29.6

2.2.1. Synthesis and characterisation of the Janus dendrimers

The synthesis of the four amphiphilic Janus dendrimers from their constituent dendrons was achieved by means of the by copper(I)-catalysed Alkyne-Azide Cycloaddition (CuAAC) reaction and the subsequent removal of the *t*-Boc protecting moieties in acidic conditions, as gathered in Scheme 2.6.

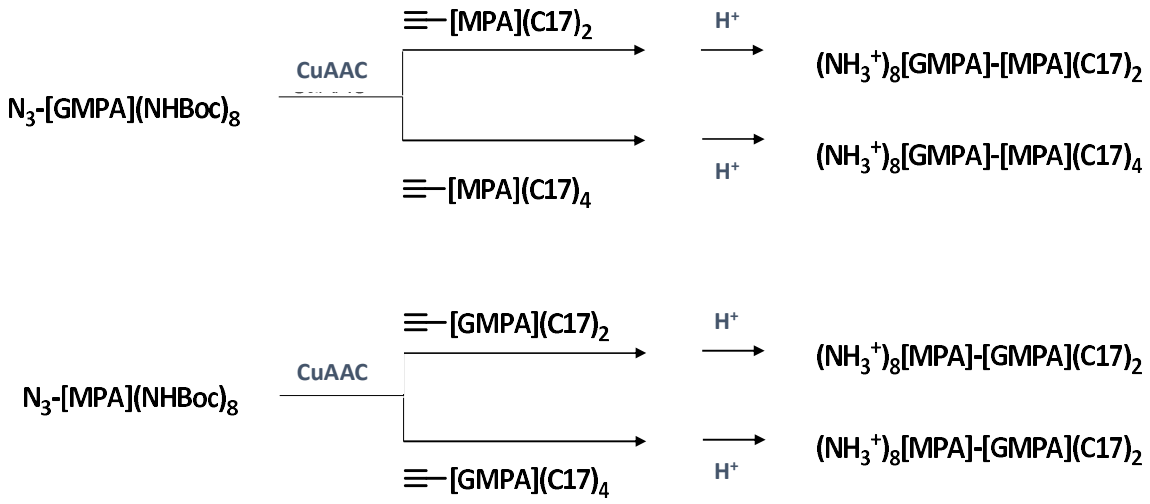

Scheme 2.6. Schematic pathway for the synthesis of the four amphiphilic Janus dendrimers.

For that purpose, the hydrophilic *t*-Boc protected and azide-functionalised dendrons were allowed to react with an excess of the corresponding lipophilic alkyne-containing dendron in dry DMF at 45 ºC (**general procedure IX**). Copper(I) was obtained *in situ* by reduction of copper(II) sulphate by (*L*)-sodium ascorbate. Tris[(1-benzyl-1*H*-1,2,3-triazol-4-yl)methyl]amine (TBTA) was added to the reaction mixture to increase the stability of copper(I), since this catalytic strategy has proven to be advantageous for the synthesis of dendrimers[10]. Additionally, after 24-48 h of reaction, an excess of Merrifield's peptide resin modified with azide groups was added to the reaction mixture to remove unreacted alkynes. The product purification was accomplished by several washing steps first with brine and then with an aqueous solution of KCN to remove the remaining copper species, followed by a flash chromatography on silica gel using a ramp with variable dichloromethane: methanol ratios (depending on the dendrimer polarity).

As last step, the *t*-Boc protecting groups were cleaved under acidic conditions to obtain the corresponding ammonium salts in quantitative yields (**general procedure VI**). Final products were dissolved in methanol and precipitated in cold ether. Finally, they were recovered by pouring the supernatant and the remaining solvent traces were removed under vacuum.

The dendrimers derived from the CuAAC coupling bearing *t*-Boc moieties in the periphery were characterised by ^{1}H NMR, ^{13}C NMR, FTIR spectroscopy, MS and SEC. The final ammonium terminated dendrimers were characterised by ^{1}H NMR, ^{13}C NMR, FTIR spectroscopy and MS. SEC analyses could not be performed with these deprotected dendrimers due to their low solubility in the elution solvent, THF[3]. The final dendrimer $(NH_3^+)_8$[GMPA]-[MPA](C17)$_4$ and its *t*-Boc protected precursor $(NHBoc)_8$[GMPA]-[MPA](C17)$_4$ are here presented as a representative example to discuss the characterisation results (Figure 2.4, Figure 2.5 and Figure 2.6).

The correct click chemistry coupling was confirmed through ^{1}H NMR (Figure 2.4a) by the presence of a peak at 8.07 ppm corresponding to proton H-3 belonging to the triazole ring. Regarding the $(NH_3^+)_8$[GMPA] block, the peaks corresponding to the protons H-2 and H-1 are shifted downfield in comparison with those in the starting dendron (from 3.27 to 4.45 ppm and from 1.61 to 1.95 ppm, respectively). With respect to the [MPA](C17)$_4$ block, the peak corresponding to the protons H-5 is also shifted downfield (from 4.72 to 5.26 ppm) in comparison with the uncoupled dendron. The other signals remain essentially unaltered and a perfect correlation is observed for the signal integrations corresponding to the two blocks. In the ^{13}C NMR spectrum, two peaks corresponding to the carbon atoms of the triazole C-3 and C-4, at 126.4 and 143.5 ppm, respectively, are observed (Figure 2.4b). In addition, two quadruplets centered at 163.1 and 118.2 ppm appeared corresponding to the carbons in the trifluoroacetate counterion (TFA^-) resulting from the deprotection method employed. Specifically, the quadruplet downfield corresponds to the carbon of the carbonyl group and the quadruplet with the highest coupling constant observed at 118.2 ppm is due to the quaternary carbon directly linked to the three fluoride atoms.

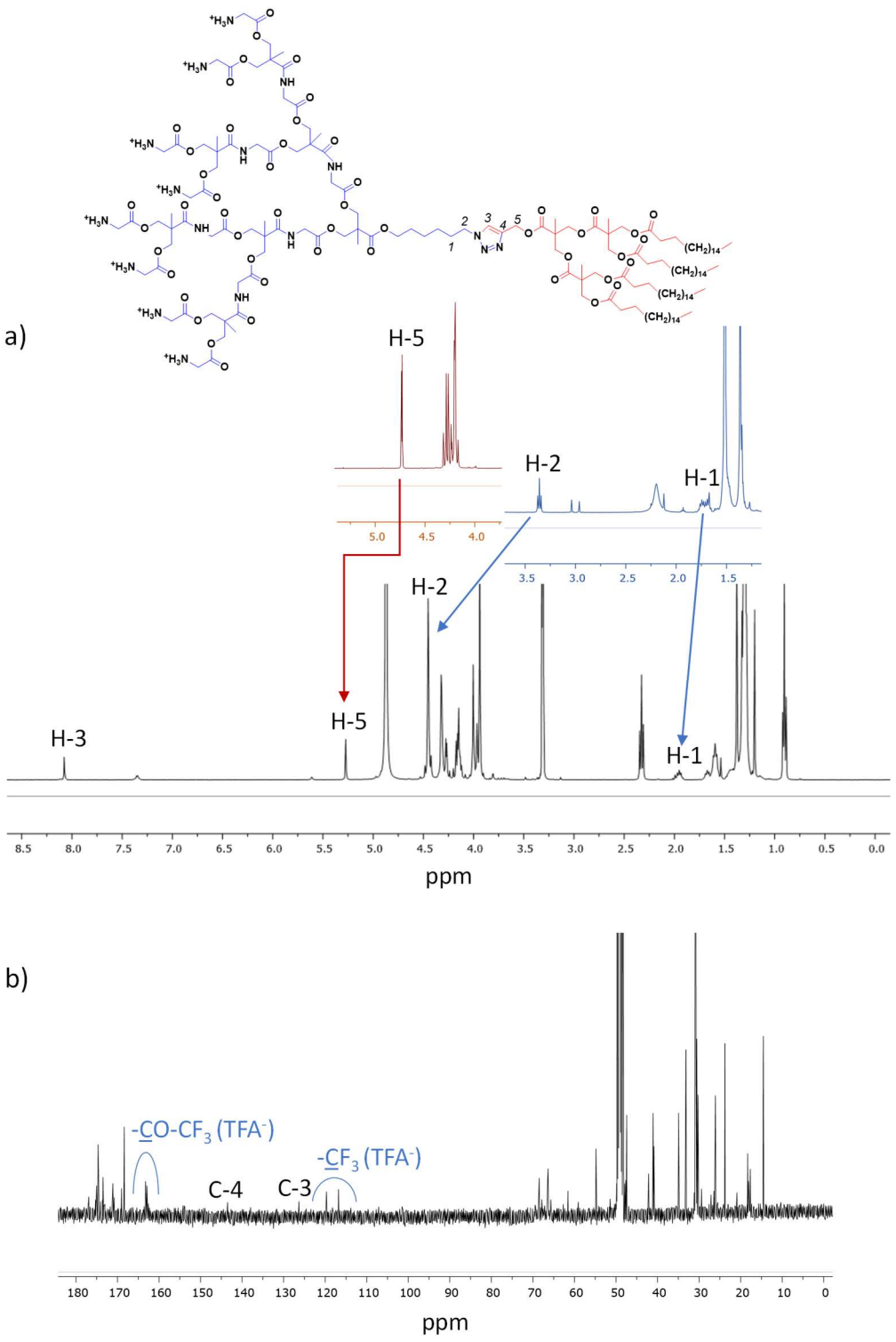

Figure 2.4. Chemical characterisation of the dendrimer $(NH_3^+)_8$[GMPA]-[MPA](C17)$_4$. a) ^{1}H NMR spectrum (CD_3OD, 400 MHz). Main chemical shifts of key signals with respect to those in the starting dendrons are also indicated with coloured fragments of each spectrum ($CDCl_3$, 400 MHz) and b) ^{13}C NMR spectrum (CD_3OD, 100 MHz).

FTIR spectroscopy showed that bands corresponding to the stretching vibrations of the azide (–N=N$^+$=N$^-$, 2106 cm^{-1}) and alkyne (≡C–H, 3292 cm^{-1} and –C≡C–, 2141 cm^{-1}) functional groups observed in the corresponding dendrons, before coupling, were not observed in the Janus dendrimer, thus indicating the formation of the triazole ring (Figure 2.5).

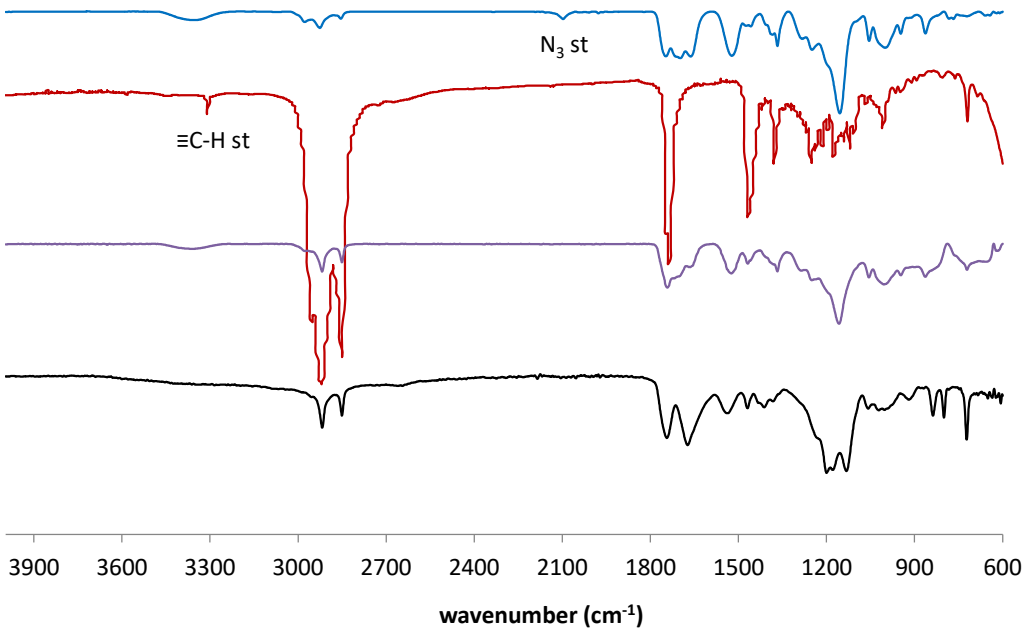

Figure 2.5. FTIR spectra in transmission mode of the dendrimer $(NH_3^+)_8$[GMPA]-[MPA](C17)$_4$ (black), the t-Boc protected dendrimer $(NHBoc)_8$[GMPA]-[MPA](C17)$_4$ (purple), and its two precursor dendrons, N_3-[GMPA]$(NHBoc)_8$ (blue) and ≡-[MPA](C17)$_4$ (red).

The molecular peaks of the dendrimers plus hydrogen and/or plus sodium were observed in the MS spectra (Figure 2.6a). Specifically, two peaks were found for $(NH_3^+)_8$[GMPA]-[MPA](C17)$_4$ dendrimer at 3225.1 (100% in intensity) and 3247.2 (92% in intensity), corresponding to the m/z ratio of the molecule ionised with hydrogen and sodium, respectively (Figure 2.6a, green spectra). Additionally, the monodispersity of the Janus dendrimers protected with *t*-Boc moieties was confirmed by SEC (Figure 2.6b). This technique showed a single and symmetrical monomodal peak for each dendrimer and also allowed us to confirm the absence of unreacted dendrons.

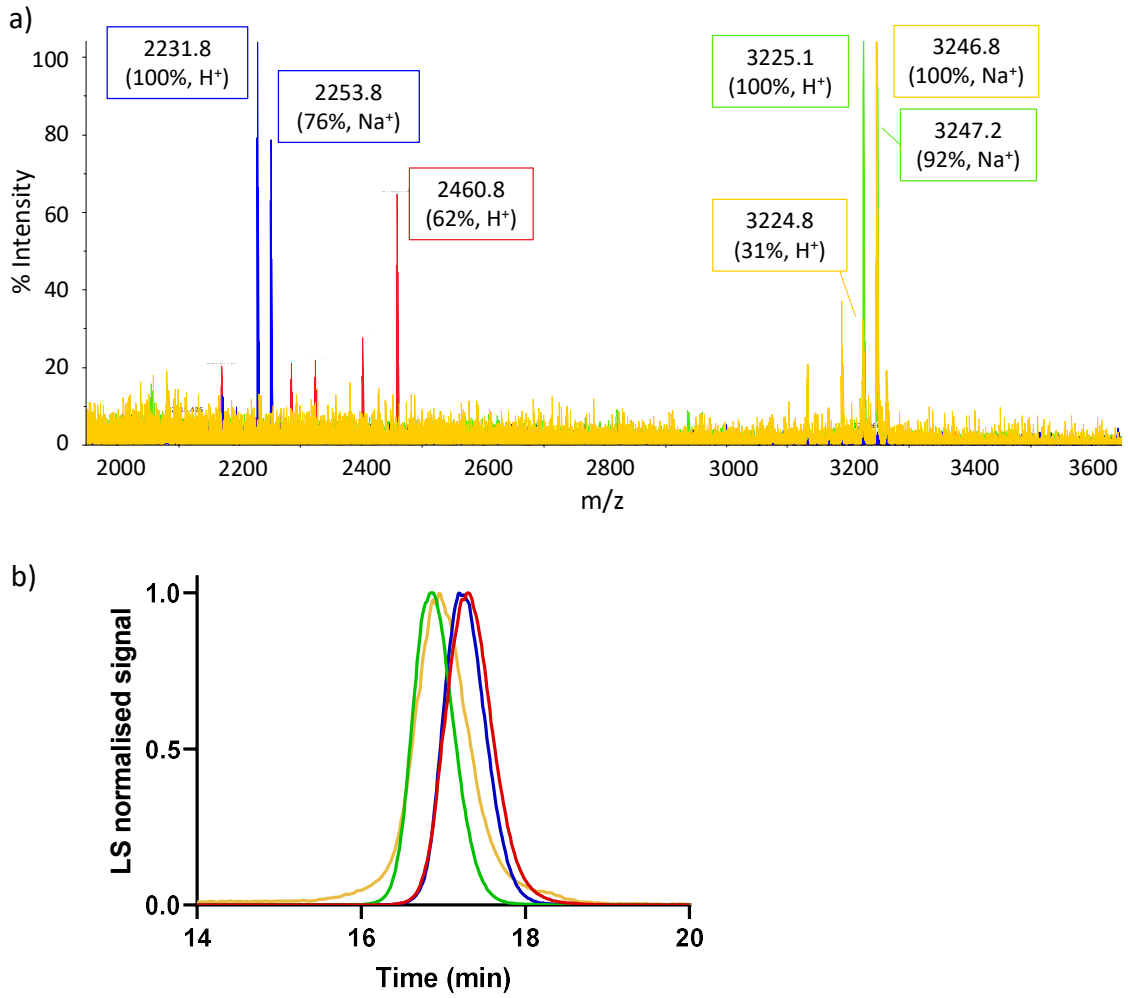

Figure 2.6. Characterisation of the four amphiphilic Janus dendrimers: a) MS spectra of the Janus dendrimers and b) SEC chromatograms of the t-Boc protected Janus dendrimers. LS: light scattering. Colour code: $(NH_3^+)_8$[GMPA]-[MPA](C17)$_2$, red; $(NH_3^+)_8$[GMPA]-[MPA](C17)$_4$, green; $(NH_3^+)_8$[MPA]-[GMPA](C17)$_2$, blue; $(NH_3^+)_8$[MPA]-[GMPA](C17)$_4$, yellow.

2.2.2. Janus self-assembly in water

The different combination of the chemical groups in the structures of the Janus dendrimers, apart from determining the lipophilic content of each dendrimer is also expected to influence the self-assembly behaviour of the Janus dendrimers and presumably, their drug loading ability and their capacity to deliver the drug in target cells in further applications.

The amphiphilic nature of these dendrimers can favour their spontaneous self-assembly in water, where the lipophilic blocks are expected to remain in the inner cavity due to hydrophobic interactions, whereas the outer side of the aggregate

would be preferentially composed by the hydrophilic blocks. Interestingly, the size and morphology of these aggregates have been shown to be reliant on the method employed for its preparation[11] and lots of efforts have been made to understand the molecules arrangement into the aqueous phase[12,13]. Some aggregate's formation methods commonly used include the film rehydration, the solvent injection, the oil-in-water emulsion or microfluidic approaches, among others.

Here, the oil-in-water method[14] has been employed to prepare the dendrimer aggregates of each amphiphilic Janus dendrimer using dichloromethane as organic solvent due to its immiscibility with water and its ability to easily evaporate. Briefly, each dendrimer was dissolved at a concentration of 1 mg/mL in dichloromethane and milliQ water was added in the appropriate volume to obtain a final concentration of 1 mg/mL. The organic solvent was completely evaporated by stirring the mixtures at room temperature with an orbital shaker under ventilation inducing the assembly of the amphiphilic molecules into the aqueous phase.

Critical aggregation concentration (CAC)

The required concentration to ensure the presence of aggregates in water was assessed by determining the critical aggregation concentration (CAC) of all the dendrimers using nile red as a solvatochromic fluorophore[15]. The solutions of the Janus dendrimers were prepared at different concentrations in the range from $1 \cdot 10^{-5}$ to 1 mg/mL, and the same amount of nile red in ethanol was added to each dendrimer solutions. After stirring the resulting solutions in the dark, the emission spectrum was recorded (λ_{max} = 635 nm and λ_{exc} = 550 nm), and the CAC was determined from the plots representing the fluorescence emission intensity of nile red as a function of the dendrimer concentration (Figure 2.7). The change of the curve slope on the graphs corresponds to the beginning of the lipophilic domain formation. The CAC for the studied Janus dendrimers are gathered in the Table 2.2 and the values are between $6.9 \cdot 10^{-6}$ and $1.2 \cdot 10^{-5}$ M, which is consistent with related dendritic structures previously reported[8].

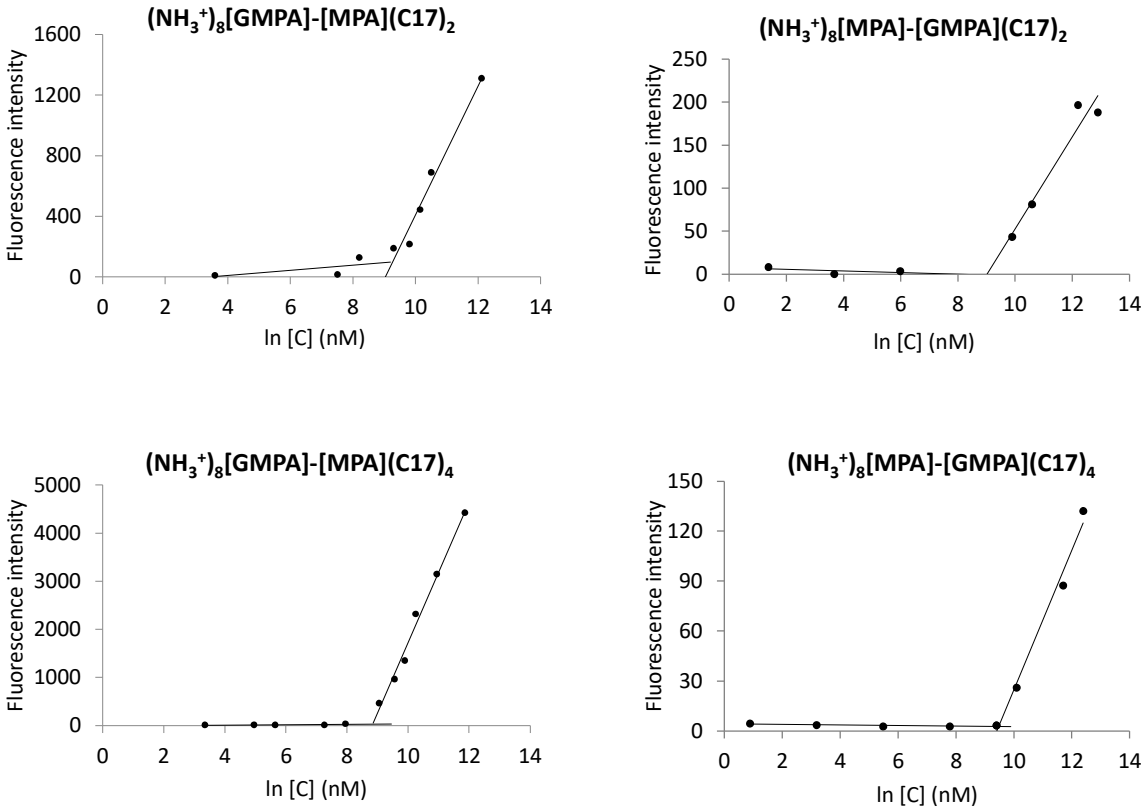

Figure 2.7. Determination of the CAC of all the Janus dendrimers by the nile red method.

Table 2.2. Critical aggregation concentration (CAC) calculations for the amphiphilic Janus dendrimers, in M.

Janus dendrimer	CAC (M)
$(NH_3^+)_8$[GMPA]-[MPA](C17)$_2$	$1.1 \cdot 10^{-5}$
$(NH_3^+)_8$[GMPA]-[MPA](C17)$_4$	$6.9 \cdot 10^{-6}$
$(NH_3^+)_8$[MPA]-[GMPA](C17)$_2$	$8.1 \cdot 10^{-6}$
$(NH_3^+)_8$[MPA]-[GMPA](C17)$_4$	$1.2 \cdot 10^{-5}$

Morphological characterisation of the aggregates

The morphology of the aggregates formed by the amphiphilic Janus dendrimers in water was studied by TEM (Figure 2.8) and their hydrodynamic diameter, D_H, was determined by DLS (Table 2.3). Dendrimers $(NH_3^+)_8$[GMPA]-[MPA](C17)$_2$, $(NH_3^+)_8$[GMPA]-[MPA](C17)$_4$, and $(NH_3^+)_8$[MPA]-[GMPA](C17)$_2$ appeared as rounded micelles in TEM images, with a homogenous size distribution, and DLS measurements gave number average D_H values of 9±1, 24±1 and 17±3 nm, respectively. Longer aggregates resembling cylindrical micelles were observed in TEM for $(NH_3^+)_8$[MPA]-[GMPA](C17)$_4$, which gave number average D_H values of 34±5 nm in DLS. The aggregates formed by the Janus dendrimers deprotected by the HCl/ethyl acetate method are shown in Annexe 1 and exhibit the same morphology.

The assembly behaviour in water of the amphiphilic dendrimers can be related to their lipophilic content (Lc) previously calculated (Table 2.1). The two dendrimers with two stearate chains, $(NH_3^+)_8$[GMPA]-[MPA](C17)$_2$ and $(NH_3^+)_8$[MPA]-[GMPA](C17)$_2$, show spherical morphology corresponding to similar and low Lc values of 19.4 and 21.4, respectively. On the other hand, both $(NH_3^+)_8$[GMPA]-[MPA](C17)$_4$ and $(NH_3^+)_8$[MPA]-[GMPA](C17)$_4$ form bigger aggregates and, interestingly, these two dendrimers assemble in a different morphology despite they display the same Lc (Lc = 29.6). In this case, the different position of the poly(esteramide) (GMPA) and polyester (MPA) dendrons with respect to the hydrophilic amino groups and lipophilic stearic acid chains seems to be responsible for the different micellar morphologies: spherical for $(NH_3^+)_8$[GMPA]-[MPA](C17)$_4$ and cylindrical for $(NH_3^+)_8$[MPA]-[GMPA](C17)$_4$. This suggests that the presence of amide groups in the GMPA dendron makes it more hydrophilic than MPA and hence their integration next to the hydrophilic outer ammonium groups enhances the hydrophilicity of this dendritic face of the Janus dendrimer. Accordingly, whereas $(NH_3^+)_8$[GMPA]-[MPA](C17)$_4$ presents a well-defined Janus structure (with two well differentiated hydrophilic and hydrophobic faces), $(NH_3^+)_8$[MPA]-[GMPA](C17)$_4$ shows an alternated sequence hydrophilic ammonium-MPA-GMPA-hydrophobic aliphatic chains which results in a less defined Janus structure. This can disrupt the hydrophobic core of rounded micelles towards wormlike micelles with bigger space occupied by the inner part

of the Janus molecules. This disrupting effect in the core of the spherical micelles is not as significant for $(NH_3^+)_8$[MPA]-[GMPA](C17)$_2$, but it could also explain why this dendrimer gives micelles almost twice in size than $(NH_3^+)_8$[GMPA]-[MPA](C17)$_2$ in spite of their similar Lc and MW.

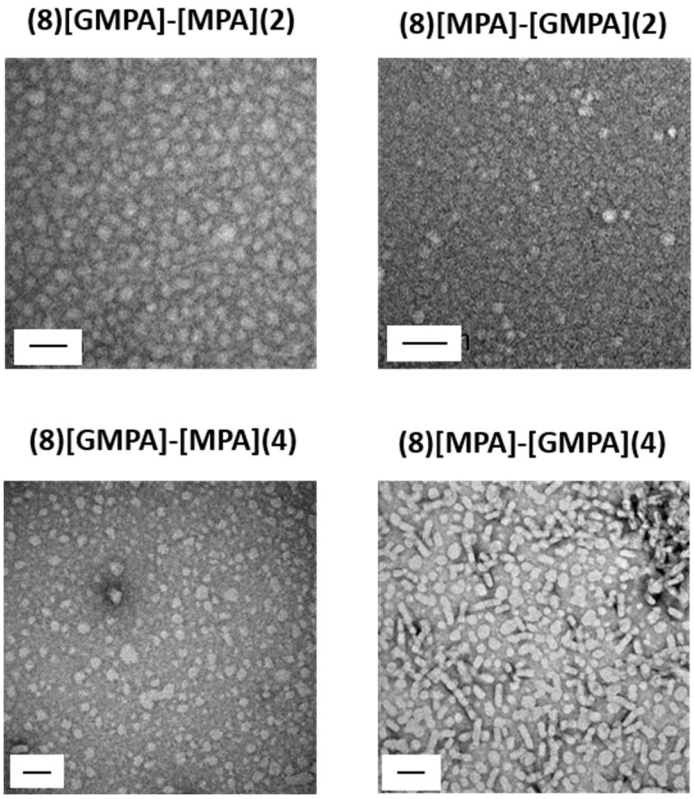

Figure 2.8. TEM images of the amphiphilic Janus aggregates obtained by the oil-in-water method. Scale bars: 50 nm.

Table 2.3. Average hydrodynamic diameters (D_H), in nm, of the dendritic aggregates measured by DLS and morphological shape observed in TEM images.

Janus dendrimer	D_H (nm)	morphology
$(NH_3^+)_8$[GMPA]-[MPA](C17)$_2$	9 ± 1	spherical micelles
$(NH_3^+)_8$[GMPA]-[MPA](C17)$_4$	24 ± 1	spherical micelles
$(NH_3^+)_8$[MPA]-[GMPA](C17)$_2$	17 ± 3	spherical micelles
$(NH_3^+)_8$[MPA]-[GMPA](C17)$_4$	34 ± 5	cylindrical micelles

2.3. Dendronized hyperbranched polymers (DHPs)

The dendronized hyperbranched polymers (DHPs) or pseudodendrimers[16] constitute the other type of dendritic structures designed in this thesis. These globular dendritic derivatives are large molecules consisting of a commercial polyester core of *bis*-MPA surrounded by multiple dendrons either of *bis*-MPA or *bis*-GMPA. The number of functional groups in the periphery exponentially grows when increasing the core or the dendron generations. In our case, the amount of desired amino-terminal groups was modulated by varying the core generation (G2, G3 or G4) while maintaining the second generation in the *bis*-MPA or *bis*-GMPA dendrons attached. In this way, a group of six DHPs have been synthesised, which can be classified into two series according to the constituent dendron (see Figure 2.9):

bis-MPA series:

- **DHP(G2)-MPA** that consists of a hyperbranched core of 2nd generation surrounded by *bis*-MPA dendrons, with a total of 64 theoretical amino terminal groups.
- **DHP(G3)-MPA** that consists of a hyperbranched core of 3rd generation surrounded by *bis*-MPA dendrons, with a total of 128 theoretical amino terminal groups.
- **DHP(G4)-MPA** that consists of a hyperbranched core of 4th generation surrounded by *bis*-MPA dendrons, with a total of 256 theoretical amino terminal groups.

bis-GMPA series:

- **DHP(G2)-GMPA** that consists of a hyperbranched core of 2nd generation surrounded by *bis*-GMPA dendrons, with a total of 64 theoretical amino terminal groups.
- **DHP(G3)-GMPA** that consists of a hyperbranched core of 3rd generation surrounded by *bis*-GMPA dendrons, with a total of 128 theoretical amino terminal groups.

- **DHP(G4)-GMPA** that consists of a hyperbranched core of 4th generation surrounded by *bis*-GMPA dendrons, with a total of 256 theoretical amino terminal groups.
-

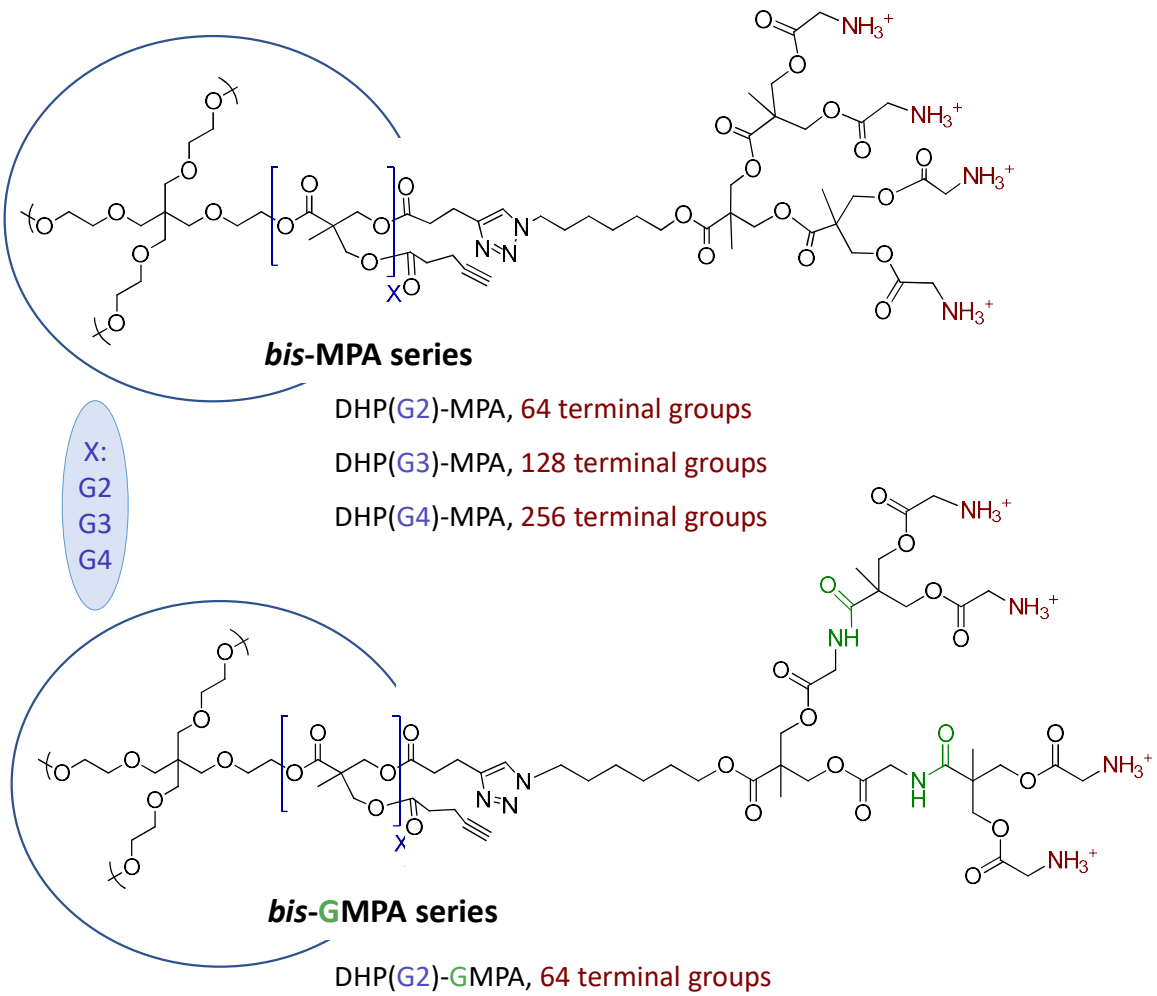

Figure 2.9. Chemical structures of the six DHPs grouped into two series, the bis-MPA and the bis-GMPA series.

2.3.1. Synthesis and characterisation of the DHPs

The attachment of dendrons to a hyperbranched core yielding the dendronized hyperbranched polymers (DHPs) allowed to obtain large molecules with a high number of amino-terminal groups in a feasible way. This strategy employed for the synthesis of the DHPs rendered structures with similar properties to those of the high generation dendrimers, with the advantage of the lower synthetic effort required[16–18].

The series of DHPs were obtained by following the synthetic steps previously reported in our group[19] and schematised in Scheme 2.7. Firstly, the commercial hyperbranched polyesters of the different generations (G2, G3 or G4) were functionalised with 4-pentynoic acid by means of Steglich's esterification to introduce alkyne groups in the periphery of the structures (**general procedure X**). These functional groups were essential to accomplish the subsequent convergent coupling of the corresponding dendron through the azide focal groups by means of the azide-alkyne 1,3-dipolar cycloaddition catalysed by Cu (I) (CuAAC) (**general procedure XI**). As in the synthesis of the Janus dendrimers, Cu (I) was obtained *in situ* from the reduction of Cu (II) in presence of *L*-ascorbate, and the tertiary amine TBTA was used to stabilise the catalytic species and favour the progress of the reaction. Finally, the *t*-Boc protecting groups were removed under acidic conditions with a mixture of $CHCl_3$:TFA (see **general procedure VI**) to obtain the amino-terminated pseudodendrimers as white solids. Note that final deprotected products are named in Scheme 2.7 as DHP(Gx)-MPA(NH_3^+) or DHP(Gx)-GMPA(NH_3^+), but they will be referred as DHP(Gx)-MPA or DHP(Gx)-GMPA in the text to simplify the nomenclature.

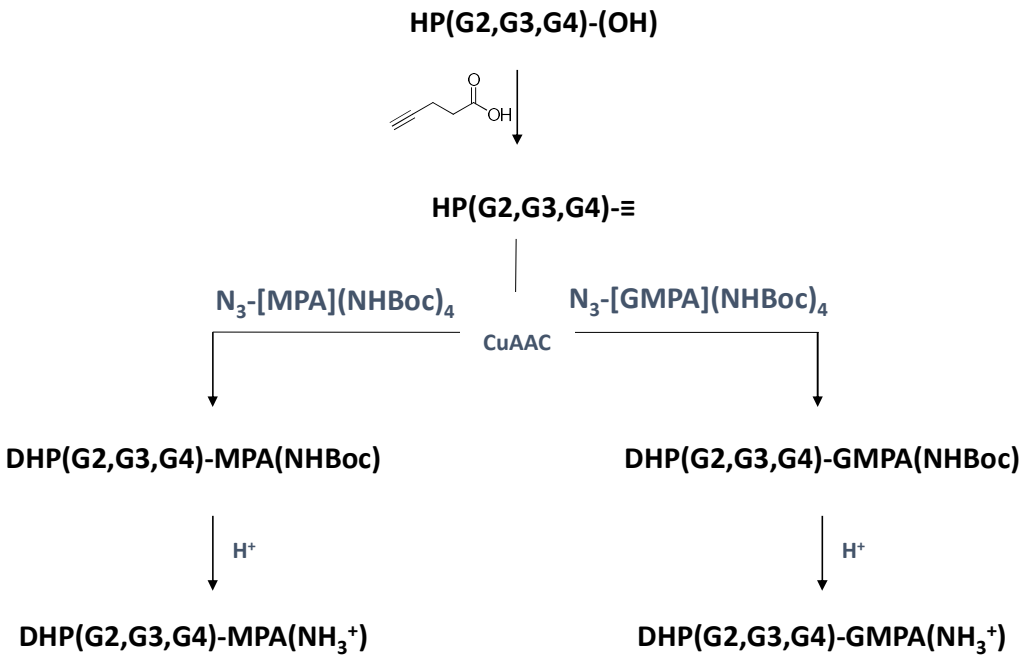

Scheme 2.7. Schematic pathway for the synthesis of the six DHPs of the bis-MPA (left) or the bis-GMPA (right) series.

All products were characterised by ^{1}H NMR, ^{13}C NMR, FTIR spectroscopy and SEC, except the final ammonium terminated DHPs, whose low solubility in the elution solvent, THF, made them not adequate to perform this chromatographic SEC analysis[3]. The pseudodendrimer DHP(G2)-MPA and their corresponding precursors, the *t*-Boc protected DHP(G2)-MPA(NHBoc) and the alkyne functionalised hyperbranched core HP(G2)-≡, are here presented as a representative example to discuss the characterisation results.

NMR spectroscopic characterisation allowed to confirm the correct product formation as well as to quantify the number of groups inserted. The alkyne incorporation was confirmed by the appearance of three peaks in the ^{1}H NMR spectrum at 2.55, 2.47 and 1.99 ppm comparing with the commercial HP, that correspond to the protons H-10', H-11' and H-13', respectively (Figure 2.10a). Moreover, their integration with respect to the unaltered methyl group in the *bis*-MPA core (H-7') at 1.24 ppm revealed that 15, 31 or 62 alkyne groups were introduced for each HP generation (G2, G3 or G4), respectively. High levels of functionalisation were reached, as observed in previous works[19], considering that

the maximum theoretical ending groups are 16, 32 and 64 for each HP generation.

After the CuAAC reaction, the ^{1}H NMR spectrum showed a chemical shift downfield of the protons adjacent to the alkyne groups as well as the inversion of their signals (Figure 2.10b). Namely, H-10' and H-11' peaks moved from 2.55 and 2.47 ppm to H-11 at 2.98 ppm and H-10 at 2.72 ppm when coupled to the dendrons. The integration of these downfield protons of the methylene signals (H-10 and H-11) and their comparison to the remaining not functionalised ones (H-10' and H-11') if any, allowed to determine the number of dendrons covalently linked by the CuAAC reaction. Apart from these modifications in the former ^{1}H NMR signals, the result of the coupling reaction could be observed by the appearance of a peak at 7.41 ppm that corresponds to the proton of the triazole ring, H-13, resulting from the cycloaddition (Figure 2.10b). The appearance of two peaks at 146.1 ppm and 121.3 ppm in the ^{13}C NMR spectrum corresponding to the triazole carbons C-12 and C-13, respectively, also corroborates the success of the coupling reaction (Figure 2.10c). According to this characterisation, the *t*-Boc protected pseudodendrimers were estimated to bear a total number of terminal amino groups as follows: the *bis*-MPA series (DHP(G2)-MPA(NHBoc), DHP(G3)-MPA(NHBoc) and DHP(G4)-MPA(NHBoc)) contained 60, 124 and 248, respectively, whereas the *bis*-GMPA series (DHP(G2)-GMPA(NHBoc), DHP(G3)-GMPA(NHBoc) and DHP(G4)-GMPA(NHBoc)) respectively included 60, 116 and 232. These slight differences between the two series degree of functionalisation in the highest HP generations could be due to steric impediments in the case of the *bis*-GMPA dendrons that may hinder the dendron access to the inner alkyne groups. Anyway, high levels of dendron attachment were reached for both series, estimated as 100% for the *bis*-MPA and higher than 94% for the *bis*-GMPA series.

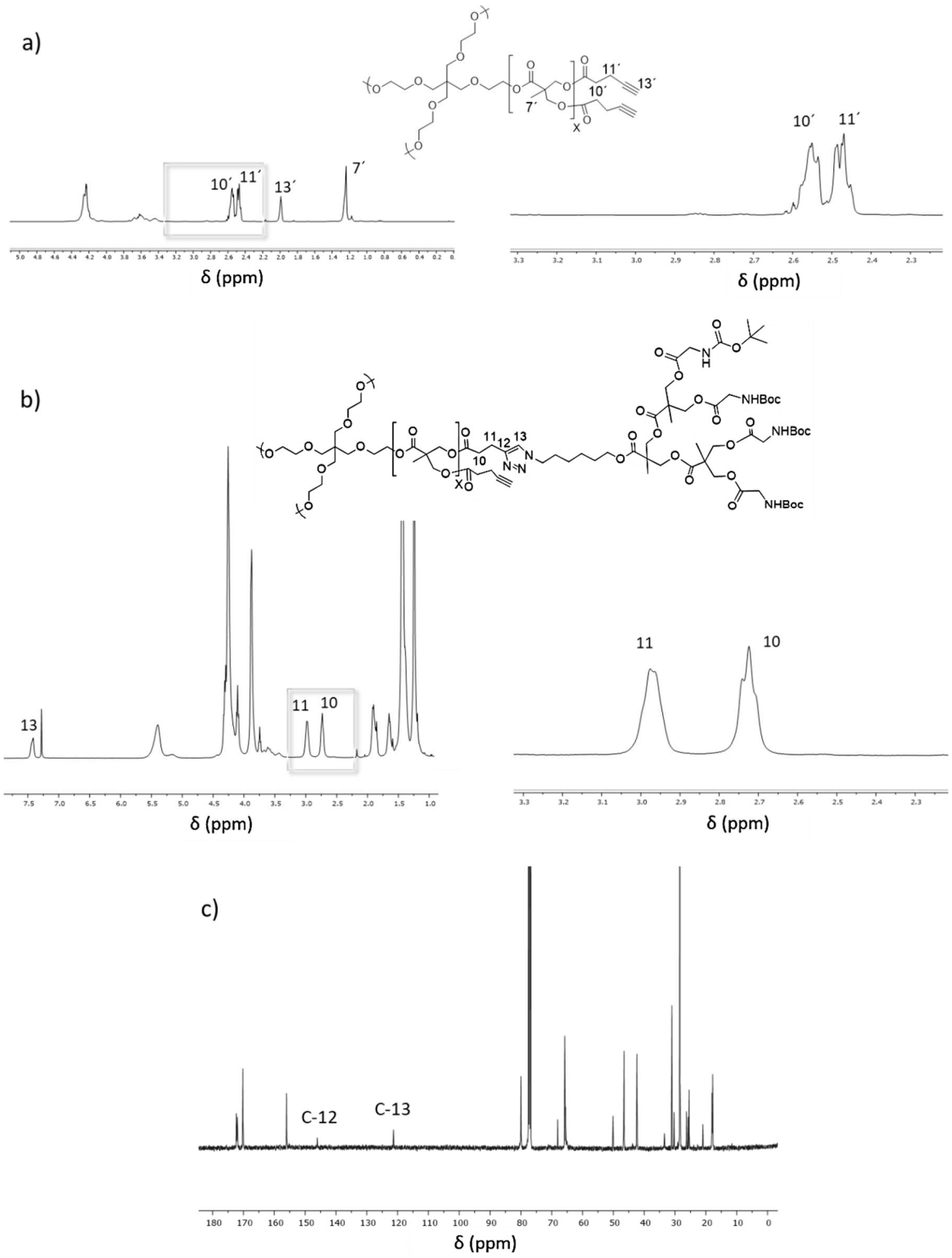

Figure 2.10. Chemical structures and shifts in ^{1}H NMR of a) HP(G2)-≡ and b) DHP(G2)-MPA(NHBoc) ($CDCl_3$, 400 MHz). Full spectra are represented in the left side, while enlargements from 3.3 to 2.3 ppm corresponding to the spectra section indicated within the boxes are represented in the right side. c) ^{13}C NMR spectrum ($CDCl_3$, 100 MHz) of DHP(G2)-MPA(NHBoc).

Further characterisation techniques were carried out to confirm the formation of the pseudodendrimers. In the FTIR spectra of DHP(G2)-MPA(NHBoc), a band at 3375 cm^{-1} corresponding to the N-H bond stretching appeared and two almost overlapped intense bands around 1700 cm^{-1} (1731 and 1710) were due to the C=O bonds of the ester groups and the carbamate groups, respectively (Figure 2.11). In addition, the bands corresponding to the stretching of the ≡C-H and C≡C bonds of the HP(G2)-≡ (3281 and 2145, respectively) and the band at 2100 cm^{-1} corresponding to the azide group of the dendron were no longer observed, thus indicating the correct coupling to the dendrons.

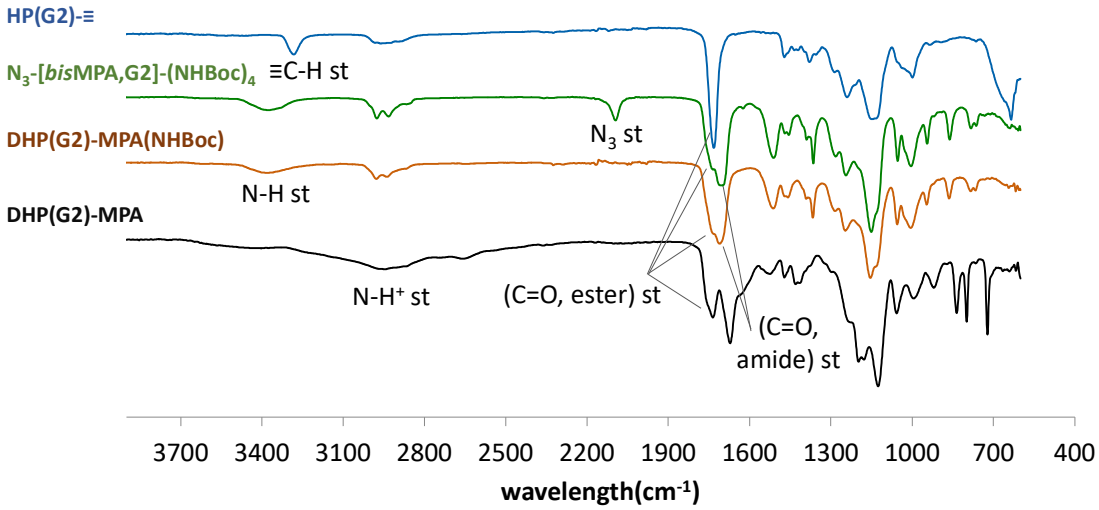

Figure 2.11. Compilation of FTIR spectra in transmission mode of HP(G2)-≡ core (blue), N_3-[bisMPA,G2]-$(NHBoc)_4$ dendron (green), DHP(G2)-MPA(NHBoc) (orange) and deprotected DHP(G2)-MPA (black).

SEC analysis of the *t*-Boc protected DHPs revealed the absence of any remaining free reactive or dendron as well as a considerable reduction in the polydispersity of the hyperbranched cores. The polydispersity values for all the *t*-Boc protected pseudodendrimers range from 1.12 to 1.23. The chemical differences between the DHPs and the polymer employed as standard reference (PMMA) may be translated into a different hydrodynamic volume and then, it is not possible to stablish a direct correlation between the retention time observed in SEC and the Mw of the molecules. However, a qualitative analysis of these data allows to infer that the decrease in the retention times comparing the

pseudodendrimers with the hyperbranched cores without dendrons covalently added is due to an increase in the Mw, as it was expected (Figure 2.12). The SEC chromatograms of the HPs functionalised with alkyne groups are shown in Annexe 2.

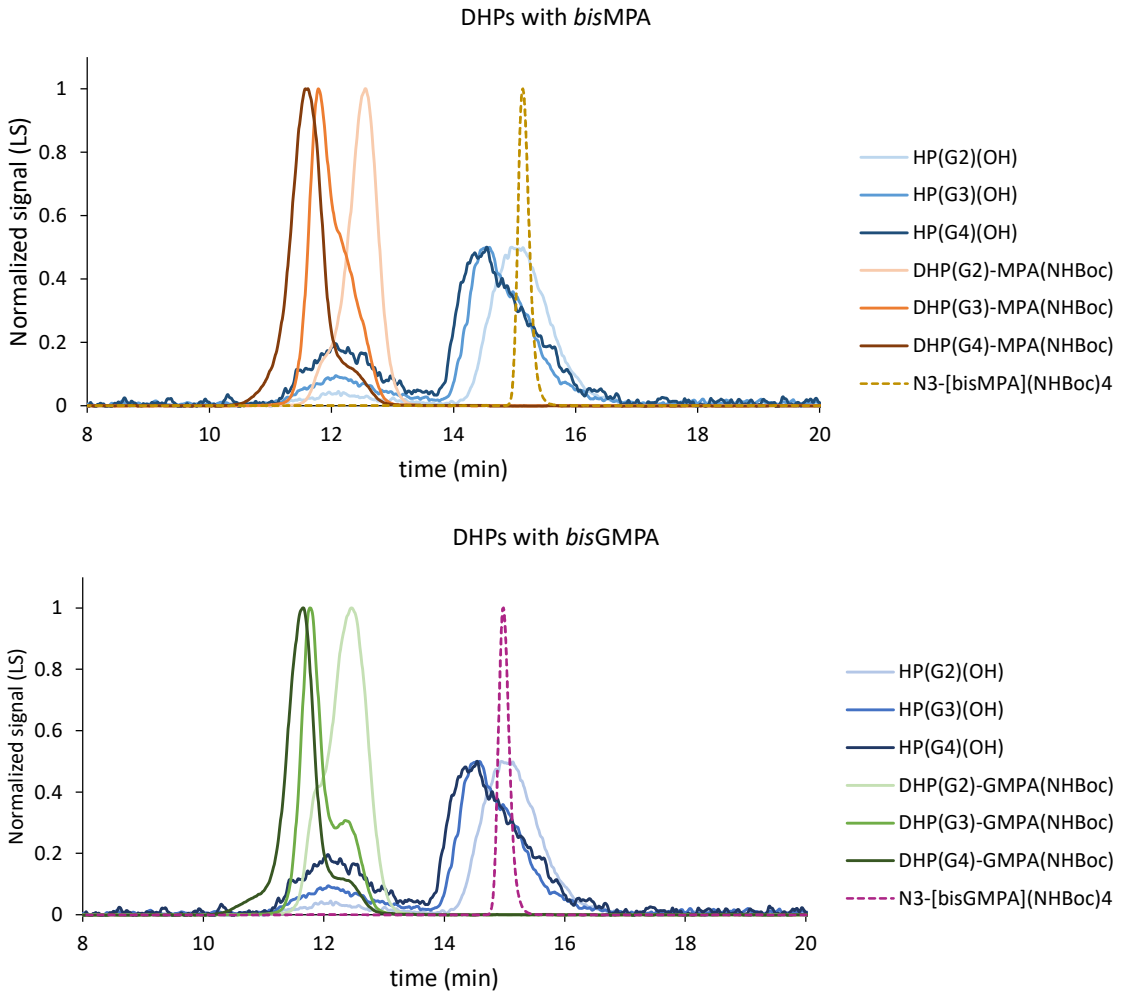

Figure 2.12. SEC chromatograms overlap of the two series of final t-Boc protected DHPs and its constituents. Above: HP(G2,G3,G4)(OH) (blue), DHP(G2,G3,G4)-MPA(NHBoc) (orange) and N_3-[bisMPA,G2]-$(NHBoc)_4$ (yellow). Below: HP(G2,G3,G4)(OH) (blue), DHP(G2,G3,G4)-GMPA(NHBoc) (green) and N_3-[bisGMPA,G2]-$(NHBoc)_4$ (purple). LS: light scattering.

The final cleavage of the *t*-Boc groups to yield the amino terminated DHP was assessed by the evolution of some signals in the NMR and FTIR spectra. On the one hand, the peak at 1.43 ppm in ^{1}H NMR and those at 156.0, 80.0 and 28.4 ppm in ^{13}C NMR corresponding to the *t*-Boc groups disappeared in these spectra (Figure 2.13a and b). In return, two quadruplets centered at 163.0 and 118.2 ppm

appeared corresponding to the carbons in the trifluoroacetate counterion (TFA^-) resulting from the deprotection method employed. Specifically, the quadruplet downfield corresponds to the carbon of the carbonyl group and the quadruplet with the highest coupling constant observed at 118.2 ppm is due to the quaternary carbon directly linked to the three fluoride atoms (Figure 2.13b). The presence of the counterion was also corroborated by ^{19}F NMR analyses (Figure 2.13c).

Regarding FTIR spectra, the removal of the *t*-Boc moieties implied the disappearance of the NC=O st band at 1710 cm^{-1} observed in DHP(G2)-MPA(NHBoc) (see Figure 2.11, black spectrum). Besides, the N-H st band around 3000 cm^{-1} got wider and more intense as a consequence of the protonation of the terminal amines.

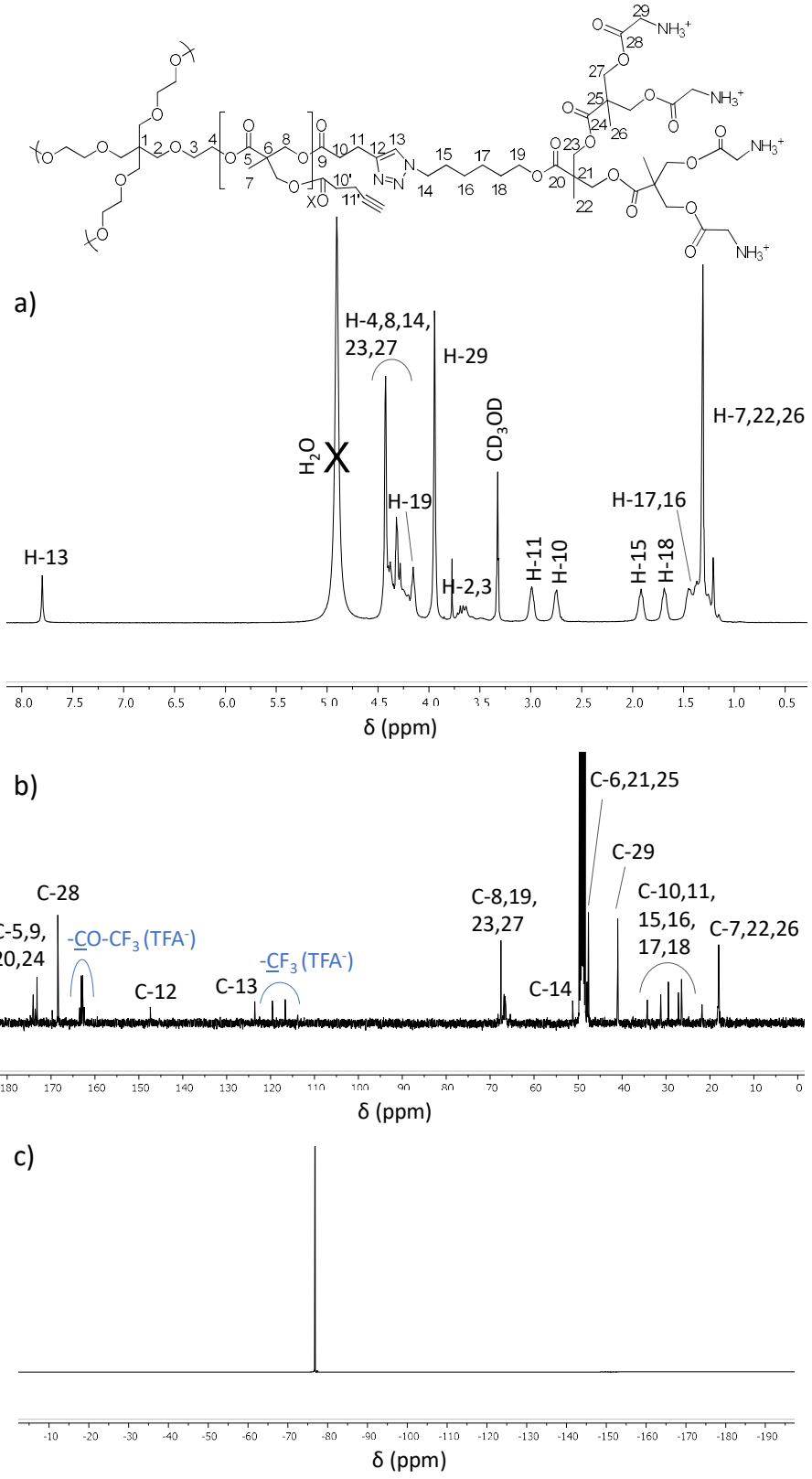

Figure 2.13. NMR spectroscopic characterisation of DHP(G2)-MPA: a) ^{1}H NMR spectrum (CD_3OD, 400 MHz), b) ^{13}C NMR spectrum (CD_3OD, 100 MHz) and c) ^{19}F NMR spectrum (CD_3OD, 376 MHz).

2.3.2. DHPs labelling with a fluorophore

In order to obtain traceable molecules that allow their visualisation during the cellular internalisation process, the DHPs were labelled with the fluorophore rhodamine B (RhB) in an amount estimated to cover around 1% of the terminal functional groups of each DHP (**general procedure XII**).

The covalent bonding took place between the carboxylic acid of the RhB and the terminal amino groups of the DHPs (Scheme 2.8). Firstly, the carboxylic acid of RhB was activated by reaction with 1,1'-carbonyldiimidazole (CDI) in anhydrous dimethylformamide (DMF). Then, the mixture was allowed to react with the terminal amino groups of the DHP dissolved in the same solvent for 24 h at 40 °C[20,21]. The amount of RhB added was selected to obtain a final functionalisation of around 1% of the amino terminal groups of each pseudodendrimer. Purification was developed by three consecutive precipitations into cold ether and further recovery by centrifugation, pouring the supernatant and keeping the pellet obtained. Lastly, products were freeze-dried to obtain the final product as a pink solid.

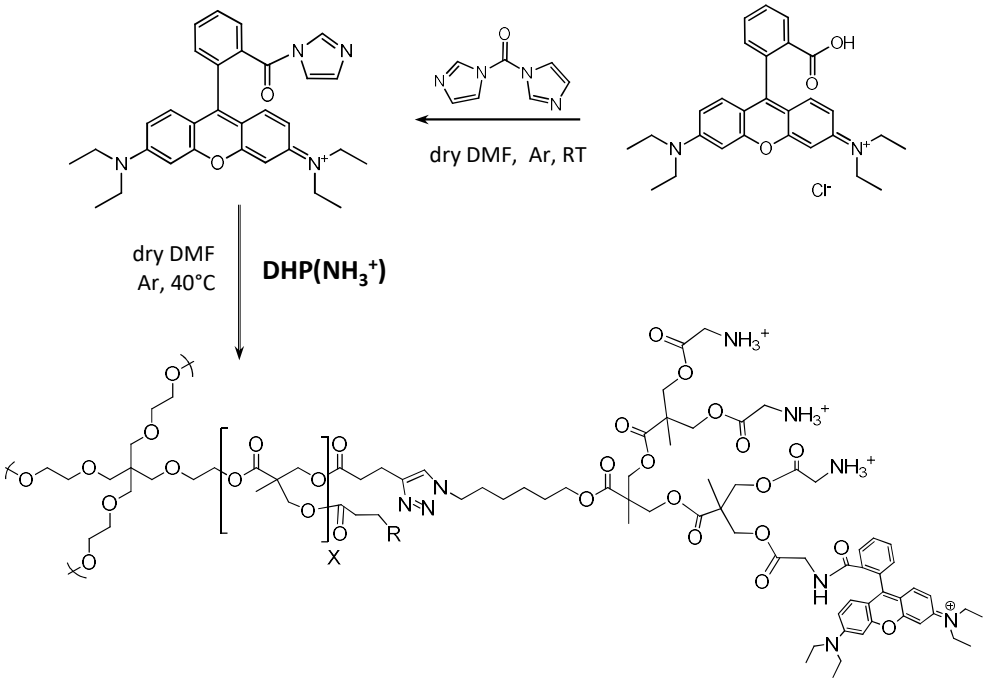

Scheme 2.8. Synthetic procedure for the covalent labelling of a DHP-MPA with rhodamine B.

The correct labelling with RhB was assessed by ^{1}H NMR characterisation (Figure 2.14). The aromatic protons of the fluorophore could be found in the region between 8.5 and 6.2 ppm in the ^{1}H NMR spectra. The methyl groups in β position from the N in the RhB are included in the up-field signal (around 1.29-1.25 ppm) together with the rest of the methyl groups of the pseudodendrimer. The number of RhB molecules in average per DHP was roughly determined by comparing the integration of the signal of the proton of the triazole at 7.8 ppm with the aromatic protons' signals, 10 protons per each RhB molecule. In this way, the degree of RhB functionalisation could be determined as the percentage of terminal amino groups functionalised with the fluorophore. The highest percentages of amino terminal groups functionalised with RhB were found for the DHPs of the smallest generation, DHP(G2)-GMPA-RhB (0.99%) and DHP(G2)-MPA-RhB (0.92%), while the rest of the functionalisation values ranged from 0.89% to 0.48%. It can be then concluded that an amount of the fluorophore within the expected limits and suitable to yield traceable molecules was finally achieved.

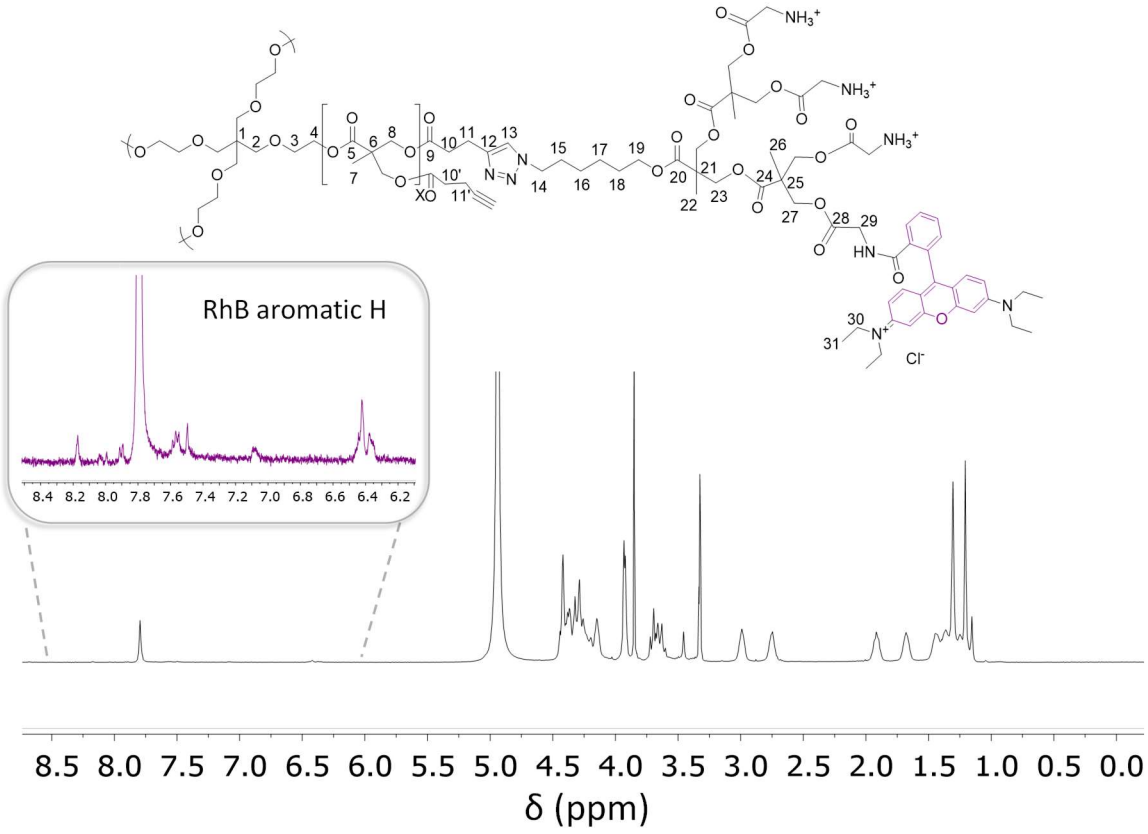

Figure 2.14. ^{1}H NMR spectrum (CD_3OD, 400 MHz) of DHP(G2)-MPA-RhB with ampliation of the 8.4-6.2 ppm region.

2.3.3. DHPs aggregation in water

The synthesised DHPs showed a complete solubilisation in water and the morphology of the resulting aggregates was studied by TEM. The spherical objects observed and their size among 10-20 nm suggest that the DHPs arrange in unimolecular micelles when dissolved in water (Figure 2.15). This unimolecular arrangement has been previously reported for similar hyperbranched polymers based on a core-shell structure[22], although it is also observed that the self-assembly into multi-micelle aggregates tends to occur at higher concentrations[23]. In addition, more compact unimolecular morphologies were observed for the *bis*-GMPA series when comparing with the *bis*-MPA derivatives, thus indicating the presence of intramolecular interactions favoured by the amide groups of the *bis*-GMPA dendrons. These observations were corroborated by DLS measurement of the hydrodynamic diameter (D_H) of the aggregates in water. D_H data analysed in intensity and number are gathered in Table 2.4, and it can be observed that the sizes observed in TEM correlate with the DLS in number, as it has been previously described, while DLS in intensity yields sizes much bigger[24]. Additionally, the ζ potential of the aggregates was measured, showing a positive surface charge in all cases. No relevant differences were found in the surface charge among the DHP of the same series, being around 6.3 for the *bis*-MPA series and around 4.5 for the *bis*-GMPA pseudodendrimers. The difference comparing both series of DHPs could be related to interactions of the terminal amino groups with the inner amide groups of the *bis*-GMPA dendrons that lead to a lesser amount of positive charges exposed to the surface and then, a decrease in their ζ potential is observed.

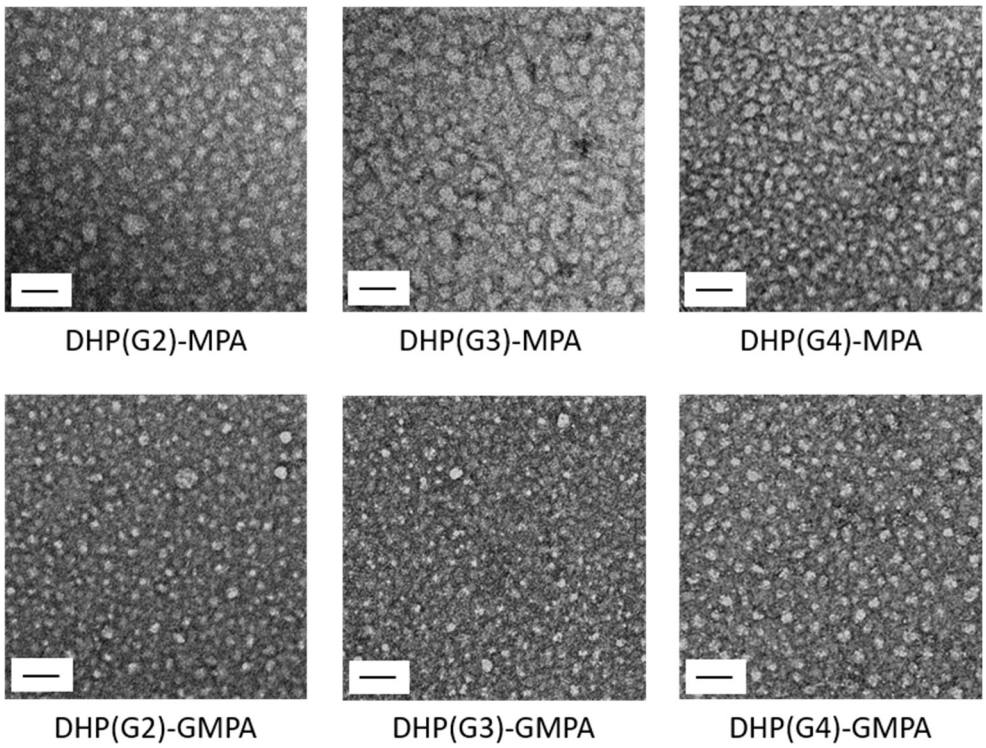

Figure 2.15. TEM images of the DHPs at 1 mg/mL in dH_2O. Scale bars: 50 nm.

Table 2.4. Hydrodynamic diameters (D_H) measured by DLS after intensity or number treatment, and ζ potential values of the DHP aggregates in water.

Pseudodendrimers	D_H intensity (nm)	D_H number (nm)	ζ potential
DHP(G2)-MPA	369 ± 19	12 ± 3	6.8
DHP(G3)-MPA	295 ± 2	15 ± 4	5.9
DHP(G4)-MPA	388 ± 5 (62) 29 ± 1 (38)	18 ± 1	6.1
DHP(G2)-GMPA	274 ± 5	7 ± 1	4.5
DHP(G3)-GMPA	335 ± 36 (90) 18 ± 3 (10)	14 ± 2	4.3
DHP(G4)-GMPA	265 ± 13 (76) 18 ± 4 (24)	9 ± 2	4.7

On the other hand, the structures formed in water by the DHPs labelled with RhB were also characterised by TEM (Figure 2.16). Similar rounded micelles were observed in this case but interestingly, more defined aggregates and slightly bigger in size were obtained after the attachment of a small amount of the fluorophore into the surface of the DHPs. Remarkably, these morphological changes were more prominent in the case of the *bis*-GMPA series of DHPs, where the increase in the size with respect to the non-labelled homologues is noteworthy.

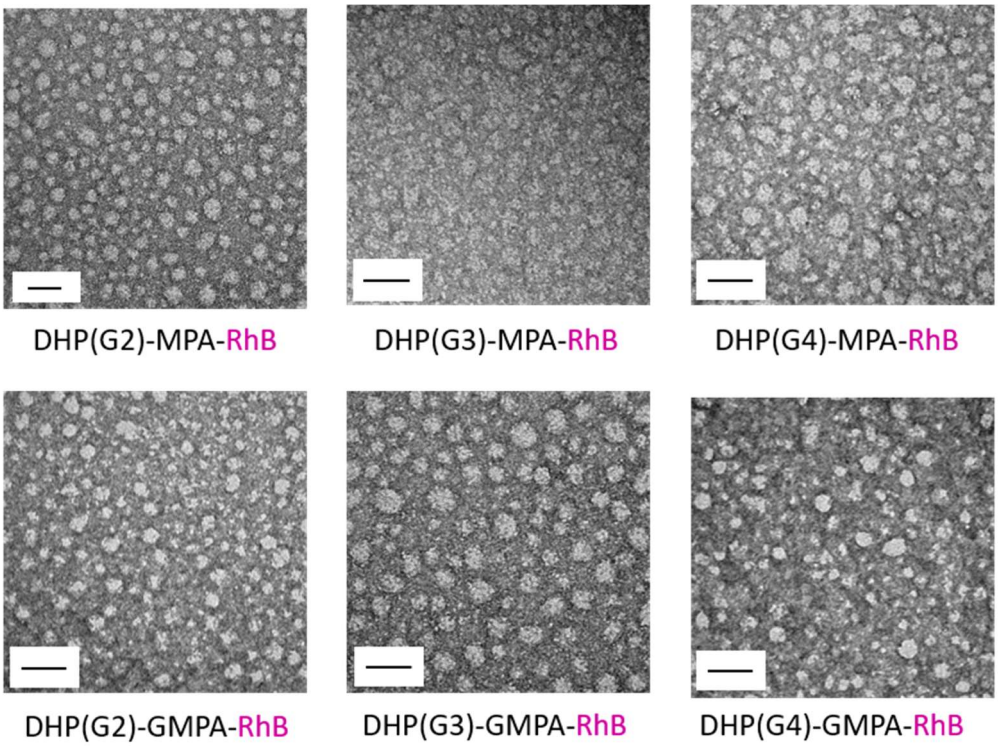

Figure 2.16. TEM images of the DHPs labelled with RhB at 1 mg/mL in dH_2O. Scale bars: 50 nm.

2.4. References

(1) Movellan, J.; Urbán, P.; Moles, E.; de la Fuente, J. M.; Sierra, T.; Serrano, J. L.; Fernàndez-Busquets, X. Amphiphilic Dendritic Derivatives as Nanocarriers for the Targeted Delivery of Antimalarial Drugs. *Biomaterials* **2014**, *35* (27), 7940–7950. https://doi.org/10.1016/j.biomaterials.2014.05.061.

(2) Fedeli, E.; Lancelot, A.; Serrano, J. L.; Calvo, P.; Sierra, T. Self-Assembling Amphiphilic Janus Dendrimers: Mesomorphic Properties and Aggregation in Water. *New J. Chem.* **2015**, *39* (3), 1960–1967. https://doi.org/10.1039/C4NJ02071E.

(3) Lancelot, A. New Dendritic Derivatives for Applications in Nanomedicine: Drug Delivery and Gene Transfection, Universidad de Zaragoza, 2017.

(4) Lancelot, A.; González-Pastor, R.; Clavería-Gimeno, R.; Romero, P.; Abian, O.; Martín-Duque, P.; Serrano, J. L.; Sierra, T. Cationic Poly(Ester Amide) Dendrimers: Alluring Materials for Biomedical Applications. *J. Mater. Chem. B* **2018**, *6* (23), 3956–3968. https://doi.org/10.1039/C8TB00639C.

(5) San Anselmo, M.; Lancelot, A.; Egido, J. E.; Clavería-Gimeno, R.; Casanova, Á.; Serrano, J. L.; Hernández-Ainsa, S.; Abian, O.; Sierra, T. Janus Dendrimers to Assess the Anti-HCV Activity of Molecules in Cell-Assays. *Pharmaceutics* **2020**, *12* (11), 1062. https://doi.org/10.3390/pharmaceutics12111062.

(6) Stenström, P.; Hjorth, E.; Zhang, Y.; Andrén, O. C. J.; Guette-Marquet, S.; Schultzberg, M.; Malkoch, M. Synthesis and in Vitro Evaluation of Monodisperse Amino-Functional Polyester Dendrimers with Rapid Degradability and Antibacterial Properties. *Biomacromolecules* **2017**, *18* (12), 4323–4330. https://doi.org/10.1021/acs.biomac.7b01364.

(7) Fernandez-Megia, E.; Correa, J.; Rodríguez-Meizoso, I.; Riguera, R. A Click Approach to Unprotected Glycodendrimers. *Macromolecules* **2006**, *39* (6), 2113–2120. https://doi.org/10.1021/ma052448w.

(8) Lancelot, A.; Clavería-Gimeno, R.; Velázquez-Campoy, A.; Abian, O.; Serrano, J. L.; Sierra, T. Nanostructures Based on Ammonium-Terminated Amphiphilic Janus Dendrimers as Camptothecin Carriers with Antiviral Activity. *European Polymer Journal* **2017**, *90* (February), 136–149. https://doi.org/10.1016/j.eurpolymj.2017.03.012.

(9) Fedeli, E.; Lancelot, A.; Dominguez, J. M.; Serrano, J. L.; Calvo, P.; Sierra, T. Self-Assembling Hybrid Linear-Dendritic Block Copolymers: The Design of Nano-Carriers for Lipophilic Antitumoral Drugs. *Nanomaterials* **2019**, *9* (2). https://doi.org/10.3390/nano9020161.

(10) Franc, G.; Kakkar, A. K. “Click” Methodologies: Efficient, Simple and Greener Routes to Design Dendrimers. *Chem. Soc. Rev.* **2010**, *39* (5), 1536–1544. https://doi.org/10.1039/B913281N.

(11) Taabache, S.; Bertin, A. Vesicles from Amphiphilic Dumbbells and Janus Dendrimers: Bioinspired Self-Assembled Structures for Biomedical Applications. *Polymers* **2017**, *9* (12), 280.

https://doi.org/10.3390/polym9070280.
(12) Gumerov, R. A.; Rudov, A. A.; Richtering, W.; Möller, M.; Potemkin, I. I. Amphiphilic Arborescent Copolymers and Microgels: From Unimolecular Micelles in a Selective Solvent to the Stable Monolayers of Variable Density and Nanostructure at a Liquid Interface. *ACS Appl. Mater. Interfaces* **2017**, *9* (37), 31302–31316. https://doi.org/10.1021/acsami.7b00772.
(13) Jiménez-Ángeles, F.; Kwon, H.-K.; Sadman, K.; Wu, T.; Shull, K. R.; Olvera de la Cruz, M. Self-Assembly of Charge-Containing Copolymers at the Liquid-Liquid Interface. *ACS Cent Sci* **2019**, *5* (4), 688–699. https://doi.org/10.1021/acscentsci.9b00084.
(14) Movellan, J.; Urbán, P.; Moles, E.; de la Fuente, J. M.; Sierra, T.; Serrano, J. L.; Fernàndez-Busquets, X. Amphiphilic Dendritic Derivatives as Nanocarriers for the Targeted Delivery of Antimalarial Drugs. *Biomaterials* **2014**, *35* (27), 7940–7950. https://doi.org/10.1016/j.biomaterials.2014.05.061.
(15) Stuart, M. C. A.; Van De Pas, J. C.; Engberts, J. B. F. N. The Use of Nile Red to Monitor the Aggregation Behavior in Ternary Surfactant-Water-Organic Solvent Systems. *Journal of Physical Organic Chemistry* **2005**, *18* (9), 929–934. https://doi.org/10.1002/poc.919.
(16) Lederer, A.; Burchard, W.; Hartmann, T.; Haataja, J. S.; Houbenov, N.; Janke, A.; Friedel, P.; Schweins, R.; Lindner, P. Dendronized Hyperbranched Macromolecules: Soft Matter with a Novel Type of Segmental Distribution. *Angew. Chem. Int. Ed. Engl.* **2015**, *54* (43), 12578–12583. https://doi.org/10.1002/anie.201504059.
(17) Lederer, A.; Hartmann, T.; Komber, H. Sphere-Like Fourth Generation Pseudo-Dendrimers with a Hyperbranched Core. *Macromolecular Rapid Communications* **2012**, *33* (17), 1440–1444. https://doi.org/10.1002/marc.201200223.
(18) Chen, P.; Li, Z. The Design of Second-Order Nonlinear Optical Dendrimers: From “Branch Only” to “Root Containing.” *Chin J Polym Sci* **2017**, *35* (7), 793–798. https://doi.org/10.1007/s10118-017-1949-y.
(19) Lancelot, A.; González-Pastor, R.; Concellón, A.; Sierra, T.; Martín-Duque, P.; Serrano, J. L. DNA Transfection to Mesenchymal Stem Cells Using a Novel Type of Pseudodendrimer Based on 2,2-Bis(Hydroxymethyl)Propionic Acid. *Bioconjugate Chem.* **2017**, *28* (4), 1135–1150. https://doi.org/10.1021/acs.bioconjchem.7b00037.
(20) Verma, S. K.; Ghorpade, R.; Pratap, A.; Kaushik, M. P. Solvent Free, N,N′-Carbonyldiimidazole (CDI) Mediated Amidation. *Tetrahedron Letters* **2012**, *53* (19), 2373–2376. https://doi.org/10.1016/j.tetlet.2012.01.125.
(21) Reul, R.; Nguyen, J.; Kissel, T. Amine-Modified Hyperbranched Polyesters as Non-Toxic, Biodegradable Gene Delivery Systems. *Biomaterials* **2009**, *30* (29), 5815–5824. https://doi.org/10.1016/j.biomaterials.2009.06.057.

(22) Sun, P.; Wang, N.; Jin, X.; Zhu, X. “Bottom-Up” Construction of Hyperbranched Poly(Prodrug- *Co* -Photosensitizer) Amphiphiles Unimolecular Micelles for Chemo-Photodynamic Dual Therapy. *ACS Appl. Mater. Interfaces* **2017**, *9* (42), 36675–36687. https://doi.org/10.1021/acsami.7b13055.
(23) Jin, X.; Sun, P.; Tong, G.; Zhu, X. Star Polymer-Based Unimolecular Micelles and Their Application in Bio-Imaging and Diagnosis. *Biomaterials* **2018**, *178*, 738–750. https://doi.org/10.1016/j.biomaterials.2018.01.051.
(24) Souza, T. G. F.; Ciminelli, V. S. T.; Mohallem, N. D. S. A Comparison of TEM and DLS Methods to Characterize Size Distribution of Ceramic Nanoparticles. *J. Phys.: Conf. Ser.* **2016**, *733*, 012039. https://doi.org/10.1088/1742-6596/733/1/012039.

Chapter 3:

Amphiphilic Janus dendrimers as drug carriers for Hepatitis C

3.1. Hepatitis C

3.1.1. Introduction

Hepatitis C is an infectious disease caused by a *Flaviviridae* RNA virus, the hepatitis C virus (HCV). The prevalence of the HCV infection is estimated to be 71 million individuals all over the world, which means 1% of the global population, although its distribution is not uniform across the globe. The HCV infection can provoke acute hepatitis C, which in a high percentage of the cases ends in chronic hepatitis C. The liver complications derived from this disease include liver fibrosis, cirrhosis, or hepatocellular carcinoma, and all together contributes to make the disease as the most frequent cause for liver transplantation in many countries. Besides, the co-infection with HCV and HIV (human immunodeficiency virus) has historically led to tricky complications and high mortality but encouragingly, it is being overcome with the development of successful treatments[1].

The HCV transmission is basically related to blood and sexual contact and it does not exist a vaccine for its prophylaxis. The existing treatments have evolved from the interferon (IFN)-based therapies to the most promising direct-acting antiviral agents (DAAs), targeting some of the multiple steps of the HCV life cycle. However, the main concerns with conventional therapies against infectious diseases are related to the viability of infected cells and the development of resistances. Although the use of combination therapies could be a solution in some cases, the discovery of effective drugs is still a need. In this sense, high-throughput screening methodologies focused on determining the interactions between the isolated target biomolecule and a potential drug constitute a helpful primary screening tool to identify potential drugs among a great amount of molecules[2–4].

Different strategies such as drug repurposing[5] or the application of mathematical models[6] have been revealed as valid strategies to identify new and effective antivirals or a combination of them. In the case of Hepatitis C, the identification of the HCV NS3 protease as a therapeutic target led to the application of a primary screening strategy to well-known compounds approved by FDA initially designed for other therapeutic purposes[7]. A screening with a battery of compounds against

partially folded NS3 allowed for the selection of a library of molecules that stabilize this inactive conformation. Among them, camptothecin (CPT), a natural alkaloid widely used in the treatment of several tumours, iopanoic acid (IA) and 3,3′,5-triiodothyroacetic acid (or tiratricol, TRIAC), these two used for thyroid-related diseases, were identified as potent bioactive allosteric inhibitors of the HCV NS3 protease (Figure 3.1). However, each of these compounds presents a series of limitations. The antitumoral CPT exhibits a low solubility, unpredictable side effects and the emergence of drug resistances, which limits its inclusion in new therapies[8]. In the case of the iodised compounds, IA and TRIAC, apart from their low water-solubility, they did not exhibit appropriate viral inhibiting activity in cell-based assays during a secondary screening[7], which was thought to be due to cell internalisation difficulties of these compounds. Far from invalidating the therapeutic possibilities of such drugs, these drawbacks fostered the search for alternative delivery strategies. In this respect, nanocarrier-based drug delivery arises as a promising approach to rescue the bioactivity observed in primary screenings[9], as it can provide a positive input on drug pharmacokinetics favouring drug bioavailability, drug targeting, cellular internalisation, and drug activity/response[10–12].

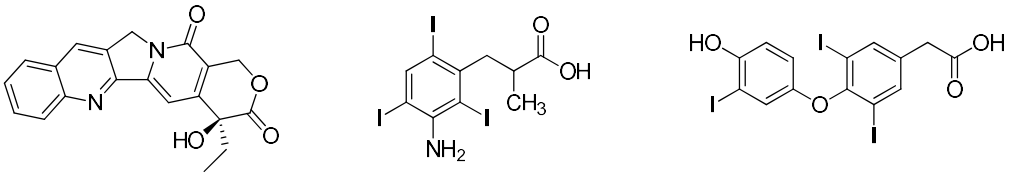

Camptothecin (CPT) | Iopanoic acid (IA) | Tiratricol (TRIAC)

Figure 3.1. Chemical structure of the allosteric inhibitors of HCV protease NS3: camptothecin (CPT), iopanoic acid (IA) and tiratricol (TRIAC).

In the search for suitable drug nanocarriers that could permit broadening the possibilities to treat viral infections revisiting drugs with promising activity, dendrimer-based nanocarriers have emerged as alluring synthetic systems because of their unique properties including controlled architecture, versatile functionalisation and cargo, and the transport and release of diverse molecules of interest[13,14]. The architecture and chemical structure of the dendritic scaffold

together with its terminal groups defines the interaction with cargo molecules and their efficient uptake by the host cells. As for delivery biomedical applications, dendrimers have been extensively investigated as drug and DNA carriers for cancer-related biomedical applications[15]. Nevertheless, there is intense research ongoing in the field of infectious diseases, where the urgent implementation of strategies for the prevention and cure is taking advantage of dendrimers as carriers for different cargos as antigens[16,17] or drugs[18,19]. The versatile self-assembly behaviour of amphiphilic Janus dendrimers has turned into a powerful approach to prepare nanocarriers[20–22], which have been shown to be advantageous for drug-delivery applications[23–26].

3.1.2. Previous work and working plan

In our group, previous works have focused on the encapsulation of CPT within polymeric structures in order to overcome the obstacles of the free administration of the drug. In this way, the first attempt was made with an amphiphilic hybrid dendritic-linear-dendritic block copolymer (HDLDBC) derived from Pluronic F127 bearing *bis*-MPA dendrons in both extremities[27] (Figure 3.2, left). The thermosensitive micelles formed by the self-assembly of these lineal structures were able to load CPT and reduce the cytotoxicity of the drug, while maintaining its antiviral activity. Moreover, other amphiphilic polymeric structures composed by hydrophilic poly(ethylene glycol) (PEG) and hydrophobic 2,6-diacylaminopyridine pendant units (DAP), PEG_x-*b*-PDAP, (Figure 3.2, right) have been studied as CPT nanocarriers with similar positive results in cellular assays[28].

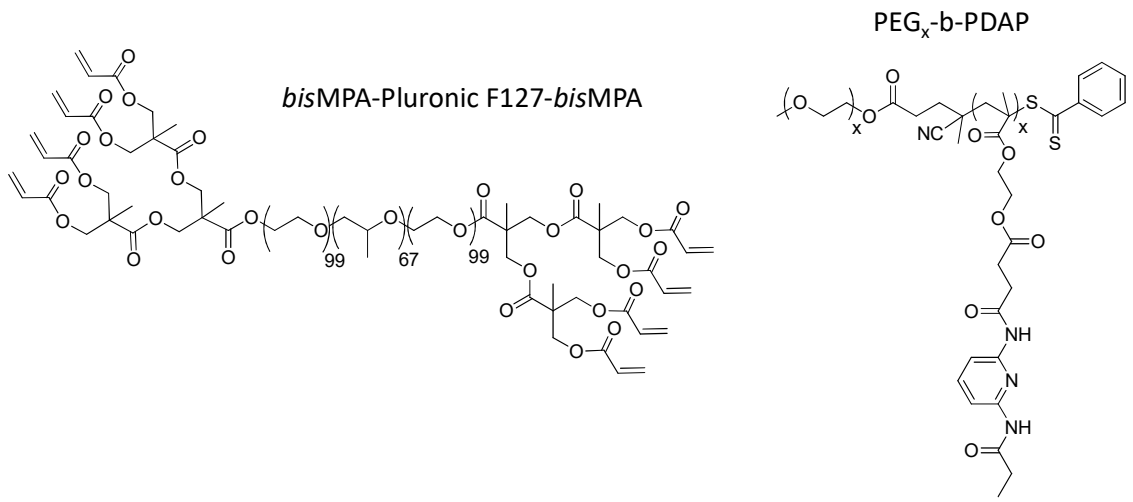

Figure 3.2. Previous polymers studied in our group as CPT nanocarriers: bisMPA-Pluronic F127-bisMPA and PEG$_x$-b-PDAP.

More recently, amphiphilic Janus dendrimers based on *bis*-MPA dendrons of different generations have been reported in our group to be useful for the delivery of CPT. Those Janus dendrimers were composed by a hydrophilic dendron terminated in amino groups and a lipophilic dendron functionalised with stearic acid chains, $(NH_3^+)[MPA]_n$-$[MPA]_n(C17)$, (Figure 3.3, upper side). Suitable combinations of the generation numbers of the hydrophilic and lipophilic dendrons provided carriers that solubilised CPT used as an anti-HCV drug, and in this case, a higher therapeutic effect than that of the free drug was achieved at low CPT doses[29]. Other interesting dendrimers based on a core of tripropargylamine surrounded by poly(ester amide) dendrons of *bis*-GMPA, $D[GMPA]_n(NH_3^+)$, (Figure 3.3, lower side) have been tested. The ability of these cationic tripodal dendrimers to load CPT and to enhance its cell viability and its antiviral activity have been also demonstrated[30].

$(NH_3^+)[MPA]_n$-$[MPA]_m(C17)$

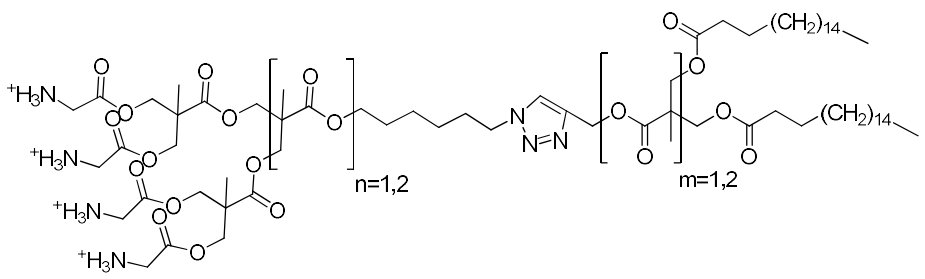

$D[GMPA]_n(NH_3^+)$

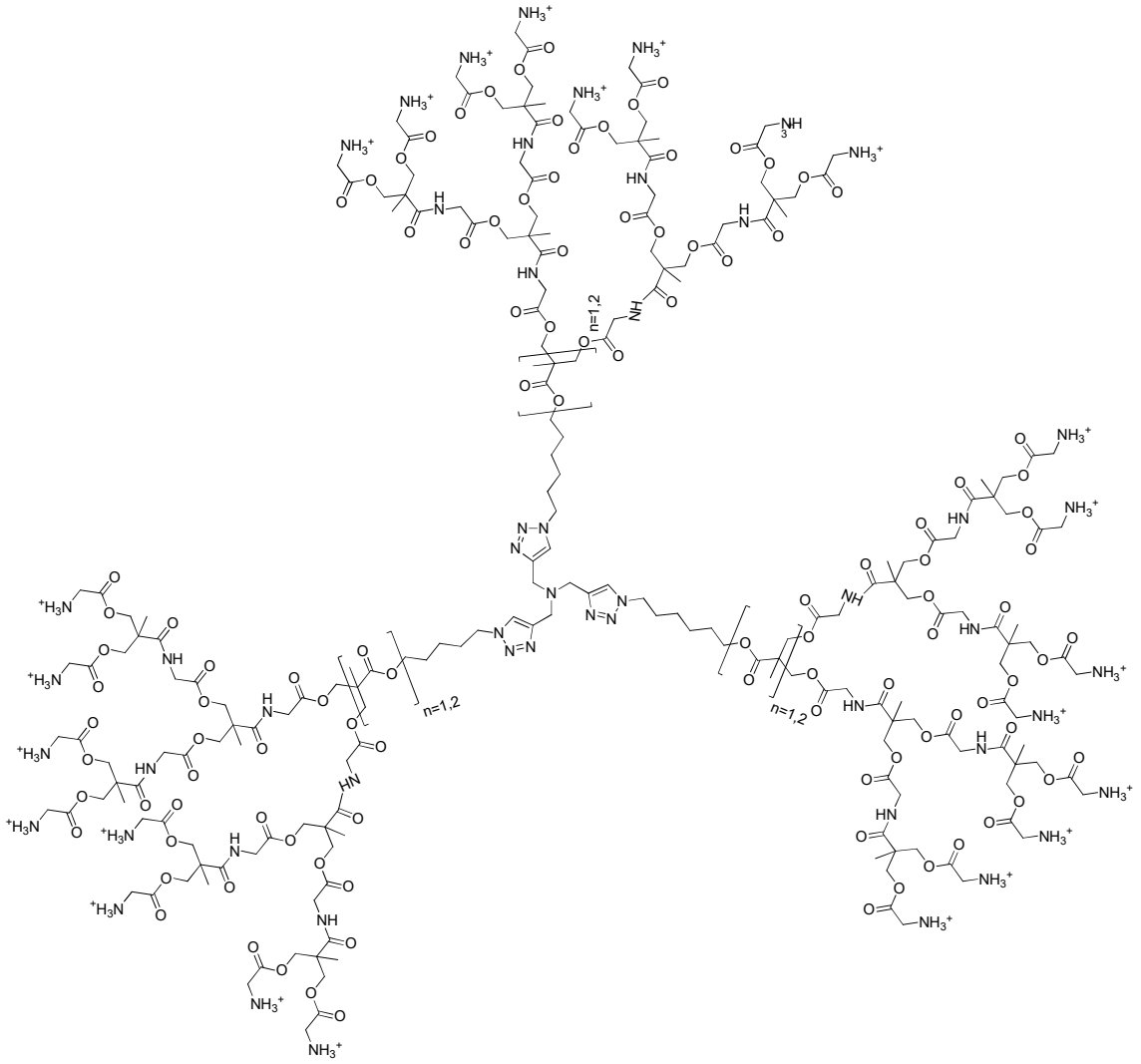

Figure 3.3. Dendritic structures previously studied in our group as CPT nanocarriers: bis-MPA Janus dendrimers with dendrons of different generations, and tripodal dendrimers derived from tripropargylamine with bis-GMPA dendrons of different generations.

With all the structures in mind that have been successful for the delivery of CPT and in particular, those that have improved the antiviral activity of the drug when encapsulated, novel structures have been designed for the delivery of the other two anti-HCV drugs selected, IA and TRIAC. The previous experience made us focus on the Janus dendrimers as promising nanocarriers to load a suitable amount of drug, and the inclusion of inner amide groups on the structure, present in the *bis*-GMPA dendrons, was thought to bring additional possibilities of interactions with cargo molecules. Thus, the four novel amphiphilic Janus dendrimers described in Chapter 2 (see figure 2.3), namely $(NH_3^+)_8$[GMPA]-[MPA](C17)$_2$, $(NH_3^+)_8$[GMPA]-[MPA](C17)$_4$, $(NH_3^+)_8$[MPA]-[GMPA](C17)$_2$, and $(NH_3^+)_8$[MPA]-[GMPA](C17)$_4$ were proposed to assess their potential in rescuing the activity of the anti-hepatitis C drugs IA and TRIAC. These dendrimers combine a *bis*-MPA dendron with a *bis*-GMPA dendron in each side of the molecule, thus taking advantage of the hydrolytic degradability of the ester linkages and the possibility to establish hydrogen bonds of the amide groups[30]. In addition, the number of aliphatic chains was varied in order to modulate the lipophilicity of the global molecule. The synthesis and characterisation of these compounds is described in chapter 2, section 2.2.1. In the following sections, their characteristics as suitable nanocarriers, including their self-assembly forming aggregates in water, their CAC values, as well as the morphology and size of the empty aggregates are also described (see section 2.2.2.).

In the present chapter, the ability of these novel Janus structures to interact with the drugs IA and TRIAC (section 3.2.1) as well as the behaviour of the drug-loaded nanocarriers is evaluated in terms of the amount of drug loaded (section 3.2.2) and the morphological features of the resulting aggregates (section 3.2.3). What is more, their ability to deliver the cargo to the target cells and their efficiency as antiviral nanocarriers is evaluated in a suitable in vitro cellular model, the Huh 5-2 cell line (section 3.3). It must be noted that among the dendrimers employed for these studies, $(NH_3^+)_8$[GMPA]-[MPA](C17)$_2$, $(NH_3^+)_8$[GMPA]-[MPA](C17)$_4$, and $(NH_3^+)_8$[MPA]-[GMPA](C17)$_2$, contain Cl^- as counterion while $(NH_3^+)_8$[MPA]-[GMPA](C17)$_4$ bears TFA^- instead, since the deprotection method to remove the ending *t*-Boc moieties was modified during the course of this thesis.

3.2. Aggregates formed by drugs and Janus dendrimers

Initially, a calorimetric study was developed to assess the thermodynamic parameters involved in the interaction between the drugs and the Janus aggregates measuring the heat transfer during the process. Then, the ability of these aggregates to load the drugs was spectroscopically determined and finally, its morphology was studied by microscopic imaging techniques.

3.2.1. Interaction studies between drugs and dendrimers

In order to test the interaction between the drugs IA and TRIAC and the Janus aggregates, Isothermal Titration Calorimetry (ITC) studies were performed. Briefly, this technique allows to determine the thermodynamic interactions between two molecules by successive injections of a ligand placed in the syringe into the sample cell containing the other molecule. A second cell with the same solvent or mixture of solvents as the sample cell is established as reference cell. The thermal power needed to maintain the reference and the sample cells at the same temperature against time is measured by the equipment after each ligand injection and the corresponding stirring. In this case, the dendritic aggregates were placed into the sample cell and the syringe was fed with the corresponding drug in each experiment, all solutions consisting of PBS/milliQ H_2O (1:1 in volume) with up to 2% of DMSO.

The thermograms represented as the raw thermal power as a function of time and the binding isotherms understood as the ligand-normalised heat effects as a function of the molar ratio were obtained for each interaction with IA (Figure 3.4) or with TRIAC (Figure 3.5). Then, the association constant (K_a) and the enthalpy change (ΔH) were estimated by fitting the titration curve (in red) through non-linear regression employing a single ligand binding site model (1:1 dendrimer aggregates:drug stoichiometry) implemented in Origin[31]. The rest of the thermodynamic parameters, ΔG and ($-T\Delta S$), were calculated with the help of the thermodynamics equations and all are gathered in Table 3.1 and graphically represented in Figure 3.6.

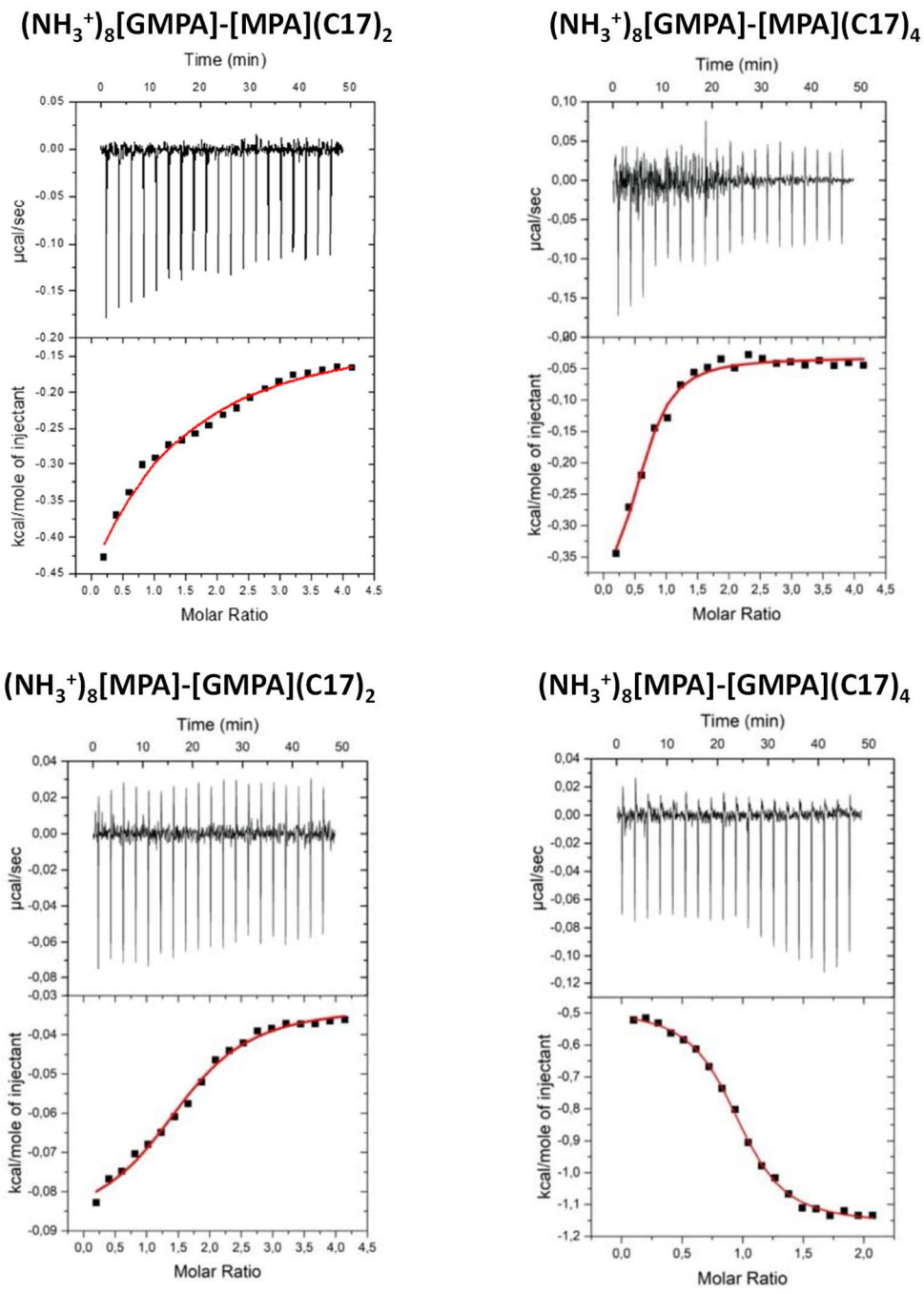

Figure 3.4. ITC thermograms (upper graphs) and binding isotherms (lower graphs) for each of the titrations measured between the dendrimer aggregates and the drug IA.

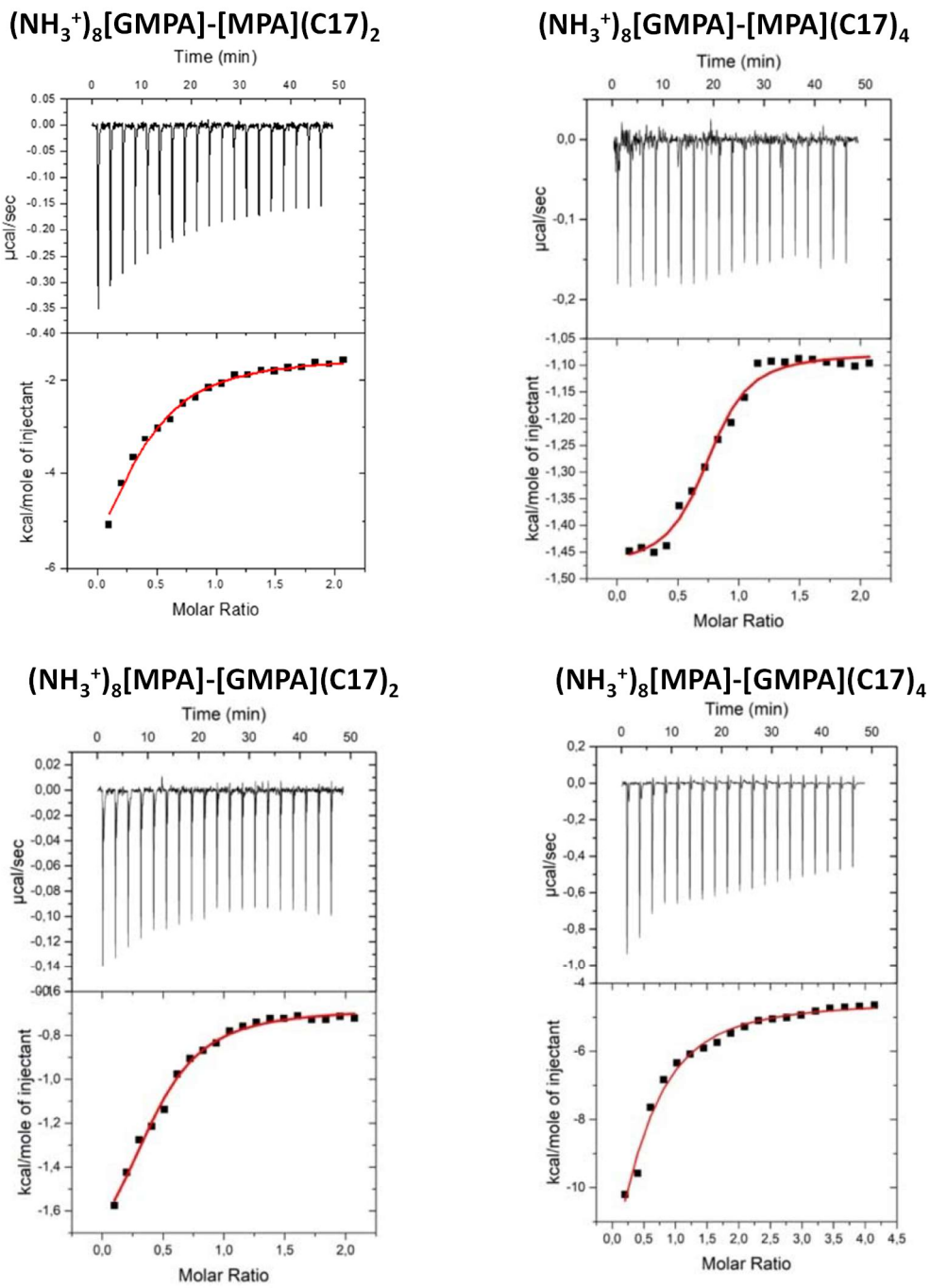

Figure 3.5. ITC thermograms (upper graphs) and binding isotherms (lower graphs) for each of the titrations measured between the dendrimer aggregates and the drug TRIAC.

From data, the spontaneous interaction between each dendrimer and each of the drugs can be confirmed, showing all negative binding Gibbs energy (ΔG) values ranging from -5.2 to -8.2 kcal/mol. Regarding the interaction with IA, the dendrimers tested present affinities with K_a ranging from 10^3 to 10^6 M^{-1} (see Table 3.1). Interestingly, the dendrimer with a lower affinity towards IA, $6.3 \cdot 10^3$ M^{-1}, was $(NH_3^+)_8$[GMPA]-[MPA](C17)$_2$, the one with a lower lipophilic content (Lc = 19.4, previously estimated in chapter 2, section 2.2). It must be noted that the ΔG obtained for this interaction indicates the lowest spontaneity of all the bindings assayed, while it remains in a negative value (-5.2 kcal/mol). With respect to TRIAC, all dendrimers exhibited a similar affinity in their interaction with the drug yielding association values in the range from 10^4 to 10^5 M^{-1}. In this case, one of the dendrimers with the highest Lc (29.6), $(NH_3^+)_8$[GMPA]-[MPA](C17)$_4$, is the one which exhibited a slightly higher affinity towards the lipophilic drug with a K_a of $6.1 \cdot 10^5$ M^{-1}. Besides, the Gibbs free energy in this intermolecular binding is the most negative among the titrations involving TRIAC and then, it is the most spontaneous interaction.

Table 3.1. Thermodynamic parameters calculated from ITC studies for the interaction between the Janus aggregates and the drugs IA or TRIAC. K_a is expressed in M^{-1}, while ΔG, ΔH and (-TΔS) are expressed in kcal/mol.

	Drug	K_a	ΔG	ΔH	-TΔS
$(NH_3^+)_8$[GMPA]-[MPA](C17)$_2$	IA	6.3×10^3	−5.2	-1.1	-4.1
	TRIAC	1.0×10^5	-6.8	-6.0	-0.8
$(NH_3^+)_8$[GMPA]-[MPA](C17)$_4$	IA	9.2×10^4	-6.8	-0.4	-6.4
	TRIAC	6.1×10^5	-7.9	-0.4	-7.5
$(NH_3^+)_8$[MPA]-[GMPA](C17)$_2$	IA	4.8×10^4	-6.4	-0.1	-6.3
	TRIAC	1.5×10^5	-7.1	-1.3	-5.8
$(NH_3^+)_8$[MPA]-[GMPA](C17)$_4$	IA	1.1×10^6	-8.2	0.7	-8.9
	TRIAC	8.8×10^4	-6.7	-15.8	9.1

On the other hand, most of the systems studied exhibited a dendrimer/drug interaction mainly driven by entropic contributions (-TΔS) (see Figure 3.6). This entropic term refers to the unspecific interactions that occur during the binding process. Briefly, two blocks of entropic contributions can be distinguished focusing on the solvent or on the molecules involved in the interaction. Firstly, the solvation entropy, which contemplates the degrees of freedom of the water molecules and usually favours the intermolecular interaction. Namely, during the binding process the water molecules localised in the surface of the two binding molecules are released to the bulk solvent and then, their degrees of freedom experiment an increase. In addition, the total molecular surface exposed to the solvent is usually reduced upon binding, and this phenomenon also contributes to explain the exchange of heat during the titration. Secondly, the conformational and roto-translational entropy, that is commonly unfavourable in the global interaction process since, upon binding, the number of accessible conformations and configurations of the interacting molecules and thus their degrees of freedom are usually reduced[32].

An exception in the kind of interactions that predominate in the binding is found for $(NH_3^+)_8$[GMPA]-[MPA]$(C17)_2$ and $(NH_3^+)_8$[MPA]-[GMPA]$(C17)_4$ with the drug TRIAC. In these interactions, enthalpic contributions (ΔH) have more importance in the resulting Gibbs energy, and notably, they are the only two in which the (-TΔS) term is positive (9.1 kcal/mol for the interaction between $(NH_3^+)_8$[MPA]-[GMPA]$(C17)_4$ and TRIAC) or nearly cero (-0.8 kcal/mol for the interaction $(NH_3^+)_8$[GMPA]-[MPA]$(C17)_2$/TRIAC) (see Table 3.1 and Figure 3.6). This may indicate the absence of any solvation favourable process in the case of $(NH_3^+)_8$[MPA]-[GMPA]$(C17)_4$/TRIAC interaction, which would be in agreement with the modest morphological changes of the aggregates observed upon the addition of the drug and the small amount of entrapped drug finally determined (these results will be next exposed in sections 3.2.2 and 3.2.3). With respect to the enthalpic term, it englobes the solvation enthalpy and the energy involved in the individual interactions between the binding molecules through hydrogen bonds, electrostatic, or van der Waals forces, among others[32]. Then, the interaction between the above cited dendrimers, $(NH_3^+)_8$[GMPA]-[MPA]$(C17)_2$ and $(NH_3^+)_8$[MPA]-[GMPA]$(C17)_4$, and TRIAC under the ITC conditions seem to

be more specific than the rest of interactions studied, where the entropic contributions were higher than the enthalpic ones[9].

Although these thermodynamic binding parameters calculated by ITC can give us an idea of the intermolecular interactions, a quantitative correlation between these data and the amount of drugs loaded within the dendrimers can not be established since the experimental conditions in both processes were not identical (concentration, time, drug addition method, volumes, etc.).

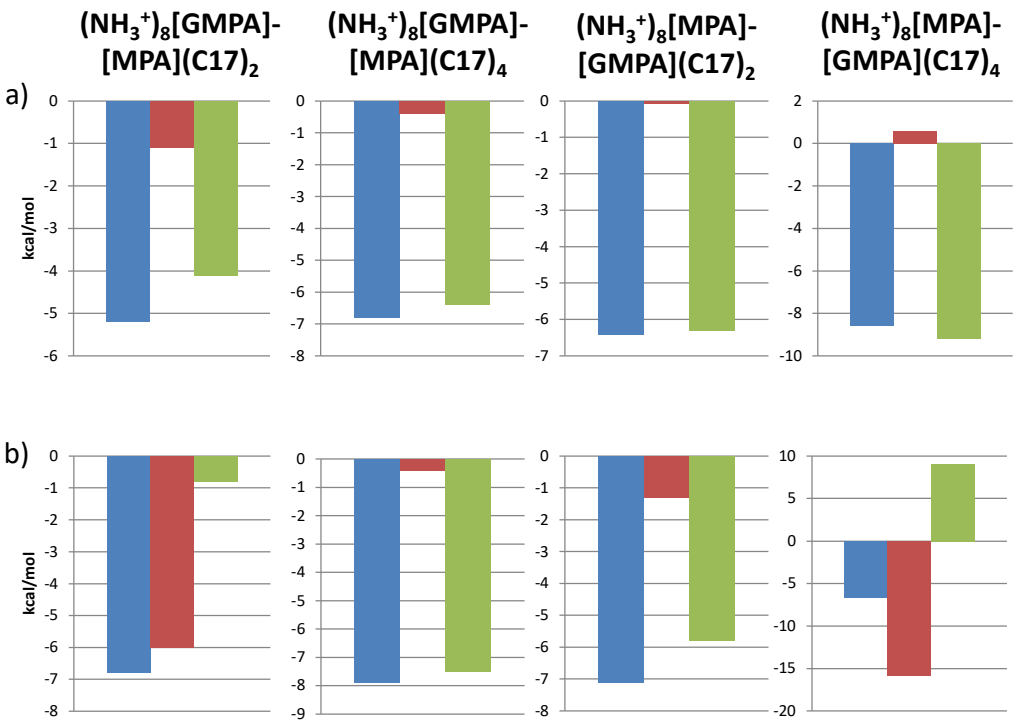

Figure 3.6. Graphical representation of thermodynamic parameters calculated from ITC assays for the interaction between Janus dendrimers and the compounds IA (a) and TRIAC (b) (extracted from Table 3.1). ΔG (blue bars), ΔH (red bars) and -TΔS (green bars) are expressed in kcal/mol.

3.2.2. Drug loading into the Janus aggregates

The lipophilic compounds IA and TRIAC were loaded within the dendritic aggregates previously formed by the oil-in-water method (see chapter 2, section 2.2.2.). This emulsion technique was employed in order to form the self-assemblies of the amphiphilic Janus dendrimers and then, the solvent diffusion technique was developed to load the drugs. This combined methodology was chosen with the aim to imitate to the extent possible the process underlying the ITC experiments, being aware that the exact reproduction of the conditions was not possible.

For the drug loading an excess of the drugs were added dissolved into DMSO to reach the starting ratio of 5 mol of drug per mol of dendrimer, ensuring also that DMSO volume in the mixture did not exceed 2.5% (v/v) in order not to interfere with the stability of the aggregates. The mixtures were stirred at 4 °C for 16 h to allow drugs to enter within the nanocarriers and then, DMSO was removed by dialysis against distilled water. The non-entrapped compounds were removed by filtration through 0.22 μm syringe filter of regenerated cellulose to obtain the drug loaded nanocarriers. Finally, the concentration of loaded drug was directly determined by UV-Vis spectroscopy (λ_{IA} = 317 nm and λ_{TRIAC} = 300 nm) after adding 75% (v/v) of spectrophotometric grade DMSO to dissociate the aggregates and allow the release of the drug. The loading process was repeated at least three times, and the drug loading content (DLC) defined as mol of loaded drug/ mol of dendrimer was calculated to estimate the success of the process. It is a useful parameter since it allows to establish a relationship between the amount of drug and nanocarrier in the same preparation and most importantly, it does not depend on the amount of drug initially provided in the loading process.

DLC values between 1.4 and 1.9 were obtained for both drugs within $(NH_3^+)_8$[GMPA]-[MPA](C17)$_2$, $(NH_3^+)_8$[GMPA]-[MPA](C17)$_4$, and $(NH_3^+)_8$[MPA]-[GMPA](C17)$_2$, whereas $(NH_3^+)_8$[MPA]-[GMPA](C17)$_4$ exhibited poor loading skills (Table 3.2). Non-significant differences were observed between IA and TRIAC DLC values when comparing within the same Janus aggregate.

Table 3.2. Determined concentration (μM) of the loaded drug into the dendritic Janus aggregates and averaged DLC in molar ratio calculated for each preparation. Lc is the lipophilic content calculated for the Janus dendrimers.

		IA		TRIAC	
Janus dendrimers	**Lc (%)**	[IA] (μM)	DLC (mol/mol)	[TRIAC] (μM)	DLC (mol/mol)
$(NH_3^+)_8$[GMPA]-[MPA]$(C17)_2$	19.4	680 ± 172	1.86	563 ± 257	1.65
$(NH_3^+)_8$[GMPA]-[MPA]$(C17)_4$	29.6	321 ± 119	1.44	505 ± 238	1.59
$(NH_3^+)_8$[MPA]-[GMPA]$(C17)_2$	21.4	641 ± 207	1.78	583 ± 167	1.81
$(NH_3^+)_8$[MPA]-[GMPA]$(C17)_4$	29.6	35 ± 16	0.19	70 ± 49	0.29

Considering that the encapsulation takes place by diffusion once the dendrimer aggregates are already formed, their initial morphology seems to be relevant during the process. In this regard, while the empty aggregates of $(NH_3^+)_8$[GMPA]-[MPA]$(C17)_2$, $(NH_3^+)_8$[GMPA]-[MPA]$(C17)_4$, and $(NH_3^+)_8$[MPA]-[GMPA]$(C17)_2$ exhibited rounded morphology, $(NH_3^+)_8$[MPA]-[GMPA]$(C17)_4$ presented a cylindrical morphology (see Figure 3.7a). It was initially considered that the amide groups present in the *bis*-GMPA dendron could facilitate the encapsulation by the establishment of hydrogen bonds with the drugs. Indeed, the inclusion of this dendritic scaffold permits suitable DLC values for antiviral activity studies, regardless its position in the Janus structure for the three dendrimers providing spherical micelles. However, this is not the case for the $(NH_3^+)_8$[MPA]-[GMPA]$(C17)_4$ dendrimer that shows poor encapsulation properties. The cylindrical shape observed for its aggregates could hamper the accessibility of the drugs to the *bis*-GMPA dendron, which is located closer to the core of the nanostructure. The fact that this dendrimer bears a different counterion in its formulation (TFA^- instead of Cl^- as the other three dendrimers), led us to question its possible implication in the drug loading process. For that reason, $(NH_3^+)_8$[GMPA]-[MPA]$(C17)_4$ aggregates prepared from the TFA^- containing dendrimer were loaded with TRIAC in order to compare its DLC value with the one obtained for the same dendrimer bearing the Cl^- counterion (see Table 3.2). The results showed a DLC value of 1.7 mol/mol of the TRIAC loaded into the TFA^- bearing $(NH_3^+)_8$[GMPA]-[MPA]$(C17)_4$, which is in the same order than the DLC for the aggregates resulting from the dendrimers having the Cl^- counterion

(1.6 mol/mol). This seems to indicate that the counterion itself does not affect the drug loading ability of this dendrimer aggregates.

Besides, the size of the hydrophilic face has been described in other studies to stabilize the dendrimer/drug aggregates once a lipophilic drug is included[29]. Then, the lower hydrophilicity and less-defined Janus structure displayed by $(NH_3^+)_8$[MPA]-[GMPA](C17)$_4$, may also increase the instability in water of the dendrimer/drug aggregates, which can also contribute to explain the poor DLC values observed (0.19 for IA and 0.29 for TRIAC). Although the decrease is not as dramatic, $(NH_3^+)_8$[GMPA]-[MPA](C17)$_4$ shows also lower DLC (1.44 for IA and 1.59 for TRIAC) than the Janus with the smallest lipophilic dendrons (DLC values above 1.65). It seems that the biggest lipophilic dendrons do not benefit the loading of the highest amount of any of these drugs. Similar observations were previously obtained for CPT, the anti-HCV lipophilic drug assayed by encapsulation on *bis*-MPA-based amphiphilic Janus dendrimers[29]. The inclusion of lipophilic molecules alters the hydrophilic/lipophilic balance of the dendrimer/drug aggregates determining the amount of drug loaded. This effect has been shown to be more significant for lower hydrophilic/lipophilic balances, that is, higher Lc.

3.2.3. Morphology of the loaded aggregates

The morphology of the drug-loaded nanocarriers was studied by TEM. Significant morphological changes compared to the empty aggregates (Figure 3.7a) were observed after the loading of the drugs into $(NH_3^+)_8$[GMPA]-[MPA](C17)$_2$, $(NH_3^+)_8$[GMPA]-[MPA](C17)$_4$, and $(NH_3^+)_8$[MPA]-[GMPA](C17)$_2$, whereas the morphology of $(NH_3^+)_8$[MPA]-[GMPA](C17)$_4$ remained almost unaltered after the drug diffusion process (Figure 3.7).

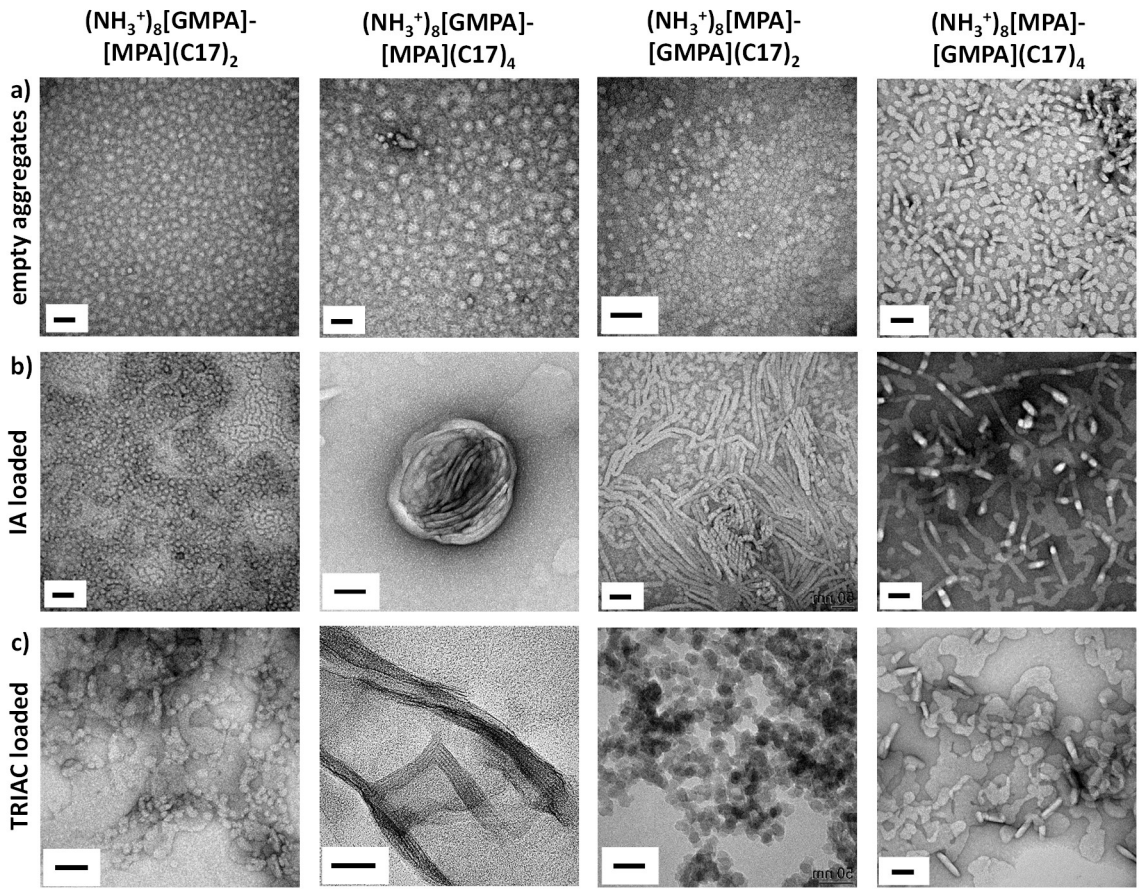

Figure 3.7. TEM images of the empty dendritic aggregates (a) or loaded with IA (b) or TRIAC (c). Scale bars: 50 nm.

The changes observed for $(NH_3^+)_8$[GMPA]-[MPA](C17)$_2$/drug (IA and TRIAC) aggregates seem related with aggregation effects of spherical micelles. No significant shape disruptions were detected, and this is in agreement with the stabilising role of its bigger hydrophilic dendron, N_3-[GMPA]$(NH_3^+)_8$, even after the increase of lipophilicity provoked by the addition of the drug. In contrast, the inclusion of each drug within the $(NH_3^+)_8$[GMPA]-[MPA](C17)$_4$ aggregates turned into the most drastic morphological changes and elongated aggregates were observed. The formation of wormlike micelles for $(NH_3^+)_8$[GMPA]-[MPA](C17)$_4$/IA and long cylindrical micelles for $(NH_3^+)_8$[GMPA]-[MPA](C17)$_4$/TRIAC can indeed be associated with a significant increase of the lipophilic contents, which is not compensated by the size of the hydrophilic dendron[33–35]. Moreover, such elongated aggregates self-arrange into large assemblies. Upon IA loading, the wormlike micelles rolled up into large spherical assemblies (see also Figure 3.8), and the TRIAC-loaded long cylindrical micelles longitudinally arrange in lamellar

structures. The formation of wormlike micelles was also detected for $(NH_3^+)_8$[MPA]-[GMPA](C17)$_2$ loaded with IA, although in this case the micelles appeared more dispersed. Upon TRIAC loading, $(NH_3^+)_8$[MPA]-[GMPA](C17)$_2$ aggregates maintained the spherical morphology. In contrast, the drug loading process carried out for $(NH_3^+)_8$[MPA]-[GMPA](C17)$_4$ only slightly affected the morphological characteristics of the aggregates, and this is consistent with the low DLC values measured (Table 3.2).

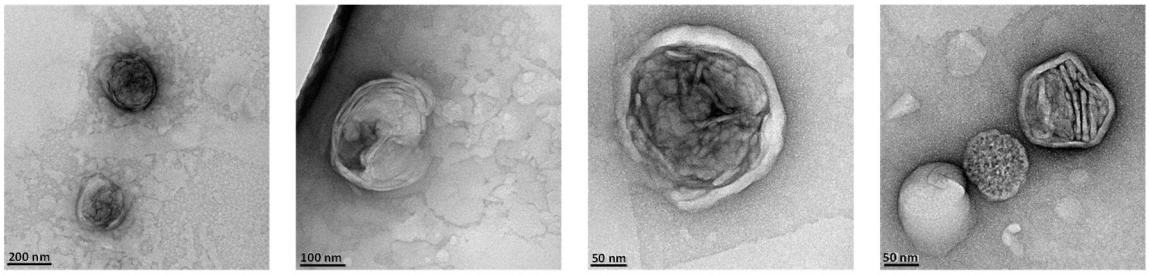

Figure 3.8. Further TEM images of the aggregates formed by $(NH_3^+)_8$[GMPA]-[MPA](C17)$_4$ and IA.

3.3. In vitro studies: cell viability and antiviral activity

The cell line employed for the in vitro studies, Huh 5-2, contains the subgenomic HCV replicon I389luc-ubi-neo/NS3-3'/5.1[36]. Its autonomous replication in the human hepatoma cell line mimics the viral replication cycle and allows to assess the anti-HCV activity of different compounds in a safe way. Among its structure, it contains the reporter gene *Photinus spyralis* luciferase[37], which will give a luminescence signal in the presence of the substrate luciferin. Since this signal is proportional to the rate of replication of the HCV replicon system, its quantification allows to determine the anti-viral effect of the compounds assayed. The 40% effective concentration (EC40) was defined as the concentration of compound that reduced the luciferase signal by 40%.

Concurrently, the cytotoxic effect of the compounds was assayed over the same cell line. CellTiter 96® AQueous One Solution Cell Proliferation Assay was employed to determine the cell viability and the CC50 was defined as the concentration at which 50% of initial cell viability was reached.

First of all, the cytotoxicity of the empty dendrimer aggregates was assayed on the Huh 5-2 cell line in order to confirm their suitability as carriers for anti-HCV drugs. The spectrophotometric results revealed that the four Janus aggregates up to 40 μM maintained the cellular viability above 85%, and only $(NH_3^+)_8$[GMPA]-[MPA](C17)$_2$ provoked the decrease of viability below 80% at the concentration of 80 μM (Figure 3.9). Then, it was demonstrated that in terms of not compromising the cell viability, the whole series of Janus dendrimers were good candidates as anti-HCV carriers. However, the dendrimer $(NH_3^+)_8$[MPA]-[GMPA](C17)$_4$ was excluded for further anti-HCV experiments due to its scarce drug loading ability.

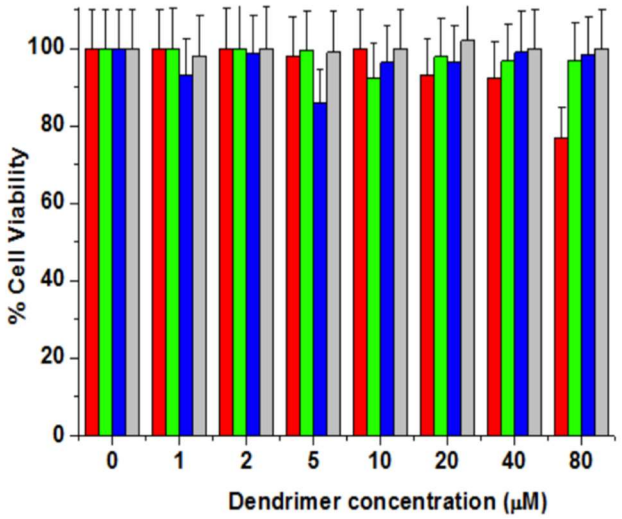

Figure 3.9. Cell Viability of empty Janus dendrimers in Huh 5-2 cell line. All the data are presented as the average ± standard deviation. Colour code: $(NH_3^+)_8$[GMPA]-[MPA](C17)$_2$, red; $(NH_3^+)_8$[GMPA]-[MPA](C17)$_4$, green; $(NH_3^+)_8$[MPA]-[GMPA](C17)$_2$, blue; $(NH_3^+)_8$[MPA]-[GMPA](C17)$_4$, grey.

The antiviral activity of the promising $(NH_3^+)_8$[GMPA]-[MPA](C17)$_2$, $(NH_3^+)_8$[GMPA]-[MPA](C17)$_4$, and $(NH_3^+)_8$[MPA]-[GMPA](C17)$_2$ dendrimers as carriers for IA and TRIAC was evaluated and compared to the free drugs, as well as the viability of the resulting aggregates. The EC40 and the CC50 values calculated from these experiments are gathered in Table 3.3.

Regarding IA, the biocompatibility of the drug remained above 80% when loaded into the three dendrimers at the highest concentrations tested (Figure 3.10a). Besides, the slight cytotoxic effect of the free drug seemed to be mostly

overcome in the dendrimer's formulations. The antiviral activity of IA did markedly improve when the drug was loaded into the dendrimer aggregates, specially into those containing the *bis*-GMPA dendron in the hydrophilic side of the Janus dendrimer, namely $(NH_3^+)_8$[GMPA]-[MPA](C17)$_2$ and $(NH_3^+)_8$[GMPA]-[MPA](C17)$_4$ (Figure 3.10b). This profile of inhibition in the viral replication allowed to calculate the EC40 for both aggregates (values between 1 and 5 μM), while the $(NH_3^+)_8$[MPA]-[GMPA](C17)$_2$/IA did not reach the inhibition level needed to calculate this parameter within the concentration of drug assayed. These EC40 values indicate a great improvement in the anti-HCV activity of the IA when loaded into the Janus dendrimers with respect to the free drug and demonstrate the suitability of these dendritic structures as nanocarriers in an *in vitro* cellular model.

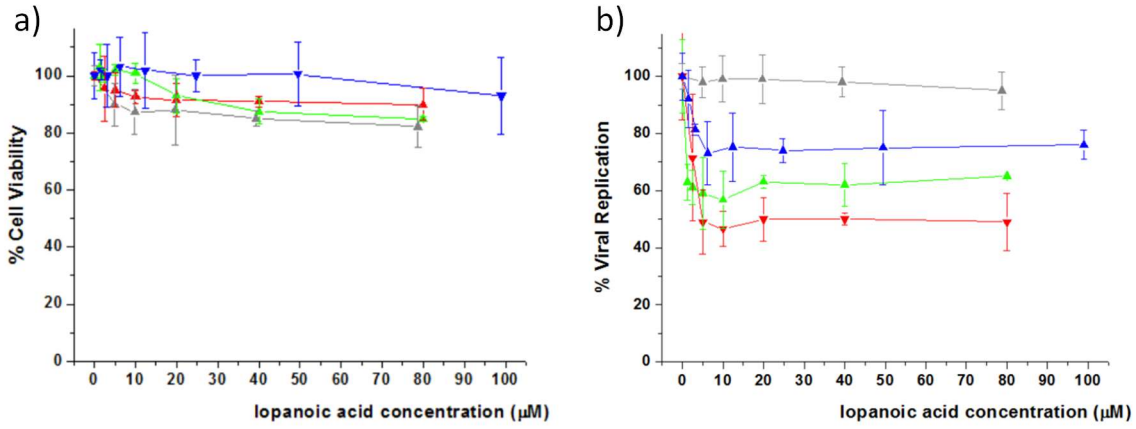

Figure 3.10. a) Cell viability and b) HCV viral replication of free IA and IA-loaded Janus dendrimers in Huh 5-2 cell line. All the data are presented as the average ± standard deviation. Colour code: free IA, grey; $(NH_3^+)_8$[GMPA]-[MPA](C17)$_2$/IA, red; $(NH_3^+)_8$[GMPA]-[MPA](C17)$_4$/IA, green; $(NH_3^+)_8$[MPA]-[GMPA](C17)$_2$/IA, blue.

On the other hand, the antiviral experiments showed that TRIAC-loaded aggregates of the dendrimers $(NH_3^+)_8$[GMPA]-[MPA](C17)$_2$ and $(NH_3^+)_8$[GMPA]-[MPA](C17)$_4$ considerably reduced the amount of drug needed to inhibit the viral replication compared with the EC40 of free TRIAC (20-40 μM) (Figure 3.11b). The EC40 values for these formulations were reached at concentrations of TRIAC between 1 and 5 μM, which means a notably enhancement of the anti-HCV of the drug with respect to its free administration. With respect to viability,

none of both systems showed cytotoxic effect up to drug concentrations of 30 μM (Figure 3.11a). Surprisingly, whereas $(NH_3^+)_8$[GMPA]-[MPA](C17)$_4$/TRIAC did not show toxicity within the full drug concentration range studied, $(NH_3^+)_8$[GMPA]-[MPA](C17)$_2$/TRIAC displayed decreased cell viability at the highest TRIAC concentration tested, i.e., 60 μM, which must be related with the increase of toxicity observed for the dendrimer itself at the highest concentration (see Figure 3.9). Anyway, this observation does not hinder its potential as effective nanocarrier given its capacity to greatly decrease the EC40 of the free drug. In contrast to dendrimers with *bis*-MPA on the lipophilic dendron, $(NH_3^+)_8$[MPA]-[GMPA](C17)$_2$ did not exhibit any benefit as carrier system for TRIAC. Their loaded aggregates do not improve the EC40 value of the free drug and moreover, the viral inhibition effect observed is likely to be due to a significant cytotoxic effect, which appears for $(NH_3^+)_8$[MPA]-[GMPA](C17)$_2$/TRIAC at a drug concentration at which the free drug is fully biocompatible.

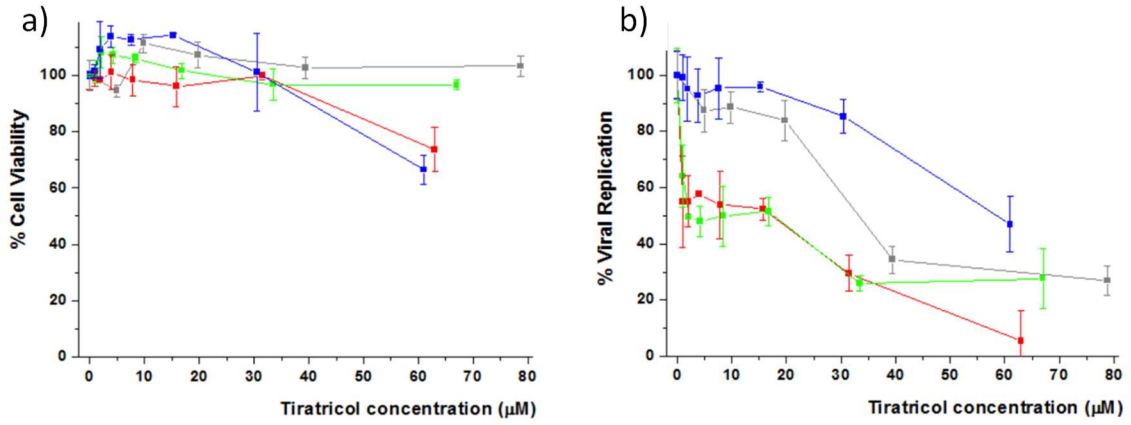

Figure 3.11. a) Cell viability and b) HCV viral replication of free TRIAC and TRIAC-loaded Janus dendrimers in Huh 5-2 cell line. All the data are presented as the average ± standard deviation. Colour code: free TRIAC, grey; $(NH_3^+)_8$[GMPA]-[MPA](C17)$_2$/TRIAC, red; $(NH_3^+)_8$[GMPA]-[MPA](C17)$_4$/TRIAC, green; $(NH_3^+)_8$[MPA]-[GMPA](C17)$_2$/TRIAC, blue.

Table 3.3. In vitro calculated CC50 and EC40 values for the dendrimer/drug aggregates compared to free drug values.

	[IA] (μM)		[TRIAC] (μM)	
	CC50	**EC40**	**CC50**	**EC40**
Free drug	300	175	188	20-40
$(NH_3^+)_8$[GMPA]-[MPA](C17)$_2$	>160	2.5–5	>63	1
$(NH_3^+)_8$[GMPA]-[MPA](C17)$_4$	>80	2.5	>67	1
$(NH_3^+)_8$[MPA]-[GMPA](C17)$_2$	>99	>99	>61	30–60

In addition, the antiviral activity of the empty dendrimer aggregates was also evaluated in the Huh 5-2 cell line to elucidate their contribution to the good values of EC40 obtained for both drugs when loaded into the aggregates. An inhibition of almost 35% in the viral replication was observed for $(NH_3^+)_8$[GMPA]-[MPA](C17)$_4$ aggregates at 15 μM, while $(NH_3^+)_8$[GMPA]-[MPA](C17)$_2$ and $(NH_3^+)_8$[MPA]-[GMPA](C17)$_2$ scarcely affected the virus life cycle in around 20% at the highest concentrations of dendrimer aggregates around 40 μM (Figure 3.12).

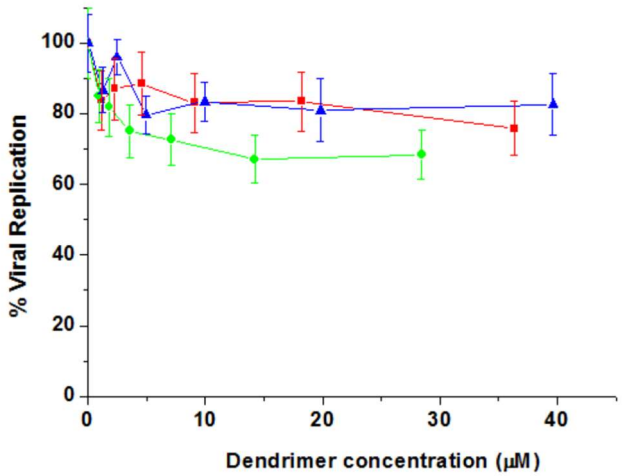

Figure 3.12. HCV viral replication of the Janus dendrimers in Huh 5-2 cell line. All the data are presented as the average ± standard deviation. Colour code: $(NH_3^+)_8$[GMPA]-[MPA](C17)$_2$, red; $(NH_3^+)_8$[GMPA]-[MPA](C17)$_4$, green and $(NH_3^+)_8$[MPA]-[GMPA](C17)$_2$, blue.

A more detailed revision of the contribution of the empty dendritic aggregates to the final antiviral activity of the drug-loaded aggregates can be done with data gathered in Table 3.4. Specifically, data for aggregates containing 10 μM IA and 30 μM TRIAC are included since those concentrations allow a proper comparative analysis. The calculation of the antiviral activity exerted by the empty dendrimers at the corresponding amount present in the samples with drug, allow to visualise their contribution to the viral replication inhibition. For instance, the aggregates $(NH_3^+)_8$[GMPA]-[MPA]$(C17)_2$/IA at 10 μM IA show a 54% of antiviral activity, while the same amount of empty dendritic aggregates just present an 11% of antiviral activity. This tendency is repeated within all samples containing IA and TRIAC, except for $(NH_3^+)_8$[MPA]-[GMPA]$(C17)_2$/TRIAC, whose antiviral activity at 30 μM of drug (16%) is worse than that of the free TRIAC (42%) and comparable to the corresponding empty dendrimer (18%).

Gathering all together, the antiviral activity due to the empty dendrimer aggregates can contribute to the good results found for the drug-loaded aggregates, specially at the lowest concentrations, but it is not enough to explain them. It is the combination of the drug with the dendrimer aggregates which is responsible of the EC40 decreases previously described. Specifically, a synergistic effect is observed for the IA-loaded aggregates, whose antiviral activity is improved with respect to the addition of the activity of the free drug and the activity of the empty dendrimer at the corresponding concentrations. However, this is not the case of the TRIAC-loaded aggregates, where just an additive effect of the activity of the two separated components seems to be responsible of the final antiviral activity of the compounds.

Table 3.4. Percentage of antiviral activity in Huh 5-2 cells of samples containing 10 μM IA or 30 μM TRIAC. The amount of dendrimer present in these samples and the corresponding antiviral activity of this amount of empty dendrimers are also indicated.

Sample	[drug] (μM)	[dendrimer] (μM)	% viral replication	% antiviral activity
Free IA	10	-	100	0
$(NH_3^+)_8$[GMPA]-[MPA]$(C17)_2$/IA	10	4.54	46	54
$(NH_3^+)_8$[GMPA]-[MPA]$(C17)_4$/IA	10	7.11	57	43
$(NH_3^+)_8$[MPA]-[GMPA]$(C17)_2$/IA	10	8.01	72	28
$(NH_3^+)_8$[GMPA]-[MPA]$(C17)_2$	-	4.54	89	11
$(NH_3^+)_8$[GMPA]-[MPA]$(C17)_4$	-	7.11	72	28
$(NH_3^+)_8$[MPA]-[GMPA]$(C17)_2$	-	8.01	82	18
Free TRIAC	30	-	58	42
$(NH_3^+)_8$[GMPA]-[MPA]$(C17)_2$/TRIAC	30	34.61	32	68
$(NH_3^+)_8$[GMPA]-[MPA]$(C17)_4$/TRIAC	30	25.46	32	68
$(NH_3^+)_8$[MPA]-[GMPA]$(C17)_2$/TRIAC	30	38.98	84	16
$(NH_3^+)_8$[GMPA]-[MPA]$(C17)_2$	-	34.61	77	23
$(NH_3^+)_8$[GMPA]-[MPA]$(C17)_4$	-	25.46	67	33
$(NH_3^+)_8$[MPA]-[GMPA]$(C17)_2$	-	38.98	82	18

3.4. General remarks

Summary

In this work, the interaction between two inhibitors of the viral protease NS3, IA and TRIAC, and the Janus aggregates has been studied by calorimetric titration. In a next step, the effective loading of the drugs into the aggregates has been determined and the morphology of the resulting aggregates has been visualised. Furthermore, the anti-HCV activity of the loaded dendritic aggregates has been determined *in vitro*, as well as their effect in the cellular viability.

Conclusions

The Janus amphiphilic dendrimers designed combining *bis*-MPA and *bis*-GMPA units on their structures have proved to be effective nanocarriers for both drugs, IA and TRIAC. The lipophilic content of the dendrimers seems to be influent in the interaction and the loading of the drugs following the diffusion technique, in which the dendritic aggregates are already formed when the drug is added. In addition, their ability to reach the Huh 5-2 cellular model and inhibit the viral replication has been demonstrated to be more efficient when the *bis*-GMPA architecture remains on the hydrophilic face of the dendrimer. Accordingly, $(NH_3^+)_8$[GMPA]-[MPA]$(C17)_2$ and $(NH_3^+)_8$[GMPA]-[MPA]$(C17)_4$ constitute promising nanocarriers that have rescued the cellular *in vitro* anti-HCV activity of both drugs, IA and TRIAC.

Future perspectives

Although successful antiviral results have been obtained with two of the dendritic aggregates, $(NH_3^+)_8$[GMPA]-[MPA]$(C17)_2$ and $(NH_3^+)_8$[GMPA]-[MPA]$(C17)_4$, as nanocarriers for IA and TRIAC; further efforts could be made in order to improve the behaviour of the other dendritic structures. For example, different methodologies could be implemented for the drug loading into the aggregates to increase the amount of drug loaded into $(NH_3^+)_8$[MPA]-[GMPA]$(C17)_4$ aggregates, such as the cosolvent method or some microfluidics approaches.

Additionally, a drug release study would help into the comprehension of the kinetics of the drugs when loaded into the nanocarriers, and *in vivo* studies would be necessary to test the activity of these formulations in a more complex model.

On the other hand, the most promising Janus dendrimers could be studied as nanocarriers for different compounds with anti-NS3 activity but rejected in the cellular screening assessed in the work by Abian *et al*[7], as it was the case for IA and TRIAC. Specifically, compounds with the size, the lipophilicity and the suitability to be determined spectrophotometrically (as they contain aromatic groups like IA and TRIAC) appear as good candidates for future studies.

Moreover, the versatility of functionalisation intrinsic to the dendrimers allows the possibility to attach a target molecule on the surface of the dendrimer to favour its route towards the tissue of interest. In this regard, the Janus dendrimers could be functionalised with specific antibodies to target the receptors overexpressed in virus infected hepatocytes, like CLDN1[38], and thus, allow a targeted drug delivery towards the hepatic infected tissue.

The results included in this chapter have been published in the journal Pharmaceutics[39]:

pharmaceutics

MDPI

Article

Janus Dendrimers to Assess the Anti-HCV Activity of Molecules in Cell-Assays

María San Anselmo [1,†], Alexandre Lancelot [1,†], Julia E. Egido [1], Rafael Clavería-Gimeno [2,3,4,‡], Álvaro Casanova [5], José Luis Serrano [1], Silvia Hernández-Ainsa [1,6,*], Olga Abian [2,3,4,7,8,*] and Teresa Sierra [1,*]

1 Instituto de Nanociencia y Materiales de Aragón (INMA), University of Zaragoza-CSIC, Pedro Cerbuna 12, 50009 Zaragoza, Spain; msananselmo@unizar.es (M.S.A.); alexandrelancelot@gmail.com (A.L.); J.EgidoEgido@umcutrecht.nl (J.E.E.); joseluis@unizar.es (J.L.S.)
2 Instituto Aragonés de Ciencias de la Salud (IACS), 50009 Zaragoza, Spain; rafacg@bifi.es
3 Institute of Biocomputation and Physics of Complex Systems (BIFI), Joint Unit IQFR-CSIC-BIFI, Universidad de Zaragoza, 50018 Zaragoza, Spain
4 Aragon Institute for Health Research (IIS Aragon), 50009 Zaragoza, Spain
5 Departamento de Farmacología y Fisiología, Facultad de Medicina, Universidad de Zaragoza, 50009 Zaragoza, Spain; alvarocasanov@gmail.com
6 ARAID Foundation, Government of Aragón, 50018 Zaragoza, Spain
7 Centro de Investigación Biomédica en Red en el Área Temática de Enfermedades Hepáticas y Digestivas (CIBERehd), 28029 Barcelona, Spain
8 Departamento de Bioquímica y Biología Molecular y Celular, Universidad de Zaragoza, 50009 Zaragoza, Spain
* Correspondence: silviamh83@unizar.es (S.H.-A.); oabifra@unizar.es (O.A.); tsierra@unizar.es or tsierra@ctq.csic.es (T.S.); Tel.: +34-876-555388 (S.H.-A.); +34-876-555417 (O.A.); +34-976-762276 (T.S.)
† These authors contribute equally to this paper.
‡ Current address: Certest Biotec S.L., 50840 Zaragoza, Spain.

Received: 16 October 2020; Accepted: 5 November 2020; Published: 7 November 2020

check for updates

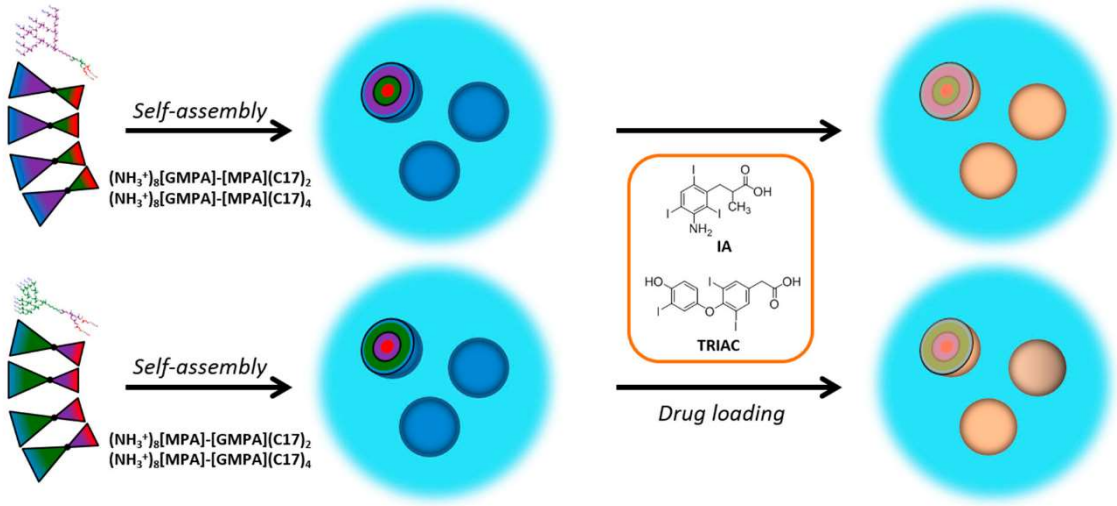

3.5. References

(1) Manns, M. P.; Buti, M.; Gane, E.; Pawlotsky, J.-M.; Razavi, H.; Terrault, N.; Younossi, Z. Hepatitis C Virus Infection. *Nat Rev Dis Primers* **2017**, *3* (1), 17006. https://doi.org/10.1038/nrdp.2017.6.

(2) Inglese, J.; Johnson, R. L.; Simeonov, A.; Xia, M.; Zheng, W.; Austin, C. P.; Auld, D. S. High-Throughput Screening Assays for the Identification of Chemical Probes. *Nature Chemical Biology* **2007**, *3* (8), 466–479. https://doi.org/10.1038/nchembio.2007.17.

(3) Bleicher, K. H.; Böhm, H.-J.; Müller, K.; Alanine, A. I. Hit and Lead Generation: Beyond High-Throughput Screening. *Nature Reviews Drug Discovery* **2003**, *2* (5), 369–378. https://doi.org/10.1038/nrd1086.

(4) Noah, J. New Developments and Emerging Trends in High-Throughput Screening Methods for Lead Compound Identification. *International Journal of High Throughput Screening* **2010**, 141. https://doi.org/10.2147/ijhts.s8683.

(5) García-Serradilla, M.; Risco, C.; Pacheco, B. Drug Repurposing for New, Effi Cient, Broad Spectrum Antivirals. *Virus Research* **2020**, *264*, 22–31. https://doi.org/10.1016/j.virusres.2019.02.011.

(6) Koizumi, Y.; Ohashi, H.; Nakajima, S.; Tanaka, Y.; Wakita, T.; Perelson, A. S.; Iwami, S.; Watashi, K. Quantifying Antiviral Activity Optimizes Drug Combinations against Hepatitis C Virus Infection. *Proceedings of the National Academy of Sciences of the United States of America* **2017**, *114* (12), 1922–1927. https://doi.org/10.1073/pnas.1610197114.

(7) Abian, O.; Vega, S.; Sancho, J.; Velazquez-Campoy, A. Allosteric Inhibitors of the NS3 Protease from the Hepatitis C Virus. *PLoS ONE* **2013**, *8* (7), 1–10. https://doi.org/10.1371/journal.pone.0069773.

(8) Martino, E.; Della Volpe, S.; Terribile, E.; Benetti, E.; Sakaj, M.; Centamore, A.; Sala, A.; Collina, S. The Long Story of Camptothecin: From Traditional Medicine to Drugs. *Bioorganic & Medicinal Chemistry Letters* **2017**, *27* (4), 701–707. https://doi.org/10.1016/j.bmcl.2016.12.085.

(9) Claveria-Gimeno, R.; Vega, S.; Grazu, V.; de la Fuente, J. M.; Lanas, A.; Velazquez-Campoy, A.; Abian, O. Rescuing Compound Bioactivity in a Secondary Cell-Based Screening by Using γ-Cyclodextrin as a Molecular Carrier. *International Journal of Nanomedicine* **2015**, *10*, 2249–2259. https://doi.org/10.2147/IJN.S79480.

(10) Torchilin, V. P. Multifunctional Nanocarriers. *Advanced Drug Delivery Reviews* **2006**, *58* (14), 1532–1555. https://doi.org/10.1016/j.addr.2006.09.009.

(11) Patil, A.; Mishra*, V.; Thakur, S.; Riyaz, B.; Kaur, A.; Khursheed, R.; Sathe, K. P. and B. Nanotechnology Derived Nanotools in Biomedical Perspectives: An Update. *Current Nanoscience* **2019**, *15* (2). https://doi.org/10.2174/1573413714666180426112851.

(12) Su, C.; Liu, Y.; Li, R.; Wu, W.; Fawcett, J. P.; Gu, J. Absorption, Distribution, Metabolism and Excretion of the Biomaterials Used in

Nanocarrier Drug Delivery Systems. *Advanced Drug Delivery Reviews* **2019**, *143*, 97–114. https://doi.org/10.1016/j.addr.2019.06.008.
(13) Sherje, A. P.; Jadhav, M.; Dravyakar, B. R.; Kadam, D. Dendrimers: A Versatile Nanocarrier for Drug Delivery and Targeting. *International Journal of Pharmaceutics* **2018**, *548* (1), 707–720. https://doi.org/10.1016/j.ijpharm.2018.07.030.
(14) Sandoval-Yañez, C.; Castro Rodriguez, C. Dendrimers: Amazing Platforms for Bioactive Molecule Delivery Systems. *Materials* **2020**, *13* (3), 570. https://doi.org/10.3390/ma13030570.
(15) Mendes, L. P.; Pan, J.; Torchilin, V. P. Dendrimers as Nanocarriers for Nucleic Acid and Drug Delivery in Cancer Therapy. *Molecules* **2017**, *22* (9), 1–21. https://doi.org/10.3390/molecules22091401.
(16) Chahal, J. S.; Khan, O. F.; Cooper, C. L.; McPartlan, J. S.; Tsosie, J. K.; Tilley, L. D.; Sidik, S. M.; Lourido, S.; Langer, R.; Bavari, S.; Ploegh, H. L.; Anderson, D. G. Dendrimer-RNA Nanoparticles Generate Protective Immunity against Lethal Ebola, H1N1 Influenza, and *Toxoplasma Gondii* Challenges with a Single Dose. *Proc Natl Acad Sci USA* **2016**, *113* (29), E4133–E4142. https://doi.org/10.1073/pnas.1600299113.
(17) Bahadoran, A.; Moeini, H.; Bejo, M. H.; Hussein, M. Z.; Omar, A. R. Development of Tat-Conjugated Dendrimer for Transdermal DNA Vaccine Delivery. *J Pharm Pharm Sci* **2016**, *19* (3), 325–338. https://doi.org/10.18433/J3G31Q.
(18) Mhlwatika, Z.; Aderibigbe, B. A. Application of Dendrimers for the Treatment of Infectious Diseases. *Molecules* **2018**, *23* (9), 2205. https://doi.org/10.3390/molecules23092205.
(19) Mintzer, M. A.; Dane, E. L.; O'Toole, G. A.; Grinstaff, M. W. Exploiting Dendrimer Multivalency To Combat Emerging and Re-Emerging Infectious Diseases. *Mol. Pharmaceutics* **2012**, *9* (3), 342–354. https://doi.org/10.1021/mp2005033.
(20) Liu, X.; Gitsov, I. Thermosensitive Amphiphilic Janus Dendrimers with Embedded Metal Binding Sites. Synthesis and Self-Assembly. *Macromolecules* **2018**, *51* (14), 5085–5100. https://doi.org/10.1021/acs.macromol.8b00700.
(21) Buzzacchera, I.; Xiao, Q.; Han, H.; Rahimi, K.; Li, S.; Kostina, N. Y.; Toebes, B. J.; Wilner, S. E.; Möller, M.; Rodriguez-Emmenegger, C.; Baumgart, T.; Wilson, D. A.; Wilson, C. J.; Klein, M. L.; Percec, V. Screening Libraries of Amphiphilic Janus Dendrimers Based on Natural Phenolic Acids to Discover Monodisperse Unilamellar Dendrimersomes. *Biomacromolecules* **2019**, *20* (2), 712–727. https://doi.org/10.1021/acs.biomac.8b01405.
(22) Sherman, S. E.; Xiao, Q.; Percec, V. Mimicking Complex Biological Membranes and Their Programmable Glycan Ligands with Dendrimersomes and Glycodendrimersomes. *Chemical Reviews* **2017**, *117* (9), 6538–6631. https://doi.org/10.1021/acs.chemrev.7b00097.

(23) Caminade, A.-M.; Laurent, R.; Delavaux-Nicot, B.; Majoral, J.-P. “Janus” Dendrimers: Syntheses and Properties. *New J. Chem.* **2012**, *36* (2), 217–226. https://doi.org/10.1039/C1NJ20458K.

(24) Sikwal, D. R.; Kalhapure, R. S.; Govender, T. An Emerging Class of Amphiphilic Dendrimers for Pharmaceutical and Biomedical Applications: Janus Amphiphilic Dendrimers. *European Journal of Pharmaceutical Sciences* **2017**, *97*, 113–134. https://doi.org/10.1016/j.ejps.2016.11.013.

(25) Taabache, S.; Bertin, A. Vesicles from Amphiphilic Dumbbells and Janus Dendrimers: Bioinspired Self-Assembled Structures for Biomedical Applications. *Polymers* **2017**, *9* (12), 280. https://doi.org/10.3390/polym9070280.

(26) Najafi, F.; Salami-Kalajahi, M.; Roghani-Mamaqani, H. Synthesis of Amphiphilic Janus Dendrimer and Its Application in Improvement of Hydrophobic Drugs Solubility in Aqueous Media. *European Polymer Journal* **2020**, *134*, 109804. https://doi.org/10.1016/j.eurpolymj.2020.109804.

(27) Jiménez-Pardo, I.; González-Pastor, R.; Lancelot, A.; Claveria-Gimeno, R.; Velázquez-Campoy, A.; Abian, O.; Ros, M. B.; Sierra, T. Shell Cross-Linked Polymeric Micelles as Camptothecin Nanocarriers for Anti-HCV Therapy. *Macromolecular Bioscience* **2015**, *15* (10), 1381–1391. https://doi.org/10.1002/mabi.201500094.

(28) Concellón, A.; Clavería-Gimeno, R.; Velázquez-Campoy, A.; Abian, O.; Piñol, M.; Oriol, L. Polymeric Micelles from Block Copolymers Containing 2,6-Diacylaminopyridine Units for Encapsulation of Hydrophobic Drugs. *RSC Adv.* **2016**, *6* (29), 24066–24075. https://doi.org/10.1039/C6RA01714B.

(29) Lancelot, A.; Clavería-Gimeno, R.; Velázquez-Campoy, A.; Abian, O.; Serrano, J. L.; Sierra, T. Nanostructures Based on Ammonium-Terminated Amphiphilic Janus Dendrimers as Camptothecin Carriers with Antiviral Activity. *European Polymer Journal* **2017**, *90* (February), 136–149. https://doi.org/10.1016/j.eurpolymj.2017.03.012.

(30) Lancelot, A.; González-Pastor, R.; Clavería-Gimeno, R.; Romero, P.; Abian, O.; Martín-Duque, P.; Serrano, J. L.; Sierra, T. Cationic Poly(Ester Amide) Dendrimers: Alluring Materials for Biomedical Applications. *Journal of Materials Chemistry B* **2018**, *6* (23), 3956–3968. https://doi.org/10.1039/c8tb00639c.

(31) Vega, S.; Abian, O.; Velazquez-Campoy, A. A Unified Framework Based on the Binding Polynomial for Characterizing Biological Systems by Isothermal Titration Calorimetry. *Methods* **2015**, *76*, 99–115. https://doi.org/10.1016/j.ymeth.2014.09.010.

(32) Velázquez Campoy, A.; Freire, E. ITC in the Post-Genomic Era…? Priceless. *Biophysical Chemistry* **2005**, *115* (2–3), 115–124. https://doi.org/10.1016/j.bpc.2004.12.015.

(33) Fedeli, E.; Lancelot, A.; Dominguez, J.; Serrano, J.; Calvo, P.; Sierra, T. Self-Assembling Hybrid Linear-Dendritic Block Copolymers: The Design of Nano-Carriers for Lipophilic Antitumoral Drugs. *Nanomaterials* **2019**, *9* (2), 161. https://doi.org/10.3390/nano9020161.

(34) del Barrio, J.; Oriol, L.; Sánchez, C.; Serrano, J. L.; Di Cicco, A.; Keller, P.; Li, M.-H. Self-Assembly of Linear−Dendritic Diblock Copolymers: From Nanofibers to Polymersomes. *J. Am. Chem. Soc.* **2010**, *132* (11), 3762–3769. https://doi.org/10.1021/ja9083946.
(35) Liu, X.; Gitsov, I. Nonionic Amphiphilic Linear Dendritic Block Copolymers. Solvent-Induced Self-Assembly and Morphology Tuning. *Macromolecules* **2019**, *52* (15), 5563–5573. https://doi.org/10.1021/acs.macromol.9b01023.
(36) Lohmann, V. Replication of Subgenomic Hepatitis C Virus RNAs in a Hepatoma Cell Line. *Science* **1999**, *285* (5424), 110–113. https://doi.org/10.1126/science.285.5424.110.
(37) Bartenschlager, R. Hepatitis C Virus Replicons: Potential Role for Drug Development. *Nature Reviews Drug Discovery* **2002**, *1* (11), 911–916. https://doi.org/10.1038/nrd942.
(38) Reynolds, G. M.; Harris, H. J.; Jennings, A.; Hu, K.; Grove, J.; Lalor, P. F.; Adams, D. H.; Balfe, P.; Hübscher, S. G.; McKeating, J. A. Hepatitis C Virus Receptor Expression in Normal and Diseased Liver Tissue. *Hepatology* **2008**, *47* (2), 418–427. https://doi.org/10.1002/hep.22028.
(39) San Anselmo, M.; Lancelot, A.; Egido, J. E.; Clavería-Gimeno, R.; Casanova, Á.; Serrano, J. L.; Hernández-Ainsa, S.; Abian, O.; Sierra, T. Janus Dendrimers to Assess the Anti-HCV Activity of Molecules in Cell-Assays. *Pharmaceutics* **2020**, *12* (11), 1062. https://doi.org/10.3390/pharmaceutics12111062.

Chapter 4:

Amphiphilic Janus dendrimers as drug carriers for Tuberculosis

4.1. Tuberculosis

4.1.1. Introduction

Tuberculosis (TB) is an infectious disease caused by *Mycobacterium tuberculosis* (*Mtb*), an intracellular pathogenic bacillus easy to disseminate from patient to patient within droplets transmitted through the air[1]. Pulmonary TB, with bacteria affecting the lungs and more specifically, the alveolar macrophages, is the most typical variant of the disease, but TB can also affect other sites (extrapulmonary TB). According to the last WHO global report about the disease[2], TB remains one of the top ten causes of death worldwide and is the leading cause of death from a single infectious disease. It is estimated that around a quarter of the world´s population, approximately 1.7 billion people, is infected by *Mtb*, being adult men of poor countries the most susceptible population, although just 5-15% of people infected will develop the disease[3].

Fortunately, there are preventive and curative treatments available, what is helping in the decrease in the mortality and morbidity, although the disease still remains as an epidemic. Since vaccination is the most effective way to control infectious diseases and there is evidence of natural human defences against TB, lots of efforts have been made towards this direction. The BCG (Bacillus Calmette–Guérin) vaccine, an attenuated form of *Mycobacterium bovis*, is the most widely used vaccine and there exist several vaccine candidates under clinical trials[3]. They can be grouped into two main categories, the whole cell-derived vaccines and the subunit vaccines. The promising vaccine MTBVAC, classified within the first group, consists of a live strain of *Mtb* attenuated by deletion of *phoP* and *fadD26*, two major virulence genes of the bacteria[4]. It has been developed at University of Zaragoza in the Group of Mycobacterium Genetics lead by Carlos Martín Montañés, and is currently in Phase IIa dose-defining trials in South Africa, while previously the safety level and the advantageous immunogenicity with respect to BCG have been demonstrated[5].

The treatment of drug susceptible TB includes four first line anti-TB medicines (see Table 4.1) for a period of two months, which is further continued four months with just two of these drugs, and this results to be successful in 85% of the patients. However, this treatment regimen is too long for many patients and lots

of efforts are being made towards safe and effective shorter regimens[6]. Regarding the administration routes of the drugs, although the first-line treatment for drug susceptible TB is given orally, the inhaled forms would be preferable in order to reach a high concentration of the drug within the lungs, thus needing a lower amount of total drug in the treatment and avoiding the side effects of the oral administration[7].

Table 4.1. Classification of the anti-TB drugs into different groups made by the WHO[8].

Groups of anti-TB drugs			
First line	**Group A**	**Group B**	**Group C**
Rifampicin	Levofloxacin	Clofazimine	Delamanid
Isoniazid	Moxifloxacin	D-cycloserine	Imipenem-Cilastatin
Ethambutol	Bedaquiline		Meropenem
Pyrazinamide	Linezolid		Amikacin
			Streptomycin
			Ethionamide
			Prothionamide
			para-aminosalicylic acid

Unfortunately, the emergence of resistant strains increases the complexity of the control of the disease. The *Mtb* isolates, according to increasing resistance to major drugs used in the treatment, can be classified into: rifampicin (RIF) resistant TB (RR-TB), multidrug resistant TB (MDR-TB) as those strains resistant to RIF and isoniazid (INH), and extensively drug resistant TB (XDR-TB)[9–13]. Very recently, in January of 2021, a definition of pre-XDR-TB has been proposed by the WHO as "TB caused by *Mtb* strains that fulfil the definition of MDR/RR-TB and which are also resistant to any fluoroquinolone". Additionally, the definition of XDR-TB has been updated to "TB caused by *Mtb* strains that fulfil the definition of

MDR/RR-TB and which are also resistant to any fluoroquinolone and at least one additional Group A drug"[14] (the fluoroquinolones recommended by the WHO for longer regimes are levofloxacin and moxifloxacin, and the different groups of anti-TB drugs are shown in Table 4.1). These resistant-TB strains require a lengthy and costly combination of drugs, which are less efficient and have more side effects than those used for the susceptible strains. For this reason, newly, shorter regimens[15] and novel therapies as the ones based on phages[16] are under examination as new strategies to deal with the resistances.

In the current therapy for treating drug susceptible TB, the combination of RIF together with INH forms the basis of the treatment because of their powerful bactericidal activity[17]. However, the bioavailability of RIF is a tricky mater and more specifically, in combined therapies with the presence of INH and pyrazinamide. Some studies points out at the existence of polymorphisms of RIF[18], which would be prompted by the presence of the other drugs[19], as the major cause of variability in its bioavailability. In contrast, other studies state that this is likely to be due to some mechanisms that enhance the degradation of RIF in presence of INH in acidic medium[19,20]. Anyway, a possible strategy to overcome this drawback would consist on the segregated administration of both drugs[19] or their protection with nanocarriers[21].

In this regard, some nanotechnological approaches have been developed with a potential use in the treatment of TB, as well as in their diagnosis and prevention[22–25]. Nanoparticles (NPs) for anti-TB drug delivery include liposomes, polymeric NPs, dendrimers, niosomes, aerosolic NPs, carbon nanotubes or the inorganic ceramic NPs[25]. Moreover, nanotechnology can bring the opportunity to co-deliver two drugs loaded together in the same nanocarrier, which could overcome the differences in the bioavailability of the single drugs *in vivo* and could allow their simultaneous release in the target tissue[26,27].

The field of the dendritic materials applied to the TB treatment has been scarcely explored to date and all examples founded are based on the physical entrapment of the drug[22,28,29]. Some attempts have been made in order to solubilise the drug RIF and then, to increase its bioavailability[30]. For example, with the additional aim to improve its internalisation into macrophages, Kumar *et al.* designed

mannosylated ethylenediamine PPI dendrimers[31] (the monosaccharide mannose specifically targets macrophages) and later, they added the PEGylation modification on the surface of the dendrimers to prolong the release of RIF[32]. The association of RIF with another type of dendrimers, PAMAM dendrimers of different generations, has been studied either with simulation[33] or experimental tools, including *in vivo* studies[34]. Other relevant drug in the TB treatment, INH, has been loaded into PAMAM dendrimers to improve their sustained delivery[35] and also PAMAM dendrimeric nanoclusters with copper and INH have been more recently studied[36].

4.1.2. Objectives and working plan

In this study, we open a research line employing *bis*-MPA and *bis*-GMPA based dendrimers in the treatment of TB. Specifically, four amphiphilic Janus dendrimers varying the *bis*-MPA/ *bis*-GMPA architecture between their sides and the generation of the lipophilic dendron have been used: $(NH_3^+)_8$[GMPA]-[MPA]$(C17)_2$, $(NH_3^+)_8$[GMPA]-[MPA]$(C17)_4$, $(NH_3^+)_8$[MPA]-[GMPA]$(C17)_2$, and $(NH_3^+)_8$[MPA]-[GMPA]$(C17)_4$ (see chapter 2). It must be noted that all dendrimers employed for this study bear TFA^- as counterion.

The objectives pursued with the employment of these amphiphilic Janus as anti-TB nanocarriers can be divided into two main blocks:

I. Previous TB studies involving dendrimers only include the drugs RIF and INH, both first line drugs. In this work, we aim to improve the bioavailability of these drugs, RIF and INH, and we will expand the study to other drugs including streptomycin (Group C) and bedaquiline (Group A) for the first time within a dendritic structure (see Table 4.1 and Figure 4.1). The interest on these two drugs (streptomycin and bedaquiline) relies in their mechanisms of action (which are different between them, and also different to those drugs used for the first line treatment), their different administration route (streptomycin must be given by intravenous injection), and the problematic side effects they exhibit. Bedaquiline, in addition, is used for the treatment of MDR and XDR TB.

II. We aim to investigate the combination of two anti-TB drugs, RIF and INH, together within a dendritic structure. These drugs are usually administered simultaneously in the regular anti-TB treatment and with their co-encapsulation in a dendritic structure, we aim to elucidate the consequences of being entrapped in a nanocarrier, in terms of their bioavailability and antimicrobial activity.

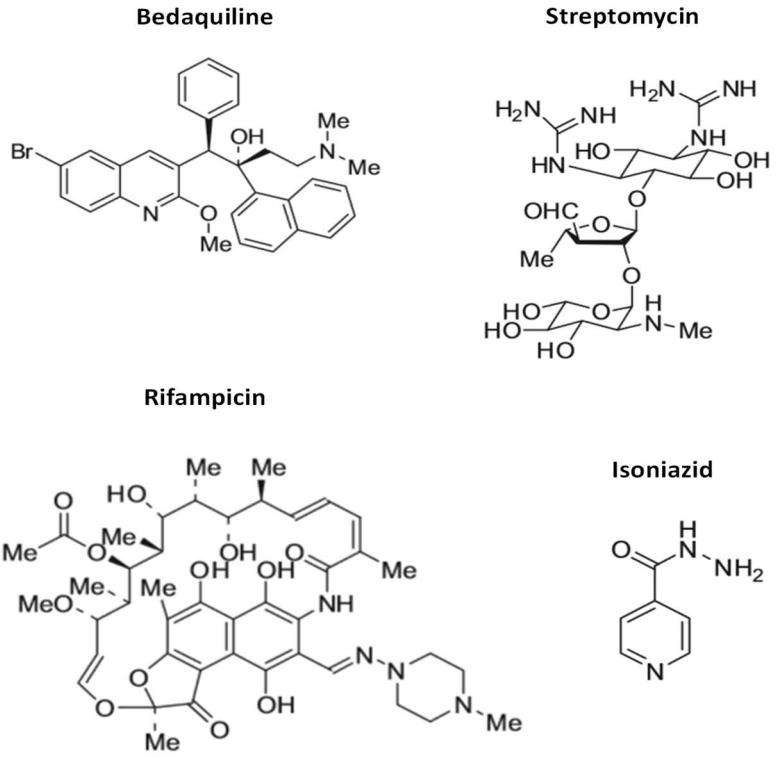

Figure 4.1. Chemical structure of the selected anti-tuberculosis agents.

The amphiphilic character of the synthesised Janus dendrimers provides a suitable environment to load both hydrophilic and lipophilic anti-TB drugs. Their ability to solubilise the proposed drugs individually or combined is presented in this chapter, as well as their antimicrobial activity against different strains of bacteria. In the following sections, the results of either single (section 4.2) or combined drugs (section 4.3) are presented, related to encapsulation ability, aggregates formation and *in vitro* antimicrobial activity determination against different strains of bacteria. Moreover, the investigation of possible synergies between drugs (section 4.3.1) and the kill curves of *Mtb* with respect to time (section 4.3.5) are also discussed.

4.2. Single drug nanocarriers based on Janus dendrimers

The following sections include the studies related to the single drugs either free or encapsulated within the Janus dendrimers. Specifically, the drug encapsulation process and quantification, their antimicrobial activity and the characterisation of the aggregates are presented.

4.2.1. Drug encapsulation and quantification

The anti-TB drugs RIF, INH, streptomycin and bedaquiline were encapsulated individually within the Janus dendritic structures at the same time as the dendritic aggregates were formed. For that purpose, the oil-in-water technique was followed by combining an organic solvent non miscible with water (DCM) and milliQ-H_2O at equal volumes. Drugs were added dissolved in one of these phases depending on their polarity, namely, RIF was dissolved in DCM and INH and streptomycin, in milliQ-H_2O. Since bedaquiline could not be dissolved in any of the two phases, DMSO was employed to dissolve it and the drug was added to the encapsulating preparation without exceeding 9% in volume. In the preparation of the aggregates, a molar ratio of 5:1 (mol of drug: mol of dendrimer) was initially used in order to have a drug excess in all cases. Then, mixtures were stirred at room temperature under ventilation until the complete evaporation of the organic phase. The required time for the complete evaporation depended on the volume of DCM added and therefore, on the amount of dendrimer, being necessary approximately one hour per mg of dendrimer. After that, the aqueous preparations were dialysed against dH_2O in order to eliminate the remaining not entrapped drugs in the case of the water-soluble drugs and the organic solvent DMSO in the case of bedaquiline encapsulation. Finally, samples were filtered through a 0.2 μm syringe filter to yield in all cases the drug loaded dendritic aggregates at a concentration of 1 mg/mL of dendrimer in milliQ-H_2O.

The amount of drug encapsulated within the dendritic aggregates was determined by High-Performance Liquid Chromatography coupled to an UV detector, HPLC/UV. The chromatographic separation was done with an analytical

cartridge C8 column (4.6 mm x 250 mm, 5 µm) with a flow rate of 1 mL/min in all cases. The mobile phase was optimised for each drug in order to reach a balance between simple eluents able to be used in the determination of various of the drugs and reasonable retention times (RT). For streptomycin and bedaquiline determination, the mobile phase was composed of methanol and a buffer of orthophosphoric acid adjusted with triethylamine to pH 3.0, at a ratio 40:60[37,38]. For the drugs INH and RIF, the eluent consisted of a mixture of acetonitrile (ACN) and the same phosphate buffer, at a ratio 60:40[39–41]. The dissolution of the aqueous loaded dendritic aggregates in the corresponding mobile phase containing methanol or ACN allowed the disruption of the aggregates and the subsequent release of the drug to properly be quantified[42,43]. The wavelengths selected for the detection of each drug were experimentally identified and they are all in the UV region of the spectra as follows: streptomycin was detected at 200 nm, bedaquiline at 225 nm, INH at 260 nm and RIF at 335 nm. Applying these conditions, the elution of the drugs in HPLC was suitable for this kind of technique, with short RT below 5 minutes in all cases. The RT found for each drug were: 2.6 min for streptomycin, 3.7 min for bedaquiline, 3.1 min for INH and 4.1 min in the case of RIF (Figure 4.2). A calibration curve was built for each drug by measuring the area below the chromatographic curve at increasing concentrations of the drugs (see Annexe 3). In the case of streptomycin (Figure 4.2a), a distorted curve was obtained by HPLC that was proportional to the concentration of drug and then, the integration of the whole signal was considered in the drug quantification.

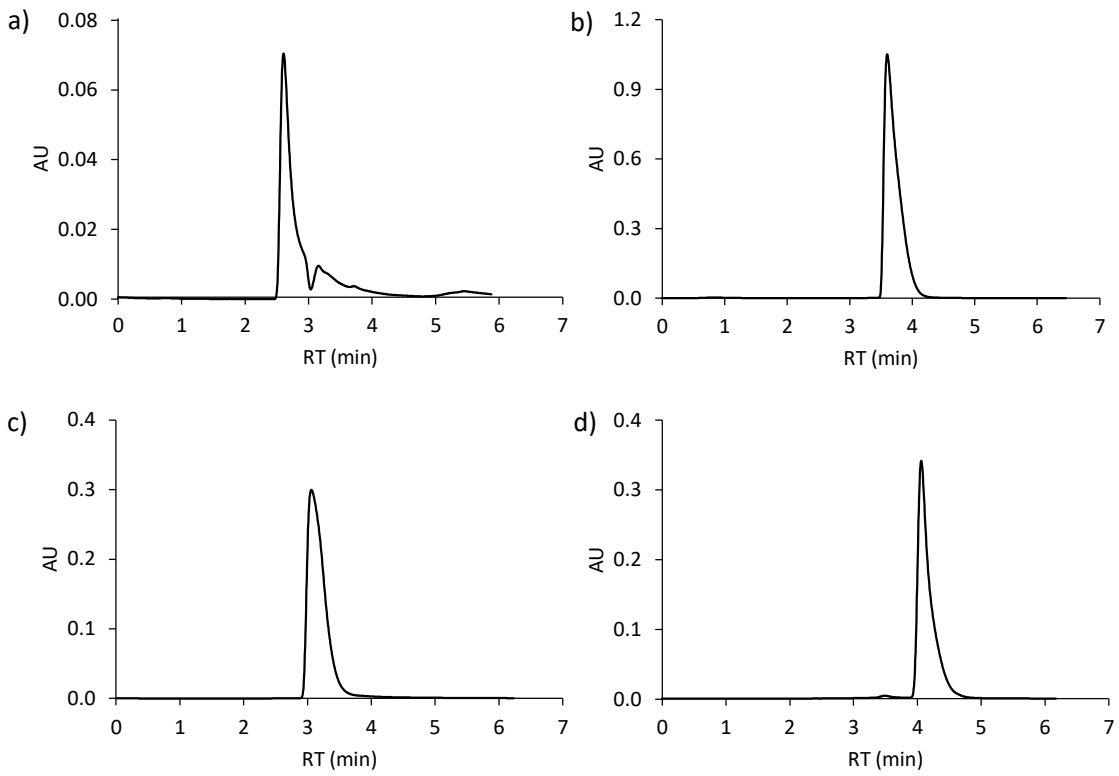

Figure 4.2. HPLC chromatograms of the single anti-tuberculosis agents: a) streptomycin, b) bedaquiline, c) INH and d) RIF.

The DLC (drug loading content) was calculated as the molar ratio between the amount of drug encapsulated within the dendrimer and the amount of dendrimer in the preparation (mol/mol). Table 4.2 gathers the quantification data of the four drugs individually encapsulated in each of the Janus dendrimers, namely, $(NH_3^+)_8$[GMPA]-[MPA](C17)$_2$, $(NH_3^+)_8$[GMPA]-[MPA](C17)$_4$, $(NH_3^+)_8$[MPA]-[GMPA](C17)$_2$, and $(NH_3^+)_8$[MPA]-[GMPA](C17)$_4$.

To provide an explanation of the encapsulation data experimentally observed, the lipophilicity of both dendrimers and drugs was taken into account. Firstly, the lipophilic content (Lc) of the dendrimers previously estimated in chapter 2 stablish the following descending order in the dendrimers regarding its Lc, in brackets: $(NH_3^+)_8$[GMPA]-[MPA](C17)$_4$ and $(NH_3^+)_8$[MPA]-[GMPA](C17)$_4$ (29.6), $(NH_3^+)_8$[MPA]-[GMPA](C17)$_2$ (21.4) and $(NH_3^+)_8$[GMPA]-[MPA](C17)$_2$ (19.4). On the other hand, the lipophilic character of the drugs was assessed by their logP value obtained from DrugBank databases and indicated in Table 4.2. It is a physicochemical parameter that indicates the preference of a solute between two

phases, usually octanol as the lipophilic phase and water as the hydrophilic one. Although it can not be considered as an absolute value able to predict the whole behaviour of a compound, it can serve as an illustrative parameter to stablish the following correlation: the higher logP value, the more lipophilic the compound is[44,45].

In general terms, proper encapsulation efficiencies were obtained for all drugs within the dendritic aggregates, except for the highly lipophilic bedaquiline (logP = 6.37), which was poorly loaded into the dendrimers. This could be due to its elevated lipophilic character or the high aromatic content in the drug structure (see Figure 4.1). Additionally, the introduction of a certain amount of DMSO may interfere with the aggregate's formation. The dendrimer $(NH_3^+)_8$[GMPA]-[MPA](C17)$_4$ is the only one that reached a DLC value above 1.00 for the bedaquiline encapsulation, and it is likely to be due to the high Lc of the dendrimer. However, the lower bedaquiline encapsulation within the other dendrimer with the same Lc, $(NH_3^+)_8$[MPA]-[GMPA](C17)$_4$, remains unexplained.

Regarding each of the drugs, similar encapsulation values within the series of dendrimers were found. This is thought to happen because the drug encapsulation process occurs while the aggregates are being formed, instead of being separated processes like in the case of the hepatitis C drug loading by diffusion[46] (see chapter 3). However, a subtle preference of the more lipophilic drugs, RIF and bedaquiline, towards the dendrimers with a higher Lc can be observed. In this line, $(NH_3^+)_8$[GMPA]-[MPA](C17)$_4$ and $(NH_3^+)_8$[MPA]-[GMPA](C17)$_4$, both with a calculated Lc of 29.6, were the Janus dendrimers which exhibited a higher DLC for the lipophilic drugs. With respect to the drugs with lower logP and then, the most hydrophilic ones, streptomycin and INH, were preferentially encapsulated within $(NH_3^+)_8$[GMPA]-[MPA](C17)$_2$, the dendrimer with the lowest Lc. The Janus dendrimer with an intermediate value of Lc of 21.4, $(NH_3^+)_8$[MPA]-[GMPA](C17)$_2$, exhibited the lowest DLC for each drug, which is in accordance with its less defined hydrophilic balance.

Table 4.2. Concentration of encapsulated drugs within the dendritic aggregates, in μg/mL, and their DLC in molar ratio. LogP for each drug was obtained from DrugBank. Lc refers to the lipophilic content estimated for each Janus dendrimer, in percentage. Mean ± SD are given for data measured in triplicate.

		Dendrimer			
Drug		**$(NH_3^+)_8$[GMPA]-[MPA](C17)$_2$** *Lc 19.4*	**$(NH_3^+)_8$[GMPA]-[MPA](C17)$_4$** *Lc 29.6*	**$(NH_3^+)_8$[MPA]-[GMPA](C17)$_2$** *Lc 21.4*	**$(NH_3^+)_8$[MPA]-[GMPA](C17)$_4$** *Lc 29.6*
Rifampicin *LogP 3.72*	[μg/mL]	395 ± 47	577 ± 107	595 ± 170	717 ± 85
	DLC	2.13 ± 0.17	2.80 ± 0.56	1.87 ± 0.99	2.83 ± 0.21
Isoniazid *LogP -0.64*	[μg/mL]	104 ± 31	44 ± 10	61 ± 15	52 ± 13
	DLC	2.61 ± 0.81	1.36 ± 0.16	1.30 ± 0.43	1.73 ± 0.85
Streptomycin *LogP -6.40*	[μg/mL]	1636	721	892	929
	DLC	3.30	1.94	1.51	1.63
Bedaquiline *LogP 6.37*	[μg/mL]	79	139	81	77
	DLC	0.57	1.16	0.54	0.64

4.2.2. Antimicrobial activity determination against BCG

The *in vitro* antimicrobial activity of each anti-TB agent either free or encapsulated was determined against *M. bovis* BCG strain, as well as the activity of the empty dendritic aggregates as controls. For that purpose, samples were assayed in two-fold serial dilutions and bacteria were inoculated at a density of 10^5 CFU/mL (colony-forming unit per mL), estimated by optical density. Finally, after 6 days of incubation at 37 ºC, the bacterial viability was assessed by a colorimetric assay, specifically by the resazurin reduction to resorufin, which triggered a colour change in the media from blue to pink in presence of viable organisms[47]. Precisely, the minimum inhibitory concentration (MIC), defined as the lowest compound concentration needed to prevent the bacterial growth, is used to evaluate the bacterial viability (Table 4.3).

Table 4.3. Minimum inhibitory concentrations (MICs) against M. bovis BCG of the free drugs and their encapsulations within the Janus dendrimers. Data are expressed in μg/mL, and at least duplicates were performed.

	MICs in BCG (μg/mL)			
	Rifampicin	**Isoniazid**	**Streptomycin**	**Bedaquiline**
Free drug	0.014	0.547	0.137	0.009
$(NH_3^+)_8$[GMPA]-[MPA](C17)$_2$	0.027-0.014	0.547	0.137	> 19.750
$(NH_3^+)_8$[GMPA]-[MPA](C17)$_4$	0.014	0.547	0.137	4.344
$(NH_3^+)_8$[MPA]-[GMPA](C17)$_2$	0.027-0.014	0.547	0.137	> 20.250
$(NH_3^+)_8$[MPA]-[GMPA](C17)$_4$	0.014	0.547	0.137	> 19.250

The encapsulation of the drug bedaquiline within the dendritic structures is one of the scarce examples found in the literature[48,49]. Apart from the low amount of drug entrapped within the dendrimers in the encapsulation process, the maintenance of its antimicrobial activity is another tricky aspect to be considered. Upon Janus dendrimer encapsulation, bedaquiline was not able to maintain its antimicrobial activity against *M. bovis* BCG. We can hypothesise that this could be due to the alteration of the stability conditions of the drug[50,51] or because of a hindered release of the drug from the dendrimers. The only combination of this drug for which the MIC could be determined was $(NH_3^+)_8$[GMPA]-[MPA](C17)$_4$/ bedaquiline, but its value, 4.344 μg/mL, was far from the MIC of the free drug (0.009 μg/mL) (Table 4.3).

The results found for the other anti-TB drugs were more promising. The activity of the encapsulated hydrophilic drugs, INH and streptomycin, was maintained unaltered with respect to the free drugs. Namely, INH showed a MIC of 0.547 μg/mL either free or encapsulated within the four dendrimers, and the fixed MIC value for streptomycin was 0.137 μg/mL in all combinations. For RIF, it was also possible to keep its antimicrobial activity after the encapsulation process, with a MIC value ranging from 0.027 to 0.014 μg/mL, a minor difference of just a dilution, which is not considered significant in this method.

In addition, the antimicrobial activity of the empty dendrimers was evaluated following the same procedure and no antimicrobial activity against *M. bovis* BCG could be detected even at the highest concentration tested (87.5 μg/mL). This is a concentration much higher than the experimentally tested with the encapsulated drugs, which is below 1 μg/mL of dendrimer in all cases. Thus, it can be affirmed that the Janus dendrimers did not show any antibacterial activity against *M. bovis* BCG by themselves.

These results obtained by the colorimetric resazurin method against *M. bovis* BCG were promising regarding the capacity of the dendrimers to entrap the drugs and solubilise them while maintaining the antimicrobial activity of RIF, INH and streptomycin.

4.2.3. Morphological study of the aggregates

The dendritic aggregates of $(NH_3^+)_8$[GMPA]-[MPA](C17)$_4$ loaded with the single drugs were characterised as a representative example of the series of dendrimers. This dendrimer was selected for further studies because it offered better antimicrobial results with all the drugs tested (see section 4.2.2). Their morphology was determined by transmission electronic microscopy (TEM), staining the samples with a solution of uranyl acetate (as described in chapter 7) and furthermore, dynamic light scattering (DLS) was developed to assess the size of the samples in solution. The results obtained by both characterisation techniques were in good agreement.

The encapsulation of the different drugs into the Janus dendrimer led to a diversity of morphologies in the resulting aggregates (Figure 4.3 and Table 4.4). On the one hand, $(NH_3^+)_8$[GMPA]-[MPA](C17)$_4$ with RIF formed small micelles with cylindrical shape (Figure 4.3b), while the cylindrical micelles observed for the dendrimer with INH were thinner and more elongated (Figure 4.3c). Different sizes for these micelles were measured by DLS, being the hydrodynamic diameter (D_H) around 13±2 nm for the micelles containing RIF and 38±7 nm in the case of the INH-containing aggregates. Since DLS assumes spherical objects in its analysis, it is reasonable to find differences in the size of these elongated cylindrical micelles determined by both techniques, TEM and DLS.

The biggest aggregates were obtained with the encapsulation of streptomycin within the dendrimer (Figure 4.3d), where two populations of rounded objects around 93±8 nm and 63±3 nm in diameter were observed by TEM and interestingly, an outer layer with a thickness of 9.8±0.6 nm with different staining contrast could be distinguished in their structure. This observation could be aligned with a disposition of the dendrimer and the drug forming nanospheres[50] with an inner space containing more organic matter where the drug would be located. The D_H measured by DLS for these structures was 48±7 nm.

Finally, the softer morphological change with respect to the empty dendrimer (Figure 4.3a) was observed after the entrapment of bedaquiline (Figure 4.3e), the drug that was encapsulated to a lesser extent. In that case, rounded micelles were also observed after the encapsulation process and their medium size just increased 3 nm in diameter with respect to the empty aggregates formed by $(NH_3^+)_8$[GMPA]-[MPA](C17)$_4$.

Table 4.4. Average hydrodynamic diameters in number measured by DLS, in nm, and morphology observed in TEM of the $(NH_3^+)_8$[GMPA]-[MPA](C17)$_4$ empty aggregates and those with the different anti-tuberculosis drugs encapsulated.

		D_H (nm)	morphology
$(NH_3^+)_8$[GMPA]-[MPA](C17)$_4$	**Empty carrier**	24 ± 1	rounded micelles
	Rifampicin	13 ± 2	cylindrical micelles
	Isoniazid	38 ± 7	elongated cylindrical micelles
	Streptomycin	48 ± 7	rounded compartmentalised nanospheres
	Bedaquiline	27 ± 5	rounded micelles

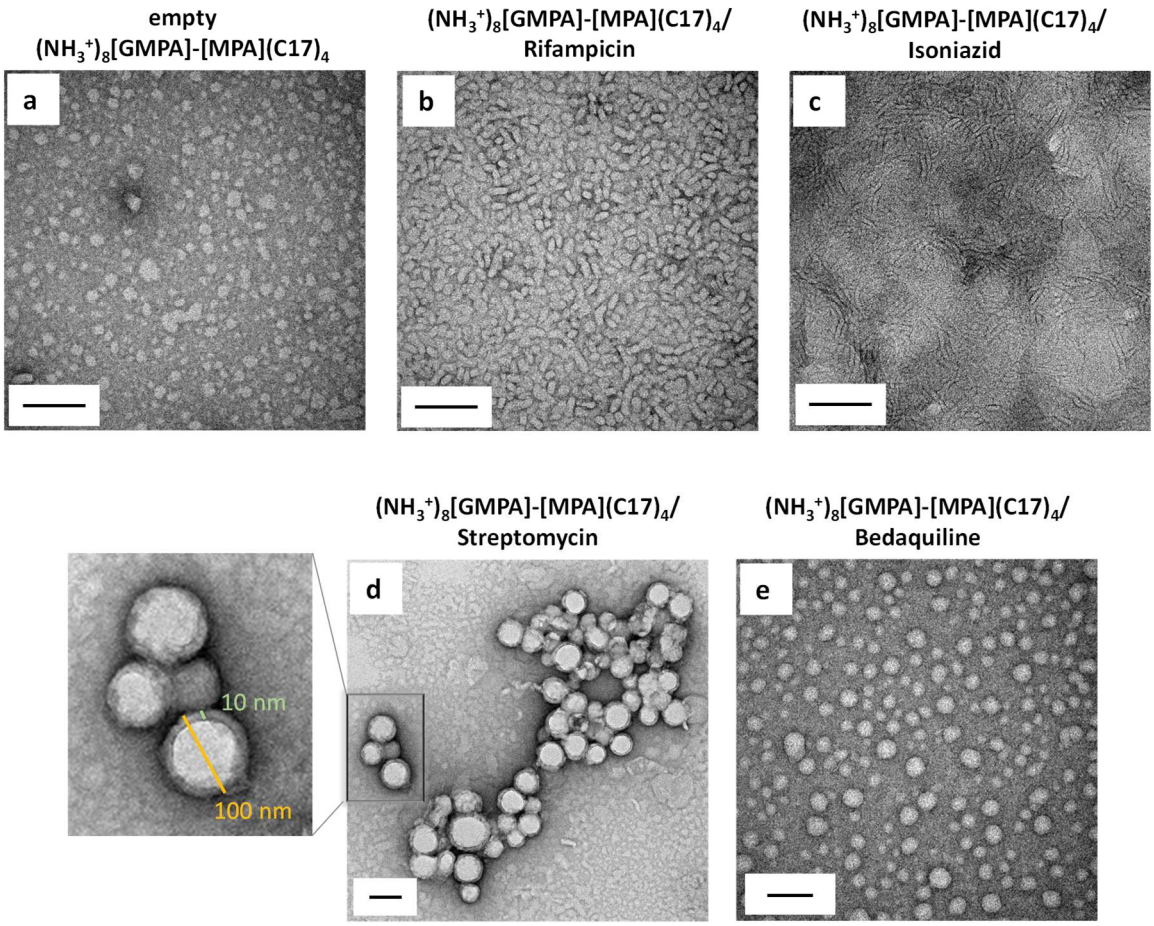

Figure 4.3. Microscopy TEM images of the aggregates formed by $(NH_3^+)_8$[GMPA]-[MPA](C17)$_4$ either empty (a) or containing the different anti-tuberculosis drugs encapsulated (b: RIF, c: INH, d: streptomycin, e: bedaquiline). Scale bars: 100 nm.

4.3. Nanocarriers co-encapsulating two drugs based on Janus dendrimers

To go a step further and to approach the real treatment regime of the disease, the effects of combining the drugs RIF and INH were studied. Initially, the possible synergistic effect between the two free drugs was assayed and then, their co-encapsulation within a dendritic nanocarrier was evaluated.

4.3.1. Determination of *in vitro* synergistic activity

Firstly, an *in vitro* assay confronting the two free drugs was performed in order to study the interaction between these anti-TB drugs against *M. bovis* BCG. Briefly, cell growth was assessed by the resazurin method[47] in a 96-well plate, where the first column showed the MIC of one of the compounds (RIF), the last row showed the MIC of the second compound (INH) and intermediate wells contain a mixture of different concentrations of the compounds. For each well in which there was no growth next to a well with growth, the fractional inhibitory concentration (FIC) was calculated using the following formulas: **FIC_{RIF}** = (MIC of RIF in the presence of INH) / MIC of RIF alone and **FIC_{INH}** = (MIC of INH in the presence of RIF) / MIC of INH alone. Both values were graphically represented to determine the shape of the curve FIC_{RIF} vs. FIC_{INH} (Figure 4.4, black curve), being the closer to the origin, the more indicative of synergy[51,52]. A synergistic profile (Figure 4.4, green) and a no interaction profile (Figure 4.4, red) are also represented as a visual guide.

Moreover, the FIC index, or **FICI**, was calculated by addition of the FIC value of each compound ($FICI = FIC_{RIF} + FIC_{INH}$), which indicates whether there is synergy ($FICI \leq 0.5$), no interaction (FICI value between 0.5 and 4) or antagonism ($FICI > 4$) between the compounds[53,54].

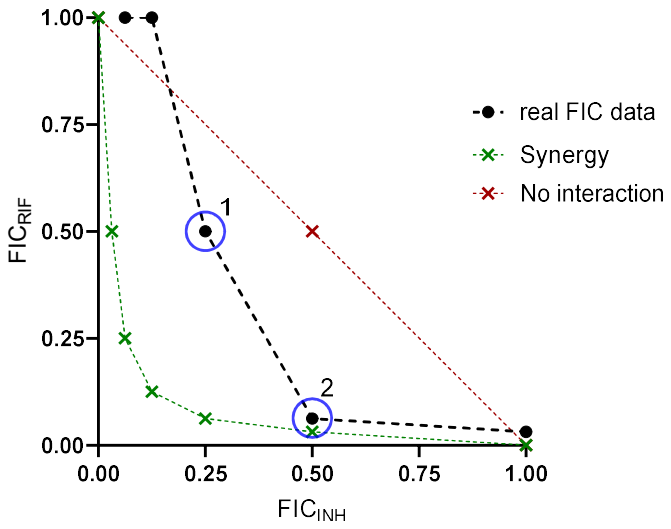

Figure 4.4. Graphical representation of FIC_{RIF} versus FIC_{INH} obtained in the synergy test to study the interaction between RIF and INH. A synergistic profile (green) and a no interaction profile (red) are also shown. Circles (1 and 2) indicate the points at which the FICI was calculated.

Since the closest points to the intersection of the axes corresponds to the most effective growth inhibitory combination, the FICI value was calculated in the two points circled in Figure 4.4. In point 1, the FICI was 0.75 while in point 2, the calculated FICI value was 0.563. It is true that this last FICI value is close to indicate a synergistic interaction between the drugs RIF and INH, but strictly talking, both FICI values are in the interval between 0.5 and 4 and thus, no interaction of the drugs is taking place against *M. bovis* BCG. This observation is in agreement with a previous study developed by Bhusal *et al.* where the combination of both drugs was interpreted as "being indifferent" against *Mtb*[55].

4.3.2. Drugs co-encapsulation and quantification

The next step consisted in the co-encapsulation of the drugs RIF and INH combined into the same dendrimer. $(NH_3^+)_8$[GMPA]-[MPA](C17)$_4$ was chosen because of its good encapsulation abilities of the single anti-TB agents (see Table 4.2) and the good antimicrobial activity of their drug-loaded aggregates against *M. bovis* BCG (see Table 4.3).

In the case of the co-encapsulation of two drugs within one dendritic structure, the same oil-in-water method was developed with the addition of each drug in the appropriate phase, depending on their polarity, to form the emulsion. For the correct quantification by HPLC of the combination of both drugs in the same sample, a change in the polarity of the mobile phase was required to fully resolve the two peaks (Figure 4.5). In the case of the individual drugs quantification, the mobile phase was composed of ACN and phosphate buffer at a ratio 60:40 (Figure 4.5a), whereas for their correct quantification in a mixture of both drugs, the ratio of solvents in the mobile phase was changed to 40:60 (Figure 4.5b). Under these chromatographic conditions, the RT for INH was maintained at 3.1 min, while the RT for RIF increased to 8.5 min and two perfectly resolved peaks were obtained (Figure 4.5b).

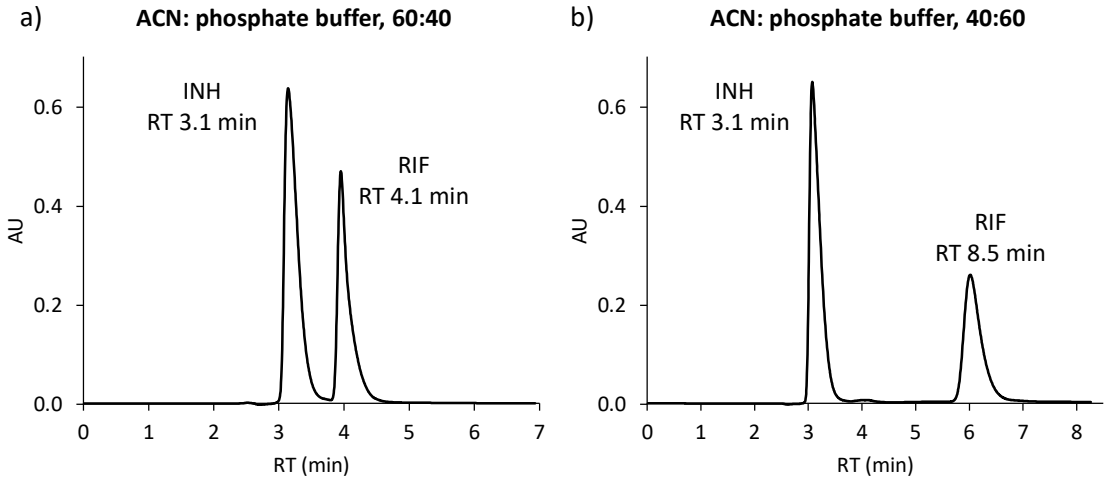

Figure 4.5. HPLC optimisation for the quantification of a mixture of RIF and INH. The mobile phase consists of ACN: phosphate buffer at a ratio a) 60:40 or b) 40:60.

The amount of each drug initially added to form the co-encapsulates followed the stablished molar ratio 5:1 with respect to the dendrimer. This 5:5:1 co-encapsulation, referred to mol INH: mol RIF: mol dendrimer, yielded similar DLC values for RIF but lower DLC values for INH compared to the values obtained for each drug individually encapsulated into the same dendritic structure, $(NH_3^+)_8$[GMPA]-[MPA](C17)$_4$ (compare Table 4.2 and Table 4.5). Namely, the single encapsulation of RIF reached the DLC value of 2.80 and in this 5:5:1 combination, the DLC was 2.93. For INH, a reduction in the DLC from 1.36 to

0.82 is observed when comparing the single and the combined encapsulation of the drug into the dendrimer. Although high concentrations of both drugs were encapsulated, the initial conditions had to be modulated since the amount of RIF encapsulated (622 µg/mL) was an order of magnitude higher than the INH (29 µg/mL) (Table 4.5). Then, it was decided to maintain the molar ratio 5:1 for the INH and decrease the ratio of RIF with respect to the dendrimer to 3:1, then obtaining the molar combination 5:3:1. With this modification, the concentration of RIF encapsulated was reduced approximately to the half (319 µg/mL), but it was still too high in comparison with the INH concentration that remained almost unaltered (26 µg/mL). Interestingly, it was observed that as the molar ratio of RIF was reduced, the DLC of INH was slightly increased (from 0.82 to 0.84). Finally, another reduction in the initial amount of RIF was tested, and the molar combination 5:1:1 was stablished as the co-encapsulating standard conditions of these two drugs into the $(NH_3^+)_8$[GMPA]-[MPA](C17)$_4$ dendrimer. In this way, a comparable amount of both drugs was encapsulated within the dendrimer, around 40 and 90 µg/mL of INH and RIF, respectively. The effect of the increase in the DLC of INH when reducing the amount of RIF added was more pronounced this time (from 0.84 to 1.44), thus indicating some type of impediment, possibly steric or driven by chemical saturation of bonding sites, for the encapsulation of INH in the presence of a high amount of RIF.

Table 4.5. Co-encapsulation of RIF and INH within the dendrimer $(NH_3^+)_8$[GMPA]-[MPA](C17)$_4$ at different initial molar ratios of each drug with respect to the dendrimer. The concentration of drug encapsulated is expressed in µg/mL and the drug loading content (DLC), in molar ratio. Mean ± SD is included for the measurements performed in triplicates.

molar combination (mol INH: mol RIF: mol dendrimer)	**drug**	**[Drug encapsulated]** (µg/mL)	**DLC**
5:5:1	INH	29	0.82
	RIF	622	2.93
5:3:1	INH	26	0.84
	RIF	319	1.74
5:1:1	INH	41 ± 9	1.44 ± 0.35
	RIF	89 ± 16	0.52 ± 0.13

4.3.3. Morphological study of the aggregates

The aggregates obtained by the combined encapsulation of INH and RIF in $(NH_3^+)_8$[GMPA]-[MPA](C17)$_4$ at the most convenient conditions, an initial molar ratio 5:1:1, were characterised by TEM (Figure 4.6a) and DLS (Figure 4.6b). The morphology of the aggregates observed by TEM resemble the cylindrical micelles obtained for the individual encapsulation of RIF but in this case, the micelles were longer (Figure 4.6a). This observation concurs with the fact that RIF is the drug encapsulated in higher concentration in these co-encapsulates. The D_H of the aggregates determined by DLS was 24±3 nm (Figure 4.6b), in between the sizes of the structures obtained for the individual encapsulation of these drugs within $(NH_3^+)_8$[GMPA]-[MPA](C17)$_4$, also determined by DLS (13±2 nm for RIF and 38±7 nm for INH).

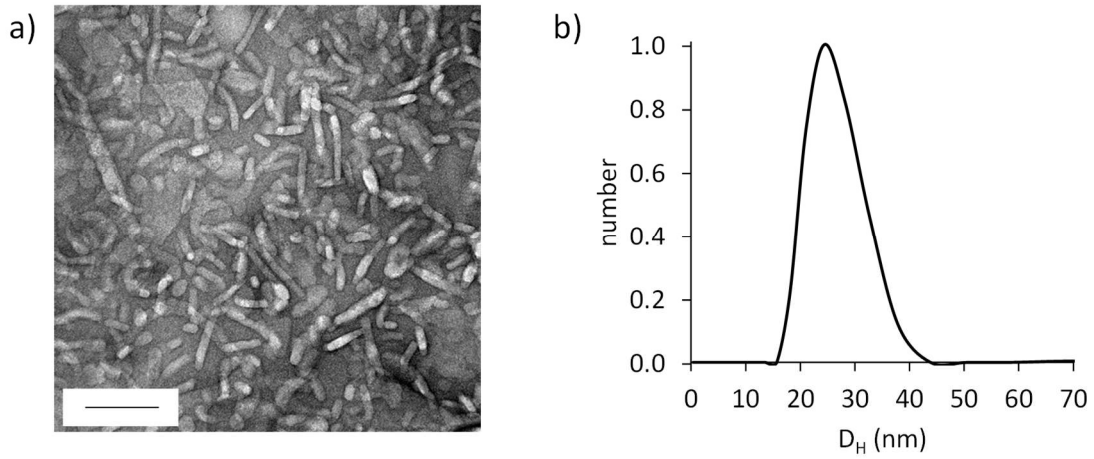

Figure 4.6. Characterisation of the combination RIF and INH co-encapsulated into $(NH_3^+)_8$[GMPA]-[MPA](C17)$_4$: a) TEM image (scale bar: 100 nm) and b) D_H measured by DLS after number treatment, in nm.

4.3.4. Antimicrobial activity determination against *M. bovis* BCG and *Mtb*

The antimicrobial activity of the drugs RIF and INH combined either free or encapsulated within the dendrimer $(NH_3^+)_8$[GMPA]-[MPA](C17)$_4$, at the same concentration of each drug in both cases, was studied against *M. bovis* BCG and *Mtb* in different environments.

Since the amount of RIF needed to kill the BCG bacteria is lower than the amount of INH (MIC_{RIF} < MIC_{INH}, see Table 4.3), and the amount of encapsulated RIF is higher than that of INH, it would be expected to observe an antimicrobial effect mainly due to the RIF present in the sample. The INH included in the combination of drugs would not be expected to decrease the MIC value of RIF because of the absence of synergy between both drugs observed in section 4.3.1. Thus, MICs results of the combinations are expressed referred to the RIF concentration (Table 4.6).

Regarding *M. bovis* BCG, the antimicrobial activity of the combination of free drugs (mixed in the same ratio as quantified in the dendrimer) against these bacteria was the same of that observed for the free RIF, 0.014 µg/mL, and this activity was maintained after being encapsulated in the dendrimer, with a MIC value of just one dilution higher (0.029 µg/mL) (these results are gathered in the BCG column of Table 4.6, together with previous data). This indicates that the combination of both drugs under the conditions assayed keep the bioavailability of RIF and does not favour the RIF degradation as it was supposed by the presence of INH[19], because its MIC is the same of that of the RIF alone, 0.014 µg/mL, highlighting the protective effect exerted by the dendritic nanocarrier.

Later, the antimicrobial activity of the selected drug combinations and their encapsulations was tested in the *Mtb* strain H37Rv. All the work related to these pathogenic bacteria was developed under extreme security measures in a biosecurity level 3 laboratory. The antimicrobial activity against *Mtb* (Table 4.6, *Mtb* column) was one order of magnitude higher than that obtained in BCG, except in the case of the INH drug, whose activity was reproducible in both bacterial species. In general terms, the same tendency was observed regarding the antimicrobial activity of each drug free and encapsulated. Namely, the MIC of

RIF was the same in both cases (free and encapsulated), 0.219 μg/mL, and also the MIC of INH was, 0.547 μg/mL; whereas the concentration of the combined drugs needed to kill the bacteria was double when encapsulated within the dendrimer.

In addition, since *Mtb* usually inhabits inside macrophages in the alveolus when infecting humans, the activity of the compounds against *Mtb*-infected macrophages was also determined. For that purpose, the monocytes THP1 were treated with phormol 12-myristate 13-acetate (PMA) for being differentiated into macrophages at the same time that they were infected by *Mtb* H37Rv. This strain of *Mtb* employed for the infection had been previously transformed with a plasmid containing the *Photinus pyralis* luciferase gene, which will allow the subsequent determination of the bacterial growth by measuring the resultant luminescent signal after addition of the substrate Bright-Glo™. The MIC values obtained in this cellular model, *Mtb*-THP1, are gathered in the corresponding column in Table 4.6 and represented in Figure 4.7. They are all in the same order of magnitude than in BCG, and the differences after encapsulating the drugs remain unaltered. The elevated susceptibility of the *Mtb* bacteria towards the drugs when infecting the macrophages compared to the free *Mtb* could be due, among other reasons, to the more acidic environment of the macrophages that would contribute to the bacterial death or to increase the drug release from dendrimers.

The antimicrobial activity of the dendrimer $(NH_3^+)_8$[GMPA]-[MPA]$(C17)_4$ by itself was also assessed but its MIC could not be determined against BCG neither *Mtb*, and it can only be concluded that it was higher than 87.5 μg/mL in both cases. In the *Mtb*-THP1 model, the MIC of the dendrimer was stablished at 32.813 μg/mL (Figure 4.7b), however, this concentration is much higher than the ones assayed in the encapsulations (0.658 μg/mL the maximum, marked with a vertical line in Figure 4.7b) and then, it can be concluded that the dendrimer itself does not have any antimicrobial activity in the aggregates dendrimer/drugs at the conditions assayed.

Table 4.6. Minimum inhibitory concentrations against different cellular species: BCG, Mtb and Mtb-THP1. The samples are the free drugs (individually or combined) and their encapsulations within the Janus dendrimer $(NH_3^+)_8$[GMPA]-[MPA](C17)$_4$. Data are expressed in μg/mL, and at least duplicates were performed. In the case of the combined drugs, the MICs are expressed referred to the RIF concentration.

	Bacterial species		
Sample	BCG	Mtb	Mtb-THP1
RIF	0.014	0.219	0.027
$(NH_3^+)_8$[GMPA]-[MPA](C17)$_4$/ RIF	0.014	0.219	0.027
INH	0.547	0.547	0.034
$(NH_3^+)_8$[GMPA]-[MPA](C17)$_4$/ INH	0.547	0.547	0.034
RIF+INH	0.014	0.219	0.014
$(NH_3^+)_8$[GMPA]-[MPA](C17)$_4$/ RIF+INH	0.029	0.438	0.041
$(NH_3^+)_8$[GMPA]-[MPA](C17)$_4$	> 87.5	> 87.5	32.813

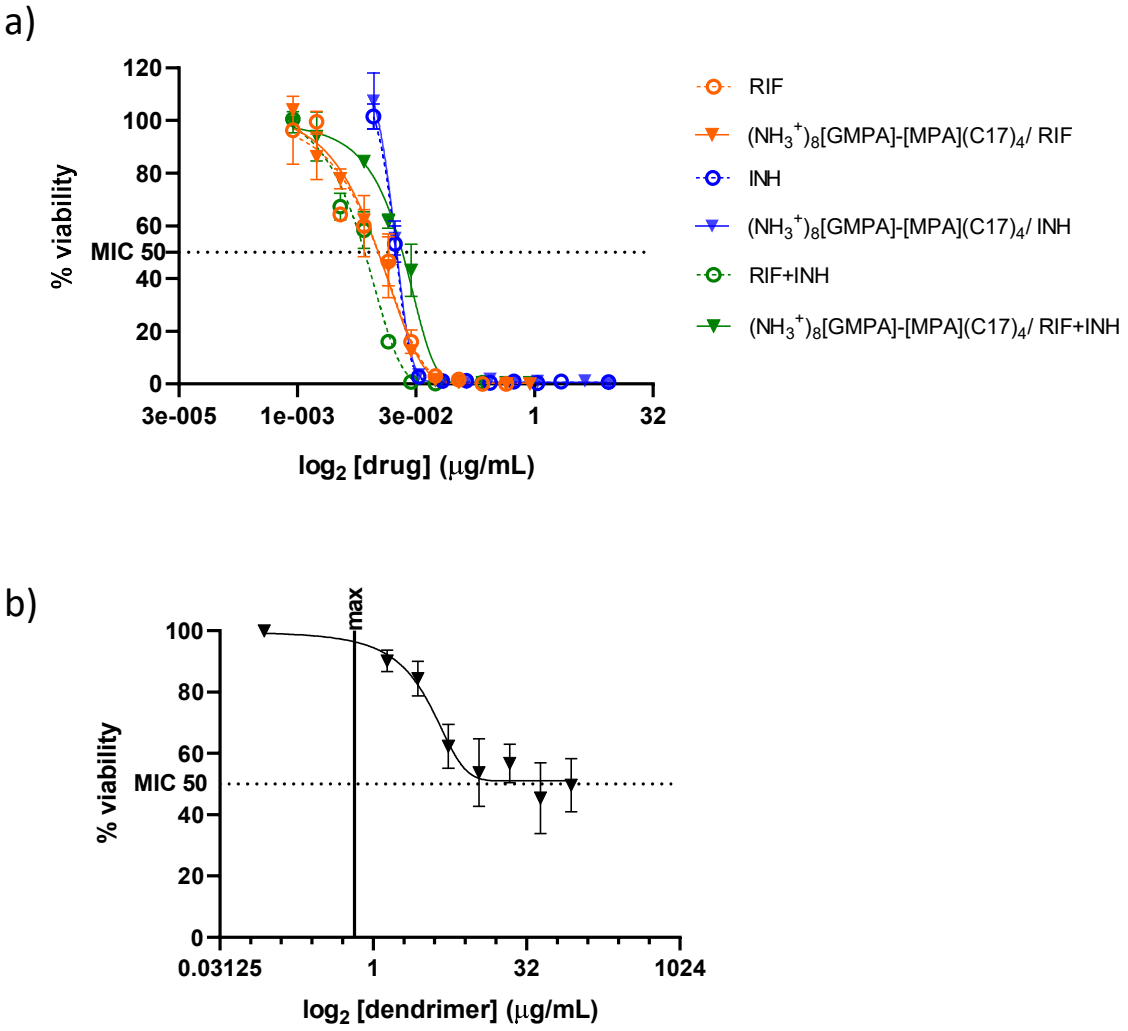

Figure 4.7. Graphical representation of the MICs against Mtb-THP1 gathered in Table 4.6: a) drugs either free (circles) or encapsulated in $(NH_3^+)_8$[GMPA]-[MPA](C17)$_4$ (triangles), and b) empty $(NH_3^+)_8$[GMPA]-[MPA](C17)$_4$. The MIC 50 is marked in both graphs with a dot line. The maximum concentration of Janus dendrimer assayed in the encapsulations in marked in graph b with a vertical solid line.

4.3.5. Kill kinetic assay in *Mtb*

The activity of the drugs encapsulated within the dendrimer, in general, is maintained with respect to the activity of the free drugs (differences of just a dilution are not considered significant in this method), as is has been observed with the MIC determination against different bacteria (see section 4.3.4). However, the MIC determination informs only of the viability of bacteria after a certain time period, but it does not inform about how fast such killing occurs nor about the possible development of drug resistances, due to the fixed timing employed for the MIC determination.

As it is widely known, the emergence of resistances towards drugs and more specifically towards antibiotics, is a dangerous issue to be concerned about[10]. The objective of this kill kinetic assay was to assess the growth evolution of *Mtb* with respect to time in presence of different concentrations of RIF, INH or the combination RIF+INH, all of them free and encapsulated in $(NH_3^+)_8$[GMPA]-[MPA](C17)$_4$. The chosen concentrations were the same (1x), 4 times (4x) and 10 times (10x) of the previously calculated MIC for each drug.

Firstly, exponentially growing cultures were diluted in 7H9-ADC-0.2% Glycerol to a cell density of 10^5 CFU/mL. These cultures were incubated at 37 °C for 3 days to restore exponential growth and then, at the denominated “day 0”, drugs were added at the designated concentrations and combinations to a total volume of 10 mL. Growth controls were included to assess the bacterial growth without antimicrobial agents as well as a control with the empty dendrimer to evaluate its influence in the bacterial growth with time. Afterwards, cultures were incubated at 37 °C and aliquots were taken at different time points to evaluate bacterial density by CFU counting. The time points set for this kinetics in *Mtb* were: -3 (growth beginning), 0 (drugs addition), 1, 2, 4, 7, 11, 16 and 22 days.

At every time point, cultures were shaken vigorously and then, samples of 100 µL were 10-fold serially diluted in 1x PBS buffer with 0.1% tyloxapol in order to break clumps. Finally, 100 µL of the dilutions were plated by duplicate on 7H10-OADC agar quad plates. After 14 - 21 days of incubation at 37 °C, CFUs were counted, and bacterial density was determined using the following formula:

$$\text{Bacterial density (CFU/mL)} = \frac{\text{Number of colonies counted}}{\text{dilution} \cdot \text{volume seeded (mL)}}$$

The bacterial density for each group of conditions, in log, was represented versus the time, in days, and the detection limit of the assay (log CFU/mL = 1) was there indicated (Figure 4.8, Figure 4.9 and Figure 4.10).

Regarding the drug **RIF** (Figure 4.8), a bacteriostatic effect, that is, an inhibition in the bacterial growth without meaning its death, can be observed at 1x MIC concentration up to day 11 when the drug is encapsulated, but for the free RIF an increase in the bacterial growth is observed at this point (Figure 4.8a). This may suggest a gradual release of RIF from the $(NH_3^+)_8$[GMPA]-[MPA](C17)4/ RIF aggregates, which provokes a more enduring effect of the drug and that is why bacterial growth is delayed with respect to the treatment with free RIF at 1x MIC. However, the most promising advantages of the RIF encapsulation into the dendrimer were shown at 4x MIC (Figure 4.8b), a concentration at which a bigger decay in the bacterial viability was obtained at day 11 with the drug encapsulated, and the subsequent bacterial growth experimented a delay with respect to the cultures treated with free RIF. This effect observed for the drug loaded dendritic aggregates at 4x MIC could be due to a delay in the emergence of RIF-resistant bacteria and/or to a slower degradation of the drug because of the protection provided by the dendrimer[19]. Nevertheless, the cause of this effect can not be elucidated from this study and further experiments would be needed, for example, by sequencing the genome of the resulting bacterial strains. Finally, at the highest concentration assayed, 10x MIC (Figure 4.8c), the RIF encapsulation within the dendrimer did not provide any benefit with respect to the same concentration of the free drug. The bacterial growth observed from day 11 could suggest that part of the drug remains entrapped within the dendrimer and then, it can not exhibit its bactericidal effect.

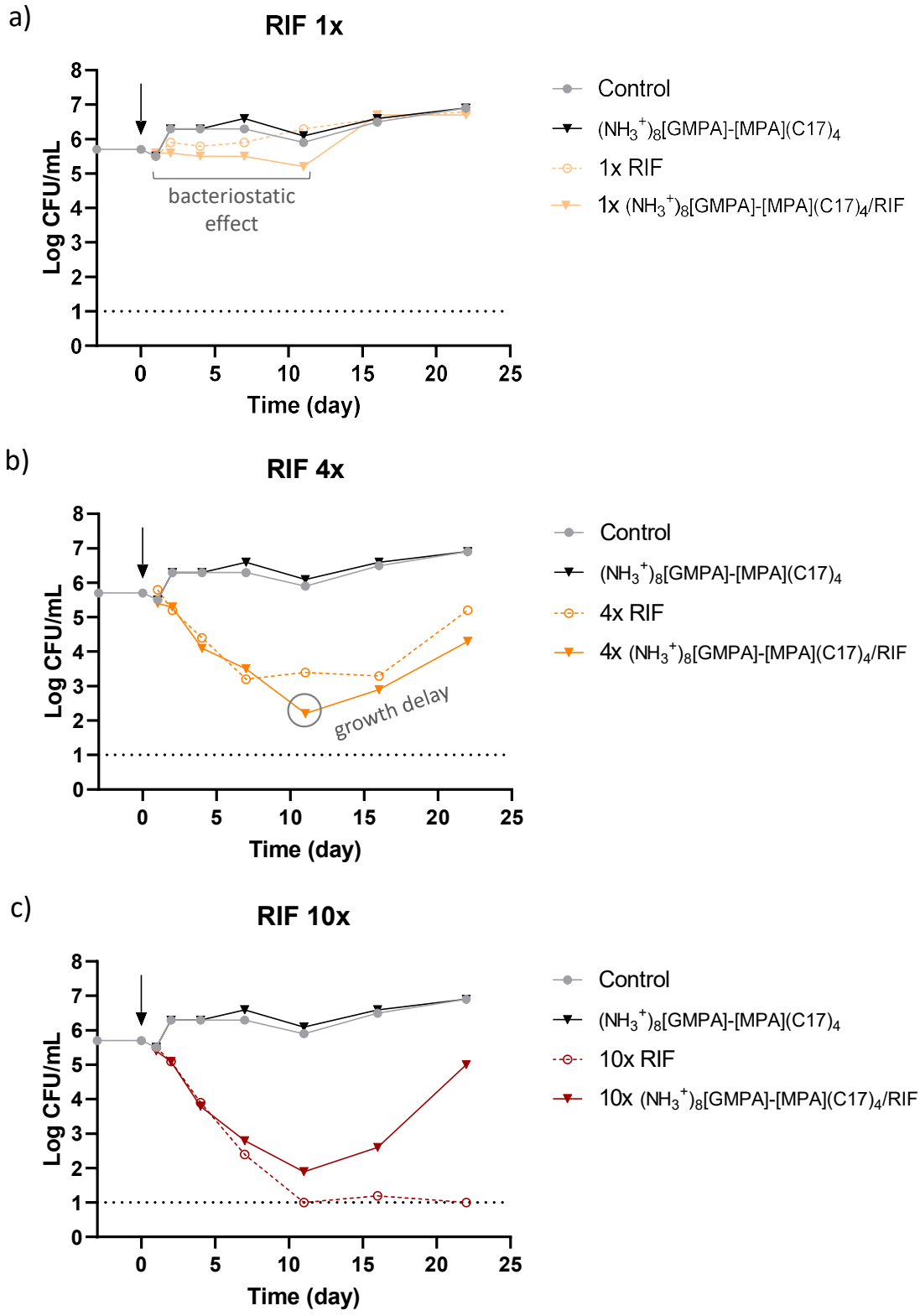

Figure 4.8. Kill kinetic assays in Mtb for RIF combinations at a) 1x MIC, b) 4x MIC and c) 10x MIC. The detection limit of the assay is marked with a dot line in each graph and the arrow indicates the drug addition. Key: colours turn darker as the drug concentration increases (1x, 4x or 10x the MIC); circle (free drug); triangle (drug encapsulated in $(NH_3^+)_8$[GMPA]-[MPA](C17)$_4$).

In the case of the **INH** treated cultures (Figure 4.9), the emergence of resistances started from day 7 after incubation with the drug. This resistance towards INH treatment is widely known, but different variants of resistant bacteria can be generated and a deeper study on their genotype would shed light on the mechanism underlying each case[56]. In the present kill kinetics study, it is observed that when incubated with 1x MIC (Figure 4.9a), the final bacterial density reached at day 22 was the same if the drug was free or encapsulated. However, the number of viable cells experimented a notable difference at day 11, being lower when treated with the aggregates $(NH_3^+)_8$[GMPA]-[MPA]$(C17)_4$/INH. This could be due again because of the gradual release of the drug from the dendritic aggregate. A similar effect was observed at 4x MIC (Figure 4.9b), whereas at 10x MIC (Figure 4.9c) the growth of the cultures treated with the free drug was slightly delayed.

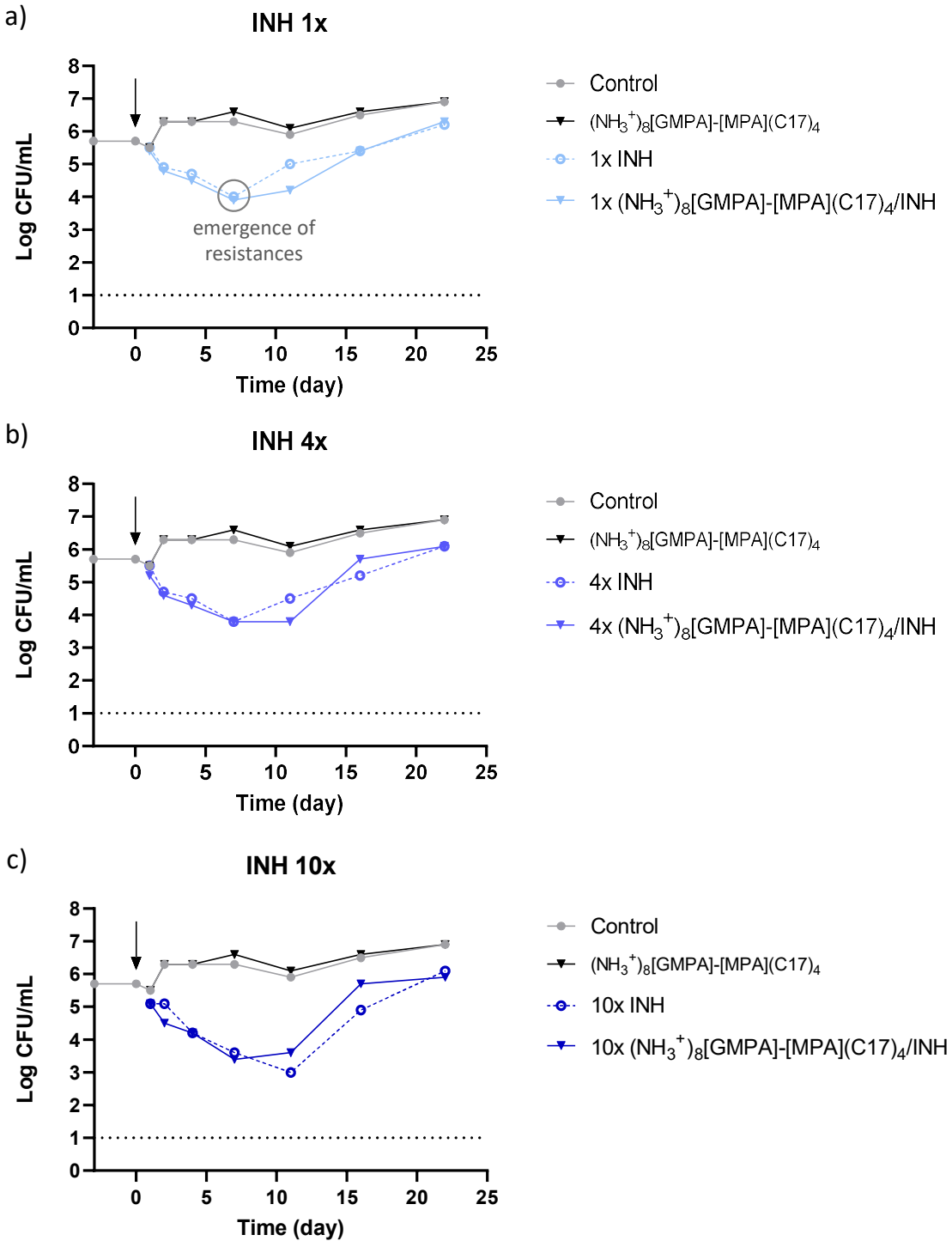

Figure 4.9. Kill kinetic assays in Mtb for INH combinations at a) 1x MIC, b) 4x MIC and c) 10x MIC. The detection limit of the assay is marked with a dot line in each graph and the arrow indicates the drug addition. Key: colours turn darker as the drug concentration increases (1x, 4x or 10x the MIC); circle (free drug); triangle (drug encapsulated in $(NH_3^+)_8$[GMPA]-[MPA](C17)$_4$).

The combination of both drugs**, RIF+INH**, was more bactericidal than the individual drugs (Figure 4.10) in the absence of any nanoparticle. At 1x MIC (Figure 4.10a), the encapsulation exhibited an apparently advantageous delay in the emergence of resistances in comparison with the free drugs, but at 4x MIC (Figure 4.10b), the dendrimer seems to be retaining part of the drugs and a bacteriostatic effect followed by a rise in the bacterial growth was observed from day 7 compared to the bactericidal effect of the naked combination of drugs; then, at these conditions, the encapsulated drugs are not sufficient to sterilise the bacterial culture. The highest concentration, the 10x MIC of RIF+INH (Figure 4.10c), is highly bactericidal for the naked and for the encapsulated combination RIF+INH. However, it can be observed that the bacterial death occurs slower in presence of the combined drugs encapsulated into the dendrimer, thus suggesting a gradual release of the drugs from $(NH_3^+)_8$[GMPA]-[MPA]$(C17)_4$/ RIF+INH.

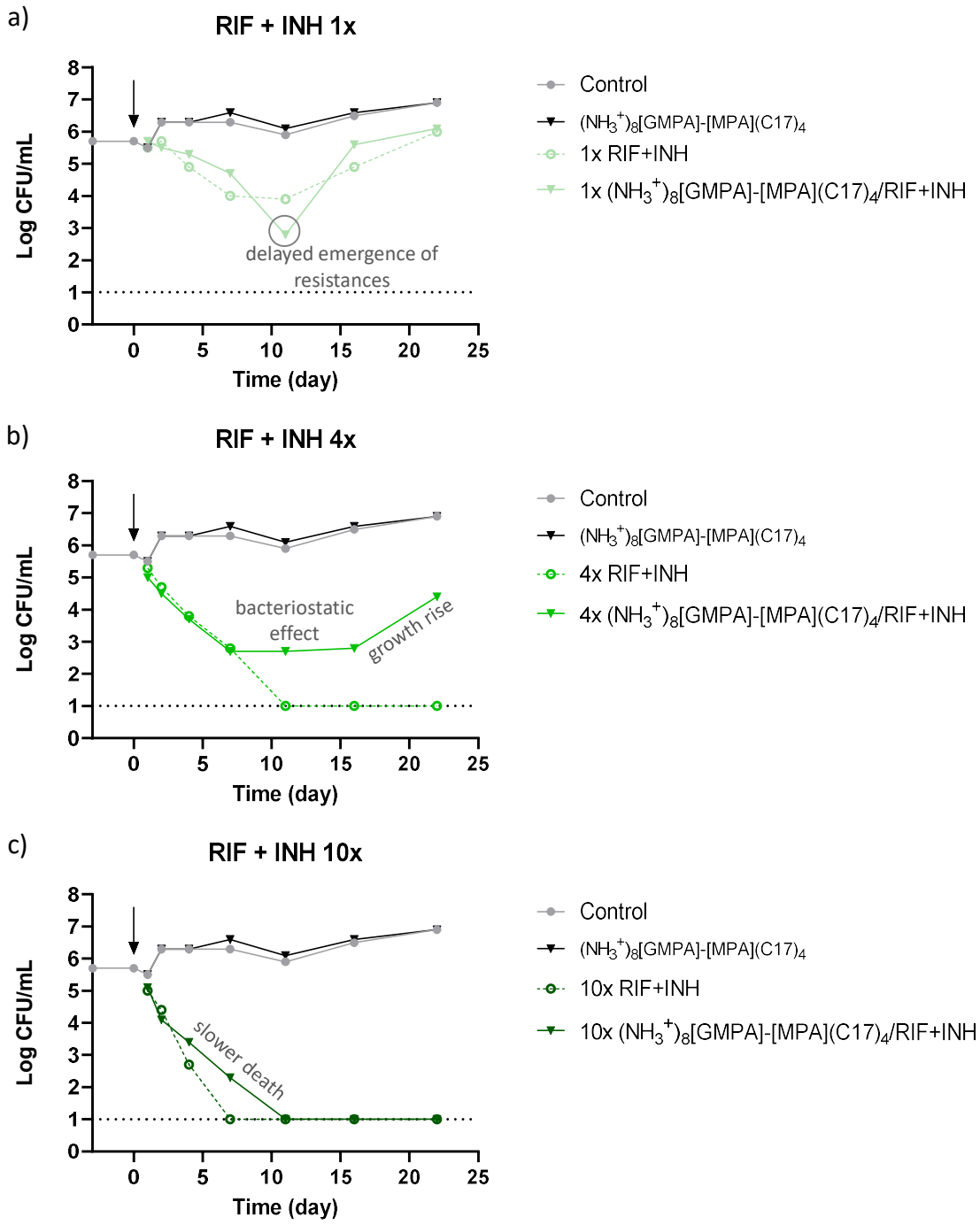

Figure 4.10. Kill kinetic assays in Mtb for RIF+INH combinations at a) 1x MIC, b) 4x MIC and c) 10x MIC. The detection limit of the assay is marked with a dot line in each graph and the arrow indicates the drug addition. Key: colours turn darker as the drug concentration increases (1x, 4x or 10x the MIC); circle (free drugs); triangle (drugs encapsulated in $(NH_3^+)_8$[GMPA]-[MPA](C17)$_4$).

Additionally, another representation of the results grouped by concentration of drugs (1x, 4x or 10x the corresponding MIC) is showed in Figure 4.11. These graphs allow to easily visualise that at 1x MIC any condition of free or encapsulated drugs can sterilise the culture (Figure 4.11a) and increasing the concentration at 4x MIC, only the combined free drugs (RIF+INH) are able to exert this sterilising effect (Figure 4.11b). Regarding the 10x MIC concentration, besides the free RIF+INH combination, the conditions able to sterilise the *Mtb* culture include the RIF+INH combination encapsulated in the dendrimer and the free RIF (Figure 4.11c).

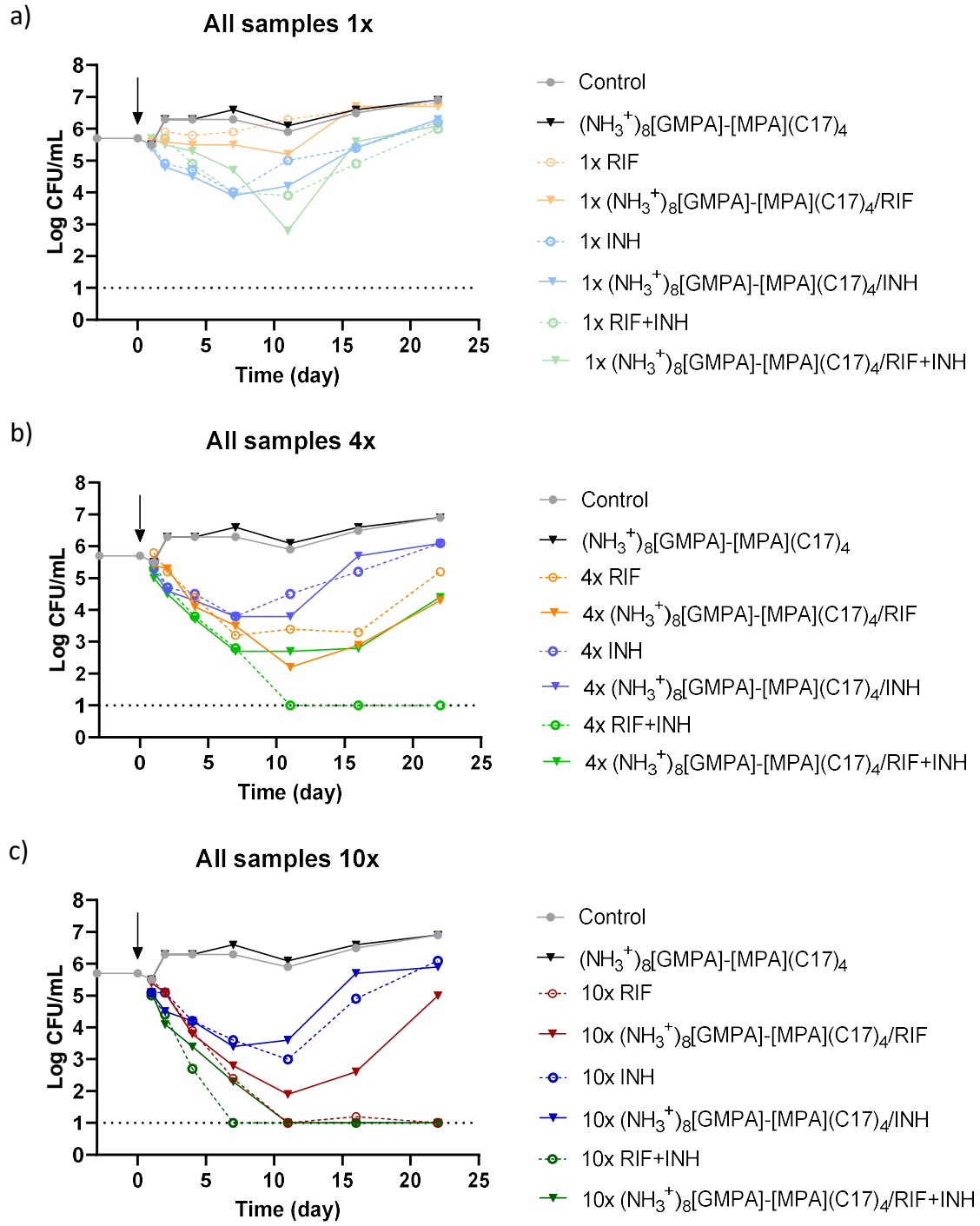

Figure 4.11. Kill kinetic assay of all samples grouped by concentrations: a) 1x MIC, b) 4x MIC and c) 10x MIC. The detection limit of the assay is marked with a dot line in each graph and the arrow indicates the drug addition. Key: colours turn darker as the drug concentration increases (1x, 4x or 10x the MIC); circle (free drugs); triangle (drugs encapsulated in $(NH_3^+)_8$[GMPA]-[MPA](C17)$_4$).

4.4. General remarks

Summary

The individual encapsulation of some anti-TB drugs (RIF, INH, streptomycin and bedaquiline) within the Janus dendrimers has been properly developed and the resulting aggregates have been studied in terms of quantification of drug loaded, morphological characterisation and *in vitro* antimicrobial activity against *M. bovis* BCG. What is more, the combination of two drugs, RIF and INH, into a dendritic nanocarrier has been explored, extending these studies to *Mtb* bacteria and *Mtb*-infected macrophages. The bacterial kill kinetics suggest that some extent of the drugs remains entrapped within the dendrimer aggregates, and the emergence of bacterial resistances is delayed under some conditions assayed.

Conclusions

Effective anti-TB drug loading has been achieved with the series of amphiphilic *bis*-MPA/*bis*-GMPA Janus dendrimers. Moreover, their antimicrobial activity against different bacterial strains is maintained after their encapsulation and, under some conditions, the treatment with the encapsulated drugs implies a delay in the emergence of resistant bacteria.

Future perspectives

As this work constitutes a novel line of research in our group, promising advances have been done while numerous ideas for future work have also emerged.

Regarding the selected anti-TB drugs, the encapsulation method of bedaquiline within the dendrimers could be improved in order to obtain loaded dendritic aggregates with more amount of drug and maintaining its antimicrobial activity[49]. Another possibility is to broaden the study to different drugs such as β-lactams[57,58] or ethambutol. The inclusion of ethambutol would be interesting since it is known to exhibit a synergistic activity when combined with other compounds[51]; in fact, an attempt to encapsulate ethambutol in our Janus

dendrimers was made but unfortunately, this had to be abandoned because of the difficulties found in its quantification.

In respect of the combination RIF+INH, different conditions of co-encapsulation increasing even more the amount of INH should be assayed in order to allow the visualisation of the effect of both drugs in the final formulation. The content of both drugs in the dendrimers should reach a ratio equivalent to that used in the treatment of TB. On the other hand, to avoid the possible RIF degradation or reduction in bioavailability while controlling the amount of INH, the combined treatment with RIF individually encapsulated within a dendrimer and INH free could be also assayed.

In addition, the genotypic sequencing of the growing bacteria after their prolongated treatment with the different combinations of drugs and dendrimers would allow to go deeper into the characterisation of the possible resistances emerged and then, into the design of more accurate treatments.

To go further, since the encapsulation within the dendrimers does not disturb the MIC activity of the drugs and in some cases, the emergence of resistances is delayed; it is proposed to assay the most promising drug-loaded dendrimers in *in vivo* models, preferentially through the intranasal administration route in order to reach quickly and selectively to the lungs. The pharmacokinetic of both drugs could be different if they are administered free or encapsulated within a dendritic nanocarrier. Moreover, the possibility to deliver both drugs in a specific tissue at the same time provided by the nanocarrier would improve the drug activity with respect to the free administration.

Finally, other dendrimers with better encapsulating abilities could be included in the study and the Janus dendritic structures could be optimised by attaching mannose residues on their surface in order to target more specifically macrophages[31,59], the usual reservoir of *Mtb* in humans.

4.5. References

(1) Seki, M.; Choi, H. J.; Kim, K.; Whang, J.; Sung, J.; Mitarai, S. Tuberculosis: A Persistent Unpleasant Neighbour of Humans. *Journal of Infection and Public Health* **2021**. https://doi.org/10.1016/j.jiph.2021.01.005.

(2) World Health Organization. Global Tuberculosis Report 2020. **2020**.

(3) Schrager, L. K.; Vekemens, J.; Drager, N.; Lewinsohn, D. M.; Olesen, O. F. The Status of Tuberculosis Vaccine Development. *The Lancet Infectious Diseases* **2020**, *20* (3), e28–e37. https://doi.org/10.1016/S1473-3099(19)30625-5.

(4) White, A. D.; Sibley, L.; Sarfas, C.; Morrison, A.; Gullick, J.; Clark, S.; Gleeson, F.; McIntyre, A.; Arlehamn, C. L.; Sette, A.; Salguero, F. J.; Rayner, E.; Rodriguez, E.; Puentes, E.; Laddy, D.; Williams, A.; Dennis, M.; Martin, C.; Sharpe, S. MTBVAC Vaccination Protects Rhesus Macaques against Aerosol Challenge with M. Tuberculosis and Induces Immune Signatures Analogous to Those Observed in Clinical Studies. *npj Vaccines* **2021**, *6* (1), 1–10. https://doi.org/10.1038/s41541-020-00262-8.

(5) Tameris, M.; Mearns, H.; Penn-Nicholson, A.; Gregg, Y.; Bilek, N.; Mabwe, S.; Geldenhuys, H.; Shenje, J.; Luabeya, A. K. K.; Murillo, I.; Doce, J.; Aguilo, N.; Marinova, D.; Puentes, E.; Rodríguez, E.; Gonzalo-Asensio, J.; Fritzell, B.; Thole, J.; Martin, C.; Scriba, T. J.; Hatherill, M.; MTBVAC Clinical Trial Team. Live-Attenuated Mycobacterium Tuberculosis Vaccine MTBVAC versus BCG in Adults and Neonates: A Randomised Controlled, Double-Blind Dose-Escalation Trial. *Lancet Respir Med* **2019**, *7* (9), 757–770. https://doi.org/10.1016/S2213-2600(19)30251-6.

(6) Update of the WHO guidance on the treatment of drug susceptible tuberculosis. https://www.who.int/news/item/16-04-2021-update-of-the-who-guidance-on-the-treatment-of-drug-susceptible-tuberculosis (accessed 2021 -05 -06).

(7) Khadka, P.; Hill, P. C.; Zhang, B.; Katare, R.; Dummer, J.; Das, S. C. A Study on Polymorphic Forms of Rifampicin for Inhaled High Dose Delivery in Tuberculosis Treatment. *International Journal of Pharmaceutics* **2020**, *587*, 119602. https://doi.org/10.1016/j.ijpharm.2020.119602.

(8) World Health Organization. Meeting Report of the WHO Expert Consultation on the Definition of Extensively Drug-Resistant Tuberculosis. **2020**.

(9) Bridget, O. N.; Prasad, R.; Onime, C.; Ali, A. A. Drug Resistant Tuberculosis Classification Using Logistic Regression. *Int. j. inf. tecnol.* **2021**. https://doi.org/10.1007/s41870-020-00592-9.

(10) Iacobino, A.; Fattorini, L.; Giannoni, F. Drug-Resistant Tuberculosis 2020: Where We Stand. *Applied Sciences* **2020**, *10* (6), 2153. https://doi.org/10.3390/app10062153.

(11) Khan, A. A.; Asghar, A. S.; Hashmi, K. U. R.; Farooq, M. S.; Shaheen, B.; Ali, I. Mycobacterium Tuberculosis: Pattern of First Line Drug Resistance. **2019**, *13* (1), 4. https://doi.org/10.29054/APMC/19.563.
(12) Lange, C.; Aarnoutse, R. E.; Alffenaar, J. W. C.; Bothamley, G.; Brinkmann, F.; Costa, J.; Chesov, D.; van, R.; Dedicoat, M.; Dominguez, J.; Duarte, R.; Grobbel, H. P.; Heyckendorf, J.; Kay, A. W.; Kirakosyan, O.; Kirk, O.; Koczulla, R. A.; Kudriashov, G. G.; Kuksa, L.; van, F.; Magis-Escurra, C.; Mandalakas, A. M.; Molina-Moya, B.; Peloquin, C. A.; Reimann, M.; Rumetshofer, R.; Schaaf, H. S. Management of Patients with Multidrug-Resistant Tuberculosis. **2019**, 19. http://dx.doi.org/10.5588/ijtld.18.0622.
(13) Mase, S. R.; Chorba, T. Treatment of Drug-Resistant Tuberculosis. *Clinics in Chest Medicine* **2019**, *40* (4), 775–795. https://doi.org/10.1016/j.ccm.2019.08.002.
(14) WHO announces updated definitions of extensively drug-resistant tuberculosis. https://www.who.int/news/item/27-01-2021-who-announces-updated-definitions-of-extensively-drug-resistant-tuberculosis (accessed 2021 -05 -06).
(15) Weng, T.; Sun, F.; Li, Y.; Chen, J.; Chen, X.; Li, R.; Ge, S.; Zhao, Y.; Zhang, W. Refining MDR-TB Treatment Regimens for Ultra Short Therapy (TB-TRUST): Study Protocol for a Randomized Controlled Trial. *BMC Infect Dis* **2021**, *21* (1), 183. https://doi.org/10.1186/s12879-021-05870-w.
(16) Allué-Guardia, A.; Saranathan, R.; Chan, J.; Torrelles, J. B. Mycobacteriophages as Potential Therapeutic Agents against Drug-Resistant Tuberculosis. *IJMS* **2021**, *22* (2), 735. https://doi.org/10.3390/ijms22020735.
(17) Kayukova, L. A.; Berikova, E. A. Modern Anti-Tuberculosis Drugs and Their Classification. Part I: First-Line Drugs. *Pharm Chem J* **2020**, *54* (6), 555–563. https://doi.org/10.1007/s11094-020-02239-2.
(18) Agrawal, S.; Ashokraj, Y.; Bharatam, P. V.; Pillai, O.; Panchagnula, R. Solid-State Characterization of Rifampicin Samples and Its Biopharmaceutic Relevance. *European Journal of Pharmaceutical Sciences* **2004**, *22* (2), 127–144. https://doi.org/10.1016/j.ejps.2004.02.011.
(19) Singh, S.; Mariappan, T. T.; Shankar, R.; Sarda, N.; Singh, B. A Critical Review of the Probable Reasons for the Poor Variable Bioavailability of Rifampicin from Anti-Tubercular Fixed-Dose Combination (FDC) Products, and the Likely Solutions to the Problem. *International Journal of Pharmaceutics* **2001**, *228* (1), 5–17. https://doi.org/10.1016/S0378-5173(01)00754-2.
(20) Mwila, C.; Walker, R. B. Improved Stability of Rifampicin in the Presence of Gastric-Resistant Isoniazid Microspheres in Acidic Media. *Pharmaceutics* **2020**, *12* (3), 234. https://doi.org/10.3390/pharmaceutics12030234.
(21) Singh, H.; Bhandari, R.; Kaur, I. P. Encapsulation of Rifampicin in a Solid Lipid Nanoparticulate System to Limit Its Degradation and Interaction with

Isoniazid at Acidic PH. *International Journal of Pharmaceutics* **2013**, *446* (1), 106–111. https://doi.org/10.1016/j.ijpharm.2013.02.012.

(22) Mignani, S.; Tripathi, R. P.; Chen, L.; Caminade, A.-M.; Shi, X.; Majoral, J.-P. New Ways to Treat Tuberculosis Using Dendrimers as Nanocarriers. *Pharmaceutics* **2018**, *10* (3). https://doi.org/10.3390/pharmaceutics10030105.

(23) Muthukrishnan, L. Multidrug Resistant Tuberculosis – Diagnostic Challenges and Its Conquering by Nanotechnology Approach – An Overview. *Chemico-Biological Interactions* **2021**, *337*, 109397. https://doi.org/10.1016/j.cbi.2021.109397.

(24) Baranyai, Z.; Soria-Carrera, H.; Alleva, M.; Millán-Placer, A. C.; Lucía, A.; Martín-Rapún, R.; Aínsa, J. A.; Fuente, J. M. de la. Nanotechnology-Based Targeted Drug Delivery: An Emerging Tool to Overcome Tuberculosis. *Advanced Therapeutics* **2021**, *4* (1), 2000113. https://doi.org/10.1002/adtp.202000113.

(25) Gupta, M.; Shivangi; Meena, L. S. Multidirectional Benefits of Nanotechnology in the Diagnosis, Treatment and Prevention of Tuberculosis. *Journal of Nanotechnology and Nanomaterials* **2020**, *1* (2). https://doi.org/10.33696/Nanotechnol.1.008.

(26) Parhi, P.; Mohanty, C.; Sahoo, S. K. Nanotechnology-Based Combinational Drug Delivery: An Emerging Approach for Cancer Therapy. *Drug Discovery Today* **2012**, *17* (17–18), 1044–1052. https://doi.org/10.1016/j.drudis.2012.05.010.

(27) Tekade, R. K.; Dutta, T.; Gajbhiye, V.; Jain, N. K. Exploring Dendrimer towards Dual Drug Delivery: PH Responsive Simultaneous Drug-Release Kinetics. *Journal of Microencapsulation* **2009**, *26* (4), 287–296. https://doi.org/10.1080/02652040802312572.

(28) Patil, K.; Bagade, S.; Bonde, S.; Sharma, S.; Saraogi, G. Recent Therapeutic Approaches for the Management of Tuberculosis: Challenges and Opportunities. *Biomedicine & Pharmacotherapy* **2018**, *99*, 735–745. https://doi.org/10.1016/j.biopha.2018.01.115.

(29) Sandoval-Yañez, C.; Castro Rodriguez, C. Dendrimers: Amazing Platforms for Bioactive Molecule Delivery Systems. *Materials* **2020**, *13* (3), 570. https://doi.org/10.3390/ma13030570.

(30) H. Malek, M. A.; M. Patel, P. Dendrimers for Drug Solubility Enhancement-A Review. *IJPSR* **2020**, *11* (2). https://doi.org/10.13040/IJPSR.0975-8232.11(2).507-23.

(31) Kumar, P. V.; Asthana, A.; Dutta, T.; Jain, N. K. Intracellular Macrophage Uptake of Rifampicin Loaded Mannosylated Dendrimers. *Journal of Drug Targeting* **2006**, *14* (8), 546–556. https://doi.org/10.1080/10611860600825159.

(32) Vijayaraj Kumar, P.; Agashe, H.; Dutta, T.; Jain, N. PEGylated Dendritic Architecture for Development of a Prolonged Drug Delivery System for an Antitubercular Drug. *CDD* **2007**, *4* (1), 11–19. https://doi.org/10.2174/156720107779314794.

(33) Bellini, R. G.; Guimarães, A. P.; Pacheco, M. A. C.; Dias, D. M.; Furtado, V. R.; de Alencastro, R. B.; Horta, B. A. C. Association of the Anti-

Tuberculosis Drug Rifampicin with a PAMAM Dendrimer. *Journal of Molecular Graphics and Modelling* **2015**, *60*, 34–42. https://doi.org/10.1016/j.jmgm.2015.05.012.

(34) Pandurangan, D.; Theivendren, P.; Kilim, D. B.; Kunjiappan, S.; Palanirajan, V. K. Formulation of Rifampicin Loaded PEGylated 5.0G EDA-PAMAM Dendrimers as Effective Long-Duration Release Drug Carriers https://www.eurekaselect.com/152972/article (accessed 2021 -03 -07).

(35) Singh, N.; Gautam, S. P.; Singh, L.; Dhiman, A.; Siddiqui, G.; Verma, A. Isoniazid Loaded Dendrimer Based Nano Carriers for the Delivery of Anti Tuberculosis. *Indian Research Journal of Pharmacy and Science* **2016**, 12.

(36) Rodrigues, B.; Shende, P. Monodispersed Metal-Based Dendrimeric Nanoclusters for Potentiation of Anti-Tuberculosis Action. *Journal of Molecular Liquids* **2020**, *304*, 112731. https://doi.org/10.1016/j.molliq.2020.112731.

(37) Ullah, A.; Urrehman, K. Simple and Rapid Method on High Performance Liquid Chromatography (HPLC) for Estimation of Streptomycin Sulphate. *World Applied Sciences Journal* **2012**, *19*, 645–649. https://doi.org/10.5829/idosi.wasj.2012.19.05.1245.

(38) Momin, M. A. M.; Rangnekar, B.; Das, S. C. Development and Validation of a RP-HPLC Method for Simultaneous Quantification of Bedaquiline (TMC207), Moxifloxacin and Pyrazinamide in a Pharmaceutical Powder Formulation for Inhalation. *Journal of Liquid Chromatography & Related Technologies* **2018**, *41* (8), 415–421. https://doi.org/10.1080/10826076.2018.1437748.

(39) Calleri, E.; De Lorenzi, E.; Furlanetto, S.; Massolini, G.; Caccialanza, G. Validation of a RP-LC Method for the Simultaneous Determination of Isoniazid, Pyrazinamide and Rifampicin in a Pharmaceutical Formulation. *Journal of Pharmaceutical and Biomedical Analysis* **2002**, *29* (6), 1089–1096. https://doi.org/10.1016/S0731-7085(02)00150-4.

(40) Kumar, G. V.; Jayaprakash, D. D. Analytical Method Development and Validation by RP-HPLC for Simultaneous Estimation of Isoniazid and Ethambutol in Combined Tablet Dosage Form. **2015**, 9.

(41) Goutal, S.; Auvity, S.; Legrand, T.; Hauquier, F.; Cisternino, S.; Chapy, H.; Saba, W.; Tournier, N. Validation of a Simple HPLC-UV Method for Rifampicin Determination in Plasma: Application to the Study of Rifampicin Arteriovenous Concentration Gradient. *Journal of Pharmaceutical and Biomedical Analysis* **2016**, *123*, 173–178. https://doi.org/10.1016/j.jpba.2016.02.013.

(42) Furman, C.; Carpentier, R.; Barczyk, A.; Chavatte, P.; Betbeder, D.; Lipka, E. Development and Validation of a Reversed-Phase HPLC Method for the Quantification of Paclitaxel in Different PLGA Nanocarriers. *Electrophoresis* **2017**, *38* (19), 2536–2541. https://doi.org/10.1002/elps.201600552.

(43) Marques, L.; Mengue, G.; de Medeiros, J.; Brussulo, T. C.; Bajerski, L.; Bender, E. A.; Haas, S. E. Validation of Analytical Method by HPLC for Determination of Dapsone in Polymeric Nanocapsules Based on Crude Rice Brain Oil. *J App Pharm Sci* **2017**.

https://doi.org/10.7324/JAPS.2017.70734.
(44) Vraka, C.; Nics, L.; Wagner, K.-H.; Hacker, M.; Wadsak, W.; Mitterhauser, M. LogP, a Yesterday's Value? *Nuclear Medicine and Biology* **2017**, *50*, 1–10. https://doi.org/10.1016/j.nucmedbio.2017.03.003.
(45) Vraka, C.; Mitterhauser, M. Reconsider LogP! *Nuclear Medicine and Biology* **2017**, *54*, 42. https://doi.org/10.1016/j.nucmedbio.2017.08.007.
(46) San Anselmo, M.; Lancelot, A.; Egido, J. E.; Clavería-Gimeno, R.; Casanova, Á.; Serrano, J. L.; Hernández-Ainsa, S.; Abian, O.; Sierra, T. Janus Dendrimers to Assess the Anti-HCV Activity of Molecules in Cell-Assays. *Pharmaceutics* **2020**, *12* (11), 1062. https://doi.org/10.3390/pharmaceutics12111062.
(47) Palomino, J.-C.; Martin, A.; Camacho, M.; Guerra, H.; Swings, J.; Portaels, F. Resazurin Microtiter Assay Plate: Simple and Inexpensive Method for Detection of Drug Resistance in Mycobacterium Tuberculosis. *Antimicrobial Agents and Chemotherapy* **2002**, *46* (8), 2720–2722. https://doi.org/10.1128/AAC.46.8.2720-2722.2002.
(48) De Matteis, L.; Jary, D.; Lucía, A.; García-Embid, S.; Serrano-Sevilla, I.; Pérez, D.; Ainsa, J. A.; Navarro, F. P.; M. de la Fuente, J. New Active Formulations against M. Tuberculosis: Bedaquiline Encapsulation in Lipid Nanoparticles and Chitosan Nanocapsules. *Chemical Engineering Journal* **2018**, *340*, 181–191. https://doi.org/10.1016/j.cej.2017.12.110.
(49) Soria-Carrera, H.; Lucía, A.; Matteis, L.; Aínsa, J. A.; la Fuente, J. M.; Martín-Rapún, R. Polypeptidic Micelles Stabilized with Sodium Alginate Enhance the Activity of Encapsulated Bedaquiline. *Macromol. Biosci.* **2019**, *19* (4), 1970012. https://doi.org/10.1002/mabi.201970012.
(50) Hernández-Ainsa, S.; Barberá, J.; Marcos, M.; Serrano, J. L. Nanoobjects Coming from Mesomorphic Ionic PAMAM Dendrimers. *Soft Matter* **2011**, *7* (6), 2560. https://doi.org/10.1039/c0sm01074j.
(51) Aguilar-Pérez, C.; Gracia, B.; Rodrigues, L.; Vitoria, A.; Cebrián, R.; Deboosère, N.; Song, O.; Brodin, P.; Maqueda, M.; Aínsa, J. A. Synergy between Circular Bacteriocin AS-48 and Ethambutol against Mycobacterium Tuberculosis. *Antimicrob Agents Chemother* **2018**, *62* (9). https://doi.org/10.1128/AAC.00359-18.
(52) De Logu, A.; Onnis, V.; Saddi, B.; Congiu, C.; Schivo, M. L.; Cocco, M. T. Activity of a New Class of Isonicotinoylhydrazones Used Alone and in Combination with Isoniazid, Rifampicin, Ethambutol, Para-Aminosalicylic Acid and Clofazimine against Mycobacterium Tuberculosis. *Journal of Antimicrobial Chemotherapy* **2002**, *49* (2), 275–282. https://doi.org/10.1093/jac/49.2.275.
(53) Odds, F. C. Synergy, Antagonism, and What the Chequerboard Puts between Them. *Journal of Antimicrobial Chemotherapy* **2003**, *52* (1), 1. https://doi.org/10.1093/jac/dkg301.
(54) European Committee for Antimicrobial SusceptibilityTesting (EUCAST) of the European Society of ClinicalMicrobiology and Infectious Diseases

(ESCMID). Terminology Relating to Methods for the Determination of Susceptibility of Bacteria to Antimicrobial Agents. **2000**, 6.

(55) Bhusal, Y.; Shiohira, C. M.; Yamane, N. Determination of in Vitro Synergy When Three Antimicrobial Agents Are Combined against Mycobacterium Tuberculosis. *International Journal of Antimicrobial Agents* **2005**, *26* (4), 292–297. https://doi.org/10.1016/j.ijantimicag.2005.05.005.

(56) Sulis, G.; Pai, M. Isoniazid-Resistant Tuberculosis: A Problem We Can No Longer Ignore. *PLoS Med* **2020**, *17* (1), e1003023. https://doi.org/10.1371/journal.pmed.1003023.

(57) Shetye, G. S.; Franzblau, S. G.; Cho, S. New Tuberculosis Drug Targets, Their Inhibitors, and Potential Therapeutic Impact. *Translational Research* **2020**, *220*, 68–97. https://doi.org/10.1016/j.trsl.2020.03.007.

(58) Solapure, S.; Dinesh, N.; Shandil, R.; Ramachandran, V.; Sharma, S.; Bhattacharjee, D.; Ganguly, S.; Reddy, J.; Ahuja, V.; Panduga, V.; Parab, M.; Vishwas, K. G.; Kumar, N.; Balganesh, M.; Balasubramanian, V. In Vitro and In Vivo Efficacy of β-Lactams against Replicating and Slowly Growing/Nonreplicating Mycobacterium Tuberculosis. *Antimicrobial Agents and Chemotherapy* **2013**, *57* (6), 2506–2510. https://doi.org/10.1128/AAC.00023-13.

(59) Kaps, L.; Leber, N.; Klefenz, A.; Choteschovsky, N.; Zentel, R.; Nuhn, L.; Schuppan, D. In Vivo SiRNA Delivery to Immunosuppressive Liver Macrophages by α-Mannosyl-Functionalized Cationic Nanohydrogel Particles. *Cells* **2020**, *9* (8), 1905. https://doi.org/10.3390/cells9081905.

Chapter 5:

Pseudodendrimers in the treatment of Malaria

5.1. Malaria

5.1.1. Introduction

Malaria is an infectious disease provoked by *Plasmodium* parasites and transmitted through the bite of female mosquitoes of the *Anopheles* genus, thus being the climatic tropical conditions a favourable factor for the spread of the disease. According to the last WHO report on the disease, the number of malaria cases have decreased in the last 20 years, from 238 million in 2000 to 229 million in 2019, and the number of endemic countries has also experimented a reduction from 108 to 87 within this period of time. However, it remains a global health threat that caused 409 000 deaths in 2019, being the African Region the most hit area with around 94% of the cases and deaths of malaria[1].

Although more than 120 species of the genus *Plasmodium* exist, five of them are the responsible of the human disease: *Plasmodium falciparum, Plasmodium vivax, Plasmodium malariae, Plasmodium ovale* and *Plasmodium knowlesi*; being *P. falciparum* the cause of the most severe forms of the disease[2]. The intracellular *Plasmodium* parasite presents a complex life cycle that can be divided between the stages in the mosquito and the stages in the human host[3,4] (Figure 5.1). Briefly, after the bite of an infected mosquito, the sporozoites of the parasite are released into the blood stream of the human until they reach the liver and infect hepatocytes. There, merozoites stages are newly released into the blood and infect red blood cells (RBCs), where the parasites evolve from ring stages to schizonts in the process of intraerythrocytic maturation. This cycle inside RBCs can be continuously repeated by invading new RBCs and it constitutes the cause of all symptoms of the disease. Just few *Plasmodium*-infected RBCs, pRBCs, progress to form the sexual forms of the parasite, the gametocytes, which will continue their life cycle in the mosquito after their ingestion through a new bite. Then, gametocytes become gametes, which will undergo different growing stages until becoming sporozoites in the mosquito salivary glands, ready to infect a human and close the cycle.

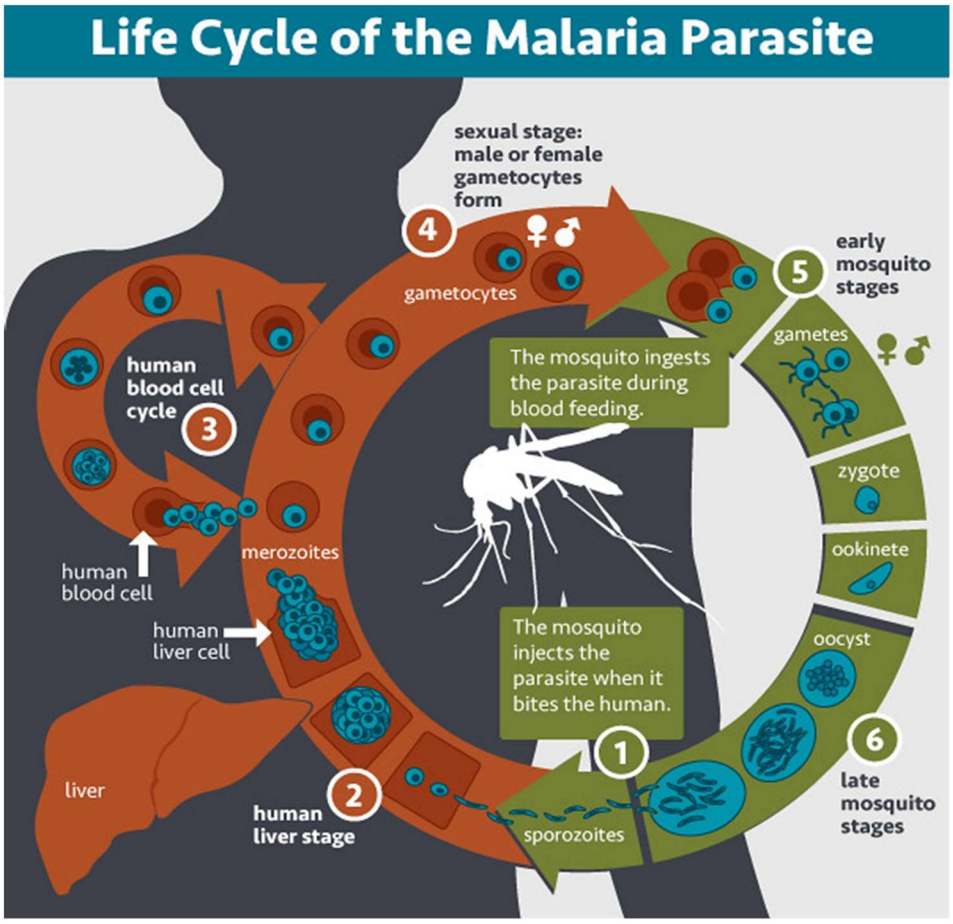

Figure 5.1. Life cycle of Plasmodium parasite. Obtained from the National Institute of Allergy and Infectious Diseases[4].

The prevention of the disease mainly consists of controlling the mosquito that acts as vector of transmission, and many efforts have been made in this direction[5–7]. Chemoprophylaxis also helps in the prevention of the infection by suppressing the blood stage of the disease, although the adherence to this preventive measure is not as good as it should be[8], and there is also some research focused on the prevention by immunization[9].

There are several agents for the treatment of malaria. Since the first used quinine, other drugs from the same aryl amino alcohols family have been used either alone or in combination with drugs with different mechanism of action[10]. The aminoquinolines such as chloroquine (CQ), quinacrine (QN) or primaquine (PQ) constitute other group of interesting active antimalarial compounds and finally, the artemisinin derivatives include compounds like artesunate, artemether, arteether or dihydroartemisinin[3,10]. The artemisinin-based combination therapies

(ACTs) became the recommended treatment for falciparum malaria worldwide in 2006 and few years later, the first ACT was approved by the FDA, i.e., artemether-lumefantrine[11]. However, the rapid spread of the disease and the emergence of resistances has continuously prompted the search for new therapeutic agents[12].

Additionally, nanotechnology has emerged as a potential tool to overcome the resistance issues in the treatment of malaria and to help in the transport of the drugs through the numerous biological membranes to be crossed to reach the parasite[13–23]. In a recently published review elaborated in collaboration with Busquets´ group[3], these nanomaterials employed in the fight against malaria have been classified according to their chemical nature. Specifically, liposomes, inorganic nanoparticles (NPs), polymeric and dendritic nanocarriers, graphene or cyclodextrins have been used to enhance the activity of previously used drugs. Different strategies such as the covalent conjugation of the drug or its physical entrapment have been reported and some issues like drug solubility, stability, toxicity and uncontrolled drug release can be overcome with the help of nanotechnology. However, there are many unsolved issues related to the most convenient administration route or the specificity of the formulations towards infected cells, without forgetting the economical drawbacks of the malaria endemic areas.

In the search for new formulations, an interesting strategy consists of the use of heparin (Figure 5.2), a negatively charged polysaccharide that has not induced resistances in the parasite and whose obtention is economically affordable[24].

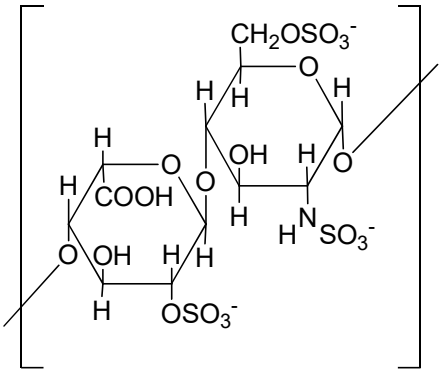

Figure 5.2. Chemical structure of the repetitive units of heparin.

The interest on this compound relies on its dual role against malaria. On the one hand, it presents antimalarial activity and in addition, it has been found to target specifically the pRBCs[24,25]. In fact, heparin was used in the treatment of severe forms of the disease, but the side effects due to its potent anticoagulant activity and the short circulation times in blood led to abandoning its use[26–29]. In this regard, several attempts have been made to exploit these unique properties of heparin as antimalarial[30,31]. The ability of the polysaccharide to block the parasite life cycle within the mosquito has been explored with encouraging results in the prevention of the human disease[32]. On the other hand, the formation of polyelectrolyte stable complexes with heparin to reduce its anticoagulant activity was firstly explored with poly(amidoamines)[33]. Moreover, the coating of drug-loaded liposomes with heparin by electrostatic bonding was explored to design nanocarriers with antimalarial activity and to specifically deliver the drug into the pRBCs and thus, reduce the drug IC_{50}[25]. Another recent study evaluated the therapeutic activity of different modified heparins and pointed out at the need of more effective nanocarriers to solve the issues of anticoagulant activity and low circulation times associated to the use of heparin as antimalarial[34].

5.1.2. Previous work and working plan

With the idea of designing effective nanostructures to serve as heparin coating nanocarriers, previous structures developed in our group with antimalarial purposes were taken into consideration.

A first study explored the ability of two Janus dendrimers based on *bis*-MPA and two HDLDBCs based on Pluronic F127 bearing also *bis*-MPA dendrons in the extremities to encapsulate and deliver the drugs CQ and PQ[35]. After the good *in vivo* and *in vitro* results obtained, new HDLDBCs bearing *bis*-GMPA dendrons were investigated as nanocarriers, broadening the study to the drug QN[23]. The inclusion of the *bis*-GMPA architecture was thought to possibly modulate the characteristics of the obtained micelles, through interactions like the hydrogen bonds allowed by the amide groups. Other dendritic structures that form unimolecular micelles in water have been studied as antimalarial drug nanocarriers in parallel[23]. Specifically, the pseudodendrimers or dendronized

hyperbranched polymers (DHPs) consisting of a *bis*-MPA core of different generations surrounded by dendrons of *bis*-MPA of the 3rd generation (Figure 5.3), that interestingly expose a large number of amino protonated groups in the periphery[36].

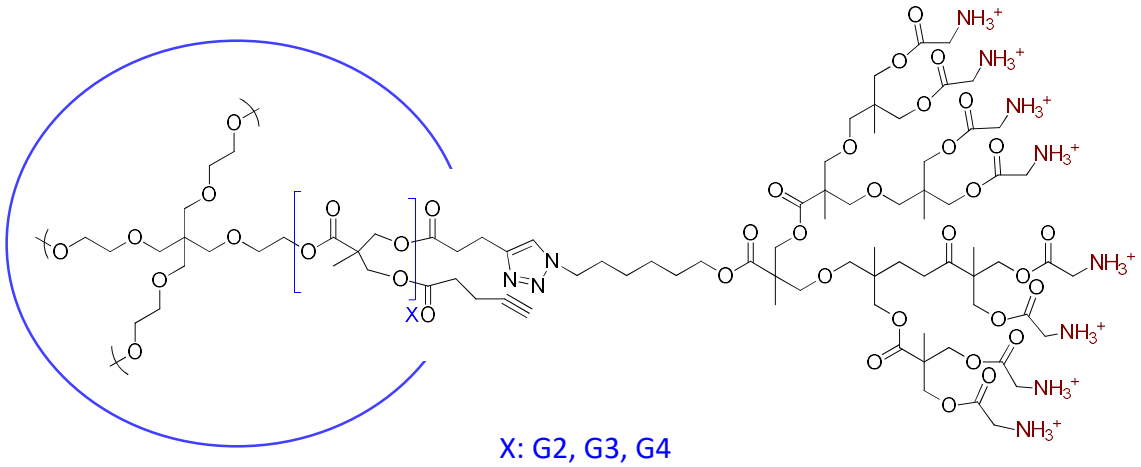

Figure 5.3. Chemical structure of the DHPs previously studied as antimalarial nanocarriers.

Finally, the properties of these polycationic DHPs have been explored to form stable complexes with heparin and enhance the activity of the encapsulated drugs[36]. The antiparasitic activity of QN was not improved by its encapsulation in the biggest DHP, DHP(G4)-MPA, but it was enhanced upon the addition of heparin to the complex, obtaining an IC_{50} reduction of 36% with respect to the free drug. Following this research line, in this thesis new pseudodendrimers or DHPs varying the dendrons covalently attached to the core have been investigated as nanostructures suitable to complex heparin and enhance its antimalarial abilities. Specifically, the series of DHPs described in chapter 2 were prepared, with dendrons of the 2nd generation either of *bis*-MPA or *bis*-GMPA. In these compounds, 64, 128 or 256 theoretical amino terminal groups have been reached when attaching the dendrons to each hyperbranched core (G2, G3 or G4, respectively), which means a high number of cationic groups able to interact with the negatively charged heparin. In addition, the inclusion of dendrons either

of *bis*-MPA or *bis*-GMPA was proposed to make a comparative study of the interaction abilities of both structures to form the complexes with heparin (section 5.2), inhibit the parasite growth (section 5.3.2), target the specific cells (section 5.3.3) or modulate the circulation time of heparin (section 5.4.1). The analogue DHPs labelled with rhodamine B (Rh) (see chapter 2, section 2.3.2.) were also included in the studies in order to obtain traceable complexes for the targeting assays.

Most of the experimental part of these chapter has been developed during a two-month research stay in the group of Nanomalaria led by Xavier Fernàndez-Busquets at ISGlobal Institute, Barcelona. Some ethical issues related to the use of human blood and the *in vivo* studies are reported in the Experimental chapter 7, section 7.2.2.4.

5.2. Complex formation and characterisation between heparin and DHPs

The formation of complexes between the negatively charged glycosaminoglycan heparin (Bioiberica) and the polycationic DHPs was studied by the methylene blue (MB) spectroscopic competition assay, adapted from Rodrigo *et al*.[37] and Al-Jamal *et al*.[38]. It consists of the competition of two species, MB and DHPs to complex heparin, which can be assessed by a colorimetric change (section 5.2.1).

After establishing the ratios of complexation between heparin and DHPs, the complexes were morphologically characterised by microscopy (TEM) (section 5.2.2) and the release of heparin from the complexes was assessed by electrophoretic separation after incubating the complexes in physiological conditions at different times (section 5.2.3).

5.2.1. Complexes formation

Briefly, free MB yields a spectrum with a maximum peak at 665 nm (solid blue line in Figure 5.4), while the maximum shifts to 565 nm when the probe is

complexed by heparin (dotted blue line in Figure 5.4). Then, the ratio between the absorbances at both wavelengths (A_{665}/A_{565}) indicates the degree of free MB in the sample. In the MB competition assay designed, a fixed amount of heparin and the corresponding amount of MB that fully complex the polysaccharide are previously established and then, the addition of the DHP compete with the MB in the heparin complexation. This displacement can be observed by the appearance of a peak at 665 nm, which indicates that the MB has been released from the complex and remains free in solution. Thus, the higher amount of free MB determined indicates that more amount of heparin has been complexed by the DHP. The corresponding controls were also assayed in order to corroborate the absence of interferences at the cited wavelengths (see Figure 5.4).

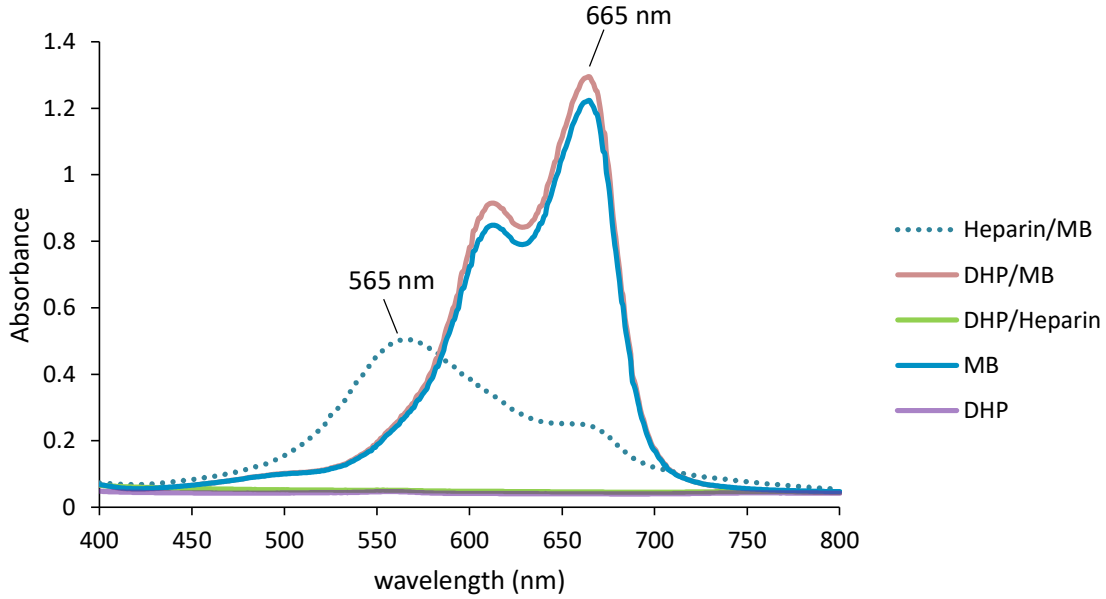

Figure 5.4. UV-Visible spectra identification of the maximum wavelength in each possible combination of the MB competition assay.

Firstly, complexes between heparin (final concentration of 10 µg/mL) and MB (final concentration of 50 µM) were formed in 96-multiwell dishes with TRIS-HCl 10 mM pH 7.4 buffer under vigorous stirring at RT for 15 minutes. Then, increasing amounts of the corresponding DHP calculated in weight ratio ($w_{DHP}/w_{heparin}$) were added and final volume was adjusted to 150 µL with milliQ-H_2O. Ratios tested include 0.25, 0.5, 1, 1.5, 2, 3, 4, 5, 7.5, 10, 15, 20, 25, 30 and 40. The mixtures were allowed to stir for another 30 minutes at RT and a

spectroscopic scanning between 400 and 800 nm was performed in an Infinite M Nano+ (TECAN) instrument. Triplicates of these experiments were performed with the six DHPs of the *bis*-MPA and *bis*-GMPA series and with the homologues containing the fluorophore rhodamine B.

The representation of the intensity ratio between the absorbances (A_{665}/A_{565}) versus the ratio in weight of both molecules involved in the complex formation ($w_{DHP}/w_{heparin}$) allows to calculate the ratio at which the heparin is completely complexed by the DHP, when the curve reached a plateau (Figure 5.5). The curves for the DHPs without (Figure 5.5a) and with rhodamine (Figure 5.5b) are represented, and $w_{DHP}/w_{heparin}$ ratios at which no heparin remains free are extrapolated from the graphs and gathered in Table 5.1.

Among the **series of DHPs**, little differences were found in their ability to complex heparin. Namely, all the DHPs of the *bis*-MPA series could totally complex heparin from a ratio 4/1 ($w_{DHP}/w_{heparin}$). Within the *bis*-GMPA series, a slight increase in the amount of DHP required to complex the heparin was observed, being the ratio 5/1 for the bigger pseudodendrimer, DHP(G4)-GMPA, and between 5/1 and 7.5/1 for DHP(G3)-GMPA.

Regarding the heparin complex formation with the **DHPs labelled with rhodamine B** (DHPs-Rh), the absorbance due to Rh at the concentrations assayed did not interfere with the measurements. A notable increment in the $w_{DHP}/w_{heparin}$ ratios was observed in some cases compared to the DHPs without the fluorophore. This increment in the amount of DHP-Rh required to fully complex the heparin could be due to the attachment of the fluorophore on the surface of the DHPs that, although is present in a small amount (less than 1% of the peripheric groups), reduces slightly the availability of the peripheric amino groups to interact with heparin due to steric hindrance. This effect due to the presence of rhodamine has been previously observed for the formation of complexes with a core of HP(G3) with *bis*-MPA 3rd generation dendrons, although in that case, the number of ammonium groups available was significantly lower when rhodamine was attached[36]. Interestingly, among the DHP(G_n)-MPA-Rh series, an influence of the HP core generation and thus, of the number of peripheric cationic groups was observed in their ability to complex heparin. As

seen in Figure 5.5b, DHP(G3)-MPA-Rh and DHP(G4)-MPA-Rh complex heparin from a similar ratio between 4/1 and 7.5/1, while the pseudodendrimer with less terminal amino groups, DHP(G2)-MPA-Rh, requires a higher amount of dendritic material to displace the MB and completely complex the heparin. The high value obtained in this last case (ratio 20/1) is more similar to those of the *bis*-GMPA series. With respect to the DHP(G_n)-GMPA-Rh series, this influence of the number of peripheric groups was also observed, although in a lower extent, with $w_{DHP}/w_{heparin}$ ratios varying from 20/1 to 15/1.

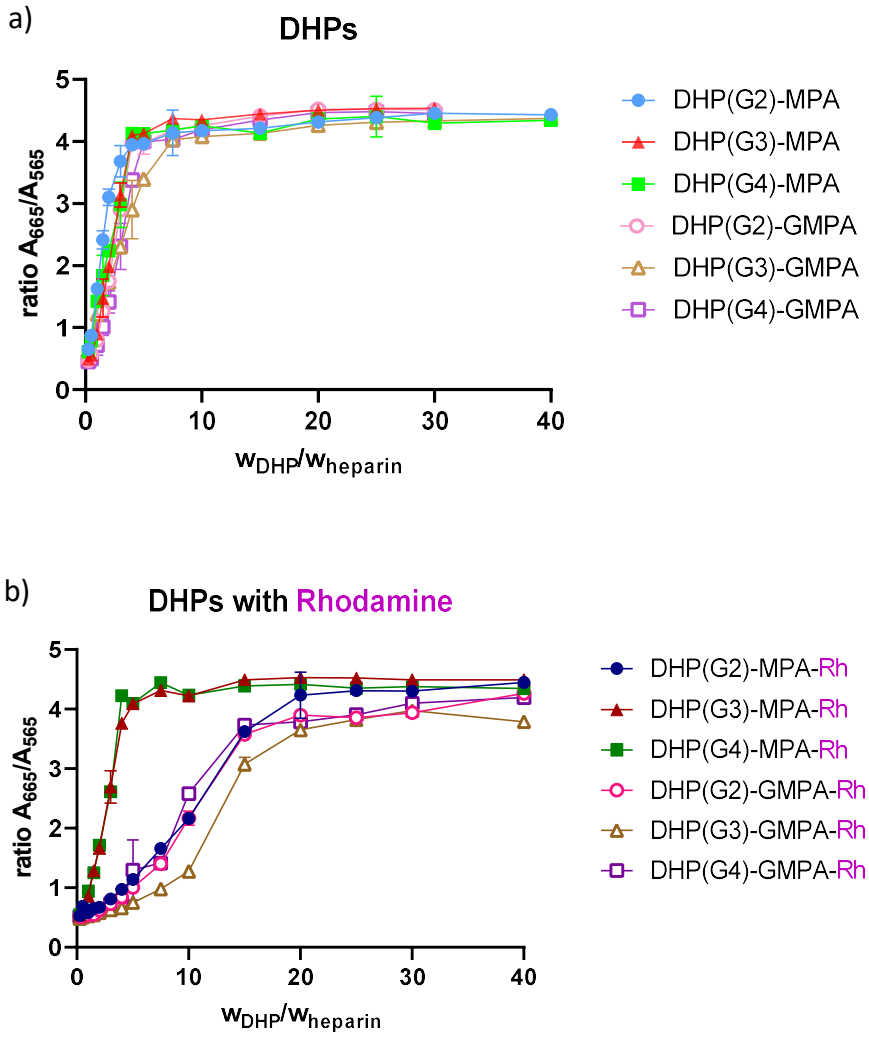

Figure 5.5. Determination of the complexation ratios between heparin and DHPs, either without (a) or with (b) rhodamine attached on the DHPs surface. Data are represented as mean ± SD (n=3).

Table 5.1. Determined $w_{DHP}/w_{heparin}$ ratios for the complexation of heparin by DHPs and DHPs-Rh, extracted from Figure 5.5.

			$w_{DHP}/w_{heparin}$	
	Pseudodendrimer	Theoretical $-NH_3^+$	Without rhodamine	With rhodamine
bis-MPA series	DHP(G2)-MPA	64	4	20
	DHP(G3)-MPA	128	4	4-7.5
	DHP(G4)-MPA	256	4	4
bis-GMPA series	DHP(G2)-GMPA	64	4	15-20
	DHP(G3)-GMPA	128	5-7.5	20
	DHP(G4)-GMPA	256	5	15

5.2.2. Complexes morphological characterisation

The morphology of the complexes formed by the biggest DHPs from the two series, namely DHP(G4)-MPA and DHP(G4)-GMPA, with heparin at the ratios established, was studied by TEM. In Figure 5.6, spherical objects can be observed for both complexes, resulting from the arrangement of the unimolecular micelles around 14 nm formed by the single DHPs in water (see chapter 2, section 2.3.3.).

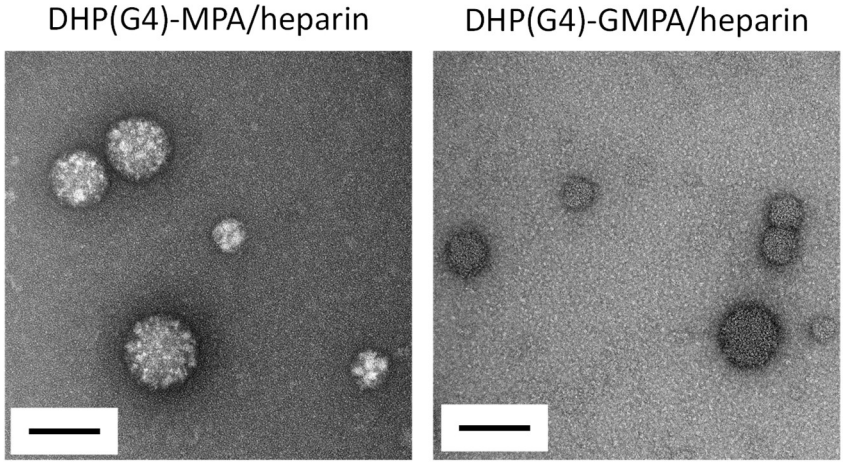

Figure 5.6. TEM images of the complexes between DHPs and heparin. Scale bars: 100 nm.

This arrangement into bigger aggregates was prompted by the complexation of heparin and yields spherical nanoobjects of different sizes, ranging from 40 to 100 nm in diameter in the case of the complexes DHP(G4)-MPA/heparin (Figure 5.6, left). The aggregates formed by the complexes DHP(G4)-GMPA/heparin are slightly smaller, from 30 to 80 nm (Figure 5.6, right), which is in agreement with the possibility offered by the inner amide groups of the *bis*-GMPA to stablish hydrogen bonds and yield more compact structures.

5.2.3. Heparin release study

The kinetics of the heparin release from the complexes with the DHPs was evaluated by incubating the complexes at physiological conditions (in RPMI media at 37 ºC under gentle stirring) for different time periods until 24 hours. After that, samples containing 20 µg of polysaccharide in all cases were loaded in a non-denaturing polyacrylamide gel and separated under an electric field. The same amount of free heparin in RPMI was used as control of the experiment. Detailed procedure for the electrophoretic assay is described in chapter 7, section 7.2.2.4.

The analysis of the gels after applying the electrophoretic field and staining with Alcian blue reveals and intense band corresponding to the free heparin while, interestingly, any signal was observed for samples with fully complexed heparin (Figure 5.7a). This could be due to the big size of the complexes that does not allow them to enter the gel or maybe due to an effect of the charges that makes the positively charged complexes move to the negative pole, that is, in the opposite direction. In any case, free or released heparin can be perfectly identified by this method and the measurement of the intensity of the bands at each time point allows to draw a graphic with the percentage of heparin released versus time (Figure 5.7b). For both complexes, DHP(G4)-MPA/heparin and DHP(G4)-GMPA/heparin, the polysaccharide was completely released after 18 hours (or 1080 min) of incubation. However, some differences can be found at shorter incubation times. Specifically, DHP(G4)-MPA/heparin complexes start to release a small amount of heparin at 75 min while DHP(G4)-GMPA/heparin complexes do not start the release until 200 min of incubation. That delayed

release is in agreement with a stronger complexation of heparin with the DHP(G4)-GMPA, probably driven by additional forces allowed by the amide groups of the *bis*-GMPA dendrons.

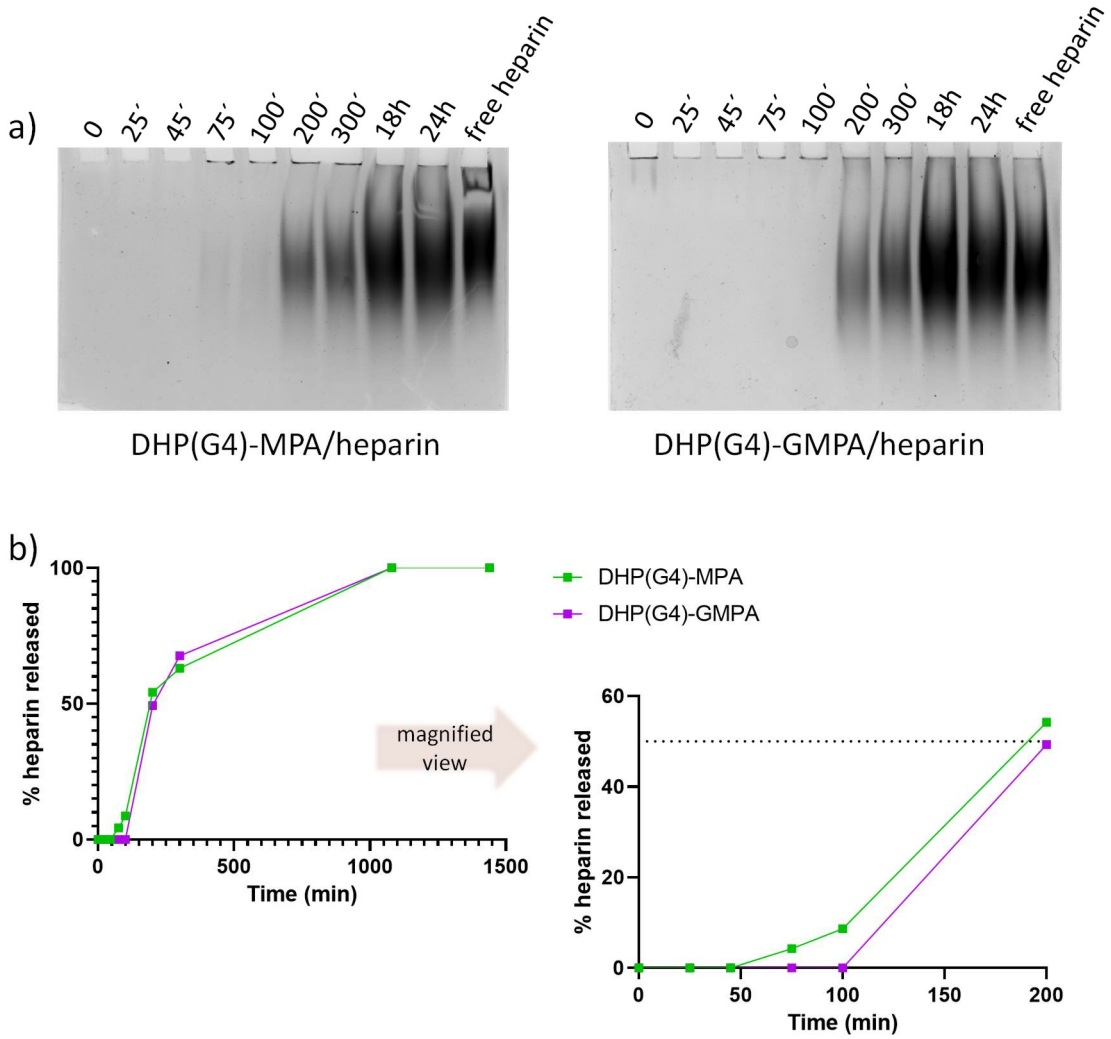

Figure 5.7. Heparin release study from complexes DHP(G4)-MPA/heparin and DHP(G4)-GMPA/heparin. a) polyacrylamide gel electrophoresis analysis of heparin after different times of incubation; b) graphical representation of the percentage of heparin released at each time point.

5.3. *In vitro* studies

Once the ratios for the complex formation between DHPs and heparin had been established, these combinations were used for the following experiments. In the next sections, the cytotoxicity of the DHPs in human cells (section 5.3.1), the ability of the complexes to inhibit *P. falciparum* growth (section 5.3.2) and the preferential targeting of the complexes towards infected or non-infected RBCs (section 5.3.3) are presented.

P. falciparum strain 3D7 was cultured in human RBCs in RPMI media (Invitrogen) supplemented with *L*-glutamine (2 mM) at 37 °C under hypoxia conditions, i.e., 94% N_2, 5% CO_2 and 3% O_2. The culture was maintained at 3% haematocrit (% in volume of RBCs) and between 0.5-3% parasitaemia (% of pRBCs with respect to RBCs) with the addition of fresh RBCs. The parasitaemia was routinely calculated by optical microscope counting after nuclei staining. Additionally, the parasites present in the culture could be synchronised at a specific stage of the parasite life cycle; namely, early stages (mostly rings) were obtained by a lysis procedure based on sorbitol[39], and mature stages were rescued by a density gradient method employing percoll[40]. For the following experiments, desynchronised cultures (Figure 5.8) were employed in order to have a representation of all the erythrocytic stages of the parasite in the culture and thus, could have an overview of the effect of the treatment over all of them.

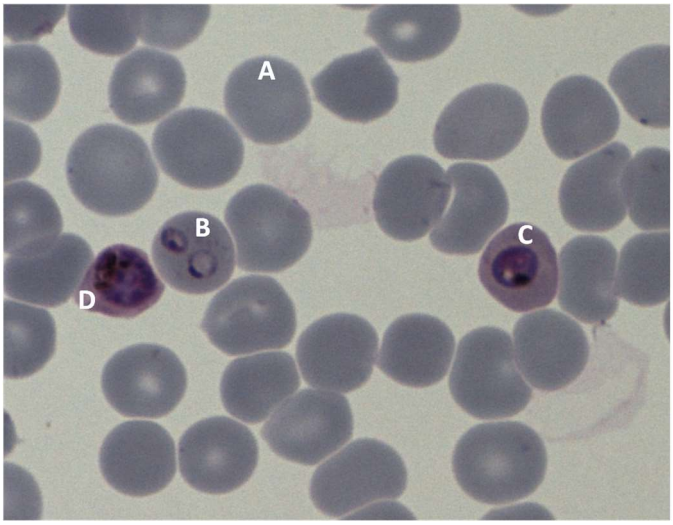

Figure 5.8. Microscopic image of a desynchronised culture of pRBCs with a representation of all the erythrocytic stages of P. falciparum. A, healthy RBC; B, ring stages; C, trophozoites; D, late trophozoite/early schizont.

5.3.1. Cytotoxicity assay

The effect of the series of DHPs and the homologues with rhodamine over the viability of human cells was evaluated in human umbilical vein endothelial cells (HUVEC). These cells were selected as a model to evaluate the cytotoxicity because of the high abundance of endothelial vessel cells in the blood stream[23]. Cultures were grown in Medium 199 (M199, LabClinics) supplemented with 10% heat inactivated FBS, 1% penicillin/streptomycin and 10 mM glutamine.

To assay the cytotoxicity of the compounds, cells were seeded at a density of 2.2×10^4 cells/mL in MW96 plates and incubated for 24 hours at 37 °C. Then, medium was replaced with samples diluted in M199 without complements and microplates were incubated for 48 hours at 37 °C. To determine the viability levels, medium was then replaced with 10% of 4-[3-(4-iodophenyl)-2-(4-nitrophenyl)-2H-5-tetrazolio]-1,3-benzene disulfonate (WST-1, Roche) in M199 and incubated at the same conditions for 4 hours. The cleavage of the tetrazolium salt WST-1 to yield formazan, occurring inside living cells, was spectrophotometrically determined by measuring the absorbance at 440 nm and 600 nm in an EPOCH plate reader (BioTeck). Wells with cells in medium without any treatment were included as positive growth control, 50% DMSO was used as negative control, and the maximum percentage of water added with the samples (5% v/v) was also assayed. Samples were assayed in triplicate.

The percentage of cellular viability versus the concentration of compound assayed is graphically represented in Figure 5.9 until 4 mg/mL. All the compounds assayed were found to be non-cytotoxic up to 444 µg/mL, with viability levels above 80% and even up to 1333 µg/mL, where the viability remains above 70%. At the highest concentration assayed, 4000 µg/mL, the DHPs exhibited a cytotoxic effect with viability levels between 40-50% (Figure 5.9a). Interestingly, the DHPs-Rh showed a lower cytotoxicity at that concentration, with viability values ranging from 50 to 70% (Figure 5.9b). It could be due to the slightly lower amount of free amino groups in the compounds that bear rhodamine on the surface, which contributes to a lower cytotoxic effect, but it is unlikely due to the low amount of functionalised amine groups. The steric hindrance provoked by the presence of rhodamine could also contribute to

explain this effect. It must be noted that the pseudodendrimers of the *bis*-MPA series labelled with rhodamine exhibited a more marked cytotoxic effect than the ones of the *bis*-GMPA series. This observation is also in agreement with the possible reduction of amino terminal groups exposed to the outer part of the pseudodendrimer in the case of the *bis*-GMPA series, probably due to intramolecular bonds favoured by the inner amides present in the *bis*-GMPA dendrons. Nevertheless, the range of concentrations assayed is wide enough, and both, the DHPs and the DHPs-Rh, have demonstrated good biocompatibility abilities.

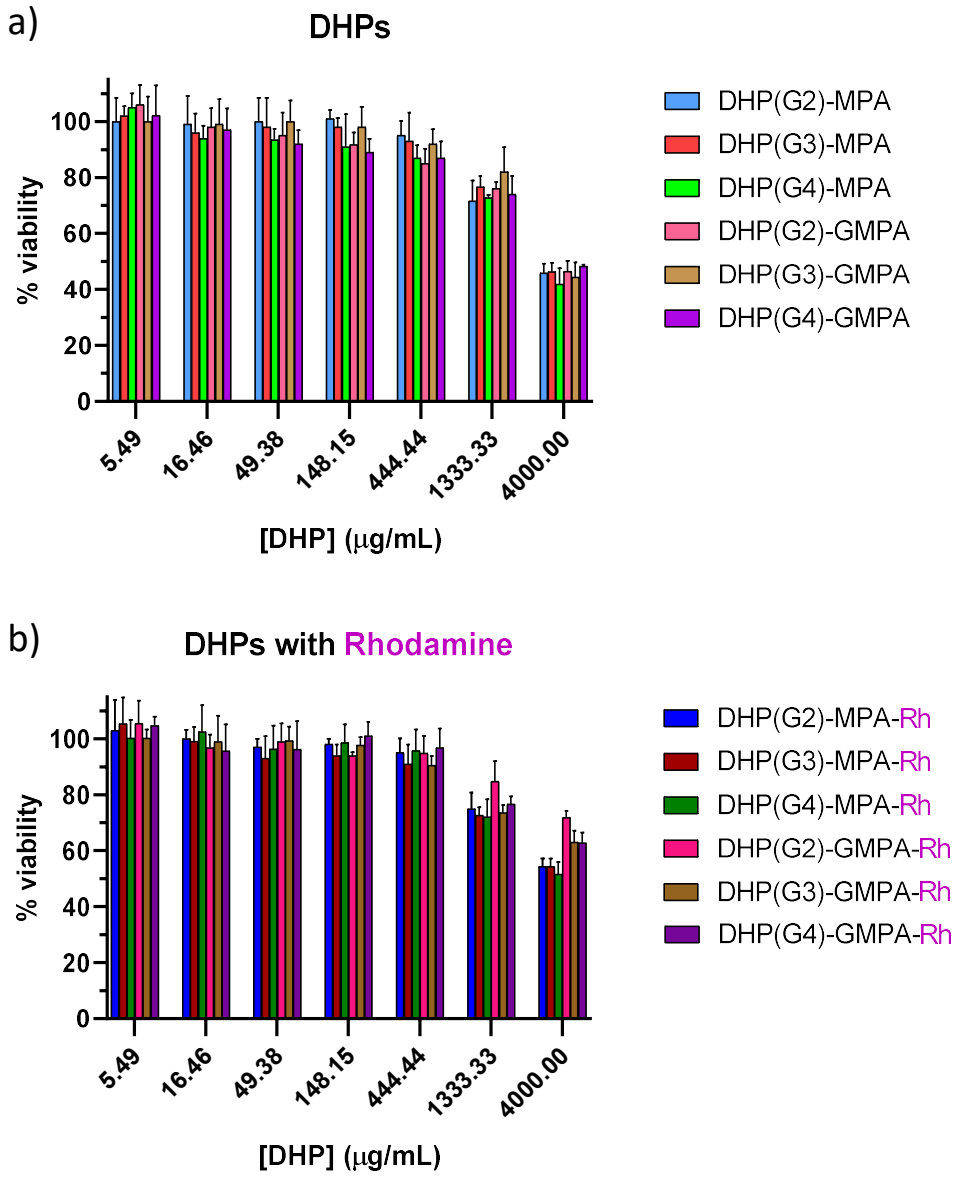

Figure 5.9. Cytotoxicity assayed in HUVEC of the series of a) DHPs and the b) DHPs with rhodamine B. Mean ± SD (n = 3).

5.3.2. *Plasmodium* inhibition assays

The absence of nuclei in the RBCs makes it possible to assess the growth of the parasite *P. falciparum* in the cultures by staining the whole culture with a nucleic acid dye and then, analysing the intensity of fluorescence by flow cytometry (pRBCs are the unique cells stained because they contain the genetic material of the parasite).

With this strategy, the potential of the complexes between DHPs or DHPs-Rh and heparin to inhibit the growth of the parasite in RBCs was evaluated by the growth inhibition assay (GIA). This assay was used to determine the concentration of a compound needed to inhibit the parasite growth in a 50%, thus defining the IC_{50}. Prior to compounds addition, culture was adjusted to 1-1.5% parasitemia and 6% hematocrit.

The inhibitory activity of the complexes DHPs/heparin and DHPs-Rh/heparin was assessed, as well as the activity of the free heparin and all the pseudodendrimers without heparin as controls. Compounds were dissolved in the minimal amount of water and the DHP/heparin complexes were incubated for 30 minutes at RT before making serial dilutions in complete RPMI, always maintaining the percentage of water under 3% (v/v) in the testing sample. Heparin concentrations tested ranged from 200 to 0.091 µg/mL and the DHP amount was accordingly adjusted considering the corresponding $w_{DHP}/w_{heparin}$ ratio previously established for each pseudodendrimer. In addition, the highest water percentage added was assayed to check its effect over the parasite growth, while not treated cells were established as positive growth controls and heparin at 200 µg/mL was employed as negative growth control. A total of 100 µL of the adjusted culture and 100 µL of the samples were added per well, in triplicate. After resuspending, they were incubated at 37 °C in hypoxia for 48 hours.

Then, samples were stained for further cytometry analysis. Namely, 2 µL of each well resuspended sample were mixed in a U-bottom 96 well plate with 198 µL of a solution of SYTO-11 in PBS (250 nM) and they were analysed through a BD LSR Fortessa 4 Laser cytometer with a HTS reader. Briefly, cell population of interest, RBCs, were selected by size (FSC, forward scatter) and complexity (SSC, side scatter) (Figure 5.10a) and afterwards, fluorescence of that population

was analysed with a laser at $\lambda_{excitation}$= 488 nm and $\lambda_{emission}$= 525 nm (Figure 5.10b). Flow rate was set at 1 µL/second and 20000 events per well were recorded. In addition, parasitemia of interesting wells was corroborated by sample staining with Giemsa followed by optical microscope analysis (NIS Elements F 3.0) and the programme PlasmaScore to facilitate the counting.

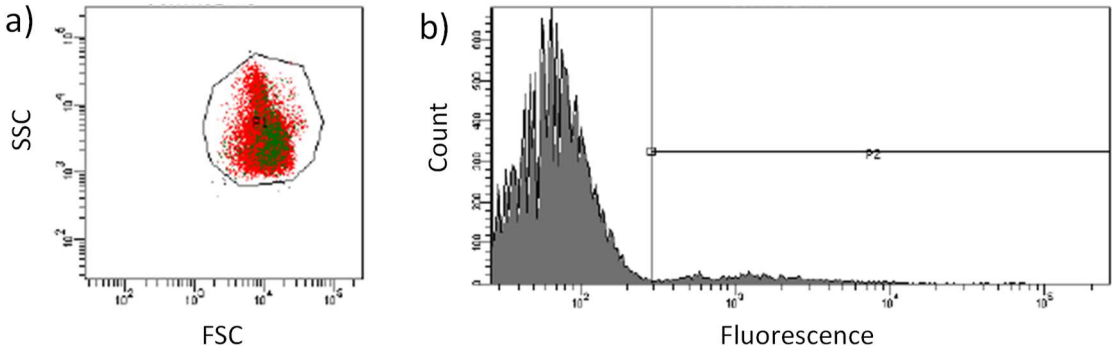

Figure 5.10. Cytometry analysis of the growth inhibition assays (GIAs): a) selection of the cellular population of interest by size and complexity, and b) analysis of the fluorescence of that population at $\lambda_{ex/em}$: 488/525 nm.

The percentage of *P. falciparum* growth inhibition vs the concentration of heparin or pseudodendrimer is graphically represented in Figure 5.11 for the combinations of DHPs, and in Figure 5.12 for the combinations of DHPs with rhodamine. In addition, Table 5.2 gathers the IC_{50} values obtained from the GIAs for all the combinations tested.

The complexes formed between the series of **DHPs** and heparin had antiparasitic activities similar of that of the free heparin, with an IC_{50} of 5.16 µg/mL. Specifically, all the pseudodendrimers of the *bis*-GMPA series in combination with heparin presented similar IC_{50} values, ranging from 5.11 to 5.42 µg/mL (see Table 5.2), whereas within the *bis*-MPA series more variations were found. In the case of the larger compound in combination with heparin, DHP(G4)-MPA/Hep, its IC_{50} (4.32 µg/mL) revealed a slight improvement of the inhibitory activity of the free heparin, while the other two complexes, DHP(G2)-MPA/Hep and DHP(G3)-MPA/Hep, did not show this effect. In addition, the *Plasmodium* growth inhibition activity of the single DHPs was assayed and it was observed that they do not exhibit antiparasitic activity by themselves (see Figure 5.11b), thus concluding

that the activity previously observed for the complexes with heparin was due to the appropriate complexation of heparin on the DHPs structures.

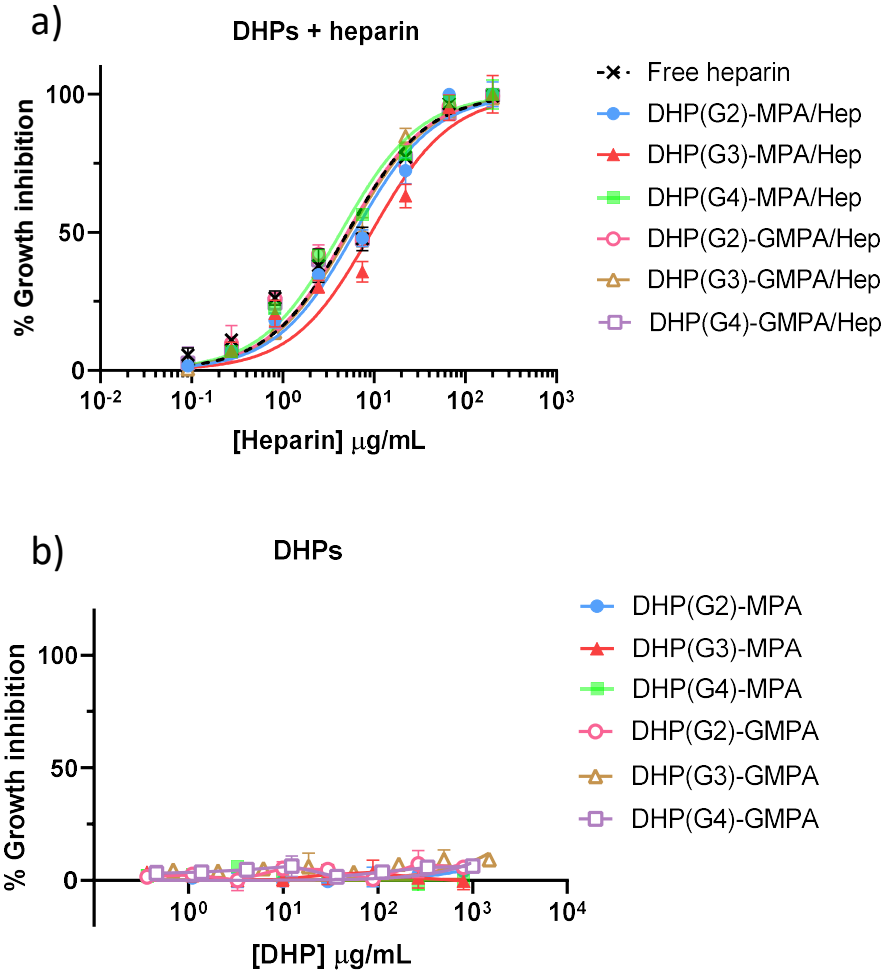

Figure 5.11. Growth inhibition assays (GIAs) of the complexes DHPs/heparin (a) and the free DHPs (b), with free heparin as control. Mean ± SD (n=3).

Table 5.2. IC_{50} values obtained from the GIAs assays for all the combinations tested.

		IC_{50} (µg/mL)
	Heparin	5.16
DHPs	DHP(G2)-MPA/Hep	6.15
	DHP(G3)-MPA/Hep	9.37
	DHP(G4)-MPA/Hep	4.32
	DHP(G2)-GMPA/Hep	5.11
	DHP(G3)-GMPA/Hep	5.42
	DHP(G4)-GMPA/Hep	5.33
DHPs with rhodamine	DHP(G2)-MPA-Rh/Hep	2.52
	DHP(G3)-MPA-Rh/Hep	12.18
	DHP(G4)-MPA-Rh/Hep	13.53
	DHP(G2)-GMPA-Rh/Hep	5.12
	DHP(G3)-GMPA-Rh/Hep	4.67
	DHP(G4)-GMPA-Rh/Hep	4.65

The series of **DHPs labelled with rhodamine** was also tested as anti-*Plasmodium* agents. The low concentration of rhodamine present in the samples did not impair the measurement of the SYTO-11 fluorescence at the selected wavelength. In this case, little variation was found again within the activity of the complexes of the *bis*-GMPA series, while more interesting results were found for the *bis*-MPA containing complexes. However, the activity of the single DHPs-Rh revealed a certain inhibitory activity due to the labelled pseudodendrimers themselves (see Figure 5.12b) and thus, the interpretation of the results must consider the amount of DHP-Rh required to form the complex with heparin. The antimalarial potential of the fluorophore rhodamine B has been previously reported[41,42]. In this regard, the combination that showed a better *Plasmodium* inhibitory performance with an IC_{50} of 2.52 µg/mL, DHP(G2)-MPA-Rh/Hep, requires a $w_{DHP}/w_{heparin}$ ratio of 20/1 to establish the complexes and then, more amount of rhodamine is finally present in the sample than in the cases of

DHP(G3)-MPA-Rh/Hep or DHP(G4)-MPA-Rh/Hep, whose complexation ratios were 7.5/1 and 4/1, respectively, and their antimalarial activities were markedly worse, with IC_{50} higher than 12 µg/mL. Surprisingly, the antiparasitic activities of the complexes DHP(G_n)-GMPA-Rh with heparin (IC_{50} between 4.65 and 5.12 µg/mL) were slightly better but did not differ too much from those of the homologues without the fluorophore (Rh), even though the ratios of complexation ($w_{DHP}/w_{heparin}$ 15/1-20/1) indicate that a high amount of rhodamine is present in the complex.

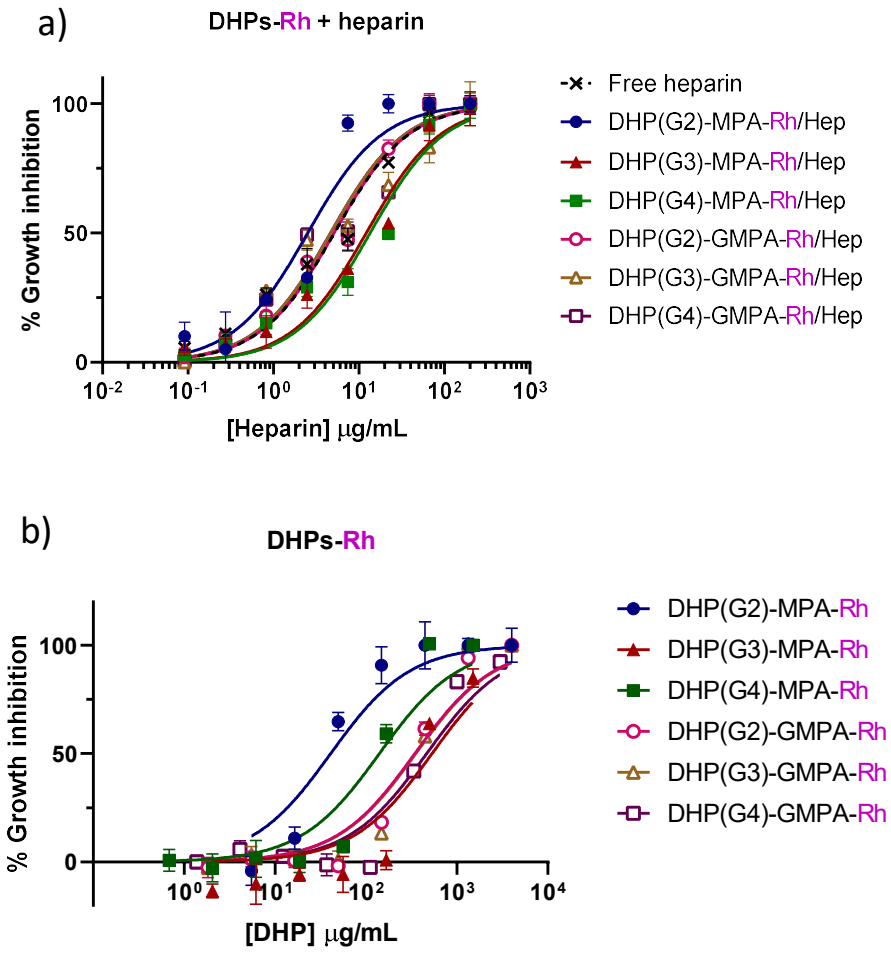

Figure 5.12. Growth inhibition assays (GIAs) of the complexes DHPs-Rh/heparin (a) and the free DHPs-Rh (b), with free heparin as control. Mean ± SD (n=3).

5.3.3. Targeting of infected RBCs

The ability of the rhodamine labelled DHPs and their complexes with heparin to target parasite infected RBCs, pRBCs, was evaluated by flow cytometry and by fluorescence microscopy. Briefly, cultures of infected RBCs were incubated at two different conditions of time and concentration with the pseudodendrimers, either with or without heparin. On the one hand, 0.5 mg/mL of DHPs-Rh were incubated for 1 h and on the other hand, 1.0 mg/mL of DHPs-Rh were incubated for 4 h with the cultures. The corresponding amount of heparin was added in each case to form the complexes. Incubation with Hoechst (0.2 µg/mL) for 30 minutes was developed to stain the parasites nuclei.

In order to determine the intensity of fluorescence by **flow cytometry**, samples were washed, diluted in PBS (1:100) and stored in darkness until their analysis. Fluorescence intensities were measured at $\lambda_{ex/em}$: 350/450 nm for Hoechst (Figure 5.13, blue population), and at $\lambda_{ex/em}$: 561/582 nm for rhodamine B (Figure 5.13, red population). 50000 events were recorded for each sample in a LSRFortessa™ flow cytometer instrument (BD Biosciences) and Flowing Software 2.5.1. was employed for further analysis.

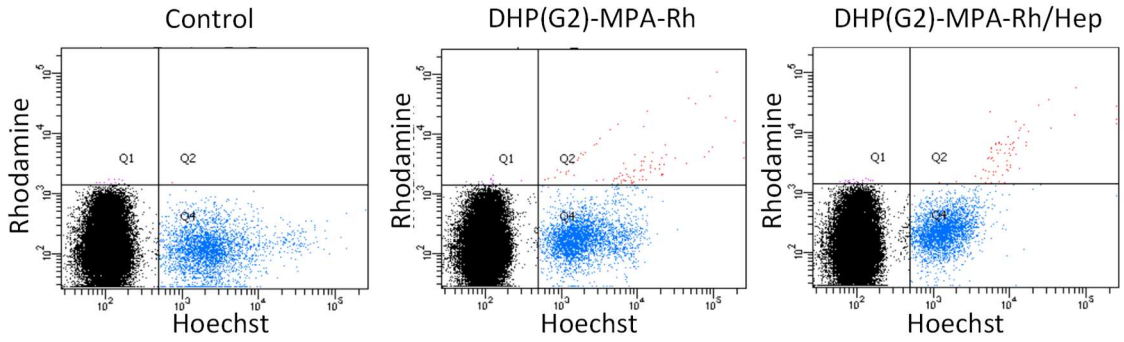

Figure 5.13. Analysis by flow cytometry of the targeting experiments. Samples include a control of the parasitised culture and cultures incubated with DHP(G2)-MPA-Rh or the complexes DHP(G2)-MPA-Rh/heparin. Experimental conditions: 1.0 mg/mL of DHP and 4 hours of incubation.

Cytometry results were interpreted considering the intensity of rhodamine B fluorescence in parasitised cells, pRBCs, (Figure 5.14, graphs on the left) and non-parasitised RBCs (Figure 5.14, graphs on the right). Both experimental conditions of sample incubation are represented in Figure 5.14 as follows: the condition (a) refers to 1 h of incubation with 0.5 mg/mL of DHP-Rh and condition (b) indicates the highest timing and concentration conditions, i.e., 4 h and 1.0 mg/mL.

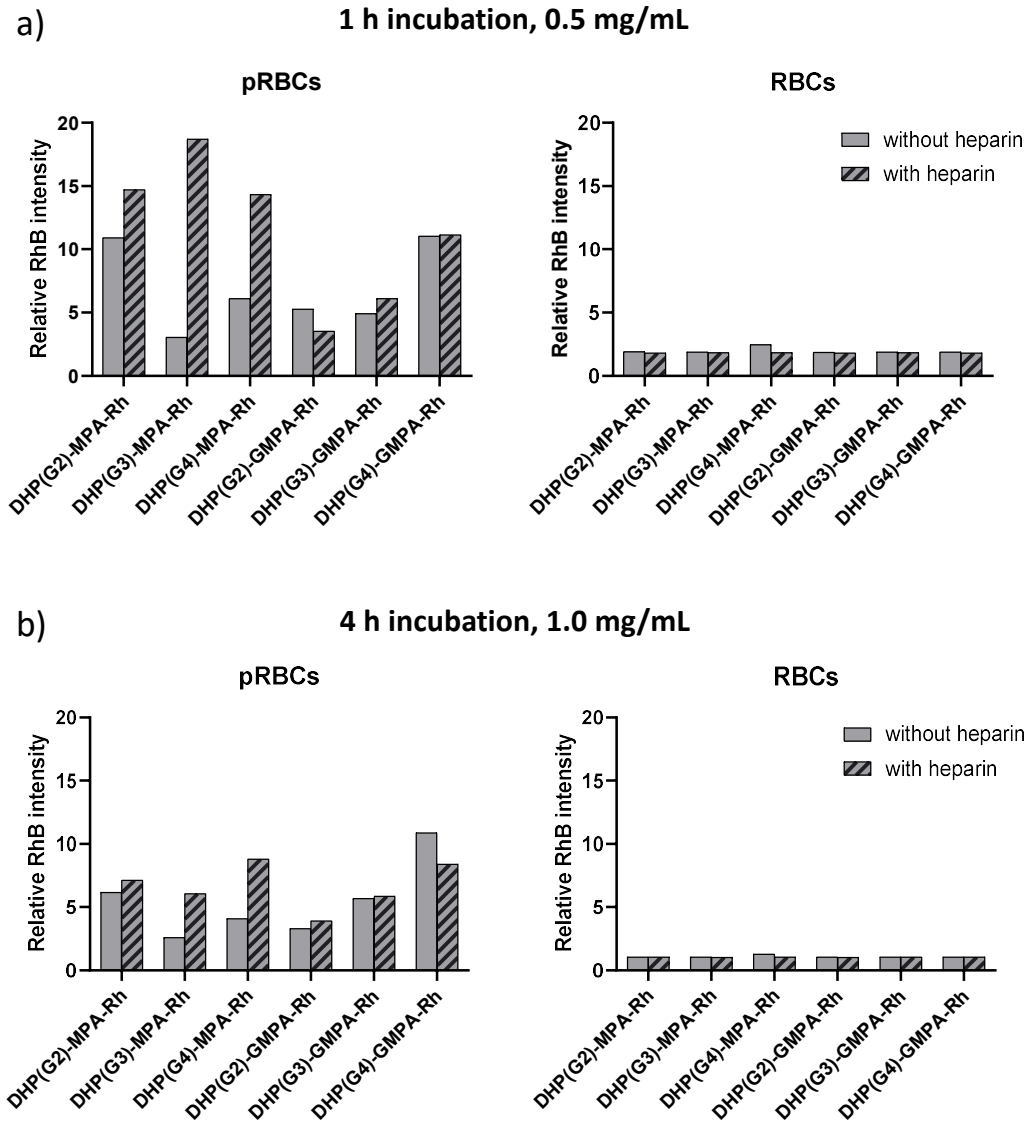

Figure 5.14. Intensity of rhodamine fluorescence in pRBCs (graphs on the left) and RBCs (graphs on the right) after incubation with samples at different conditions: a) 1 h at 0.5 mg/mL or b) 4 h at 1.0 mg/mL. Samples of DHPs-Rh without (plain grey bars) or with heparin (striped grey bars) were assayed.

Regarding the targeting towards the different cellular populations, pRBCs or RBCs, the preference of the samples towards the pRBCs (see Figure 5.14, graphs on the left) is predominant under both incubation conditions, since the intensity of rhodamine is higher within this cellular population compared to the healthy RBCs, where the intensity of rhodamine remains below 2.5 a.u. in all cases (see Figure 5.14, graphs on the right). Between both incubation conditions, the increasing of the time and the concentration of DHP-Rh was not translated into a higher intensity of rhodamine in the cells of interest, thus pointing at the conditions of 1 h and 0.5 mg/mL as the most favourable to observe the targeting effect (Figure 5.14a). This could be related to the increased probability to suffer degradation or to a higher cellular excretion when increasing the incubation time. Among the compounds tested, the single DHPs-Rh (plain grey bars) exhibited some targeting activity themselves towards the pRBCs, with intensities up to 11 a.u. Interestingly, complexation with heparin (striped grey bars) enhanced this affinity towards pRBCs for the DHP-MPA-Rh series, reaching intensity values of 18.7 a.u., whereas the heparin scarcely affected the targeting of the DHP-GMPA-Rh series complexes towards the pRBCs.

Samples were also visualised by **fluorescence microscopy** with an inverted Olympus Ix51 microscope. Non fixed samples were washed with incomplete RPMI medium and placed in an 8-well Ibitreat chamber slide system (Ibidi, catalog number 80826). The fluorescence of Hoechst was observed at $\lambda_{ex/em}$: 350/420 nm and rhodamine was identified at $\lambda_{ex/em}$: 553/590 nm. Figure 5.15 gathers the fluorescence microscopy images for the incubation of the cultures with DHP(G2)-MPA-Rh and their complexes with heparin. This pseudodendrimer has been chosen as a representative example of the whole series of DHPs with rhodamine since it exhibited good targeting abilities towards pRBCs, with and without complexing heparin (see Figure 5.14). No relevant differences were found between the fluorescence images at the two experimental conditions, namely, 1 h at 0.5 mg/mL (Figure 5.15a) and 4 h at 1.0 mg/mL (Figure 5.15b), neither between the samples with or without heparin. In general terms, the fluorescence microscopy images show that the rhodamine of the DHP(G2)-MPA-Rh (red fluorescence) overlapped with extracellular forms of the parasite (stained in blue). Only in the sample of DHP(G2)-MPA-Rh incubated for 1 h at 0.5 mg/mL, an

aggregate with red fluorescence was found attached to the surface of a pRBC (marked with a white arrow in Figure 5.15a).

In conclusion, the pseudodendrimer is able to target both, the intracellular forms of the parasite, pRBCs, and the extracellular forms. This information is given by the different complementary techniques employed to evaluate the targeting, flow cytometry analysis and fluorescence microscopy, although in microscopic images the targeting towards the extracellular forms of the parasite are principally observed.

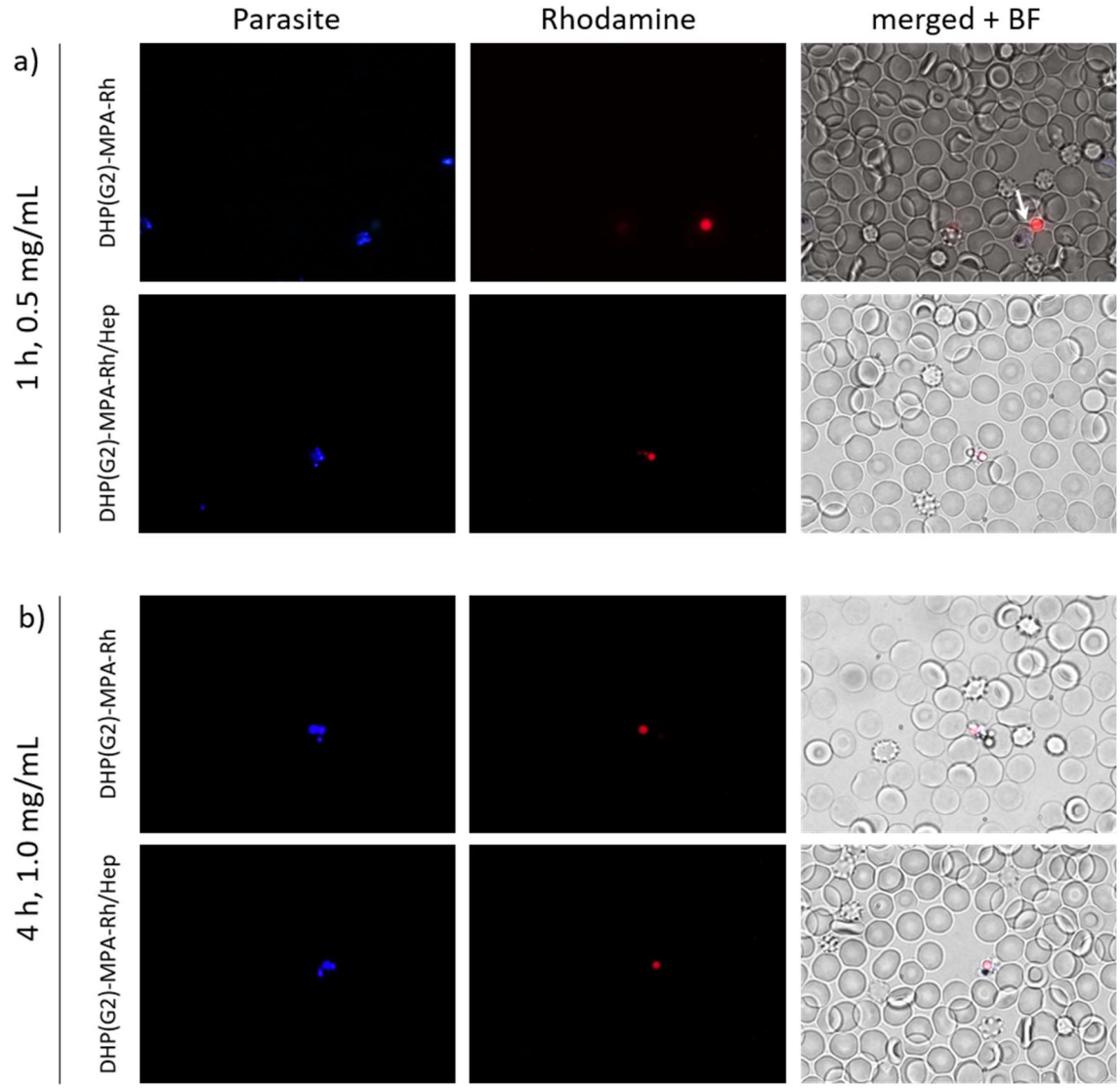

Figure 5.15. Fluorescence microscopy images for the incubation of the cultures with DHP(G2)-MPA-Rh and their complexes with heparin under the two experimental conditions: 1 h at 0.5 mg/mL (a) and 4 h at 1.0 mg/mL (b). Nuclei of the parasite are represented in blue and rhodamine in red. The RBCs diameter is around 5 - 7.5 μm. BF: bright field.

5.4. *In vivo* studies

The *in vitro* activity testing of the compounds constitutes a compulsory step in the search for new formulations, however *in vivo* models are of great help in order to elucidate their performance in a more complex organism and can give a better approximation to their final behaviour in humans. On the other hand, the use of animals for research purposes is a highly controversial issue and must always be developed respecting at least the three Rs principles of replacement, reduction and refinement stated by Russel and Burch in 1959, and always looking after the animal welfare[43].

The rapid elimination of heparin from the blood circulation constitutes a disadvantage for the antimalarial activity of the polysaccharide, considering the life cycle of the parasite in the intraerythrocytic stage. For that reason, heparin formulations that increase its blood circulation times would be beneficial to favour the therapeutic activity of heparin[34].

The *in vivo* assays developed in this thesis had the objective to evaluate the ability of the pseudodendrimers to increase the residence time of heparin in plasma. This is a prior step to the antimalarial activity evaluation *in vivo*, which requires the previous infection of the animal model with the parasite. Then, this further study would be later carried out with the DHP/heparin formulation that showed the more prolongated heparin plasma half-life, in favour of reducing the number of infected mice.

5.4.1. Determination of heparin half-life in plasma

The residence time of heparin in circulation was evaluated in inbred BALB/c female mice of 20 g in average, purchased from Charles River, and under an approved licence. Mice were housed under standard conditions of light and temperature at the Animal Facilities of the Clinic Hospital of Barcelona, and they were fed a commercial diet *ad libitum.* Firstly, intraperitoneal administration of the compounds was developed and then, blood extractions at different time points were carried out to monitor the amount of heparin in plasma with respect to time. Specifically, 100 µL of a solution of the compounds in PBS were injected

(calculated to administered 3.7 mg heparin/kg) and six temporal points were selected, 20, 45, 75, 100, 200 and 300 minutes after compounds injection. Three mice were employed to test each compound (Table 5.3), and another mouse without any treatment was employed to extract the blood and use it for the calibration standard curve for further heparin quantification.

Table 5.3. Distribution of the experimental conditions and the animals employed to test each compound.

Time points (min)			
Mouse 1	Mouse 2	Mouse 3	blood extraction
20	45	75	100 µL from tail
100	200	300	800 µL intracardiac

In this way, each mouse yielded the blood needed for two time points; firstly, 100 µL of blood were extracted from the tail and finally, 800 µL of intracardiac blood from previously anaesthetised animals, which meant the endpoint for the animal. The anaesthesia was intraperitoneally administered before intracardiac puncture, and it consisted of 200 µL of a mixture of ketamine (Imalgene, 100 mg/kg) and xylazine (Rompun, 10 mg/kg) in sterile water for injections (Meinsol). Euthanasia was performed by the cervical dislocation method[44] to guarantee the minimal animal distress. Blood samples were collected in eppendorfs with sodium citrate buffer 3.8% (w/v) pH 7.2 (an anticoagulant) at ratio 1:9; 10 µL for the first blood extraction (100 µL) and 80 µL for the last one (800 µL). Samples were centrifuged for 10 minutes at 500 g to obtain the plasma (the supernatant) and they were stored at -80 ºC for further quantification of heparin.

The determination of the amount of heparin present in each sample of plasma was performed with the Heparin Red® assay (Redprobes)[45]. Briefly, it consists of a polycationic fluorescent probe that in presence of the polyanionic heparin tends to aggregate and its fluorescence is quenched (Figure 5.16).

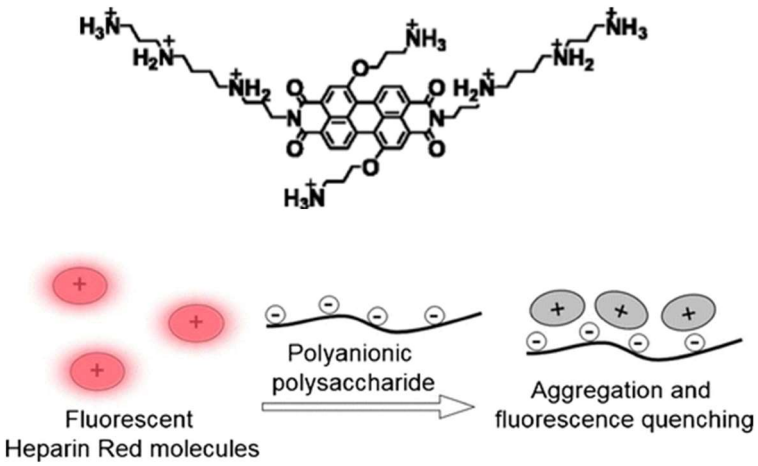

Figure 5.16. Heparin Red chemical structure (above) and scheme of the quenching reaction occurring during the heparin red assay (below). Adapted from Warttinger et al.[45]

20 µL of each sample (plasma containing different concentrations of heparin added for the calibration curve or plasma extracted from the treated mice) were placed in duplicates per mouse and time point in a black MW96 plate with clear bottom (Costar) and 80 µL of the kit solution mixture (enhancer solution:Heparin Red 1000:9) were added to each well. Then, plates were shaken for 2 min and the fluorescence was measured at $\lambda_{ex/em}$: 570/605 nm in a microplate reader (Infinite M Nano+,TECAN). The calibration curve with known amounts of heparin in mice plasma (0, 1.5, 3, 7.5, 15, 30, 40 and 50 µg/mL) was developed under the same experimental conditions (Figure 5.17), observing a decay in the intensity of fluorescence as the concentration of heparin is raised. Samples were assayed in duplicates per time point or without replicates in the cases when the volume of biological sample was a limiting factor.

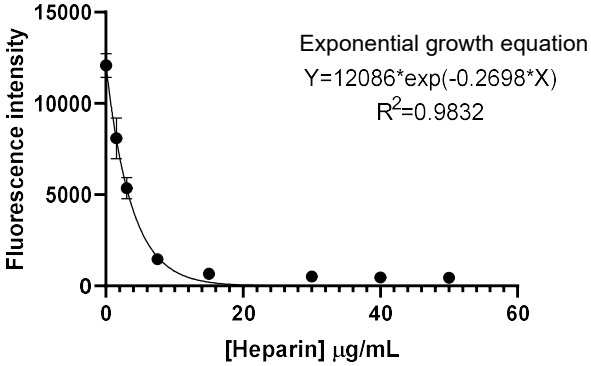

Figure 5.17. Calibration curve for the concentration of heparin in plasma. The intensity of fluorescence was measured at 570 nm and 605 nm. Mean ± SD (n = 2).

The circulation time in plasma of intraperitoneally injected heparin is represented in Figure 5.18 for all the complexes between the DHPs and heparin, and the corresponding heparin half-lives ($t_{1/2}$) in minutes are gathered in Table 5.4. $t_{1/2}$ is calculated adjusting the experimental data to a one phase exponential decay equation (Y=a*exp(-K*X) + b) using GraphPad Prism 8.0.2. software. It must be noted that the curve of the free heparin is not present in Figure 5.18 because there were experimental problems in its quantification, and it should be repeated. However, the $t_{1/2}$ for the free commercial heparin was obtained from another experiment developed in the same laboratory[34] and it is included in Table 5.4 as a reference value (25.7 min).

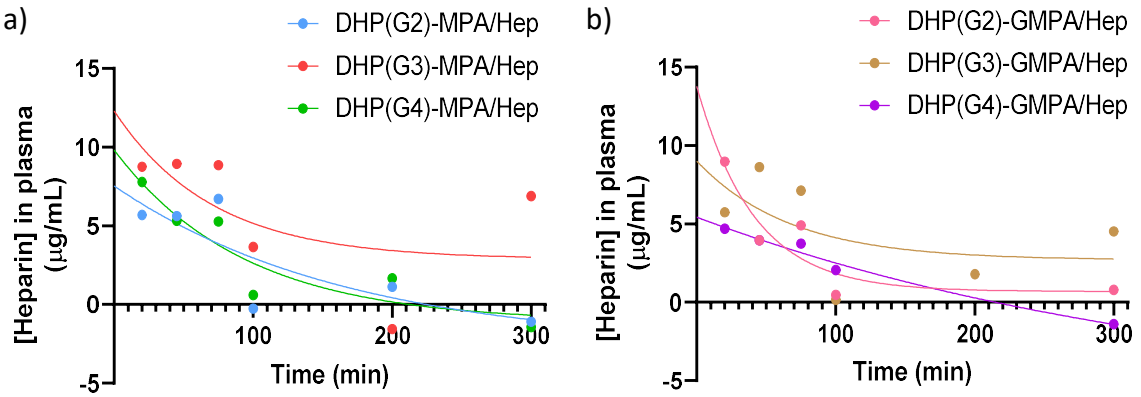

Figure 5.18. Determination of the concentration of heparin in plasma with respect to time for all the complexes between the DHPs and heparin: a) complexes with DHPs of the bis-MPA series and b) bis-GMPA series.

*Table 5.4. Heparin half-life ($t_{1/2}$) determination, in minutes, calculated from Figure 5.18 for all the complexes between DHPs and heparin. *The value for commercial heparin was obtained from Lantero et al.[34]*

complexes	Heparin $t_{1/2}$ (min)
DHP(G2)-MPA/Hep	117.00
DHP(G3)-MPA/Hep	48.86
DHP(G4)-MPA/Hep	64.71
DHP(G2)-GMPA/Hep	28.53
DHP(G3)-GMPA/Hep	46.60
DHP(G4)-GMPA/Hep	253.60
*Commercial heparin	25.74

The circulation times of heparin when administered complexed by the DHPs, DHP/Hep, (Figure 5.18) follow similar descending profiles that the profile of the free heparin (curve not shown). In most cases, the amount of heparin in plasma was detectable up to 75-100 min after the intraperitoneal administration, whereas it became undetectable or not following any clear trend from this time point. It may indicate a rapid clearance from blood, possibly related with common interactions with components of the plasma.

The $t_{1/2}$ values extracted from the fitted curves reveal an increase on the circulating time of the heparin when forming complexes with the DHPs (Table 5.4), however, the abnormal quantification of heparin at long times is thought to be the mayor cause for these huge increments on the $t_{1/2}$ observed. In conclusion, this preliminary study has allowed to stablish the experimental conditions for the heparin quantification of different heparin-containing formulations in mice plasma and at least, the half-life of heparin in circulation has been shown not to decrease. However, further research would be required to refine and corroborate these results.

5.5. General remarks

Summary

The ability of pseudodendrimers consisting of a hyperbranched core of *bis*-MPA of different generations bearing either *bis*-MPA or *bis*-GMPA dendrons to complex the polysaccharide heparin has been demonstrated and characterised. After evaluating the cytotoxic effect of these pseudodendrimers in human endothelial cells, the anti-*Plasmodium* activity of the complexes has been assayed *in vitro.* Additionally, their preferential targeting towards infected or non infected RBCs has been tested and finally, the circulation time of heparin when administered within the complexes has been determined in mice.

Conclusions

All the pseudodendrimers studied have demonstrated a good heparin complexation at ratios ranging from 4/1 to 7.5/1 in weight ($w_{DHP}/w_{heparin}$) for DHPs, and at higher ratios (4/1–20/1) for DHPs labelled with Rh, maybe due to steric hindrance in presence of Rh on the surface of the DHPs. Moreover, the heparin release study points out at a stronger interaction of heparin with DHP(G4)-GMPA compared to DHP(G4)-MPA, which may be due to the enhanced interaction possibilities offered by the amide groups in the *bis*-GMPA dendron.

On the other hand, the biocompatibility of the pseudodendrimers in human endothelial cells has been verified. In addition, the anti-*Plasmodium* activity of the free heparin is mostly maintained or enhanced within some of these formulations. The preferential targeting of the dendritic structures with and without heparin towards infected RBCs has been demonstrated by flow cytometry. A significant enhancement of these addressing is observed in the DHPs of the *bis*-MPA series when heparin is complexed. Lastly, the circulation time of the complexed heparin within the series of DHPs has been evaluated in a preliminary study *in vivo*, revealing promising results in terms of not decreasing the half-life in blood of free administered heparin. Regarding the *in vivo* results (section 5.4.1) and the anti-*Plasmodium* activity obtained in the GIAs experiments *in vitro* (section 5.3.2), we adventure to postulate DHP(G4)-MPA/Hep and DHP(G2)-GMPA/Hep, with IC_{50}

values of 4.32 and 5.11 μg/mL, respectively, as the most promising formulations for further *in vivo* experiments.

Future perspectives

It would be interesting to study the activity of the complexes in cultures synchronised in late stages of the parasite in the intraerythrocytic form, since it is known that heparin has more targeting towards trophozoites and mostly, towards schizonts.

Regarding the results obtained from the *in vivo* study, it should be advisable to repeat the circulation time determination of heparin administered free and complexed within the two most promising DHPs, DHP(G4)-MPA and DHP(G2)-GMPA. In addition, further *in vivo* experiments could be carried out in order to determine the anti-*Plasmodium* activity of the selected formulations in an *in vivo* model. For that purpose, mice must be previously infected with the appropriate species of the parasite, *P. yoelii* or *P. berghei*, then, the testing formulations are injected and finally, blood extractions allow to monitor the evolution of the provoked disease by analysing the percentage of pRBCs in blood.

On the other hand, the anticoagulant activity of the heparin complexed by the DHPs should be assessed. Moreover, the complexes obtained between heparin and DHPs could be loaded with other antimalarial drugs in order to enhance its activity within the nanocarriers, taking advantage of their targeting abilities.

5.6. References

(1) World Malaria Report **2020**: 20 Years of Global Progress and Challenges. 299.

(2) Carter, R.; Mendis, K. N. Evolutionary and Historical Aspects of the Burden of Malaria. *Clin Microbiol Rev* **2002**, *15* (4), 564–594. https://doi.org/10.1128/CMR.15.4.564-594.2002.

(3) Neves Borgheti-Cardoso, L.; San Anselmo, M.; Lantero, E.; Lancelot, A.; Serrano, J. L.; Hernández-Ainsa, S.; Fernàndez-Busquets, X.; Sierra, T. Promising Nanomaterials in the Fight against Malaria. *J. Mater. Chem. B* **2020**, 10.1039.D0TB01398F. https://doi.org/10.1039/D0TB01398F.

(4) Malaria Parasite, Mosquito, and Human Host | NIH: National Institute of Allergy and Infectious Diseases https://www.niaid.nih.gov/diseases-conditions/malaria-parasite (accessed Mar 24, 2021).

(5) Barik, T. K.; Kamaraju, R.; Gowswami, A. Silica Nanoparticle: A Potential New Insecticide for Mosquito Vector Control. *Parasitol. Res.* **2012**, *111* (3), 1075–1083. https://doi.org/10.1007/s00436-012-2934-6.

(6) Benelli, G.; Govindarajan, M.; Kadaikunnan, S.; Alharbi, N. S. What Kind of Reducing Botanical? High Mosquitocidal Efficacy of a Silver Nanocomposite Synthesized Using a Leaf Aqueous Extract of Fumaria Indica. *J Clust Sci* **2017**, *28* (1), 637–643. https://doi.org/10.1007/s10876-017-1159-3.

(7) Benelli, G.; Maggi, F.; Pavela, R.; Murugan, K.; Govindarajan, M.; Vaseeharan, B.; Petrelli, R.; Cappellacci, L.; Kumar, S.; Hofer, A.; Youssefi, M. R.; Alarfaj, A. A.; Hwang, J.-S.; Higuchi, A. Mosquito Control with Green Nanopesticides: Towards the One Health Approach? A Review of Non-Target Effects. *Environ Sci Pollut Res* **2018**, *25* (11), 10184–10206. https://doi.org/10.1007/s11356-017-9752-4.

(8) Ahluwalia, J.; Brooks, S. K.; Weinman, J.; Rubin, G. J. A Systematic Review of Factors Affecting Adherence to Malaria Chemoprophylaxis amongst Travellers from Non-Endemic Countries. *Malaria Journal* **2020**, *19* (1), 16. https://doi.org/10.1186/s12936-020-3104-4.

(9) Cockburn, I. A.; Seder, R. A. Malaria Prevention: From Immunological Concepts to Effective Vaccines and Protective Antibodies. *Nature Immunology* **2018**, *19* (11), 1199–1211. https://doi.org/10.1038/s41590-018-0228-6.

(10) Tse, E. G.; Korsik, M.; Todd, M. H. The Past, Present and Future of Anti-Malarial Medicines. *Malaria Journal* **2019**, *18* (1), 93. https://doi.org/10.1186/s12936-019-2724-z.

(11) Ashley, E. A.; Phyo, A. P. Drugs in Development for Malaria. *Drugs* **2018**, *78* (9), 861–879. https://doi.org/10.1007/s40265-018-0911-9.

(12) Wells, T. N. C.; van Huijsduijnen, R. H.; Van Voorhis, W. C. Malaria Medicines: A Glass Half Full? *Nature Reviews Drug Discovery* **2015**, *14* (6), 424–442. https://doi.org/10.1038/nrd4573.

(13) Barabadi, H.; Alizadeh, Z.; Rahimi, M. T.; Barac, A.; Maraolo, A. E.; Robertson, L. J.; Masjedi, A.; Shahrivar, F.; Ahmadpour, E. Nanobiotechnology as an Emerging Approach to Combat Malaria: A Systematic Review. *Nanomedicine: Nanotechnology, Biology and Medicine* **2019**, *18*, 221–233. https://doi.org/10.1016/j.nano.2019.02.017.

(14) Mvango, S.; Matshe, W. M. R.; Balogun, A. O.; Pilcher, L. A.; Balogun, M. O. Nanomedicines for Malaria Chemotherapy: Encapsulation vs. Polymer Therapeutics. *Pharm Res* **2018**, *35* (12), 237. https://doi.org/10.1007/s11095-018-2517-z.

(15) Rai, M.; Ingle, A. P.; Paralikar, P.; Gupta, I.; Medici, S.; Santos, C. A. Recent Advances in Use of Silver Nanoparticles as Antimalarial Agents. *International Journal of Pharmaceutics* **2017**, *526* (1), 254–270. https://doi.org/10.1016/j.ijpharm.2017.04.042.

(16) Thakkar, M.; S., B. Combating Malaria with Nanotechnology-Based Targeted and Combinatorial Drug Delivery Strategies. *Drug Deliv. and Transl. Res.* **2016**, *6* (4), 414–425. https://doi.org/10.1007/s13346-016-0290-2.

(17) Amolegbe, S. A.; Hirano, Y.; Adebayo, J. O.; Ademowo, O. G.; Balogun, E. A.; Obaleye, J. A.; Krettli, A. U.; Yu, C.; Hayami, S. Mesoporous Silica Nanocarriers Encapsulated Antimalarials with High Therapeutic Performance. *Scientific Reports* **2018**, *8* (1), 3078. https://doi.org/10.1038/s41598-018-21351-8.

(18) Martí Coma-Cros, E.; Biosca, A.; Marques, J.; Carol, L.; Urbán, P.; Berenguer, D.; Riera, M. C.; Delves, M.; Sinden, R. E.; Valle-Delgado, J. J.; Spanos, L.; Siden-Kiamos, I.; Pérez, P.; Paaijmans, K.; Rottmann, M.; Manfredi, A.; Ferruti, P.; Ranucci, E.; Fernàndez-Busquets, X. Polyamidoamine Nanoparticles for the Oral Administration of Antimalarial Drugs. *Pharmaceutics* **2018**, *10* (4), 225. https://doi.org/10.3390/pharmaceutics10040225.

(19) Mhlwatika, Z.; Aderibigbe, B. A. Polymeric Nanocarriers for the Delivery of Antimalarials. *Molecules* **2018**, *23* (10), 2527. https://doi.org/10.3390/molecules23102527.

(20) Velasques, K.; Maciel, T. R.; de Castro Dal Forno, A. H.; Teixeira, F. E. G.; da Fonseca, A. L.; Varotti, F. de P.; Fajardo, A. R.; Ávila, D. S. de; Haas, S. E. Co-Nanoencapsulation of Antimalarial Drugs Increases Their in Vitro Efficacy against Plasmodium Falciparum and Decreases Their Toxicity to Caenorhabditis Elegans. *European Journal of Pharmaceutical Sciences* **2018**, *118*, 1–12. https://doi.org/10.1016/j.ejps.2018.03.014.

(21) Alven, S.; Aderibigbe, B. A.; Balogun, M. O.; Matshe, W. M. R.; Ray, S. S. Polymer-Drug Conjugates Containing Antimalarial Drugs and Antibiotics. *Journal of Drug Delivery Science and Technology* **2019**, *53*, 101171. https://doi.org/10.1016/j.jddst.2019.101171.

(22) Jawahar, N.; Baruah, U. K.; Singh, V. Co-Delivery of Chloroquine Phosphate and Azithromycin Nanoparticles to Overcome Drug Resistance in Malaria through Intracellular Targeting; **2019**.

(23) Martí Coma-Cros, E.; Lancelot, A.; San Anselmo, M.; Neves Borgheti-Cardoso, L.; Valle-Delgado, J. J.; Serrano, J. L.; Fernàndez-Busquets, X.; Sierra, T. Micelle Carriers Based on Dendritic Macromolecules Containing

Bis-MPA and Glycine for Antimalarial Drug Delivery. *Biomater. Sci.* **2019**, *7* (4), 1661–1674. https://doi.org/10.1039/C8BM01600C.
(24) Boyle, M. J.; Richards, J. S.; Gilson, P. R.; Chai, W.; Beeson, J. G. Interactions with Heparin-like Molecules during Erythrocyte Invasion by Plasmodium Falciparum Merozoites. *Blood* **2010**, *115* (22), 4559–4568. https://doi.org/10.1182/blood-2009-09-243725.
(25) Marques, J.; Moles, E.; Urbán, P.; Prohens, R.; Busquets, M. A.; Sevrin, C.; Grandfils, C.; Fernàndez-Busquets, X. Application of Heparin as a Dual Agent with Antimalarial and Liposome Targeting Activities toward Plasmodium-Infected Red Blood Cells. *Nanomedicine: Nanotechnology, Biology and Medicine* **2014**, *10* (8), 1719–1728. https://doi.org/10.1016/j.nano.2014.06.002.
(26) Smitskamp, H.; Wolthuis, F. H. New Concepts in Treatment of Malignant Tertian Malaria with Cerebral Involvement. **1971**, 3.
(27) Muñir, M.; Tjandra, H.; Rampengan, T. H.; Mustadjab, I.; Wulur, F. H. Heparin in the treatment of cerebral malaria. *Paediatrica Indonesiana* **1980**, *20* (1/2), 47–50.
(28) World Health Organization Malaria Action Programme. Severe and Complicated Malaria. *Transactions of The Royal Society of Tropical Medicine and Hygiene* **1986**, *80*.
(29) Leitgeb, A. M.; Blomqvist, K.; Cho-Ngwa, F.; Samje, M.; Nde, P.; Titanji, V.; Wahlgren, M. Low Anticoagulant Heparin Disrupts Plasmodium Falciparum Rosettes in Fresh Clinical Isolates. *The American Journal of Tropical Medicine and Hygiene* **2011**, *84* (3), 390–396. https://doi.org/10.4269/ajtmh.2011.10-0256.
(30) Fernàndez-Busquets, X. Heparin-Functionalized Nanocapsules: Enabling Targeted Delivery of Antimalarial Drugs. *Future Medicinal Chemistry* **2013**, *5* (7), 737–739. https://doi.org/10.4155/fmc.13.53.
(31) Fernàndez-Busquets, X. Novel Strategies for Plasmodium-Targeted Drug Delivery. *Expert Opinion on Drug Delivery* **2016**, *13* (7), 919–922. https://doi.org/10.1517/17425247.2016.1167038.
(32) Lantero, E.; Fernandes, J.; Aláez-Versón, C. R.; Gomes, J.; Silveira, H.; Nogueira, F.; Fernàndez-Busquets, X. Heparin Administered to Anopheles in Membrane Feeding Assays Blocks Plasmodium Development in the Mosquito. *Biomolecules* **2020**, *10* (8), 1136. https://doi.org/10.3390/biom10081136.
(33) Urbán, P.; Ranucci, E.; Fernàndez-Busquets, X. Polyamidoamine Nanoparticles as Nanocarriers for the Drug Delivery to Malaria Parasite Stages in the Mosquito Vector. *Nanomedicine* **2015**, *10* (22), 3401–3414. https://doi.org/10.2217/nnm.15.174.
(34) Lantero, E.; Aláez-Versón, C. R.; Romero, P.; Sierra, T.; Fernàndez-Busquets, X. Repurposing Heparin as Antimalarial: Evaluation of Multiple Modifications Toward In Vivo Application. *Pharmaceutics* **2020**, *12* (9), 825. https://doi.org/10.3390/pharmaceutics12090825.
(35) Movellan, J.; Urbán, P.; Moles, E.; de la Fuente, J. M.; Sierra, T.; Serrano, J. L.; Fernàndez-Busquets, X. Amphiphilic Dendritic Derivatives as

Nanocarriers for the Targeted Delivery of Antimalarial Drugs. *Biomaterials* **2014**, *35* (27), 7940–7950. https://doi.org/10.1016/j.biomaterials.2014.05.061.

(36) Lancelot, A. New Dendritic Derivatives for Applications in Nanomedicine: Drug Delivery and Gene Transfection, Universidad de Zaragoza, **2017**.

(37) Rodrigo, A. C.; Barnard, A.; Cooper, J.; Smith, D. K. Self-Assembling Ligands for Multivalent Nanoscale Heparin Binding. *Angewandte Chemie International Edition* **2011**, *50* (20), 4675–4679. https://doi.org/10.1002/anie.201100019.

(38) Al-Jamal, K. T.; Al-Jamal, W. T.; Kostarelos, K.; Turton, J. A.; Florence, A. T. Anti-Angiogenic Poly-L-Lysine Dendrimer Binds Heparin and Neutralizes Its Activity. *Results Pharma Sci* **2012**, *2*, 9–15. https://doi.org/10.1016/j.rinphs.2011.12.002.

(39) Lambros, C.; Vanderberg, J. P. Synchronization of Plasmodium Falciparum Erythrocytic Stages in Culture. *The Journal of Parasitology* **1979**, *65* (3), 418–420. https://doi.org/10.2307/3280287.

(40) Dluzewski, A. R.; Ling, I. T.; Rangachari, K.; Bates, P. A.; Wilson, R. J. M. A Simple Method for Isolating Viable Mature Parasites of Plasmodium Falciparum from Cultures. *Transactions of The Royal Society of Tropical Medicine and Hygiene* **1984**, *78* (5), 622–624. https://doi.org/10.1016/0035-9203(84)90221-9.

(41) Tanabe, K. Inhibitory Effect of Rhodamine 123 on the Growth of the Rodent Malaria Parasite, *Plasmodium Yoelii* 1. *The Journal of Protozoology* **1984**, *31* (2), 310–313. https://doi.org/10.1111/j.1550-7408.1984.tb02968.x.

(42) Wadi, I.; Singh, P.; Nath, M.; Anvikar, A. R.; Sinha, A. Malaria Transmission-Blocking Drugs: Implications and Future Perspectives. *Future Medicinal Chemistry* **2020**, fmc-2020-0026. https://doi.org/10.4155/fmc-2020-0026.

(43) Lee, K. H.; Lee, D. W.; Kang, B. C. The 'R' Principles in Laboratory Animal Experiments. *Lab Anim Res* **2020**, *36* (1), 45. https://doi.org/10.1186/s42826-020-00078-6.

(44) Euthanasia https://www.research.psu.edu/animalresourceprogram/euthanasia (accessed Mar 22, 2021).

(45) Warttinger, U.; Giese, C.; Harenberg, J.; Holmer, E.; Krämer, R. A Fluorescent Probe Assay (Heparin Red) for Direct Detection of Heparins in Human Plasma. *Anal Bioanal Chem* **2016**, *408* (28), 8241–8251. https://doi.org/10.1007/s00216-016-9940-y.

Chapter 6:

Pseudodendrimers as vectors for gene transfection

6.1. Gene transfection

6.1.1. Introduction

Gene therapy is a promising approach in biomedical research to treat some diseases by the insertion of genetic information into cells[1]. The earliest experiments of Griffith in 1928 evidenced for the first time the transfer of genetic material in *Streptococcus pneumoniae* and laid the foundation for this promising field based on genetic transfer[2]. This technology has evolved thanks to the progress made in the genetic material understanding, the improvements in its manipulation and the development of diverse methods to mediate the process. The first protocol of gene transfer without therapeutic purpose approved in human dates from 1988 and it was only two years later when the first gene therapy trial to overcome an enzymatic deficiency was approved by the FDA[3,4]. Since that historic event, gene therapy has gained importance in the treatment of several disorders including various types of cancer, monogenic, cardiovascular or infectious diseases among others[5]. A very latest example of this technology can be found in the emergent vaccines against COVID-19 pandemic that focus on the delivery of different constructs of genetic material that encode for the virulent protein spike to fight the disease; a pioneer strategy in licensed vaccines to date[6].

The development of ingenious methodologies to deliver genetic material inside the cells of interest has considerably improved the efficacy of the gene therapy-based treatments. Physical methods as electroporation, ultrasound, hydrodynamic, needle injection or the gene gun immunisation are included among the various approaches studied mostly for *ex vivo* applications[7,8], whereas for *in vitro* and *in vivo* purposes the biggest attention is focused on chemical-based vectors for gene delivery since they protect nucleic acids from degradation and define complexes suitable for cell internalisation[9].

The first vectors employed in gene therapy were based on adenoviruses and afterwards, a wide range of viral vectors have been explored as genetic vehicles, namely adeno-associated viruses (AAV), alphaviruses, flaviviruses, herpes simplex viruses (HSV), measles viruses, rhabdoviruses, retroviruses, lentiviruses (LV), Newcastle disease virus (NDV), poxviruses or picornaviruses[10]. The initial

safety drawbacks concerning viral vectors have been mostly overcome thanks to the progress made in vector engineering, what allowed the approval of the first gene therapy treatment in 2017, i.e. Luxturna, based on the AAV delivery method to treat a retinal dystrophy[11]. However, there are still some issues to take into account related with the immune response provoked by the viral-based vectors in the host tissues[12], its safety and some manufacturing limits[9].

Non-viral vectors constitute an alternative to mediate the gene delivery overcoming those undesired aspects although their transfection efficiency can be compromised due to the endocytosis process by which they enter living cells[13]. Among them, two main chemical structures can be found: lipids and polymers, with the corresponding formation of lipoplexes or polyplexes when electrostatically interacting with the nucleic acid. These cationic vectors exhibit versatility in the type and size of genetic material complexed and in the attachment of specific targeting ligands[14]. Some cationic polymers studied as non-viral gene delivery systems include polyamines as poly(ethylenimine) (PEI) derivatives, polyesters like poly-DL-lactide (PLA), polysaccharides as chitosan or pectin, polypeptides as poly-*L*-lysine (PLL) or the structurally controlled dendrimers[13–15]. The low polydispersity exhibited by dendrimers and the possibility to functionalise them with diverse ligands on the surface[16] postulate them as promising candidates for gene therapy[17]. Some recent successful examples of gene transfection include dendrimers based on poly(amidoamine) (PAMAM)[18], poly(propylene imine) (PPI)[19], polyesters (2,2´-*bis*(hydroxymethyl)propionic acid or *bis*-MPA)[20] and polyesteramides (2,2´-*bis*(glycyloxymethyl)propionic acid or *bis*-GMPA)[21], carbosilane[22,23], ornithine[24], guanidinylated[25], phosphorous[26,27] or triazine[28] containing dendrimers.

6.1.2. Previous work and working plan

Previous works in our group have explored the ability of different globular dendritic materials as vectors for gene transfer. In the first study reported, ionic dendrimers derived either from *bis*-MPA or PAMAM were designed[29]. In both cases, hydrophilic chains of 2-[2-(2-methoxyethoxy)ethoxy]acetic acid were added as counterions to increase the solubility and biocompatibility of the

compounds. Specifically, the *bis*-MPA derivative consists of four dendrons of *bis*-MPA of the 2nd generation attached to a tetrafunctional core derived from pentaerythritol, functionalised with an acid chain in each of the amino terminal groups (Figure 6.1a). The PAMAM derivatives were of the 2nd and 5th generation, and two ionic derivatives were prepared for each generation. That is, derivatives of PAMAM with only the external amino groups functionalised with acid chains were prepared (Figure 6.1b) and also derivatives with both, external and internal amino groups functionalised with the acid moieties (Figure 6.1c).

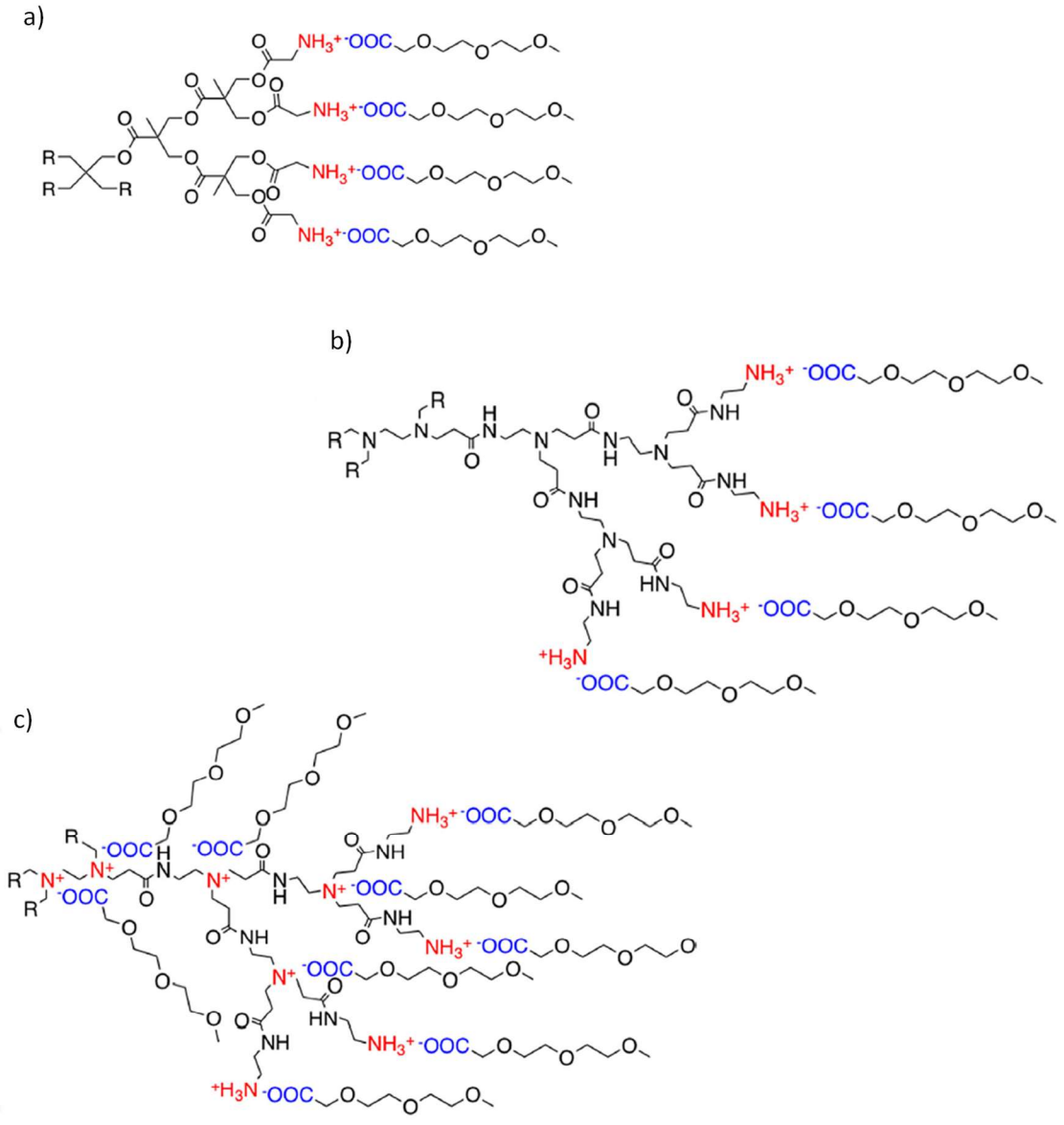

Figure 6.1. Dendritic ionic structures functionalised with 2-[2-(2-methoxyethoxy)ethoxy]acetic acid moieties. a) bis-MPA derivative, b) PAMAM of 2nd generation with external amines functionalised, and c) PAMAM of 2nd generation with both, external and internal amines functionalised. R: repetition of the drawn part of the molecule.

Although all the ionic structures tested were able to complex a plasmid DNA (pDNA), PAMAM derivatives were discarded due to their high cytotoxicity levels. The ionic *bis*-MPA dendrimer exhibited a lower complexation ability, but its high biocompatibility postulated it as a promising vector for gene transfer.

In a further study, globular structures based on *bis*-MPA were proposed due to the good biocompatibility results obtained with this polyester architecture and the high complexation abilities of the globular PAMAM previously studied. Specifically, the three DHPs also cited in chapter 5 for the encapsulation of antimalarial drugs were proposed, based on a hyperbranched core of *bis*-MPA of different generations (G2, G3 or G4) surrounded by *bis*-MPA dendrons of the 3rd generation[20] (Figure 6.2).

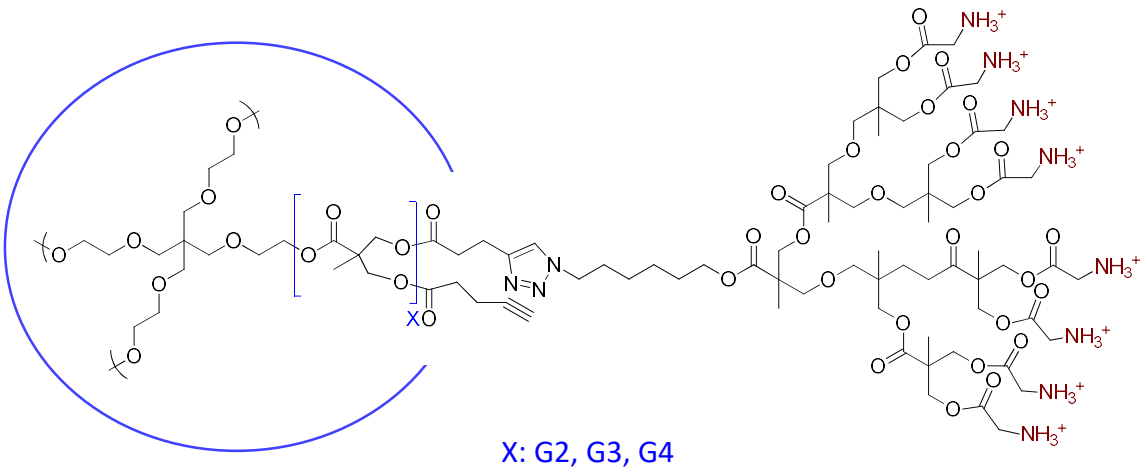

Figure 6.2. Hyperbranched bis-MPA structures previously used in our group for plasmid DNA transfection.

These pseudodendritic structures were found to be efficient vectors for gene transfection and the number of terminal cationic moieties was found to be relevant[20]. In the latest study regarding gene transfection within our group, globular tripodal dendrimers were designed[21]. Briefly, these cationic structures consisted of a tripropargylamine core decorated with *bis*-GMPA dendrons of the

3rd or 4th generation (Figure 6.3). The inclusion of the *bis*-GMPA architecture was thought to increase the interactions with the genetic material by the possibility to stablish H-bonding interactions through the inner amide groups, while a high number of cationic groups was maintained (24 and 48, respectively). These dendritic structures have been also cited in section 3.1.2. (previous work) in chapter 3 for the encapsulation of the anti-HCV drug CPT[21]. Regarding their application as gene vectors, the dendrimer with more cationic groups showed good abilities to complex pDNA and small interference RNA (siRNA), while the smallest dendrimer just complexed pDNA and at higher ratios. However, a limited cellular internalisation led to poor transfection efficiencies in the case of the complexes with pDNA, and only positive transfection levels were obtained for the complexes with siRNA[21].

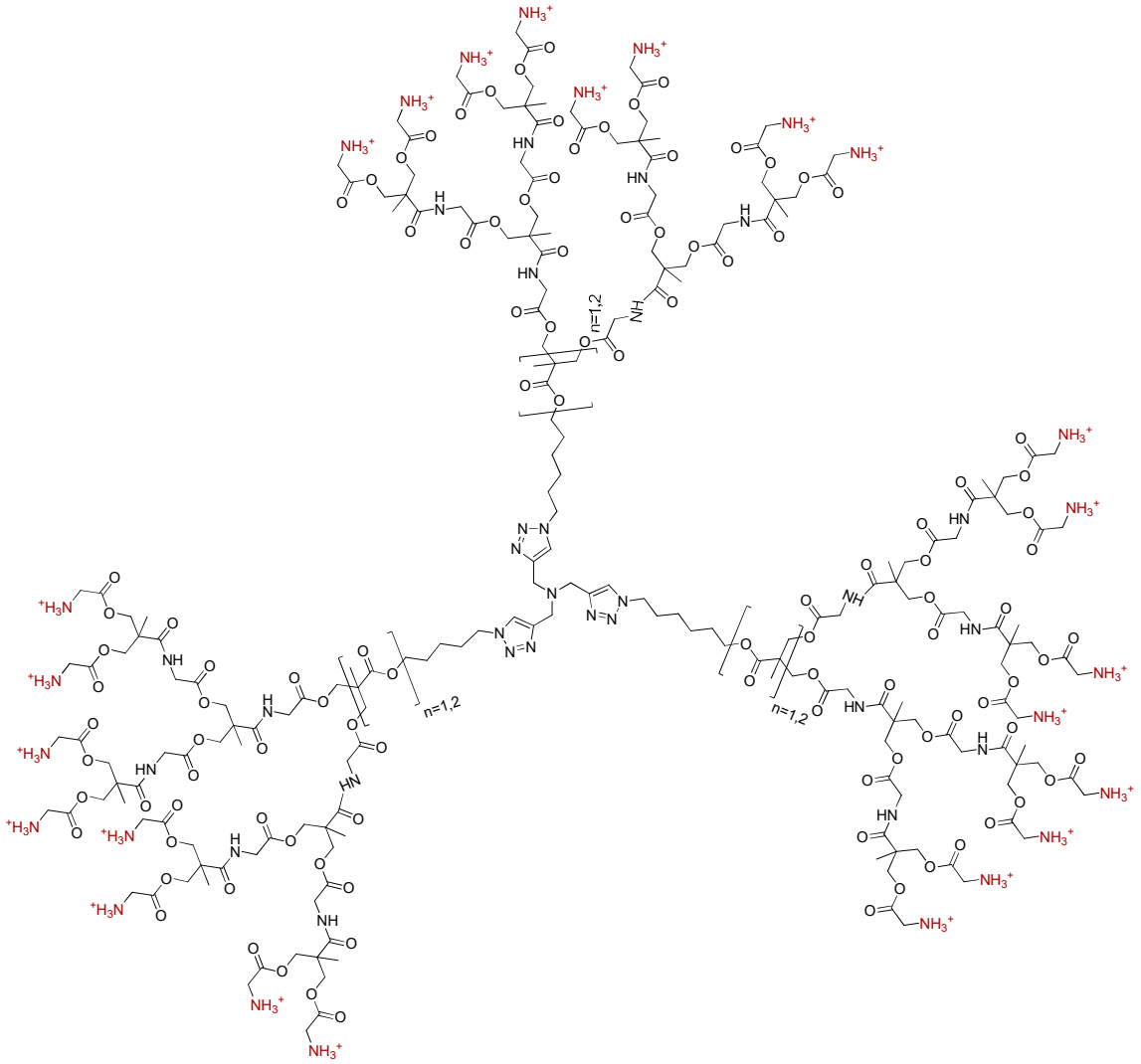

Figure 6.3. Tripodal polycationic dendrimers with bis-GMPA dendrons previously used for gene transfection.

All these results indicate that a high biocompatibility and a terminal polycationic composition are required to effectively complex the anionic nucleic acids[30]. In addition, the *bis*-GMPA architecture has been barely studied and their possibilities to reinforce the interactions with the nucleic acids seems to be interesting. For these reasons, the series of novel pseudodendrimers described in chapter 2 is here proposed as efficient non-viral vectors for gene transfection. Namely, the *bis*-MPA series: DHP(G2)-MPA, DHP(G3)-MPA and DHP(G4)-MPA and, on the other hand, the *bis*-GMPA series: DHP(G2)-GMPA, DHP(G3)-GMPA and DHP(G4)-GMPA. The elevated number of polycationic terminal groups (ca. 64, 128 or 256 for the different generations) makes them suitable to complex nucleic acids, while their chemical composition allows good biocompatibility levels. In addition, the two series with either dendrons of *bis*-MPA or *bis*-GMPA in the periphery was thought to make a comparative study and elucidate whether the substitution of the *bis*-MPA dendrons by the *bis*-GMPA ones improves the transfection efficiency of the resulting DHPs.

To evaluate their gene transfection abilities, two different types of genetic material were employed in order to express (pDNA) or silence the expression (siRNA) of a specific protein as a proof of concept. Namely, the green fluorescent protein (GFP) was selected as reporter and then, the pDNA is hereinafter named as pGFP and the siRNA is referred as siGFP. In the following sections, the studies concerning the application of the DHPs as vectors for gene transfection are presented. Firstly, the buffering ability of the DHPs was evaluated according to some endosomal scape theories. Then, the formation of complexes between the DHPs and the nucleic acids (i.e., dendriplexes) was determined by gel retardation assays and the resulting dendriplexes were characterised by DLS, ζ potential and AFM. After that, the transfection efficiency of the DHPs as gene vectors was assessed in both tumoral and mesenchymal stem cells, while the effect of the formulations on the cellular viability was also determined. Finally, the internalisation of the complexes was assessed by confocal imaging.

6.2. Buffering ability of the DHPs

Thinking about the application of the polycationic DHPs as gene transfer vectors, a limiting step in the effective delivery of genetic material inside the cell is its successful scape from the endosomes to the cytosol after their entrance by endocytosis to avoid their degradation in lysosomes. One possible mechanism of endosomal scape consists on the proton sponge effect[31,32], in which an agent with buffering and flexibility to swell capacities is required. According to this hypothesis, the low pH in the endosomal environment induces the protonation of these entrapped agents, which leads to the massive inflow of ions and water. Finally, the endosome membrane is disrupted through osmotic swelling and its content is released into the cytosolic space[33].

Aiming to study the buffering capacity of the DHPs, a pH titration assay was developed, revealing a mild buffering ability for all DHPs at physiological pH compared to the NaCl solution. However, an interesting slight increase of that effect was observed at acidic conditions below pH 6 (Figure 6.4). Commercial PAMAM of the 5th generation, PAMAM(G5), was chosen as positive buffering control since its number of terminal amine groups, 128, is the average of those in the studied DHPs. No relevant differences in the buffering ability were found among the different generations of DHPs neither between the *bis*-MPA and the *bis*-GMPA pseudodendrimer series, thus indicating that the total number of amino-terminal groups or the inner amides do not interfere in this protonation process. As it has been reported, the introduction of secondary and mostly tertiary amines in the chemical structure, as in the case of the positive control PAMAM[34], would help to achieve this buffering ability, although cytotoxic side effects must be also taken into consideration. Nevertheless, lots of studies have been developed to elucidate the endosomal scape mechanism to cytosol and the proton sponge is not the unique possible pathway[35]. Thus, this pH titration study can only suggest that once internalised by the cell, a similar endosomal scape to the intracellular space would be expected for all empty DHPs regarding the proton sponge theory. However, the dendriplexes formation between DHPs and nucleic acids will be later studied, and multiple factors can influence the complex

mechanisms by which the genetic material is finally delivered into the cell and develop its function.

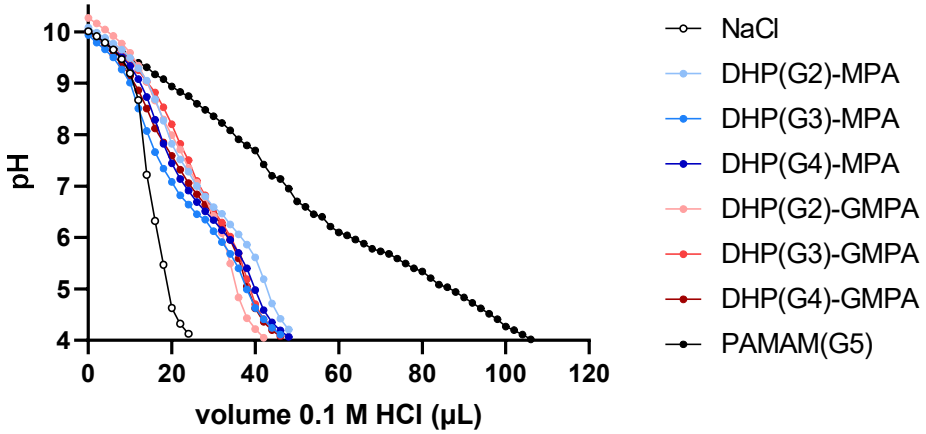

Figure 6.4. Buffering ability assay of the DHPs from pH 10 to 4, adjusting pH with 0.1 M HCl. Negative control: 0.1 M NaCl, positive control: PAMAM(G5).

6.3. Dendriplexes formation and characterisation

The pGFP employed was the pAcGFP1-N1 vector (Clontech) of 4.7 kb, which encodes a GFP from Aequorea coerulescens ($\lambda_{ex/em}$: 475/505 nm). Among its characteristics, this vector contains a multiple cloning site that allows gene fusions to the AcGFP1 gene at the N-terminus, yielding a fusion protein that maintains the fluorescent properties. Interestingly, this plasmid is suitable for the transfection into a wide range of mammalian cells and here, it has been used as a transfection marker in tumoral and pluripotent cell lines.

The siGFP selected to silence GFP in those lines expressing the protein was the GFP Duplex I (Horizon, Dharmacon). The genomic structure is formed by the hybridisation of two RNA strands of 22 nucleotides each, whose targeting sequence is 5'-GCA AGC UGA CCC UGA AGU UC-3'. This RNA was directly used after resuspension in the correspondent 1X siRNA buffer (Horizon, Dharmacon) up to 20 µM. Both nucleic acids were stored at -20 °C following commercial specifications.

Lipofectamine 3000 (Invitrogen) and Superfect (Quiagen) were employed as control transfection reagents of different chemical nature, being the first one a

commonly used lipidic transfectant whereas the second one is based on a dendritic globular structure more similar to the DHPs under evaluation.

Firstly, the formation of dendriplexes was studied by the agarose gel retardation assay and then, dendriplexes were characterised by a combination of techniques such as DLS, ζ potential or AFM.

6.3.1. Dendriplexes formation

Dendriplexes were freshly formed before each experiment. Pseudodendrimers and nucleic acids were softly mixed by pipetting in serum free DMEM medium (SFM) to avoid protein interferences during complex formation. Then, they were incubated during 20 minutes at RT. Different N/P ratios were assayed to stablish the minimum amount of dendritic material needed to complex a fixed amount of genetic material (0.2 μg of pGFP and 0.225 μg of siGFP). The number of N^+ terminal groups of each molecule of DHP and the P^- groups of the nucleic acids were considered in the N/P ratio determination.

Complexes between Lipofectamine 3000 or Superfect and nucleic acids were formed under the same experimental conditions, and the ratio in weight (w/w) was used to stablish their complexation abilities.

6.3.1.1. Gel retardation assay

The gel retardation assay based on the agarose electrophoresis mobility of the molecules allowed to identify the minimum N/P ratios at which the nucleic acids were totally complexed by the pseudodendrimers. The commercial transfectant reagents Lipofectamine 3000 (lipidic formulation) and Superfect (dendritic formulation) were used under supplier specifications and their w/w ratios for nucleic acid complexation were determined following the same procedure. As seen in Figure 6.5a, pGFP was totally complexed at N/P ratio 25 by all the DHPs studied, when no band of free pGFP was observed, although partial complexation could be observed from lower ratios specially for the biggest DHPs generation. Even though the majority of the siGFP was complexed by the pseudodendrimers

at N/P ratio 100, more markedly for G4-DHPs, the N/P complexation ratio was stablished at 150 in all cases to assure whole nucleic acid capture (Figure 6.5b). Higher ratios were tested for both nucleic acids without observing changes once the dendriplex was already formed (data not shown in Figure 6.5).

The complexation involving the commercial reagents also needed more amount of polycationic carrier in the case of siGFP (w/w ratio 7 for Lipofectamine and 3 for Superfect) than for pGFP (w/w ratios 1.5 and 2 for Lipofectamine and Superfect, respectively). These prominent differences between nucleic acids complexation ratios have been previously described to reside in the size and rigidity of each construct[36,37]. The pGFP employed is a bigger and more flexible molecule (it consists of 4700 base pairs versus the short duplex siGFP of 22 base pairs) able to form stable dendriplexes requiring less amount of positively charged material to be fully complexed. Considering that all pseudodendrimers have a similar number of N^+ per mass unit (between $1.5 \cdot 10^{18}$ and $1.8 \cdot 10^{18}$ N^+/mg), differences in the total number of peripheric amino groups have shown not to have a strong influence on the N/P ratio of dendriplexes formation for the range of pseudodendrimer generations studied. On the other hand, the presence of inner amido groups in the series of pseudodendrimers containing the *bis*-GMPA dendron (DHP(G2)-GMPA, DHP(G3)-GMPA and DHP(G4)-GMPA) seems not to affect the amount of pseudodendrimer required to form the complexes compared to the *bis*-MPA pseudodendrimer series (DHP(G2)-MPA, DHP(G3)-MPA and DHP(G4)-MPA). A slight difference is only observed in G3-DHPs, since the DHP(G3)-GMPA starts the pGFP complexation at N/P ratio 1 whereas its *bis*-MPA homologous needs to increase N/P ratio to 5 to modify the electrophoretic mobility of the nucleic acid (see Figure 6.5a).

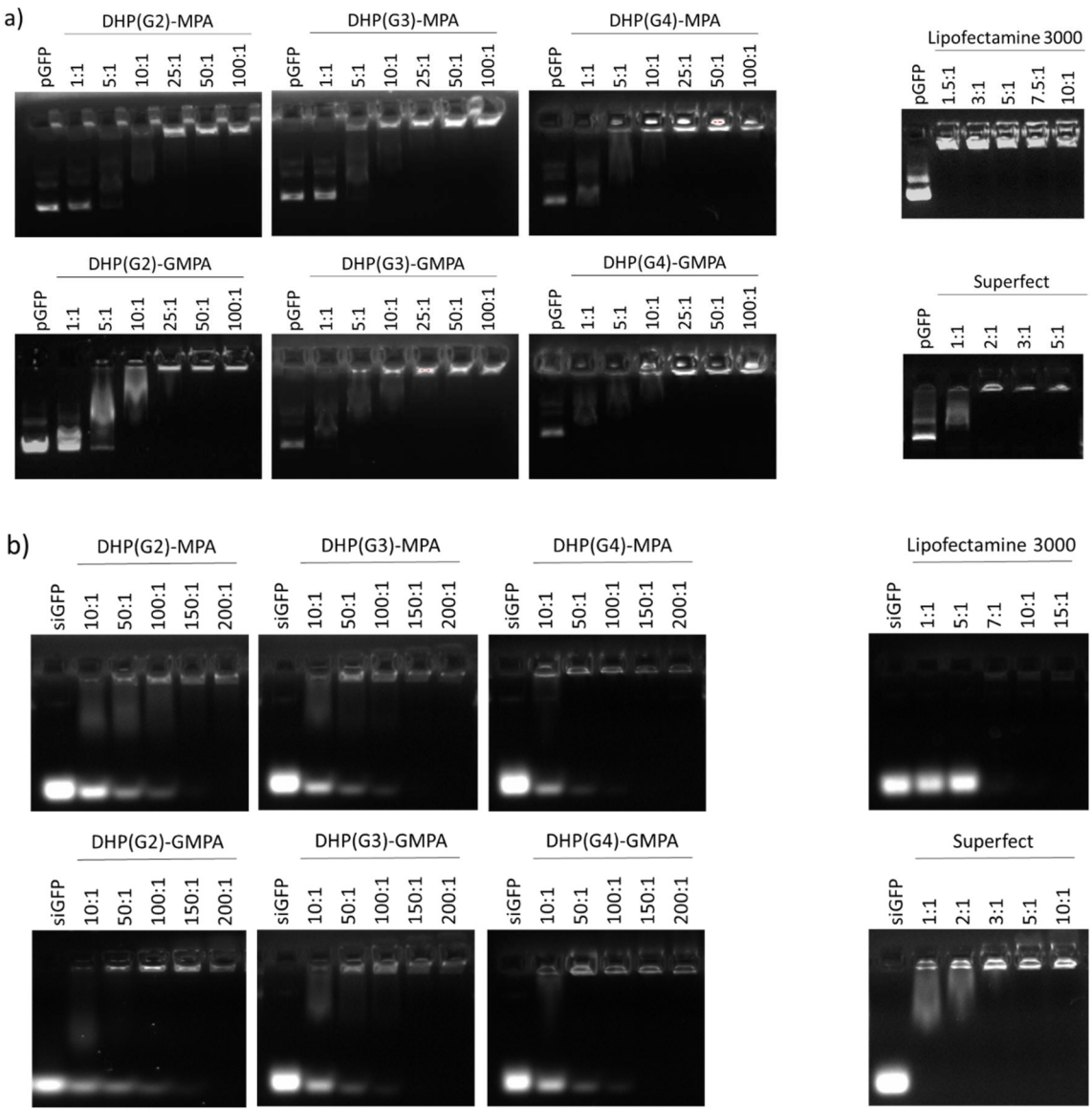

Figure 6.5. Complex formation between polycationic carriers and nucleic acids. a) Gel retardation of pGFP in presence of increasing amounts of pseudodendrimers or the commercial transfectants Lipofectamine 3000 and Superfect. b) Gel retardation of siGFP in presence of increasing amounts of pseudodendrimers or the commercial reagents.

6.3.2. Dendriplexes morphological characterisation

The morphological characterisation of the dendriplexes at different N/P ratios was carried out by different techniques: dynamic light scattering (DLS), ζ potential and atomic force microscopy (AFM). In all cases, complexes were formed by soft mixing and incubating 20 minutes at RT.

6.3.2.1. DLS and ζ potential

The hydrodynamic diameters (D_H) of the dendriplexes were determined by **DLS** measurements in a Malvern Instruments Nano ZS, with a 633 nm wavelength laser and a 173° angle detection. Dendriplexes were prepared in distilled water, fixing the concentrations of pGFP at 20 μg/mL and siGFP at 5.7 μg/mL. DHPs concentrations ranged from 0.5 to 11.3 mg/mL to stablish the N/P ratios 25 or 500 for pGFP, and 150 or 750 for siGFP, the ones at which the complexes are completely formed (see Figure 6.5) and the most effective ones in terms of transfection activity (data present in further sections). Disposable ZEN0040 cuvettes were employed and a series of three measurements of five runs each were performed for each sample. D_H, in nm, were obtained by the size distributions measured in intensity.

Sizes determined by DLS in intensity (Table 6.1) showed two populations of nanoparticles for the majority of dendriplexes involving pGFP, while only one population was observed for the siGFP dendriplexes. This may be related to the more flexibility exhibited by the plasmid DNA that allows more possibilities of conformation. The bigger population of dendriplexes with pGFP at the forming ratio (N/P 25) displayed sizes below 210 nm that predominated in abundance over the smaller population (around 30 nm), but it is important to consider that DLS in intensity tends to overestimate the population of particles with larger size in detriment to the smaller ones[38]. Comparing the diameters of the empty carriers in water with those at the N/P ratio at which the dendriplexes with pGFP start to be formed (N/P 25), the decrease in size suggests a compaction of the structures when adding pGFP. As expected, these diameters were incremented when the ratio N/P was raised to 500. siGFP dendriplexes experimented less size variations once the complexes were already formed, observing diameters around

250 nm for all dendriplexes at N/P ratio 150 and more compact structures around 200 nm at the highest ratio assayed (N/P 750).

Table 6.1. DLS of the dendriplexes with pGFP (N/P ratios 25 and 500) and siGFP (N/P ratios 150 and 750). The hydrodynamic diameters (D_H) were calculated in intensity and data are given as mean ± SD (in nm) and the percentage of each population is included in brackets if applicable.

		pGFP		siGFP	
Pseudodendrimers	Empty carriers	Dendriplexes N/P 25	Dendriplexes N/P 500	Dendriplexes N/P 150	Dendriplexes N/P 750
DHP(G2)-MPA	369 ± 19	197 ± 8 (91) 32 ± 4 (9)	349 ± 15 (92) 12 ± 2 (8)	236 ± 15	164 ± 6
DHP(G3)-MPA	295 ± 2	210 ± 18 (92) 29 ± 3 (8)	251 ± 5 (100)	269 ± 7	224 ± 16
DHP(G4)-MPA	388 ± 5 (62) 29 ± 1 (38)	166 ± 19 (85) 29 ± 8 (15)	271 ± 18 (72) 22 ± 3 (28)	259 ± 14	165 ± 10
DHP(G2)-GMPA	274 ± 5	183 ± 18 (89) 34 ± 12 (11)	248 ± 12 (82) 4 ± 1 (18)	253 ± 15	184 ± 7
DHP(G3)-GMPA	335 ± 36 (90) 18 ± 3 (10)	190 ± 40 (69) 42 ± 6 (31)	371 ± 14 (85) 43 ± 5 (15)	234 ± 13	171 ± 4
DHP(G4)-GMPA	265 ± 13 (76) 18 ± 4 (24)	128 ± 1 (88) 19 ± 2 (12)	243 ± 9 (78) 15 ± 1 (22)	251 ± 9	276 ± 15

ζ potential measurements were performed in a Malvern Instruments Nano ZS in PBS buffer pH 7.4. Samples were prepared with 1 μg/mL of pGFP and 0.3 μg/mL of siGFP, with DHPs ranging from 26.3 to 565 μg/mL to form the same N/P ratios described for DLS measurements. DTS1070 cuvettes were employed and three measurements of ten runs were developed for each sample.

The measurement of the ζ potential (Table 6.2) revealed that all the dendriplexes presented a positive surface charge, thus indicating that the nucleic acid had been completely complexed, as it was evidenced by gel retardation assays (see Figure 6.5). Besides, a general increase in the charge was observed when increasing the N/P ratio due to the presence of a higher number of molecules of

the positively charged pseudodendrimers. Regarding both DHPs series, dendriplexes with DHP-GMPA vectors presented lower ζ potential values than those with DHP-MPA of the same generation. This could be due to the location of the terminal amino groups of the DHP in a more internal cavity of the complex and it may be related to interactions with the inner amide groups of the *bis*-GMPA dendrons as the reason for this conformation. Anyway, all the dendriplexes studied exhibited suitable surfaces to favour their cellular uptake by electrostatic attraction with the negatively charged cellular membranes[39].

Table 6.2. ζ potential of the dendriplexes with pGFP (N/P ratios 25 and 500) and siGFP (N/P ratios 150 and 750). Results are expressed as the average in mV.

		pGFP		siGFP	
Pseudodendrimers	Empty carriers	Dendriplexes N/P 25	Dendriplexes N/P 500	Dendriplexes N/P 150	Dendriplexes N/P 750
DHP(G2)-MPA	6.8	3.7	6.5	8.1	12.1
DHP(G3)-MPA	5.9	4.6	12.3	12.8	13.5
DHP(G4)-MPA	6.1	5.5	13.1	11.2	10.6
DHP(G2)-GMPA	4.5	3.6	3.6	6.4	5.0
DHP(G3)-GMPA	4.3	2.5	8.5	9.3	6.0
DHP(G4)-GMPA	4.7	0.6	4.1	7.0	7.4

6.3.2.2. AFM

The formation of the dendriplexes between pGFP or siGFP and the biggest pseudodendrimer of the *bis*-MPA series, DHP(G4)-MPA, was further confirmed by AFM (Figure 6.6). As observed in DLS measurements, two sizes populations were found for the complexes involving pGFP. Namely, for DHP(G4)-MPA/pGFP dendriplexes at N/P ratio 25, some large aggregates around 200 nm in length were found, while a more abundant population of small, rounded structures ca. 20 nm was observed (Figure 6.6b). The images revealed by AFM for the dendriplexes with pGFP at N/P ratio 500 were similar to those at N/P ratio 25, although the small population was even more predominant in this case (Figure

6.6c). The discordance between the abundance of populations observed between DLS and AFM is commonly observed, since the DLS technique measured in intensity tends to overestimate the presence of the biggest population. However, the DLS in number reflects more accurately these AFM sizes, yielding D_H below 33±2 nm for all the dendriplexes with pGFP (data shown in annexe 5).

On the other hand, the siGFP dendriplexes at N/P ratio 150 (Figure 6.6d) yielded larger structures between 100-200 nm in AFM, with the presence of some clusters of dendriplexes as well that may explain the bigger sizes determined by DLS, i.e., 259±14 nm (see Table 6.1). These observations in AFM are in good agreement with the data determined by DLS.

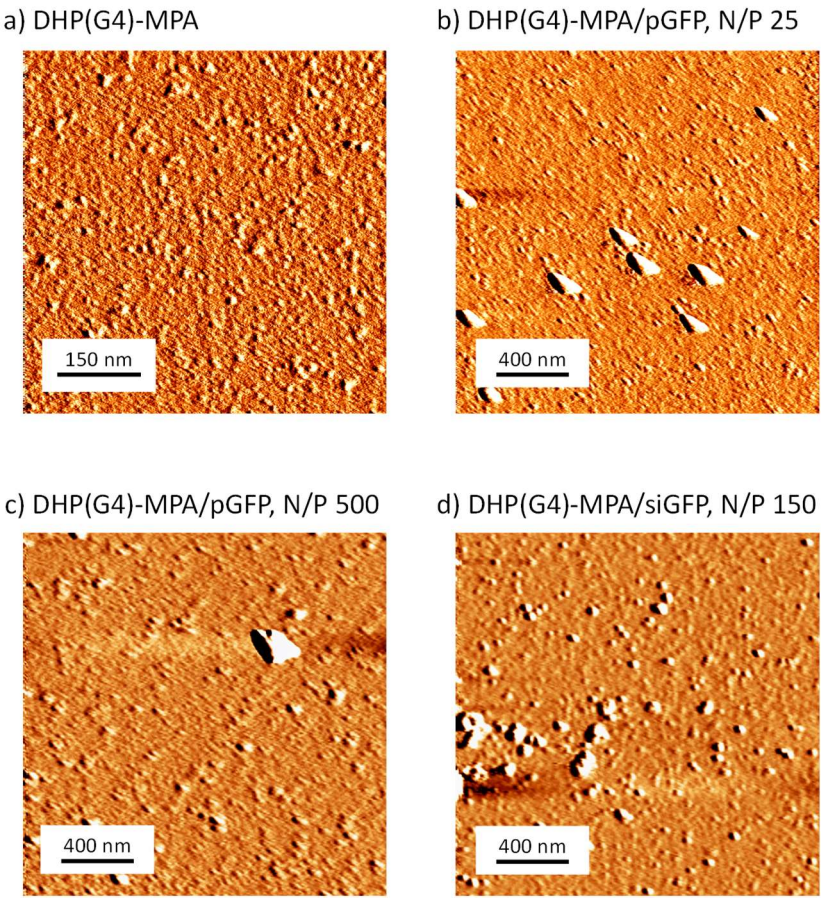

Figure 6.6. AFM topographic images of the DHP(G4)-MPA empty aggregates (a), and the dendriplexes formed with pGFP at N/P ratios 25 (b) and 500 (c), and dendriplexes with siGFP at N/P ratio 150 (d).

6.4. Transfection and viability experiments

Cell lines and culture

Human cervix cancer cell line HeLa and that transformed to intrinsically express the GFP protein, HeLa-GFP, were grown in DMEM (high glucose with *L*-glutamine) supplemented with 10% FBS, and 1% antibiotics (penicillin, streptomycin, amphotericin) at 37 °C and 5% CO_2 in a humidified atmosphere. Mesenchymal stem cells from mouse (mMSCs) and those stably expressing GFP, mMSCs-GFP, were maintained under the same experimental conditions with their specific MesenCult™ Expansion Medium for mouse (StemCell) supplemented with *L*-glutamine.

Transfection experiments

For pGFP transfection, HeLa or mMSCs cells were seeded at a density of $1 \cdot 10^4$ cells per well in 96 multiwell culture plates in their respective culture medium. After 24 h incubation at 37 °C, culture medium was removed and 50 µL of dendriplexes already formed in SFM as described above were added per well in triplicate. 0.2 µg of pGFP per well were added in all cases while the amount of dendrimer was adjusted to cover a wide range of N/P ratios (25, 50, 100, 250, 500). Complexes were incubated for 4, 8 or 24 h at 37 °C and then, compounds were replaced with 100 µL fresh medium. After 48 h incubation, GFP expression was evaluated by fluorescence microscopy (NIS-Elements, Nikon) and quantified by fluorimetric determination at 485/20 excitation, 516/20 emission wavelengths in a microplate reader (Synergy HT). Transfection experiments with siGFP were similarly performed into HeLa-GFP and mMSCs-GFP cell lines, stablishing 200 nM as the fixed concentration of siGFP per well. N/P ratios tested were 150, 300, 500 and 750. Finally, the GFP-expression decrease was determined following the same procedures. For positive controls, the commercial reagents Lipofectamine 3000 and Superfect were incubated with nucleic acids at the corresponding ratios previously stablished following the supplier recommendations. Naked nucleic acids were also tested at the same concentrations and no treated cells were included as negative controls for transfection experiments.

Viability experiments

The evaluation of the cytotoxic effect of the compounds was carried out by the Alamar Blue assay. Briefly, cells were seeded at a density of $1 \cdot 10^4$ cell per well in 96 multiwell culture plates and after 24 h of incubation at 37 °C, medium was replaced by 50 µL of the testing compounds dissolved in SFM per well, in triplicates. After 4, 8 or 24 h of incubation, the solutions were removed and 100 µL of fresh complete medium were added and incubated for another 48 h. After that, medium was replaced by a 10% (v/v) Alamar Blue dye solution in complete DMEM and allow to react for 2 h at 37 °C. Then, absorbance at 570 and 600 nm was read in a Multiskan GO (ThermoScientific) plate reader.

6.4.1. Optimisation of transfection conditions

Different parameters were initially optimised using DHP(G4)-MPA in order to find the appropriate conditions to perform a comparative study on the transfection ability of the different pseudodendrimers.

On the one hand, the effect of modifying the incubation time of the dendriplexes with cells was evaluated for the complexes between DHP(G4)-MPA and pGFP at the N/P ratio 500. Namely, 4, 8 or 24 h of incubation in HeLa were assayed and the results were evaluated in terms of fluorescence increase (transfection efficiency) and cell viability, comparing with the commercial reagent Lipofectamine 3000 (Figure 6.7a). The highest fluorescence levels (8.7 a.u.) were found after 8 h of incubation with the dendriplexes although the viability of the host cells was affected as a result, yielding 60% of viability. This cytotoxic effect was overcome after 24 h of incubation, when the transfection effectivity remained at high levels (7.3 a.u.) and the viability above 80%. We hypothesize that this extra-time may allow the culture to recover after the pGFP internalisation and then, the number of viable cells increases compared to 8 h. However, the commercial transfectant was not adequate as reference under these experimental conditions since its cytotoxic activity provokes an almost complete elimination of cellular viability. The fluorescence levels obtained for DHP(G4)-MPA after 4 h of incubation were comparable to those observed for Lipofectamine (5.2 a.u. and 6.0 a.u., for DHP(G4)-MPA and lipofectamine

respectively), and the 22% of viability for the commercial reagent still allows comparisons between both gene delivery vectors at these conditions.

On the other hand, the amount of pGFP per well was varied between 0.2 and 0.4 µg following previous studies[20]. In Figure 6.7b, data for dendriplexes with DHP(G4)-MPA and pGFP at different N/P ratios (25, 50, 100, 250 and 500) with the different amounts of pGFP are shown. Despite the highest transfection efficiencies were reached with 0.4 µg of pGFP, more specifically at the ratio N/P 250, the low viability exhibited for these complexes (around 50%) discard these conditions for the later transfection assays. The amount of 0.2 µg of pGFP allowed relevant fluorescence levels when increasing the N/P ratio to 500 while the cell viability was maintained above 86%.

Within these studies, 4 h of incubation and 0.2 µg of pGFP were stablished as the most appropriate parameters to carry on the comparative study of transfection ability on the pseudodendrimers.

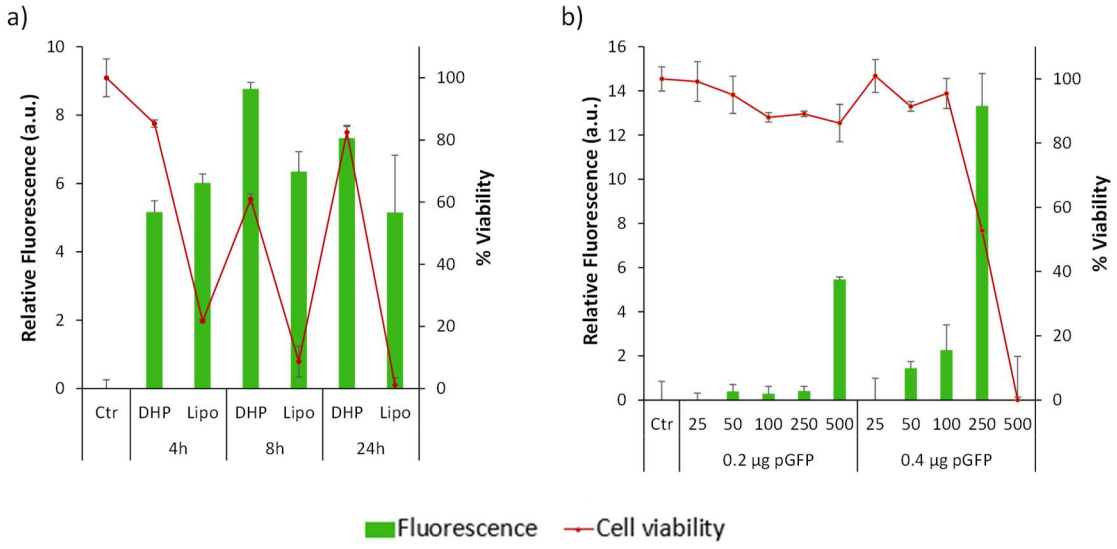

Figure 6.7. Optimisation of the transfection experimental conditions in HeLa. a) Different incubation times (4, 8 or 24h) of the dendriplexes between DHP(G4)-MPA and pGFP at ratio N/P 500. Complexes between Lipofectamine 3000 and pGFP were included as transfection controls at each incubation time. b) Transfection experiments with 0.2 or 0.4 µg of pGFP per sample. Besides controls, dendriplexes with DHP(G4)-MPA at different N/P ratios (25, 50, 100, 250 and 500) were assayed. Error bars denote the standard deviation (n=3). Ctr: control of cells without any treatment. Lipo: lipofectamine 3000.

6.4.2. *In vitro* pGFP transfection

We initially confirmed that the naked pGFP did not have any transfection ability by itself under these conditions, corroborating the necessity to employ a vector to facilitate its delivery into the cells.

The ability of all the DHPs as gene delivery vectors for pGFP in a broad range of N/P ratios was evaluated in two different cell lines: HeLa, a tumoral cell line, and the mesenchymal cells mMSCs. The transfection and viability results in both cell lines with the DHPs and the pGFP at ratios N/P 25, 50, 100, 250 and 500 are shown in Figure 6.8. In general terms, better transfection results were obtained within the mesenchymal cell line, thus opening a promising landscape for gene delivery into these pluripotent cells with a wide range of further applications[40]. Since the comparison between DHPs series (*bis*-MPA and *bis*-GMPA), generations (G2, G3 and G4) and N/P ratios follow the same tendency in terms of non-viral vectors efficiency within the two cell lines, the discussion will be focused on the most promising results in the mMSCs cells (Figure 6.8b).

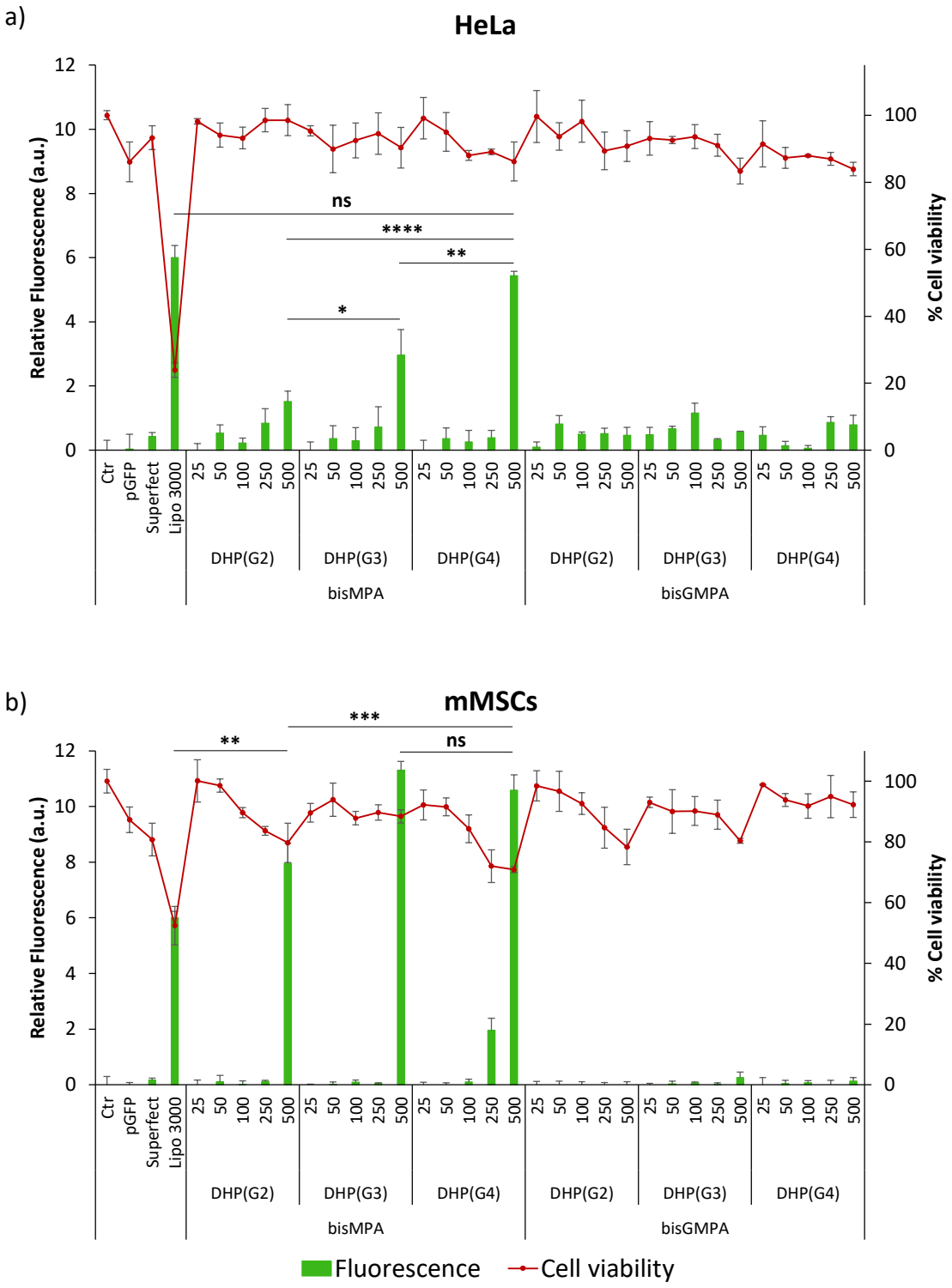

*Figure 6.8. Transfection experiments with pGFP in a) HeLa and b) mMSCs cell lines. All the DHPs of the bis-MPA and bis-GMPA series were assayed as vectors at N/P ratios 25, 50, 100, 250 and 500. Controls without treatment, naked pGFP, with Superfect and with Lipofectamine 3000 are also included for each cell lines. Green bars show transfection efficiency and red points indicate cell viability. Error bars indicate the standard deviation (SD) (n= 3). Statistical analysis was performed by one-way ANOVA; ns, $p > 0.05$; *, $p < 0.05$; **, $p < 0.01$; ***, $p < 0.001$; ****, $p < 0.0001$.*

Comparing the two DHP series (*bis*-MPA and *bis*-GMPA), it is remarkable the absence of any transfection activity with those DHPs including the *bis*-GMPA dendron (DHP(G2)-GMPA, DHP(G3)-GMPA and DHP(G4)-GMPA). Although, according to the gel retardation assay (see Figure 6.5), the dendriplexes were all successfully formed at the N/P ratio 25, their final transfection activity showed significant differences (see Figure 6.8). Indeed, the data seem to suggest that the inner amido groups of the *bis*-GMPA dendrons hinder somehow the final expression of the GFP protein since lower values (below 0.3 a.u.) are observed in all cases comprising DHPs-GMPA (see Figure 6.8). A plausible explanation could be related to the establishment of hydrogen bonds between the *bis*-GMPA dendrons and the nucleic acid, which could render more stable dendriplexes thus hampering subsequent pGFP release and deliver to the nucleus[30,41]. In addition, the lower ζ potential values observed for DHPs-GMPA compared to DHPs-MPA (see Table 6.2), could also reduce their cellular uptake.

The DHPs of the *bis*-MPA series presented good characteristics as non-viral pGFP vectors as they reached higher transfection efficiencies than Superfect, a commercially available gene delivery vector with dendritic structure. Besides, at the highest ratio tested (N/P 500, see Figure 6.8), the results obtained for the DHPs were even higher than that for the lipid based Lipofectamine 3000 control. In this line, larger transfection efficiencies were observed when the N/P ratio was significantly higher than the stablished as the minimum for dendriplexes formation, which had been previously observed in other studies[20]. This observation could suggest a benefited cytosolic release of the endosome content when increasing the pseudodendrimer dose with respect to the nucleic acid, which indeed is translated into an increase in the ζ potential for all the dendriplexes with pGFP studied[42] (see Table 6.2). Among the *bis*-MPA series, even the small DHP(G2)-MPA at N/P ratio 500 showed better transfection efficiency than the commercial lipidic Lipofectamine 3000 (8.0 a.u. versus 6.0 a.u.). Besides, the bigger polyester core generation, the more activity it exhibited as pGFP vector. It is interesting to note that no significant differences in the levels of transfection were found at N/P ratio 500 for DHP(G3)-MPA and DHP(G4)-MPA (11.3 a.u. and 10.6 a.u., respectively), whereas the biggest DHP also presented some transfection activity (2.0 a.u.) when decreasing the N/P ratio to 250. The ζ

potential values of these two dendriplexes formed between DHP(G3)-MPA or DHP(G4)-MPA with pGFP at N/P ratio 500 are the highest ones among the pGFP complexes (12.3 and 13.1 mV, respectively, see Table 6.2), which may contribute to a more favourable cellular uptake, thus benefiting subsequent transfection activity. The low cytotoxicity of these dendritic vectors, remaining above 70% viability in all cases, arose as another advantageous feature compared to commercial Lipofectamine vector.

Fluorescence microscopy was used to corroborate the spectroscopical results. As a representative example, the fluorescence on mMSCs after transfection with DHP(G4)-MPA and pGFP at different N/P ratios is shown in Figure 6.9. Namely, the expression of green fluorescence was observed to increase when raising the N/P ratio from 100 to 500. While scarce fluorescence was observed at N/P 100, at the highest ratio assayed, N/P 500, the levels of GFP expression were higher than those of the cells transfected with the commercial Lipofectamine 3000 as vector. These qualitative results are in good agreement with the previous spectroscopical data measured (see Figure 6.8b).

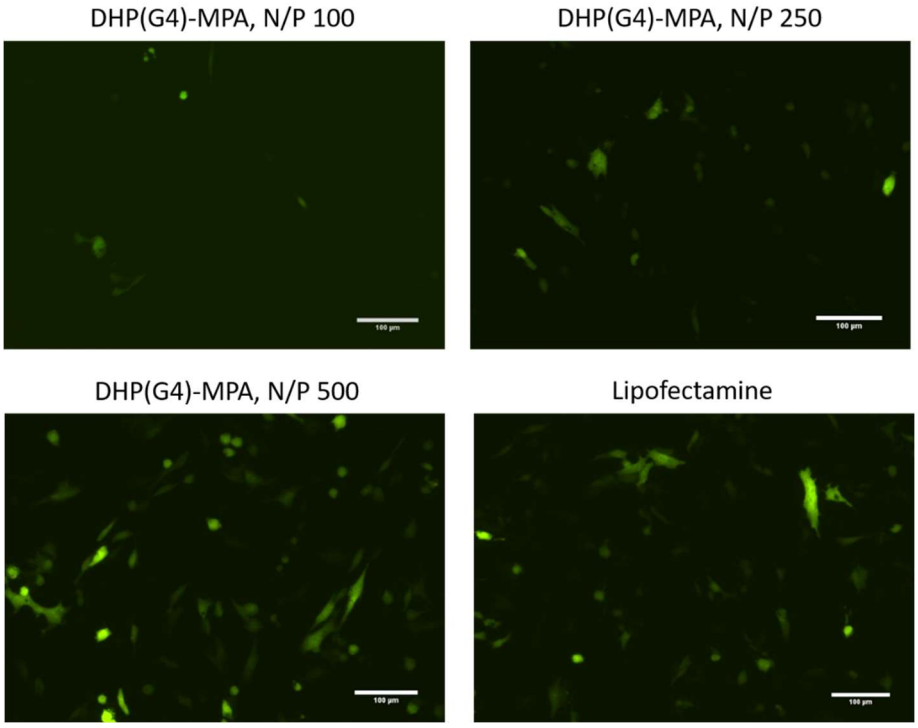

Figure 6.9. Fluorescence images of mMSCs cells expressing GFP after incubation with the pGFP in combination with DHP(G4)-MPA at N/P ratios 100, 250 or 500, and the pGFP with Lipofectamine 3000 as control. Scale bars: 100 μm.

6.4.3. *In vitro* siGFP transfection

siGFP effective transfection leads to the reduction of the fluorescence intensity in GFP-expressing cell lines. Cell death can also result into the reduction of GFP expression. Therefore, it is important to assess both characteristics simultaneously in order to avoid misleading results. The microscopic observation allowed to qualitatively corroborate those fluorescence levels.

The two cell lines studied, HeLa-GFP and mMSCs-GFP, showed similar transfection levels for the siGFP delivered into de DHPs at the broad range of N/P ratios tested. Specifically, the results at N/P ratios 150, 300, 500 and 750 are shown in Figure 6.10.

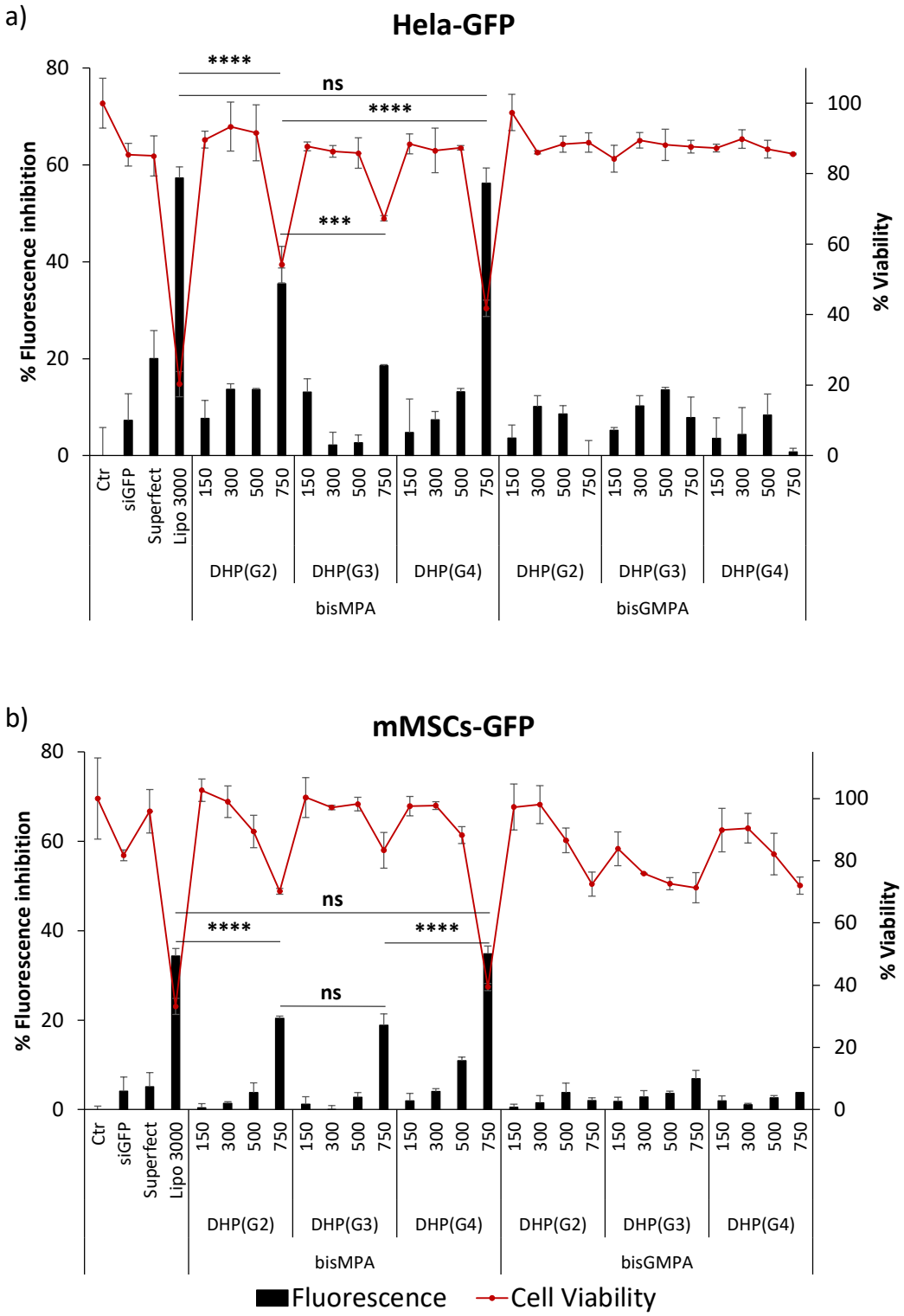

*Figure 6.10. Transfection experiments with siGFP in a) HeLa-GFP and b) mMSCs-GFP cell lines. All the DHPs of the bis-MPA and bis-GMPA series were assayed as vectors at N/P ratios 150, 300, 500 and 750. Controls without treatment, naked siGFP, with Superfect and with Lipofectamine 3000 are also included for each cell lines. Black bars show transfection efficiency and red points indicate cell viability. Error bars indicate the standard deviation (SD) (n= 3). Statistical analysis was performed by one-way ANOVA; ns, $p > 0.05$; ***, $p < 0.001$; ****, $p < 0.0001$.*

The most relevant results in the mesenchymal cell line, mMSCs-GFP, will be here discussed. Among the DHP series, *bis*-MPA derivatives showed better transfection activity than their *bis*-GMPA counterparts. Focusing on the DHPs-MPA series, a core generation dependence was observed again, being the levels of DHP(G4)-MPA fluorescence inhibition at N/P ratio 750 (35%) comparable to those of Lipofectamine (34%). An improvement in the transfection efficiency was observed when increasing the N/P ratio, but the cell viability levels were also compromised. The dendriplex formulation that yielded the higher rate of fluorescence inhibition, DHP(G4)-MPA/siGFP at N/P ratio 750, was also responsible for a 60% decay in cell viability (see Figure 6.10b). Reducing the N/P ratio of DHP(G4)-MPA to 500 allowed a 11% of fluorescence inhibition without negatively affecting cell viability (levels above 88%). Non-significant differences were found in the activity of DHP(G2)-MPA and DHP(G3)-MPA as siGFP vectors at N/P ratio 750 (20% and 19% of fluorescence inhibition, respectively) but the differences in cell viability postulate DHP(G3)-MPA as a better vector.

The levels of green fluorescence expression were also assessed by **fluorescence microscopy**. Apart from Lipofectamine 3000-transfected cells, a control of the wild type mMSCs-GFP cells was included to visualize the highest level of fluorescence reached within this cell line. As a representative example, images of the transfection with DHP(G4)-MPA and siGFP at different N/P ratios (300, 500 and 750) are shown in Figure 6.11. As previously observed in the spectroscopic fluorescence determination (see Figure 6.10), the increase in the N/P ratio from 300 to 750 was translated into a decrease of the fluorescence levels, that is, an improvement on the siGFP silencing activity. The highest GFP expression inhibition in mMSCs-GFP with a DHP vector was reached after transfection with DHP(G4)-MPA/siGFP at N/P ratio 750, whose levels of fluorescence were comparable to those of the mMSCs-GFP cells transfected with Lipofectamine 3000 as vector.

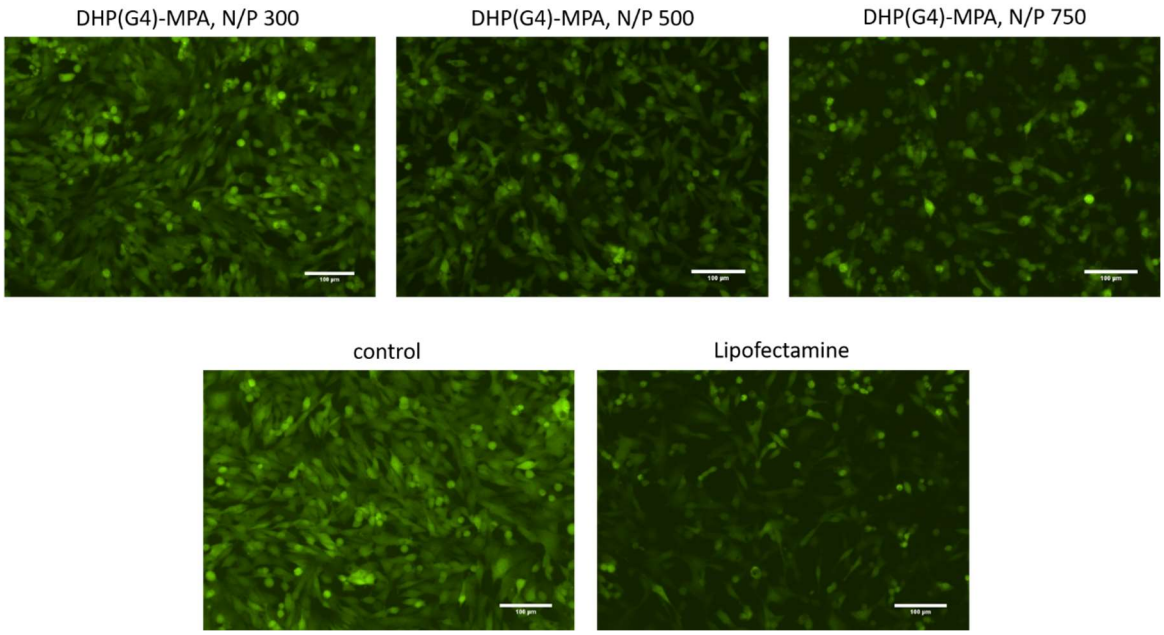

Figure 6.11. Fluorescence images of mMSCs-GFP cells showing a reduction in the GFP expression after incubation with the siGFP in combination with DHP(G4)-MPA at N/P ratios 300, 500 or 750. siGFP with Lipofectamine 3000 and the wild type cells are included as controls. Scale bars: 100 µm.

6.5. Internalisation and cellular distribution

The most promising DHPs combinations with pGFP were evaluated in terms of cell internalisation and intracellular distribution in both cell lines, HeLa and mMSCs. Namely, dendriplexes between DHP(G4)-MPA or DHP(G4)-GMPA and pGFP at N/P ratios 500 were chosen to carry out this assay. In order to visualise the dendriplexes within the intracellular compartments by confocal microscopy, the pseudodendrimers were previously labelled with the fluorophore rhodamine B (as explained in chapter 2, section 2.3.2). Actin filaments and nuclei were properly stained to allow the cellular visualisation too (see chapter 7, section 7.2.2.5.). Analogue conditions as those employed in the transfection experiments were assayed for the intracellular observation of the dendriplexes.

The internalisation visualised of the dendriplexes containing DHP(G4)-MPA-RhB or DHP(G4)-GMPA-RhB was low in both cell lines. A lower number of rhodamine-labelled aggregates were found in the case of HeLa (Figure 6.12a) compared to the mesenchymal cell line (Figure 6.12b), thus indicating a lower efficiency on their cellular uptake after 4 h of incubation.

Interestingly, few dendriplexes composed by DHP(G4)-MPA-RhB were found within the HeLa cell line whereas the confocal microscopy did not show any DHP(G4)-GMPA-RhB dendriplexes inside these cells (Figure 6.12a). The preferent internalisation of the DHP(G4)-MPA-RhB dendriplexes over the DHP(G4)-GMPA-RhB ones was also observed in the mesenchymal cell line (Figure 6.12b). In this case, a high number of dendriplexes containing the pseudodendrimer DHP(G4)-MPA-RhB were found inside the mMSCs, while just few DHP(G4)-GMPA-RhB dendriplexes were found on the cellular surface. Moreover, the location of the DHP(G4)-MPA-RhB dendriplexes revealed their distribution along the cellular morphology, with the presence of some aggregates collocating with actin in the peripheric cytoplasm (white arrows) and others in the surroundings of the cellular nucleus (yellow arrows). This indicates the effective internalisation of the aggregates after the incubation time assayed with different rates of progression in their pathway towards the nucleus for the final delivery of the plasmid.

The results obtained by confocal microscopy are in good agreement with the transfection efficiencies previously measured (see Figure 6.8). Specifically, the better internalisation of the pGFP dendriplexes by the mesenchymal cell line contributes to explain the highest transfection efficiencies found within this cell line. On the other hand, the absence of DHP(G4)-GMPA-RhB aggregates inside the HeLa cells and their scarce presence on the surface of the mMSCs could be explained by their lower positive surface charge (4.1 mV versus 13.1 mV of the dendriplexes with DHP(G4)-MPA, see Table 6.2), which would affect the electrostatic attraction between the aggregates and the negatively charged cellular membranes[39]. This, together with the hypothesis of the stronger interaction between the *bis*-GMPA dendrons and the nuclei acids that hinders its final dissociation, may contribute to the lower transfection efficiencies yielded by the dendriplexes with DHP(G4)-GMPA.

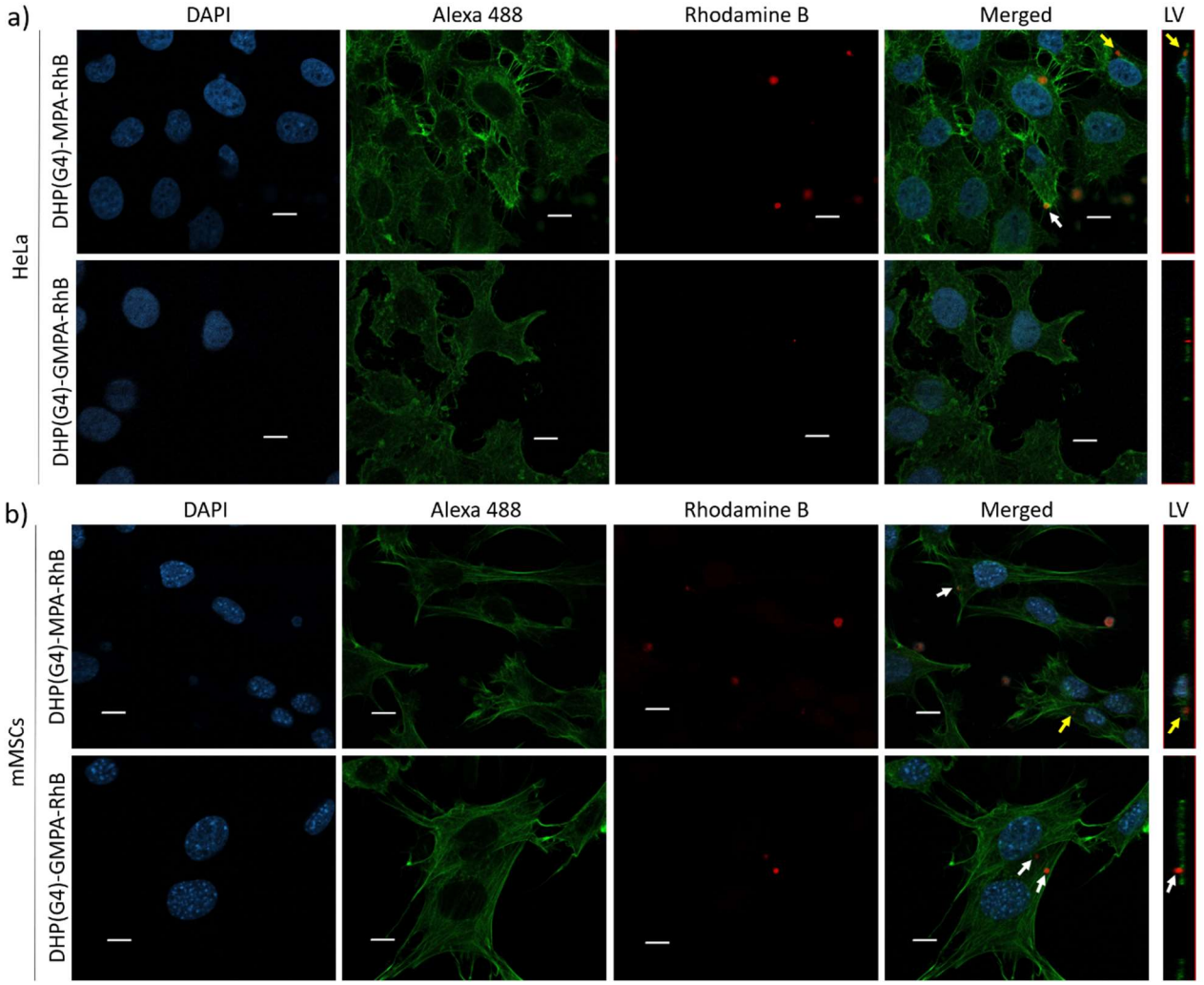

Figure 6.12. Confocal z-stack projections of the internalisation of DHP(G4)-MPA-RhB or DHP(G4)-GMPA-RhB dendriplexes with pGFP at N/P ratio 500 in HeLa (a) and mMSCs (b). Scale bars: 10 μm. Color code: blue, nuclei; green, actin; red, rhodamine B. Single images for each channel are represented as well as all channels merged and some representative lateral views (LV). White arrows indicate dendriplexes inside the cells or on the surface, and yellow arrows indicate dendriplexes near the nucleus.

6.6. General remarks

Summary

The ability of the pseudodendrimers of the *bis*-MPA and *bis*-GMPA series as vectors for gene delivery has been explored. Firstly, their buffering response to pH has been evaluated and then, their capacity to complex nucleic acids yielding dendriplexes has been tested in a wide range of ratios N/P. After the characterisation of the resulting dendriplexes, their final behaviour as gene vectors has been assayed in two different cell lines, tumoral and mesenchymal cells, while the biocompatibility was determined. Finally, the internalisation of the dendriplexes was visualised by microscopical techniques.

Conclusions

The ability of the pseudodendrimers to complex pGFP and siGFP has been demonstrated. Their transfection activity as non-viral vectors has revealed the greater convenience of the DHP-MPA pseudodendrimers over their DHP-GMPA homologues and most remarkable, over other highly efficient commercial dendritic-based reagent. Most interestingly, transfection levels even as good as the lipidic commercial Lipofectamine 3000 were reached for the siGFP transfection with DHP(G4)-MPA at N/P ratio 750 and almost a 2-fold improvement in the pGFP transfection efficiency of Lipofectamine 3000 has been achieved with DHP(G3)-MPA and DHP(G4)-MPA at N/P ratio 500. A generation dependence has been observed as well as the influence of some parameters like N/P ratios or incubation times in the transfection efficiency. The lower efficiency obtained for the DHP-GMPA series as gene delivery vectors compared to the DHP-MPA series is proposed to occur by the combination of various factors related with the chemical composition of the structures and the physico-chemical properties of the resulting aggregates. They include a stronger interaction between the *bis*-GMPA dendrons and the nucleic acids that hinders their subsequent release to accomplish their cellular function and their lower cellular internalisation probably due to the lower positive charges on the surface of the dendriplexes. Finally, the gene delivery results are more promising within the

mesenchymal cell lines than the tumoral ones, regarding both, internalisation rates and final transfection activities.

Future perspectives

The pluripotency of the mesenchymal cells points them as a powerful tool that is gaining interest in the biomedical fields of regenerative medicine and oncology[40]. For that reason, after having found competent vectors for the transfection on this kind of cells and having set the optimal conditions, we envision as interesting next step to assess the subsequent differentiation of these transfected cells into a cell of interest, e.g., a hepatocyte, by the addition of the required factors. Then, the analysis of the phenotypic and genotypic characteristics of the resulting cultures would allow to confirm the correct differentiation and to use these cells with regenerative purposes.

6.7. References

(1) Kaestner, L.; Scholz, A.; Lipp, P. Conceptual and Technical Aspects of Transfection and Gene Delivery. *Bioorganic & Medicinal Chemistry Letters* **2015**, *25* (6), 1171–1176. https://doi.org/10.1016/j.bmcl.2015.01.018.

(2) Griffith, Fred. The Significance of Pneumococcal Types. *J Hyg (Lond)* **1928**, *27* (2), 113–159.

(3) Blaese, R. M.; Culver, K. W.; Miller, A. D.; Carter, C. S.; Fleisher, T.; Clerici, M.; Shearer, G.; Chang, L.; Chiang, Y.; Tolstoshev, P.; Greenblatt, J. J.; Rosenberg, S. A.; Klein, H.; Berger, M.; Mullen, C. A.; Ramsey, W. J.; Muul, L.; Morgan, R. A.; Anderson, W. F. T Lymphocyte-Directed Gene Therapy for ADA- SCID: Initial Trial Results After 4 Years. *Science* **1995**, *270* (5235), 475–480. https://doi.org/10.1126/science.270.5235.475.

(4) Aiuti, A.; Roncarolo, M. G.; Naldini, L. Gene Therapy for ADA-SCID, the First Marketing Approval of an Ex Vivo Gene Therapy in Europe: Paving the Road for the next Generation of Advanced Therapy Medicinal Products. *EMBO Molecular Medicine* **2017**, *9* (6), 737–740. https://doi.org/10.15252/emmm.201707573.

(5) Wirth, T.; Parker, N.; Ylä-Herttuala, S. History of Gene Therapy. *Gene* **2013**, *525* (2), 162–169. https://doi.org/10.1016/j.gene.2013.03.137.

(6) Bennet, B. M.; Wolf, J.; Laureano, R.; Sellers, R. S. Review of Current Vaccine Development Strategies to Prevent Coronavirus Disease 2019 (COVID-19). *Toxicol Pathol* **2020**, *48* (7), 800–809. https://doi.org/10.1177/0192623320959090.

(7) Razi Soofiyani, S.; Baradaran, B.; Lotfipour, F.; Kazemi, T.; Mohammadnejad, L. Gene Therapy, Early Promises, Subsequent Problems, and Recent Breakthroughs. *Adv Pharm Bull* **2013**, *3* (2), 249–255. https://doi.org/10.5681/apb.2013.041.

(8) Lostalé-Seijo, I.; Montenegro, J. Synthetic Materials at the Forefront of Gene Delivery. *Nature Reviews Chemistry* **2018**, *2* (10), 258–277. https://doi.org/10.1038/s41570-018-0039-1.

(9) Nyamay'Antu, A.; Dumont, M.; Kedinger, V.; Erbacher, P. Non-Viral Vector Mediated Gene Delivery: The Outsider to Watch Out For in Gene Therapy. *Cell Gene Therapy Insights* **2019**, *5* (S1), 51–57. https://doi.org/10.18609/cgti.2019.007.

(10) Lundstrom, K. Viral Vectors in Gene Therapy. *Diseases* **2018**, *6* (2), 42. https://doi.org/10.3390/diseases6020042.

(11) Prado, D. A.; Acosta-Acero, M.; Maldonado, R. S. Gene Therapy beyond Luxturna: A New Horizon of the Treatment for Inherited Retinal Disease. *Current Opinion in Ophthalmology* **2020**, *31* (3), 147–154. https://doi.org/10.1097/ICU.0000000000000660.

(12) Shirley, J. L.; de Jong, Y. P.; Terhorst, C.; Herzog, R. W. Immune Responses to Viral Gene Therapy Vectors. *Molecular Therapy* **2020**, *28* (3), 709–722. https://doi.org/10.1016/j.ymthe.2020.01.001.

(13) Ramamoorth, M.; Narvekar, A. Non Viral Vectors in Gene Therapy- An Overview. *J Clin Diagn Res* **2015**, *9* (1), GE01–GE06. https://doi.org/10.7860/JCDR/2015/10443.5394.
(14) Sung, Y.; Kim, S. Recent Advances in the Development of Gene Delivery Systems. *Biomater Res* **2019**, *23* (1), 8. https://doi.org/10.1186/s40824-019-0156-z.
(15) Patil, S.; Gao, Y.-G.; Lin, X.; Li, Y.; Dang, K.; Tian, Y.; Zhang, W.-J.; Jiang, S.-F.; Qadir, A.; Qian, A.-R. The Development of Functional Non-Viral Vectors for Gene Delivery. *International Journal of Molecular Sciences* **2019**, *20* (21), 5491. https://doi.org/10.3390/ijms20215491.
(16) Yang, J.; Zhang, Q.; Chang, H.; Cheng, Y. Surface-Engineered Dendrimers in Gene Delivery. *Chem. Rev.* **2015**, *115* (11), 5274–5300. https://doi.org/10.1021/cr500542t.
(17) Palmerston Mendes, L.; Pan, J.; Torchilin, V. P. Dendrimers as Nanocarriers for Nucleic Acid and Drug Delivery in Cancer Therapy. *Molecules* **2017**, *22* (9). https://doi.org/10.3390/molecules22091401.
(18) Hu, H.; Wang, H.; Liang, S.; Li, X.; Wang, D. Synthesis and Characterization of a PAMAM Dendrimer Nanocarrier Functionalized by HA for Targeted Gene Delivery Systems and Evaluation in Vitro. *Journal of Biomaterials Science, Polymer Edition* **2020**, *0* (0), 1–24. https://doi.org/10.1080/09205063.2020.1827921.
(19) Laskar, P.; Somani, S.; Mullin, M.; J. Tate, R.; Warzecha, M.; Bowering, D.; Keating, P.; Irving, C.; Y. Leung, H.; Dufès, C. Octadecyl Chain-Bearing PEGylated Poly(Propyleneimine)-Based Dendrimersomes: Physicochemical Studies, Redox-Responsiveness, DNA Condensation, Cytotoxicity and Gene Delivery to Cancer Cells. *Biomaterials Science* **2021**. https://doi.org/10.1039/D0BM01441A.
(20) Lancelot, A.; González-Pastor, R.; Concellón, A.; Sierra, T.; Martín-Duque, P.; Serrano, J. L. DNA Transfection to Mesenchymal Stem Cells Using a Novel Type of Pseudodendrimer Based on 2,2-Bis(Hydroxymethyl)Propionic Acid. *Bioconjugate Chem.* **2017**, *28* (4), 1135–1150. https://doi.org/10.1021/acs.bioconjchem.7b00037.
(21) Lancelot, A.; González-Pastor, R.; Clavería-Gimeno, R.; Romero, P.; Abian, O.; Martín-Duque, P.; Serrano, J. L.; Sierra, T. Cationic Poly(Ester Amide) Dendrimers: Alluring Materials for Biomedical Applications. *J. Mater. Chem. B* **2018**, *6* (23), 3956–3968. https://doi.org/10.1039/C8TB00639C.
(22) Gómez, R.; Mata, F. J. de la; Jiménez-Fuentes, J. L.; Ortega, P.; Klajnert, B.; Pedziwiatr-Werbicka, E.; Shcharbin, D.; Bryszewska, M.; Maly, M.; Maly, J.; Serramía, M. J.; Lorente, R.; Muñoz-Fernández, M. A. Cationic Carbosilane Dendrimers as Non-viral Vectors of Nucleic Acids (Oligonucleotide or SiRNA) for Gene Therapy Purposes. In *Dendrimers in Biomedical Applications*; 2013; pp 40–55. https://doi.org/10.1039/9781849737296-00040.
(23) Serramía, M. J.; Álvarez, S.; Fuentes-Paniagua, E.; Clemente, M. I.; Sánchez-Nieves, J.; Gómez, R.; de la Mata, J.; Muñoz-Fernández, M. Á.

In Vivo Delivery of SiRNA to the Brain by Carbosilane Dendrimer. *Journal of Controlled Release* **2015**, *200*, 60–70. https://doi.org/10.1016/j.jconrel.2014.12.042.

(24) Saviano, F.; Lovato, T.; Russo, A.; Russo, G.; Bouton, C. R.; Shattock, R. J.; Alexander, C.; Quaglia, F.; Blakney, A. K.; Gurnani, P.; Conte, C. Ornithine-Derived Oligomers and Dendrimers for *in Vitro* Delivery of DNA and *Ex Vivo* Transfection of Skin Cells *via* SaRNA. *J. Mater. Chem. B* **2020**, *8* (22), 4940–4949. https://doi.org/10.1039/D0TB00942C.

(25) Zhou, J.; Ma, S.; Zhang, Y.; He, Y.; Yang, J.; Zhang, H.; Luo, K.; Gu, Z. Tunable Membrane-Penetrating Bioreductive Nanogels Based on Guanidinylated Dendrimers for Programmable Gene Delivery. *Applied Materials Today* **2020**, *20*, 100646. https://doi.org/10.1016/j.apmt.2020.100646.

(26) Shcharbin, D.; Dzmitruk, V.; Shakhbazau, A.; Goncharova, N.; Seviaryn, I.; Kosmacheva, S.; Potapnev, M.; Pedziwiatr-Werbicka, E.; Bryszewska, M.; Talabaev, M.; Chernov, A.; Kulchitsky, V.; Caminade, A.-M.; Majoral, J.-P. Fourth Generation Phosphorus-Containing Dendrimers: Prospective Drug and Gene Delivery Carrier. *Pharmaceutics* **2011**, *3* (3), 458–473. https://doi.org/10.3390/pharmaceutics3030458.

(27) Ihnatsyeu-Kachan, A.; Dzmitruk, V.; Apartsin, E.; Krasheninina, O.; Ionov, M.; Loznikova, S.; Venyaminova, A.; Miłowska, K.; Shcharbin, D.; Mignani, S.; Muñoz-Fernández, M. A.; Majoral, J.-P.; Bryszewska, M. Multi-Target Inhibition of Cancer Cell Growth by SiRNA Cocktails and 5-Fluorouracil Using Effective Piperidine-Terminated Phosphorus Dendrimers. *Colloids and Interfaces* **2017**, *1* (1), 6. https://doi.org/10.3390/colloids1010006.

(28) Wang, Y.; Li, L.; Shao, N.; Hu, Z.; Chen, H.; Xu, L.; Wang, C.; Cheng, Y.; Xiao, J. Triazine-Modified Dendrimer for Efficient TRAIL Gene Therapy in Osteosarcoma. *Acta Biomaterialia* **2015**, *17*, 115–124. https://doi.org/10.1016/j.actbio.2015.01.007.

(29) Movellan, J.; González-Pastor, R.; Martín-Duque, P.; Sierra, T.; de la Fuente, J. M.; Serrano, J. L. New Ionic Bis-MPA and PAMAM Dendrimers: A Study of Their Biocompatibility and DNA-Complexation: New Ionic Bis-MPA and PAMAM Dendrimers: A Study …. *Macromol. Biosci.* **2015**, *15* (5), 657–667. https://doi.org/10.1002/mabi.201400422.

(30) Thomas, T. J.; Tajmir-Riahi, H. A.; Thomas, T. Polyamine–DNA Interactions and Development of Gene Delivery Vehicles. *Amino Acids* **2016**, *48* (10), 2423–2431. https://doi.org/10.1007/s00726-016-2246-8.

(31) Behr, J.-P. The Proton Sponge: A Trick to Enter Cells the Viruses Did Not Exploit. *CHIMIA International Journal for Chemistry* **1997**, *51* (1–2), 34–36.

(32) Yang, S.; May, S. Release of Cationic Polymer-DNA Complexes from the Endosome: A Theoretical Investigation of the Proton Sponge Hypothesis. *J. Chem. Phys.* **2008**, *129* (18), 185105. https://doi.org/10.1063/1.3009263.

(33) Varkouhi, A. K.; Scholte, M.; Storm, G.; Haisma, H. J. Endosomal Escape Pathways for Delivery of Biologicals. *Journal of Controlled Release* **2011**, *151* (3), 220–228.

https://doi.org/10.1016/j.jconrel.2010.11.004.
(34) Lin, C.; Engbersen, J. F. J. Effect of Chemical Functionalities in Poly(Amido Amine)s for Non-Viral Gene Transfection. *Journal of Controlled Release* **2008**, *132* (3), 267–272. https://doi.org/10.1016/j.jconrel.2008.06.022.
(35) Ahmad, A.; Khan, J. M.; Haque, S. Strategies in the Design of Endosomolytic Agents for Facilitating Endosomal Escape in Nanoparticles. *Biochimie* **2019**, *160*, 61–75. https://doi.org/10.1016/j.biochi.2019.02.012.
(36) Kang, H. C.; Bae, Y. H. Co-Delivery of Small Interfering RNA and Plasmid DNA Using a Polymeric Vector Incorporating Endosomolytic Oligomeric Sulfonamide. *Biomaterials* **2011**, *32* (21), 4914–4924. https://doi.org/10.1016/j.biomaterials.2011.03.042.
(37) Ziebarth, J. D.; Kennetz, D. R.; Walker, N. J.; Wang, Y. Structural Comparisons of PEI/DNA and PEI/SiRNA Complexes Revealed with Molecular Dynamics Simulations. *J Phys Chem B* **2017**, *121* (8), 1941–1952. https://doi.org/10.1021/acs.jpcb.6b10775.
(38) Malvern. Zetasizer Nano User Manual. Malvern Instruments Ltd. **2013**.
(39) Zhang, D.; Wei, L.; Zhong, M.; Xiao, L.; Li, H.-W.; Wang, J. The Morphology and Surface Charge-Dependent Cellular Uptake Efficiency of Upconversion Nanostructures Revealed by Single-Particle Optical Microscopy. *Chemical Science* **2018**, *9* (23), 5260–5269. https://doi.org/10.1039/C8SC01828F.
(40) Andrzejewska, A.; Lukomska, B.; Janowski, M. Concise Review: Mesenchymal Stem Cells: From Roots to Boost. *STEM CELLS* **2019**, *37* (7), 855–864. https://doi.org/10.1002/stem.3016.
(41) Cheng, Y.; Sellers, D. L.; Tan, J.-K. Y.; Peeler, D. J.; Horner, P. J.; Pun, S. H. Development of Switchable Polymers to Address the Dilemma of Stability and Cargo Release in Polycationic Nucleic Acid Carriers. *Biomaterials* **2017**, *127*, 89–96. https://doi.org/10.1016/j.biomaterials.2017.02.036.
(42) Zhou, J.; Wu, Y.; Wang, C.; Cheng, Q.; Han, S.; Wang, X.; Zhang, J.; Deng, L.; Zhao, D.; Du, L.; Cao, H.; Liang, Z.; Huang, Y.; Dong, A. PH-Sensitive Nanomicelles for High-Efficiency SiRNA Delivery in Vitro and in Vivo: An Insight into the Design of Polycations with Robust Cytosolic Release. *Nano Lett.* **2016**, *16* (11), 6916–6923. https://doi.org/10.1021/acs.nanolett.6b02915.

Chapter 7:

Experimental section

7.1. Chemical synthesis and characterisation

7.1.1. Materials and equipments

The commercial reagents used in this thesis were acquired from Sigma Aldrich® or Acros Organics™, solvents were obtained from Sigma Aldrich® or Scharlab and dialysis membranes were purchased from Spectra/Por™.

^{1}H NMR, **^{13}C NMR** and **^{19}F NMR** experiments were performed in a Bruker AV-400 (^{1}H: 400 MHz, ^{13}C: 100 MHz, ^{19}F: 376 MHz) spectrometer employing deuterated solvents. The chemical shifts are given in ppm and the coupling constants in Hz.

Mass spectrometry (MS) were performed using an ESI Bruker Esquire 300^{+} or a Bruker Microflex system employing the MALDI-TOF technique with nitrogen laser (337 nm) and dithranol as matrix.

Fourier transformed infrared (FTIR) spectra were performed using a Bruker Vertex 70 spectrophotometer in attenuated total reflection (ATR) mode and recorded between 4000 and 600 cm^{-1}.

Size exclusion chromatography (SEC) was performed on a Waters e2695 Alliance system with two Styragel columns HR4 and HR1 (500 and 104 Å of pore size) in series and a Waters 2424 evaporation light scattering detector. Samples were dissolved into THF (HPLC grade) at the concentration of 1 mg/mL. The flow rate was set at 1 mL/min and the temperature at 35 °C. Poly(methyl methacrylate) (PMMA) was used as standard for calibration.

7.1.2. *bis*-MPA and *bis*-GMPA dendrons

7.1.2.1. *bis*-MPA dendrons

General procedure I: Steglich's esterification

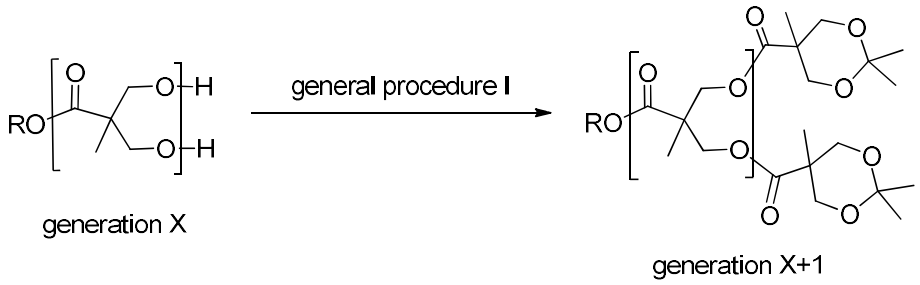

The hydroxy terminated dendron (1.00 mol) was dissolved into dry DCM and then, *bis*-MPA acetal (1.10 (G1), 1.05 (G2) or 1.50 (G3) mol per hydroxyl groups according to the dendron generation) and DPTS (0.40 mol per hydroxyl groups) were added. The reaction mixture was stirred under argon atmosphere and cooled down to 0 ºC. A solution of DCC (1.10, 1.05 or 1.50 mol per hydroxyl group according to the dendron generation) in dry DCM was added dropwise and the reaction mixture was stirred under argon atmosphere at room temperature. The time of reaction varies from overnight to 3 days and it is specified for each molecule. The white precipitate appeared, N,N'-dicyclohexylurea (DCU), was filtered off and the solvent was evaporated under vacuum to get a mixture of oil and solid. DCU was newly precipitated into hexane and filtered off, with the subsequent solvent evaporation under reduced pressure. The crude product was purified though silica gel column chromatography with mixtures of hexane and ethyl acetate as eluent (specific proportions indicated in the description of each compound).

General procedure II: deprotection of the hydroxyl groups

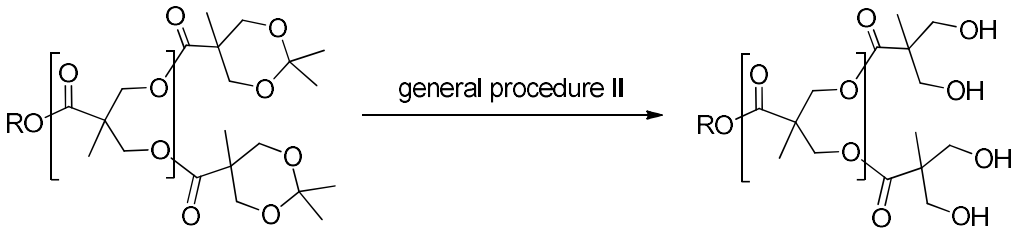

Dowex® proton exchange resin (50% in weight) was previously washed in MeOH for 30 minutes and recovered by filtration. The acetal protected dendron (1.00 mol) was dissolved in MeOH and then, the washed Dowex resin H^+ was added. The reaction mixture was stirred during the indicated time depending on the dendron generation, and the resin was filtered off. The pure product was obtained after solvent evaporation under vacuum.

General procedure III: protection with *t*-Boc moieties

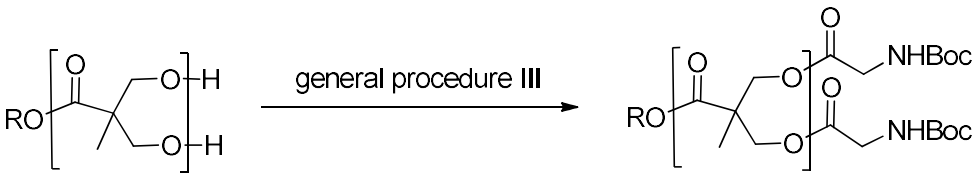

The hydroxy terminated dendron (1.00 mol) was dissolved into dry DCM, together with GlyBoc(OH) (1.25 mol per hydroxyl groups) and DMAP (0.40 mol per hydroxyl groups). This mixture was stirred under argon atmosphere and cooled down to 0 °C. A solution of DCC (1.25 mol per hydroxyl groups) in dry DCM was added dropwise. The reaction mixture was then allowed to stir under argon atmosphere at room temperature for 24 or 48 hours. The white precipitate which appeared, DCU, was removed by filtration. The solvent of the resulting mixture was evaporated under vacuum. A mixture of hexane and ethyl acetate was added to provoke further precipitation of DCU, which was filtered off. The solvent was evaporated under reduced pressure and the crude product was purified twice through silica gel column chromatography (hexane: ethyl acetate mixtures as eluent).

General procedure IV: functionalisation of *bis*-MPA dendrons with stearic acid chains

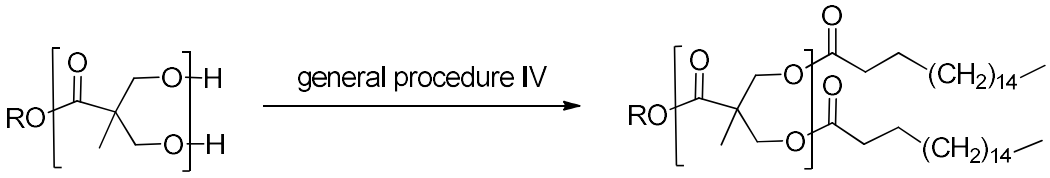

The hydroxy terminated dendron (1.00 mol) was dissolved intro dry DCM and then, stearic acid (1.50 mol per hydroxyl groups) and DMAP (0.40 mol per hydroxyl groups) were added, stirred under argon atmosphere and cooled down to 0 °C. After that, a solution of DCC (2.00 (G1) or 1.50 (G2) mol per hydroxyl groups according to the dendron generation) in dry DCM was added dropwise and the reaction mixture was stirred under argon atmosphere at room temperature for 2-7 days. The DCU precipitated was removed by filtration and the solvent was evaporated under reduced pressure. The mixture of oil and solid obtained was diluted into hexane to provoke the further DCU precipitation, and the filtration and evaporation steps were repeated. Finally, the crude product was purified by precipitating it into cold acetone twice.

***bis*-MPA acetal**

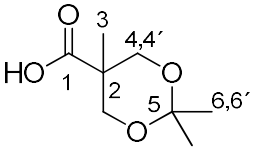

2,2´-bis(hydroxymethyl)propionic acid (30.10 g, 219.92 mmol, 1.00 eq.), 2,2´-dimethoxypropane (41.4 mL, 329.95 mmol, 1.50 eq.) and TsOH·H_2O (2.30 g, 11.91 mmol, 0.05 eq.) were dissolved together into dry acetone (150 mL). The reaction mixture was stirred for 2 hours at room temperature and then, the reaction was neutralised with a solution of 80% of NH_3 in H_2O (25%), and 20% of EtOH. After that, the solvent was evaporated under vacuum and a white solid was got. It was dissolved in ethyl acetate (100 mL) and was washed twice with distilled water. The organic phase was dried over anhydrous $MgSO_4$, and solvent was evaporated under vacuum to get a white powder (24.90 g, 65 %). ^{1}H NMR (400 MHz, $CDCl_3$) δ (ppm): 11.69 (bs, -COOH), 4.19 (d, *J* = 12.0 Hz, 2H, H-4'),

3.66 (d, *J* = 12.0 Hz, 2H, H-4), 1.44 (s, 3H, H-6'), 1.41 (s, 3H, H-6), 1.21 (s, 3H, H-3). ^{13}C NMR (100 MHz, $CDCl_3$) δ (ppm): 180.5, 98.5, 65.9, 41.9, 25.3, 22.2, 18.6. MS (ESI^+) *m/z (%):* found *197.1 (100),* calculated for $[C_8H_{14}O_4,Na]^+$ *197.1*. FTIR (v_{max}/cm^{-1}, ATR): 3136 (COO-H st), 2984-2891 (C-H st), 1718 (C=O st), 1456 (CH_2, CH_3 δ).

6-azidohexan-1-ol

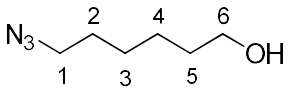

NaN_3 (20.70 g, 318.42 mmol, 2.10 eq.) was dissolved in DMF (60 mL) and 6-chlorohexan-1-ol (20.23 mL, 151.63 mmol, 1.00 eq.) was added. The reaction mixture was stirred at 130 ºC for 36 hours and then, it was allowed to cool down. Et_2O (200 mL) and H_2O (400 mL) were added, and the product was extracted three times with Et_2O (3 x 200 mL). Organic phases were collected together, washed twice with brine (2 x 200 mL) and dried over anhydrous $MgSO_4$. Solvent was evaporated under vacuum to give an orange oil. This crude product was purified on silica gel (hexane:ethyl acetate = 7:3) to yield a light-yellow oil (18.67 g, 86 %). ^{1}H NMR (400 MHz, $CDCl_3$) δ (ppm): 3.65 (t, *J* = 6.5 Hz, 2H, H-6), 3.27 (t, *J* = 6.9 Hz, 2H, H-1), 1.60 (m, 4H, H-2 and H-5), 1.47 (bs, -OH), 1.40 (m, 4H, H-3 and H-4). ^{13}C NMR (400 MHz, $CDCl_3$) δ (ppm): 62.9, 51.5, 32.7, 28.9, 26.7, 25.5. MS (ESI^+) *m/z (%):* found *166.0 (100),* calculated for $[C_6H_{13}N_3O,Na]^+$ *166.1*. FTIR (v_{max}/cm^{-1}, ATR): 3339 (O-H st), 2933-2862 (C-H st), 2091 (N_3 st), 1456 (CH_2, CH_3 δ).

N_3-[MPA,G1]-(acetal)$_1$

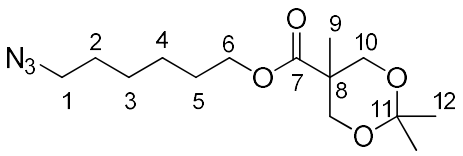

General procedure I. 6-azidohexan-1-ol (12.68 g, 88.60 mmol, 1.00 eq.), *bis*-MPA acetal (16.97 g, 97.42 mmol, 1.10 eq.), DPTS (10.43 g, 35.43 mmol, 0.40 eq.), DCC (20.10 g, 97.42 mmol, 1.10 eq.), dry DCM (300 mL). Time of reaction: overnight. The crude product was purified on silica gel (hexane:ethyl acetate = 8:2) to give a light-yellow oil (22.50 g, 85 %). ^{1}H NMR (400 MHz, $CDCl_3$) δ (ppm):

4.17 (d, *J* = 11.8 Hz, 2H, H-10'), 4.13 (t, *J* = 6.7 Hz, 2H, H-6), 3.62 (d, *J* = 11.8 Hz, 2H, H-10), 3.25 (t, *J* = 6.9 Hz, 2H, H-1), 1.66 (m, 2H, H-5), 1.60 (m, 2H, H-2), 1.42 (s, 3H, H-12'), 1.39 (m, 4H, H-3 and H-4), 1.37 (s, 3H, H-12), 1.17 (s, 3H, H-9). ^{13}C NMR (100 MHz, $CDCl_3$) δ (ppm): 174.4, 98.1, 66.2, 64.8, 51.4, 41.9, 28.8, 28.6, 26.4, 25.5, 24.7, 22.8, 18.8. MS (ESI$^+$) *m/z (%):* found *322.2 (100),* calculated for $[C_{14}H_{25}N_3O_4,Na]^+$ *322.2*. FTIR (ν_{max}/cm^{-1}, ATR): 2935-2866 (C-H st), 2095 (N_3 st), 1728 (C=O st), 1456 (CH_2, CH_3 δ), 1256 (CO-O st), 1157 (C-O st).

N_3-[MPA,G1]-$(OH)_2$

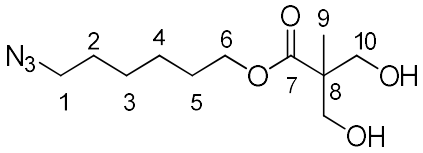

General procedure II. N_3-[MPA,G1]-$(acetal)_1$ (22.50 g, 75.15 mmol, 1.00 eq.), ion exchange resin Dowex H$^+$ (12.13 g, 50 % mass equivalent), MeOH (350 mL). Time of reaction: 5 hours. The product was obtained as a colourless oil (19.40 g, quantitative yield). ^{1}H NMR (400 MHz, $CDCl_3$) δ (ppm): 4.16 (t, *J* = 6.6 Hz, 2H, H-6), 3.80 (ABq, *J* = 11.3 Hz, ΔvAB = 76.0 Hz, 4H, H-10), 3.27 (t, *J* = 6.9 Hz, 2H, H-1), 2.67 (bs, -OH), 1.68 (m, 2H, H-5), 1.60 (m, 2H, H-2), 1.40 (m, 4H, H-3 and H-4), 1.05 (s, 3H, H-9). ^{13}C NMR (100 MHz, $CDCl_3$) δ (ppm): 176.0, 68.5, 64.9, 51.3, 49.1, 28.7, 28.4, 26.3, 25.4, 17.1. MS (ESI$^+$) *m/z (%):* found *282.2 (100)*, calculated for $[C_{11}H_{21}N_3O_4,Na]^+$ *282.3.* FTIR (ν_{max}/cm^{-1}, ATR): 3358 (O-H st), 2976-2937 (C-H st), 2096 (N_3 st), 1703 (C=O st), 1456 (CH_2,CH_3 δ), 1250 (CO-O st), 1155 (C-O st).

N_3-[MPA,G2]-$(acetal)_2$

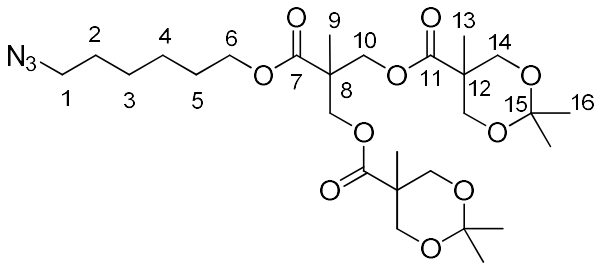

General procedure I. N_3-[MPA,G1]-$(OH)_2$ (6.00 g, 23.14 mmol, 1.00 eq.), *bis*-MPA acetal (8.46 g, 48.59 mmol, 2.10 eq.), DPTS (5.45 g, 18.51 mmol, 0.80 eq.),

DCC (10.03 g, 48.59 mmol, 2.10 eq.), dry DCM (90 mL). Time of reaction: 24 hours. The crude product was purified on silica gel (hexane:ethyl acetate = 7:3) to give a colourless oil (10.69 g, 81 %). ^{1}H NMR (400 MHz, $CDCl_3$) δ (ppm): 4.32 (s, 4H, H-10), 4.14 (d, *J* = 11.8 Hz, 4H, H-14'), 4.11 (t, *J* = 6.7 Hz, 2H, H-6), 3.61 (d, *J* = 12.5 Hz, 4H, H-14), 3.27 (t, *J* = 6.9 Hz, 2H, H-1), 1.65 (m, 2H, H-5), 1.60 (m, 2H, H-2), 1.41 (s, 6H, H-16'), 1.39 (m, 4H, H-3 and H-4), 1.35 (s, 6H, H-16), 1.28 (s, 3H, H-9), 1.15 (s, 6H, H-13). ^{13}C NMR (100 MHz, $CDCl_3$) δ (ppm): 173.5, 172.6, 98.1, 65.9, 65.3, 65.2, 51.3, 46.7, 42.0, 28.7, 28.4, 26.3, 25.5, 24.9, 22.3, 18.5, 17.7. MS (ESI^+) *m/z (%):* found *594.4 (100)*, calculated for $[C_{27}H_{45}N_3O_{10},Na]^+$ *594.3*. FTIR (ν_{max}/cm^{-1}, ATR): 2941-2864 (C-H st), 2096 (N_3 st), 1734 (C=O st), 1456 (CH_2, CH_3 δ), 1240 (CO-O st), 1122 (C-O st).

N_3-[MPA,G2]-$(OH)_4$

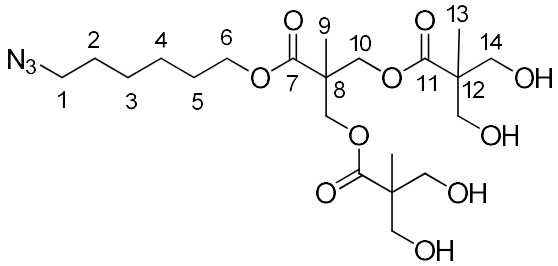

General procedure II. N_3-[MPA,G1]-$(acetal)_2$ (8.50 g, 14.87 mmol, 1.00 eq.), ion exchange resin Dowex H^+ (4.25 g, 50 % mass equivalent), MeOH (120 mL). Time of reaction: 20 hours. The product was obtained as a white solid (7.27 g, quantitative yield). ^{1}H NMR (400 MHz, $CDCl_3$) δ (ppm): 4.37 (ABq, *J* = 11.1 Hz, $\Delta\nu_{AB}$ = 15.1 Hz, 4H, H-10), 4.15 (t, *J* = 6.6 Hz, 2H, H-6), 3.72 (ABq, *J* = 11.4 Hz, $\Delta\nu_{AB}$ = 26.7 Hz, 8H, H-14), 3.28 (t, *J* = 6.8 Hz, 2H, H-1), 1.67 (m, 2H, H-5), 1.61 (m, 2H, H-2), 1.40 (m, 4H, H-3 and H-4), 1.31 (s, 3H, H-9), 1.05 (s, 6H, H-13). ^{13}C NMR (100 MHz, $CDCl_3$) δ (ppm): 175.1, 173.0, 67.9, 65.4, 64.8, 51.3, 49.7, 46.3, 28.7, 28.4, 26.3, 25.4, 18.1, 17.1. MS (ESI^+) *m/z (%):* found *514.3 (100)*, calculated for $[C_{21}H_{37}N_3O_{10},Na]^+$ *514.3*. FTIR (ν_{max}/cm^{-1}, ATR): 3286 (O-H st), 2980-2937 (C-H st), 2096 (N_3 st), 1730 (C=O st), 1462 (CH_2, CH_3 δ), 1238 (CO-O st), 1119 (C-O st).

N_3-[MPA,G3]-$(acetal)_4$

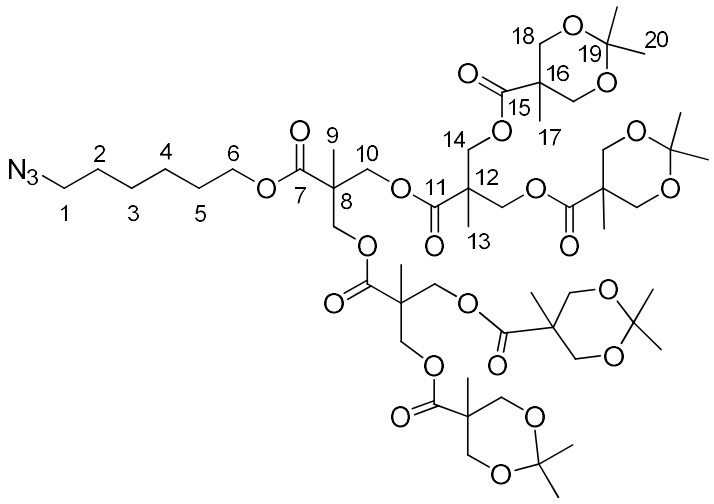

General procedure I. N_3-[MPA,G2]-$(OH)_4$ (3.12 g, 6.35 mmol, 1.00 eq.), *bis*-MPA acetal (6.63 g, 38.07 mmol, 6.00 eq.), DPTS (2.99 g, 10.15 mol, 1.60 eq.), DCC (7.86 g, 38.07 mmol, 6.00 eq.), dry DCM (120 mL). Time of reaction: 3 days. The crude product was purified twice on silica gel (firstly, hexane:ethyl acetate = 7:3 and finally, hexane:ethyl acetate = ramp from 7:3 to 5:5) to give a colourless gel (5.32 g, 75 %). ^{1}H NMR (400 MHz, $CDCl_3$) δ (ppm): 4.28 (m, 12H, H-10 and H-14), 4.13 (d, *J* = 12.9 Hz, 8H, H-18'), 4.10 (t, *J* = 7.2 Hz, 2H, H-6), 3.61 (d, *J* = 12.6 Hz, 8H, H-18), 3.27 (t, *J* = 6.8 Hz, 2H, H-1), 1.65 (m, 2H, H-5), 1.60 (m, 2H, H-2), 1.40 (m, 16H, H-3, H-4 and H-20'), 1.34 (s, 12H, H-20), 1.26 (s, 6H, H-13), 1.25 (s, 3H, H-9), 1.13 (s, 12H, H-17). ^{13}C NMR (100 MHz, $CDCl_3$) δ (ppm): 173.5, 172.1, 171.8, 98.1, 66.0, 65.9, 65.4, 64.9, 51.3, 46.8, 46.6, 42.0, 28.7, 28.4, 26.3, 25.4, 25.1, 22.1, 18.5, 17.7, 17.1. MS (ESI^+) *m/z (%):* found *1138.6 (100)* and *580.8 (16)*, calculated for $[C_{53}H_{85}N_3O_{22},Na]^+$ *1138.6.* FTIR (ν_{max}/cm^{-1}, ATR): 2989-2941-2874 (C-H st), 2096 (N_3 st), 1734 (C=O st), 1456 (CH_2, CH_3 δ), 1240 (CO-O st), 1130 (C-O st).

N_3-[MPA,G3]-$(OH)_8$

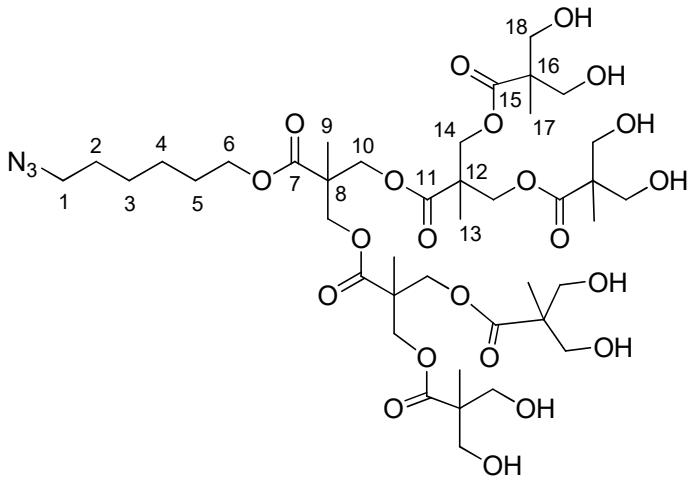

General procedure II. N_3-[MPA,G3]-$(acetal)_4$ (5.26 g, 4.71 mmol, 1.00 eq.), ion exchange resin Dowex H^+ (2.67 g, 50 % mass equivalent), MeOH (100 mL). Time of reaction: 24 hours. The product was obtained as a white solid (4.13 g, 92 %). ^{1}H NMR (400 MHz, CD_3OD) δ (ppm): 4.29 (m, 12H, H-10 and H-14), 4.17 (t, *J* = 6.6 Hz, 2H, H-6), 3.64 (ABq, *J* = 10.8 Hz, $\Delta\nu_{AB}$ = 42.4 Hz, 16H, H-18), 3.31 (t, *J* = 6.8 Hz, H-1)*, 1.70 (m, 2H, H-5), 1.62 (m, 2H, H-2), 1.44 (m, 4H, H-3 and H-4), 1.30 (s, 3H, H-9), 1.29 (s, 6H, H-13), 1.15 (s, 12H, H-17). *H-1 signal in ^{1}H NMR is overlapped with the solvent signal, but the correlation between H-1 and H-2 was checked in ^{1}H-^{1}H COSY and the ^{1}H NMR in $CDCl_3$ allowed to measure the multiplicity and the *J* of the signal. ^{13}C NMR (100 MHz, CD_3OD) δ (ppm): 175.9, 174.0, 173.7, 67.3, 66.6, 66.2, 65.8, 52.4, 51.8, 47.9, 29.8, 29.5, 27.4, 26.6, 18.3, 18.1, 17.3. MS (ESI^+) *m/z (%):* found *978.5 (100)*, calculated for $[C_{41}H_{69}N_3O_{22},Na]^+$ *978.4*. FTIR (ν_{max}/cm^{-1}, ATR): 3283 (O-H st), 2978-2939-2883 (C-H st), 2104 (N_3 st), 1732 (C=O st), 1473 (CH_2, CH_3 δ), 1234 (CO-O st), 1130 (C-O st).

N_3-[MPA,G2]-$(NHBoc)_4$

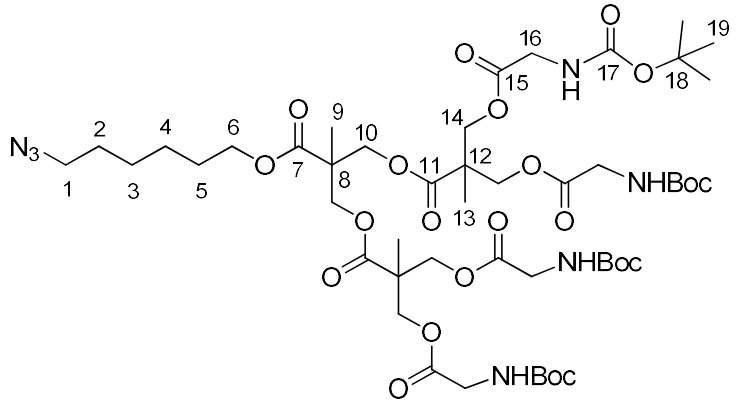

General procedure III. N_3-[MPA,G2]-$(OH)_4$ (5.00 g, 10.17 mmol, 1.00 eq.), Glyboc(OH) (8.91 g, 50.86 mmol, 5.00 eq.), DMAP (1.99 g, 16.28 mmol, 1.60 eq.), DCC (10.49 g, 50.86 mmol, 5.00 eq.), dry DCM (300 mL). Time of reaction: 24 hours. The crude product was purified twice on silica gel (firstly, hexane:ethyl acetate = ramp from 7:3 to 5:5 and finally, hexane:ethyl acetate = 6:4) to get a colourless solid (9.72 g, 85 %). ^{1}H NMR (400 MHz, $CDCl_3$) δ (ppm): 5.25 (bs, -NH), 4.25 (m, 12H, H-10 and H-14), 4.11 (t, *J* = 6.7 Hz, 2H, H-6), 3.88 (d, *J* = 5.8 Hz, 8H, H-16), 3.27 (t, *J* = 6.8 Hz, 2H, H-1), 1.66 (m, 2H, H-5), 1.60 (m, 2H, H-2), 1.43 (m, 40H, H-3, H-4 and H-19), 1.24 (s, 3H, H-9), 1.23 (s, 6H, H-13). ^{13}C NMR (100 MHz, $CDCl_3$) δ (ppm): 172.2-171.8, 170.0, 155.6, 79.9, 65.7-65.5, 51.5, 46.6, 46.4, 42.2, 28.7, 28.3, 26.4, 25.4, 17.9, 17.7. MS (MALDI$^+$) *m/z (%):* found *1142.4 (100)*, calculated for $[C_{49}H_{81}N_7O_{22},Na]^+$ *1142.5*. FTIR (ν_{max}/cm^{-1}, ATR): 3379 (N-H st), 2976-2935 (C-H st), 2098 (N_3 st), 1738 (C=O st ester), 1703 (C=O st carbamate), 1514 (N-H δ), 1462 (CH_2, CH_3 δ), 1242 (CO-O st), 1153 (NCO-O st), 1132 (C-O st). SEC (*ref PMMA*): Mw 1070 g·mol^{-1}; Đ (dispersity) 1.01.

N_3-[MPA,G3]-$(NHBoc)_8$

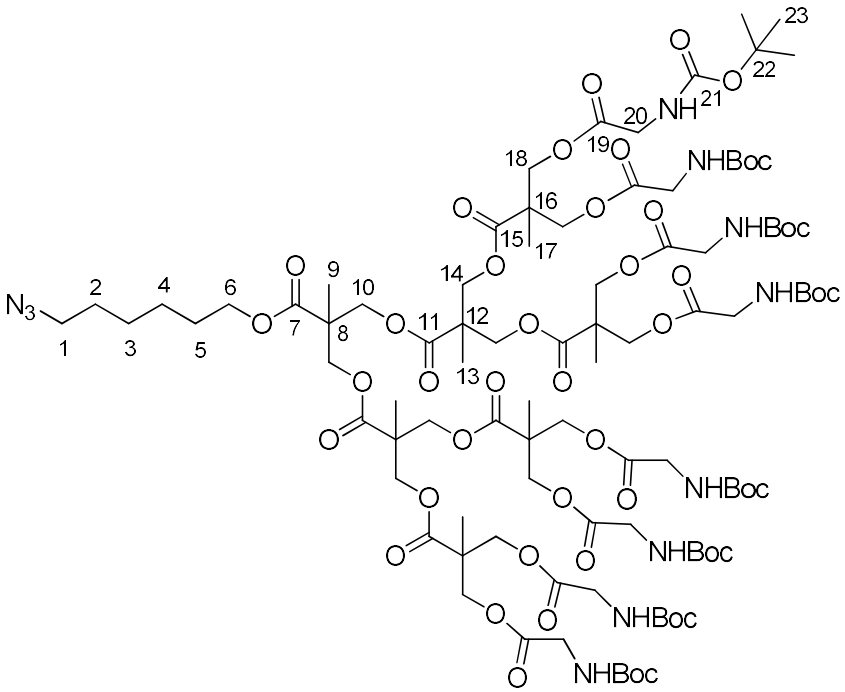

General procedure III. N_3-[MPA,G3]-$(OH)_8$ (3.59 g, 3.75 mmol, 1.00 eq.), Glyboc(OH) (6.58 g, 37.56 mmol, 10.00 eq.), DMAP (1.47 g, 12.02 mmol, 3.20 eq.), DCC (7.75 g, 37.56 mmol, 10.00 eq.), dry DCM (100 mL). Time of reaction: 48 hours. The crude product was purified twice on silica gel (hexane:ethyl acetate = ramp from 7:3 to 4:6) to get a light-yellow solid (2.07 g, 25 %). ^{1}H NMR (400 MHz, $CDCl_3$) δ (ppm): 5.33 (bs, -NH), 4.26 (m, 28H, H-10, H-14 and H-18), 4.12 (t, *J* = 7.1 Hz, 2H, H-6), 3.88 (d, *J* = 5.6 Hz, 16H, H-20), 3.29 (t, *J* = 6.8 Hz, 2H, H-1), 1.67 (m, 2H, H-5), 1.61 (m, 2H, H-2), 1.44 (s, 72H, H-23), 1.40 (m, 4H, H-3 and H-4), 1.28 (s, 3H, H-9), 1.26 (s, 6H, H-13), 1.24 (s, 12H, H-17). ^{13}C NMR (100 MHz, $CDCl_3$) δ (ppm): 171.9, 170.1, 155.9, 80.0, 65.7-64.8, 51.3, 46.7-46.4, 42.2, 28.7, 28.3, 26.3, 25.4, 17.9-17.5. MS (MALDI$^+$) *m/z (%):* found *2236.3 (86)*, calculated for $[C_{97}H_{157}N_{11}O_{46},Na]^+$ *2235.0*. FTIR (ν_{max}/cm^{-1}, ATR): 3356 (N-H st), 2980-2935 (C-H st), 2102 (N_3 st), 1738 (C=O st ester), 1695 (C=O st carbamate), 1508 (N-H δ), 1458 (CH_2, CH_3 δ), 1367 (C-N st), 1240 (CO-O st), 1151 (NCO-O st), 1126 (C-O st). SEC (*ref PMMA*): Mw 2877 g·mol^{-1}; Đ 1.04.

≡-[MPA,G1]-(acetal)$_1$

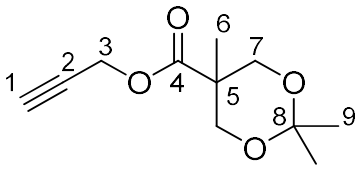

General procedure I. Propargyl alcohol (2.54 mL, 43.54 mmol, 1.05 eq.), *bis*-MPA acetal (7.81 g, 41.47 mmol, 1.00 eq.), DPTS (4.88 g, 16.59 mmol, 0.40 eq.), DCC (8.98 g, 43.54 mmol, 1.05 eq.), dry DCM (80 mL). Time of reaction: 24 hours. The crude product was purified on silica gel (hexane:ethyl acetate = 8:2) to give a light-yellow oil (6.14 g, 70 %). ^{1}H NMR (400 MHz, $CDCl_3$) δ (ppm): 4.70 (d, *J* = 2.5 Hz, 2H, H-3), 4.16 (d, *J* = 11.9 Hz, 2H, H-7), 3.62 (d, *J* = 11.9 Hz, 2H, H-7´), 2.45 (t, *J* = 2.5 Hz, 1H, H-1), 1.39 (s, 3H, H-9), 1.35 (s, 3H, H-9´), 1.17 (s, 3H, H-6). ^{13}C NMR (100 MHz, $CDCl_3$) δ (ppm): 173.5, 98.1, 77.4, 75.0, 65.9, 52.5, 41.8, 24.5, 22.7, 18.5. MS (ESI$^+$) *m/z* (%): found *235.0 (25),* calculated for $[C_{11}H_{16}O_4,Na]^+$ *235.1*. FTIR (ν_{max}/cm^{-1}, ATR): 3267 (≡C-H st), 2945 (C-H st), 2127 (C≡C st), 1724 (C=O st), 1429 (CH_2, CH_3 δ).

≡-[MPA,G1]-(OH)$_2$

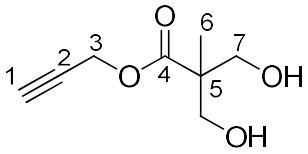

General procedure II. ≡-[MPA,G1]-(acetal)$_1$ (5.54 g, 26.11 mmol, 1.00 eq.), Dowex resin H$^+$ (2.93 g, 50% mass equivalent), MeOH (80 mL). Time of reaction: 5 hours. The product was obtained as a light-yellow oil (4.52 g, quantitative yield). ^{1}H NMR (400 MHz, $CDCl_3$) δ (ppm): 4.75 (d, *J* = 2.5 Hz, 2H, H-3), 3.91 (d, *J* = 11.3 Hz, 2H, H-7), 3.72 (d, *J* = 11.3 Hz, 2H, H-7´), 2.79 (bs, 2H, -OH), 2.49 (t, *J* = 2.5 Hz, 1H, H-1), 1.09 (s, 3H, H-6). ^{13}C NMR (100 MHz, $CDCl_3$) δ (ppm): 175.2, 77.4, 75.4, 68.0, 52.6, 49.5, 17.1. MS (ESI$^+$) *m/z (%)*: found *194.9 (100)*, calculated for $[C_8H_{12}O_4,Na]^+$ *195.1*. FTIR (ν_{max}/cm^{-1}, ATR): 3292 (O-H st), 2943 (C-H st), 2127 (C≡C st), 1730 (C=O st), 1462 (CH_2, CH_3 δ).

≡-[MPA,G2]-(acetal)$_2$

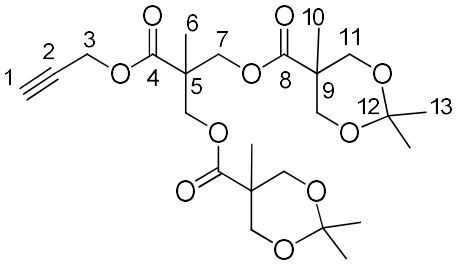

General procedure I. ≡-[MPA,G1]-(OH)$_2$ (6.87 g, 38.70 mmol, 1.00 eq.), *bis*-MPA acetal (15.30 g, 81.30 mmol, 2.10 eq.), DPTS (9.11 g, 30.70 mmol, 0.80 eq.), DCC (16.77 g, 81.30 mmol, 2.10 eq.), dry DCM (200 mL). Time of reaction: overnight. The crude product was purified on silica gel (hexane:ethyl acetate = 7:3) to obtain a white powder (18.57 g, 99 %). ^{1}H NMR (400 MHz, $CDCl_3$) δ (ppm): 4.72 (d, *J* = 2.4 Hz, 2H, H-3), 4.33 (s, 4H, H-7), 4.16 (d, *J* = 12.0 Hz, 4H, H-11'), 3.62 (d, *J* = 12.3 Hz, 4H, H-11), 2.47 (t, *J* = 2.4 Hz, 1H, H-1), 1.41 (s, 6H, H-13'), 1.39 (s, 6H, H-13), 1.20 (s, 3H, H-6), 1.16 (s, 6H, H-10). ^{13}C NMR (100 MHz, $CDCl_3$) δ (ppm): 173.5, 171.8, 98.1, 77.2, 75.2, 65.9, 65.2, 52.6, 46.8, 42.0, 24.9, 22.2, 18.5, 17.6. MS (MALDI$^+$) *m/z (%)*: found *507.2 (100),* calculated for $[C_{24}H_{36}O_{10},Na]^+$ *507.2*. FTIR (ν_{max}/cm^{-1}, ATR): 3249 (≡C-H st), 2923 (C-H st), 2121 (C≡C st), 1733 (C=O st), 1458 (CH_2, CH_3 δ).

≡-[MPA,G2]-(OH)$_4$

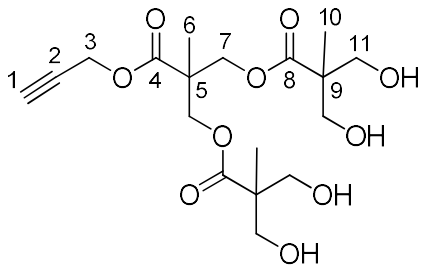

General procedure II. ≡-[MPA,G2]-(acetal)$_2$ (17.17 g, 35.44 mmol, 1.00 eq.) Dowex resin H$^+$ (8.59 g, 50 % mass equivalent), MeOH (200 mL). Time of reaction: 10 hours. The product was obtained as a white powder (13.03 g, 91 %). ^{1}H NMR (400 MHz, CD_3OD) δ (ppm): 4.76 (d, *J* = 2.4 Hz, 2H, H-3), 4.29 (ABq, *J* = 10.8 Hz, $\Delta\nu_{AB}$ = 9.8 Hz, 4H, H-7), 3.64 (ABq, *J* = 11.2 Hz, $\Delta\nu_{AB}$ = 25.3 Hz, 8H, H-11), 2.96 (t, *J* = 2.4 Hz, 1H, H-1), 1.31 (s, 3H, H-6), 1.15 (s, 6H, H-10). ^{13}C NMR (100 MHz, CD_3OD) δ (ppm): 175.9, 173.7, 78.6, 76.7, 66.4, 65.8, 51.8, 47.9, 40.5, 18.1, 17.3. MS (MALDI$^+$) *m/z (%)*: found *427.2 (100),* calculated for

$[C_{18}H_{28}O_{10},Na]^+$ *427.2*. FTIR (ν_{max}/cm^{-1}, ATR): 3403 (O-H st), 2923 (C-H st), 2125 (C≡C st), 1732 (C=O st), 1461 (CH_2, CH_3 δ).

≡-[MPA,G1]-(C17)$_2$

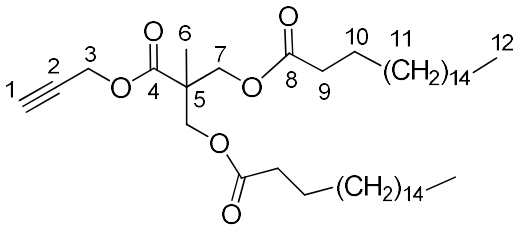

General procedure IV. ≡-[MPA,G1]-(OH)$_2$ (3.00 g, 17.49 mmol, 1.00 eq.), stearic acid (14.93 g, 52.47 mmol, 3.00 eq.), DMAP (1.71 g, 13.99 mmol, 0.80 eq.), DCC (10.83 g, 52.47 mmol, 4.00 eq.), dry DCM (150 mL). Time of reaction: 2 days. The product was obtained as a white powder (7.73 g, 63%). ^{1}H NMR (400 MHz, $CDCl_3$) δ (ppm): 4.71 (d, *J* = 2.1 Hz, 2H, H-3), 4.23 (ABq, *J* = 11.4 Hz, $\Delta\nu_{AB}$ = 6.0 Hz, 4H, H-7), 2.45 (t, *J* = 2.1 Hz, 1H, H-1), 2.30 (t, *J* = 7.5 Hz, 4H, H-9), 1.59 (m, 4H, H-10), 1.25 (m, 59H, H-6 and H-11), 0.88 (t, *J* = 6.3 Hz, 6H, H-12). ^{13}C NMR (100 MHz, $CDCl_3$) δ (ppm): 173.2, 172.1, 77.2, 75.1, 65.1, 52.5, 46.4, 34.1, 31.9, 29.7-29.1, 24.9, 22.7, 17.7, 14.1. MS (MALDI$^+$) *m/z (%)*: found *727.6 (100),* calculated for $[C_{44}H_{80}O_6,Na]^+$ *727.6*. FTIR (ν_{max}/cm^{-1}, ATR): 3294 (≡C-H st), 2916 (C-H st), 2129 (C≡C st), 1734 (C=O st), 1473 (CH_2, CH_3 δ), 1250 (CO-O st), 1132 (C-O st). SEC (*ref PMMA*): Mw 1408 g·mol^{-1}; Đ 1.06.

≡-[MPA,G2]-(C17)$_4$

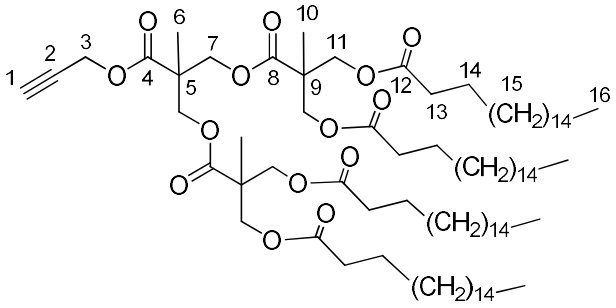

General procedure IV. ≡-[MPA,G2]-(OH)$_4$ (1.50 g, 3.71 mmol, 1.00 eq.), stearic acid (6.33 g, 22.26 mmol, 6.00 eq.), DMAP (7.25 g, 5.94 mmol, 1.60 eq.), DCC (4.59 g, 22.27 mmol, 6.00 eq.), dry DCM (100 mL). Time of reaction: 7 days. The product was obtained as a white powder (3.67 g, 67 %). ^{1}H NMR (400 MHz,

$CDCl_3$) δ (ppm): 4.72 (d, *J* = 2.4 Hz, H-3), 4.26 (ABq, *J* = 8.1 Hz, $\Delta\nu_{AB}$ = 12.0 Hz, H-7), 4.19 (ABq, *J* = 10.5 Hz, $\Delta\nu_{AB}$ = 6.8 Hz, 8H, H-11), 2.50 (t, *J* = 2.4 Hz, 1H, H-1), 2.29 (t, *J* = 7.5 Hz, 8H, H-13), 1.58 (m, 8H, H-14), 1.25 (m, 121H, H-6, H-10 and H-15), 0.88 (t, *J* = 6.6 Hz, 12H, H-16). ^{13}C NMR (100 MHz, $CDCl_3$) δ (ppm): 173.1, 172.0, 171.4, 77.1, 75.4, 65.6, 65.0, 52.8, 46.7, 46.4, 34.0, 31.9, 29.7-29.1, 24.8, 22.7, 17.8, 17.4, 14.1. MS (MALDI$^+$) *m/z (%)*: found *1492.4 (100)*, calculated for $[C_{90}H_{164}O_{14},Na]^+$ *1492.2*. FTIR (ν_{max}/cm^{-1}, ATR): 3292 (≡C-H st), 2916 (C-H st), 2141 (C≡C st), 1736 (C=O st), 1472 (CH_2, CH_3 δ), 1236 (CO-O st), 1119 (C-O st). SEC (*ref PMMA*): Mw 2783 g·mol^{-1}; Đ 1.04.

7.1.2.2. *bis*-GMPA dendrons

General procedure V: esterification coupling for the growing of the *bis*-GMPA dendrons

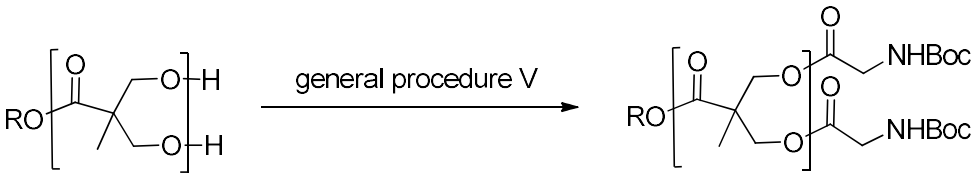

The hydroxy terminated dendron (1.00 mol) was dissolved into dry DCM, together with Glyboc(OH) (1.25 mol per hydroxyl groups) and DPTS (0.40 mol per hydroxyl groups). This mixture was stirred under argon atmosphere and cooled down to 0 °C. A solution of DCC (1.25 mol per hydroxyl groups) in dry DCM was added dropwise. The reaction mixture was then allowed to stir under argon atmosphere for 1-4 days at room temperature. The white precipitate appeared, DCU, was removed by filtration and the solvent was evaporated under vacuum. A mixture of hexane and ethyl acetate (4:1) was added to provoke further precipitation of the DCU, which was newly filtered off. The solvent was evaporated under reduced pressure and the crude product was purified through silica gel column chromatography with mixtures of hexane:ethyl acetate at different ratios depending on the dendron.

General procedure VI: deprotection of terminal amino groups

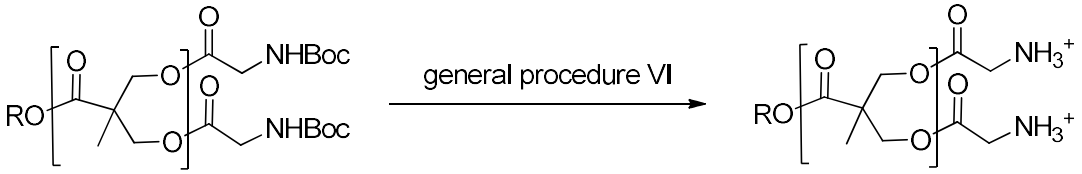

The *t*-Boc protective groups were removed under mild-acidic conditions. The *t*-Boc protected dendron (1.00 mol) was dissolved in a mixture of chloroform ($CHCl_3$) and trifluoroacetic acid (TFA), 1:1 in volume, and the reaction occurred after 3-3.5 hours at room temperature. After that, the solvent and the excess of TFA were removed under vacuum. The product was then dissolved in the minimal amount of methanol and precipitated into cold ether. The precipitate was finally recovered by centrifugation for 5 min at 4000 rpm.

General procedure VII: amide coupling for the growing of the *bis*-GMPA dendrons

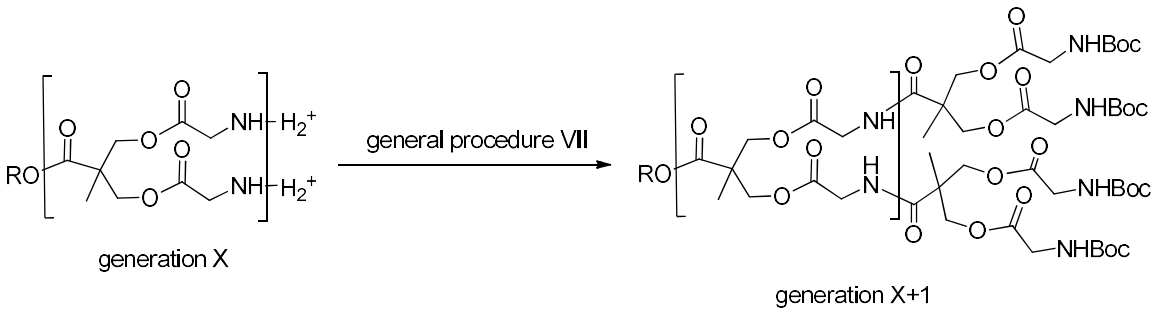

The amino terminated dendron (1.00 mol) was dissolved into a mixture of dry DMF and dry DCM. *bis*-GMPA monomer (1.10 or 1.50 mol per amino groups according to the dendron generation), HOBt·nH_2O (1.10 or 1.50 mol per amino groups according to the dendron generation) and DMAP (1.40 mol per amino groups) were added, and the reaction mixture was stirred under argon atmosphere and cooled down to 0 ºC. A solution of DCC (1.10 or 1.50 mol per amino groups according to the dendron generation) in dry DCM was added dropwise to the reaction mixture and it was stirred under argon atmosphere at room temperature for 3-5 days. The white precipitated DCU was filtered off and the solvent was evaporated under vacuum. A mixture of hexane and ethyl acetate was added to provoke the precipitation of remaining DCU and HOBt, which were filtered off. The organic phase was washed three times with brine, dried over anhydrous $MgSO_4$ and the solvent was evaporated. Remaining HOBt was precipitated into cold ethyl acetate, filtered off and the solvent was evaporated under reduced pressure. Finally, the crude product was purified through silica gel column chromatography with mixtures of hexane:ethyl acetate or DCM:MeOH as eluent, depending on the dendron generation.

General procedure VIII: functionalisation of *bis*-GMPA dendrons with stearic acid chains

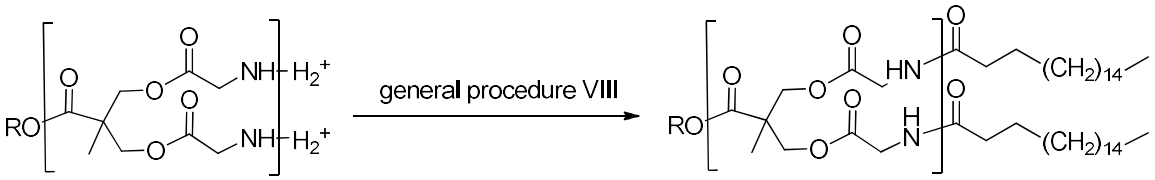

Stearic acid (1.50 mol per amino groups), DMAP (0.40 mol per amino group), HOBt·nH_2O (1.50 mol per amino groups) and DCC (1.50 mol per amino groups) were dissolved into dry DCM. The amino terminated dendron (1.00 mol) and an excess of DMAP (1.00 mol per amino groups) were dissolved in anhydrous DMSO and added dropwise to the reaction mixture. The final reaction mixture was stirred at room temperature under argon atmosphere for 48 hours. The white precipitate appeared, DCU, was filtered off and the solvent was evaporated under vacuum. The crude product was dissolved into the minimal volume of DCM and purified by precipitation into cold acetone overnight. The precipitate was further purified through silica gel column chromatography with mixtures of DCM:MeOH under the conditions specified in the description of each compound.

BnOOC-[MPA,G1]-$(OH)_2$

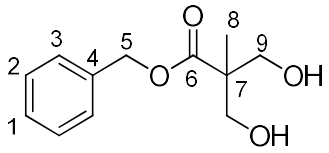

Bis-MPA (20.00 g, 149.14 mmol, 1.00 eq.) and KOH (10.20 g, 178.97 mmol, 1.20 eq.) were dissolved in DMF (100 mL). The reaction mixture was stirred at 100 ºC for 1 hour and then, BnBr (26.55 mL, 223.71 mmol, 1.50 eq.) was added dropwise. The reaction mixture was stirred at 100 ºC overnight. The white precipitate appeared was filtered off. Water (450 mL) was added, and the product was extracted three times with ethyl acetate (3 x 200 mL). The organic phases were collected and washed three times with brine (3 x 150 mL) to give a yellow oil. The crude product was purified by recrystallisation into toluene to yield white crystals (17.64 g, 53 %). ^{1}H NMR (400 MHz, $CDCl_3$) δ (ppm): 7.36 (m, 5H, H-1, H-2 and H-3), 5.21 (s, 2H, H-5), 3.93 (dd, *J* = 11.3 Hz, *J* = 7.2 Hz, 2H, H-9'), 3.73

(dd, *J* = 11.3 Hz, *J* = 6.9 Hz, 2H, H-9), 2.86 (bs, -OH), 1.08 (s, 3H, H-8). ^{13}C NMR (100 MHz, $CDCl_3$) δ (ppm): 175.9, 135.8, 128.8, 128.5, 128.0, 68.7, 66.9, 49.4, 17.2. MS (ESI^+) *m/z* (%): found *247.1 (100),* calculated for $[C_{12}H_{16}O_4,Na]^+$ *247.1*. FTIR (v_{max}/cm^{-1}, ATR): 3358 (O-H st), 2943-2885 (C-H st and C-H_{ar} st), 1703 (C=O st).

BnOOC-[MPA,G1]-$(NHBoc)_2$

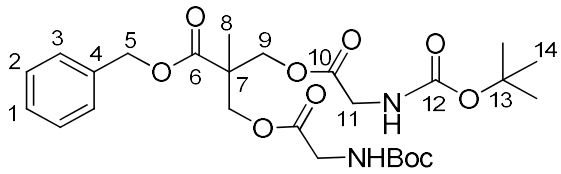

General procedure V. BnOOC-[MPA,G1]-$(OH)_2$ (10.86 g, 48.42 mmol, 1.00 eq.), Glyboc(OH) (21.25 g, 121.04 mmol, 2.50 eq.), DPTS (11.46 g, 38.74 mmol, 0.80 eq.), DCC (24.98 g, 121.04 mmol, 2.50 eq.), dry DCM (300 mL). Time of reaction: overnight. The crude powder was purified on silica gel (hexane:ethyl acetate = 8:2) to get a colourless oil (24.11 g, 92 %). ^{1}H NMR (400 MHz, $CDCl_3$) δ (ppm): 7.41-7.29 (m, 5H, H-1, H-2 and H-3), 5.16 (s, 2H, H-5), 4.98 (bs, -NH), 4.31 (ABq, *J* = 10.4 Hz, Δv_{AB} = 37.4 Hz, 4H, H-9), 3.79 (d, *J* = 3.8 Hz, 4H, H-11), 1.44 (s, 18H, H-14), 1.26 (s, 3H, H-8). ^{13}C NMR (100 MHz, $CDCl_3$) δ (ppm): 172.2, 169.9, 155.6, 135.4, 128.6, 128.5, 128.3, 80.0, 67.0, 65.8, 46.3, 42.2, 28.3, 17.9. MS (ESI^+) *m/z* (%): found *561.3 (100),* calculated for $[C_{26}H_{38}N_2O_{10},Na]^+$ *561.3*. FTIR (v_{max}/cm^{-1}, ATR): 3375 (N-H st), 2972-2932 (C-H st and C-H_{ar} st), 1724 (C=O st ester), 1711 (C=O st carbamate), 1518 (N-H δ), 1456 (CH_2, CH_3 δ), 1367 (C-N st), 1254 (CO-O st), 1153 (NCO-O st), 1134 (C-O st).

***t*-Boc protected *bis*-GMPA monomer**

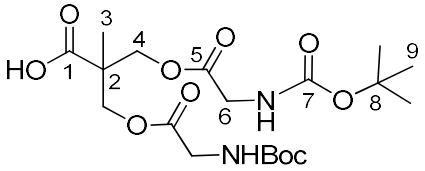

$BnOOC-[MPA,G1]-(NHBoc)_2$ (15.05 g, 27.95 mmol, 1.00 eq.) was dissolved into ethyl acetate (150 mL) under argon atmosphere by making several cycles argon-vacuum. Pd/C (785 mg, 0.05 eq. in weight) was carefully added to the reaction

mixture and the atmosphere was replaced by H_2. Firstly, three cycles argon-vacuum were made and then, three cycles vacuum-H_2. The reaction mixture was stirred overnight under H_2 pressure. Then, it was filtered through celite© with ethyl acetate as eluent. The solvent was evaporated under reduced pressure and the product was obtained as a colourless gel (10.59 g, 85 %). ^{1}H NMR (400 MHz, $CDCl_3$) δ (ppm): 5.22 (bs, -NH), 4.31 (ABq, *J* = 11.2 Hz, $\Delta\nu_{AB}$ = 39.8 Hz, 4H, H-4), 3.90 (d, *J* = 5.4 Hz, 4H, H-6), 1.44 (s, 18H, H-9), 1.28 (s, 3H, H-3). ^{13}C NMR (100 MHz, $CDCl_3$) δ (ppm): 176.0, 170.1, 155.9, 80.2, 65.8, 45.9, 42.3, 28.3, 17.8. MS (ESI^+) *m/z* (%): found *471.2 (100),* calculated for $[C_{19}H_{32}N_2O_{10},Na]^+$ *471.2*. FTIR (ν_{max}/cm^{-1}, ATR): 3362 (N-H st), 2980-2939 (C-H st), 1738 (C=O st ester), 1697 (C=O st carbamate), 1516 (N-H δ), 1456 (CH_2, CH_3 δ), 1367 (C-N st), 1240 (CO-O st), 1157 (NCO-O st), 1057 (C-O st).

N_3-[GMPA,G1]-$(NHBoc)_2$

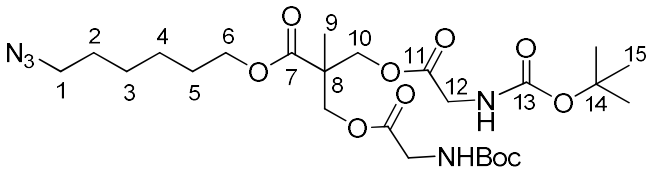

General procedure V. N_3-[MPA,G1]-$(OH)_2$ (7.99 g, 30.82 mmol, 1.00 eq.), Glyboc(OH) (13.50 g, 77.05 mmol, 2.50 eq.), DPTS (7.26 g, 24.66 mmol, 0.80 eq.), DCC (15.90 g, 77.05 mmol, 2.50 eq.), dry DCM (225 mL). Time of reaction: 3 days. The crude product was purified on silica gel (hexane:ethyl acetate = ramp from 8:2 to 7:3) to give a colourless waxy oil (13.58 g, 77 %). ^{1}H NMR (400 MHz, $CDCl_3$) δ (ppm): 5.08 (bs, -NH), 4.30 (ABq, *J* = 11.1 Hz, $\Delta\nu_{AB}$ = 42.1 Hz, 4H, H-10), 4.12 (t, *J* = 6.5 Hz, 2H, H-6), 3.88 (d, *J* = 5.7 Hz, 4H, H-12), 3.27 (t, *J* = 6.8 Hz, 2H, H-1), 1.64 (m, 2H, H-5), 1.60 (m, 2H, H-2), 1.44 (s, 18H, H-15), 1.38 (m, 4H, H-3 and H-4), 1.24 (s, 3H, H-9). ^{13}C NMR (100 MHz, $CDCl_3$) δ (ppm): 171.1, 170.0, 155.7, 80.0, 65.7, 65.2, 51.3, 46.2, 42.2, 28.7, 28.3, 26.3, 25.4, 18.0. MS (ESI^+) *m/z* (%): found *596.2 (84)*, calculated for $[C_{25}H_{43}N_5O_{10},Na]^+$ *596.3*. FTIR (ν_{max}/cm^{-1}, ATR): 3410-3342 (N-H st), 2982-2945-2870 (C-H st), 2093 (N_3 st), 1761 and 1757 (C=O st ester), 1722 and 1688 (C=O st carbamate), 1537-1508 (N-H δ), 1472 (CH_2, CH_3 δ), 1367 (C-N st), 1288 (CO-O st), 1159 (NCO-O st), 1130 (C-O st).

N_3-[GMPA,G1]-$(NH_3^+)_2$

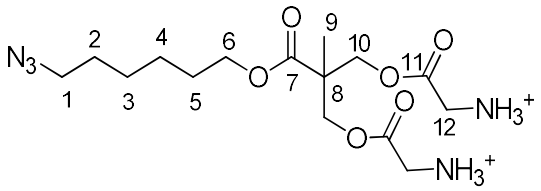

General procedure VI. N_3-[GMPA,G1]-$(NHBoc)_2$ (13.17 g, 22.96 mmol, 1.00 eq.), $CHCl_3$:TFA (1:1) (30 mL). Time of reaction: 3 hours. A dark amber oil was obtained (6.98 g, 51 %). ^{1}H NMR (400 MHz, $(CD_3)_2SO$) δ (ppm): 8.39 (bs, -NH), 4.33 (ABq, *J* = 10.9 Hz, $\Delta\nu_{AB}$ = 25.9 Hz, 4H, H-10), 4.08 (t, *J* = 6.5 Hz, 2H, H-6), 3.84 (s, 4H, H-12), 3.32 (t, *J* = 6.8 Hz, 2H, H-1), 1.57 (m, 2H, H-5), 1.54 (m, 2H, H-2), 1.33 (m, 4H, H-3 and H-4), 1.22 (s, 3H, H-9). ^{13}C NMR (100 MHz, $(CD_3)_2SO$) δ (ppm): 172.4, 165.3, 162.9 (q, $^1J_{FC}$ = 34.5 Hz), 118.1 (q, $^2J_{CF}$ = 292.6 Hz), 67.7, 66.7, 52.1, 47.1, 40.9, 29.6, 29.2, 27.4, 26.4, 17.9. MS (ESI^+) *m/z* (%): found *374.2 (86)*, calculated for $[C_{15}H_{27}N_5O_6,H]^+$ *374.2*. FTIR (ν_{max}/cm^{-1}, ATR): 3435-2650 (N-H^+), 2939-2867-2754-2652 (C-H st), 2098 (N_3 st), 1739 (C=O st ester), 1641-1526 (N-H^+ δ), 1460 (CH_2, CH_3 δ), 1439 (C-N st), 1243 (CO-O st), 1176 (C-O st).

N_3-[GMPA,G2]-$(NHBoc)_4$

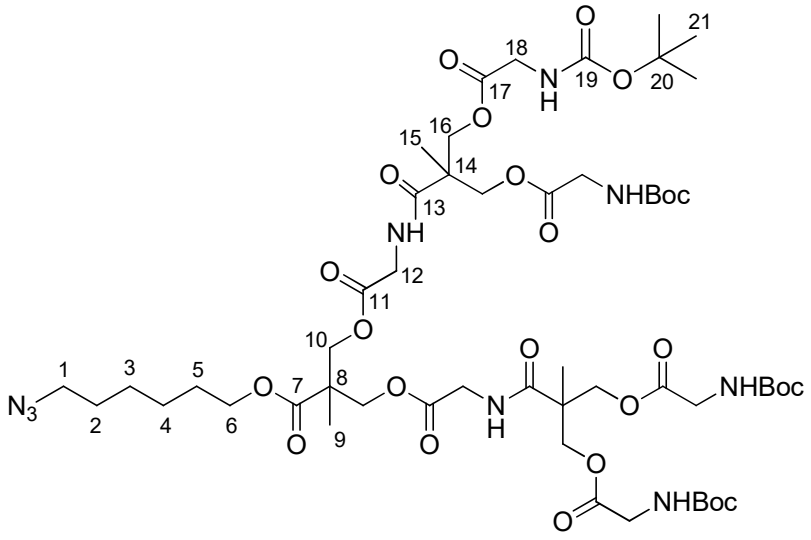

General procedure VII. N_3-[GMPA,G1]-$(NH_3^+)_2$ (3.29 g, 5.47 mmol, 1.00 eq.), *bis*-GMPA monomer (5.39 g, 12.03 mmol, 2.20 eq.), HOBt·H_2O (1.63 g, 12.03 mmol, 2.20 eq.), DMAP (1.87 g, 15.31 mmol, 2.80 eq.), DCC (2.48 g, 12.03 mmol, 2.20 eq.), dry DMF (20 mL), dry DCM (95 mL). Time of reaction: 3 days.

The crude product was purified on silica gel (hexane:ethyl acetate = ramp from 1:1 to 1:9) to obtain a yellow oil (2.68 g, 40 %). ^{1}H NMR (400 MHz, $CDCl_3$) δ (ppm): 7.09 (bs, -NHCO), 5.27 (bs, -NHBoc), 4.40-4.20 (m, 10H, H-10' and H-16), 4.17 (m, 2H, H-10), 4.14 (t, *J* = 6.4 Hz, 2H, H-6), 3.97 (d, *J* = 5.2 Hz, 4H, H-12), 3.91 (s, 8H, H-18), 3.27 (t, *J* = 6.8 Hz, 2H, H-1), 1.66 (m, 2H, H-5), 1.61 (m, 2H, H-2), 1.43 (s, 36H, H-21), 1.39 (m, 4H, H-3 and H-4), 1.28 (s, 6H, H-15), 1.26 (s, 3H, H-9). ^{13}C NMR (100 MHz, $CDCl_3$) δ (ppm): 172.9, 172.5, 170.6, 169.8, 156.0, 80.2, 66.7, 65.3, 65.0, 51.3, 46.4, 46.1, 42.4, 40.9, 28.8, 28.5, 26.5, 25.6, 18.1, 17.9. MS (MALDI$^+$) *m/z* (%): found *1256.6 (17)*, calculated for $[C_{53}H_{87}N_9O_{24},Na]^+$ *1256.6*. FTIR (ν_{max}/cm^{-1}, ATR): 3360 (N-H st), 2978-2939-2864 (C-H st), 2098 (N_3 st), 1741 (C=O ester st), 1699 (C=O st carbamate), 1674 (C=O st amide), 1520 (N-H δ), 1456 (CH_2, CH_3 δ), 1367 (C-N st), 1248 (CO-O st), 1155 (NCO-O st). SEC (*ref PMMA*): Mw 1675 g·mol^{-1}; Đ 1.08.

N_3-[GMPA,G2]-(NH_3^+)$_4$

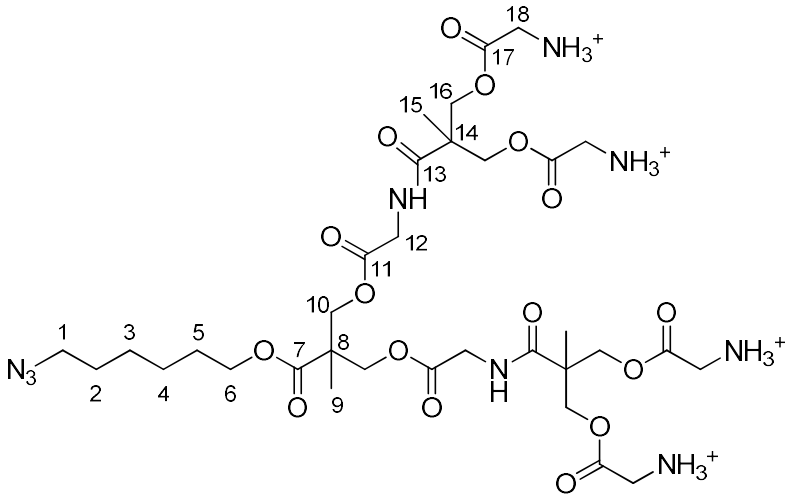

General procedure VI. N_3-[GMPA,G2]-(NHBoc)$_4$ (2.50 g, 2.03 mmol, 1.00 eq.), $CHCl_3$:TFA (1:1) (12.6 mL).Time of reaction: 3.5 hours. A yellow solid was obtained (2.54 g, 97 %). ^{1}H NMR (400 MHz, CD_3OD) δ (ppm): 8.36 (bs, -NHCO), 4.48-4.37 (m, 8H, H-16), 4.35-4.27 (m, 4H, H-10), 4.15 (t, *J* = 6.5 Hz, 2H, H-6), 3.94 (s, 4H, H-12), 3.91 (m, 8H, H-18), 3.30 (t, *J* = 6.9 Hz, 2H, H-1)*, 1.68 (m, 2H, H-5), 1.61 (m, 2H, H-2), 1.44 (m, 4H, H-3 and H-4), 1.36 (s, 6H, H-15), 1.27 (s, 3H, H-9). *H-1 signal in ^{1}H NMR is overlapped with the solvent signal, but the correlation between H-1 and H-2 was checked in ^{1}H-^{1}H COSY and the ^{1}H NMR in

$(CD_3)_2CO$ allowed to measure the multiplicity and the *J* of the signal. ^{13}C NMR (100 MHz, CD_3OD) δ (ppm): 174.9, 174.1, 170.8, 168.1, 163.0 (q, $^1J_{FC}$ = 34.6 Hz), 118.2 (q, $^2J_{CF}$ = 292.7 Hz), 68.4, 67.2, 66.6, 52.3, 47.6, 47.3, 42.0, 41.1, 29.7, 29.3, 27.3, 26.5, 18.1, 17.9. MS (MALDI$^+$) *m/z* (%): found *834.7 (81),* *c*alculated for $[C_{33}H_{55}N_9O_{16},H]^+$ *834.4*. FTIR (ν_{max}/cm^{-1}, ATR): 3369 (N-H st), 2941-2638 (C-H st and N-H$^+$ st), 2102 (N_3 st), 1749 (C=O st ester), 1668 (C=O st amide and N-H$^+$ δ), 1541 (N-H δ), 1474 (CH_2, CH_3 δ), 1433 (C-N st), 1184 (CO-O st), 1136 (C-O st).

N_3-[GMPA,G3]-$(NHBoc)_8$

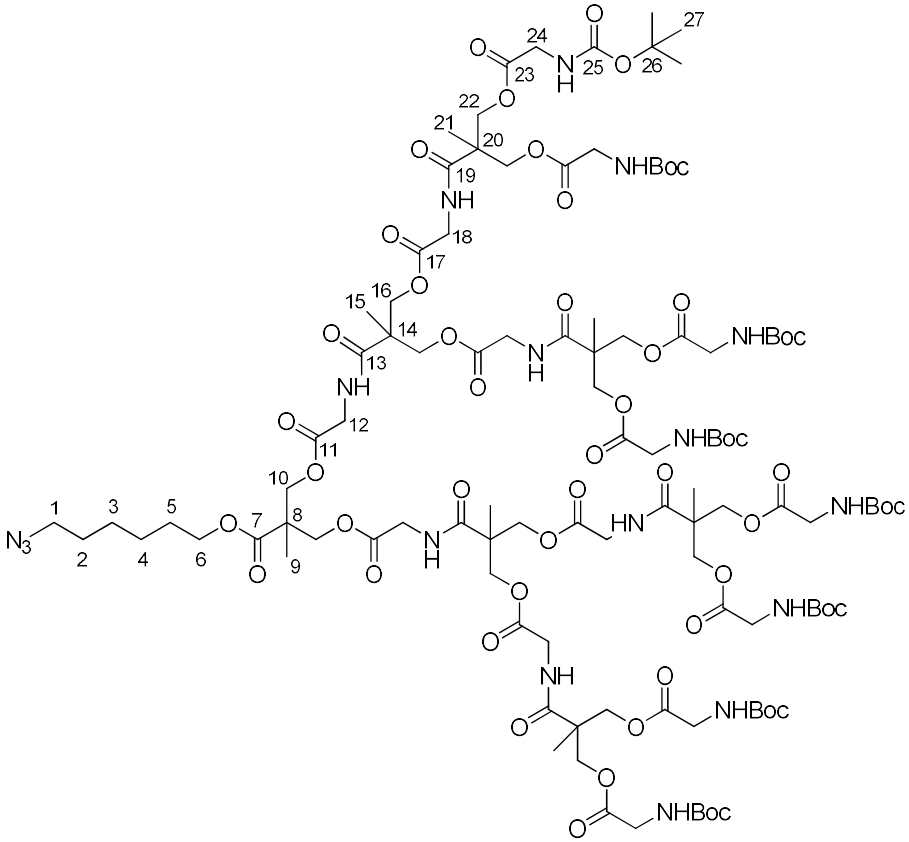

General procedure VII. N_3-[GMPA,G2]-$(NH_3^+)_4$ (2.00 g, 2.04 mmol, 1.00 eq.), *bis*-GMPA monomer (5.50 g, 12.25 mmol, 6.00 eq.), HOBt·nH_2O (1.88 g, 12.25 mmol, 6.00 eq.), DMAP (1.40 mg, 11.43 mmol, 5.60 eq.), DCC (2.53 g, 12.25 mmol, 6.00 eq.), dry DMF (33 mL), dry DCM (66 mL). The crude product was purified on silica gel (DCM:MeOH = 95:5) to obtain a white solid (3.88 g, 74 %). ^1H NMR (400 MHz, $CDCl_3$) δ (ppm): 7.19 (bs, -NHCO), 5.42 (bs, -NHBoc), 4.38-4.20 (m, 28H, H-10, H-16 and H-22), 4.13 (t, *J* = 6.4 Hz, 2H, H-6), 4.00 (d, *J* = 5.2

Hz, 8H, H-18), 3.95 (d, *J* = 5.2 Hz, 4H, H-12), 3.90 (d, *J* = 5.2 Hz, 16H, H-24), 3.27 (t, *J* = 6.8 Hz, 2H, H-1), 1.66 (m, 2H, H-5), 1.61 (m, 2H, H-2), 1.44 (m, 76H, H-3, H-4 and H-27), 1.28 (s, 12H, H-21), 1.26 (s, 3H, H-9), 1.25 (s, 6H, H-15). ^{13}C NMR (100 MHz, $CDCl_3$) δ (ppm): 172.8, 172.5, 170.6, 156.0, 80.0, 66.4, 65.2, 51.2, 46.1, 46.0, 42.3, 41.3, 28.6, 28.3, 26.2, 25.3, 18.3, 18.0, 17.7. MS (MALDI$^+$) *m/z* (%): found *2578.7 (100)*, calculated for $[C_{109}H_{175}N_{17}O_{52},Na]^+$ *2577.2*. FTIR (ν_{max}/cm^{-1}, ATR): 3356 (N-H st), 2978-2928-2854 (C-H st), 2106 (N_3 st), 1742 and 1718 (C=O ester st), 1699 (C=O carbamate st), 1664 (C=O amide st), 1528 (N-H δ), 1458 (CH_2, CH_3 δ), 1367 (C-N st), 1250 (CO-O st), 1157 (NCO-O st). SEC (*ref PMMA*): Mw 2966 g·mol^{-1}; Đ 1.02.

≡-[GMPA,G1]-(NHBoc)$_2$

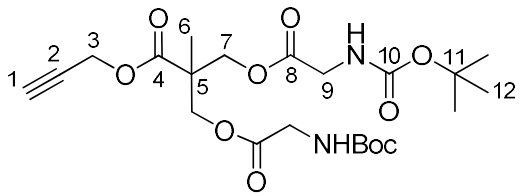

General procedure V. ≡-[MPA,G1]-(OH)$_2$ (3.80 g, 22.06 mmol, 1.00 eq.), Glyboc(OH) (9.66 g, 55.16 mmol, 2.50 eq.), DPTS (5.20 g, 17.65 mmol, 0.80 eq.), DCC (11.38 g, 55.16 mmol, 2.50 eq.) and dry DCM (120 mL). Time of reaction: 4 days. The crude product was purified on silica gel (hexane:ethyl acetate = ramp from 9:1 to 7:3). A white waxy solid was obtained (10.19 g, 95 %). ^{1}H NMR (400 MHz, $CDCl_3$) δ (ppm): 5.09 (bs, -NH), 4.72 (d, *J* = 2.5 Hz, 2H, H-3), 4.32 (ABq, *J* = 11.1 Hz, $\Delta\nu_{AB}$ = 37.6 Hz, 4H, H-7), 3.89 (d, *J* = 5.9 Hz, 4H, H-9), 2.51 (t, *J* = 2.5 Hz, 1H, H-1), 1.44 (s, 18H, H-12), 1.27 (s, 3H, H-6). ^{13}C NMR (100 MHz, $CDCl_3$) δ (ppm): 171.7, 170.1, 155.8, 80.1, 77.5, 75.5, 65.7, 52.8, 46.4, 42.3, 28.4, 17.9. MS (ESI$^+$) *m/z (%)*: found *509.0 (100)*, calculated for $[C_{22}H_{34}N_2O_{10},Na]^+$ *509.2*. FTIR (ν_{max}/cm^{-1}, ATR): 3420 (N-H st), 3317 (≡C-H st), 2976-2934 (C-H st), 2139 (C≡C st), 1724 and 1715 (C=O st ester), 1682 (C=O st carbamate), 1512 (N-H δ), 1367 (C-N st), 1286 (CO-O st), 1155 (C-O st).

≡-[GMPA,G1]-(NH_3^+)$_2$

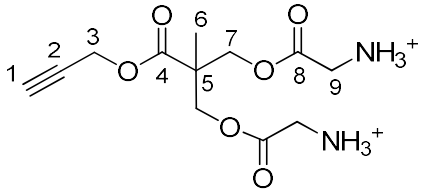

General procedure VI. ≡-[GMPA,G1]-(NHBoc)$_2$ (7.75 g, 15.93 mmol, 1.00 eq.), $CHCl_3$:TFA (1:1) (16 mL). Time of reaction: 3.5 hours. The final product was obtained as a yellow oil (6.26 g, 76 %). ^{1}H NMR (400 MHz, (CD_3OD) δ (ppm): 4.89 (bs, -NH), 4.78 (d, *J* = 2.5 Hz, 2H, H-3), 4.45 (s, 4H, H-7), 3.88 (s, 4H, H-9), 3.00 (t, *J* = 2.5 Hz, 1H, H-1), 1.33 (s, 3H, H-6). ^{13}C NMR (100 MHz, (CD_3OD) δ (ppm): 171.2, 167.1, 163.0 (q, $^1J_{FC}$ = 34.2 Hz), 118.2 (q, $^2J_{CF}$ = 292.3 Hz), 78.2, 78.0, 65.8, 52.8, 45.9, 39.5, 17.2. MS (ESI^+) *m/z (%)*: found *286.9 (100)*, calculated for $[C_{12}H_{18}N_2O_6,H]^+$ *287.1*. FTIR (ν_{max}/cm^{-1}, ATR): 3298 (≡C-H st), 3232-2588 (bs N-H$^+$ st), 1761 and 1726 (C=O st ester), 1553 (N-H$^+$ δ), 1502 (CH_2, CH_3 δ), 1404 (C-N st), 1213 (C-O st).

≡-[GMPA,G2]-(NHBoc)$_4$

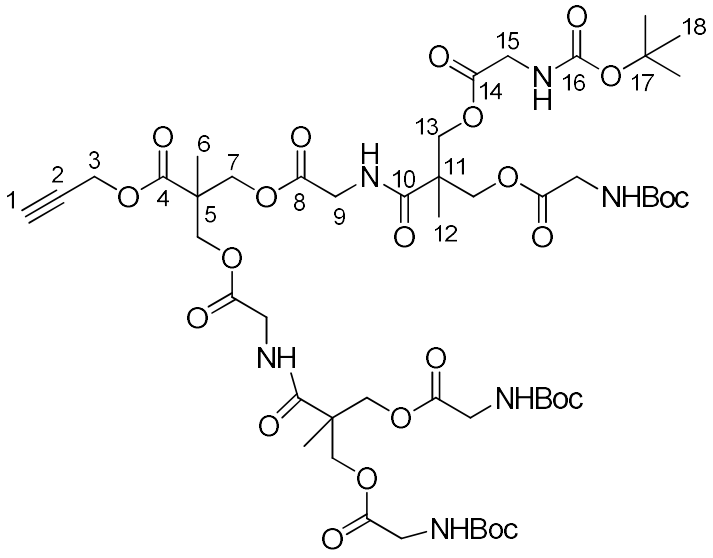

General procedure VII. ≡-[GMPA,G1]-(NH_3^+)$_2$ (2.00 g, 5.57 mmol, 1.00 eq.), *bis*-GMPA monomer (5.49 g, 12.25 mmol, 2.20 eq.), HOBt·nH_2O (1.66 g, 12.25 mmol, 2.20 eq.), DMAP (1.91 g, 15.59 mmol, 2.80 eq.), DCC (2.53 g, 12.25 mmol, 2.20 eq.), dry DMF (80 mL), dry DCM (120 mL). Time of reaction: 5 days. The crude product was purified on silica gel (hexane:ethyl acetate = 3:7) to get a

white powder (3.44 g, 54 %). ^{1}H NMR (400 MHz, $CDCl_3$) δ (ppm): 8.02 (bs, -NHCO), 5.28 (bs, -NHBoc), 4.73 (d, *J* = 2.4 Hz, 2H, H-3), 4.43-4.18 (m, 12H, H-7 and H-13), 3.98 (d, *J* = 5.3 Hz, 4H, H-9), 3.92 (d, *J* = 4.7 Hz, 8H, H-15), 2.52 (t, *J* = 2.4 Hz, 1H, H-1), 1.43 (s, 36H, H-18), 1.28 (s, 9H, H-6 and H-12). ^{13}C NMR (100 MHz, CD_3OD) δ (ppm): 178.1, 173.0, 171.8, 170.4, 155.9, 80.3, 78.3, 75.7, 67.5, 66.7, 52.9, 47.7-46.0, 42.5, 41.2, 33.0, 28.5, 28.1, 26.7, 26.1, 18.2, 17.9. MS (MALDI$^+$) *m/z (%):* found *1169.6 (100),* calculated for $[C_{50}H_{78}N_6O_{24},Na]^+$ *1169.5.* FTIR (ν_{max}/cm^{-1}, ATR): 3479-3192 (N-H st and ≡C-H st), 2980 and 2937 (C-H st), 1745 (C=O st ester), 1697 (C=O st carbamate), 1668 (C=O st amide), 1519 (N-H δ), 1367 (C-N st), 1283 and 1250 (CO-O st), 1153 (C-O st).

≡-[GMPA,G2]-$(NH_3^+)_4$

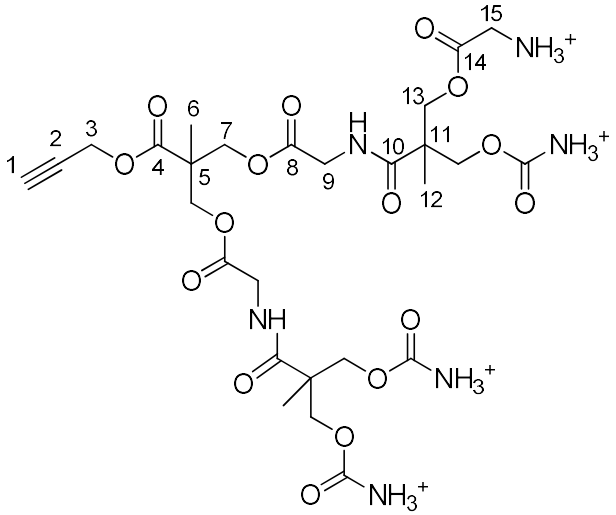

General procedure VI. ≡-[GMPA,G2]-$(NHBoc)_4$ (1.43 g, 1.24 mmol, 1.00 eq.), $CHCl_3$:TFA (1:1) (3 mL). Time of reaction: 3 hours. A white sticky solid was obtained (1.19 g, 80 %). ^{1}H NMR (400 MHz, CD_3OD) δ (ppm): 4.77 (d, *J* = 2.5 Hz, 2H, H-3), 4.48-4.37 (m, 8H, H-13), 4.32 (s, 4H, H-7), 3.95 (s, 4H, H-9), 3.91 (s, 8H, H-15), 2.99 (t, *J* = 2.4 Hz, 1H, H-1), 1.36 (s, 6H, H-12), 1.29 (s, 3H, H-6). ^{13}C NMR (100 MHz, CD_3OD) δ (ppm): 175.0-168.3, 162.9 (q, $^{1}J_{FC}$ = 34.3 Hz), 118.1 (q, $^{2}J_{CF}$ = 292.5 Hz), 78.4, 76.8, 68.5-66.9, 53.7, 47.7, 47.4, 42.0, 41.0, 28.0, 17.8, 17.6. MS (MALDI$^+$) *m/z (%)*: found *747.6 (77),* calculated for $[C_{30}H_{46}N_6O_{16},H]^+$ *747.3*. FTIR (ν_{max}/cm^{-1}, ATR): 3371-2547 (bs N-H$^+$ st and ≡C-H st), 1730 (C=O st ester), 1670 and 1637 (C=O st amide), 1537 (N-H$^+$ δ), 1413 (C-N st), 1190 and 1136 (C-O st).

≡-[GMPA,G1]-(C17)$_2$

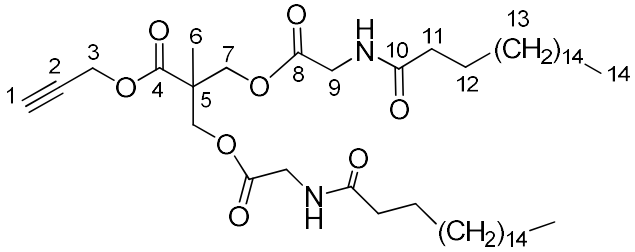

General procedure VIII. Stearic acid (2.37 g, 8.34 mmol, 3.00 eq.), DMAP (0.27 g, 2.22 mmol, 0.80 eq.), HOBt (1.28 g, 8.34 mmol, 3.00 eq.), DCC (1.72 g, 8.34 mmol, 3.00 eq.), dry DCM (90 mL), ≡-[GMPA,G1]-(NH_3^+)$_2$ (1.00 g, 2.78 mmol, 1.00 eq.), DMAP (0.68 g, 5.56 mmol, 2.00 eq.), anhydrous DMSO (10 mL). The precipitate was further purified on silica gel (DCM:MeOH = 98:2) to give a brown solid (1.86 g, 82 %). ^{1}H NMR (400 MHz, $CDCl_3$) δ (ppm): 6.16 (bs, -NH), 4.72 (d, *J* = 2.4 Hz, 2H, H-3), 4.32 (m, 4H, H-7), 4.01 (d, *J* = 5.4 Hz, 4H, H-9), 2.50 (t, *J* = 2.4 Hz, 1H, H-1), 2.24 (t, *J* = 7.7 Hz, 4H, H-11), 1.63 (m, 4H, H-12), 1.28 (s, 3H, H-6), 1.24 (m, 56H, H-13), 0.87 (t, *J* = 6.8 Hz, 6H, H-14). ^{13}C NMR (100 MHz, $CDCl_3$) δ (ppm): 173.7, 171.8, 169.8, 75.6, 65.8, 52.9, 46.3, 41.2, 36.5, 32.1, 29.9-29.3, 25.7, 22.8, 18.2, 14.3. MS (ESI^+) *m/z (%)*: found *841.5 (100)*, calculated for $[C_{48}H_{86}N_2O_8,Na]^+$ *841.6*. FTIR (ν_{max}/cm^{-1}, ATR): 3294 (N-H st), 2955-2916 (C-H st), 1744 (C=O ester st), 1645 (C=O amide st), 1555 (N-H δ), 1470 (CH_2, CH_3 δ), 1203 (CO-O st). SEC (*ref PMMA*): Mw 1710 g·mol^{-1}; Đ 1.05.

≡-[GMPA,G2]-(C17)$_4$

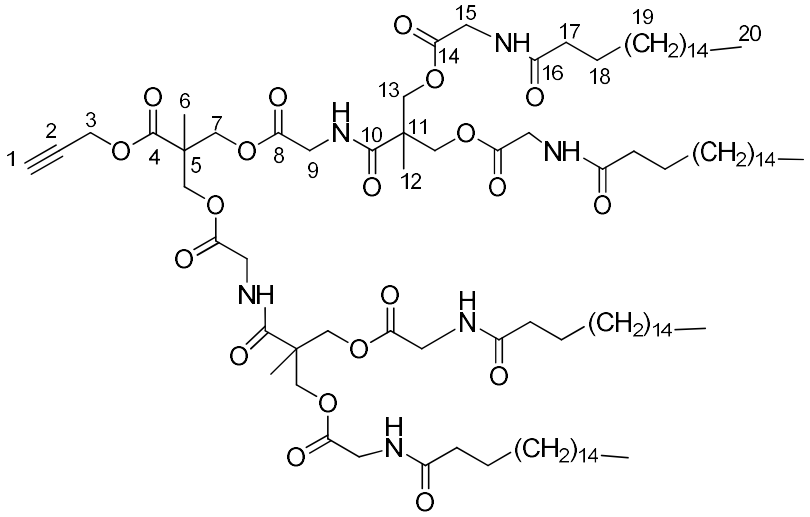

General procedure VIII. Stearic acid (1.68 g, 5.91 mmol, 6.00 eq.), DMAP (0.19 g, 1.57 mmol, 1.60 eq.), HOBt (0.80 g, 5.91 mmol, 6.00 eq.), DCC (1.22 g, 5.91 mmol, 6.00 eq.), dry DCM (45 mL), ≡-[GMPA,G2]-(NH_3^+)$_4$ (1.18 g, 0.98 mmol, 1.00 eq.), DMAP (0.48 g, 3.94 mmol, 4.00 eq.), anhydrous DMSO (5 mL). Time of reaction: The precipitate was further purified by two consecutives silica gel columns (firstly, DCM:MeOH = 98:2 and secondly, DCM:MeOH = ramp from 100:0 to 98:2). A yellow waxy solid was obtained (0.55 g, 31 %). ^{1}H NMR (400 MHz, $CDCl_3$) δ (ppm): 6.52 (bs, -NH), 4.74 (d, *J* = 2.4 Hz, 2H, H-3), 4.41-4.20 (m, 12H, H-7 and H-13), 4.02 (d, *J* = 5.6 Hz, 8H, H-15), 3.97 (d, *J* = 5.6 Hz , 4H, H-9), 2.53 (t, *J* = 2.4 Hz, 1H, H-1), 2.24 (t, *J* = 7.7 Hz, 8H, H-17), 1.62 (m, 8H, H-18), 1.25 (s, 121H, H-6, H-12 and H-19), 0.88 (t, *J* = 6.8 Hz, 12H, H-20). ^{13}C NMR (100 MHz, $CDCl_3$) δ (ppm): 174.2, 173.0, 171.9, 169.9, 169.5, 75.7, 66.8, 65.3, 52.9, 46.1, 41.5, 36.4, 32.1, 29.8-29.5, 25.7, 22.8, 18.1, 14.2. MS (MALDI$^+$) *m/z (%):* found *1835.8 (100)*, calculated for $[C_{102}H_{182}N_6O_{20},Na]^+$ *1834.3.* FTIR (ν_{max}/cm^{-1}, ATR): 3449-3211 (N-H st and ≡C-H st), 2916 and 2851 (C-H st), 1745 (C=O ester st), 1645 (C=O amide st), 1537 (N-H δ), 1468 (CH_2, CH_3 δ), 1200 (C-O st). SEC (*ref PMMA*): Mw 3231 g·mol^{-1}; Đ 1.04.

7.1.3. Amphiphilic Janus dendrimers

General procedure IX: copper(I) azide-alkyne cycloaddition reaction (CuAAC) for the synthesis of the Janus dendrimers

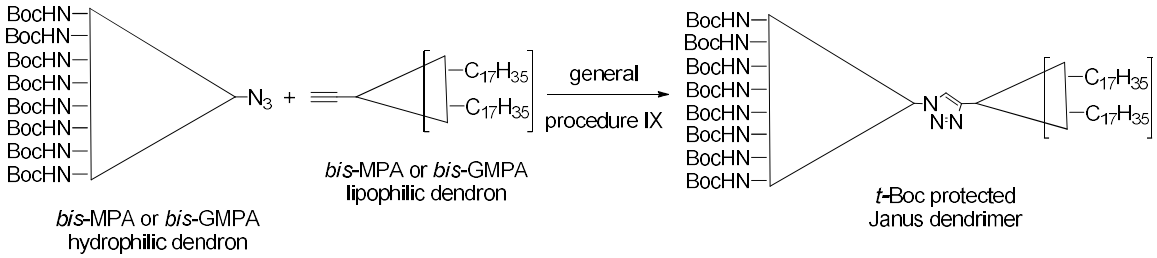

$CuSO_4 \cdot 5H_2O$ (0.10 mol), (*L*)-ascorbate (0.20 mol) and TBTA (0.10 mol) were dissolved into dry DMF in a Schlenk flask. Three vacuum-argon cycles were carried out to purge the flask form air and the solution was stirred at 45 °C under argon atmosphere for at least 15 min, until it turns yellow in colour. The azide (1.00 mol) and alkyne (1.20 mol) dendrons were dissolved into dry DMF at 45 °C in another Schlenk flask and three vacuum-argon cycles were carried out. The previously prepared copper solution was added to the azide-alkyne mixture through a cannula and the reaction mixture was stirred at 45 °C for 24-48 hours under argon atmosphere. Then, an excess of Merrifield´s peptide resin modified with azide groups was added to the reaction mixture and after three vacuum-argon cycles, it was stirred at 45 °C for another 24 hours in order to remove unreacted alkynes. After that, the reaction mixture was filtered off and the resin was washed with ethyl acetate. 100 mL of brine were added and the product was extracted twice with ethyl acetate (2 x 70 mL). Organic phases were combined and washed three times with brine (3 x 100 mL), then once with a KCN aqueous solution (15 mg into 100 mL of water) and finally twice with brine (2 x 100 mL), dried over anhydrous $MgSO_4$ and the solvent was evaporated under reduced pressure. Finally, the crude product was purified on silica gel using a variable DCM:MeOH ramp ratio (depending on the dendrimer polarity) to give a white or yellow solid.

(NHBoc)$_8$[GMPA]-[MPA](C17)$_2$

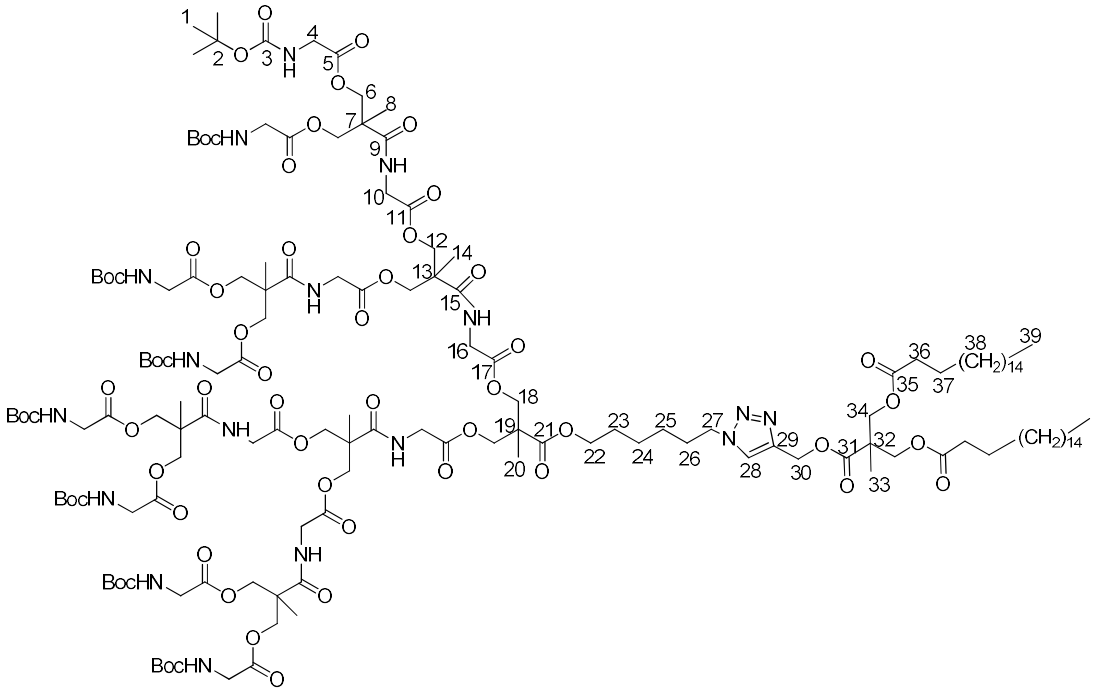

General procedure IX. N_3-[GMPA](NHBoc)$_8$ (400 mg, $1.57 \cdot 10^{-1}$ mmol, 1.00 eq.), ≡-[MPA]-(C17)$_2$ (133 mg, $1.88 \cdot 10^{-1}$ mmol, 1.20 eq.), $CuSO_4 \cdot 5H_2O$ (3.9 mg, $1.57 \cdot 10^{-2}$ mmol, 0.10 eq.), (*L*)-ascorbate (6.2 mg, $3.13 \cdot 10^{-2}$ mmol, 0.20 eq.) and TBTA (8.3 mg, $1.57 \cdot 10^{-2}$ mmol, 0.10 eq.) into dry DMF (8 mL). The crude product was purified on silica gel (DCM:MeOH = ramp from 98:2 to 95:5) to give a yellow solid (310 mg, 61 %). ^{1}H NMR (400 MHz, $CDCl_3$) δ (ppm): 7.65 (s, 1H, H-28), 7.20 (bs, -NHCO), 5.42 (bs, -NHBoc), 5.26 (s, 2H, H-30), 4.40-4.21 (m, 30H, H-6, H-12, H-18 and H-27), 4.18 (ABq, *J* = 11.1 Hz, $\Delta\nu_{AB}$ = 19.7 Hz, 4H, H-34), 4.13 (t, *J* = 6.2 Hz, 2H, H-22), 4.00 (d, *J* = 5.2 Hz, 8H, H-10), 3.95 (d, *J* = 4.8 Hz, 4H, H-16), 3.90 (d, *J* = 6.0 Hz, 16H, H-4), 2.25 (t, *J* = 7.6 Hz, 4H, H-36), 1.94 (m, 2H, H-26), 1.65 (m, 2H, H-23), 1.56 (m, 4H, H-37), 1.43 (s, 72H, H-1), 1.38 (m, 4H, H-24 and H-25), 1.28 (s, 12H, H-8), 1.26 (m, 65H, H-14, H-20 and H-38), 1.21 (s, 3H, H-33), 0.87 (t, *J* = 6.8 Hz, 6H, H-39). ^{13}C NMR (100 MHz, $CDCl_3$) δ (ppm): 173.6-173.1, 170.9, 170.3-170.2, 156.6, 142.9, 124.3, 80.3, 67.1-65.5, 58.9, 50.8, 47.7, 46.8-46.6, 42.9, 41.9, 41.8, 34.5, 32.5, 30.6, 30.3-29.7, 28.8, 28.6, 26.5, 25.8, 25.4, 23.3, 18.7-18.1, 14.4. MS (MALDI$^+$) *m/z (%):* found *3283.3 (46)*, calculated for $[C_{153}H_{255}N_{17}O_{58},Na]^+$ *3281.8.* FTIR (ν_{max}/cm^{-1}, ATR): 3468-3246 (N-H st), 2961, 2922, 2853 (C-H st), 1744 (C=O st ester), 1703 (C=O st carbamate), 1663 (C=O st amide), 1526 (N-H δ), 1458 (CH_2, CH_3 δ), 1367 (C-N st), 1250 (CO-O st), 1157 (NCO-O st). SEC (*ref PMMA*): Mw 4072 g·mol^{-1}; Đ 1.04.

(NHBoc)$_8$[GMPA]-[MPA](C17)$_4$

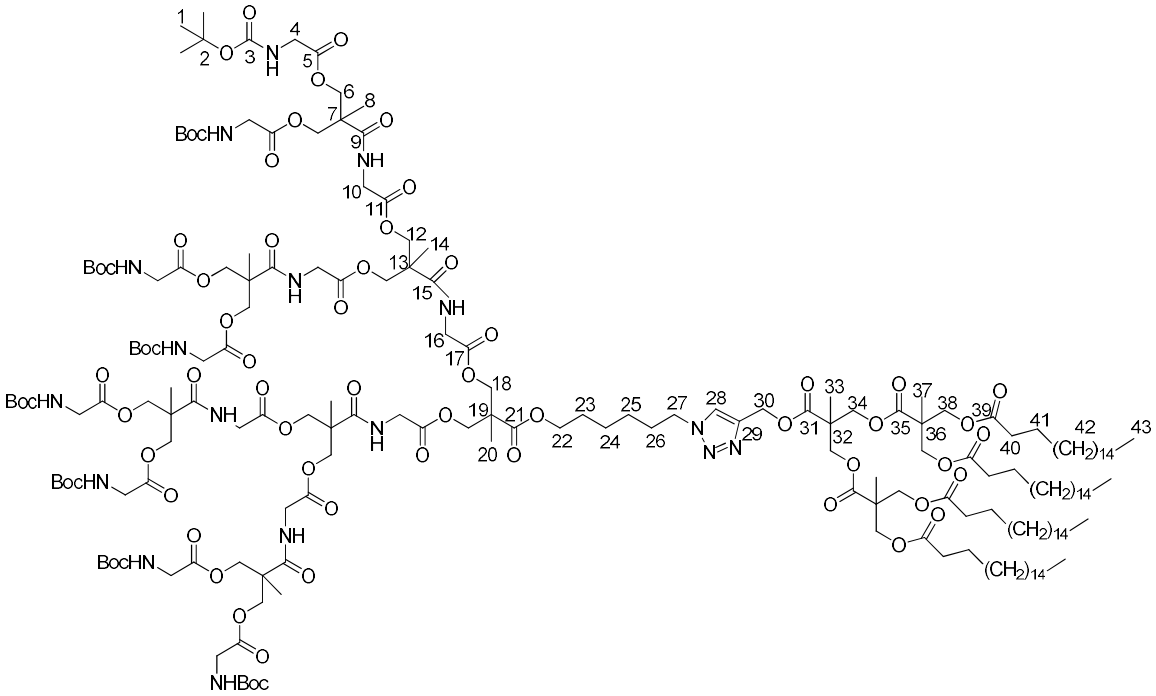

General procedure IX. N_3-[GMPA](NHBoc)$_8$ (1000 mg, $3.91 \cdot 10^{-1}$ mmol, 1.00 eq.), ≡-[MPA](C17)$_4$ (690 mg, $4.69 \cdot 10^{-1}$ mmol, 1.20 eq.), $CuSO_4 \cdot 5H_2O$ (11.5 mg, $3.91 \cdot 10^{-2}$ mmol, 0.10 eq.), (*L*)-ascorbate (15.5 mg, $7.82 \cdot 10^{-2}$ mmol, 0.20 eq.) and TBTA (20.8 mg, $3.91 \cdot 10^{-2}$ mmol, 0.10 eq.) into dry DMF (10 mL). The crude product was purified on silica gel (DCM:MeOH = ramp from 98:2 to 95:5) to give a yellow solid (1070 mg, 68 %). ^{1}H NMR (400 MHz, $CDCl_3$) δ (ppm): 7.67 (s, 1H, H-28), 7.19 (bs, -NHCO), 5.25 (bs, -NHBoc), 5.22 (s, 2H, H-30), 4.37-4.19 (m, 34H, H-6, H-12, H-18, H-27 and H-34), 4.12 (ABq, *J* = 11.2 Hz, $\Delta\nu_{AB}$ = 9.8 Hz, 8H, H-38), 4.11 (t, *J* = 6.0 Hz, 2H, H-22), 3.98 (d, *J* = 5.2 Hz, 8H, H-10), 3.94 (d, *J* = 5.2 Hz, 4H, H-16), 3.88 (d, *J* = 5.6 Hz, 16H, H-4), 2.27 (t, *J* = 7.6 Hz, 8H, H-40), 1.92 (m, 2H, H-26), 1.63 (m, 2H, H-23), 1.56 (m, 8H, H-41), 1.44 (s, 72H, H-1), 1.37 (m, 4H, H-24 and H-25), 1.27 (s, 12H, H-8), 1.26-1.16 (m, 130H, H-14, H-20, H-33, H-37 and H-42), 0.86 (t, *J* = 6.4 Hz, 12H, H-43). ^{13}C NMR (100 MHz, $CDCl_3$) δ (ppm): 173.1-169.5, 156.0, 141.9, 124.1, 80.0, 66.7-64.9, 58.4, 50.1, 46.6-46.0, 42.3, 41.3-41.2, 34.0, 31.9, 30.1, 29.7-29.1, 28.3, 26.0, 25.2, 24.8, 22.7, 18.3-17.7, 14.1. MS (MALDI$^+$) *m/z (%):* found *4047.9 (32)*, calculated for $[C_{199}H_{339}N_{17}O_{66},Na]^+$ *4046.4.* FTIR (ν_{max}/cm^{-1}, ATR): 3362 (N-H st), 2976, 2918, 2851 (C-H st), 1744 (C=O st ester), 1717 (C=O st carbamate), 1663 (C=O st amide), 1526 (N-H δ), 1470 (CH_2, CH_3 δ), 1367 (C-N st), 1252 (CO-O st), 1159 (NCO-O st). SEC (*ref PMMA*): Mw 5551 g·mol^{-1}; Đ 1.03.

$(NHBoc)_8$[MPA]-[GMPA]$(C17)_2$

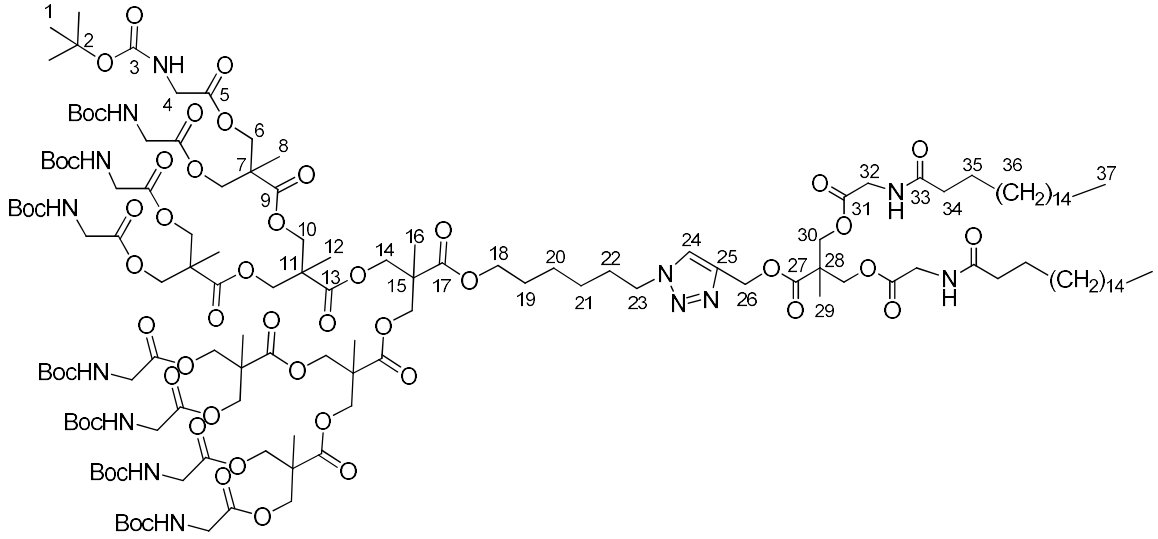

General procedure IX. N_3-[MPA]$(NHBoc)_8$ (1576 mg, $7.12 \cdot 10^{-1}$ mmol, 1.00 eq.), ≡-[GMPA]$(C17)_2$ (700 mg, $8.55 \cdot 10^{-1}$ mmol, 1.20 eq.), $CuSO_4 \cdot 5H_2O$ (17.8 mg, $7.12 \cdot 10^{-2}$ mmol, 0.10 eq.), *(L)*-ascorbate (28.2 mg, $1.42 \cdot 10^{-1}$ mmol, 0.20 eq.) and TBTA (37.8 mg, $7.12 \cdot 10^{-2}$ mmol, 0.10 eq.) into dry DMF (19 mL). The crude product was purified through silica gel column chromatography (DCM: MeOH = ramp from 100:0 to 96:4) to obtain a white powder (588 mg, 27 %). ^{1}H NMR (400 MHz, $CDCl_3$) δ (ppm): 7.91 (s, 1H, H-24), 6.70 (bs, -NHCO), 5.37 (bs, -NHBoc), 5.27 (s, 2H, H-26), 4.44 (t, *J* = 6.5 Hz, 2H, H-23), 4.25 (m, 32H, H-6, H-10, H-14 and H-30), 4.11 (t, *J* = 6.6 Hz, 2H, H-18), 3.95 (s, 4H, H-32), 3.88 (s, 16H, H-4), 2.27 (t, *J* = 7.7 Hz, 4H, H-34), 1.96 (m, 2H, H-22), 1.64 (m, 6H, H-19 and H-35), 1.43 (s, 72H, H-1), 1.26 (s, 12H, H-8), 1.24 (s, 72H, H-12, H-16, H-20, H-21, H-29, H-36), 0.86 (t, *J* = 6.9 Hz, 6H, H-37). ^{13}C NMR (100 MHz, $CDCl_3$) δ (ppm)**:** 173.9, 172.4, 172.2, 172.0, 171.7, 170.2, 169.7, 156.0, 80.1, 65.8, 65.5, 46.5, 42.4, 41.2, 36.4, 32.0, 29.8, 29.7, 28.5, 25.7, 22.8, 18.1, 17.7, 14.2. MS (MALDI$^+$) *m/z (%):* found *3054.8 (6)*, calculated for $[C_{145}H_{243}N_{13}O_{54},Na]^+$ *3053.7.* FTIR (ν_{max}/cm^{-1}, ATR): 3497-3207 (N-H st), 2918 and 2851 (C-H st), 1738 (C=O st ester), 1718 (C=O st carbamate), 1518 (N-H δ), 1470 (CH_2, CH_3 δ), 1367 (C-N st), 1157 (NCO-O st). SEC (*ref PMMA*): Mw 4234 g·mol^{-1}; Đ 1.04.

$(NHBoc)_8$[MPA]-[GMPA]$(C17)_4$

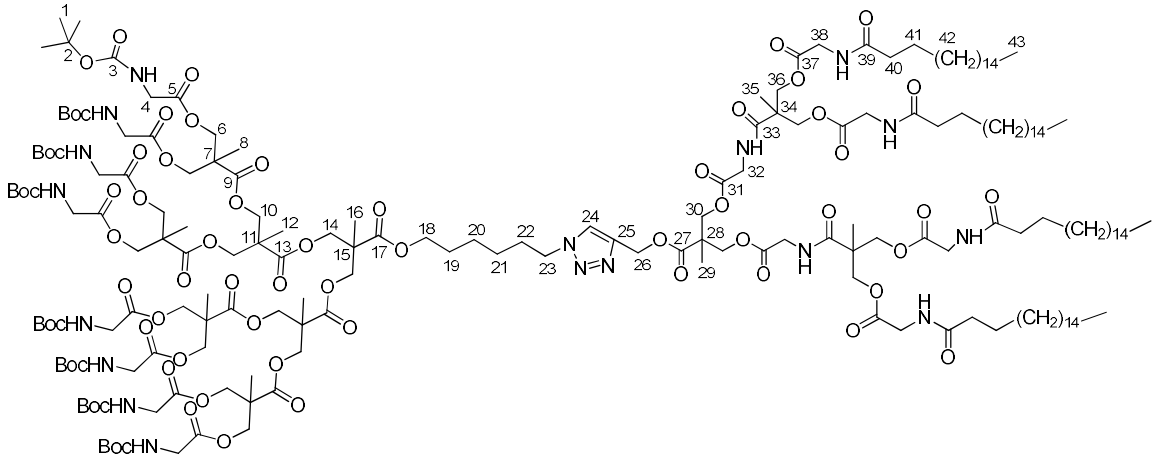

General procedure IX. N_3-[MPA]$(NHBoc)_8$ (334 mg, $1.51 \cdot 10^{-1}$ mmol, 1.00 eq.), ≡-[GMPA]$(C17)_4$ (328 mg, $1.81 \cdot 10^{-1}$ mmol, 1.20 eq.), $CuSO_4 \cdot 5H_2O$ (3.8 mg, $1.51 \cdot 10^{-2}$ mmol, 0.10 eq.), (*L*)-ascorbate (6.0 mg, $3.02 \cdot 10^{-2}$ mmol, 0.20 eq.) and TBTA (8.0 mg, $1.51 \cdot 10^{-2}$ mmol, 0.10 eq.) into dry DMF (10 mL). The crude product was purified on silica gel (DCM: MeOH = ramp from 100:0 to 98:2) to give a yellow solid (380 mg, 63 %). ^{1}H NMR (400 MHz, $CDCl_3$) δ (ppm): 7.76 (s, 1H, H-24), 6.62 (bs, -NHCO), 5.39 (bs, -NHBoc), 5.25 (s, 2H, H-26), 4.39 (t, *J* = 7.4 Hz, 2H, H-23), 4.35-4.18 (m, 40H, H-6, H-10, H-14, H-30 and H-36), 4.13 (t, *J* = 6.8 Hz, 2H, H-18), 4.03 (d, *J* = 6.2 Hz, 8H, H-38), 3.94 (d, *J* = 5.6 Hz, 4H, H-32), 3.87 (d, *J* = 6.2 Hz, 16H, H-4), 2.24 (t, *J* = 7.7 Hz, 8H, H-40), 1.94 (m, 2H, H-22), 1.62 (m, 10H, H-19 and H-41), 1.44 (s, 72H, H-1), 1.28 (s, 12H, H-8), 1.25 (s, 134H, H-12, H-16, H-20, H-21, H-29, H-35 and H-42), 0.87 (t, *J* = 7.1 Hz, 12H, H-43). ^{13}C NMR (100 MHz, $CDCl_3$) δ (ppm): 174.4-169.3, 155.9, 80.0, 65.9-65.4, 46.7, 46.4, 45.9, 42.2, 41.4, 36.2, 31.9, 29.7-29.4, 28.3, 25.7, 22.7, 18.1-17.6, 14.1. MS (MALDI$^+$) *m/z (%):* found *4043.0 (94)*, calculated for $[C_{199}H_{339}N_{17}O_{66},Na]^+$ *4046.4.* FTIR (ν_{max}/cm^{-1}, ATR): 3468-3221 (N-H st), 2960-2918-2850 (C-H st), 1735 (C=O st ester), 1718 (C=O st carbamate), 1656 (C=O st amide), 1521 (N-H δ), 1467 (CH_2, CH_3 δ), 1367 (C-N st), 1265-1220 (CO-O st), 1157 (NCO-O st). SEC (*ref PMMA*): Mw 5231 g·mol^{-1}; Đ 1.05.

$(NH_3^+)_8$[GMPA]-[MPA](C17)$_2$

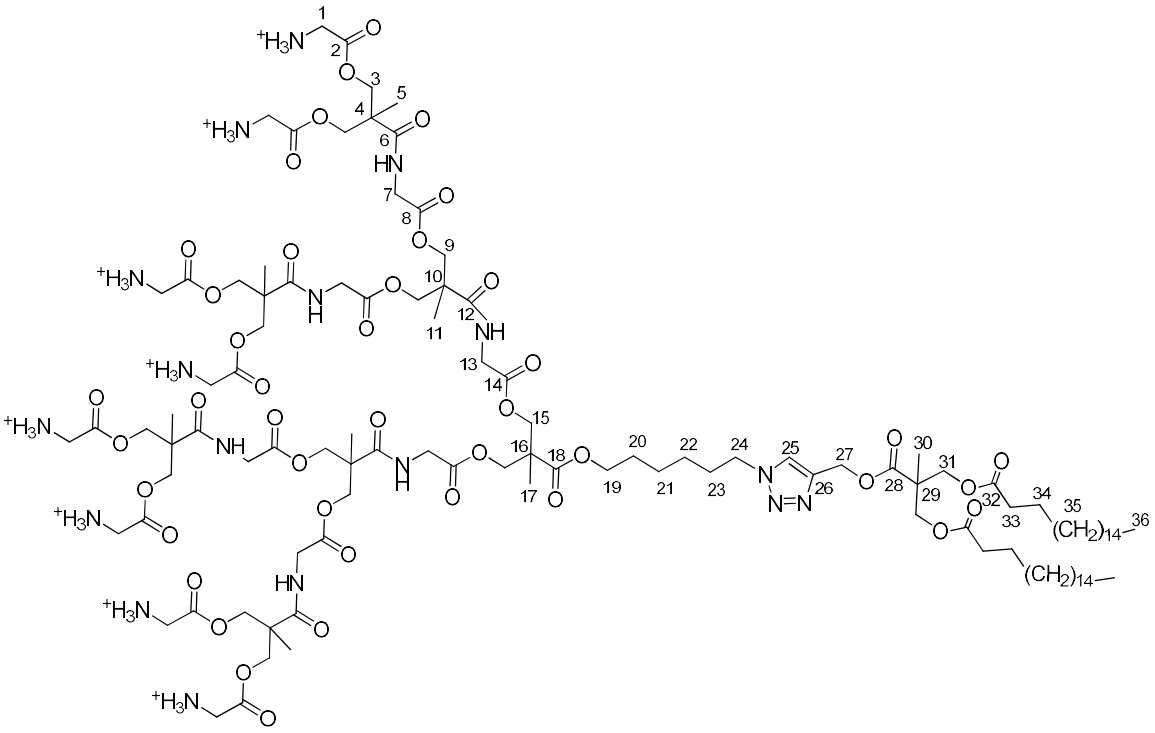

General procedure VI. $(NHBoc)_8$[GMPA]-[MPA](C17)$_2$ (285 mg, $8.74 \cdot 10^{-2}$ mmol, 1.00 eq.). $CHCl_3$:TFA (1:1) (3 mL). Time of reaction: 3.5 hours. The product was obtained as a white solid (293 mg, quantitative yield). ^{1}H NMR (400 MHz, CD_3OD) δ (ppm): 8.04 (s, 1H, H-25), 5.25 (s, 2H, H-27), 4.44 (m, 18H, H-3 and H-24), 4.31 (m, 12H, H-9 and H-15), 4.21 (ABq, *J* = 11.1 Hz, $\Delta\nu_{AB}$ = 39.5 Hz, 4H, H-31), 4.09 (t, *J* = 7.8 Hz, 2H, H-19), 3.98 (s, 8H, H-7), 3.95 (s, 4H, H-13), 3.92 (s, 16H, H-1), 2.26 (t, *J* = 7.3 Hz, 4H, H-33), 1.94 (m, 2H, H-23), 1.66 (m, 2H, H-20), 1.56 (m, 4H, H-34), 1.43 (m, 4H, H-21 and H-22), 1.36 (s, 12H, H-5), 1.31 (s, 6H, H-11), 1.29 (m, 56H, H-35), 1.27 (s, 3H, H-17), 1.24 (s, 3H, H-30), 0.90 (t, J = 6.9 Hz, 6H, H-36). ^{13}C NMR (100 MHz, CD_3OD) δ (ppm): 175.3-174.0, 171.1-170.8, 168.3, 162.9 (q, $^1J_{FC}$ = 34.7 Hz), 143.5, 126.2, 118.1 (q, $^2J_{CF}$ = 291.8 Hz), 68.5, 67.8, 67.2, 66.4-66.2, 58.9, 51.3, 47.7-47.4, 42.1, 41.0, 34.8, 33.1, 31.1, 30.8-30.2, 29.4, 27.0, 26.4, 26.0, 23.7, 18.1-17.7, 14.5. MS (MALDI$^+$) *m/z (%):* found *2460.8 (62)*, calculated for $[C_{113}H_{191}N_{17}O_{42},H]^+$ *2459.4*. FTIR (ν_{max}/cm^{-1}, ATR): 3630-2600 (bs N-H$^+$ st), 2920 and 2851 (C-H st), 1749 (C=O st ester), 1670 (C=O st amide and N-H$^+$ δ), 1537 (N-H δ), 1437 (CH_2, CH_3 δ), 1178 (CO-O st), 1132 (C-O st).

$(NH_3^+)_8$[GMPA]-[MPA](C17)$_4$

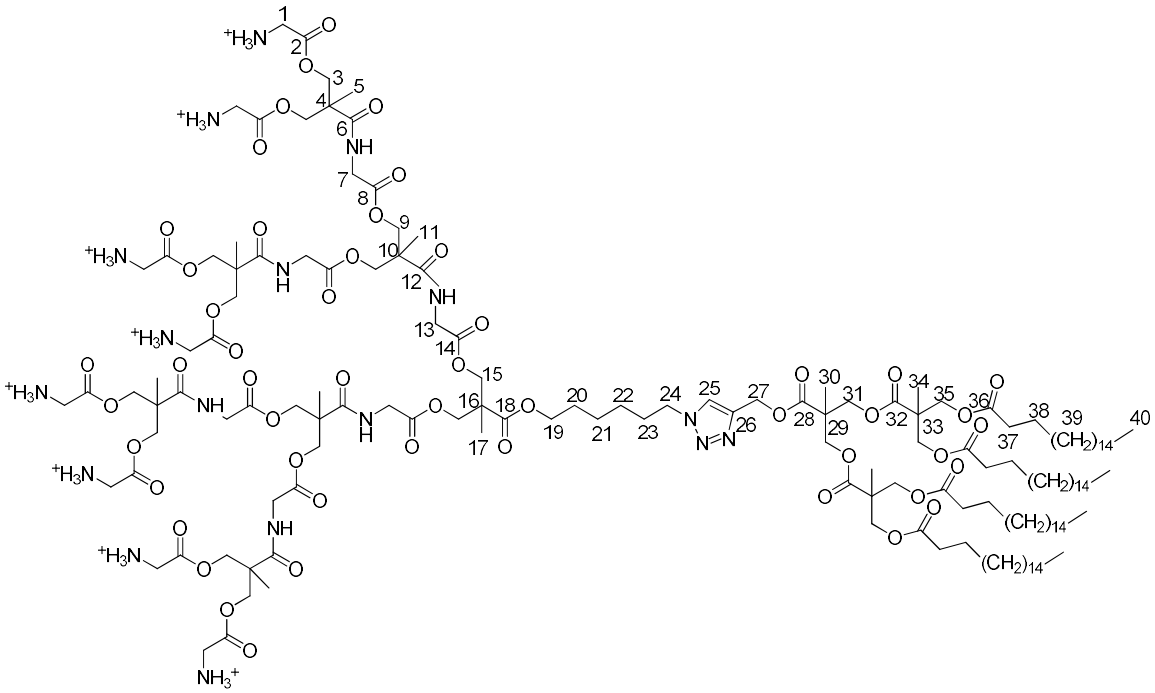

General procedure VI. $(NHBoc)_8$[GMPA]-[MPA](C17)$_4$ (637 mg, $1.58 \cdot 10^{-1}$ mmol, 1.00 eq.). $CHCl_3$:TFA (1:1) (3 mL). Time of reaction: 4.5 hours. The product was obtained as a white solid (650 mg, quantitative yield). ^{1}H NMR (400 MHz, CD_3OD) δ (ppm): 8.06 (s, 1H, H-25), 7.34 (bs, -NHCO), 5.27 (s, 2H, H-27), 4.44 (m, 18H, H-3 and H-24), 4.31 (m, 12H, H-9 and H-15), 4.27 (ABq, 4H, H-31), 4.15 (m, 10H, H-19 and H-35), 3.98 (m, 8H, H-7), 3.95 (m, 4H, H-13), 3.92 (s, 16H, H-1), 2.33 (t, *J* = 7.4 Hz, 8H, H-37), 1.95 (m, 2H, H-23), 1.67 (m, 2H, H-20), 1.59 (m, 8H, H-38), 1.44 (m, 4H, H-21 and H-22), 1.36 (s, 12H, H-5), 1.33-1.25 (m, 124H, H-11, H-17, H-30, and H-39), 1.20 (s, 6H, H-34), 0.90 (t, J = 6.9 Hz, 12H, H-40). ^{13}C NMR (100 MHz, CD_3OD) δ (ppm): 175.3-170.8, 168.9-168.3, 163.1 (q, $^1J_{FC}$ = 34.6 Hz), 143.5, 126.3, 118.2 (q, $^2J_{CF}$ = 293.3 Hz), 68.5-66.3, 59.0, 51.3, 47.9-47.4, 42.1, 41.1-40.9, 34.9, 33.1, 31.1, 30.9-30.2, 29.4, 27.1, 26.4, 26.1, 23.8, 18.3-17.8, 14.5. MS (MALDI$^+$) *m/z (%):* found *3225.1 (100),* calculated for $[C_{159}H_{275}N_{17}O_{50},H]^+$ *3224.0* and found *3247.2 (92),* calculated for $[C_{159}H_{275}N_{17}O_{50},Na]^+$ *3246.0.* FTIR (ν_{max}/cm^{-1}, ATR): 3653-2600 (bs N-H$^+$ st), 2943, 2918 and 2851 (C-H st), 1745 (C=O st ester), 1674 (C=O st amide and N-H$^+$ δ), 1537 (N-H δ) 1470 (CH_2, CH_3 δ), 1200 (CO-O st), 1132 (C-O st).

$(NH_3^+)_8$[MPA]-[GMPA](C17)$_2$

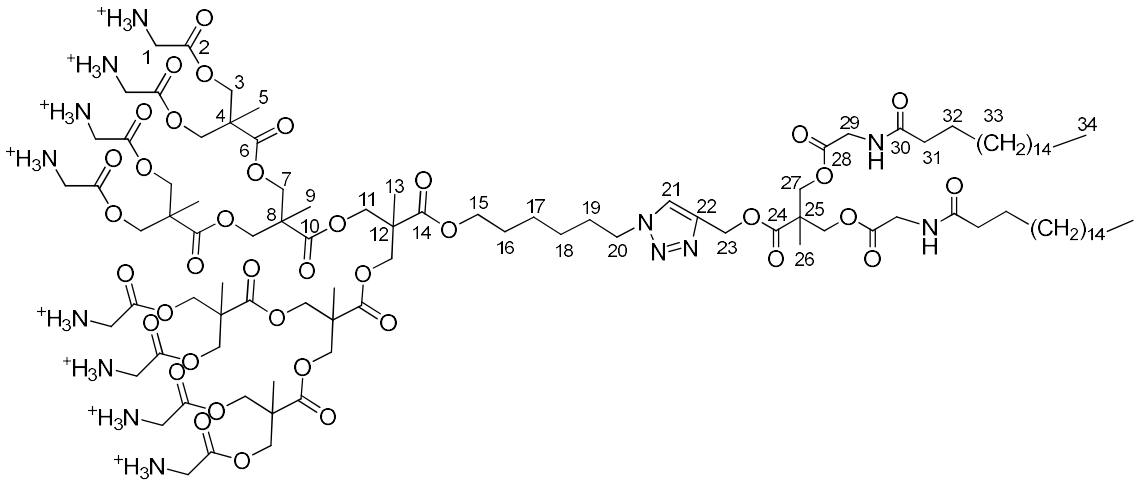

General procedure VI. $(NHBoc)_8$[MPA]-[GMPA](C17)$_2$ (588 mg, $1.94 \cdot 10^{-1}$ mmol, 1.00 eq.). $CHCl_3$:TFA (1:1) (2.5 mL). Time of reaction: 4.5 hours. The product was obtained as a white solid (610 mg, quantitative yield). ^{1}H NMR (400 MHz, CD_3OD) δ (ppm): 8.07 (s, 1H, H-21), 5.26 (s, 2H, H-23), 4.46-4.39 (m, 18H, H-3 and H-20), 4.38-4.23 (m, 16H, H-7, H-11 and H-27), 4.14 (t, *J* = 6.5 Hz, 2H, H-15), 3.93 (s, 16H, H-1), 3.87 (s, 4H, H-29), 2.25 (t, *J* = 7.6 Hz, 4H, H-31), 1.94 (m, 2H, H-19), 1.68 (m, 2H, H-16), 1.62 (m, 4H, H-32), 1.45 (m, 4H, H-17 and H-18), 1.33 (s, 12H, H-5), 1.32-1.26 (m, 65H, H-9, H-13 and H-33), 1.25 (s, 3H, H-26), 0.90 (t, *J* = 6.9 Hz, 6H, H-34). ^{13}C NMR (100 MHz, CD_3OD) δ (ppm): 176.8, 174.7-173.1, 170.8, 169.0-168.5, 163.0 (q, $^1J_{FC}$ = 34.6 Hz), 143.6, 126.2, 118.2 (q, $^2J_{CF}$ = 293.7 Hz), 67.5-65.2, 59.0, 51.3, 48.0-47.7, 41.9, 41.0-40.8, 36.8, 33.1, 31.1, 30.8-30.3, 29.4, 27.0, 26.9, 26.4, 23.7, 18.1-17.7, 14.5. MS (MALDI$^+$) *m/z (%):* found *2231.8 (100),* calculated for $[C_{105}H_{179}N_{13}O_{38},H]^+$ *2231.3* and found *2253.8 (76),* calculated for $[C_{105}H_{179}N_{13}O_{38},Na]^+$ *2253.3.* FTIR (ν_{max}/cm^{-1}, ATR): 3650-2600 (bs N-H$^+$ st), 2924 and 2853 (C-H st), 1742 (C=O st ester), 1672 (C=O amide st and N-H$^+$ δ), 1529 (N-H δ), 1470 (CH_2, CH_3 δ), 1200 (CO-O st), 1126 (C-O st).

$(NH_3^+)_8$[MPA]-[GMPA](C17)$_4$

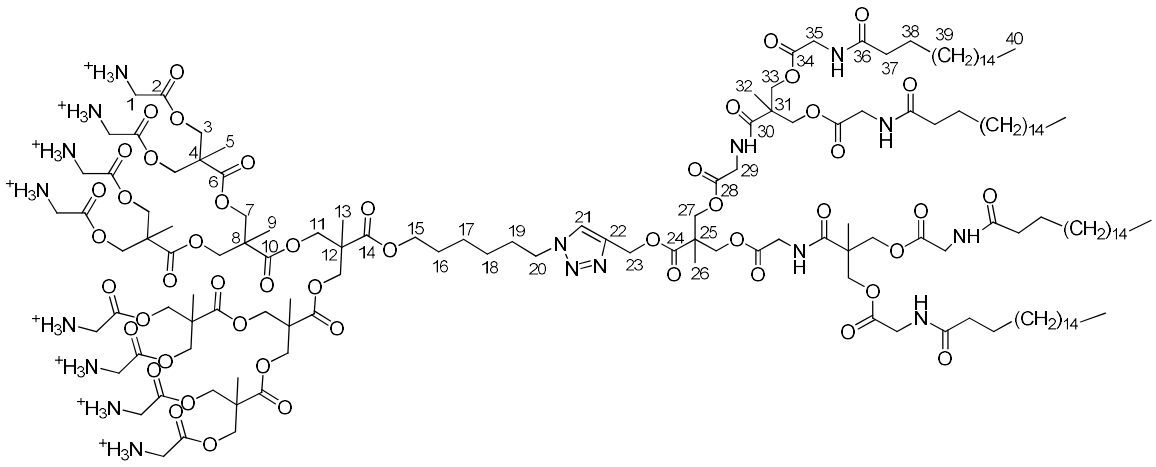

General procedure VI. $(NHBoc)_8$[MPA]-[GMPA](C17)$_4$ (360 mg, $8.9 \cdot 10^{-2}$ mmol, 1.00 eq.). $CHCl_3$:TFA (1:1) (2 mL). Time of reaction: 5.5 hours. The product was obtained as a white solid (290 mg, quantitative yield). ^{1}H NMR (400 MHz, CD_3OD) δ (ppm): 8.09 (s, 1H, H-21), 5.27 (s, 2H, H-23), 4.49-4.39 (m, 18H, H-3 and H-20), 4.37-4.22 (m, 24H, H-7, H-11, H-27 and H-33), 4.14 (t, *J* = 6.5 Hz, 2H, H-15), 3.95 (s, 8H, H-35), 3.94 (s, 16H, H-1), 3.90 (s, 4H, H-29), 2.26 (t, *J* = 7.6 Hz, 8H, H-37), 1.95 (m, 2H, H-19), 1.68 (m, 2H, H-16), 1.62 (m, 8H, H-38), 1.45 (m, 4H, H-17 and H-18), 1.34-1.27 (m, 139H, H-5, H-9, H-13, H-32 and H-39), 1.26 (s, 3H, H-26), 0.90 (t, *J* = 6.9 Hz, 12H, H-40). ^{13}C NMR (100 MHz, CD_3OD) δ (ppm): 176.8, 175.3-173.2, 171.0, 170.7, 168.5, 162.9 (q, $^1J_{FC}$ = 35.0 Hz), 143.6, 126.2, 118.1 (q, $^2J_{CF}$ = 292.6 Hz), 67.7-65.9, 59.1, 51.3, 48.1-47.3, 42.1, 41.0, 36.8, 33.1, 31.1, 30.8-30.4, 29.4, 27.0-26.4, 23.7, 18.2-17.7, 14.5. MS (MALDI$^+$) *m/z (%):* found *3224.8 (31)*, calculated for $[C_{159}H_{275}N_{17}O_{50},H]^+$ *3224.0* and found *3246.8 (100)*, calculated for $[C_{159}H_{275}N_{17}O_{50},Na]^+$ *3246.0*. FTIR (ν_{max}/cm^{-1}, ATR): 3623-2352 (bs N-H$^+$ st), 2918 and 2850 (C-H st), 1745 (C=O st ester), 1674 (C=O st amide and N-H$^+$ δ), 1537 (N-H δ), 1469 (CH_2, CH_3 δ), 1199 (CO-O st), 1130 (C-O st).

7.1.4. Dendronized hyperbranched polymers (DHPs)

The representation of the structures of the DHPs and the integration of the large signals of the protons in ^{1}H NMR have been made approximately and considering that these compounds are irregular because of their nature of hyperbranched polymers.

General procedure X: alkyne functionalisation of the commercial HPs

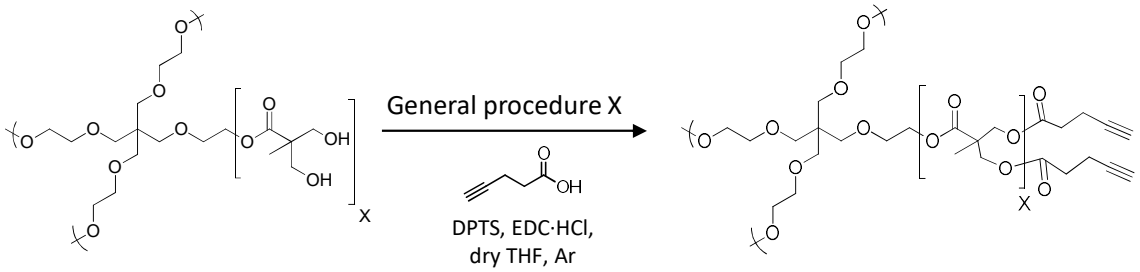

Commercial hyperbranched polyesters of different generations (G2, G3 or G4) (1.00 mol) were dissolved into dry THF. DPTS (0.50 mol per hydroxyl groups) and 4-pentynoic acid (1.25 mol per hydroxyl groups) were also dissolved. The reaction mixture was stirred under argon atmosphere and was cooled down to 0 °C. EDC·HCl (1.25 mol per hydroxyl groups) was added. The mixture was stirred under argon atmosphere at room temperature for 72 hours. Then, solvent was evaporated, and the resulting product was dissolved in DCM (100 mL) and washed twice with water (2 x 70 mL) and once with brine (70 mL). The organic phase was dried over anhydrous $MgSO_4$, and solvent was partially evaporated. It was precipitated into cold hexane and recovered by further centrifugation for 30 min at 4000 rpm. The alkyne functionalised hyperbranched polymer was finally washed twice with cold hexane and an amber solid was obtained.

General procedure XI: copper(I) azide-alkyne cycloaddition reaction (CuAAC) for the synthesis of the DHPs

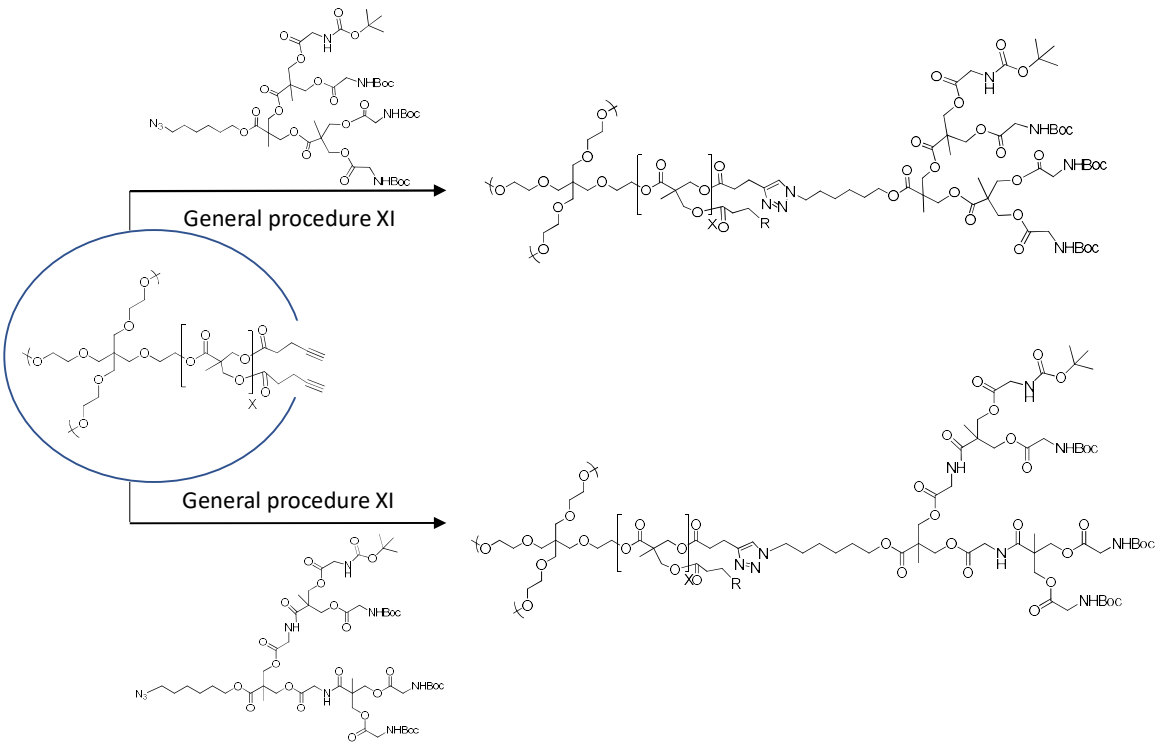

Alkyne functionalised hyperbranched polymer (1.00 mol) and the corresponding *t*-Boc protected dendron with azide in the focal point (N_3-[MPA,G2]-$(NHBoc)_4$ or N_3-[GMPA,G2]-$(NHBoc)_4$ (1.20 mol per mol of alkyne group) were dissolved into dry DMF in a Schlenk flask. Three cycles vacuum-argon were made. $CuSO_4 \cdot 5H_2O$ (0.10 mol per mol of alkyne group), (*L*)-ascorbate (0.20 mol per mol of alkyne group) and TBTA (0.10 mol per mol of alkyne group) were dissolved into dry DMF in a second Schlenk flask and the same procedure was developed to remove the O_2. It was allowed to stir at 45 °C for approximately 1 hour, time when Cu (I) was obtained and the solution turns yellow in colour. Then, it was added through a cannula to the first reaction mixture (the azide-alkyne) and was stirred all together under argon atmosphere at 45 °C for 2 days. Brine (250 mL) was added to the reaction mixture and the product was extracted three times with ethyl acetate (3 x 150 mL). Organic phases were collected and three further washings with brine (3 x 200 mL) were done. The organic phase was dried over anhydrous $MgSO_4$ and solvent was evaporated under reduced pressure to give a yellow oil. The crude product was filtrated through silica gel with DCM as eluent and the solvent was evaporated to give a light-yellow oil. The product was then

dissolved in ethyl acetate (250 mL) and was washed twice with a solution of KCN in water (15 mg in 150 mL) and twice with brine (2 x 150 mL). The organic phase was dried over anhydrous $MgSO_4$ and concentrated by evaporation under reduced pressure. Purification was carried out by precipitation into a mixture of hexane: ethyl acetate (9:1) and recovery by filtration. Products were obtained as white solids.

HP[G2,G3,G4]-≡

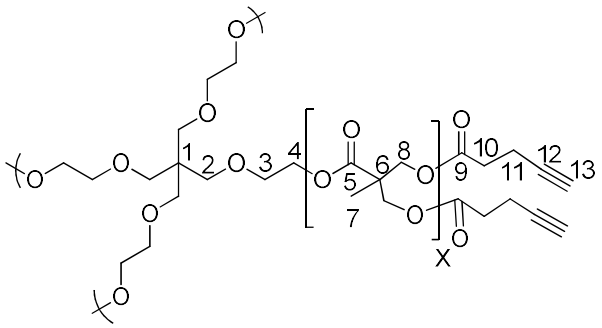

HP[G2]-≡

General procedure X. Commercial HP[G2]-$(OH)_{16}$ (1.13 g, 0.65 mmol, 1.00 eq), DPTS (2.29 g, 7.77 mmol, 12.00 eq), 4-pentynoic acid (1.22 g, 12.44 mmol, 20.00 eq) and EDC·HCl (2.38 g, 12.44 mmol, 20.00 eq) into dry THF (90 mL). The product was obtained as an amber solid (1.68 g, 88%). ^{1}H NMR (400 MHz, $CDCl_3$) δ (ppm): 4.23 (m, 53H, H-4 and H-8), 3.62 (m, 16H, H-2 and H-3), 2.55 (m, 30H, H-10), 2.47 (m, 30H, H-11), 1.99 (m, 15H, H-13), 1.24 (m, 36H, H-7). ^{13}C NMR (100 MHz, $CDCl_3$) δ (ppm): 171.3, 82.5, 69.5, 65.5, 46.7, 33.3, 17.9, 14.4. FTIR (ν_{max}/cm^{-1}, ATR): 3281 (≡C-H st), 2145 (C≡C st), 1732 (C=O st), 1240 (CO-O st). SEC (*ref PMMA*): Mw 3313 g·mol^{-1}; Đ 1.19.

HP[G3]-≡

General procedure X. Commercial HP[G3]-$(OH)_{32}$ (1.25 g, 0.35 mmol, 1.00 eq), DPTS (1.63 g, 5.54 mmol, 16.00 eq), 4-pentynoic acid (1.36 g, 13.86 mmol, 40.00 eq) and EDC·HCl (2.66 g, 13.86 mmol, 40.00 eq) into dry THF (100 mL). The product was obtained as an amber solid (1.60 g, 75%). ^{1}H NMR (400 MHz,

$CDCl_3$) δ (ppm): 4.24 (m, 114H, H-4 and H-8), 3.62 (m, 16H, H-2 and H-3), 2.56 (m, 64H, H-10), 2.47 (m, 64H, H-11), 2.00 (m, 31H, H-13), 1.25 (m, 84H, H-7). ^{13}C NMR (100 MHz, $CDCl_3$) δ (ppm): 171.3, 82.5, 69.5, 65.5, 46.7, 33.3, 17.9, 14.4. FTIR (ν_{max}/cm^{-1}, ATR): 3281 (≡C-H st), 2132 (C≡C st), 1730 (C=O st), 1240 (CO-O st). SEC (*ref PMMA*): Mw 5368 g·mol^{-1}; Đ 1.27.

HP[G4]-≡

General procedure X. Commercial HP[G4]-$(OH)_{64}$ (1.25 g, 0.17 mmol, 1.00 eq), DPTS (1.71 g, 5.46 mmol, 32.00 eq), 4-pentynoic acid (1.34 g, 13.66 mmol, 80.00 eq) and EDC·HCl (2.62 g, 13.66 mmol, 80.00 eq) into dry THF (100 mL). The product was obtained as an amber solid (1.40 g, 67%). ^1H NMR (400 MHz, $CDCl_3$) δ (ppm): 4.24 (m, 248H, H-4 and H-8), 3.63 (m, 16H, H-2 and H-3), 2.56 (m, 128H, H-10), 2.48 (m, 128H, H-11), 2.00 (m, 61H, H-13), 1.25 (m, 180H, H-7). ^{13}C NMR (100 MHz, $CDCl_3$) δ (ppm): 171.3, 82.5, 69.5, 65.5, 46.7, 33.3, 17.9, 14.4. FTIR (ν_{max}/cm^{-1}, ATR): 3281 (≡C-H st), 2136 (C≡C st), 1730 (C=O st), 1240 (CO-O st). SEC (*ref PMMA*): Mw 12843 g·mol^{-1}; Đ 1.62.

DHP[G2,G3,G4 + MPA,G2](NHBoc)

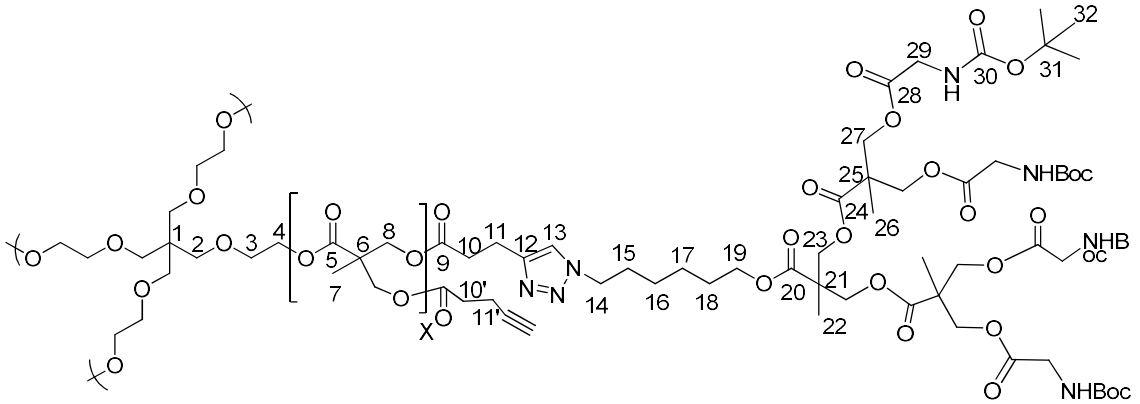

DHP[G2+MPA,G2](NHBoc)

General procedure XI. HP[G2]-≡ (381 mg, 0.13 mmol, 1.00 eq), N_3-[MPA,G2]-$(NHBoc)_4$ (2600 mg, 2.32 mmol, 18.00 eq), $CuSO_4 \cdot 5H_2O$ (48.4 mg, 0.19 mmol, 1.50 eq), (*L*)-ascorbate (76.7 mg, 0.39 mmol, 3.00 eq), TBTA (102.9 mg, 0.19

mmol, 1.50 eq) and dry DMF (17 mL). A white solid was obtained (1.34 g, 53%). ^{1}H NMR (400 MHz, $CDCl_3$) δ (ppm): 7.41 (s, 15H, H-13), 5.39 (bs, -NHBoc), 4.25 (m, 250H, H-4, H-8, H-14, H-23, H-27), 4.09 (m, 31H, H-19), 3.87 (d, J = 5.0 Hz, 120H, H-29), 3.61 (m, 16H, H-2 and H-3), 2.98 (m, 29H, H-11), 2.72 (m, 29H, H-10), 1.89 (m, 29H, H-15), 1.64 (m, 29H, H-18), 1.43 (s, 540H, H-32), 1.23 (s, 243H, H-7, H-16, H-17, H-22, H-26). ^{13}C NMR (100 MHz, $CDCl_3$) δ (ppm): 172.3, 171.9, 170.2, 156.0, 146.1, 121.3, 80.0, 68.1, 65.8, 65.5, 50.1, 46.7, 46.5, 42.4, 33.5, 30.3, 28.4, 26.3, 25.7, 25.4, 20.9, 18.0, 17.8. FTIR (ν_{max}/cm^{-1}, ATR): 3375 (N-H st), 2979 and 2937 (C-H st), 1731 (C=O st ester), 1710 (C=O st carbamate), 1515 (N-H δ), 1456 (CH_2, CH_3 δ), 1367 (C-N st), 1245 (CO-O st), 1153 (NCO-O st), 1132 (C-O st). SEC (*ref PMMA*): Mw 14045 g·mol^{-1}; Đ 1.12.

DHP[G3+MPA,G2](NHBoc)

General procedure XI. HP[G3]-≡ (274 mg, $4.5 \cdot 10^{-2}$ mmol, 1.00 eq), N_3-[MPA,G2]-$(NHBoc)_4$ (1937 mg, 1.73 mmol, 38.40 eq), $CuSO_4 \cdot 5H_2O$ (36 mg, 0.14 mmol, 3.20 eq), (*L*)-ascorbate (57 mg, 0.29 mmol, 6.40 eq), TBTA (76.4 mg, 0.14 mmol, 3.20 eq) and dry DMF (15 mL). A white solid was obtained (0.64 g, 35%). ^{1}H NMR (400 MHz, $CDCl_3$) δ (ppm): 7.44 (s, 31H, H-13), 5.42 (bs, -NHBoc), 4.25 (m, 506H, H-4, H-8, H-14, H-23, H-27), 4.10 (t, J = 6.7 Hz, 62H, H-19), 3.87 (d, J = 5.9 Hz, 247H, H-29), 3.60 (m, 16H, H-2 and H-3), 2.97 (m, 62H, H-11), 2.73 (m, 62H, H-10), 1.89 (m, 62H, H-15), 1.64 (m, 62H, H-18), 1.43 (s, 1116H, H-32), 1.24 (s, 499H, H-7, H-16, H-17, H-22, H-26). ^{13}C NMR (100 MHz, $CDCl_3$) δ (ppm): 172.4, 172.0, 170.2, 156.1, 146.1, 121.4, 80.0, 65.8, 65.5, 50.2, 46.7, 46.5, 42.4, 33.4, 30.3, 28.5, 26.3, 25.4, 20.9, 18.1, 17.8. FTIR (ν_{max}/cm^{-1}, ATR): 3375 (N-H st), 2977 and 2937 (C-H st), 1724 (C=O st ester), 1710 (C=O st carbamate), 1510 (N-H δ), 1459 (CH_2, CH_3 δ), 1367 (C-N st), 1245 (CO-O st), 1153 (NCO-O st), 1132 (C-O st). SEC (*ref PMMA*): Mw 23052 g·mol^{-1}; Đ 1.13.

DHP[G4+MPA,G2](NHBoc)

General procedure XI. HP[G4]-≡ (303 mg, $2.5 \cdot 10^{-2}$ mmol, 1.00 eq), N_3-[MPA,G2]-$(NHBoc)_4$ (2122 mg, 1.89 mmol, 76.80 eq), $CuSO_4 \cdot 5H_2O$ (40 mg, 0.16 mmol, 6.40 eq), (*L*)-ascorbate (63 mg, 0.32 mmol, 12.80 eq), TBTA (84 mg, 0.16 mmol, 6.40 eq) and dry DMF (15 mL). A white solid was obtained (1.15 g, 56%). ^{1}H NMR (400 MHz, $CDCl_3$) δ (ppm): 7.43 (s, 62H, H-13), 5.42 (bs, -NHBoc), 4.24 (m, 1004H, H-4, H-8, H-14, H-23, H-27), 4.08 (m, 124H, H-19), 3.85 (s, 496H, H-29), 3.59 (m, 16H, H-2 and H-3), 2.95 (m, 124H, H-11), 2.71 (m, 124H, H-10), 1.88 (m, 124H, H-15), 1.63 (m, 124H, H-18), 1.42 (s, 2232H, H-32), 1.22 (s, 998H, H-7, H-16, H-17, H-22, H-26). ^{13}C NMR (100 MHz, $CDCl_3$) δ (ppm): 172.4, 172.0, 170.2, 156.1, 146.0, 121.4, 80.0, 65.8, 65.5, 50.1, 46.7, 46.5, 42.4, 33.4, 30.3, 29.8, 28.5, 26.3, 25.4, 21.0, 18.0, 17.8. FTIR (ν_{max}/cm^{-1}, ATR): 3382 (N-H st), 2977 and 2937 (C-H st), 1724 (C=O st ester), 1710 (C=O st carbamate), 1513 (N-H δ), 1456 (CH_2, CH_3 δ), 1367 (C-N st), 1245 (CO-O st), 1153 (NCO-O st), 1132 (C-O st). SEC (*ref PMMA*): Mw 41530 g·mol^{-1}; Đ 1.17.

DHP[G2,G3,G4 + GMPA,G2](NHBoc)

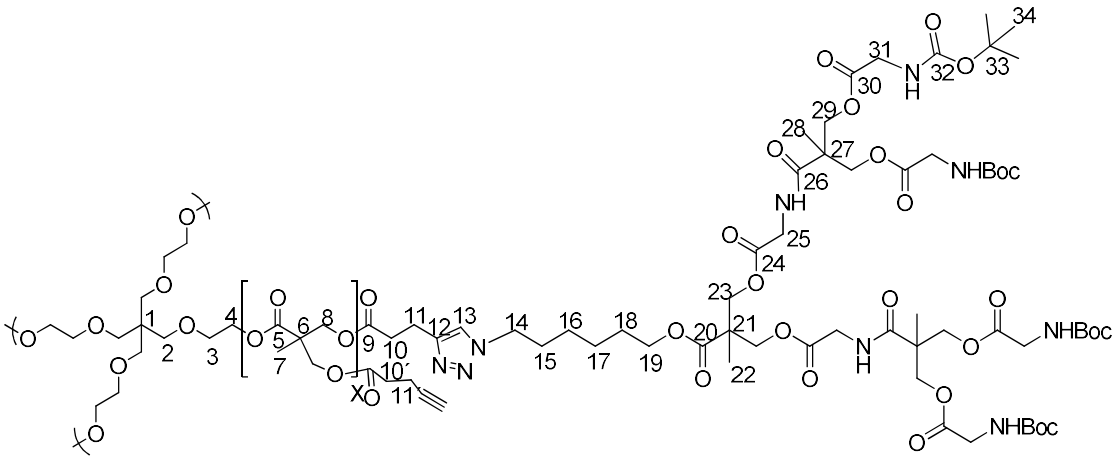

DHP[G2+GMPA,G2](NHBoc)

General procedure XI. HP[G2]-≡ (134 mg, $4.6 \cdot 10^{-2}$ mmol, 1.00 eq), N_3-[GMPA,G2]-$(NHBoc)_4$ (1011 mg, 0.82 mmol, 18.00 eq), $CuSO_4 \cdot 5H_2O$ (17 mg, $6.8 \cdot 10^{-2}$ mmol, 1.50 eq), (*L*)-ascorbate (27 mg, 0.14 mmol, 3.00 eq), TBTA (36

mg, $6.8 \cdot 10^{-2}$ mmol, 1.50 eq) and dry DMF (10 mL). A white solid was obtained (0.48 g, 49%). ^{1}H NMR (400 MHz, $CDCl_3$) δ (ppm): 7.42 (s, 15H, H-13), 5.44 (bs, -NHBoc), 4.29 (m, 280H, H-4, H-8, H-14, H-19, H-23, H-29), 3.94 (s, 60H, H-25), 3.89 (s, 120H, H-31), 3.60 (m, 16H, H-2 and H-3), 2.96 (m, 30H, H-11), 2.71 (m, 30H, H-10), 2.52 (m, 1H, H-10´), 2.43 (m, 1H, H-11´), 1.88 (m, 30H, H-15), 1.62 (m, 30H, H-18), 1.42 (s, 540H, H-34), 1.35 (m, 60H, H-16, H-17), 1.27 (s, 93H, H-7, H-22), 1.24 (s, 90H, H-28). ^{13}C NMR (100 MHz, $CDCl_3$) δ (ppm): 173.0, 172.7, 172.2, 170.5, 169.7, 156.2, 146.1, 121.5, 80.1, 66.6, 65.3, 50.1, 46.4, 46.2, 42.5, 41.2, 33.4, 30.2, 29.2, 28.5, 26.2, 25.4, 22.8, 21.0, 18.5, 17.9. FTIR (ν_{max}/cm^{-1}, ATR): 3361 (N-H st), 2977 and 2937 (C-H st), 1720 (C=O st ester), 1704 (C=O st carbamate), 1670 (C=O st amide), 1521 (N-H δ), 1458 (CH_2, CH_3 δ), 1367 (C-N st), 1245 (CO-O st), 1153 (NCO-O st), 1054 (C-O st). SEC (*ref PMMA*): Mw 15482 g·mol^{-1}; Đ 1.12.

DHP[G3+GMPA,G2](NHBoc)

General procedure XI. HP[G3]-≡ (134 mg, $2.2 \cdot 10^{-2}$ mmol, 1.00 eq), N_3-[GMPA,G2]-$(NHBoc)_4$ (1013 mg, 0.82 mmol, 37.20 eq), $CuSO_4 \cdot 5H_2O$ (17 mg, $6.8 \cdot 10^{-2}$ mmol, 3.10 eq), (*L*)-ascorbate (27 mg, 0.14 mmol, 6.20 eq), TBTA (36 mg, $6.8 \cdot 10^{-2}$ mmol, 3.10 eq) and dry DMF (10 mL). A white solid was obtained (0.22 g, 23%). ^{1}H NMR (400 MHz, $CDCl_3$) δ (ppm): 7.44 (s, 29H, H-13), 5.45 (bs, -NHBoc), 4.30 (m, 536H, H-4, H-8, H-14, H-19, H-23, H-29), 3.95 (s, 116H, H-25), 3.89 (s, 232H, H-31), 3.60 (m, 16H, H-2 and H-3), 2.96 (m, 58H, H-11), 2.72 (m, 58H, H-10), 2.52 (m, 4H, H-10´), 2.43 (m, 4H, H-11´), 1.87 (m, 58H, H-15), 1.63 (m, 58H, H-18), 1.42 (s, 1044H, H-34), 1.36 (m, 116H, H-16, H-17), 1.26 (s, 183H, H-7, H-22), 1.24 (s, 174H, H-28). ^{13}C NMR (100 MHz, $CDCl_3$) δ (ppm): 173.1, 172.7, 170.5, 169.7, 156.2, 146.1, 121.6, 80.1, 66.6, 65.3, 50.2, 46.4, 46.2, 42.6, 41.2, 33.5, 30.3, 29.2, 28.5, 26.2, 25.4, 22.8, 21.0, 18.5, 17.9. FTIR (ν_{max}/cm^{-1}, ATR): 3361 (N-H st), 2977 and 2937 (C-H st), 1720 (C=O st ester), 1710 (C=O st carbamate), 1670 (C=O st amide), 1521 (N-H δ), 1456 (CH_2, CH_3 δ), 1367 (C-N st), 1249 (CO-O st), 1153 (NCO-O st), 1054 (C-O st). SEC (*ref PMMA*): Mw 25411 g·mol^{-1}; Đ 1.23.

DHP[G4+GMPA,G2](NHBoc)

General procedure XI. HP[G4]-≡ (168 mg, $1.37 \cdot 10^{-2}$ mmol, 1.00 eq), N_3-[GMPA,G2]-$(NHBoc)_4$ (1258 mg, 1.02 mmol, 74.40 eq), $CuSO_4 \cdot 5H_2O$ (21.2 mg, $8.5 \cdot 10^{-2}$ mmol, 6.20 eq), (*L*)-ascorbate (34 mg, 0.17 mmol, 12.40 eq), TBTA (45 mg, $8.5 \cdot 10^{-2}$ mmol, 6.20 eq) and dry DMF (12 mL). A white solid was obtained (0.70 g, 58%). ^{1}H NMR (400 MHz, $CDCl_3$) δ (ppm): 7.45 (s, 58H, H-13), 5.47 (bs, -NHBoc), 4.29 (m, 1064H, H-4, H-8, H-14, H-19, H-23, H-29), 3.94 (s, 232H, H-25), 3.89 (s, 464H, H-31), 3.60 (m, 16H, H-2 and H-3), 2.95 (m, 116H, H-11), 2.71 (m, 116H, H-10), 2.52 (m, 8H, H-10´), 2.43 (m, 8H, H-11´), 1.88 (m, 116H, H-15), 1.62 (m, 116H, H-18), 1.42 (s, 2088H, H-34), 1.36 (m, 232H, H-16, H-17), 1.27 (s, 366H, H-7, H-22), 1.24 (s, 348H, H-28). ^{13}C NMR (100 MHz, $CDCl_3$) δ (ppm): 173.1, 172.7, 170.5, 169.6, 156.2, 146.1, 121.5, 80.1, 66.6, 65.3, 50.1, 46.3, 46.2, 42.5, 41.2, 36.2, 33.5, 31.7, 30.3, 29.2, 28.5, 26.2, 25.4, 22.8, 21.0, 18.5, 17.9. FTIR (ν_{max}/cm^{-1}, ATR): 3369 (N-H st), 2977 and 2937 (C-H st), 1741 (C=O st ester), 1710 (C=O st carbamate), 1670 (C=O st amide), 1523 (N-H δ), 1456 (CH_2, CH_3 δ), 1367 (C-N st), 1243 (CO-O st), 1155 (NCO-O st), 1054 (C-O st). SEC (*ref PMMA*): Mw 47197 g·mol^{-1}; Đ 1.19.

DHP[G2,G3,G4 + MPA,G2](NH_3^+)

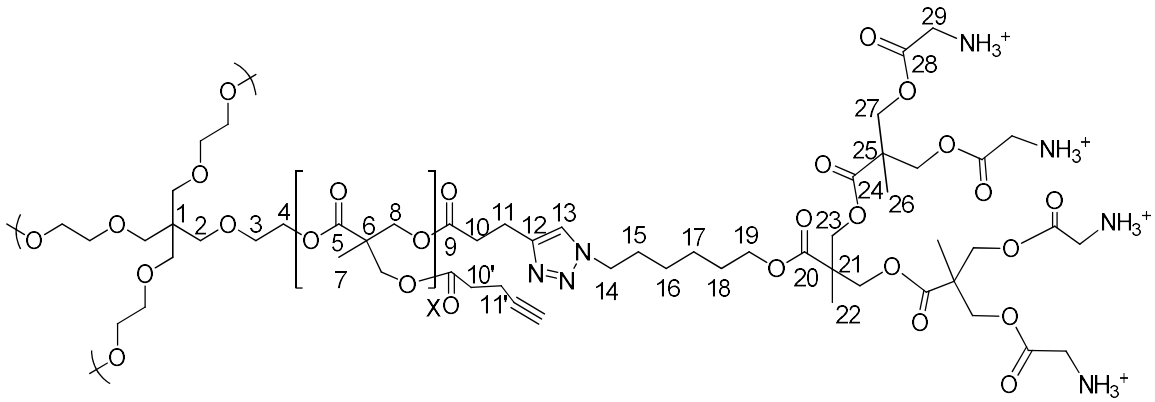

DHP[G2+MPA,G2](NH_3^+)

General procedure VI. DHP[G2+MPA,G2](NHBoc) (764.7 mg, $3.88 \cdot 10^{-2}$ mmol) and $CHCl_3$:TFA, 1:1 in volume (2 mL). A white solid was obtained (614 mg, 77%).

^{1}H NMR (400 MHz, CD_3OD) δ (ppm): 7.78 (s, 15H, H-13), 4.41 (m, 250H, H-4, H-8, H-14, H-23, H-27), 4.14 (m, 30H, H-19), 3.93 (s, 120H, H-29), 3.65 (m, 16H, H-2 and H-3), 2.98 (m, 29H, H-11), 2.74 (m, 29H, H-10), 1.90 (m, 29H, H-15), 1.67 (m, 29H, H-18), 1.43 (m, 30H, H-17), 1.35 (m, 30H, H-16), 1.29 (m, 183H, H-7, H-22, H-26). ^{13}C NMR (100 MHz, CD_3OD) δ (ppm): 174.0, 173.2, 169.7, 168.4, 162.9 (q, $^{1}J_{FC}$ = 34.7 Hz), 147.4, 123.6, 118.1 (q, $^{2}J_{CF}$ = 292.3 Hz), 67.6, 66.9, 66.6, 51.2, 48.0, 47.7, 41.0, 40.9, 34.3, 31.2, 29.5, 27.2, 26.4, 18.0, 17.7. FTIR (ν_{max}/cm^{-1}, ATR): 3300-2600 (bs, N-H^{+} st), 2972 and 2941 (C-H st), 1735 (C=O st ester), 1670-1558 (N-H^{+} δ), 1436 (CH_2, CH_3 δ), 1429 (C-N st), 1197 (CO-O st), 1132 (C-O st).

DHP[G3+MPA,G2](NH$_3^+$)

General procedure VI. DHP[G3+MPA,G2](NHBoc) (496.3 mg, 1.22·10^{-2} mmol) and $CHCl_3$:TFA, 1:1 in volume (2 mL). A white solid was obtained (494 mg, 95%). ^{1}H NMR (400 MHz, CD_3OD) δ (ppm): 7.78 (s, 31H, H-13), 4.41 (m, 506H, H-4, H-8, H-14, H-23, H-27), 4.14 (m, 62H, H-19), 3.93 (s, 248H, H-29), 3.65 (m, 16H, H-2 and H-3), 2.97 (m, 62H, H-11), 2.73 (m, 62H, H-10), 1.90 (m, 62H, H-15), 1.67 (m, 62H, H-18), 1.43 (m, 62H, H-17), 1.35 (m, 62H, H-16), 1.29 (m, 375H, H-7, H-22, H-26). ^{13}C NMR (100 MHz, CD_3OD) δ (ppm): 174.0, 173.2, 168.4, 163.0 (q, $^{1}J_{FC}$ = 34.4 Hz), 147.4, 123.6, 117.8 (q, $^{2}J_{CF}$ = 292.8 Hz), 67.6, 66.9, 66.6, 51.3, 48.0, 47.7, 41.0, 34.3, 31.2, 29.5, 27.2, 26.4, 21.8, 18.0. FTIR (ν_{max}/cm^{-1}, ATR): 3300-2600 (bs, N-H^{+} st), 2972 and 2945 (C-H st), 1735 (C=O st ester), 1670-1596 (N-H^{+} δ), 1471 (CH_2, CH_3 δ), 1429 (C-N st), 1178 (CO-O st), 1132 (C-O st).

DHP[G4+MPA,G2](NH$_3^+$)

General procedure VI. DHP[G4+MPA,G2](NHBoc) (742.4 mg, 9.08·10^{-3} mmol) and $CHCl_3$:TFA, 1:1 in volume (2 mL). A white solid was obtained (701 mg, 91%). ^{1}H NMR (400 MHz, CD_3OD) δ (ppm): 7.79 (s, 62H, H-13), 4.41 (m, 1004H, H-4, H-8, H-14, H-23, H-27), 4.14 (m, 124H, H-19), 3.94 (s, 496H, H-29), 3.65 (m, 16H, H-2 and H-3), 2.97 (m, 124H, H-11), 2.73 (m, 124H, H-10), 1.89 (m, 124H, H-15), 1.67 (m, 124H, H-18), 1.41 (m, 124H, H-17), 1.36 (m, 124H, H-16), 1.29

(m, 750H, H-7, H-22, H-26). ^{13}C NMR (100 MHz, CD_3OD) δ (ppm): 174.0, 173.2, 168.5, 163.0 (q, $^{1}J_{FC}$ = 34.6 Hz), 147.5, 123.6, 118.2 (q, $^{2}J_{CF}$ = 293.1 Hz), 67.6, 66.9, 66.6, 51.3, 48.0, 47.7, 41.0, 34.3, 31.2, 29.5, 27.2, 26.4, 21.8, 18.0. FTIR (ν_{max}/cm^{-1}, ATR): 3300-2600 (bs, N-H$^+$ st), 2986 and 2918 (C-H st), 1735 (C=O st ester), 1672-1560 (N-H$^+$ δ), 1471 (CH_2, CH_3 δ), 1429 (C-N st), 1197 (CO-O st), 1126 (C-O st).

DHP[G2,G3,G4 + GMPA,G2](NH$_3^+$)

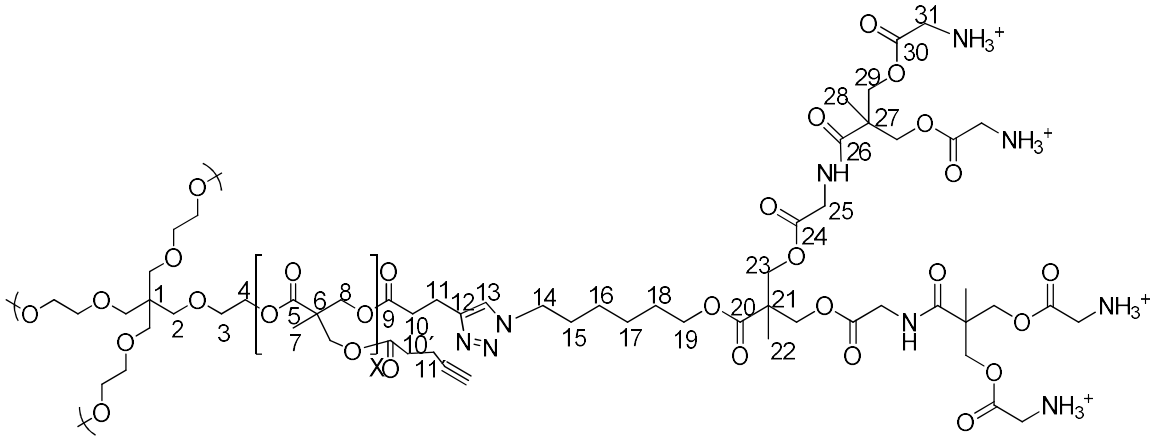

DHP[G2+GMPA,G2](NH$_3^+$)

General procedure VI. DHP[G2+GMPA,G2](NHBoc) (404.3 mg, 1.88·10^{-2} mmol) and $CHCl_3$:TFA, 1:1 in volume (1.5 mL). A white solid was obtained (293 mg, 70%). ^{1}H NMR (400 MHz, CD_3OD) δ (ppm): 7.78 (s, 15H, H-13), 4.43 (m, 250H, H-4, H-8, H-14, H-23, H-29), 4.12 (m, 30H, H-19), 3.93 (m, 180H, H-25, H-31), 3.62 (m, 16H, H-2 and H-3), 2.97 (m, 30H, H-11), 2.73 (m, 30H, H-10), 2.53 (m, 1H, H-10´), 2.44 (m, 1H, H-11´), 1.90 (m, 30H, H-15), 1.64 (m, 30H, H-18), 1.35 (m, 153H, H-7, H-16, H-17, H-22), 1.25 (m, 90H, H-28). ^{13}C NMR (100 MHz, CD_3OD) δ (ppm): 174.1, 173.6, 171.0, 168.4, 163.0 (q, $^{1}J_{FC}$ = 34.5 Hz), 147.4, 123.6, 118.2 (q, $^{2}J_{CF}$ = 292.9 Hz), 68.5, 67.2, 66.4, 51.3, 47.6, 47.4, 42.1, 41.1, 40.9, 34.3, 31.2, 29.4, 27.1, 26.4, 21.8, 18.2, 17.7. FTIR (ν_{max}/cm^{-1}, ATR): 3300-2600 (bs, N-H$^+$ st), 2983 and 2931 (C-H st), 1745 (C=O st ester), 1670 (C=O st amide), 1537 (N-H δ), 1436 (CH_2, CH_3 δ), 1411 (C-N st), 1182 (CO-O st), 1137 (NCO-O st), 1126 (C-O st).

DHP[G3+GMPA,G2](NH$_3^+$)

General procedure VI. DHP[G3+GMPA,G2](NHBoc) (167 mg, $3.8 \cdot 10^{-3}$ mmol) and $CHCl_3$:TFA, 1:1 in volume (1 mL). A white solid was obtained (152 mg, 87%). ^{1}H NMR (400 MHz, CD_3OD) δ (ppm): 7.78 (s, 29H, H-13), 4.43 (m, 478H, H-4, H-8, H-14, H-23, H-29), 4.12 (m, 58H, H-19), 3.93 (m, 348H, H-25, H-31), 3.66 (m, 16H, H-2 and H-3), 2.97 (m, 58H, H-11), 2.73 (m, 58H, H-10), 2.51 (m, 4H, H-10´), 2.44 (m, 4H, H-11´), 1.89 (m, 58H, H-15), 1.64 (m, 58H, H-18), 1.35 (m, 299H, H-7, H-16, H-17, H-22), 1.25 (m, 174H, H-28). ^{13}C NMR (100 MHz, CD_3OD) δ (ppm): 174.1, 173.6, 171.0, 168.4, 163.0 (q, $^1J_{FC}$ = 34.5 Hz), 147.4, 123.6, 118.3 (q, $^2J_{CF}$ = 293.2 Hz), [69.3-65.6], 51.3, 47.6, 47.4, 42.1, 41.1, 40.9, 34.3, 31.2, 29.4, 27.1, 26.4, 21.8, 18.2, 17.8. FTIR (ν_{max}/cm^{-1}, ATR): 3300-2600 (bs, N-H$^+$ st), 2975 and 2942 (C-H st), 1741 (C=O st ester), 1670 (C=O st amide), 1537 (N-H δ), 1473 (CH_2, CH_3 δ), 1413 (C-N st), 1182 (CO-O st), 1174 (NCO-O st), 1126 (C-O st).

DHP[G4+GMPA,G2](NH$_3^+$)

General procedure VI. DHP[G4+GMPA,G2](NHBoc) (601 mg, $6.8 \cdot 10^{-3}$ mmol) and $CHCl_3$:TFA, 1:1 in volume (2 mL). A white solid was obtained (585 mg, 93%). ^{1}H NMR (400 MHz, CD_3OD) δ (ppm): 7.78 (s, 58H, H-13), 4.43 (m, 948H, H-4, H-8, H-14, H-23 and H-29), 4.12 (m, 116H, H-19), 3.94 (m, 696H, H-25 and H-31), 3.66 (m, 16H, H-2 and H-3), 2.97 (m, 116H, H-11), 2.73 (m, 116H, H-10), 2.51 (m, 8H, H-10´), 2.44 (m, 8H, H-11´), 1.89 (m, 116H, H-15), 1.65 (m, 116H, H-18), 1.35 (m, 598H, H-7, H-16, H-17 and H-22), 1.25 (m, 348H, H-28). ^{13}C NMR (100 MHz, CD_3OD) δ (ppm): 176.9, 175.0, 174.1, 171.0, 169.0, 168.4, 163.0 (q, $^1J_{FC}$ = 34.1 Hz), 147.4, 123.6, 118.4 (q, $^2J_{CF}$ = 293.6 Hz), [69.3-65.7], 51.3, 47.6, 47.4, 42.1, 41.1, 40.9, 34.3, 31.2, 29.4, 27.2, 26.4, 21.8, 18.3, 17.8. FTIR (ν_{max}/cm^{-1}, ATR): 3300-2600 (bs, N-H$^+$ st), 2995 and 2950 (C-H st), 1745 (C=O st ester), 1670 (C=O st amide), 1539 (N-H δ), 1436 (CH_2, CH_3 δ), 1413 (C-N st), 1182 (CO-O st), 1176 (NCO-O st), 1128 (C-O st).

7.1.4.1. Rhodamine B labelled DHPs

General procedure XII: functionalisation of the deprotected DHPs with rhodamine B

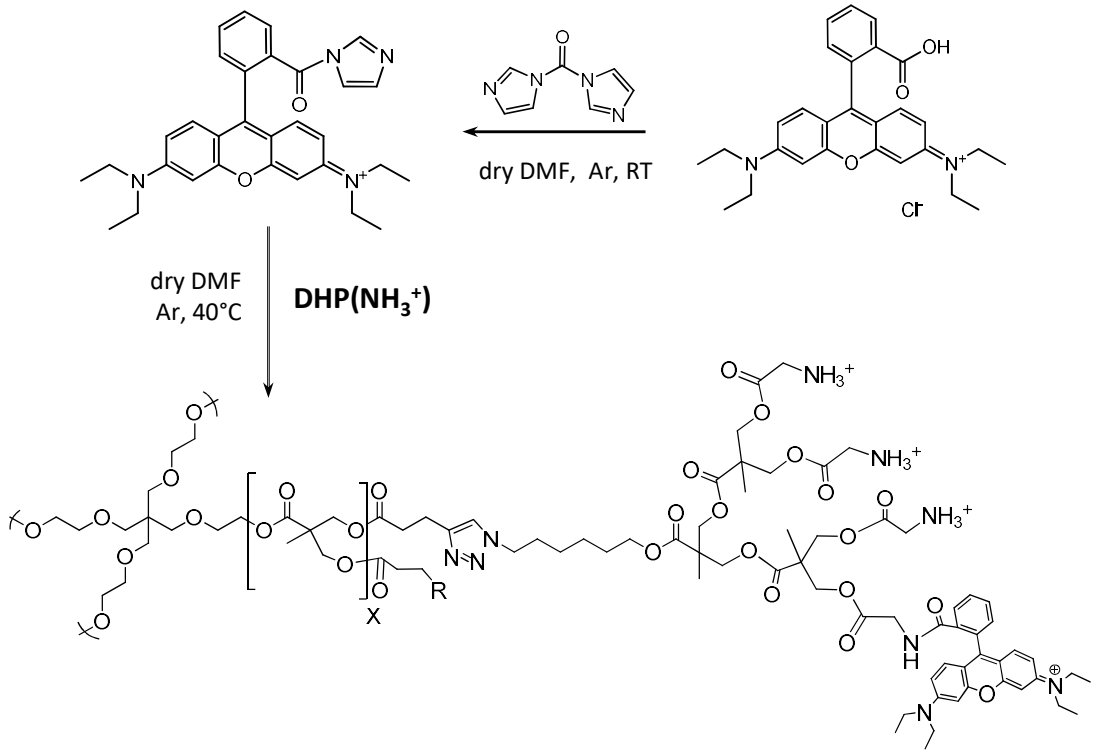

Firstly, the carboxylic acid of rhodamine B (RhB) (0.01 equivalent per amino terminal group) was activated by reaction with 1,1´-carbonyldiimidazole (CDI) (0.0103 equivalent per amino terminal group) in anhydrous DMF for 1 hour at RT. Then, the mixture was allowed to react with terminal amino groups of the DHP (1.00 equivalent) dissolved in the same solvent for 24 h at 40 °C. The amount of RhB added was estimated to obtain a final functionalisation around 1% of the amino terminal groups of each pseudodendrimer. Purification was developed by three consecutive precipitations into cold ether and further recovery by centrifugation. Finally, products were freeze-dried to obtain the final product as a pink solid.

DHP[G2,G3,G4 + MPA,G2](NH$_3^+$)-RhB

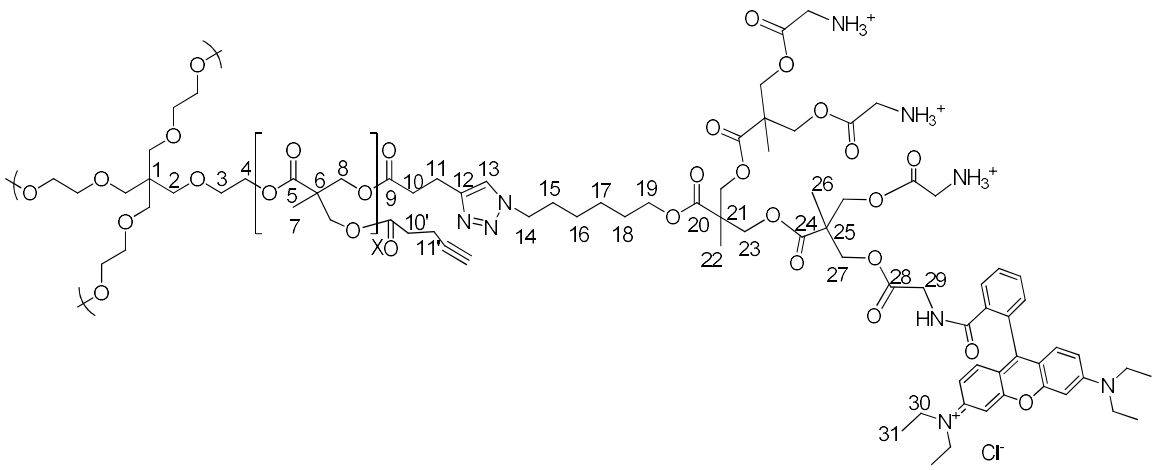

DHP(G2)-MPA-RhB

General procedure XII. DHP(G2)-MPA (250.0 mg, $1.22 \cdot 10^{-2}$ mmol, 1.00 eq), RhB (3.2 mg, $6.72 \cdot 10^{-3}$ mmol, 0.60 eq), CDI (1.9 mg, $1.17 \cdot 10^{-2}$ mmol, 0.62 eq) and dry DMF (5 mL). A pink solid was obtained (99 mg, 0.92% functionalisation). ^{1}H NMR (400 MHz, CD_3OD) δ (ppm): [8.20-6.30] (m, H_{ar} RhB), 7.78 (s, 15H, H-13), 4.41 (m, 250H, H-4, H-8, H-14, H-23 and H-27), 4.14 (m, 30H, H-19), 3.92-3.84 (m, 120H, H-29), 3.65 (m, 16H, H-2 and H-3), 2.97 (m, 29H, H-11), 2.74 (m, 29H, H-10), 1.90 (m, 29H, H-15), 1.66 (m, 29H, H-18), 1.43 (m, 30H, H-17), 1.35 (m, 30H, H-16), 1.31-1.10 (m, 189H, H-7, H-22, H-26 and H-31). FTIR (ν_{max}/cm^{-1}, ATR): 3600-2430 (bs, N-H$^+$ st), 2941 and 2887 (C-H st), 1728 (C=O st ester), 1674 (N-H$^+$ δ), 1466 (CH_2, CH_3 δ), 1411 (C-N st), 1184 (CO-O st), 1130 (C-O st).

DHP(G3)-MPA-RhB

General procedure XII. DHP(G3)-MPA (399.0 mg, $9.38 \cdot 10^{-3}$ mmol, 1.00 eq), RhB (5.6 mg, $1.16 \cdot 10^{-2}$ mmol, 1.24 eq), CDI (1.95 mg, $1.20 \cdot 10^{-2}$ mmol, 1.28 eq) and dry DMF (5 mL). A pink solid was obtained (260 mg, 0.48% functionalisation). ^{1}H NMR (400 MHz, CD_3OD) δ (ppm): [8.20-6.30] (m, H_{ar} RhB), 7.78 (s, 31H, H-13), 4.41 (m, 506H, H-4, H-8, H-14, H-23 and H-27), 4.14 (m, 62H, H-19), 3.93-3.85 (m, 248H, H-29), 3.65 (m, 16H, H-2 and H-3), 2.97 (m, 62H, H-11), 2.73 (m, 62H, H-10), 1.90 (m, 62H, H-15), 1.67 (m, 62H, H-18), 1.43 (m, 62H, H-17), 1.35 (m, 62H, H-16), 1.32-1.12 (m, 381H, H-7, H-22, H-26 and H-31). FTIR (ν_{max}/cm^{-1}, ATR): 3600-2430 (bs, N-H$^+$ st), 2941 and 2881 (C-H st),

1730 (C=O st ester), 1672 (N-H^+ δ), 1471 (CH_2, CH_3 δ), 1433 (C-N st), 1182 (CO-O st), 1126 (C-O st).

DHP(G4)-MPA-RhB

General procedure XII. DHP(G4)-MPA (552.0 mg, $6.48 \cdot 10^{-3}$ mmol, 1.00 eq), RhB (7.7 mg, $1.61 \cdot 10^{-2}$ mmol, 2.48 eq), CDI (2.7 mg, $1.65 \cdot 10^{-2}$ mmol, 2.55 eq) and dry DMF (5 mL). A pink solid was obtained (422 mg, 0.65% functionalisation). ^{1}H NMR (400 MHz, CD_3OD) δ (ppm): [8.20-6.30] (m, H_{ar} RhB), 7.79 (s, 62H, H-13), 4.41 (m, 1004H, H-4, H-8, H-14, H-23 and H-27), 4.14 (m, 124H, H-19), 3.94-3.84 (m, 496H, H-29), 3.65 (m, 16H, H-2 and H-3), 2.97 (m, 124H, H-11), 2.73 (m, 124H, H-10), 1.89 (m, 124H, H-15), 1.67 (m, 124H, H-18), 1.41 (m, 124H, H-17), 1.36 (m, 124H, H-16), 1.32-1.09 (m, 766H, H-7, H-22, H-26 and H-31). FTIR (v_{max}/cm^{-1}, ATR): 3650-2400 (N-H^+ st), 2947 and 2881 (C-H st), 1730 (C=O st ester), 1672 (N-H^+ δ), 1471 (CH_2, CH_3 δ), 1432 (C-N st), 1184 (CO-O st), 1128 (C-O st).

DHP[G2,G3,G4 + GMPA,G2](NH_3^+)-RhB

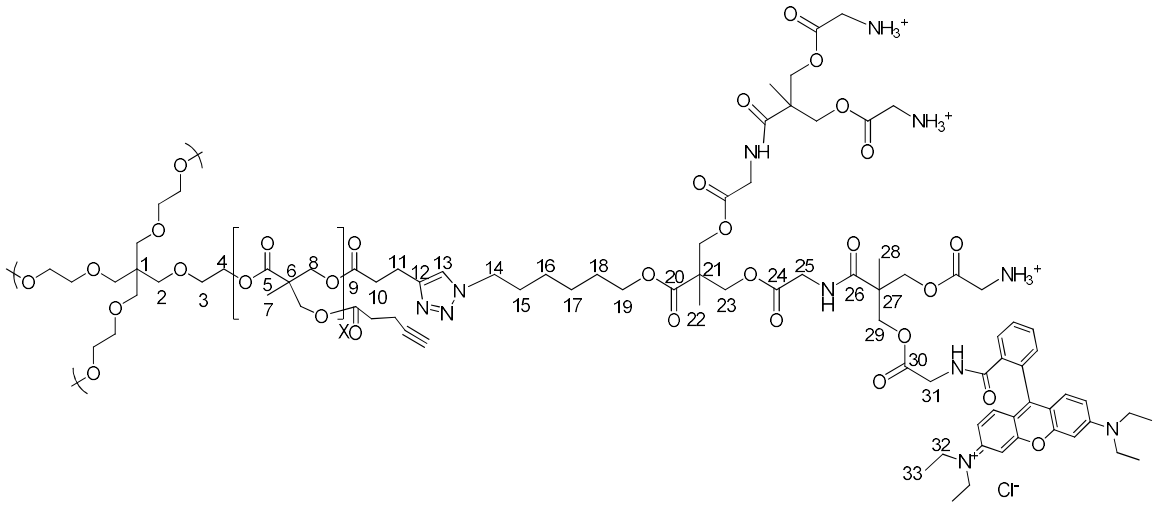

DHP(G2)-GMPA-RhB

General procedure XII. DHP(G2)-GMPA (256.0 mg, $1.15 \cdot 10^{-2}$ mmol, 1.00 eq), RhB (4.2 mg, $6.90 \cdot 10^{-3}$ mmol, 0.60 eq), CDI (1.2 mg, $7.13 \cdot 10^{-3}$ mmol, 0.62 eq)

and dry DMF (5 mL). A pink solid was obtained (211 mg, 0.99% functionalisation). ^{1}H NMR (400 MHz, CD_3OD) δ (ppm): [8.38-6.32] (m, H_{ar} RhB), 7.78 (s, 15H, H-13), 4.47-4.15 (m, 250H, H-4, H-8, H-14, H-23 and H-29), 4.12 (m, 30H, H-19), 3.99-3.82 (m, 180H, H-25 and H-31), 3.62 (m, 16H, H-2 and H-3), 2.97 (m, 30H, H-11), 2.73 (m, 30H, H-10), 2.53 (m, 1H, H-10´), 2.44 (m, 1H, H-11´), 1.90 (m, 30H, H-15), 1.64 (m, 30H, H-18), 1.35 (m, 153H, H-7, H-16, H-17and H-22), 1.25 (m, 98H, H-28 and H-33). FTIR (v_{max}/cm^{-1}, ATR): 3650-2400 (bs, N-H$^+$ st), 2941 and 2881 (C-H st), 1730 (C=O st ester), 1668 (C=O st amide), 1533 (N-H δ), 1472 (CH_2, CH_3 δ), 1411 (C-N st), 1184 (CO-O st), 1130 (C-O st).

DHP(G3)-GMPA-RhB

General procedure XII. DHP(G3)-GMPA (141.0 mg, $3.06 \cdot 10^{-3}$ mmol, 1.00 eq), RhB (2.3 mg, $3.79 \cdot 10^{-3}$ mmol, 1.24 eq), CDI (1.2 mg, $3.92 \cdot 10^{-3}$ mmol, 1.28 eq) and dry DMF (5 mL). A pink solid was obtained (110 mg, 0.89% functionalisation). ^{1}H NMR (400 MHz, CD_3OD) δ (ppm): [8.40-6.32] (m, H_{ar} RhB), 7.78 (s, 29H, H-13), 4.48-4.15 (m, 478H, H-4, H-8, H-14, H-23, H-29), 4.12 (m, 58H, H-19), 4.00-3.80 (m, 348H, H-25 and H-31), 3.66 (m, 16H, H-2 and H-3), 2.97 (m, 58H, H-11), 2.73 (m, 58H, H-10), 2.51 (m, 4H, H-10´), 2.44 (m, 4H, H-11´), 1.89 (m, 58H, H-15), 1.64 (m, 58H, H-18), 1.35 (m, 299H, H-7, H-16, H-17, H-22), 1.25 (m, 186H, H-28 and H-33). FTIR (v_{max}/cm^{-1}, ATR): 3670-2340 (bs, N-H$^+$ st), 2935 and 2881 (C-H st), 1728 (C=O st ester), 1670 (C=O st amide), 1541 (N-H δ), 1471 (CH_2, CH_3 δ), 1412 (C-N st), 1184 (CO-O st), 1134 (C-O st).

DHP(G4)-GMPA-RhB

General procedure XII. DHP(G4)-GMPA (534.0 mg, $5.79 \cdot 10^{-3}$ mmol, 1.00 eq), RhB (6.5 mg, $1.34 \cdot 10^{-2}$ mmol, 2.32 eq), CDI (2.24 mg, $1.38 \cdot 10^{-2}$ mmol, 2.39 eq) and dry DMF (6 mL). A pink solid was obtained (399 mg, 0.59% functionalisation). ^{1}H NMR (400 MHz, CD_3OD) δ (ppm): [8.34-6.30] (m, H_{ar} RhB), 7.78 (s, 58H, H-13), 4.48-4.16 (m, 948H, H-4, H-8, H-14, H-23 and H-29), 4.12 (m, 116H, H-19), 4.00-3.82 (m, 696H, H-25 and H-31), 3.66 (m, 16H, H-2 and H-3), 2.97 (m, 116H, H-11), 2.73 (m, 116H, H-10), 2.51 (m, 8H, H-10´), 2.44 (m, 8H,

H-11´), 1.89 (m, 116H, H-15), 1.65 (m, 116H, H-18), 1.35 (m, 598H, H-7, H-16, H-17 and H-22), 1.25 (m, 364H, H-28 and H-33). FTIR (ν_{max}/cm^{-1}, ATR): 3650-2600 (bs, N-H^+ st), 2976 and 2896 (C-H st), 1738 (C=O st ester), 1643 (C=O st amide), 1528 (N-H δ), 1439 (CH_2, CH_3 δ), 1377 (C-N st), 1188 (CO-O st), 1178 (NCO-O st), 1128 (C-O st).

7.2. Procedures and equipments

7.2.1. General procedures and equipments

Transmission electron microscopy (TEM)

Electron Microscopy images were recorded on a FEI TECNAI T20 system with a beam power of 200 kV. For TEM, a droplet (10 µL) of the freshly prepared sample at 1 mg/mL was deposited on a Formvar (10 nm)/Carbon Film (1 nm) coated 400 mesh coppered grid (ANAME) and 1% aqueous uranyl acetate solution was used as negative stain.

Atomic Force Microscopy (AFM)

AFM measurements were carried out in a Veeco-Bruker Multimode 8 instrument using a cantilever with a force constant of 22-100 N/m (NT-NMD Spectrum Instruments). 4 µL of samples in distilled water were deposited into previously exfoliated mica substrate and allowed to fix for 5 minutes. Then, three consecutive washes with filtered milliQ-H_2O were performed and samples were softly dried with a N_2 flux for 3 minutes. Soft tapping mode in air was employed for the measurements (150-800 kHz) and software WSxM 4.0 Beta 9.3[1] was used for further image analysis.

Dynamic light scattering (DLS)

The hydrodynamic diameters of the samples in aqueous solution were measured with a Malvern Instruments Nano ZS with a 633 nm wavelength laser and a detection angle of 173°. Disposable ZEN0040 cuvettes were employed and a series of three measurements of five runs each were performed for each sample. Average hydrodynamic diameters (in nm) were obtained after applying intensity and number data treatment. Unless otherwise indicated, samples were dissolved in distilled water at the concentration of 1 mg/mL.

Fluorescence and absorbance

The fluorescence emission spectra were obtained on a Perkin-Elmer-Ls 55 system. The UV-Vis absorbance of the samples was measured with a Varian Cary 100 probe UV-Vis spectrophotometer.

Formation of the dendrimer aggregates

The formation of the nanoaggregates from the amphiphilic Janus dendrimer was carried out by the oil-in-water method. Each dendrimer was dissolved at a concentration of 1 mg/mL in DCM, a volatile and water-immiscible solvent. An appropriate volume of distilled water was added to obtain a final concentration of 1 mg/mL in water. The mixtures were stirred at room temperature with an orbital shaker until the organic solvent had completely evaporated.

Critical aggregation concentration (CAC) determination

The critical aggregation concentration (CAC) of the amphiphilic Janus dendrimer was measured using the nile red fluorescence technique[2]. Samples with a volume of 2 mL and a concentration in the range from $1 \cdot 10^{-5}$ to 1 mg/mL were prepared. Nile red was dissolved in ethanol at a concentration of $2.5 \cdot 10^{-1}$ mM and 10 µL of this solution was added to the dendrimer solutions. The mixtures were stirred at room temperature for 1 hour in the dark using an IKA KS 130 basic orbital shaker. The emission spectrum was measured (λ_{max1} = 653 nm, λ_{max2} = 635 nm and λ_{exc} = 550 nm). The CAC was determined by plotting the fluorescence emission intensity of nile red at 635 nm as a function of the dendrimer concentration. The change of the curve slope corresponds to the beginning of lipophilic domain formation.

7.2.2. Specific procedures in the biomedical applications

7.2.2.1. Materials

The material for cellular culture was obtained from TPP® or Thermo Fisher Scientific™; culture media DMEM, PBS and trypsin-EDTA 0.25% from Gibco™; FBS from Fisher™; PBS 5x with EDTA from Alfa Aesar; MesenCult™ Expansion Kit (Mouse) from Stemcell; plasmid DNA from Clontech; siRNA from Horizon Dharmacon; Alamar Blue and Lipofectamine 3000 from Invitrogen™ and Superfect from Quiagen.

The drugs iopanoic acid, tiratricol, rifampicin, streptomycin sulphate and bedaquiline were obtained from Sigma Aldrich®; isoniazid from FLUKA and heparin from Bioiberica.

7.2.2.2. Study of the Janus dendrimers in hepatitis C

Isothermal titration calorimetry (ITC)

Drug binding to dendritic aggregates was studied by ITC with an Auto-iTC200 Isothermal Titration Calorimetry (MicroCal, GE Healthcare). Drug samples and reference solutions were properly degassed and carefully loaded into the cells to avoid bubble formation during stirring. Experiments were performed with freshly prepared drug solutions, at 25°C in PBS/milliQ-H_2O (1:1 in volume) with up to 2% of DMSO. The solutions with the dendritic aggregates at 20-80 μM concentration were placed in the calorimetric cell and titrated with the solution containing the drug at 200-1600 μM, always being the syringe solution ten or twenty times higher than the dendritic aggregates solution in each experiment. Control experiments were performed under the same experimental conditions. The heat evolved after each drug-containing solution injection was obtained from the integral of the calorimetric signal. The heat due to the binding reaction was obtained as the difference between the reaction heat and the corresponding heat of dilution, the latter estimated as a constant heat throughout the experiment and included as an adjustable parameter in the analysis. The association constant (K_a) and the enthalpy change (ΔH) were obtained through non-linear regression of experimental data to a model with a single ligand binding site. Data were analysed using the software developed in the laboratory of Dra. Olga Abian implemented in Origin 7.0 (OriginLab, USA).

Drug loading and quantification

The solvent diffusion technique was employed to encapsulate the compounds iopanoic acid (IA) and 3,5,3'-triiodothyroacetic acid (TRIAC) within the dendritic aggregates previously formed, thus mimicking the process that undergoes during the ITC technique. Firstly, compounds were dissolved into DMSO at the high concentration of 50 mg/mL (87.58 mM IA and 80.39 mM TRIAC, respectively)

and the corresponding volume of each solution was added to the previously prepared aggregates to reach the ratio of 5 mol of drug per mol of dendrimer, at the same time that DMSO volume does not exceed 2.5% (v/v). The mixtures were stirred at 4°C for 16 hours to allow drugs to enter within the aggregates. DMSO was removed by dialysis against distilled water in sink conditions at 4°C using a MWCO 1000 Dalton membrane replacing dialysis medium up to 48 hours. The non-encapsulated compounds were removed by filtration through 0.22 µm syringe filter to obtain the dendrimer/drug conjugates.

The concentration of encapsulated drug was directly measured by absorbance ($\lambda_{iopanoic\ acid}$ = 317 nm and $\lambda_{tiratricol}$ = 300 nm) adding 75% (v/v) of spectrophotometric grade DMSO (Sigma Aldrich®) to dissociate the aggregates and allow the release of the drug. In each case, the absorbance was compared with a calibration curve in the range between 15 and 250 µg/mL of the corresponding drug. The encapsulation process was repeated at least three times, and the average drug loading content was determined as the quantity in mol of encapsulated drug per mole of Janus dendrimer.

Cells and Replicon System

The highly permissive cell clone Huh 7-Lunet, as well as Huh 7 cells containing subgenomic HCV replicons I389luc-ubi-neo/NS3-3'/5.1 (Huh 5-2), I377NS3-3'/wt (Huh 9-13), or I389/hygro-ubi-NS3-3/5.1 (a kind gift from Dr. V. Lohmann and Dr. R. Bartenschlager) has been previously described[3–6]. Briefly, this system allowed the efficient propagation of genetically modified HCV RNAs (replicons) in a human hepatoma cell line (Huh). The amount of RNA that has been transcribed and translated is determined through the quantification of a reporter contained in the replicon system (luciferase). The amount of luminescence detected (after adding the substrate specific for this enzyme) is proportional to the virus replication rate. Cells were grown in Dulbecco's Modified Eagle's Medium (DMEM) supplemented with 10% heat-inactivated fetal bovine serum, 1X non-essential amino acids, 100 IU/mL penicillin, 100 µg/mL streptomycin and 250 µg/mL geneticin (G418).

Antiviral Assay with Huh 5-2 Cells

Antiviral assays for assessing the efficacy of the drug-dendrimer systems were performed as described in the literature[3–7]. Briefly, Huh 5-2 cells were seeded at a density of $7 \cdot 10^3$ cells per well in a tissue culture-treated white 96-well view plate (Techno Plastic Products AG) in complete DMEM supplemented with 250 µg/mL G418. After incubation for 24 h at 37 °C, the medium was removed and two-fold serial dilutions in complete DMEM (without G418) of the drug-dendrimer nanocarriers were added to a total volume of 100 µL. Final drug concentrations up to 160 µM for IA and up to 67 µM for TRIAC were tested, the maximum assayed concentration depended on the loading efficiency. Specifically, 160, 80, 99 µM of IA loaded into $(NH_3^+)_8$[GMPA]-[MPA]$(C17)_2$, $(NH_3^+)_8$[GMPA]-[MPA]$(C17)_4$ or $(NH_3^+)_8$[MPA]-[GMPA]$(C17)_2$, respectively, were assayed. For TRIAC, 63, 67 and 61 µM were tested within the previous dendrimer nanocarriers. After 3 days of incubation at 37 °C, luciferase activity was determined using the Bright-Glo™ Luciferase Assay System (30 µL). The luciferase signal was measured using a Synergy HT 50 Multimode Reader (BioTek Instruments). Luminescence signal levels obtained in each assay were normalised using internal patterns previously determined in Huh 5-2 cells. The 40% effective concentration (EC40) was defined as the concentration of compound that reduced the luciferase signal by 40%.

Viability Assay

Cytotoxicity assays for assessing the cell viability of all the dendrimer/drug aggregates were performed as described in the literature. Briefly, Huh5-2 cell lines were seeded at a density of $7 \cdot 10^3$ cells per well of a 96-well plate in complete DMEM with the appropriate concentration of G418. Serial dilutions of the dendrimer/drug aggregates in complete DMEM (without G418) were added 24 h after seeding. Cells were allowed to proliferate for 3 days at 37 °C. Cell culture medium was removed and cell number was determined by CellTiter 96® AQueous One Solution Cell Proliferation Assay. The 50% cytotoxic concentration (CC50) was determined employing the dose-response equation (i.e., Hill equation). All experiments on Huh5-2 cells were carried out in triplicate.

7.2.2.3. Study of the Janus dendrimers in tuberculosis

Drug loading and quantification

The oil-in-water technique was employed to encapsulate the compounds RIF, INH, streptomycin and bedaquiline while the dendritic aggregates were formed. Compounds were dissolved either in DCM (RIF), in milliQ-H_2O (INH and streptomycin) or DMSO (bedaquiline), and a molar ratio 5:1 with respect to the dendrimer was stablished. Volumes of water and DCM were adjusted to be equal and mixtures were stirred at RT under ventilation until the complete evaporation of DCM. Then, samples were dialysed against dH_2O (MWCO = 1 KDa) and filtered off (0.2 µm syringe filter).

The concentration of encapsulated drug was directly measured by HPLC/UV with analytical cartridge C8 column (4.6 mm x 250 mm, 5 µm, Waters) and a flow rate of 1 mL/min. The mobile phase for streptomycin and bedaquiline determination was methanol: orthophosphoric acid buffer pH 3.0, 40:60[8,9]. For the drugs INH and RIF, the eluent consisted of acetonitrile: orthophosphoric acid buffer pH 3.0, 60:40[10–12]. For the combination RIF+INH, the mobile phase was acetonitrile: orthophosphoric acid buffer pH 3.0, 40:60. The conditions for each drug identification were: streptomycin (200 nm, 2.6 min), bedaquiline (225 nm, 3.7 min), INH (260 nm, 3.1 min) and RIF (335 nm, 4.1 min). In the mixture RIF+INH, the RT of RIF increased to 8.5 min. The average drug loading content was determined in µg/mL and the DLC was calculated as the quantity in mol of encapsulated drug per mole of Janus dendrimer.

Bacterial strains and culture

The attenuated Calmette and Guerin bacillus (BCG) and *Mycobacterium tuberculosis* strains were provided by the Mycobacteria's Genetics group of University of Zaragoza. They were grown at 37 °C in Middlebrook 7H9 medium supplemented with 10% ADC (albumin, dextrose, catalase) and 0.05% Tween 80. In the case of *M. tuberculosis*, all the experiments were carried out in a biosafety level 3 laboratory (BSL-3).

Antimicrobial determination

BCG strain was firstly selected to assess the minimum inhibitory concentration (MIC) of the whole battery of compounds: free drugs, empty dendritic aggregates and aggregates containing one drug or a combination of drugs. Then, the antimicrobial activity of a selection of compounds was also determined in *M. tuberculosis* following the same procedure, as it is described below.

Serial dilutions of the compounds dissolved in 100 µL of Middlebrook 7H9 medium supplemented with 0.5% glycerol and 10% ADC were added in 96 multiwell microplates in duplicates. The same volume of the corresponding bacteria was inoculated at $2 \cdot 10^5$ CFU/mL (determined by optical density measurement at 590 nm), so as the final cell density assayed was 10^5 CFU/mL. After incubating plates for 6 days at 37 °C, 30 µL per well of resazurin (0.01 % w/v) were added and the mixtures were incubated for another 48 hours. The presence of metabolically active bacteria was translated into a colour change of the suspension from blue to pink, due to the reduction of the resazurin. Thus, the MIC value was stablished as the lowest concentration (blue in colour) of the compound tested that provoked the inhibition in bacterial growth[13]. In the case of the assays with *M. tuberculosis*, the antimicrobial activity revealed by the reduction of the resazurin was more precisely determined by fluorescence measurement at λ_{exc}: 530 and λ_{em}: 590 nm.

Synergy test

This assay was used to study the interaction between two compounds against a particular bacterial strain. It allows calculation of the fractional inhibitory concentration index, FICI, which indicates whether there is synergy, no interaction or antagonism between the compounds. It was carried out in a 96-well plates format and cell growth assessed by the resazurin assay.

Antibiotic stock: in fresh medium prepare a solution with 4x highest concentration of the compound to be tested. For each 96-well plate prepare 1.5 mL of antibiotic “A” stock solution (4x) and 0.7 mL of antibiotic “B” stock solution (4x).

1. Add 100 µL of fresh medium to each well except wells A2 to G2.
2. Add 50 µL of fresh media to wells A2 to F2.
3. Add 100 µL of 4x antibiotic “A” stock solution from G1 to G12.

4. Add 100 µL of 4x antibiotic “B” stock solution from H2 to G2.
5. Add 50 µL of 4x antibiotic “B” stock solution from F2 to A2.
6. Make 2-fold serial dilutions of compound “A” (from G1-G12 to A1-A12). Discard the last 100 µL.
7. Make 2-fold serial dilutions of compound “B” (from A2-H2 to A12-H12). Discard the last 100 µL. Wells G2 to A2 remain empty.
8. Add 100 µL of the $2 \cdot 10^5$ CFU/mL bacterial cell inoculum to each well.

FICI index analysis

FIC index (FICI) is calculated as follows: $FICI = FIC_A + FIC_B$

$FIC_{A \text{ or } B}$ = (MIC of A or B in the presence of B or A) / MIC of A or B alone.

a. Column A1-H1 indicates MIC for “A”.
b. Row H1-H12 indicates MIC for “B”.
c. Determine for each row and column those wells with the lowest concentration for each of both compounds which is inhibiting cell growth.
d. Calculate $FIC_{A \text{ and } B}$ for each well.
e. Plot values FIC_A vs FIC_B to determine the shape of the curve. The closer to origin, the more synergistic the interaction is.

7.2.2.4. Study of the DHPs in malaria

Polyacrylamide gel electrophoresis

Samples of DHPs/heparin and free heparin were incubated in RPMI at 37 ºC under gentle stirring for different time periods and then, they were separated by non-denaturing electrophoresis. For that, 6% polyacrylamide gels were prepared and 20 µg of polysaccharide at 1 mg/mL were loaded into each well with TRIS-HCl 20 mM pH 8.8 as running buffer[14]. Then, electrophoresis was performed in a Bio-Rad equipment at 100 V for 40 min. Gels were later stained with 0.5% Alcian Blue solution in 3% acetic acid/ 25% isopropanol for 30 min with gentle stirring. Finally, they were de-stained in 10% acetic acid/ 40% ethanol overnight changing three times the media, and they were digitalised in a ChemiDoc equipment. ImageJ software was employed to quantify the intensity of the bands.

Ethical issues for the use of human blood and *in vivo* studies

The human blood used in this work was from voluntary donors and commercially obtained from the *Banc de Sang i Teixits* (www.bancsang.net). Blood was not collected specifically for this research; the purchased units had been discarded for transfusion, usually because of an excess of blood relative to anticoagulant solution. Prior to their use, blood units underwent the analytical checks specified in the current legislation. Before being delivered to the laboratory, unit data were anonymised and irreversibly dissociated, and any identification tag or label had been removed in order to guarantee the non-identification of the blood donor. No blood data were or will be supplied, in accordance with the current *Ley Orgánica de Protección de Datos* and *Ley de Investigación Biomédica*. The blood samples will not be used for studies other than those made explicit in this research.

Mice (18-20 g) were maintained under standard environmental conditions: 20-24 °C and 12/12 h light/dark cycle, with *ad libitum* access to a semi-solid diet and water during the duration of the experiments. In the presence of toxic effects including, among others, >20% reduction in animal weight, aggressive and unexpected animal behaviour or the presence of blood in faeces, animals were immediately anesthetised using a 100 mg/kg Ketolar plus 5 mg/kg Midazolan mixture and sacrificed by cervical dislocation. The animal care and use protocols followed adhered to the specific national and international guidelines specified in the Spanish Royal Decree 53/2013, which is based on the European regulation 2010/63/UE. The studies reported here were performed under protocols reviewed and approved by the Ethical Committee on Clinical Research from the *Hospital Clínic de Barcelona* (Reg. HCB/2018/1223, January 23, 2019).

7.2.2.5. Study of the DHPs in gene transfection

Buffering ability determination

In order to determine the buffering ability of the pseudodendrimers, 1 mg of each compound or PAMAM as positive control was dissolved in 10 mL of 0.1 M NaCl. pH was adjusted to 10 with 0.1 M NaOH solution and then, successive additions of 0.1 M HCl were done until the pH value of 5 was reached. 0.1 M NaCl was

assayed as negative control and all the titrations were represented as the pH value with respect to the added volume of 0.1M HCl, in µL. pH was monitored with a sensION^{TM} + PH31 pH-meter and a HACH electrode.

Plasmid DNA amplification and purification

The commercial pAcGFP1-N1 plasmid (pGFP) was transformed into *Escherichia coli* DH5α and propagated in LB medium with kanamycin, firstly in LB-agar overnight at 37 °C to obtain isolated colonies and then, the selected colonies were grown in liquid LB for 24 hours at 37 °C. Then, plasmid DNA was purified with the PureLink Expi Endotoxin-Free Maxi Plasmid Purification Kit (ThermoFisher). Digestion with the restriction enzyme Not I (ThermoFisher) followed by gel electrophoresis (0.8% agarose) was performed to evaluate the extracted plasmid purity. Its concentration was spectroscopically determined in a nanodrop ND1000 Spectrophotometer (Nano Drop®).

Dendriplexes formation

Dendriplexes, namely, complexes between dendritic structures and genetic material, were freshly formed before each experiment. Pseudodendrimers and nucleic acids were softly mixed by pipetting in serum free DMEM medium (SFM) to avoid protein interferences during complex formation. Then, they were incubated during 20 minutes at room temperature. Different N/P ratios were assayed to stablish the minimum amount of dendritic material needed to complex a fixed amount of genetic material (0.2 µg of pGFP and 0.225 µg of siGFP). The number of N^+ terminal groups of each molecule of DHP and the P^- groups of the nucleic acids were considered in the N/P ratio determination. Lipofectamine 3000 and Superfect were employed as control transfection reagents of different chemical nature, being the first one a commonly used lipidic transfectant whereas the second one is based on a dendritic globular structure more similar to the DHPs under evaluation.

Gel retardation assay

Gel retardation assay was performed in order to check the complete nucleic acids complexation. 0.8% (w/v) agarose gels stained with 3 µL of GelRed were prepared in 1x TAE buffer. Different N/P ratios were assayed with a fixed amount

of nucleic acid and increasing amounts of pseudodendrimer in a total volume of 12 µL of SFM. Specifically, 0.2 µg of pGFP and 0.225 µg of siGFP were fixed considering commercial recommendations and the sensitivity of the technique. Electrophoresis was run at 90-100 V for 20-30 min in a Bio-Rad equipment and a GelDoc (Bio-Rad) was employed to digitalise the gels.

DLS measurements

In the specific case of the dendriplexes, the sample preparation for hydrodynamic diameter measurement was done by fixing the concentrations of pGFP and siGFP at 20 µg/mL and 5.7 µg/mL, respectively. DHPs concentrations ranged from 0.5 to 11.3 mg/mL to stablish the N/P ratios 25 or 500 for pGFP, and 150 or 750 for siGFP, the ones at which the complexes are completely formed and the most effective ones in terms of transfection activity. Complexes were softly mixed and incubated for 20 minutes at room temperature. Empty DHPs were measured at 0.5 mg/mL under the same conditions.

ζ potential titration

Measurements were performed in a Malvern Instruments Nano ZS in PBS buffer pH 7.4. Samples were prepared with 1 µg/mL of pGFP and 0.3 µg/mL of siGFP, with DHPs ranging from 26.3 to 565 µg/mL to form the same N/P ratios described for DLS measurements. Complexes were softly mixed and incubated for 20 minutes at room temperature. DTS1070 cuvettes were employed and three measurements of ten runs were developed for each sample.

Cell lines and culture

Human cervix cancer cell line HeLa and that transformed to intrinsically express the GFP protein, HeLa-GFP, were grown in DMEM (high glucose with *L*-glutamine) supplemented with 10% FBS, and 1% antibiotics (penicillin, streptomycin, amphotericin) at 37 °C and 5% CO_2 in a humidified atmosphere. Mesenchymal stem cells from mouse (mMSCs) and those stably expressing GFP, mMSCs-GFP, were maintained under the same experimental conditions with their specific MesenCult™ Expansion Medium for mouse (StemCell) supplemented with *L*-glutamine.

Viability assay

The evaluation of the cytotoxic effect of the compounds was carried out by the Alamar Blue assay. Briefly, cells were seeded at a density of $1 \cdot 10^4$ cell per well in 96 multiwell culture plates and after 24 hours of incubation at 37 °C, medium was replaced by 50 µL of the testing compounds dissolved in SFM per well, in triplicates. After 4, 8 or 24 h of incubation, the solutions were removed and 100 µL of fresh complete medium were added and incubated for another 48 hours. After that, medium was replaced by a 10% (v/v) Alamar Blue dye solution in complete DMEM and allow to react for 2 hours at 37 °C. Then, absorbance at 570 and 600 nm was read in a Multiskan GO (ThermoScientific) plate reader.

Transfection experiments

For pGFP transfection, HeLa or mMSCs cells were seeded at a density of $1 \cdot 10^4$ cells per well in 96 multiwell culture plates in their respective culture medium. After 24 h incubation at 37 °C, culture medium was removed and 50 µL of dendriplexes already formed in SFM as described above were added per well in triplicate. 0.2 µg of pGFP per well were added in all cases while the amount of dendrimer was adjusted to cover a wide range of N/P ratios (25, 50, 100, 250, 500). Complexes were incubated for 4, 8 or 24 h at 37 °C and then, compounds were replaced with 100 µL fresh medium. After 48 h incubation, GFP expression was evaluated by fluorescence microscopy (NIS-Elements, Nikon) and quantified by fluorimetric determination at 485/20 excitation, 516/20 emission wavelengths in a microplate reader (Synergy HT). Transfection experiments with siGFP were similarly performed into HeLa-GFP and mMSCs-GFP cell lines, stablishing 200 nM as the fixed concentration of siGFP per well. N/P ratios tested were 150, 300, 500 and 750. Finally, the GFP-expression decrease was determined following the same procedures. For positive controls, the commercial reagents Lipofectamine 3000 and Superfect were incubated with nucleic acids at the corresponding ratios previously stablished following the supplier recommendations. Naked nucleic acids were also tested at the same concentrations and no treated cells were included as negative controls for transfection experiments.

Internalisation and intracellular distribution by confocal microscopy

To evaluate the intracellular distribution of the rhodamine labelled DHPs with pGFP, they were visualised by confocal laser scanning microscopy after incubation with cells. Briefly, HeLa cells were seeded at a density of $4 \cdot 10^4$ cells per well and mMSCs at $8 \cdot 10^4$ cells per well over sterile glass covers on 24 multiwell plates and incubated for 24 h at 37 °C. Then, medium was replaced with 500 µL of the corresponding dendriplexes in SFM at N/P ratio 500, with 0.5 µg of pGFP per well. After 4 h of incubation at 37 °C, cells were washed three times with PBS, fixed with 4% (v/v) paraformaldehyde and washed twice with PBS. Cell permeabilisation was accomplished with a PBS plus 1% BSA and 0.1% saponin solution and then, actin filaments staining was performed by incubating 1 h in the dark with phalloidin-Alexa Fluor 488 diluted in the permeabilisation solution (1:200). Further washings were performed and then, nuclei were stained at the same time as slides were mounted with a solution of DAPI in Fluoromount-G mounting medium (1:250). Samples thus prepared were allowed to dry in the dark and sealed for later microscopic observation in a Confocal Zeiss LSM 880 with the 63x oil immersion objective. DAPI fluorescence was observed at λ_{exc}: 405 nm, λ_{em}: 453 nm; Alexa Fluor 488 at λ_{exc}: 488 nm, λ_{em}: 526 nm and finally, the Rhodamine of the labelled DHPs was examined under λ_{exc}: 561 nm, λ_{em}: 635 nm. Zen Blue 2.3 software and Image J were employed for image analysis.

Statistical analysis

Results are reported as mean ± SD (standard deviation) and data were analysed by one-way analysis of variance (ANOVA) with Tukey post-hoc testing using GraphPad Prism 8.0.2 software. $p < 0.05$, *; $p < 0.01$, **; $p < 0.001$, *** and $p < 0.0001$, **** were considered to be statistically significant.

7.3. References

(1) Horcas, I.; Fernández, R.; Gómez-Rodríguez, J. M.; Colchero, J.; Gómez-Herrero, J.; Baro, A. M. WSXM: A Software for Scanning Probe Microscopy and a Tool for Nanotechnology. *Review of Scientific Instruments* **2007**, *78* (1), 013705. https://doi.org/10.1063/1.2432410.

(2) Stuart, M. C. A.; van de Pas, J. C.; Engberts, J. B. F. N. The Use of Nile Red to Monitor the Aggregation Behavior in Ternary Surfactant-Water-Organic Solvent Systems. *J. Phys. Org. Chem.* **2005**, *18* (9), 929–934. https://doi.org/10.1002/poc.919.

(3) Courcambeck, J.; Bouzidi, M.; Perbost, R.; Jouirou, B.; Amrani, N.; Cacoub, P.; Pèpe, G.; Sabatier, J.-M.; Halfon, P. Resistance of Hepatitis C Virus to NS3-4A Protease Inhibitors: Mechanisms of Drug Resistance Induced by R155Q, A156T, D168A and D168V Mutations. *Antivir. Ther. (Lond.)* **2006**, *11* (7), 847–855.

(4) Susser, S.; Vermehren, J.; Forestier, N.; Welker, M. W.; Grigorian, N.; Füller, C.; Perner, D.; Zeuzem, S.; Sarrazin, C. Analysis of Long-Term Persistence of Resistance Mutations within the Hepatitis C Virus NS3 Protease after Treatment with Telaprevir or Boceprevir. *Journal of Clinical Virology* **2011**, *52* (4), 321–327. https://doi.org/10.1016/j.jcv.2011.08.015.

(5) Blight, K. J.; McKeating, J. A.; Rice, C. M. Highly Permissive Cell Lines for Subgenomic and Genomic Hepatitis C Virus RNA Replication. *J Virol* **2002**, *76* (24), 13001–13014. https://doi.org/10.1128/JVI.76.24.13001-13014.2002.

(6) Lohmann, V. Replication of Subgenomic Hepatitis C Virus RNAs in a Hepatoma Cell Line. *Science* **1999**, *285* (5424), 110–113. https://doi.org/10.1126/science.285.5424.110.

(7) Urbani, A.; Bazzo, R.; Nardi, M. C.; Cicero, D. O.; De Francesco, R.; Steinkühler, C.; Barbato, G. The Metal Binding Site of the Hepatitis C Virus NS3 Protease: A SPECTROSCOPIC INVESTIGATION. *J. Biol. Chem.* **1998**, *273* (30), 18760–18769. https://doi.org/10.1074/jbc.273.30.18760.

(8) Ullah, A.; Urrehman, K. Simple and Rapid Method on High Performance Liquid Chromatography (HPLC) for Estimation of Streptomycin Sulphate. *World Applied Sciences Journal* **2012**, *19*, 645–649. https://doi.org/10.5829/idosi.wasj.2012.19.05.1245.

(9) Momin, M. A. M.; Rangnekar, B.; Das, S. C. Development and Validation of a RP-HPLC Method for Simultaneous Quantification of Bedaquiline (TMC207), Moxifloxacin and Pyrazinamide in a Pharmaceutical Powder Formulation for Inhalation. *Journal of Liquid Chromatography & Related Technologies* **2018**, *41* (8), 415–421. https://doi.org/10.1080/10826076.2018.1437748.

(10) Calleri, E.; De Lorenzi, E.; Furlanetto, S.; Massolini, G.; Caccialanza, G. Validation of a RP-LC Method for the Simultaneous Determination of Isoniazid, Pyrazinamide and Rifampicin in a Pharmaceutical Formulation. *Journal of Pharmaceutical and Biomedical Analysis* **2002**, *29* (6), 1089–1096. https://doi.org/10.1016/S0731-7085(02)00150-4.

(11) Kumar, G. V.; Jayaprakash, D. D. Analytical Method Development and Validation by RP-HPLC for Simultaneous Estimation of Isoniazid and Ethambutol in Combined Tablet Dosage Form. **2015**, 9.
(12) Goutal, S.; Auvity, S.; Legrand, T.; Hauquier, F.; Cisternino, S.; Chapy, H.; Saba, W.; Tournier, N. Validation of a Simple HPLC-UV Method for Rifampicin Determination in Plasma: Application to the Study of Rifampicin Arteriovenous Concentration Gradient. *Journal of Pharmaceutical and Biomedical Analysis* **2016**, *123*, 173–178. https://doi.org/10.1016/j.jpba.2016.02.013.
(13) Soria-Carrera, H.; Lucía, A.; Matteis, L.; Aínsa, J. A.; la Fuente, J. M.; Martín-Rapún, R. Polypeptidic Micelles Stabilized with Sodium Alginate Enhance the Activity of Encapsulated Bedaquiline. *Macromol. Biosci.* **2019**, *19* (4), 1970012. https://doi.org/10.1002/mabi.201970012.
(14) Marques, J.; Vilanova, E.; Mourão, P. A. S.; Fernàndez-Busquets, X. Marine Organism Sulfated Polysaccharides Exhibiting Significant Antimalarial Activity and Inhibition of Red Blood Cell Invasion by Plasmodium. *Sci Rep* **2016**, *6* (1), 24368. https://doi.org/10.1038/srep24368.

Chapter 8:

Resumen y

conclusiones generales

8.1. Resumen

En el marco de las posibilidades ofrecidas por la nanotecnología, los **materiales dendríticos** presentan un gran interés debido a su gran potencial como transportadores de moléculas de diversa naturaleza. En este sentido, los dendrímeros y materiales derivados han sido ampliamente utilizados en **biomedicina** como transportadores de **fármacos** y de **material genético**. Dentro de la gran variedad de dendrímeros existente, la presente tesis doctoral se ha centrado en el estudio de materiales dendríticos basados en el ácido 2,2´-*bis*(hidroximetil)propiónico (***bis*-MPA**) y el ácido 2,2'-*bis*(gliciloximetil)propiónico (***bis*-GMPA**) (Figura 8.1). Éste último incluye grupos amida internos potencialmente capaces de establecer puentes de hidrógeno con las moléculas que aloje en su interior y reforzar de esta manera su interacción para una encapsulación más eficiente.

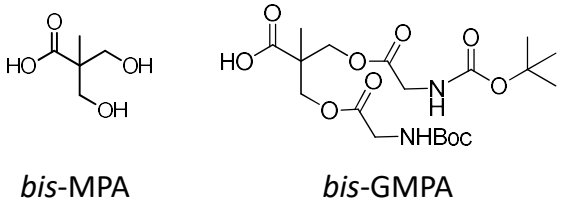

Figura 8.1. Estructura química de las unidades repetitivas de bis-MPA y bis-GMPA.

Basados en estas unidades mínimas, se han diseñado dos tipos de materiales dendríticos: **dendrímeros de tipo Jano** anfífilos y **polímeros hiperramificados dendronizados** (DHPs, por sus siglas en inglés) (Figura 8.2).

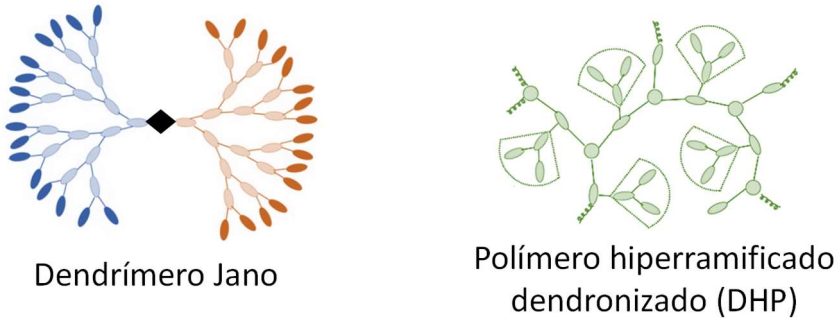

Figura 8.2. Representación esquemática de dendrímeros tipo Jano y polímeros hiperramificados dendronizados.

Los **dendrímeros tipo Jano** anfífilos combinan una cara hidrófila con una lipófila y en esta tesis doctoral, se ha alternado la composición *bis*-MPA/ *bis*-GMPA entre ambas caras. Además, también se ha modificado el número de cadenas lipófilas (2 ó 4), alterando de esta manera el balance hidrófilo del dendrímero resultante. En concreto, los dendrímeros Jano sintetizados han sido:

- **$(NH_3^+)_8$[GMPA]-[MPA](C17)$_2$** que consiste en un dendrón hidrófilo de *bis*-GMPA 3ª generación y un dendrón lipófilo de *bis*-MPA de 1ª generación,
- **$(NH_3^+)_8$[GMPA]-[MPA](C17)$_4$** que consiste en un dendrón hidrófilo de *bis*-GMPA 3ª generación y un dendrón lipófilo de *bis*-MPA de 2ª generación,
- **$(NH_3^+)_8$[MPA]-[GMPA](C17)$_2$** que consiste en un dendrón hidrófilo de *bis*-MPA 3ª generación y un dendrón lipófilo de *bis*-GMPA de 1ª generación,
- **$(NH_3^+)_8$[MPA]-[GMPA](C17)$_4$** que consiste en un dendrón hidrófilo de *bis*-MPA 3ª generación y un dendrón lipófilo de *bis*-GMPA de 2ª generación.

Por otra parte, los **DHPs** sintetizados consisten en un núcleo hiperramificado de *bis*-MPA de diferentes generaciones (G2, G3 o G4) en el cual se han insertado dendrones de *bis*-MPA o de *bis*-GMPA, obteniendo en ambos casos macromoléculas globulares policatiónicas. Esta última característica es de gran interés para acomplejar electrostáticamente diversas moléculas de naturaleza aniónica. Específicamente, se han sintetizado seis DHPs que se pueden clasificar de la siguiente manera según los dendrones componentes:

Serie *bis*-MPA:

- **DHP(G2)-MPA** que consiste en un núcleo hiperramificado de 2ª generación rodeado de dendrones de *bis*-MPA, con un total de 64 grupos amino terminales teóricos,
- **DHP(G3)-MPA** que consiste en un núcleo hiperramificado de 3ª generación rodeado de dendrones de *bis*-MPA, con un total de 128 grupos amino terminales teóricos,
- **DHP(G4)-MPA** que consiste en un núcleo hiperramificado de 4ª generación rodeado de dendrones de *bis*-MPA, con un total de 256 grupos amino terminales teóricos.

Serie *bis*-GMPA:

- **DHP(G2)-GMPA** que consiste en un núcleo hiperramificado de 2ª generación rodeado de dendrones de *bis*-GMPA, con un total de 64 grupos amino terminales teóricos,
- **DHP(G3)-GMPA** que consiste en un núcleo hiperramificado de 3ª generación rodeado de dendrones de *bis*-GMPA, con un total de 128 grupos amino terminales teóricos,
- **DHP(G4)-GMPA** que consiste en un núcleo hiperramificado de 4ª generación rodeado de dendrones de *bis*-GMPA, con un total de 256 grupos amino terminales teóricos.

En todos los casos, la estrategia empleada para la unión de los dendrones entre sí o la unión de los dendrones al núcleo hiperramificado ha sido la reacción de cicloadición 1,3-dipolar entre grupos azida y alquino catalizada por Cu (I), CuAAC, dando lugar a un anillo de triazol.

Tras sintetizar, caracterizar y estudiar las propiedades de ambos tipos de materiales dendríticos en medio acuoso (capítulo 2), se ha realizado un estudio más específico de los dendrímeros tipo Jano como transportadores de fármacos anti-hepatitis C (capítulo 3) y anti-tuberculosos (capítulo 4); mientras que los DHPs se han explorado como vectores de heparina en el tratamiento de la malaria (capítulo 5) y como vectores de material genético dentro de la estrategia denominada transfección génica (capítulo 6).

El estudio de la **hepatitis C** se ha focalizado en rescatar la actividad antiviral de dos compuestos que inhiben la actividad de la proteasa viral NS3 *in vitro*, pero que presentan escasa actividad en estudios celulares. Estos compuestos son el ácido iopanoico (IA) y el tiratricol (TRIAC), y ambos se han solubilizado con la ayuda de dendrímeros Jano como nanotransportadores. Inicialmente, se ha realizado un estudio calorimétrico para evaluar la interacción entre los compuestos y los agregados dendríticos, y posteriormente, se han incorporado dichos compuestos mediante difusión en los agregados dendríticos previamente formados. Estos agregados cargados con los compuestos se han caracterizado morfológicamente y se ha evaluado su actividad antiviral al mismo tiempo que se

ha estudiado su efecto citotóxico sobre las células. Los dendrímeros más prometedores para esta aplicación han sido $(NH_3^+)_8$[GMPA]-[MPA](C17)$_2$ y $(NH_3^+)_8$[GMPA]-[MPA](C17)$_4$, consiguiendo reducir considerablemente la EC40 de los fármacos libres.

En cuanto a la **tuberculosis**, el carácter anfífilo de los dendrímeros Jano se ha aprovechado para encapsular fármacos de diferente naturaleza de manera individual (rifampicina (RIF), isoniazida (INH), estreptomicina o bedaquilina) y combinaciones de ellos (RIF+INH). Los agregados resultantes se han caracterizado y la cantidad de fármaco encapsulada se ha cuantificado mediante HPLC. Adicionalmente, se ha evaluado la actividad antimicrobiana de todos los fármacos libres y encapsulados individualmente en los cuatro dendrímeros Jano frente a *M. bovis* BCG, comprobando que se mantiene de manera generalizada la actividad de los fármacos tras su encapsulación excepto en el caso de la bedaquilina. Posteriormente y tras comprobar la ausencia de sinergismo entre RIF e INH libres, se ha seleccionado el dendrímero $(NH_3^+)_8$[GMPA]-[MPA](C17)$_4$ para realizar la co-encapsulación de ambos (RIF+INH), y tras la correspondiente caracterización de los nanoagregados resultantes, se ha explorado su actividad antimicrobiana frente a diferentes cepas (*M. bovis* BCG, *M. tuberculosis y Mtb*-THP1*).* Otro estudio interesante realizado ha consistido en la evaluación de la cinética de muerte de *Mtb* con el tiempo frente a las diferentes combinaciones de fármacos libres y encapsulados en el dendrímero, lo que permite visualizar la aparición de resistencias bacterianas. En este sentido, ciertas condiciones de fármacos encapsulados han permitido retrasar la aparición de resistencias bacterianas, lo cual es muy positivo e interesante de cara a posibles estudios *in vivo*.

El estudio sobre la **malaria** se ha centrado en mejorar las propiedades ventajosas del polisacárido heparina como agente antimalárico y como molécula de direccionamiento hacia glóbulos rojos infectados por el parásito. Para ello, se han empleado los DHPs como vectores capaces de acomplejar la heparina y potencialmente capaces de reducir los efectos laterales perjudiciales del tratamiento con el polisacárido (fuerte actividad anticoagulante que puede derivar en hemorragias cerebrales, escaso tiempo de circulación en sangre, etc.). En primer lugar, se han formado los complejos DHP/heparina mediante

interacciones electrostáticas y se han caracterizado morfológicamente. A continuación, se ha estudiado la cinética de liberación de la heparina de los complejos, observando un posible efecto de las amidas del *bis*-GMPA como grupos capaces de establecer puentes de hidrógeno y retener en mayor medida el polisacárido. La actividad antiparasitaria de todos los complejos DHP/heparina formados, así como la de los complejos entre la heparina y los DHPs marcados con el fluoróforo rodamina (DHP-Rh/heparina), ha revelado buenos niveles de actividad de la heparina acomplejada, mejorando la IC50 de la heparina libre en algunos casos. Además, se ha estudiado mediante distintas técnicas el direccionamiento preferencial de los complejos DHPs-Rh/heparina frente a glóbulos rojos sanos o infectados por el parásito. Por último, se ha estudiado el tiempo de circulación en plasma de la heparina libre y formando complejos con los DHPs en un modelo animal *in vivo.*

Los DHPs también se han explorado como vectores no virales para introducir material genético en células tumorales (HeLa) y mesenquimales (mMSCs); es decir, para la aplicación denominada **transfección génica.** En primer lugar, se han establecido los ratios N/P a los cuales se forman los dendriplejos (complejos entre dendrímero y material genético) con pDNA y siRNA. Tras caracterizar los dendriplejos mediante diversas técnicas fisico-químicas, se ha evaluado su actividad como vectores génicos en las correspondientes líneas celulares, empleando la proteína verde fluorescente (GFP) como marcador. La valoración de los resultados de transfección (sobreexpresión de GFP con pDNA o inhibición de GFP con siRNA) junto a la toxicidad producida en las líneas celulares, postulan a los DHPs de la serie de *bis*-MPA como mejores candidatos, ya que los homólogos de la serie *bis*-GMPA presentan una actividad prácticamente despreciable, probablemente debido a su menor internalización celular y a una menor disociación del material genético del dendriplejo. En concreto, la actividad como vector de transfección mejora conforme aumenta la generación del núcleo hiperramificado y son necesarios ratios N/P elevados para alcanzar buenos niveles de transfección e incluso superar a agentes comerciales muy eficaces.

8.2. Conclusiones generales

Se han sintetizado de manera satisfactoria la serie de materiales dendríticos descritos anteriormente, dendrímeros de tipo Jano y DHPs, y se ha evaluado su comportamiento en medio acuoso, así como su biocompatibilidad hasta concentraciones suficientemente elevadas con vistas a las aplicaciones biomédicas.

De los resultados obtenidos pueden extraerse las siguientes conclusiones:

Dendrímeros tipo Jano

1. El carácter anfífilo de los dendrímeros de tipo Jano permite la encapsulación individual y combinada de diferentes fármacos, manteniendo e incluso mejorando su actividad celular.

2. La estructura de los fármacos utilizados condiciona la morfología de los agregados resultantes, lo que resulta fundamental en sus aplicaciones.

3. La presencia de *bis*-GMPA en la cara lipófila del dendrímero altera la clara distinción entre los bloques hidrófilo y lipófilo del dendrímero y distorsiona la morfología de los agregados que forman los dendrímeros en agua, lo que se traduce en una menor capacidad de carga de fármacos mediante el método de difusión. Por lo que estos dendrímeros no favorecen la carga de los fármacos.

4. Por otro lado, los dendrímeros con los grupos amida del *bis*-GMPA en la cara hidrófila, $(NH_3^+)_8$[GMPA]-[MPA](C17)$_2$ y $(NH_3^+)_8$[GMPA]-[MPA](C17)$_4$, son más adecuados como nanotransportadores de fármacos, lo que los hace mucho más interesantes para futuros estudios.

Polímeros Hiperramificados Dendronizados

5. Se ha comprobado que la liberación de la heparina de los complejos DHP-GMPA/heparina es más lenta que la liberación de los complejos con *bis*-MPA. Este hecho permitirá utilizar un material u otro según la aplicación buscada.

6. Los DHPs de la serie *bis*-MPA han demostrado ser vectores no virales muy eficientes para introducir material genético en el interior de células tumorales y más interesantemente, en células mesenquimales. Este hecho abre la puerta a múltiples posibilidades terapéuticas debido a su capacidad de diferenciación en varios tejidos celulares diferentes.

7. Por el contrario, la inclusión de dendrones de *bis*-GMPA en los DHPs incrementa las interacciones entre el pseudodendrímero y el material genético, lo que dificulta su disociación posterior y disminuye su capacidad de internalización celular. Como consecuencia, se obtienen menores niveles de transfección génica, por lo que esta estrategia sintética no es favorable para esta aplicación.

Annexes

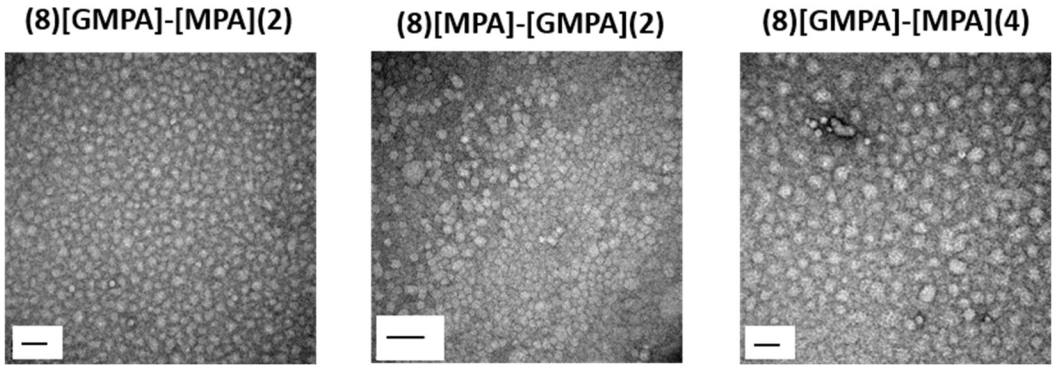

Annexe 1. TEM images of the aggregates formed by the Janus dendrimers deprotected by the HCl/ethyl acetate method. Scale bars: 50 nm.

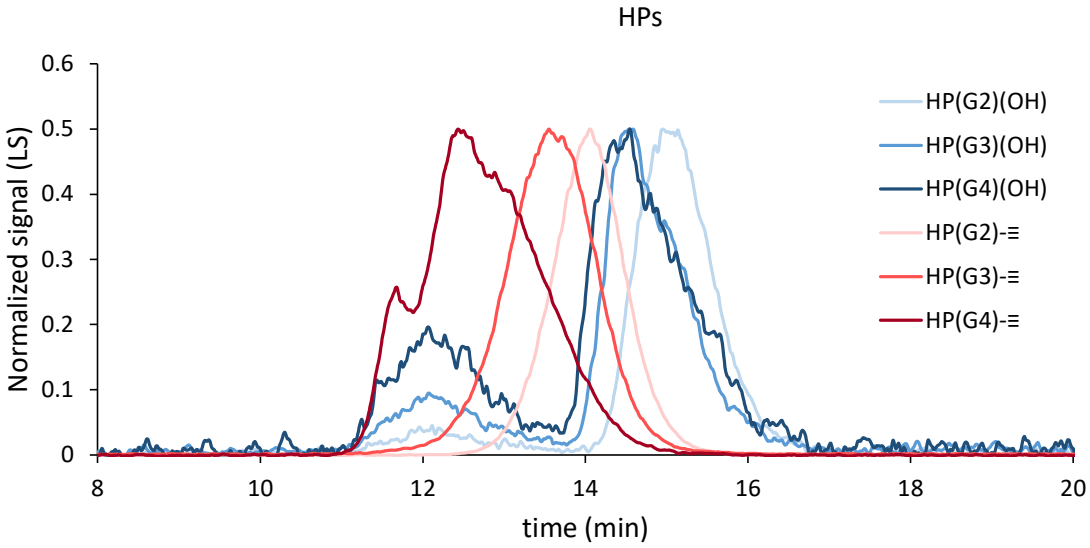

Annexe 2. SEC chromatograms overlap of the commercial HP(G2,G3,G4)(OH) (blue) and the HPs functionalised with alkyne groups, HP(G2,G3,G4)-≡ (red). LS: light scattering.

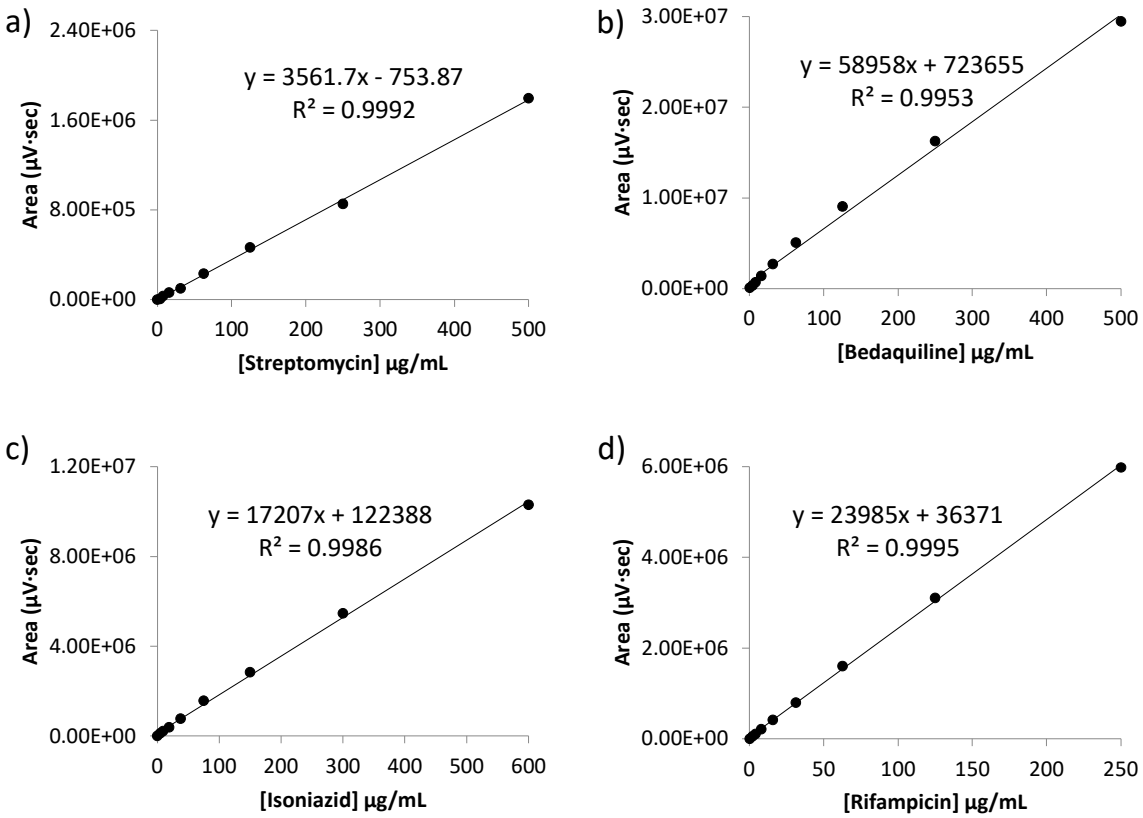

Annexe 3. Calibration curves for the anti-tuberculosis drugs measured by HPLC: a) streptomycin, b) bedaquiline, c) isoniazid and d) rifampicin.

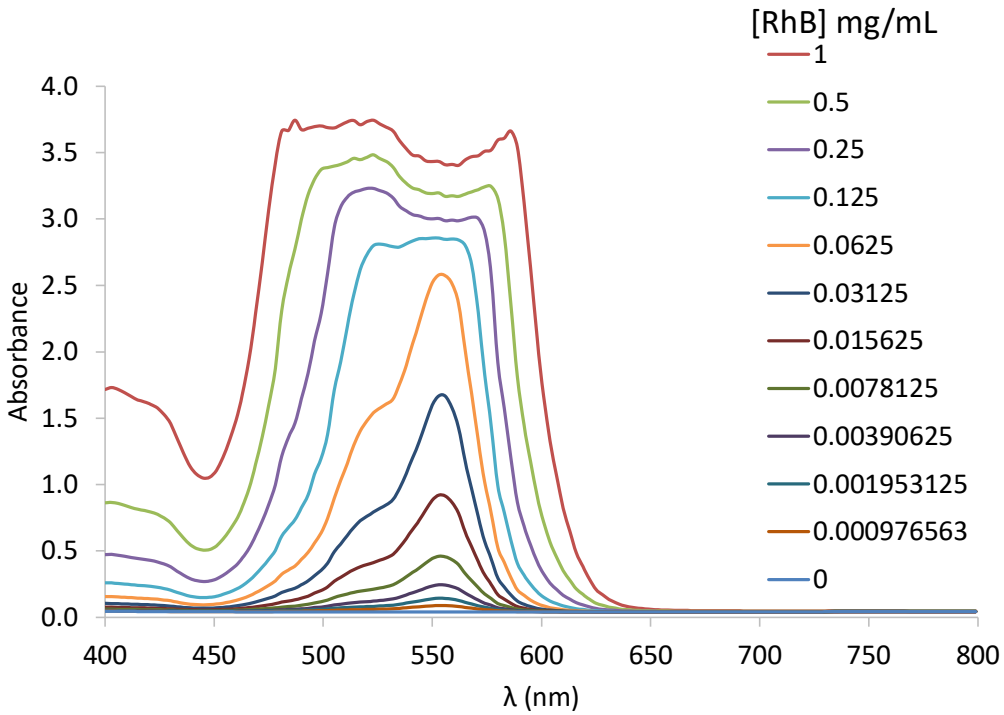

Annexe 4. Absorbance scan spectra of Rhodamine B at different concentrations in milliQ-H_2O. Triplicates were measured in an Infinite M Nano+ (TECAN) instrument.

		pGFP		siGFP	
Pseudodendrimers	Empty carriers	Dendriplexes N/P 25	Dendriplexes N/P 500	Dendriplexes N/P 150	Dendriplexes N/P 750
DHP(G2)-MPA	12 ± 3	27 ± 5	9 ± 3	190 ± 10	113 ± 5
DHP(G3)-MPA	15 ± 4	26 ± 5	25 ± 4	233 ± 5	157 ± 13
DHP(G4)-MPA	18 ± 1	27 ± 5	17 ± 2	209 ± 9	77 ± 14
DHP(G2)-GMPA	7 ± 1	32 ± 7	3 ± 1	178 ± 8	112 ± 4
DHP(G3)-GMPA	14 ± 2	32 ± 4	31 ± 7	178 ± 11	121 ± 7
DHP(G4)-GMPA	9 ± 2	33 ± 2	12 ± 2	230 ± 9	172 ± 18

Annexe 5. Hydrodynamic diameters (in nm) of the empty DHPs and the dendriplexes DHP/genetic material at different N/P ratios, measured by DLS in number. Data are represented as mean ± SD (n=3).